WHOI-94-12
1993

DTIC
SELECTED
JUL 2 1 1995
G

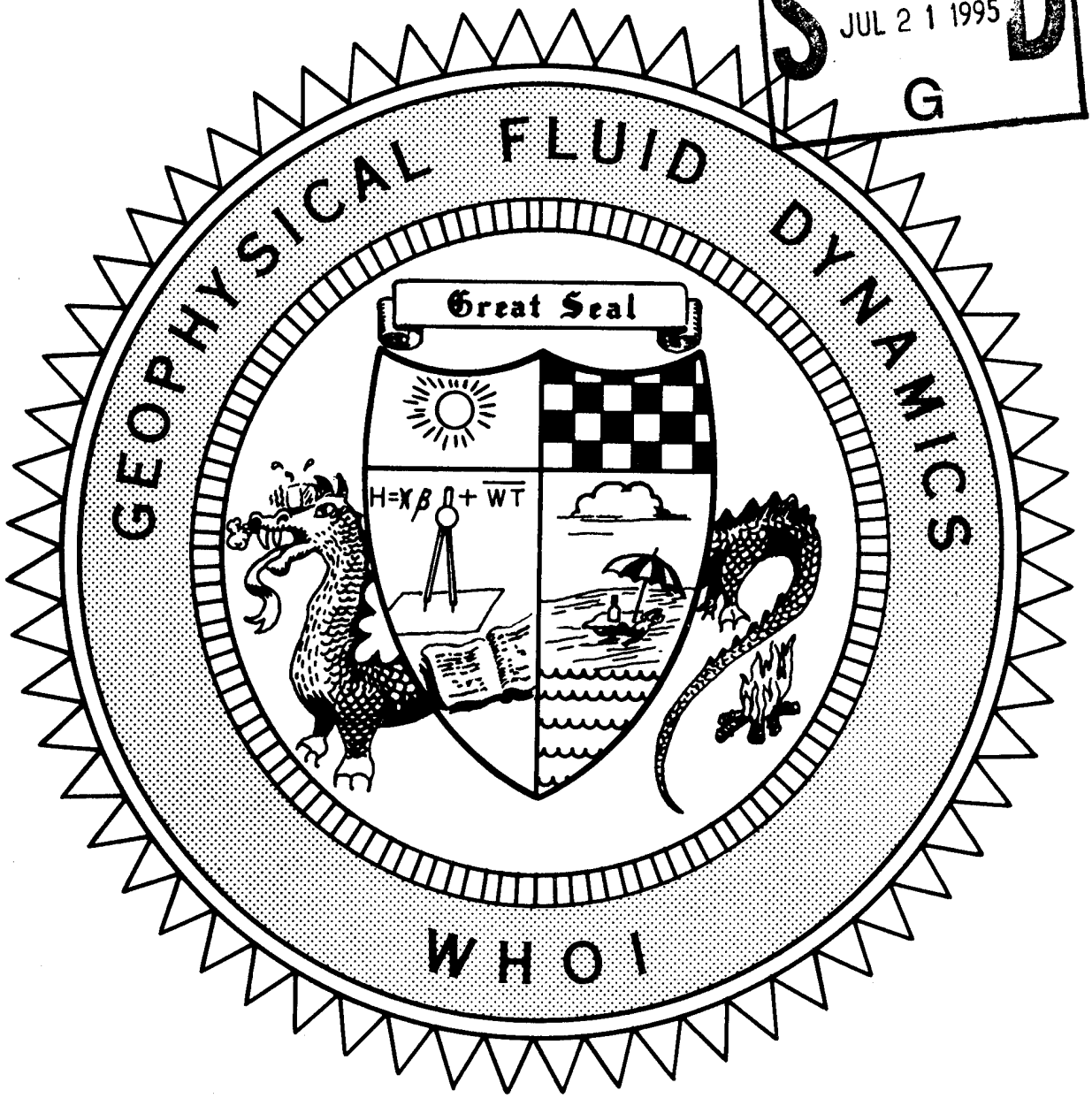

DISTRIBUTION STATEMENT A
Approved for public release;
Distribution Unlimited

DTIC QUALITY INSPECTED 5

19950720 011

Course Lectures
Abstracts of Participants
Fellows Project Reports

WHOI-94-12

"Geometrical Methods In Fluid Dynamics"
1993 Summer Study Program in Geophysical Fluid Dynamics

by

Rick Salmon, Director
and
Barbara Ewing-Deremer, Staff Assistant

Woods Hole Oceanographic Institution
Woods Hole, Massachusetts 02543

Accesion For
NTIS CRA&I [X]
DTIC TAB [ ]
Unannounced [ ]
Justification
By
Distribution /
Availability Codes
Dist | Avail and / or Special
A-1

Summer 1993

Technical Report

Funding was provided by the National Science Foundation
under Grant No. OCE-8901012.

Reproduction in whole or in part is permitted for any purpose of the United States Government. This report should be cited as Woods Hole Oceanog. Inst. Tech. Rept., WHOI-94-12.

Approved for public release; distribution unlimited.

Approved for Distribution:

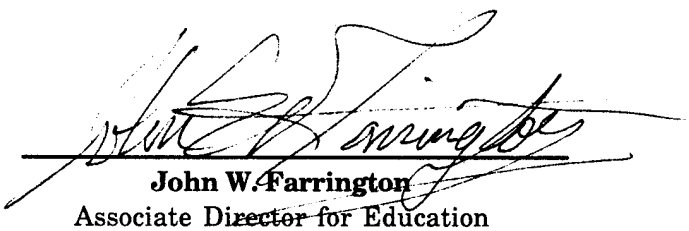

John W. Farrington
Associate Director for Education
Dean of Graduate Studies

Contents

Group Photograph 6
Director's message 7
1993 GFD Participants 8
1993 Lecture Schedule 10

Photo: Principal Lecturer Phil Morrison 16

Principal Lectures by Philip J. Morrison:
HAMILTONIAN DESCRIPTION OF THE IDEAL FLUID

Introduction 17

I. Rudiments of few degree-of-freedom systems illustrated by passive advection in two-dimensional fluids

A. Model for two-dimensional fluid motion 21
B. Passive advection 23
C. Integrable systems: one degree of freedom 24
D. Chaotic dynamics: two degrees of freedom 26
E. "Diffusion": three degrees of freedom 31

II. Functional differentiation, two action principles of mechanics and the action principle and canonical Hamiltonian description of the ideal fluid

A. Functional calculus 34
B. Two action principles of mechanics 41
C. Action principle and canonical Hamiltonian description of the ideal fluid in Lagrangian or material variables 44

III. Noncanonical Hamiltonian dynamics — Examples

A. Noncanonical Hamiltonian dynamics 50
B. Examples
1. Free rigid body 57
2. Korteweg-deVries equation 58
3. 1-D pressureless fluid 59
4. 1-D compressible fluid 60
5. 2-D Euler scalar vortex dynamics 61
6. 3-D ideal fluid 63
7. General comments 66

IV. Tutorial on Lie groups and algebras, reduction—realization, and Clebsch variables

A. Tutorial on Lie groups and algebras 67
B. Reduction—realization
1. Reduction of finite dimensional systems 75
2. Standard reduction 76
3. Reduction of the free rigid body 78
4. Reduction for the ideal fluid: Lagrangian to Eulerian variables 80
C. Clebsch variables
1. Clebsch variables for finite systems 83
2. Clebsch variables for infinite systems 84
3. Fluid examples 86
4. Semidirect product relations 88
5. Other Clebsch reductions: the ideal fluid 88

V. Stability and Hamiltonian systems

A. Stability and canonical Hamiltonian systems 91
B. Stability and noncanonical Hamiltonian systems 100
C. Dynamical accessibility 105

Photo: Principal Lecturer Ted Shepherd 112

Principal Lectures by Theodore G. Shepherd:
APPLICATIONS OF HAMILTONIAN THEORY TO GFD

1. Generalized Hamiltonian dynamics
1.1 Introduction 113
1.2 Dynamics 114
1.3 Steady states and conditional extrema 115
1.4 Example: barotropic vorticity equation 116
1.5 Symmetries and conservation laws 118
1.6 Steadily translating solutions 120

2. Hamiltonian structure of quasi-geostrophic flow
2.1 The two-layer model 121
2.2 Continuously stratified flow over topography 123

3. Pseudoenergy and available potential energy
3.1 Disturbances to basic states 125
3.2 APE of internal gravity waves 126
3.3 Pseudoenergy 127
3.4 Example: stratified Boussinesq flow 129
3.5 Nonlinear static stability 131
3.6 Nonlinear saturation of instabilities 132

4. Pseudoenergy and Arnol'd's stability theorems
4.1 Arnol'd's stability theorems 134
4.2 Andrews' theorem 137
4.3 Available energy 138
4.4 Nonlinear saturation of baroclinic instability 139

5. Pseudomomentum
5.1 General construction 142
5.2 Example: barotropic vorticity equation 143
5.3 Wave, mean-flow interaction 145
5.4 Wave action 147
5.5 Instabilities 148

Reports of the Fellows

A nonlinear wave in rotating shallow water
Oliver Bühler 153

Drop formation from viscous fingering 160
Silvana S. S. Cardoso

A study of a shell model of fully developed turbulence 170
Diego del-Castillo-Negrete

Gravity wave generation by quasi-geostrophic point vortices 185
Geoffrey T. Dairiki

A periodic orbit expansion of the Lorenz system 199
Sean McNamara

Elliptical vortices in shear:
Hamiltonian formulation, vortex merger and chaos 211
Keith Ngan

A Hamiltonian weak-wave model for shallow water flow 224
Caroline L. Nore

Dissipative quantum chaos 239
Dean Petrich

Moisture and available potential energy 248
Kyle Swanson

On aspects of Benney's equation 257
Rodney A. Worthing

Other Lectures

Coherent structures and homoclinic orbits 266
N. J. Balmforth

Intergyre water exchange of combined wind and buoyancy forcing 271
Liang Gui Chen

Fast dynamos near integrability 275
Steve Childress

Pressure fluctuations in swirling turbulent flows 277
Stephan Fauve

Gulf Stream meandering: Some physics and some biology 282
Glenn Flierl and Cabell Davis

Generation of solitary waves by external forcing 283
Roger Grimshaw

Solitary waves with oscillatory tails and exponential asymptotics Roger Grimshaw 292

Vertical temperature gradient finestructure spectra in the Gulf of California 299
Juan A. Rodrigues-Sero and Myrl C. Hendershott

On the representation of a magnetic field as a vector product of two gradients Louis N. Howard 300

Why do synoptic scale eddies like to go to the tropics? 304
R. Kimura and H. B. Cheong

Short wavelength instabilities of Riemann ellipsoids 309
Norman R. Lebovitz

Vorticity coordinates and a canonical form
for balanced models 312
Gudrun Magnusdottir

Necessary conditions for statistical stability:
with applications to large scale flow due to convection 317
Willem V. R. Malkus

Three-dimensional, Hamiltonian vortices 322
Steve Meacham

Higher order models for water waves 327
Peter J. Olver

Hamiltonian GFD and stability 332
Pedro Ripa

Structure of the canonical transformation 337
Ian Roulstone and Michael J. Sewell

On the Hamiltonian structure of semi-geostrophic theory 342
Ian Roulstone and John Norbury

Linear and nonlinear baroclinic wave packets:
atmospheric cyclogenesis and storm tracks 347
Kyle Swanson

Instability in extended systems 351
L. Tao and E. A. Spiegel

The fluid dynamics of crystal slurries 360
Andrew W. Woods and Richard A. Jarvis

A laboratory model of cooling over the continental shelf 362
J. A. Whitehead

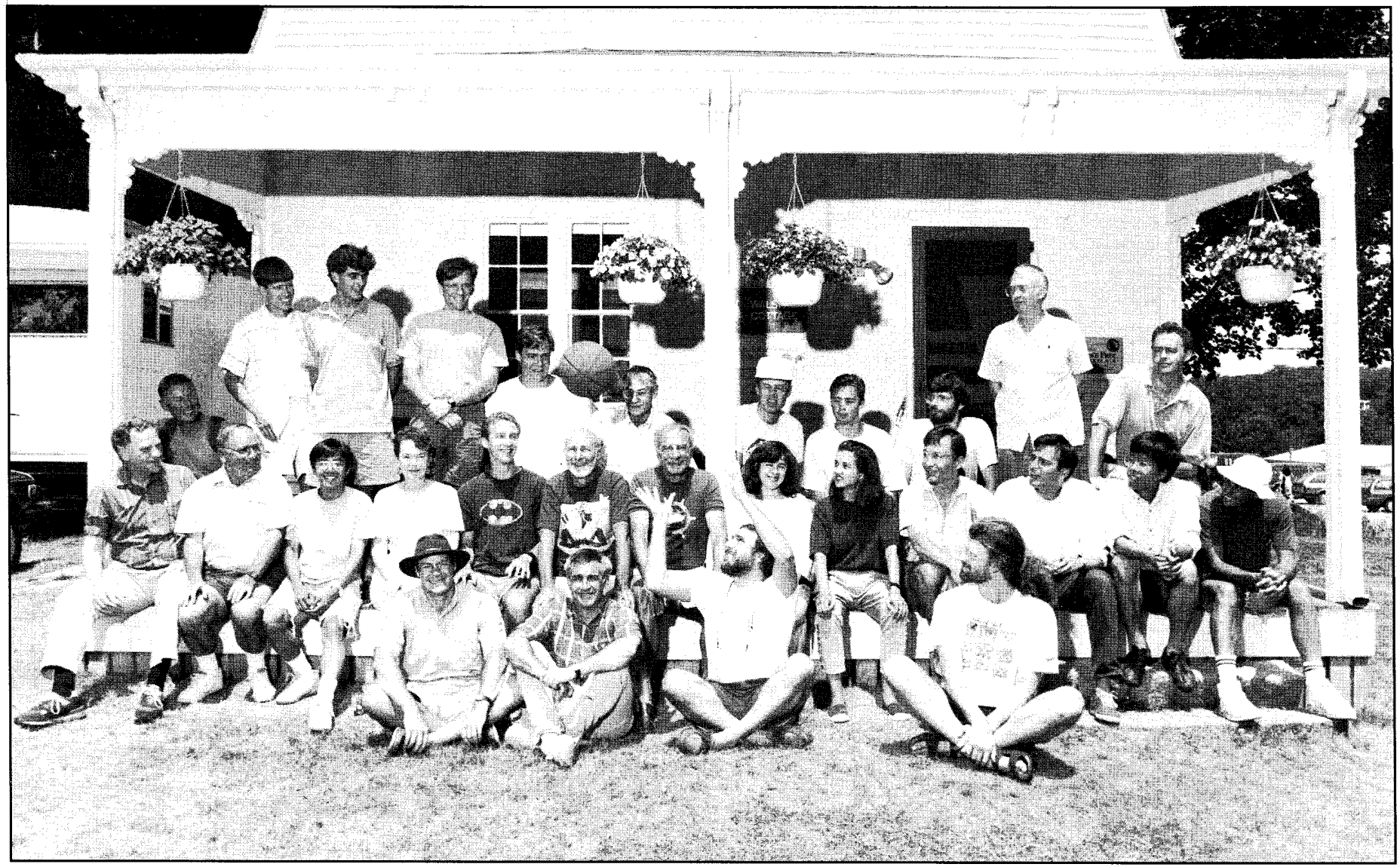

Front Row: Shepherd, Salmon, Morrison, Bokhove

Middle Row: Spiegel, Frazell, Tao, Ewing-DeRemer, Petrich, Keller, Veronis, Cardoso, Nore, Dairiki, Buhler, Ngan, Worthing

Back Row: Whitehead, McNamara, Woods, Del-Castillo, Swanson, Lebovitz, Ierley, Balmforth, Meacham, Malkus, Vallis

Director's message

"Geometrical methods in fluid dynamics" were the subject of the 1993 GFD session, a mathematical summer in which the inhabitants of Walsh Cottage explored applications of Hamiltonian fluid mechanics and related ideas about symmetry and conservation laws to practical problems in geophysical fluid dynamics. Experts Phil Morrison and Ted Shepherd set the pace with an intensive introductory course, leaving themselves exhausted and the rest of us greatly stimulated. Subsequent lecturers "fanned out" to cover the spectrum of currently interesting topics, from *slow manifolds* to *fast dynamos.*

The 1993 session attracted an extraordinary number of visitors, forcing the director to abandon his early promise of "no afternoon lectures after the first few weeks." But despite the heavy schedule, lots of work got done, especially by our fellows, several of whom apparently discovered the secret of going entirely without sleep. This year we stretched our meager resources to accept 10 fellows from a group of 45 outstanding applicants. However, I must sincerely apologize to the many excellent young scientists who had to be turned down.

This year, in an effort to decrease the 1993 volume's size while increasing its archival value, I mildly discouraged participants from submitting abstracts of work that would soon be published in a regular journal. Therefore, readers should be sure to scan the "1993 Lecture Schedule" to get a complete picture of what went on at the cottage.

Once again, it is a great pleasure to thank the Woods Hole Oceanographic Institution for its warm hospitality, and Jake Peirson and the staff of the WHOI Education office for their indispensable help. Very special thanks go to our administrative assistant, Barbara Ewing-DeRemer; to our crisis-management specialist, Bob Frazell; and to Steve Meacham and Glenn Flierl, who kept things running smoothly in the computer trailer. We gratefully acknowledge the continuing support of the National Science Foundation and the Office of Naval Research.

Rick Salmon
1993 Director

1993 GFD Participants

The Fellows

Oliver Bühler	Germany
Diego del-Castillo-Negrete	Mexico
Silvana Cardoso	Portugal
Geoffrey Dairiki	USA
Sean McNamara	USA
Keith Ngan	Canada
Caroline Nore	France
Dean Petrich	USA
Kyle Swanson	USA
Rodney Worthing	USA

The Staff and Visitors

James Anderson	Stevens Institute of Technology
Neil Balmforth	Columbia University
Janet Becker	University of California, San Diego
Onno Bokhove	University of Toronto
Sally Bower	University of Cambridge
Paola Cessi	University of California, San Diego
Eric Chassignet	Univeristy of Miami
Liang Gui Chen	University of California, San Diego
Steven Childress	New York University
John David Crawford	University of Pittsburgh
Anders Engqvist	Stockholm University
Stephan Fauve	Ecole Normale Superieure de Lyon
Glenn Flierl	Massachusetts Institute of Technology
Roger Grimshaw	Monash University
Karl Helfrich	Woods Hole Oceanographic Institution
Myrl Hendershott	University of California, San Diego
Louis Howard	Florida State University
Glenn Ierley	University of California, San Diego
Joseph Keller	Stanford University
Ryuji Kimura	University of Tokyo
Norman Lebovitz	University of Chicago
Gudrun Magnusdottir	University of Cambridge
Willem Malkus	Massachusetts Institute of Technology
Josep Massaguer	Universitat Politecnica Catalunya
Steve Meacham	Florida State University

Philip Morrison	University of Texas
Peter Olver	University of Minnesota
Joseph Pedlosky	Woods Hole Oceanographic Institution
R. James Purser	National Meteorological Center
Pedro Ripa	Centro de Investigacion Cientifica y de Educacion Superior de Ensenada
Claes Rooth	University of Miami
Robert Rosner	University of Chicago
Ian Roulstone	Meteorological Office (U.K.)
Rick Salmon	University of California, San Diego
Bradley Shadwick	University of Texas
Julio Sheinbaum	Centro de Investigacion Cientifica y de Educacion Superior de Ensenada
Ted Shepherd	University of Toronto
Sergio Signorini	National Science Foundation
Edward Spiegel	Columbia University
Melvin Stern	Florida State University
Louis Tao	University of Chicago
Geoffrey Vallis	University of California, Santa Cruz
George Veronis	Yale University
Fabian Waleffe	Massachusetts Institute of Technology
Tom Warn	McGill University
Jack Whitehead	Woods Hole Oceanographic Institution
Andrew Woods	Cambridge University
William Young	University of California, San Diego

Lecture Schedule

Mon. June 21, 10 AM
Rudiments of few-degree-of-freedom systems, chaotic advection
Phil Morrison

Tues. June 22, 10 AM
Functional differentiation, two mechanical action principles, action for a fluid
Phil Morrison

Wed. June 23, 10 AM
Noncanonical mechanics
Phil Morrison

Wed. June 23, 2 PM
Generation of solitary waves by external forcing and mesoscale variability
Roger Grimshaw

Thurs. June 24, 10 AM
Lie algebras, Poisson maps, reduction, Clebsch variables
Phil Morrison

Fri. June 25, 10 AM
Linear Hamiltonian systems, variational principles for equilibrium and stability
Phil Morrison

Fri. June 25, 2 PM
Parametrically excited quasi-patterns
Stephan Fauve

Mon. June 28, 10 AM
Generalized Hamiltonian dynamics: extremal properties, symmetries, and conservation laws
Ted Shepherd

Mon. June 28, 2 PM
Vorticity coordinates, transformed primitive equations, and a generalized form for balanced models
Gudrun Magnusdottir

Tue. June 29, 10 AM
Examples from geophysical fluid dynamics
Ted Shepherd

Wed. June 30, 10 AM
Pseudoenergy and available potential energy
Ted Shepherd

Wed. June 30, 2 PM
Averaging and adiabatic invariants for Hamiltonian systems
Norman Lebovitz

Thurs. July 1, 10 AM

Pseudoenergy and nonlinear stability
Ted Shepherd

Thurs. July 1, 2 PM

Putting some thermodynamics into simple ocean models
Pedro Ripa

Fri. July 2, 10 AM

Pseudomomentum and wave, mean-flow interaction
Ted Shepherd

Fri. July 2, 2 PM

Success and failure of Arnol'd's method
Pedro Ripa

Mon. July 5, 10 AM

A tutorial on Lie groups and algebras
Phil Morrison

Tue. July 6, 10 AM

Contour dynamics: Why are Hamiltonian approaches useful?
Glenn Flierl, Steve Meacham, and Phil Morrison

Tue. July 6, 1:30 PM

Exponential asymptotics and weakly nonlocal solitary waves
Roger Grimshaw

Wed. July 7, 10 AM

Introduction to symmetry methods
Peter Olver

Thurs. July 8, 10 AM

Large-scale flows, resonances and waves in two-dimensional thermal convection
Josep Massaguer

Thurs. July 8, 2 PM

Existence and non-existence of solitary waves
Peter Olver

Fri. July 9, 10 AM

The KdV equation and vortex patch dynamics
Dean Petrich

Mon. July 12, 10 AM

Inshore continental inertial boundary layers
Melvin Stern

Tues. July 13, 10 AM

Stability of shear flows
Joe Keller

Tues. July 13, 1:30 PM
Temperature finestructure in the Gulf of California
Myrl Hendershott

Wed. July 14, 10 AM
Astro-mathematics of the solar cycle
Ed Spiegel

Wed. July 14, 2 PM
Short wavelength instabilities of two-dimensional flows
Norman Lebovitz

Thurs. July 15, 10 AM
Fluid dynamics of crystal slurries
Andrew Woods

Fri. July 16, 10 AM
Hamiltonian quasigeostrophic vortices
Steve Meacham

Mon. July 19, 10 AM
Coherent structures and homoclinic orbits
Neil Balmforth

Tue. July 20, 10 AM
Introduction to center manifolds and normal forms
John David Crawford

Wed. July 21, 10 AM
Basic states in rotationally symmetric systems
John David Crawford

Wed. July 21, 1:30 PM
Center manifolds for extended systems
Ed Spiegel

Thurs. July 22, 10 AM
A model of Gulf Stream recirculation and separation
George Veronis

Thurs. July 22, 2 PM
Bifurcations with circular symmetry and rotational symmetry
John David Crawford

Fri. July 23, 10 AM
A numerical study of hydrodynamics using the nonlinear Schrodinger equation
Caroline Nore

Mon. July 26, 10 AM
Instability of shear flows
Fabian Waleffe

Tues. July 27, 10 AM

Linear and nonlinear baroclinic wavepackets: Atmospheric cyclogenesis and storm tracks

Kyle Swanson

Wed. July 28, 10 AM

Fast dynamos near integrability

Steve Childress

Wed. July 28, 2 PM

Intergyre water exchange of combined wind and buoyancy forcing

Lianggui Chen

Thurs. July 29, 10 AM

Marginally stable solitary waves

Joe Pedlosky

Fri. July 30, 10 AM

Berry phase in Hamiltoniam systems

James Anderson

Mon. Aug. 2, 10 AM

Gulf Stream meandering: some physics and some biology

Glenn Flierl

Tues. Aug. 3, 10 AM

Explosive resonant triads in a continuously stratified shear flow

Janet Becker

Wed. Aug. 4, 10 AM

How to make transient growth persist

Lou Howard

Thurs. Aug. 5, 10 AM

Necessary conditions for statistical stability applied to mean flows caused by convection

Willem Malkus

Fri. Aug. 6, 10 AM

Time-dependent exchange flows

Karl Helfrich

Mon. Aug. 9, 10 AM

A view of dynamical approximations

Rick Salmon

Mon. Aug. 9, 2 PM

Anatomy of the canonical transformation

Ian Roulstone

Tues. Aug. 10, 10 AM
Hamiltonian structure of the semigeostrophic equations
Ian Roulstone

Tues. Aug. 10, 2PM
Hamiltonian balanced dynamics and the slow manifold
Onno Bokhove

Wed. Aug. 11, 10 AM
Contact transformations and the construction of consistent semigeostrophic theories
James Purser

Wed. Aug. 11, 7 PM
A night in the center manifold
Ed Spiegel

Thurs. Aug. 12, 10 AM
Fast algorithms for the construction of finite-element semigeostrophic solutions
James Purser

Fri. Aug. 13, 10 AM
Mechanisms of dense water removal from the continental shelf
Jack Whitehead

Mon. Aug. 16, 10 AM
On geometric constraints for the diffusion of vector fields
Robert Rosner

Tue. Aug. 17, 10 AM
Chaotic transport by travelling waves in shear flow
Diego del-Castillo

Wed. Aug. 18, 10 AM
Cancelling the dynamo
Louis Tao

Thurs. Aug. 19, 10 AM
Why do synoptic-scale atmospheric eddies in mid-latitude like to go to the tropics?
Ryuji Kimura

Tues. Aug. 24, 10 AM
Dissipative quantum chaos
Dean Petrich

Tues. Aug. 24, 11:15 AM
Gravity-wave generation by (pseudo) quasigeostrophic vortices
Jeff Dairiki

Tues. Aug. 24, 2 PM
Waves in label-space
Oliver Bühler

Tues. Aug. 24, 3:15 PM

Drop formation from viscous fingering
Silvana Cardoso

Wed. Aug. 25, 10 AM

A study of intermittency in a shell model of fully-developed turbulence
Diego del Castillo

Wed. Aug. 25, 11:15 AM

Elliptical vortices in shear: Hamiltonian formulation, vortex merger, and chaos
Keith Ngan

Wed. Aug. 25, 2 PM

Hamiltonians and moisture: Generalizations of convective available potential energy
Kyle Swanson

Thurs. Aug. 25, 10 AM

A Hamiltonian weak-wave model for shallow-water flow
Caroline Nore

Thurs. Aug. 25, 11:15 AM

Pulsating pulses
Rodney Worthing

Thurs. Aug. 25, 2 PM

Application of the periodic-orbit expansion to the Lorenz system
Sean McNamara

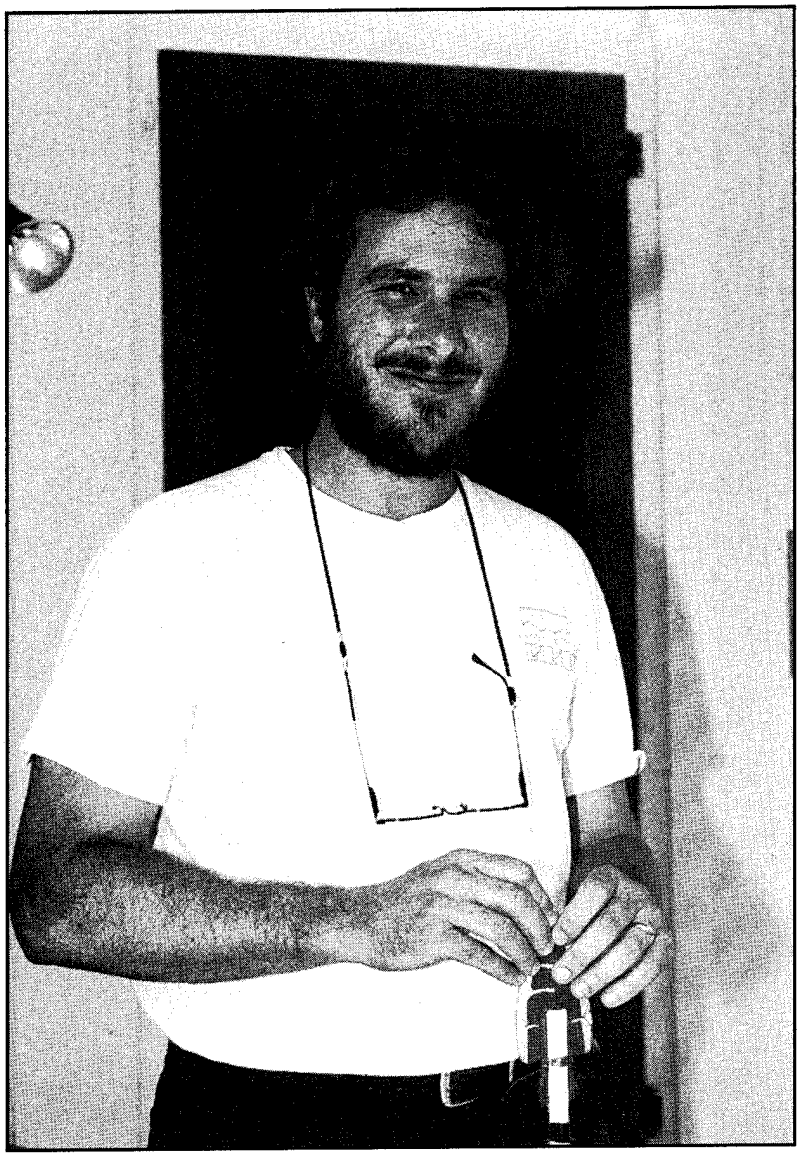

Principal Lecturer Phil Morrison

Hamiltonian Description of the Ideal Fluid

P. J. MORRISON
Department of Physics and Institute for Fusion Studies
The University of Texas at Austin
Austin, Texas 78712
morrison@hagar.ph.utexas.edu

Introduction

Why look at fluid mechanics from a Hamiltonian perspective? The simple answer is because it is there and it is beautiful. For ideal fluids the Hamiltonian form is not artificial or contrived, but something that is basic to the model. However, if you are a meteorologist or an oceanographer, perhaps what you consider to be beautiful is the ability to predict the weather next week or to understand transport caused by ocean currents. If this is the case, a more practical answer may be needed. Below, in the remainder of this Introduction, I will give some arguments to this effect. However, I have observed that the Hamiltonian philosophy is like avocado: you either like it or you don't. In any event, over the past 13 years I have also observed a strong development in this field, and this is very likely to continue.

One practical reason for the Hamiltonian point of view is that it provides a unifying framework. In particular, when solving "real" problems one makes approximations about what the dominant physics is, considers different geometries, defines small parameters, expands, etc. In the course of doing this there are various kinds of calculations that are done again and again, for example, calculations regarding:

1. waves and instabilities by means of linear eigenanalyses;
2. parameter dependencies of eigenvalues as obtained by such eigenanalyses;
3. stability that are based on arguments involving energy or other invariants;
4. various kinds of perturbation theory;
5. approximations that lead to low degree-of-freedom dynamics.

After a while one discovers that certain things happen over and over again in the above calculations, for example:

1. the nature of the spectrum is not arbitrary, but possesses limitations;
2. upon collision of eigenvalues only certain types of bifurcations can occur;
3. the existence of Rayleigh type stability criteria (these occur for a wide variety of fluid and plasma problems);
4. simplifications based on common patterns;
5. common methods for reducing the order of systems.

By understanding the Hamiltonian perspective, one knows in advance (within bounds) what answers to expect and what kinds of procedures can be performed.

In cases where dissipation is not important and approximations are going to be made, it is, in my opinion, desirable to have the approximate model retain the Hamiltonian structure of the primitive model. One may not want to introduce spurious unphysical dissipation. Understanding the Hamiltonian structure allows one to make Hamiltonian approximations. In physical situations where dissipation is important, I believe it is useful to see in which way the dynamics differ from what one expects for the ideal (dissipationless) model. The Hamiltonian model thus serves as a sort of benchmark. Also, when approximating models with dissipation we can isolate which part is dissipative and make sure that the Hamiltonian part retains its Hamiltonian structure and so on.

It is well-know that Hamiltonian systems are not structurally stable in a strict mathematical sense (that I won't define here). However, this obviously does not mean that Hamiltonian systems are not important; the physics point of view can differ from the mathematics. A simple linear oscillator with very small damping can behave, over long periods of time, like an undamped oscillator, even though the topology of its dynamics is quite different.

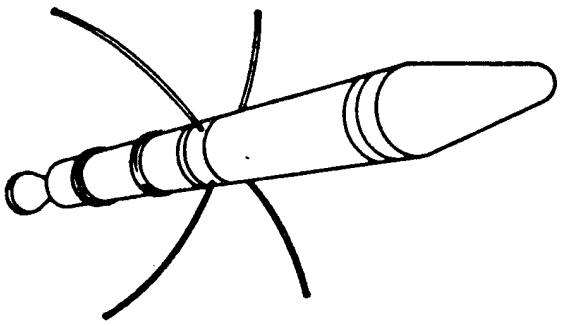

Figure 1:

To say that a Hamiltonian system is structurally unstable is not enough. A favorite example of mine that illustrates this point concerns the first U.S. satellite, Explorer I, which was launched in 1958 (see Figure 1). This spacecraft was designed so that its attitude would be stabilized by spin about its symmetry axis. However, the intended spin-stabilized state did not persist and the satellite soon began to tumble. The reason for this is attributed

to energy dissipation in the small antennae shown in the figure. Thus unlike the simple oscillator, where the addition of dissipation has a small effect, here the addition of dissipation had a catastrophic effect. Indeed, this was a most expensive experiment on *negative energy modes*, a universal phenomenon in fluids that I will discuss.

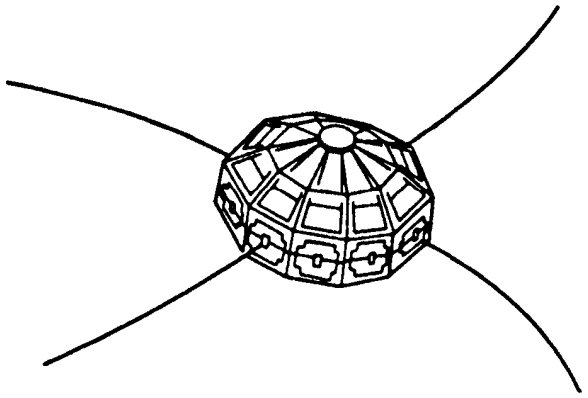

Figure 2:

After Explorer I, in 1962 Alouette I was launched (see Figure 2)*, which has an obvious design difference. This satellite behaved like the damped linear oscillator in the sense that dissipation merely caused it to spin down. I would like to emphasize that the difference between the behavior of Explorer I and Alouette I lies in a mathematical property of the Hamiltonian dynamics of these spacecraft; it could have been predicted.

So, the purpose of my lectures is to describe the Hamiltonian point of view in fluid mechanics, and to do so in an accessible language. It is to give you some fairly general tools and tricks. I am not going to solve a single "real" problem; however, you will see specific examples of problems throughout the summer. Lecture I is somewhat different in flavor from the others. Imagine that you have succeeded in obtaining a finite Hamiltonian system out of some fluid model, the Kida vortex being a good example. What should you expect of the dynamics? Lecture I, being a sketch of low degree-of-freedom Hamiltonian dynamics, answers this to some degree. The remaining four lectures are concerned with the structure of infinite degree-of-freedom Hamiltonian systems, although I will often use finite systems for means of exposition. To see how the Lectures are organized, consult the Table of Contents.

References are given both as footnotes and at the end of various sections. Those at the ends of sections are typically of a more general and comprehensive nature. The referencing should not be taken as complete, but as a guide to the literature.

Acknowledgments

First and foremost I would like to thank Rick Salmon for being an excellent Director of the summer program and for facilitating this cathartic outburst. I would like to thank the Fellows for being a jolly good audience and for their aid in the preparation of this

*Both Figures 1 and 2 are after P. W. Likins, AGARD Lecture Series, 3b-1 (1971).

document. In particular, Oliver Buhler and Caroline Nore helped with the Introduction and Lecture IV, Diego del-Castillo-Negrete helped with Lecture I, Geoffrey Dairiki and Keith Ngan helped with Lecture II, Sean McNamara and Dean Petrich helped with Lecture III, and Kyle Swanson and Rodney Worthing helped with Lecture V. Thanks also are given to Brad Shadwick for help with the figures, aid with TEX, and for general discussion pertaining to the text. I would like to give a blanket thanks to all the other participants for their role in creating the splendid "GFD environment." The Rambo-style proofreading efforts of L. C. Morrison are dearly appreciated. The hospitality of the Woods Hole Oceanographic Institution is greatly acknowledged, along with the support of the US Department of Energy under contract No. DE-FG05-80ET-53088.

I. Rudiments of Few Degree-of-Freedom Hamiltonian Systems Illustrated by Passive Advection in Two-Dimensional Fluids

In this introductory lecture we will review some basic aspects of Hamiltonian systems with a finite number of degrees of freedom. We illustrate, in particular, properties of one, two, and three degree-of-freedom systems by considering the passive advection of a tracer in two-dimensional incompressible fluid flow. The tracer is something that moves with, but does not influence, the fluid flow; examples include neutrally buoyant particles and colored dye. The reason for mixing Hamiltonian system phenomenology with fluid advection is that the latter provides a nice framework for visualization, since as we shall see the phase space of the Hamiltonian system is in fact the physical space occupied by the fluid.

A point of view advocated in this lecture series is that an understanding of finite Hamiltonian systems is useful for the eventual understanding of infinite degree-of-freedom systems, such as the equations of various ideal fluid models. Such infinite systems are the main subject of these lectures. It is important to understand that the infinite systems are distinct from the passive advection problem that is treated in this lecture; the former is governed by partial differential equations while the later is governed by ordinary differential equations.

A. A Model for Two-Dimensional Fluid Motion

In various situations fluids are adequately described by models were motion only occurs in two spatial dimensions. An important example is that of rotating fluids where the dominant physics is governed by geostrophic balance, where the pressure force is balanced by the Coriolis force. For these types of flows the well-known Taylor-Proudman* theorem states that the motion is predominantly two-dimensional. A sort of general model that describes a variety of two-dimensional fluid motion is given by the following:

$$\frac{\partial q}{\partial t} + [\psi, q] = \mathcal{S} + \mathcal{D}, \tag{I.1}$$

where $q(x,y,t)$ is a vorticity-like variable, $\psi(x,y,t)$ is a stream function, both of which are functions of the spatial variable $(x,y) \in D$, where D is some spatial domain, and t is time. The quantities $\mathcal{S}$ and $\mathcal{D}$ denote sources and sinks, respectively. Examples of $\mathcal{S}$ include the input of vorticity by means of pumping or stirring, while examples of $\mathcal{D}$ include viscous dissipation and Ekman drag. Above, the Poisson bracket notation, which is also the Jacobian, is used:

$$[f,g] := \frac{\partial f}{\partial x}\frac{\partial g}{\partial y} - \frac{\partial f}{\partial y}\frac{\partial g}{\partial x}, \tag{I.2}$$

and we have assumed incompressible flow, which implies that the two components of the velocity field are given by

$$(u,v) = \left(-\frac{\partial \psi}{\partial y}, \frac{\partial \psi}{\partial x}\right). \tag{I.3}$$

*J. Pedlosky, *Geophysical Fluid Dynamics*, 2nd ed. (Springer-Verlag, New York, 1987).

In order to close the system a "self-consistency" condition that relates q and ψ is required. We signify this by $q = \mathcal{L}\psi$. Examples include:

- The two-dimensional Euler equation where $q = \nabla^2\psi$.
- The rotating fluid on the β-plane where $q = \nabla^2\psi + \beta y$.

In the former case q is the vorticity, while in the latter case q is the potential vorticity.

For convenience we will suppose that the domain D is an annular region as depicted in Figure 1 below. Many experiments have been performed in this geometry* where the fluid swirls about in the θ and r directions and is predominantly two-dimensional. The geometry of the annulus suggests the use of polar coordinates, which are given here by the formulas: $x = r\sin\theta$ and $y = r\cos\theta$. In terms of r and θ the bracket of (I.2) becomes

$$[f,g] = \frac{1}{r}\left(\frac{\partial f}{\partial\theta}\frac{\partial g}{\partial r} - \frac{\partial f}{\partial r}\frac{\partial g}{\partial\theta}\right). \tag{I.4}$$

The spatial variables (x,y) play the role below of canonical coordinates, with x being the configuration space variable and y being the canonical momentum. The transformation from (x,y) to (r,θ) is a noncanonical transformation and so the form of the Poisson bracket is altered as manifest by the factor of $1/r$. (In Lecture III we will discuss this in detail.) To preserve the canonical form we replace r by a new coordinate $J := r^2/2$ and the bracket becomes

$$[f,g] = \frac{\partial f}{\partial\theta}\frac{\partial g}{\partial J} - \frac{\partial f}{\partial J}\frac{\partial g}{\partial\theta}. \tag{I.5}$$

These coordinates are convenient, since they can be action-angle variables, as we will see.

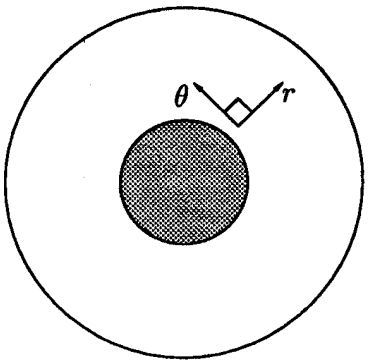

Figure 1:

A solution to (I.1) provides a stream function, $\psi(\theta, J, t)$. In this lecture we will assume that various forms of ψ are known, without going into detail as to whether or not these forms are solutions with particular choices of $\mathcal{L}$, $\mathcal{S}$, or $\mathcal{D}$. Here we will just suppose that the tracers

*See e.g. H. P. Greenspan, *Theory of Rotating Fluids* (Cambridge Univ. Press, Cambridge, 1968) and J. Sommeria, S. D. Meyers and H. L. Swinney, *Nonlinear Topics in Ocean Physics*, edited by A. Osborne, (North-Holland, Amsterdam, 1991).

in the fluid, specks of dust if you like, follow particular assumed forms for the velocity field of the flow. The stream function gives a means for visualizing this. Setting ψ=constant for some particular time defines an instantaneous stream line whose tangent is the velocity field. (See Figure 2 below.)

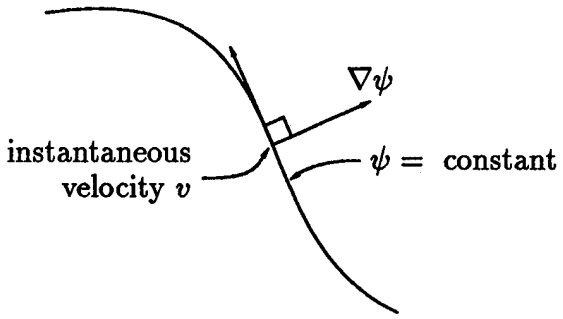

Figure 2:

B. Passive Advection

Imagine that a tiny piece of the fluid is labeled, somehow, in a way that it can be followed. As mentioned above, a small neutrally buoyant sphere or a small speck of dust might serve this purpose. Since such a tracer, the sphere or the speck, moves with the fluid its dynamics is governed by

$$\dot{x} = u = -\frac{\partial\psi}{\partial y} = [x,\psi]\,, \qquad \dot{y} = v = \frac{\partial\psi}{\partial x} = [y,\psi] \tag{I.6}$$

or in terms of the (θ, J) variables

$$\dot{J} = -\frac{\partial\psi}{\partial\theta}\,, \qquad \dot{\theta} = \frac{\partial\psi}{\partial J}\,. \tag{I.7}$$

These are special cases of Hamilton's equations, which are usually written as

$$\dot{p}_i = [p_i, H] = -\frac{\partial H}{\partial q_i}\,, \qquad \dot{q}_i = [q_i, H] = \frac{\partial H}{\partial p_i}, \qquad i = 1,2,\ldots N\,, \tag{I.8}$$

where [,], the *Poisson bracket*, is defined by

$$[f,g] = \sum_{i=1}^{n}\left(\frac{\partial f}{\partial q_i}\frac{\partial g}{\partial p_i} - \frac{\partial f}{\partial p_i}\frac{\partial g}{\partial q_i}\right)\,. \tag{I.9}$$

Here (q_i, p_i) constitutes a canonically conjugate pair with q_i being the canonical coordinate and p_i being the canonical momentum. Together they are coordinates for the $2N$ dimensional *phase space*. The function $H(q,p,t)$ is the Hamiltonian. Observe that y (or J), which physically is a coordinate, here plays the role of momentum, and $-\psi$ is the Hamiltonian.

We emphasize, once again, that the coordinates (x, y) are coordinates for something labelling a fluid element, and the motion of the fluid element is determined by a prescribed velocity field. This is to be distinguished from the Lagrangian variable description of the ideal fluid, which we treat in Lecture III, where the goal is to describe the velocity field as determined by the solution of a partial differential equation.

Before closing this subsection we give a bit of terminology. A single *degree of freedom* corresponds to each (q, p) pair. However, some account should be given as to whether or not H depends explicitly upon time. It is well-known that nonautonomous ordinary differential equations can be converted into autonomous ones by adding a dimension. Therefore, researchers sometimes count a half of a degree of freedom for this. Thus (I.7) is a $1\frac{1}{2}$ degree-of-freedom system if ψ depends explicitly upon time, otherwise it is a one degree-of-freedom system. This accounting is not so precise, since one might want to distinguish between different types of time dependencies. We will return to this point later.

C. Integrable Systems: One Degree of Freedom

All one degree-of-freedom systems are integrable. However, integrable systems of higher dimension are rare in spite of the fact that old-fashioned mechanics texts make them the center piece (if not the only piece). A theorem often credited to Siegel* shows how integrable systems are of measure zero. What exactly it means to be integrable is an active area of research with a certain amount of subjectivity. For us integrable systems will be those for which the motion is determined by the evaluation of N integrals. When this is the case, the motion is "simple."

More formally, a system with a time independent Hamiltonian, $H(q, p)$, with N degrees of freedom is said to be *integrable* if there exist N independent, smooth constants of motion I_i, i.e.,

$$\frac{dI_i}{dt} = [I_i, H] = 0\,, \qquad i, j = 1, 2, ...N\,, \tag{I.10}$$

that are in *involution*, i.e.,

$$[I_i, I_j] = 0\,, \qquad i, j = 1, 2, ...N\,. \tag{I.11}$$

The reason that the constants are required to be smooth and independent is that the equations $I_i = c_i$, where the c_i's are constants, must define N different surfaces of dimension $2N - 1$ in the $2N$ dimensional phase space. The reason for the constants to be in involution is that one wants to use the I's (or combinations of them) as momenta and momenta must pairwise commute. In coordinates of this type the motion is quite simple.

Sometimes additional requirements are added in definitions of integrability. For example, one can add the requirements that the surfaces I_i = constant for $i = 1, 2, ...N$ be *compact* and *connected.* If this is the case the motion takes place on an N-torus and there exist *action-angle* variables J_i, θ_i in terms of which Hamilton's equations have the form

$$\frac{dJ_i}{dt} = -\frac{\partial H}{\partial \theta_i} = 0\,, \qquad \frac{d\theta_i}{dt} = \frac{\partial H}{\partial J_i} = \Omega_i(J)\,, \qquad i, j = 1, 2, ...N\,. \tag{I.12}$$

*See e.g. J. Moser, *Stable and Random Motions in Dynamical Systems*, (Princeton University Press, Princeton, 1973).

The first of Eqs. (I.12) implies $H = H(J)$ alone. When H does not depend upon a coordinate, the coordinate is said to be *ignorable* and its conjugate momentum is a constant of motion. In action-angle variables all coordinates are ignorable and the second of Eqs. (I.12) is easy to integrate, yielding

$$\theta_i = \theta_i^0 + \Omega_i(J)t \qquad i,j = 1,2,...N\,, \tag{I.13}$$

where θ_i^0 is the integration constant, θ is defined modulo 2π, and $\Omega_i(J) := \partial H/\partial J_i$ are the frequencies of motion around the N-torus.

A good deal of the machinery of Hamiltonian mechanics was developed to try and reduce equations to the action-angle form above. If one could find a coordinate transformation, in particular a canonical transformation (c.f. Lecture III), that takes the system of interest into the form of (I.12), then one could simply integrate and then map back to get the solution in closed form. The theory of canonical transformations, Hamilton-Jacobi theory, etc. sprang up because of this idea. However, now it is known that this procedure is not possible in general because generically Hamiltonian systems are not integrable. Typically systems are *chaotic*, i.e., trajectories wander in a seemingly random way in phase space rather that lying on an N-dimensional torus. A distinct feature of trajectories is that they display *sensitive dependence* on initial conditions. We will say a little about this below.

To conclude this section we return to our fluid mechanics example, in which context we show how all one degree-of-freedom systems are integrable. In the case where ψ is time independent, we clearly have a single degree of freedom with one constant of motion, viz. ψ:

$$\dot{\psi} = \frac{\partial\psi}{\partial x}\,\dot{x} + \frac{\partial\psi}{\partial y}\,\dot{y} = 0\,, \tag{I.14}$$

which follows upon substitution of the equations of motion for the tracer, (I.6). To integrate the system one solves

$$\psi(x,y) = \psi_0 \tag{I.15}$$

for $x = f(\psi_0, y)$, which is in principle (if not in practice) possible, and then inserts the result as follows:

$$\dot{y} = \frac{\partial\psi}{\partial x}(x,y)\Big|_{x=f(\psi_0,y)} =: D(\psi_0,y)\,. \tag{I.16}$$

Equation(I.16) is separable, which implies

$$\int_{y_0}^{y} \frac{dy'}{D(\psi_0,y)} = \int_{t_0}^{t} dt'\,. \tag{I.17}$$

Thus we have reduced the system to the evaluation of a single integral, a so-called quadrature. There are some sticky points, though, since $x = f(\psi_0, y)$ may not be single-valued or even invertible explicitly, and usually one cannot do the integral explicitly. Moreover, afterwards one must invert (I.17) to obtain the trajectory. These are only technical problems, ones that are easily surmounted with modern computers.

Generally equations of the form of (I.1) possess equilibrium solutions when ψ and q depend upon only a single coordinate. The case of special interest here is when the domain is the annulus discussed above, polar coordinates are used, and ψ depends only upon r (or equivalently the canonical variable J). Physically this corresponds to a purely azimuthally symmetric, sheared fluid flow, where $v_\theta = v_\theta(r)$. In this case stream lines are "energy surfaces," which are merely concentric circles as depicted in Figure 3 below. The counterpart of (I.13), the equations of motion for the speck of dust in the fluid, are

$$\theta = \theta_0 + \Omega(r)\, t\,, \qquad\qquad r = r_0 \tag{I.18}$$

where $v_\theta = \Omega r$. Note the speck goes round and round at a rate dependent upon its radius, but does not go in or out.

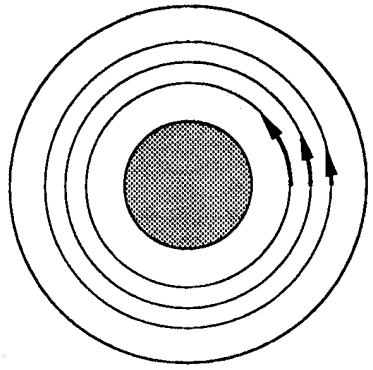

Figure 3:

D. Chaotic Dynamics: Two Degrees of Freedom

As noted, one degree-of-freedom systems are always integrable, but two degree-of-freedom systems typically are not. Nonintegrable systems exhibit chaos which is briefly described.

Systems with two degrees of freedom have a four dimensional phase space, which is difficult to visualize, so we do something else. A convenient artifice is the *surface of section* or as it is sometimes called the Poincaré section. Suppose the surface $H(q_1, q_2, p_1, p_2) =$ constant $=: E$ is compact (i.e. contained within a three sphere). Since the motion is restricted to this surface p_2 can be eliminated in lieu of E, which we keep fixed. We could then plot the trajectory in the space with the coordinates (q_1, q_2, p_1), but simpler pictures are obtained if we instead plot a point in the (q_1, p_1) plane whenever q_2 returns to its initial value, say $q_2 = 0$.

We also require that it pierce this plane with the momentum p_2 having the same sign upon each piercing. This separates out the branches of the surface $H = E$. That q_2 will return is almost assured, since the Poincaré recurrence theorem tells us that almost any orbit will return to within any ϵ-ball (points interior to a sphere of radius ϵ). It is unlikely it will traverse the ball without piercing q_2=0. (If there are no fixed points within the ball the

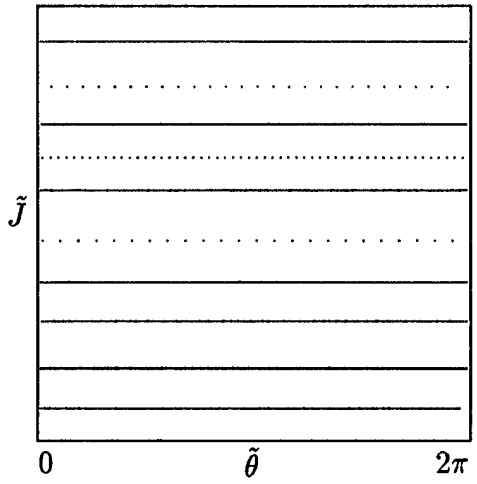

Figure 4:

vector field can be locally rectified and unless there is no component normal to the (q_1, p_1) plane, which is unlikely, it will pierce.)

For integrable systems an orbit either eventually returns to itself, in which case we have a *periodic orbit* or it maps out a curve, which is an example of an *invariant set.* The latter case is typical as illustrated in Figure 4. In nonintegrable or chaotic systems this is not true as is illustrated Figures 5(a) and 5(b), where it is seen that orbits make "erratic" patterns.

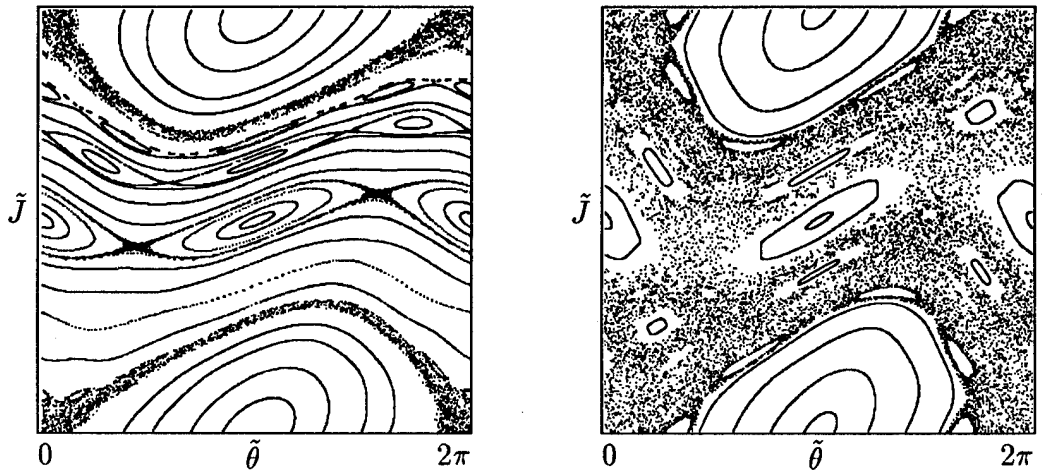

Figure 5:

Now what about the fluid mechanics illustration? Can chaos exist? How can we have a two degree-of-freedom system when we only have the two spatial coordinates, say (θ, J)? The answer is that explicit time dependence in ψ, the extra half of degree of freedom, is enough for chaos. There is, in fact, a trick for *puffing up* a $1\frac{1}{2}$ degree-of-freedom system and making it look like a two degree-of-freedom system, and vice verse.

Let s correspond to a fake time variable, set $t = \phi$, where ϕ is going to be a new canonical coordinate, and define a new Hamiltonian by

$$H(\theta, J, \phi, I) = \psi(\theta, J, \phi) + I\,. \tag{I.19}$$

The equations of motion for this Hamiltonian are

$$\frac{d\theta}{ds} = \frac{\partial H}{\partial J} = \frac{\partial \psi}{\partial J}\,, \qquad \frac{dJ}{ds} = -\frac{\partial H}{\partial \theta} = -\frac{\partial \psi}{\partial \theta}\,; \tag{I.20}$$

$$\frac{d\phi}{ds} = \frac{\partial H}{\partial I} = 1\,, \qquad \frac{dI}{ds} = -\frac{\partial H}{\partial \phi} = -\frac{\partial \psi}{\partial \phi}\,. \tag{I.21}$$

The first of Eqs. (I.21) tells us that $\phi = s + s_0 = t$; we set $s_0 = 0$. Thus we obtain what we already knew, namely, that $\phi = t$ and that Eqs. (I.20) give the correct equations of motion. What is the role of the second of Eqs. (I.21)? This equation merely tells us that I has to change so as to make H=constant.

The above trick becomes particularly useful when ψ is a periodic function of time: $\psi(\theta, J, t) = \psi(\theta, J, t + T)$. In this case it makes sense to identify $\phi + T$ with ϕ, because the force or vector field is the same at these points. With this identification done, it is clear that a surface of section is obtained by plotting (θ, J) at intervals of T.

We will leave it as an exercise to show how to construct $1\frac{1}{2}$ degree-of-freedom Hamiltonian systems from two degree-of-freedom Hamiltonian systems.

Now suppose the stream function is composed of an azimuthal shear flow plus a propagating wave:

$$\psi(J, \theta, t) = \psi_0(J) + \psi_1(J)\cos\left(m_1(\theta - \omega_1 t)\right)\,, \tag{I.22}$$

where $m_1 \in \mathbb{N}$ and ψ_1 is assumed small in comparison to ψ_0. Here $\psi_0(J)$ represents the azimuthal background shear flow and the second term represents the wave, with ψ_1, m_1 and ω_1 being the radial eigenfunction, mode number and frequency of the wave, respectively.

This system might look like a $1\frac{1}{2}$ degree-of-freedom system, but it is in fact integrable. The easiest way to see this is to boost into the frame of reference rotating with the wave. In this frame the stream function becomes

$$\tilde{\psi}(\tilde{J}, \tilde{\theta}, t) = \psi_0(\tilde{J}) + \psi_1(\tilde{J})\cos\left(m_1\tilde{\theta}\right) - \omega_1\tilde{J}\,, \tag{I.23}$$

where the canonical transformation is $\tilde{J} = J$, $\tilde{\theta} = \theta - \omega_1 t$. This transformation is derivable from the mixed variable generating function $F(\theta, \tilde{J}) = \tilde{J}(\theta - \omega_1 t)$. Note the term $-\omega_1\tilde{J}$ accounts for the azimuthal rigid rotation generated from the frame shift.

In the absence of the wave it is clear that the trajectories in phase space are just circles as shown in Figure 3 (or straight lines as plotted in Figure 4). However, from the form of (I.22) it is clear that something interesting is going to happen at stagnation points, that is, where

$$\frac{\partial \psi}{\partial \tilde{\theta}} = \frac{\partial \psi}{\partial \tilde{J}} = 0\,. \tag{I.24}$$

Stagnation points occur at places where the phase velocity of the wave matches the background azimuthal velocity. Here a *critical layer* opens up into an island chain. In the terminology of Hamiltonian dynamics this is called a *resonance* and looks as depicted in Figure 6 below.

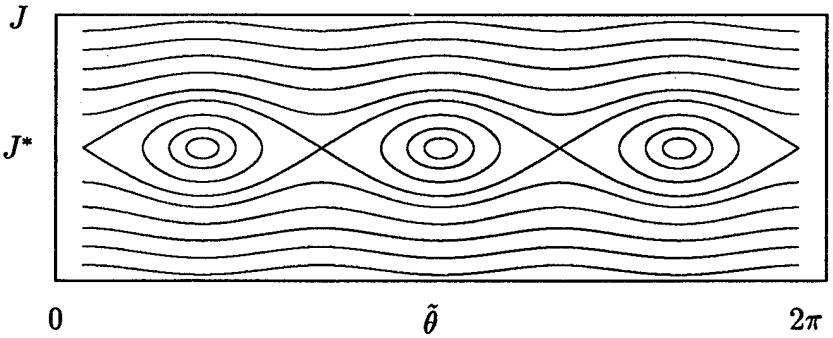

Figure 6:

From the picture it is clear that orbits lie on surfaces and from the form of the stream function given by Eq. (I.23) it is clear that the motion can be solved by quadrature. The use of the coordinate $\tilde{\theta} = \theta - \omega_1 t$ reduces this system to a single degree of freedom.

As noted above, the fact that we could reduce the $1\frac{1}{2}$ degree-of-freedom system to a single degree of freedom is the exception rather than the rule, generically it is not possible to get rid of time dependence by changing coordinates. This is the case, for example, for an azimuthal shear flow with the presence of two waves with *different* phase velocities, which has the stream function

$$\psi(J,\theta,t) = \psi_0(J) + \psi_1(J)\cos\left(m_1(\theta - \omega_1 t)\right) + \psi_2(J)\cos\left(m_2(\theta - \omega_2 t)\right) . \qquad \text{(I.25)}$$

It is clear that in this case a frame no longer exists in which the flow is stationary. In general there will be chaotic motion of a tracer particle. In a frame moving at a phase velocity ω_1 a tracer particle wants to execute its integrable motion, as described above, however it is perturbed by a time dependent wave propagating by at a speed $|\omega_1 - \omega_2|$. In a frame moving at ω_2 the situation is reversed. A plot of both of the integrable motions, in their respective frames, is shown below in Figure 7. This is a plot of (I.23) for the first wave superimposed on a plot of the same function for the second wave, but with ψ_1, m_1 and ω_1 replaced by ψ_2, m_2 and ω_2. The form of ψ_1 and ψ_2 is chosen in this figure to be proportional to sech^2; the angle $\tilde{\theta}$ is $\theta - \omega_1 t$ for the first wave and $\theta - \omega_2 t$ for the second. If the distance between the island chains is well separated, then this figure closely approximates the surface of section. The figure, in fact, suggests a basic mechanism of Hamiltonian chaos, the competition between resonances. If the resonances are close enough together a trajectory, in a sense, flips back and forth between the two integrable motions. When this happens a given trajectory may no longer map out a continuous curve. Generally separatrices become fuzzy, but some continuous curves still exists as shown in Figure 5.

As stated above, Figure 7 is not a surface of section, because the resonances were plotted independently, but if they are far apart and the amplitude of the resonances are both small it looks about right. To see the real surface of section one could integrate the differential

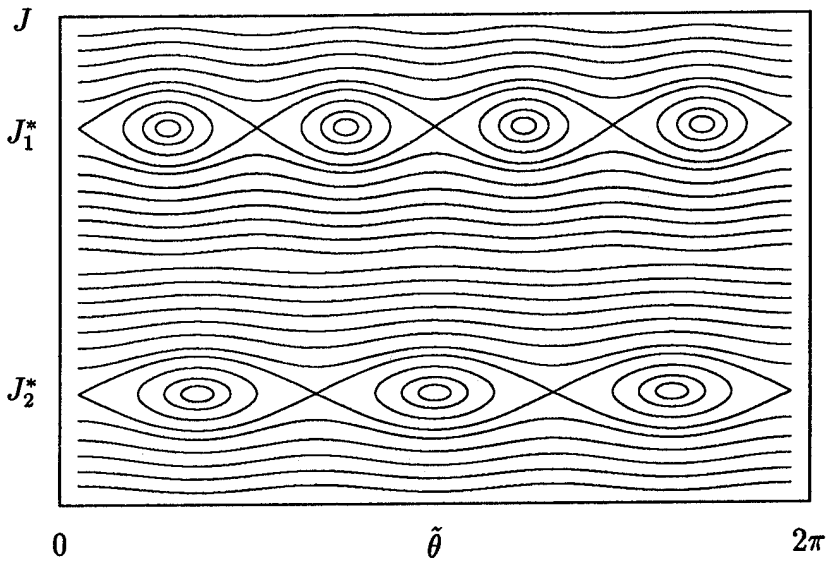

Figure 7:

equations numerically *. Instead of doing this you can consider the following toy, actually a serious toy, called the *standard map* (which is sometimes called the Chirikov-Taylor map):

$$\tilde{\theta}_{n+1} = \tilde{\theta}_n + \tilde{J}_{n+1}$$
$$\tilde{J}_{n+1} = \tilde{J}_n - k\ \sin(\tilde{\theta})\,, \qquad \text{(I.26)}$$

where $\tilde{J}$ and $\tilde{\theta}$ are computed mod-2π. This is an example of an area preserving map; it was, in fact, used to obtain Figures 4, 5(a), and 5(b). Area preserving maps are nice because the surface of section can be obtained without having to iterate differential equations. Importantly, the standard map describes *generic* behavior of Hamiltonian systems near resonances—it is the prototype of area preserving maps.

I recommend that you examine the standard map starting from $k = 0$, gradually increasing k. The case where $k = 0$ was shown in Figure 4, which clearly indicates integrable behavior. For $k \neq 0$ some of the invariant sets (continuous curves) are broken. As $k \to 0$ the measure of invariant sets approaches unity. This is in essence the celebrated KAM theorem. For larger k more and more curves are broken, but some still exist (see Figure 5(a) where $k = .80$ and Figure5(b) where $k = 1.2$). At a critical value of $k_c \approx .97$, curves that span $0 < \tilde{\theta} \leq 2\pi$ no longer exist. The critical value k_c was calculated by Greene* to many decimal places.

The question of when the last continuous curve breaks is an important one of Hamiltonian dynamics theory. In particular, it is of importance in the passive advection fluid mechanics

*To do this one can use standard Runge-Kutta packages. However, now more sophisticated *symplectic* integration algorithms exist. See e.g. C. Kueny, "Nonlinear Instability and Chaos in Plasma Wave-Wave Interactions," Ph.D. Thesis, University of Texas at Austin (1993) and many references cited therein.

*J. M. Greene, J. Math. Phys. **20**, 1183 (1979).

problem since these curves are barriers to transport. One is interested in when these curves break as the sizes and positions of the resonances change. The method developed by Greene gives a precise answer to this question, but requires some effort. A simple but rough criterion that yields an estimate for when the continuous curves between two resonances cease to persist is given by the *Chirikov overlap criterion.* According to this criterion the last curve separating two resonances will be destroyed when the sum of the half-widths of the two resonances (calculated independently) equals the distance between the resonances; that is,

$$\frac{W_1}{2} + \frac{W_2}{2} = |J_1^* - J_2^*| \tag{I.27}$$

where W_1 and W_2 denote the widths of the resonances while J_1^* and J_2^* denote their positions. This criterion is straightforward to apply and usually gives reasonable results. However, it must be borne in mind that it is only a rough estimate and as such has limitations. As noted above, more sophisticated criteria exist.

The study of two degree-of-freedom Hamiltonian systems is a richly developed yet still open area of research. Unfortunately, in only a single lecture it is only possible to scratch the surface and hopefully whet your appetite. Conspicuously absent from this lecture is any discussion of the notions of universality and renormalization. There is much to be learned from the references given below.

E. "Diffusion": Three Degrees of Freedom

In closing we mention something about three degree-of-freedom systems. For these systems the invariant sets that are remnants of the integrable N-tori do not divide the phase space. For three degree-of-freedom systems the phase space is six dimensional and the corresponding three dimensional invariant tori do not isolate regions. Because of this trajectories are not confined and can wander around the tori. This phenomenon is generally called *Arnold diffusion.* A cartoon of this is shown in Figure 8 below.

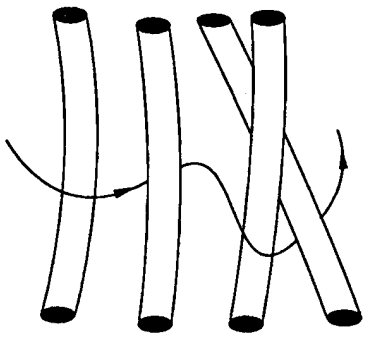

Figure 8:

There is a great deal of literature dealing with the chaotic advection of a passive tracer in two-dimensional fluid systems. These studies typically involve model stream functions that are time periodic, and hence are nonintegrable. For these systems the diffusion phenomenon

mentioned above cannot occur. However, it is possible that the solution of (I.1) is not periodic, but *quasiperiodic*, a special case of which is represented by the following:

$$\psi(\theta, J, t) = f(\theta, J, \omega_2 t, \omega_3 t)\,, \tag{I.28}$$

where f is a function that satisfies

$$f(\theta, J, \omega_2 t, \omega_3 t) = f(\theta, J, \omega_2 t + 2\pi, \omega_3 t) = f(\theta, J, \omega_2 t, \omega_3 t + 2\pi)\,. \tag{I.29}$$

If ω_1/ω_2 is irrational, then ψ is not periodic.

One can puff up a system with a Hamiltonian of the form of (I.28) into a three degree-of-freedom system by a technique similar to that described above. Let $\theta =: \theta_1$, $J =: J_1$, and define

$$H(\theta_1, J_1, \theta_2, J_2, \theta_3, J_3) = f(\theta_1, J_1, \theta_2, \theta_3) + \omega_2 J_2 + \omega_3 J_3\,, \tag{I.30}$$

and introduce the false time s as before. Note the last two terms of (I.30) are just the Hamiltonian for two linear oscillators in action-angle form, but here they are coupled to each other and to oscillator "1" through f. Hamilton's equations are

$$\frac{d\theta_1}{ds} = \frac{\partial f}{\partial J_1}\,, \qquad \frac{d\theta_2}{ds} = \omega_2\,, \qquad \frac{d\theta_3}{ds} = \omega_3\,; \tag{I.31}$$

$$\frac{dJ_1}{ds} = -\frac{\partial f}{\partial \theta_1}\,, \qquad \frac{dJ_2}{ds} = -\frac{\partial f}{\partial \theta_2}\,, \qquad \frac{dJ_3}{ds} = -\frac{\partial f}{\partial \theta_3}\,. \tag{I.32}$$

It is clear how the last two equations of (I.31) can be collapsed back down. The last two equations of (I.32) guarantee that J_2 and J_3 will vary so as to make H conserved.

The kind of quasiperiodic system treated in this section is undoubtedly relevant for the study of transport in two dimensional fluids. Solutions of (I.1) are more likely quasiperiodic than periodic. A stream function that describes an azimuthally symmetric shear flow plus three waves with different speeds is quasiperiodic. Transport in systems like this and its generalization to more frequencies is not well understood.

References

[1] V. I. Arnold, "Small Denominators and Problems of Stability of Motion in Classical Celestial Motion," Usp. Mat. Nauk. **18**, 85-191 (1963).

[2] M. V. Berry, "Regular and Irregular Motion," in *Mathematical Methods in Hydrodynamics and Integrability in Dynamical Systems*, eds. M. Tabor and Y. Treve, AIP Conf. Proc. 88 (AIP, New York, 1982), pp. 16-120.

[3] J. D. Meiss, "Symplectic Maps, Variational Principles, and Transport," Rev. Mod. Phys. **64**, 795-848 (1992).

[4] R. S. MacKay, "Renormalization in Area-Preserving Maps," Ph.D. Thesis, Princeton University (1982).

[5] J. M. Ottino, "Mixing, Chaotic Advection and Turbulence," Ann. Rev. Fluid Mech. **22**, 207 (1990).

[6] D. del-Castillo-Negrete and P. J. Morrison, "Chaotic Advection by Rossby Waves in Shear Flow," Phys. Fluids A **5**, 948-965 (1993).

II. Functional Calculus, Two Action Principles of Mechanics, and the Action Principle and Canonical Hamiltonian Description of the Ideal Fluid

A. Functional Calculus

A *functional* is a map that takes functions into real numbers. Describing them correctly requires defining a function space, which is the domain of the functional, and the rule that assigns the real number. Like ordinary functions, functionals have notions of continuity, differentiability, the chain rule, etc. In this section we will not be concerned with rigor, but with learning how to perform various formal manipulations.

As an example of a functional consider the kinetic energy of a constant density, one-dimensional, bounded fluid:

$$T[u] = \tfrac{1}{2}\int_{x_0}^{x_1} \rho_0 u^2 \, dx. \tag{II.1}$$

Here T is a functional of u which is indicated by the "[ ]" notation, a notation that we use in general to denote functionals. The function $u(x)$ is the fluid velocity, which is defined on $x \in (x_0, x_1)$, and ρ_0 is a constant fluid density. Given a function $u(x)$ we could put it in (II.1), do the integral, and get a number.

We would like to know in general how the value of a functional $K[u]$ changes as $u(x)$ changes a little, say $u(x) \to u(x) + \epsilon\,\delta u(x)$, where $u + \epsilon\,\delta u$ must still be in our domain. The first order change in K induced by δu is called the *first variation*, δK, which is given by

$$\begin{aligned}\delta K[u;\delta u] &:= \lim_{\epsilon\to 0}\frac{K[u+\epsilon\,\delta u]-K[u]}{\epsilon} = \frac{d}{d\epsilon}K[u+\epsilon\,\delta u]\Big|_{\epsilon=0} \\ &=: \int_{x_0}^{x_1}\delta u\,\frac{\delta K}{\delta u(x)}\,dx =: \left\langle \frac{\delta K}{\delta u}, \delta u\right\rangle .\end{aligned} \tag{II.2}$$

We will assume that the limit exists and that there are no problems with the equalities above; later, however, we will give an exercise where something "interesting" happens.

The notation $\delta K[u;\delta u]$ is used because there is a difference in the behavior of the two arguments: generally δK is a linear functional in δu, but not so in u. The quantity $\delta K/\delta u(x)$ of (II.2) is the *functional derivative* of the functional K. This notation for the functional derivative is chosen since it emphasizes the fact that $\delta K/\delta u$ is a gradient in function space. The reason why the arguments of u are sometimes displayed will become clear below.

For the example of (II.1) the first variation is given by

$$\delta T[u;\delta u] = \int_{x_0}^{x_1}\rho_0 u\,\delta u\,dx\,, \tag{II.3}$$

and hence the functional derivative is given by

$$\frac{\delta T}{\delta u} = \rho_0 u\,. \tag{II.4}$$

To see that the functional derivative is a gradient, let us take a side track and consider the first variation of a function of n variables, $f(x_1, x_2, \ldots, x_n) = f(x)$:

$$\delta f(x;\delta x) = \sum_{i=1}^{n} \frac{\partial f(x)}{\partial x_i}\,\delta x_i =: \nabla f \cdot \delta x\,. \tag{II.5}$$

It is interesting to compare the definition of (II.5) with the last definition of (II.2). The "$\cdot$" in (II.5) is analogous to the pairing $\langle\ ,\ \rangle$, while δx is analogous to δu. In fact, the index i is analogous to x, the argument of u. Finally, the gradient ∇f is analogous to $\delta K/\delta u$.

Consider now a more general functional, one of the form

$$F[u] = \int_{x_0}^{x_1} \mathcal{F}(x, u, u_x, u_{xx}, \ldots)\,dx\,, \tag{II.6}$$

where $\mathcal{F}$ is an ordinary, sufficiently differentiable, function of its arguments. Note $u_x := du/dx$, etc. The first variation of (II.6) yields

$$\delta F[u;\delta u] = \int_{x_0}^{x_1} \left[\frac{\partial \mathcal{F}}{\partial u}\delta u + \frac{\partial \mathcal{F}}{\partial u_x}\delta u_x + \frac{\partial \mathcal{F}}{\partial u_{xx}}\delta u_{xx} + \cdots\right] dx\,, \tag{II.7}$$

which upon integration by parts becomes

$$\delta F[u;\delta u] = \int_{x_0}^{x_1} \left[\frac{\partial \mathcal{F}}{\partial u} - \frac{d}{dx}\frac{\partial \mathcal{F}}{\partial u_x} + \frac{d^2}{dx^2}\frac{\partial \mathcal{F}}{\partial u_{xx}} - \cdots\right] \delta u\,dx \;+\; \left[\frac{\partial \mathcal{F}}{\partial u_x}\delta u + \cdots\right]\Bigg|_{x_0}^{x_1}. \tag{II.8}$$

Usually the variations δu are chosen so that the last term, the boundary term, vanishes; e.g. $\delta u(x_0) = \delta u(x_1) = 0$, $\delta u_x(x_0) = \delta u_x(x_1) = 0$, etc. Sometimes the integrated term vanishes without a condition on δu because of the form of $\mathcal{F}$. When this happens the boundary conditions are called *natural*. Assuming, for one reason or the other, the boundary term vanishes, (II.8) becomes

$$\delta F[u;,\delta u] = \left\langle \frac{\delta F}{\delta u}, \delta u \right\rangle\,, \tag{II.9}$$

where

$$\frac{\delta F}{\delta u} = \frac{\partial \mathcal{F}}{\partial u} - \frac{d}{dx}\frac{\partial \mathcal{F}}{\partial u_x} + \frac{d^2}{dx^2}\frac{\partial \mathcal{F}}{\partial u_{xx}} - \cdots\,. \tag{II.10}$$

The main objective of the calculus of variations is the extremization of functionals. A common terminology is to call a function $\hat{u}$, which is a point in the domain, an *extremal point* if $\delta F[\hat{u}]/\delta u = 0$. It could be a maximum, a minimum, or an inflection point. If the extremal point $\hat{u}$ is a minimum or maximum, then such a point is called an *extremum*.

The standard example of a functional that depends on the derivative of a function is the arc length functional,

$$L[u] = \int_{x_0}^{x_1} \sqrt{1 + u_x^2}\,dx\,. \tag{II.11}$$

We leave it to you to show that the shortest distance between two points is a straight line.

Another example is the functional defined by evaluating the function u at the point x'. This can be written as

$$u(x') = \int_{x_0}^{x_1} \delta(x - x')\, u(x)\, dx\,, \tag{II.12}$$

where $\delta(x - x')$ is the Dirac delta function and where we have departed from the "[ ]" notation. Applying the definition of (II.2) yields

$$\frac{\delta u(x')}{\delta u(x)} = \delta(x - x')\,. \tag{II.13}$$

This is the infinite dimensional analogue of $\partial x_i/\partial x_j = \delta_{ij}$.

The generalizations of the above ideas to functionals of more than one function and to more than a single spatial variable are straightforward. An example is given by the kinetic energy of a three-dimensional compressible fluid,

$$T[\rho, v] = \tfrac{1}{2}\int_D \rho v^2\, d^3x\,, \tag{II.14}$$

where the velocity has three Cartesian components $v = (v_1, v_2, v_3)$ that depend upon $x = (x_1, x_2, x_3) \in D$ and $v^2 = v \cdot v = v_1^2 + v_2^2 + v_3^2$. The functional derivatives are

$$\frac{\delta T}{\delta v_i} = \rho v_i\,, \qquad \frac{\delta T}{\delta \rho} = \frac{v^2}{2}\,. \tag{II.15}$$

We will use these later.

For a more general functional $F[\psi]$, where $\psi(x) = (\psi_1, \psi_2, \ldots, \psi_\nu)$ and $x = (x_1, x_2, \ldots, x_n)$, the analogue of (II.2) is

$$\delta F[\psi; \delta\psi] = \int_D \delta\psi_i \frac{\delta F}{\delta \psi_i(x)}\, d^n x =: \left\langle \frac{\delta F}{\delta \psi}, \delta\psi \right\rangle . \tag{II.16}$$

Here and henceforth we sum repeated indices.

As an exercise consider the pathological functional.

$$P[\psi] = \int_{-1}^{1} \mathcal{P}(\psi_1, \psi_2)\, dx\,, \tag{II.17}$$

where

$$\mathcal{P} = \begin{cases} \dfrac{\psi_1 \psi_2^2}{\psi_1^2 + \psi_2^4}\,, & \psi_1 \neq 0 \\[2ex] 0\,, & \psi_1 = 0\,. \end{cases} \tag{II.18}$$

Calculate $\delta P[0, 0; \delta\psi_1, \delta\psi_2]$. Part of this problem is to figure out what the problem is.

Next, we consider the important *functional chain rule*, which is a simple idea that underlies a great deal of literature relating to the Hamiltonian structure of fluids and plasmas.

Suppose we have a functional $F[u]$ and we know u is related to another function w by means of a linear operator

$$u = \mathcal{O} w . \tag{II.19}$$

As an example, u and w could be real valued functions of a single variable, x, and

$$\mathcal{O} := \sum_{k=0}^{n} a_k(x) \frac{d^k}{dx^k} , \tag{II.20}$$

where, as usual, u, w, and a_k have as many derivatives as needed. We can define a functional on w by inserting (II.19) into $F[u]$:

$$\bar{F}[w] := F[u] = F[\mathcal{O} w]. \tag{II.21}$$

Equating variations yields

$$\left\langle \frac{\delta \bar{F}}{\delta w}, \delta w \right\rangle = \left\langle \frac{\delta F}{\delta u}, \delta u \right\rangle , \tag{II.22}$$

where the equality makes sense if δu and δw are connected by (II.19), i.e.

$$\delta u = \mathcal{O}\, \delta w, \tag{II.23}$$

where we assume an arbitrary δw induces a δu.

Inserting (II.23) into (II.22) yields

$$\begin{aligned} \left\langle \frac{\delta \bar{F}}{\delta w}, \delta w \right\rangle &= \left\langle \frac{\delta F}{\delta u}, \mathcal{O}\, \delta w \right\rangle \\ &= \left\langle \mathcal{O}^\dagger \frac{\delta F}{\delta u}, \delta w \right\rangle , \end{aligned} \tag{II.24}$$

where $\mathcal{O}^\dagger$ is the formal adjoint of $\mathcal{O}$. Since δw is arbitrary

$$\frac{\delta \bar{F}}{\delta w} = \mathcal{O}^\dagger \frac{\delta F}{\delta u} . \tag{II.25}$$

This follows from the DuBois-Reymond lemma, which is proven by assuming (II.25) does not hold at some point x, selecting δw to be localized about the point x, and establishing a contradiction. A physicist would just set δw equal to the Dirac delta function to obtain the result.

Notice that nowhere did we assume that $\mathcal{O}$ was invertible—it needn't be for the chain rule to work in one direction. Functionals transform in the other direction. Given a relation $\psi[\chi]$ we can calculate an expression for $\delta F/\delta \chi$, where F is a functional of χ through ψ. However, given an arbitrary functional of χ, we cannot obtain a functional of ψ.

The above was clearly a special case in that the two functions u and w were linearly related. More generally, consider the functional $F[\psi]$ and suppose ψ is related to $\chi = (\chi_1, \chi_1, \ldots, \chi_\mu)$ in an arbitrary, not necessarily linear, way:

$$\psi_i = \psi_i[\chi] , \qquad i = 1, 2, \ldots, \nu . \tag{II.26}$$

This "[ ]" notation could be confusing, but we have already stated that ψ and χ are functions. A variation of ψ induced by χ requires linearization of (II.26), which we write as

$$\delta\psi_i = \frac{\delta\psi_i}{\delta\chi}[\chi;\delta\chi]\,, \qquad i = 1,2,\ldots,\nu\,, \tag{II.27}$$

or simply, since $\delta\psi/\delta\chi$ is a linear operator on $\delta\chi$,

$$\delta\psi_i = \frac{\delta\psi_i}{\delta\chi_j}\,\delta\chi_j \qquad i = 1,2,\ldots,\nu; \quad j = 1,2,\ldots,\mu\,. \tag{II.28}$$

Inserting (II.28) into (II.22) implies

$$\left\langle \frac{\delta F}{\delta\chi}, \delta\chi \right\rangle = \left\langle \left(\frac{\delta\psi}{\delta\chi}\right)^{\dagger} \frac{\delta F}{\delta\psi}, \delta\chi \right\rangle\,, \tag{II.29}$$

whence it is seen that

$$\frac{\delta F}{\delta\chi_j} = \left(\frac{\delta\psi_i}{\delta\chi_j}\right)^{\dagger} \frac{\delta F}{\delta\psi_i} \qquad i = 1,2,\ldots,\nu; \quad j = 1,2,\ldots,\mu\,. \tag{II.30}$$

Here we have dropped the overbar on F, as is commonly done. In (II.30) it is important to remember that δ(function)/δ(function) is a linear operator acting to its right, as opposed to δ(functional)/δ(function), which is a gradient.

As an example consider functionals that depend upon the two components of the velocity field for an incompressible fluid in two dimensions, $u(x,y)$ and $v(x,y)$. These are linearly related to the stream function ψ by $u = -\partial\psi/\partial y$ and $v = \partial\psi/\partial x$. For this case (II.27) becomes

$$\delta u = \frac{\delta u}{\delta\psi}\,\delta\psi = -\frac{\partial}{\partial y}\,\delta\psi$$

$$\delta v = \frac{\delta v}{\delta\psi}\,\delta\psi = \frac{\partial}{\partial x}\,\delta\psi\,, \tag{II.31}$$

and

$$\frac{\delta F}{\delta\psi} = \frac{\partial}{\partial y}\frac{\delta F}{\delta u} - \frac{\partial}{\partial x}\frac{\delta F}{\delta v}\,. \tag{II.32}$$

Now consider the *second variation*, $\delta^2 F$, and *second functional derivative*, $\delta^2 F/\delta\psi\delta\psi$. Since the first variation, $\delta F[\psi;\delta\psi]$, is a functional of ψ, a second variation can be made in this argument:

$$\delta^2 F[\psi;\delta\psi,\delta\hat{\psi}] = \left.\frac{d}{d\eta}\delta F[\psi+\eta\delta\hat{\psi};\delta\psi]\right|_{\eta=0}$$

$$=: \int_D \delta\psi_i\,\frac{\delta^2 F}{\delta\psi_i\delta\psi_j}\,\delta\hat{\psi}_j\,d^n x =: \left\langle \delta\psi, \frac{\delta^2 F}{\delta\psi\delta\psi}\delta\hat{\psi} \right\rangle\,. \tag{II.33}$$

Observe that $\delta^2 F$ is a bilinear functional in $\delta\psi$ and $\delta\hat{\psi}$. If we set $\delta\hat{\psi} = \delta\psi$ we obtain a quadratic functional. Equation (II.33) defines $\delta^2 F/\delta\psi\delta\psi$, which is a linear operator that acts on $\delta\hat{\psi}$ but depends nonlinearly on ψ. It possesses a symmetry analogous to the interchange of the order of second partial differentiation. To see this observe

$$\delta^2 F[\psi; \delta\psi, \delta\hat{\psi}] = \frac{\partial^2}{\partial\eta\partial\epsilon} F[\psi + \eta\delta\hat{\psi} + \epsilon\delta\psi]\Big|_{\epsilon=0,\,\eta=0} . \tag{II.34}$$

Since the order of differentiation in (II.33) is immaterial it follows that

$$\left(\frac{\delta^2 F}{\delta\psi_i \delta\psi_j}\right)^\dagger = \frac{\delta^2 F}{\delta\psi_j \delta\psi_i} , \qquad i = 1, 2, \ldots, \nu . \tag{II.35}$$

This relation is necessary for establishing the Jacobi identity of noncanonical Poisson brackets.

As an example consider the second variation of the arc length functional of (II.11). Performing the operations of (II.34) yields

$$\delta^2 L[u; \delta u; \delta\hat{u}] = \int_{x_0}^{x_1} \delta u_x \, \frac{1}{(1 + u_x^2)^{3/2}} \, \delta\hat{u}_x \, dx . \tag{II.36}$$

Thus

$$\frac{\delta^2 L}{\delta u^2} = \frac{d}{dx} \, \frac{1}{(1 + u_x^2)^{3/2}} \, \frac{d}{dx} . \tag{II.37}$$

For an important class of function spaces, one can convert functionals into functions of a countably infinite number of arguments. This is a method for proving theorems concerning functionals and can also be useful for establishing formal identities. One way to do this would be to convert the integration of a functional into a sum by finite differencing. Another way to do this, for example for functionals of the form of (II.6), is to suppose $(x_0, x_1) = (-\pi, \pi)$ and expand in a Fourier series,

$$u(x) = \sum_{k=-\infty}^{\infty} u_k \, e^{ikx} . \tag{II.38}$$

Upon inserting (II.38) into (II.6) one obtains an expression for the integrand which is, in principle, a known function of x. Integration then yields a function of the Fourier amplitudes, u_k. Thus we obtain

$$F[u] = F(u_0, u_1, u_{-1}, \ldots) . \tag{II.39}$$

In closing this discussion of functional calculus we consider a functional, one expressed as a function of an infinite number of arguments, that demonstrates an "interesting" property. The functional is given by

$$F(x_1, x_2, \ldots) = \sum_{k=1}^{\infty} \left(\tfrac{1}{2} a_k \, x_k^2 - \tfrac{1}{4} b_k \, x_k^4\right) , \tag{II.40}$$

where the domain of F is composed of sequences $\{x_k\}$, and the coefficients are given by

$$a_k = \frac{1}{k^6}\,, \qquad b_k = \frac{1}{k^2}\,. \tag{II.41}$$

Assuming that (II.40) converges uniformly, the first variation yields

$$\delta F = \sum_{k=1}^{\infty} \left(a_k\, x_k - b_k\, x_k^3\right) \delta x_k\,, \tag{II.42}$$

which has three extremal points

$$x_k^{(0)} = 0, \qquad x_k^{(\pm)} = \pm(a_k/b_k)^{1/2}\,, \tag{II.43}$$

for all k. It is the first of these that will concern us. The second variation evaluated at $x_k^{(0)}$ is

$$\delta^2 F = \sum_{k=1}^{\infty} a_k (\delta x_k)^2\,. \tag{II.44}$$

where we assume (II.42) converges uniformly for x_k and δx_k. Since $a_k > 0$ for all k, (II.44) is positive definite; i.e.

$$\delta^2 F > 0 \quad \text{for} \quad \delta x_k \neq 0\,, \quad \text{for all} \quad k\,. \tag{II.45}$$

However, consider ΔF defined by

$$\Delta F = F(x^{(0)} + \Delta x) - F(x^{(0)}) = \sum_{k=1}^{\infty} \left[\tfrac{1}{2} a_k\, (\Delta x_k)^2 - \tfrac{1}{4} b_k\, (\Delta x_k)^4\right]\,, \tag{II.46}$$

which we evaluate at

$$\Delta x_k = \begin{cases} \dfrac{1}{m}\,, & k = m \\[2ex] 0\,, & k \neq m\,, \end{cases} \tag{II.47}$$

and obtain

$$\Delta F < 0\,, \tag{II.48}$$

provided $m > 1$. Since m can be made as large as desired, we have shown that inside any neighborhood of $x^{(0)}$, no matter how small, $\Delta F < 0$. Therefore, this extremal point is not a minimum — even though $\delta^2 F$ is positive definite.

A sufficient condition for proving that an extremal point is an extremum is afforded by a property known as *strong positivity*. If $\hat{\psi}$ is an extremal point and the quadratic functional $\delta^2 F[\hat{\psi}; \delta\psi]$ satisfies

$$\delta^2 F[\hat{\psi}; \delta\psi] \geq c \|\delta\psi\|^2\,,$$

where $c = \text{const.} > 0$ and "$\|\ \|$" is a norm defined on the domain of F, then $\delta^2 F[\hat{\psi}; \delta\psi]$ is strongly positive. This is sufficient for $\hat{\psi}$ to be an minimum. We will leave it to you to explain why the functional $F(x_1, x_2, \ldots)$ is not strongly positive. This example points to a mathematical technicality that is encountered when proving stability by Liapunov's method (cf. Lecture V).

References

[1] R. Courant and D. Hilbert, *Methods of Mathematical Physics* (Wiley Interscience, New York, 1953) Vol. I Chapt.IV.

[2] I. M. Gelfand and S. V. Fomin, *Calculus of Variations* (Prentice-Hall, Englewood Cliffs, N. J., 1963.)

B. Two Action Principles of Mechanics

Physicists have had a long lasting love affair with the idea of generating physical laws by setting the derivative of some functional to zero. This is called an *action principle.* The most famous action principle is Hamilton's principle, which produces Lagrange's equations of mechanics upon variation. One reason action principles are appreciated is because they give a readily covariant theory and means have been developed for building in symmetries. However, it should be pointed out that the use of continuous symmetry groups in this context is only a limited part of a deep and beautiful theory that was initiated by Sophus Lie and others. Perhaps the most convincing deep reason for action principles is the cleanliness and utility of Feynman's path integral formulation. The utility of action principles should not be understated. Indeed, they provide a good starting place for making approximations. However, a quote from Truesdell can't be resisted:

> A fully conservative situation can be described by an action principle, which has the advantage of making the theory accessible also to physicists. *

In any event, Hamilton's principle is an important prototype upon which modern theories are in part built. Shortly, we will show how this story goes for the ideal fluid, but first we review some mechanics.

One approach to producing the equations of motion for a mechanics problem is to first identify the configuration space, Q, with coordinates $q = (q_1, q_2, \ldots, q_N)$. Then based on physical intuition, write down the kinetic and potential energies, T and V, respectively. The equations of motion then follow upon setting the functional derivative of the following action functional to zero:

$$S[q] = \int_{t_0}^{t_1} L(q, \dot{q}, t)\, dt\,, \tag{II.49}$$

where $L := T - V$ is the Lagrangian function. The functions $q(t)$ over which we are extremizing must satisfy the fixed end conditions $q(t_0) = q_0$ and $q(t_1) = q_1$. Thus $\delta q(t_0) = \delta q(t_1) = 0$. The functional derivative relations

$$\frac{\delta S[q]}{\delta q_i} = 0 \tag{II.50}$$

imply Lagrange's equations,

$$\frac{\partial L}{\partial q_i} = \frac{d}{dt}\frac{\partial L}{\partial \dot{q}_i}\,. \tag{II.51}$$

*C. Truesdell, *Six Lectures on Modern Natural Philosophy* (Springer-Verlag, New York, 1966.)

This is Hamilton's principle.

Since for particles in rectangular coordinates usually

$$T = \tfrac{1}{2}\sum_i m_i \dot{q}_i^2 \qquad\qquad V = V(q)\,, \tag{II.52}$$

Eqs. (II.51) yield

$$m_i \ddot{q}_i = -\frac{\partial V}{\partial q_i}\,, \qquad\qquad i = 1, 2, \ldots, N\,. \tag{II.53}$$

This is just Newton's second law with a conservative force. You will notice that Hamilton's principle does not yield Hamilton's equations—one way to get them is via the Legendre transformation.

The *Legendre transformation* is a trick for transferring functional dependence. Generally it is used in physics when one has a sort of "fundamental" function that describes a theory, whether it be thermodynamics or, as is the case here, dynamics. It has a nice geometric interpretation, but we will skip this. Here we will use it to transform the N second order differential equations of (II.53) into the $2N$ first order equations of Hamilton.

Define a quantity $p_i := \partial L/\partial \dot{q}_i$, which is the canonical momentum, and consider

$$\bar{H}(q, p, \dot{q}, t) := \sum_i p_i \dot{q}_i - L(q, \dot{q}, t)\,. \tag{II.54}$$

Now we ask the question: how does $\bar{H}$ change if we independently change q, $\dot{q}$, p, and t a little? Evidently

$$\begin{aligned}\delta\bar{H} &= \sum_i \left[\frac{\partial \bar{H}}{\partial q_i}\delta q_i + \frac{\partial \bar{H}}{\partial \dot{q}_i}\delta \dot{q}_i + \frac{\partial \bar{H}}{\partial p_i}\delta p_i\right] + \frac{\partial \bar{H}}{\partial t}\delta t \\ &= \sum_i \left[-\frac{\partial L}{\partial q_i}\delta q_i + (p_i - \frac{\partial L}{\partial \dot{q}_i})\delta \dot{q}_i + \dot{q}_i \delta p_i\right] - \frac{\partial L}{\partial t}\delta t.\end{aligned} \tag{II.55}$$

The first thing to notice is that if $\delta q = \delta p = \delta t = 0$, i.e. we only vary $\delta\dot{q}$, then $\delta\bar{H} = 0$, since $p_i = \partial L/\partial \dot{q}_i$. This means $\bar{H}$ is independent of $\dot{q}$, so we drop the overbar and write $H(q, p, t)$. Equating the remaining coefficients of the variations yields

$$\frac{\partial H}{\partial q_i} = -\frac{\partial L}{\partial q_i}\,; \qquad \frac{\partial H}{\partial p_i} = \dot{q}_i\,; \qquad \frac{\partial H}{\partial t} = -\frac{\partial L}{\partial t}\,. \tag{II.56}$$

Lagrange's equations, (II.51), together with the definition of p_i and the middle of (II.56) give Hamilton's equations:

$$\dot{p}_i = -\frac{\partial H}{\partial q_i}\,, \qquad\qquad \dot{q}_i = \frac{\partial H}{\partial p_i}\,. \tag{II.57}$$

In order to explicitly calculate $H(p, q, t)$ in the standard case of mechanics, one uses $p_i = \partial L/\partial \dot{q}_i$ to solve for $\dot{q} = \dot{q}(p)$ and then inserts this into (II.54). This requires L to be

convex in $\dot{q}$. Since there exist important physical cases where L is not convex, Dirac and others developed a theory to handle this. An interesting new application of Dirac's constraint theory for filtering out fast motion in GFD models has recently been developed*.

Now consider another action principle which is sometimes called the *phase space action.* This one, which directly yields Hamilton's equations, is given by

$$S[q,p] = \int_{t_0}^{t_1} \left[\sum_i p_i \dot{q}_i - H(q,p,t) \right] \, dt \,, \tag{II.58}$$

where S is a functional of q and p, independently. The end conditions are $q(t_0) = q_0$ and $q(t_1) = q_1$, i.e. q is fixed as before. However, the boundary condition on p is natural in that nothing is required of it at the ends. One has a sort of "clothesline" boundary condition as depicted in Figure 1 below, where the curve is free to slide along the lines of constant q in the p-direction.

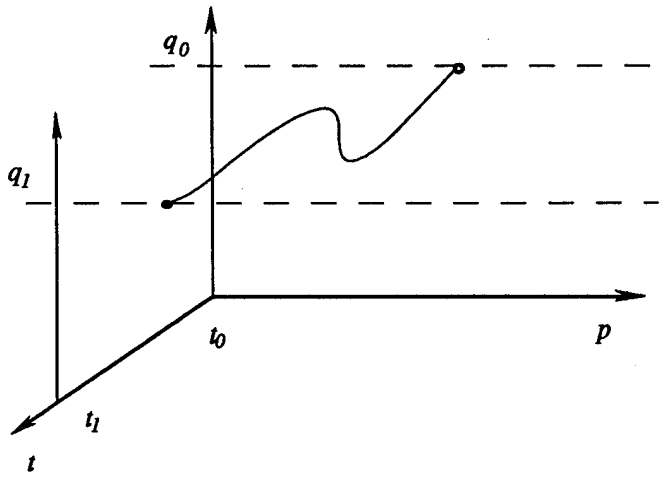

Figure 1:

Variation of S with respect to q and p yields, respectively,

$$\dot{p}_i = -\frac{\partial H}{\partial q_i} \,, \qquad\qquad \dot{q}_i = \frac{\partial H}{\partial p_i} \,. \tag{II.59}$$

Thus the phase space action yields directly Hamilton's equations as the extremal condition.

*R. Salmon, J. Fluid Mech. **196**, 345 (1988).

References

[1] E. Saletan and A. Cromer, *Theoretical Mechanics* (John Wiley, New York, 1971.)

[2] E. C. G. Sudarshan and N. Mukunda, *Classical Dynamics: A Modern Perspective* (John Wiley, New York, 1974.)

C. Action Principle and Canonical Hamiltonian Description of the Ideal Fluid in Lagrangian or Material Variables

Now we are in a position to talk about fluid mechanics, but we're going to do so in terms of variables that might be new to you. Often, fluid mechanics is taught entirely in terms of Eulerian variables. In what follows, *Lagrangian variables*, or as they are sometimes called, material variables, will be central.

The idea we are going to pursue is a simple one. *If a fluid is described as a collection of fluid particles or elements, then both the Hamiltonian and the Lagrangian formalism that we have described above can be adapted to describe the ideal fluid.* The adaptation requires an extension to an infinite number of degrees of freedom in order to describe a continuum of fluid elements. This means that a fluid element is shrunk to zero size and that there is one for each point of the fluid. This is an idealization since in reality, fluid elements don't exist: if they were of macroscopic size, they wouldn't maintain their integrity forever, and if they were of microscopic size, we would be outside the realm of fluid mechanics. However, there exists a precise Eulerian state corresponding to a Lagrangian state. It should be kept in mind that the above limitations apply to the fluid description in general, whether it be in Lagrangian or Eulerian variables.

Suppose the position of a fluid element, referred to a fixed rectangular coordinate systems, is given by

$$q = q(a,t)\,, \tag{II.60}$$

where $q = (q_1, q_2, q_3)$. This is the material or Lagrangian variable. Here $a = (a_1, a_2, a_3)$ is any label that identifies a fluid particle, which is often taken to be the position of the fluid particle at time $t = 0^*$. The quantities $q_i(a,t)$ are coordinates for the configuration space $\mathcal{Q}$, which is in fact a function space because in addition to the three indices "i" there is the continuum label a. We assume that a varies over a fixed domain, D, which is completely filled with fluid, and that the functions q map D onto itself. We will assume that as many derivatives of q with respect to a as needed exist, but we won't say more about $\mathcal{Q}$; in fact, not that much is known about the solution space for the 3-D fluid equations in Lagrangian variables. At this stage we will assume that the configuration space has been specified and proceed to discuss the potential energy of the fluid.

*Note, however, that the freedom to relabel particles is associated in an important way with the Casimir invariants that are discussed below. See e.g. M. Calkin, Can. J. Phys. **41**, 2241 (1963); P. Ripa, AIP Conf. Proc. **76** (1981); R. Salmon, AIP Conf. Proc. **88**, 127 (1982).

The fluid approximation assumes local thermodynamic equilibrium in spite of the fact that the fluid can flow at nonzero velocity. Potential energy is stored in terms of pressure and temperature. More precisely we adapt the energy representation of thermodynamics where the extensive energy is treated as a function of the extensive variables, viz. the entropy and the volume. For a fluid it is convenient to consider the energy per unit mass, which we denote by U to be a function of the entropy per unit mass, s, and the mass density, ρ. The inverse of the later quantity is a measure of the volume. The intensive quantities, pressure and temperature, are obtained as follows:

$$T = \frac{\partial U}{\partial s}(s,\rho)\,, \qquad p = \rho^2 \frac{\partial U}{\partial \rho}(s,\rho)\,. \tag{II.61}$$

The second of (II.61) is a bit peculiar—it arises because the volume, the usual thermodynamics variable, is proportional to ρ^{-1}. Note also that special choices for U produce specific fluid flows: barotropic flow, adiabatic flow, etc.

The quantities ρ and s are in fact Eulerian variables which we must, in order to move ahead, describe in terms of Lagrangian variables. With this goal in mind, let us sidetrack for a moment and discuss the Lagrangian-Eulerian map. The difference between the two types of variables can be elucidated by describing two ways of watching fish. In the Eulerian picture one stays at a point and watches whatever fish happen by; in the Lagrangian picture one picks out a particular fish and keeps track of where it goes. Note that this analogy gets better if the fish are very small, neutrally buoyant, and dead!

Call r the *spatial* variable, i.e. the Eulerian point of observation. The Eulerian density is then related to the Lagrangian variable q as follows:

$$\rho(r,t) = \int_D \delta(r - q(a,t))\, \rho_0(a)\, d^3a\,. \tag{II.62}$$

Here $\delta(r-q)$ is a three-dimensional Dirac delta-function and $\rho_0(a)$ is an initial configuration of mass density ascribed to the particle labeled by a. It is akin to knowing the mass of the particle labeled by "i" in conventional particle mechanics.

Equation (II.62) embodies mass conservation. This can be seen by using a property of the δ-function: $\delta(f(x)) = \delta(x - x_0)/\mid f'(x_0)\mid$ where x_0 is the only place where $f(x_0) = 0$. In three dimensions this yields

$$\rho(r,t) = \left.\frac{\rho_0(a)}{\mathcal{J}(a,t)}\right|_{a=q^{-1}(r,t)}\,, \tag{II.63}$$

where the Jacobian $\mathcal{J} = \det(\partial q_i/\partial a_j)$. That this is local mass conservation follows from

$$\rho\, d^3q = \rho_0\, d^3a\,, \tag{II.64}$$

where d^3a is an initial volume element that maps into d^3q at time t, and $d^3q = \mathcal{J}\, d^3a$. (When integrating over D we will replace d^3q by d^3r.)

In addition to the mass ascribed to a fluid particle, one could ascribe other quantities, e.g. color, smell or what have you. In the ideal fluid, the entropy per unit mass s is such

a quantity. We suppose that initially $s = s_0(a)$ and that it remains so. A form similar to (II.62) corresponding to this statement is given by

$$\sigma(r,t) = \int_D \sigma_0(a)\delta(r - q(a,t))\, d^3a\,, \tag{II.65}$$

where $\sigma(r,t) = \rho(r,t)\, s(r,t)$ is the entropy per unit volume and $\sigma_0 = \rho_0(a)s_0(a)$. Thus the counterpart of (II.63) is

$$s(r,t) = s_0(a)|_{a=q^{-1}(r,t)}\,. \tag{II.66}$$

This is merely the statement that the quantity s stays put on a fluid particle.

Completing the Lagrange-Euler map requires the specification of the Eulerian velocity field, something that is not needed now, but which we record here for later reference. By now you will have noticed that the Euler-Lagrange map naturally takes the Lagrangian variables into Eulerian densities. Thus we consider the momentum density $M := \rho v$. A form for M similar to (II.62) and (II.65) is given by the following:

$$M(r,t) = \int_D \dot{q}(a,t)\, \delta(r - q(a,t))\, \rho_0(a)\, d^3a\,. \tag{II.67}$$

Performing the integration produces the counterpart of (II.63) and (II.64), viz.

$$v(r,t) = \dot{q}(a,t)|_{a=q^{-1}(r,t)}\,, \tag{II.68}$$

which is the usual relation between the Lagrangian variable and the Eulerian velocity field.

Now we can return to our quest for the potential energy. Since the energy per unit volume is given by ρU, the total potential energy function is evidently

$$V[q] = \int_D \rho_0 U(s_0, \rho_0/\mathcal{J})\, d^3a\,. \tag{II.69}$$

Observe that (II.69) is a functional of q that depends only upon $\mathcal{J}$ and hence only upon $\partial q/\partial a$.

The next step required for constructing Hamilton's principle is to obtain an expression for the kinetic energy functional. This is clearly given by

$$T[q] = \tfrac{1}{2}\int_D \rho_0\, \dot{q}^2\, d^3a\,. \tag{II.70}$$

Observe that (II.70) is a functional of q that depends only upon $\dot{q}$.

From (II.69) and (II.70) the Lagrangian functional is obtained,

$$L[q,\dot{q}] = \int_D \left[\, \tfrac{1}{2}\rho_0\, \dot{q}^2 - \rho_0 U(s_0, \rho_0/\mathcal{J})\right]\, d^3a \tag{II.71}$$

$$=: \int_D \mathcal{L}(q, \dot{q}, \partial q/\partial a, t)\, d^3a\,,$$

where $\mathcal{L}(q, \dot{q}, \partial q/\partial a, t)$ is the Lagrangian density. Thus the action functional is given by

$$S[q] = \int_{t_0}^{t_1} L[q, \dot{q}]\, dt = \int_{t_0}^{t_1} \int_D \left[\tfrac{1}{2}\, \rho_0\, \dot{q}^2 - \rho_0 U\right]\, d^3a\,. \tag{II.72}$$

Observe that this action functional is like that for finite degree-of-freedom systems, as treated above, except that the sum over particles is replaced by integration over D, i.e.

$$\int_D d^3a \leftrightarrow \sum_i\,. \tag{II.73}$$

The mass of each "particle" of the continuum corresponds to $\rho_0\, d^3a$.

The end conditions for Hamilton's principle for the fluid are the same as before,

$$\delta q(a, t_0) = \delta q(a, t_1) = 0. \tag{II.74}$$

However, in addition, boundary conditions are needed because there is now going to be integration by parts with respect to a. It is assumed that these are such that all surface terms vanish. Later we will see what this implies.

In order to apply Hamilton's principle, we must functionally differentiate (II.72), thus, it is necessary to know something about differentiating determinants. Recall

$$\frac{\partial q_k}{\partial a_j}\frac{A_{ki}}{\mathcal{J}} = \delta_{ij} \tag{II.75}$$

where A_{ki} is the cofactor of $\partial q_k/\partial a_i =: q_{k,i}$. (Remember repeated indices are to be summed.) A convenient expression for A_{ki} is given by

$$A_{ki} = \tfrac{1}{2}\, \epsilon_{kjl}\epsilon_{imn}\frac{\partial q_j}{\partial a_m}\frac{\partial q_l}{\partial a_n}\,, \tag{II.76}$$

where ϵ_{ijk} is the skew symmetric tensor (density), which vanishes if any two of i, j, k are equal, is equal to 1 if i, j, k are unequal and a cyclic permutation of $1, 2, 3$, and is otherwise equal to -1. In functionally differentiating (II.72) we will require the following relation:

$$\frac{\partial \mathcal{J}}{\partial q_{i,j}} = A_{ij}\,, \tag{II.77}$$

which follows from (II.75).

For Lagrangian density functionals of the form $\mathcal{L}(q, \dot{q}, \partial q/\partial a, t)$, the functional derivative $\delta S/\delta q(a, t) = 0$ implies

$$\frac{d}{dt}\left(\frac{\partial \mathcal{L}}{\partial \dot{q}_i}\right) + \frac{\partial}{\partial a_j}\left(\frac{\partial \mathcal{L}}{\partial q_{i,j}}\right) - \frac{\partial \mathcal{L}}{\partial q_i} = 0\,, \tag{II.78}$$

provided the surface integral vanishes:

$$\int_{t_0}^{t_1} \int_{\partial D} p\, \delta q_i A_{ij} n_j\, d^2a = \int_{t_0}^{t_1} \int_{\partial D} p\, \delta q \cdot \hat{n}\, d^2q\,. \tag{II.79}$$

The equality above follows upon changing from integration over a to integration over q. Note $A_{ij} d^2a = d^2q$. Evidently the surface term vanishes if any of the following are true on ∂D:

(i) $\delta q_i = 0$

(ii) $p = (\rho_0^2/\mathcal{J}^2)\,(\partial U/\partial \rho) = 0$

(iii) $\delta q \cdot \hat{n} = 0$,

where p is the pressure and $\hat{n}$ is a unit normal vector to ∂D. While all of these possibilities result in the vanishing of the surface term, (i) is clearly more than is necessary, in light of (iii), which merely states that fluid particles are not forced through the boundary. In the case where D is a box and periodic boundary conditions are imposed, the vanishing of the surface term is automatic. In the case where D is "all space" the physical boundary condition is (ii), which asserts that the pressure vanishes at infinity.

From (II.78) the equation of motion is obtained,

$$\rho_0 \ddot{q}_i - A_{ij} \frac{\partial}{\partial a_j} \left(\frac{\rho_0^2}{\mathcal{J}^2} \frac{\partial U}{\partial \rho} \right) = 0 \,. \tag{II.80}$$

Here we have used $\partial A_{ij}/\partial a_j = 0$, which you can work out using (II.76). Alternatively, upon using (II.75) the equation of motion can be written in the form

$$\rho_0 \ddot{q}_j \frac{\partial q_j}{\partial a_i} - \mathcal{J} \frac{\partial}{\partial a_i} \left(\frac{\rho_0^2}{\mathcal{J}^2} \frac{\partial U}{\partial \rho} \right) = 0 \,. \tag{II.81}$$

We leave it to you to show that (II.80) can be transformed into Eulerian form:

$$\rho \left(\frac{\partial v}{\partial t} + v \cdot \nabla v \right) = -\nabla p \,, \tag{II.82}$$

where $v = v(r,t)$. A useful identity in this regard is

$$\frac{\partial}{\partial q_k} = \frac{1}{\mathcal{J}} A_{ki} \frac{\partial}{\partial a_i} \,. \tag{II.83}$$

With (II.83) it is clear that (II.80) is of the form of Newton's second law. The Legendre transform follows easily. The canonical momentum density is

$$\pi_i(a,t) := \frac{\delta L}{\delta \dot{q}_i(a)} = \rho_0 \dot{q}_i \,, \tag{II.84}$$

and

$$H[\pi, q] = \int d^3a \, [\pi \cdot q - \mathcal{L}] = \int d^3a \, \left[\frac{\pi^2}{2\rho_0} + \rho_0 U \right] \,. \tag{II.85}$$

Hamilton's equations are then

$$\dot{\pi}_i = -\frac{\delta H}{\delta q_i} \,; \qquad \dot{q}_i = \frac{\delta H}{\delta \pi_i} \,. \tag{II.86}$$

These equations can also be written in terms of the Poisson bracket

$$\{F, G\} = \int \left[\frac{\delta F}{\delta q} \cdot \frac{\delta G}{\delta \pi} - \frac{\delta G}{\delta q} \cdot \frac{\delta F}{\delta \pi} \right] d^3a \tag{II.87}$$

viz.,

$$\dot{\pi}_i = \{\pi_i, H\}\,; \qquad \dot{q}_i = \{q_i, H\}\,. \tag{II.88}$$

Here $\delta q_i(a)/\delta q_j(a') = \delta_{ij}\delta(a-a')$ has been used, a relation that is analogous to $\partial q_j/\partial q_i = \delta_{ij}$ for finite systems [recall (II.13)].

In conclusion we point out that variational principles similar to that given above exist for essentially *all* ideal fluid models, including incompressible flow, magnetohydrodynamics, etc. One can even obtain directly two-dimensional scalar vortex dynamics by considering constrained variations.

References

[1] J. Serrin, "Mathematical Principles of Classical Fluid Mechanics," in *Handbuch der Physik* VIII pt.1, ed. S. Flügge (Springer-Verlag, Berlin, 1959) pp. 125-263.

[2] C. Eckart, "Variation Principles of Hydrodynamics," Phys. Fluids **3**, 421-427 (1960).

[3] W.A. Newcomb, "Lagrangian and Hamiltonian Methods in Magnetohydrodynamics," Nuclear Fusion Supplement, pt. 2, 451-463 (1962).

[4] R. Salmon, "Hamilton's Principle and Ertel's Theorem," in *Mathematical Methods in Hydrodynamics and Integrability in Dynamical Systems*, eds. M. Tabor and Y. Treve, AIP Conf. Proc. 88 (AIP, New York, 1982), pp. 127-135.

III. Noncanonical Hamiltonian Dynamics —Examples

A. Noncanonical Hamiltonian Dynamics

Let us start out by playing a sort of game. Suppose we have a system of ordinary differential equations:

$$\dot{z}^i = V^i(z), \quad i = 1, 2 \ldots M. \tag{III.1}$$

How would you know if this system is a Hamiltonian system? If you came upon the equations during research you might have some idea based upon the physics, but assume that this is not the case here. What would you do?

One thing you might try is to check *Liouville's theorem.* Hamilton's equations have the property

$$\sum_i \left[\frac{\partial \dot{q}_i}{\partial q_i} + \frac{\partial \dot{p}_i}{\partial p_i}\right] = \sum_i \left[\frac{\partial^2 H}{\partial q_i \partial p_i} - \frac{\partial^2 H}{\partial p_i \partial q_i}\right] = 0\,, \tag{III.2}$$

from which one can show that phase space volume is conserved; i.e. if

$$\mathcal{V}(t) = \int_{S(t)} \prod_{i=1}^{N} dp_i\, dq_i\,, \tag{III.3}$$

where $S(t)$ is a surface that bounds an arbitrary volume, then

$$\frac{d\mathcal{V}}{dt} = 0\,. \tag{III.4}$$

The surface may distort, and in general it will do so in a major way, but the volume inside remains constant. The analogous statement for the system of (III.1) is incompressibility of the vector field; i.e.

$$\sum_i \frac{\partial V^i}{\partial z^i} = 0\,, \tag{III.5}$$

whence it follows that

$$\mathcal{V}(t) = \int_{S(t)} \prod_{i=1}^{N} dz_i \tag{III.6}$$

is constant in time.

Suppose (III.5) is not true, as is the case for the following example:

$$\dot{z}_1 = -\frac{z_2^3}{3} - z_2\,,$$

$$\dot{z}_2 = \frac{z_1}{z_2^2 + 1}\,. \tag{III.7}$$

For this system

$$\frac{\partial \dot{z}_1}{\partial z_1} + \frac{\partial \dot{z}_2}{\partial z_2} = -\frac{2z_1 z_2}{(z_2^2+1)^2} \neq 0\,. \tag{III.8}$$

You would be mistaken if, based on (III.8), you concluded that (III.7) is not Hamiltonian. In fact this system is a disguised simple harmonic oscillator. It has been disguised by making a noncanonical coordinate change, something that we will discuss below.

So, is there a method for determining whether a system is Hamiltonian in general? Probably the answer is no, since one must first find a Hamiltonian and this requires a technique for finding constants of motion. There is no completely general way for doing this.* Nevertheless we can say some things; however, to do so we must investigate Hamiltonian systems in arbitrary coordinates.

You might wonder, why would equations ever arise in noncanonical variables? Surely the physics would make things come out right. To the contrary, variables that are the most physically compelling need not be canonical variables. *The Eulerian variables that describe ideal continuous media are in general noncanonical.* This includes Liouville's equation for the dynamics of the phase space density of a collection of particles, the BBGKY hierarchy, the Vlasov equation, ideal fluid dynamics and various approximations thereof, magnetized fluids, ...; it includes essentially every fundamental equation for classical media.

So with the above motivation, let us turn to discussing noncanonical Hamiltonian dynamics for finite degree of freedom systems, a formalism that extends back to Sophus Lie. The first step is to write Hamilton's equations in covariant form. Thus define

$$z^i = \begin{cases} q_i & \text{for } i = 1, 2, \ldots N, \\ p_{i-N} & \text{for } i = N+1, \ldots 2N\,. \end{cases} \tag{III.9}$$

The z^i are coordinates on phase space which we denote by $\mathcal{Z}$. In terms of the z's Hamilton's equations take the compact form

$$\dot{z}^i = J_c^{ij} \frac{\partial H}{\partial z^j} = [z^i, H]\,, \tag{III.10}$$

where the Poisson bracket is given by

$$[f, g] = \frac{\partial f}{\partial z^i} J_c^{ij} \frac{\partial g}{\partial z^j}\,, \tag{III.11}$$

with

$$(J_c^{ij}) = \begin{pmatrix} 0_N & I_N \\ -I_N & 0_N \end{pmatrix}\,. \tag{III.12}$$

Above, the repeated indices are to be summed over $1, 2, \ldots 2N$. In (III.12), 0_N is an $N \times N$ matrix of zeros and I_N is the $N \times N$ unit matrix. The subscript c of J_c indicates that the system is written in terms of canonical coordinates. It is important to realize that we have only rewritten Hamilton's equations in new notation, albeit in a form that is suggestive.

*Techniques for finding constants of motion do exist, but necessarily possess limitations. See e.g. A. Ramani, B. Gramniaticos, and T. Bountis, Phys. Rep. **180**, 161 (1989), and references therein.

Now consider a general, time independent change of coordinates

$$\bar{z}^i = \bar{z}^i(z)\,. \tag{III.13}$$

The Hamiltonian H transforms as a scalar:

$$H(z) = \bar{H}(\bar{z})\,. \tag{III.14}$$

Taking time derivatives of (III.13) yields

$$\dot{\bar{z}}^l = \frac{\partial \bar{z}^l}{\partial z^i}\dot{z}^i = \frac{\partial \bar{z}^l}{\partial z^i}J_c^{ij}\frac{\partial H}{\partial z^j} = \left[\frac{\partial \bar{z}^l}{\partial z^i}J_c^{ij}\frac{\partial \bar{z}^m}{\partial z^j}\right]\frac{\partial \bar{H}}{\partial \bar{z}^m}\,. \tag{III.15}$$

Defining

$$J^{lm} := \frac{\partial \bar{z}^l}{\partial z^i}J_c^{ij}\frac{\partial \bar{z}^m}{\partial z^j}\,, \tag{III.16}$$

we see Hamilton's equations are covariant and that J^{lm}, which is called the *cosymplectic form*, transforms as a contravariant tensor of second rank. In the new variables, Hamilton's equations become

$$\dot{\bar{z}}^l = J^{lm}(\bar{z})\frac{\partial \bar{H}}{\partial \bar{z}^m} = [\bar{z}^l, H]\,, \tag{III.17}$$

where the Poisson bracket is now given by

$$[f,g] = \frac{\partial f}{\partial \bar{z}^l}J^{lm}\frac{\partial g}{\partial \bar{z}^m}\,. \tag{III.18}$$

Notice in (III.17) we have displayed the explicit $\bar{z}$ dependence in J^{lm}. This was done to emphasize an important distinction—that between *covariance* and *form invariance*. Equation (III.16) is a statement of covariance, while a statement of form invariance is given by

$$J_c^{lm} = \frac{\partial \bar{z}^l}{\partial z^i}J_c^{ij}\frac{\partial \bar{z}^m}{\partial z^j}\,. \tag{III.19}$$

This is in fact the definition of a canonical transformation. Form invariance here means that the form of the J^{ij}, and hence Hamilton's equations remains the same. Evidently, the first N of $\bar{z}^l$ are coordinates, while the second N are momenta, so it is a simple matter to revert to the usual form of Hamilton's equations in the new canonical variables $\bar{z}^l$.

Let us now return to Liouville's theorem. Taking the divergence of (III.17) yields

$$\frac{\partial \dot{\bar{z}}^l}{\partial \bar{z}^l} = \frac{\partial J^{lm}}{\partial \bar{z}^l}\frac{\partial \bar{H}}{\partial \bar{z}^m} + J^{lm}\frac{\partial^2 \bar{H}}{\partial \bar{z}^l \partial \bar{z}^m}\,. \tag{III.20}$$

The second term vanishes because J^{lm} is antisymmetric and $\partial^2\bar{H}/\partial\bar{z}^l\partial\bar{z}^m$ is symmetric. This is all there is for the usual Liouville's theorem, since in the canonical case J^{lm} is constant so

the first term vanishes. However, for Hamilton's equations written in noncanonical coordinates the following is typically (but not necessarily) true:

$$\frac{\partial \dot{\bar{z}}^l}{\partial \bar{z}^l} = \frac{\partial J^{lm}}{\partial \bar{z}^l}\frac{\partial \bar{H}}{\partial \bar{z}^m} \neq 0\,. \tag{III.21}$$

This was the situation for our little example of (III.7).

It might have occurred to you that changing the coordinates may hide but cannot destroy volume preservation. This is clear if we simply change coordinates in (III.3):

$$\mathcal{V}(t) = \int_{S(t)} \mathcal{J} \prod_{l=1}^{2N} d\bar{z}^l\,. \tag{III.22}$$

If we include the Jacobian $\mathcal{J} := \det(\partial z^i/\partial \bar{z}^j)$ in the integrand, then Liouville's theorem is still satisfied. There is a nice formula relating $\mathcal{J}$ and J, which is obtained by taking the determinant of (III.16) and using the determinant product rule:

$$\mathcal{J} = \frac{1}{\sqrt{\det J}}\,. \tag{III.23}$$

Observe that there are many J's with the same $\mathcal{J}$.

Before leaving this discussion of Liouville's theorem we mention that even though J is a function of $\bar{z}$, it is still possible for $\partial \dot{\bar{z}}^l/\partial \bar{z}^l = 0$. This can happen because $\bar{H}$ is such that the two vectors of (III.21) are perpendicular or it may happen that $\partial J^{lm}/\partial \bar{z}^l = 0$, even though J is a function of $\bar{z}$. The latter case occurs for fluid models and underlies attempts to describe turbulence by using statistical mechanics concepts.*

Now it is clear that the essence of what it means to be Hamiltonian does not lie in the canonical form. Where does it lie? It lies in some coordinate invariant properties of J. To illustrate this we will play another sort of game. Suppose you have a system of the form of (III.1) and you want to know if it is Hamiltonian. Moreover, suppose you are clever enough to realize that Liouville is not the answer, because you know that Hamiltonian systems in noncanonical coordinates look like (III.17) with Poisson brackets like (III.18). Finally, suppose somehow you have found a constant of motion, call it H, and you think this is the energy and therefore a good bet for the Hamiltonian. Then you can write

$$V^i(z) = J^{ij}\frac{\partial H}{\partial z^j} \qquad i = 1, 2, \ldots M\,. \tag{III.24}$$

Everything in (III.24) is known except J^{ij}, which is required to be antisymmetric because of (III.16). The antisymmetry automatically makes $dH/dt = 0$, and leaves M equations for $(M^2 - M)/2$ unknown quantities in J^{ij}. Suppose that with some fiddling around you have found a candidate J. [Try this for the simple example of (III.8).] Does a transformation exist such that you can transform the candidate J back to J_c?

*See e.g. D. Montgomery and R. Kraichnan, Rep. Prog. Phys. **43**, 35 (1979).

The answer to this question is given by an old theorem that is credited to Darboux. If the J^{ij} you have found makes a good Poisson bracket; that is, when (III.18) is assembled it satisfies

$$[f,g] = -[g,f] \qquad \forall\, f,g \tag{III.25}$$

$$[f,[g,h]] + [g,[h,f]] + [h,[f,g]] = 0 \qquad \forall\, f,g \tag{III.26}$$

and moreover if $\det J \neq 0$, then Darboux says there exists a transformation (at least locally) where $J \to J_c$. Note, a requirement for $\det J \neq 0$ is that $M = 2N$, since odd dimensional antisymmetric matrices have zero determinant. We will not prove Darboux's theorem, but will mention that Eq. (III.26) is the important ingredient. This is an integrability condition known as the Jacobi identity; it is the central identity of a Lie algebra—a nonassociative algebra—which has a product with properties (III.25) and (III.26), and elements that are functions defined on the phase space. We will say more about this later.

The bracket properties, (III.25) and (III.26), can be translated into properties required of the cosymplectic form. The first is evidently

$$J^{ij} = -J^{ji}\,. \tag{III.27}$$

The second, with a little work, can be shown to be equivalent to

$$S^{ijk} = J^{il}\frac{\partial J^{jk}}{\partial z^l} + J^{jl}\frac{\partial J^{ki}}{\partial z^l} + J^{kl}\frac{\partial J^{ij}}{\partial z^l} = 0\,. \tag{III.28}$$

In going from (III.26) to (III.28) it is observed that all the terms involving second derivatives that arise upon calculating $[f,[g,h]] + [g,[h,f]] + [h,[f,g]]$ cancel; only the terms where the derivative of the outer bracket acts upon the J of the inner bracket survive. This fact makes life much easier when verifying the Jacobi identity.

Now suppose everything worked out right except the J you found had $\det J = 0$, with some rank $2N < M$. What then? A generalization of the Darboux theorem, which was proven* at least by the 1930's, says that J can be transformed into the following form:

$$(J_c) = \begin{pmatrix} 0_N & I_N & 0 \\ -I_N & 0_N & 0 \\ 0 & 0 & 0_{M-2N} \end{pmatrix}. \tag{III.29}$$

Interesting things happen in places where the rank of J changes. Later we will say something about this, too.

From (III.29) it is clear that in the right coordinates the system is an N degree-of-freedom system with some extraneous coordinates, $M - 2N$ in fact. The geometrical picture is as depicted below in Figure 1.

Through any point of the M dimensional phase space $\mathcal{Z}$ there exists a regular Hamiltonian phase space $\mathcal{P}$ of dimension $2N$. These surfaces are called *symplectic leaves.* A consequence of the degeneracy is that there exists a special class of invariants that are built into the phase space. They are called *Casimir invariants*, a name which derives from the Lie algebra for

*See e.g. L. P. Eisenhart, *Continuous Groups of Transformations* (Dover, New York, 1961) and R. Littlejohn, AIP Conf. Proc. **88**, 47 (1982).

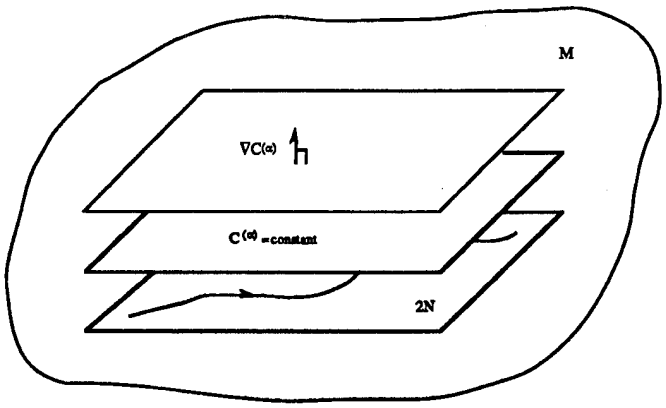

Figure 1:

angular momentum. Since the rank of J is $2N$ there exists possibly $M-2N$ independent null eigenvectors. A consequence of the Jacobi identity is that this is the case and, moreover, the null space can in fact be spanned by the gradients of the Casimir invariants, which satisfy

$$J^{ij}\frac{\partial C^{(\alpha)}}{\partial z^j} = 0\,, \tag{III.30}$$

where $\alpha = 1, 2, 3, ..., M-2N$. That the Casimir invariants are constants of motion follows from

$$\dot{C}^{(\alpha)} = \frac{\partial C^{(\alpha)}}{\partial z^i} J^{ij}\frac{\partial H}{\partial z^j} = 0\,. \tag{III.31}$$

Note that they are constants of motion for *any* Hamiltonian; they are as noted above built into the phase space and are in this sense kinematical constants of motion. The dynamics is determined by the Hamiltonian H. Note that the surfaces $\mathcal{P}$ of dimension $2N$ in the figure are the intersections of the $M-2N$ surfaces defined by $C^{(\alpha)} =$ constant. Dynamics generated by any H that begins on a particular $\mathcal{P}$ surface remains there.

The picture we have described above is the finite dimensional analogue of the Hamiltonian form possessed by Eulerian continuous media theories. We will describe the Poisson brackets for some of them soon, but now we mention that for these theories the J^{ij} has a special form that is linear in the z^k, i. e.

$$J^{ij} = c^{ij}_k z^k\,, \tag{III.32}$$

where the c^{ij}_k are constants—in fact, structure constants for a Lie algebra. In light of (III.27) and (III.28) they must satisfy

$$c^{ij}_k = -c^{ji}_k \tag{III.33}$$

and

$$c^{ij}_m c^{mk}_l + c^{jk}_m c^{mi}_l + c^{ki}_m c^{mj}_l = 0\,. \tag{III.34}$$

Brackets of the form of (III.32) are called *Lie-Poisson.*

It is interesting to reexamine the condition for Liouville's theorem (III.21) for J's of the above form,

$$\frac{\partial J^{lm}}{\partial z^l}\frac{\partial H}{\partial z^m} = c_l^{lm}\frac{\partial H}{\partial z^m} = 0\,. \tag{III.35}$$

In general, structure constants do not possesses antisymmetry or symmetry upon interchange of an up with a down index. However sometimes they do, as in the case of $so(3)$ [see (III.B)]. In general semisimple Lie algebras can, by a coordinate change, be brought into a form where the structure constants are completely antisymmetric.* In these coordinates there is Liouville's theorem without the need for inserting a Jacobian as in (III.23). This, as noted above, is typically the case for fluid theories in Eulerian variables.

In infinite dimensions the analogue of (III.18) is given by

$$\{F,G\} = \int_D \frac{\delta F}{\delta \psi^i}\mathfrak{J}^{ij}\frac{\delta G}{\delta \psi^j}\,d\mu =: \left\langle \frac{\delta F}{\delta \psi}, \mathfrak{J}\frac{\delta G}{\delta \psi}\right\rangle , \tag{III.36}$$

where $\psi^i(\mu,t)$, and $\mu = (\mu_1,...,\mu_n)$ is a "spatial" or Eulerian observation variable, and ψ^i, $i = 1,...,n$ are n components of the field. Now $\mathfrak{J}$ is an operator, and we require

$$\{F,G\} = -\{G,F\} \qquad \forall\ F,G \tag{III.37}$$

$$\{F,\{G,H\}\} + \{G,\{H,F\}\} + \{H,\{F,G\}\} = 0 \qquad \forall\ F,G,H \tag{III.38}$$

where F and G are now functionals. Analogous to (III.27) the antisymmetry condition of (III.37) requires $\mathfrak{J}$ to be *skew-symmetric*, i.e.

$$\langle f, \mathfrak{J}\, g\rangle = \left\langle \mathfrak{J}^\dagger f, g\right\rangle = -\langle g, \mathfrak{J}\, f\rangle\ . \tag{III.39}$$

The Jacobi identity (III.38) for infinite dimensional systems has a condition analogous to (III.28); one need only consider functional derivatives of $\mathfrak{J}$ when calculating $\{F,\{G,H\}\} + \{G,\{H,F\}\} + \{H,\{F,G\}\}$†. For Eulerian media, as noted above, the *cosymplectic operator* typically has the Lie-Poisson form

$$\mathfrak{J}^{ij} = \mathcal{C}_k^{ij}\psi^k\,, \tag{III.40}$$

where $\mathcal{C}_k^{ij}$ are *structure operators*. We will clarify the meaning of these structure operators by examples; a bit more will be said in Lecture IV.

---

*N. Jacobson, *Lie Algebras* (Wiley Interscience, New York, 1962).

†See e.g. P. J. Morrison (1982), *Ref. III A*.

References

[1] E. C. G. Sudarshan and N. Mukunda, *Classical Dynamics: A Modern Perspective,* (John Wiley, New York, 1974.)

[2] P. J. Morrison, "Poisson Brackets for Fluids and Plasmas," in *Mathematical Methods in Hydrodynamics and Integrability in Related Dynamical Systems*, eds. M. Tabor and Y. Treve, AIP Conference Proceedings **88**, La Jolla, 1982, p. 13.

[3] R. Salmon, Ann. Rev. Fluid Mech. **20**, 225 (1988).

B. Examples

Below the noncanonical Poisson brackets for several systems are presented. The first, the free rigid body, is a finite dimensional system, the others are infinite dimensional. We present the brackets here and refer the reader to the references* for a discussion of the Jacobi identity.

1. Free Rigid Body

The equations that govern the motion of the free rigid body are Euler's equations, the following three-dimensional system:

$$\dot{\ell}_1 = \ell_2\ell_3\left(\frac{1}{I_3} - \frac{1}{I_2}\right),$$

$$\dot{\ell}_2 = \ell_3\ell_1\left(\frac{1}{I_1} - \frac{1}{I_3}\right),$$

$$\dot{\ell}_3 = \ell_1\ell_2\left(\frac{1}{I_2} - \frac{1}{I_1}\right), \tag{III.41}$$

which correspond to the statement of torque-free motion in a frame frozen into the body with axes aligned with the principal axes. (See Lecture IV for more details.) The energy is purely rotational kinetic energy; since the axes are principal axes it takes the form

$$H = \tfrac{1}{2}\sum_{i=1}^{3}\frac{\ell_i^2}{I_i}. \tag{III.42}$$

The function H is easily seen to be a constant of motion upon differentiating with respect to time and making use of (III.41). The Poisson bracket for this system is of Lie-Poisson type

$$[f,g] = -\epsilon_{ijk}\ell_k\frac{\partial f}{\partial \ell_i}\frac{\partial g}{\partial \ell_j}. \tag{III.43}$$

*See e.g. Morrison (1982), *l.c.*

The structure constants are ϵ_{ijk}, which are those of $SO(3)$, that is, the group of rotations. The Jacobi identity is assured since the ϵ_{ijk}, being structure constants, satisfy (III.34)—something that is not difficult to verify directly. It is evident upon substituting (III.42) into (III.43), that

$$\dot{\ell}_i = [\ell_i, H]\,, \tag{III.44}$$

is equivalent to (III.41). This system possesses the Casimir invariant

$$C = \tfrac{1}{2}\sum_{i=1}^{3} \ell_i^2\,, \tag{III.45}$$

which satisfies

$$[C, f] = 0\,, \qquad \forall\, f\,. \tag{III.46}$$

Thus the global picture of the phase space $\mathcal{Z}$, which here corresponds to Figure 1, is one where the symplectic leaves are nested two-dimensional spheres in the three-dimensional space with coordinates (ℓ_1, ℓ_2, ℓ_3).

2. Korteweg-deVries Equation

We write the famous Korteweg-deVries (KdV) equation*, which describes long wavelength water waves and ion-acoustic waves in plasmas, in the following form:

$$\frac{\partial u}{\partial t} + u\frac{\partial u}{\partial x} + \frac{\partial^3 u}{\partial x^3} = 0\,. \tag{III.47}$$

Here $x \in D$, which can be (and typically is) chosen to be $(-\infty, \infty)$ or $(-\pi, \pi)$. In the former case the appropriate boundary condition is $u(\pm\infty) = 0$, while in the later case periodic boundary conditions are appropriate. The KdV equation possesses a countable infinity of constants of motion, but the one that is of interest now is the following:

$$H = \int_D \left[\tfrac{1}{6}u^3 - \tfrac{1}{2}\left(\frac{\partial u}{\partial x}\right)^2\right] dx\,. \tag{III.48}$$

The noncanonical Poisson bracket, due to Gardner†, is given by

$$\{F, G\} = -\int_D \frac{\delta F}{\delta u}\frac{\partial}{\partial x}\frac{\delta G}{\delta u} dx\,, \tag{III.49}$$

from which it is seen that the cosymplectic operator is

$$\mathfrak{J} = -\frac{\partial}{\partial x}\,. \tag{III.50}$$

*See e.g. G. Whitham, *Linear and Nonlinear Waves* (Wiley-Interscience, New York, 1974).
†C. S. Gardner, J. Math. Phys. **12**, 1548 (1971).

The skew-symmetry of (III.49) follows upon integration by parts; the Jacobi identity can be shown to be automatic since the cosymplectic operator is independent of u. Inserting the functional derivative of (III.48),

$$\frac{\delta H}{\delta u} = \left(\tfrac{1}{2}u^2 + \frac{\partial^2 u}{\partial x^2}\right) \tag{III.51}$$

into (III.49), yields

$$\frac{\partial u}{\partial t} = -\frac{\partial}{\partial x}\left(\tfrac{1}{2}u^2 + \frac{\partial^2 u}{\partial x^2}\right) = -u\frac{\partial u}{\partial x} - \frac{\partial^3 u}{\partial x^3}. \tag{III.52}$$

This bracket possesses one Casimir invariant,

$$C[u] = \int_D u\, dx\,. \tag{III.53}$$

It is easily verified that $\{C, F\} = 0$ for all functionals F. The phase space $\mathcal{Z}$ in this case is infinite dimensional—it being a function space composed of all admissible functions u. The symplectic leaves are of one fewer dimension, but they are also infinite dimensional.

Note that the bracket above is not linear in u and is therefore not of Lie-Poisson form, in spite of the fact that we have claimed that the standard Hamiltonian form for theories of media is of this type. You may know that the KdV equation is special—it being integrable by the inverse scattering method—so it is not too surprising that it has a Hamiltonian structure that is inconsistent with the credo. Although the basic equations that describe media in terms of Eulerian variables has the Lie-Poisson form, when approximations are made this form can change.

3. 1-D Pressureless Fluid

Now we consider an equation even simpler than the KdV equation, that of a one-dimensional pressureless fluid,

$$\frac{\partial u}{\partial t} + u\frac{\partial u}{\partial x} = 0\,. \tag{III.54}$$

This equation has, in jest, been referred to as both the dispersionless KdV equation and the inviscid Burger's equation. That it models a fluid suggests that the Hamiltonian ought to be just the kinetic energy functional,

$$H[u] = \int_D \tfrac{1}{2}u^2 dx\,, \tag{III.55}$$

there being no internal energy. The following bracket, with the above Hamiltonian, produces (III.54):

$$\{F, G\} = -\tfrac{1}{3}\int_D u\left[\frac{\delta F}{\delta u}\frac{\partial}{\partial x}\frac{\delta G}{\delta u} - \frac{\delta G}{\delta u}\frac{\partial}{\partial x}\frac{\delta F}{\delta u}\right] dx\,; \tag{III.56}$$

that is

$$\frac{\partial u}{\partial t} = \{u, H\} = -\tfrac{1}{3}\left(u\frac{\partial u}{\partial x} + \frac{\partial (u^2)}{\partial x}\right) = -u\frac{\partial u}{\partial x}\,. \tag{III.57}$$

The cosymplectic operator is evidently given by

$$\mathfrak{J} = -\tfrac{1}{3}\left(u\frac{\partial}{\partial x} + \frac{\partial}{\partial x}u\right) = -\tfrac{1}{3}\left(2u\frac{\partial}{\partial x} + \frac{\partial u}{\partial x}\right). \tag{III.58}$$

The following Casimir invariant is easily obtained by solving $\{C, F\} = 0$ for all functionals F; i.e., by searching for null eigenvectors of (III.58) and undoing the functional derivative:

$$C = \int_D |u|^{1/2}\, dx\,. \tag{III.59}$$

It is evident that the following Hamiltonian:

$$H[u] = \tfrac{1}{6}\int_D u^3 dx\,, \tag{III.60}$$

together with the bracket (III.49) will also produce (III.54). Thus it is possible for a system to have two Hamiltonian structures: two functionally independent Hamiltonians with two distinct Poisson brackets. This rarity occurs for the above system, the KdV equation and other systems. It is a symptom of integrability*.

4. 1-D Compressible Fluid

Now we consider a somewhat more complicated model, that of a one-dimensional compressible fluid with a pressure the depends only upon the density. The equations of motion for this system are the following:

$$\begin{aligned}\frac{\partial u}{\partial t} &= -u\frac{\partial u}{\partial x} - \frac{1}{\rho}\frac{\partial p}{\partial x}\\ \frac{\partial \rho}{\partial t} &= -\frac{\partial(\rho u)}{\partial x}\,.\end{aligned} \tag{III.61}$$

The Hamiltonian has a kinetic energy part plus an internal energy part,

$$H[\rho, u] = \int_D \left[\tfrac{1}{2}\rho u^2 + \rho U(\rho)\right] dx\,, \tag{III.62}$$

and the Poisson bracket is given by

$$\{F, G\} = -\int_D \left[\frac{\delta F}{\delta \rho}\frac{\partial}{\partial x}\frac{\delta G}{\delta u} - \frac{\delta G}{\delta \rho}\frac{\partial}{\partial x}\frac{\delta F}{\delta u}\right] dx\,. \tag{III.63}$$

The cosymplectic operator

$$\left(\mathfrak{J}^{ij}\right) = \begin{pmatrix} 0 & \frac{\partial}{\partial x} \\ \frac{\partial}{\partial x} & 0 \end{pmatrix}, \tag{III.64}$$

*See F. Magri, J. Math. Phys. **19**, 1156 (1978).

is seen to be skew-symmetric upon integration by parts and systematic neglect of the surface terms. The Jacobi identity, follows since the cosymplectic operator is independent of the dynamical variables.

Observe that this bracket, like the two above, is not Lie-Poisson. However, upon transforming from the dependent variables (u,ρ) to (M,ρ), where $M=\rho u$, it obtains the Lie-Poisson form. We won't do this transformation here but consider this below when we treat the ideal fluid in three spatial dimensions.

Setting $\{F,C\}=0$ for all F yields two equations

$$\frac{\partial}{\partial x}\frac{\delta C}{\delta \rho}=0\,, \qquad \frac{\partial}{\partial x}\frac{\delta C}{\delta u}=0\,, \tag{III.65}$$

from which we obtain the following Casimir invariants:

$$C_1[u]=\int_D u\,dx\,, \qquad C_2[\rho]=\int_D \rho\,dx\,. \tag{III.66}$$

Using

$$\begin{aligned}\frac{\delta H}{\delta u}&=\rho u\,,\\ \frac{\delta H}{\delta \rho}&=\tfrac{1}{2}u^2+h(\rho)\,,\end{aligned} \tag{III.67}$$

where $h(\rho):=\rho U_\rho+U$ is the enthalpy (note that $\delta H/\delta\rho=$ constant is Bernoulli's law), in (III.63) produces

$$\begin{aligned}\frac{\partial u}{\partial t}&=\{u,H\}=-\frac{\partial}{\partial x}\left(\tfrac{1}{2}u^2+U+\rho U_\rho\right)\,,\\ \frac{\partial \rho}{\partial t}&=\{\rho,H\}=-\frac{\partial}{\partial x}(\rho u)\,.\end{aligned} \tag{III.68}$$

These equations are seen to be equivalent to (III.61) upon making use of $h_x=p_x/\rho$ (recall $p=\rho^2U_\rho$).

5. 2-D Euler Scalar Vortex Dynamics

The vortex dynamics we consider here, unlike the examples above, has two spatial variables, $r:=(x,y)\in D$, in addition to time; that is, it is a $2+1$ theory. The noncanonical Poisson bracket possessed by this system* is the prototype of $2+1$ theories, it being shared by the 1-D Vlasov-Poisson equation†, quasigeostrophy or the Hasegawa-Mima equation, and others.

*P. J. Morrison, "Hamiltonian field description of two-dimensional vortex fluids an guiding center plasmas," Princeton University Plasma Physics Laboratory Report, PPPL-1783 (1981) (Available as American Institute of Physics Document No. PAPS-PFBPE-04-771, AIP Auxiliary Publication Service, 335 East 45th Street, New York, NY 10017) and P. J. Olver, J. Math. Anal. Appl. **89**, 233 (1982).

†P. J. Morrison, Phys. Lett. **80A**, 383 (1980).

The single dynamical variable for the 2-D Euler equation is the scalar vorticity, defined by

$$\omega(r,t) := \hat{z} \cdot \nabla \times v \,, \tag{III.69}$$

where v is the Eulerian velocity field and $\hat{z}$ is the ignored coordinate. The velocity field is assumed to be incompressible, $\nabla \cdot v = 0$, and hence the streamfunction, ψ, is introduced:

$$v = \left(-\frac{\partial \psi}{\partial y}, \frac{\partial \psi}{\partial x} \right) , \tag{III.70}$$

which is related to the vorticity through

$$\omega = \nabla^2 \psi \,. \tag{III.71}$$

The equation of motion for this system is

$$\frac{\partial \omega}{\partial t} = -v \cdot \nabla \omega = -\left[\psi, \omega\right] , \tag{III.72}$$

where

$$[f,g] = \frac{\partial f}{\partial x}\frac{\partial g}{\partial y} - \frac{\partial f}{\partial y}\frac{\partial g}{\partial x} \,. \tag{III.73}$$

There is some subtlety with the boundary conditions. The physical boundary condition for the ideal fluid is that no flow penetrates the boundary; i.e. the normal component of v vanishes. This amounts to ψ = constant on ∂D. Since ω is the dynamical variable one might expect the boundary condition to be, ω = constant on ∂D. Then it is natural to set variations of ω to zero on the boundary to eliminate surface terms obtained upon integration by parts. Although this boundary condition is correct for the Vlasov-Poisson equation, it is unphysical for the ideal fluid where the vorticity at a point on the boundary need not be constant. When boundary terms do not vanish with physical boundary conditions, generally the mathematics is signalling something physical. In this case it is signalling the fact that surfaces of constant vorticity possess dynamics, an idea that is the basis of the "contour dynamics" approximation technique. To describe this is beyond the scope of these notes. However, all these complications can be avoided by choosing the domain D to be a finite box and impose periodic boundary conditions. Alternatively, D can be chosen to be $\mathbb{R}^2$ with vanishing vorticity at infinity; however, as is well-known in electrostatics, this requires a potential that diverges logarithmically.

The energy in this model is purely kinetic, thus the Hamiltonian is given by

$$\begin{aligned} H[\omega] &= \tfrac{1}{2}\int_D v^2 \, d^2r = \tfrac{1}{2}\int_D |\nabla\psi|^2 \, d^2r \\ &= \int\int \omega(r)\, K(r|r')\, \omega(r')\, d^2r = -\tfrac{1}{2}\int_D \omega\psi \, d^2r \,, \end{aligned} \tag{III.74}$$

where K is defined by

$$\psi(r) = -\int \omega(r) K(r|r') \omega(r') \, d^2r \,. \tag{III.75}$$

Observe that in the case where $D = \mathbb{R}^2$ the last equality requires the elimination of the logarithmic singularity. The noncanonical Poisson bracket for this system is given by

$$\{F, G\} = \int_D \omega \left[\frac{\delta F}{\delta \omega}, \frac{\delta G}{\delta \omega}\right] d^2 r\,, \tag{III.76}$$

which is of the Lie-Poisson form. The cosymplectic operator in this case is

$$\mathfrak{J} = -[\omega, \cdot\,]\,. \tag{III.77}$$

Skew-symmetry follows from

$$\int_D f[g, h]\, d^2 r = -\int_D g[f, h]\, d^2 r\,, \tag{III.78}$$

which is obtained upon integration by parts and neglect of the boundary terms. The Jacobi identity for $\mathfrak{J}$ is inherited from that for $[\,,\,]$, as is generally the case for Lie-Poisson brackets. The Casimir invariant for the bracket of (III.76) is given by

$$C[\omega] = \int \mathcal{C}(\omega)\, d^2 r\,, \tag{III.79}$$

where $\mathcal{C}$ is an arbitrary function. Since $\mathcal{C}$ is arbitrary C in fact constitutes an infinity of constants of motion. These arise form the incompressibility of phase space*. We mention that even though there are an infinity of constants this is insufficient for the 2-D Euler equations to be integrable. In order to obtain the equations of motion we require

$$\frac{\delta H}{\delta \omega} = -\psi\,. \tag{III.80}$$

Evidently,

$$\frac{\partial \omega}{\partial t} = \{\omega, H\} = -[\omega, \frac{\delta H}{\delta \omega}] = [\omega, \psi]\,, \tag{III.81}$$

which is equivalent to (III.72).

6. 3-D Ideal Fluid

For this last example we consider the ideal fluid in three-dimensions, our first example of a $3 + 1$ theory where the spatial variables are the Cartesian coordinates $r := (x, y, z) =: (x_1, x_2, x_3) \in D$. The dynamical variables used are the same as those discussed in Lecture II: the three components of the Eulerian velocity field, v, the density ρ and the entropy per unit mass s. We use s rather than the pressure p, but it is a simple matter to alter this. The equations of motion are

$$\frac{\partial v}{\partial t} = -v \cdot \nabla v - \frac{1}{\rho}\nabla p\,, \tag{III.82}$$

$$\frac{\partial \rho}{\partial t} = -\nabla \cdot (\rho v)\,, \tag{III.83}$$

$$\frac{\partial s}{\partial t} = -v \cdot \nabla s\,. \tag{III.84}$$

*For a physical explanation see P. J. Morrison, Zeitshrift für Naturforschung **42a**, 1115 (1987).

Recall that the thermodynamics is embodied in an internal energy function $U(\rho, s)$, from which in addition to the pressure $p = \rho^2 U_\rho$, the temperature is given by $T = U_s$.

The Hamiltonian functional is given by

$$H[v, \rho, s] = \int_D \left(\tfrac{1}{2}\rho v^2 + \rho U(\rho, s) \right) \, d^3 r \,, \tag{III.85}$$

and the noncanonical Poisson bracket* is

$$\{F, G\} = -\int_D \left[\left(\frac{\delta F}{\delta \rho} \nabla \cdot \frac{\delta G}{\delta v} - \frac{\delta F}{\delta \rho} \nabla \cdot \frac{\delta G}{\delta v} \right) + \left(\frac{\nabla \times v}{\rho} \cdot \frac{\delta F}{\delta v} \times \frac{\delta G}{\delta v} \right) \right.$$
$$\left. + \frac{\nabla s}{\rho} \cdot \left(\frac{\delta F}{\delta s} \frac{\delta G}{\delta v} - \frac{\delta F}{\delta s} \frac{\delta G}{\delta v} \right) \right] d^3 r \,. \tag{III.86}$$

This bracket is familiar in that the first term is the generalization to three-dimensions of that for the $1+1$ compressible fluid given above. Similarly, recognizing that via the chain rule $\delta F/\delta v = \nabla \times \delta F/\delta \omega$, the second term is seen to be a generalization of that for the $2+1$ scalar vortex dynamics given above†. The third term is not familiar, but had we included entropy in our $1+1$ fluid theory its one-dimensional counterpart would have been present.

Using

$$\frac{\delta H}{\delta v} = \rho v \,, \qquad \frac{\delta H}{\delta \rho} = \tfrac{1}{2} v^2 + (\rho U)_\rho \,, \qquad \frac{\delta H}{\delta s} = \rho U_s \,, \tag{III.87}$$

Eqs.(III.84) are seen to be equivalent to

$$\frac{\partial v}{\partial t} = \{v, H\} \,, \qquad \frac{\partial \rho}{\partial t} = \{\rho, H\} \,, \qquad \frac{\partial s}{\partial t} = \{s, H\} \,. \tag{III.88}$$

In order to obtain the equations of motion from the above and in order to prove the Jacobi identity, integrations by parts must be performed and surface terms involving functionals must be neglected. The boundary condition appropriate for the ideal fluid, as noted above, is $\hat{n} \cdot v = 0$ on ∂D, but this is a boundary condition on v not on the functionals directly. The function space of functionals must be such that these terms vanish for all functionals. In the case where D is a finite domain there is a complication with the vanishing of these terms, as in the case for the 2-D Euler equations. This problem is not an issue when periodic boundary conditions are used or when $D = \mathbb{R}^3$, for in these cases the space of functionals can be defined appropriately. However, when D is a finite domain there is difficulty. One might try to eliminate the surface terms by requiring all functionals to satisfy $\hat{n} \cdot \delta F/\delta v = 0$, but this space of functionals is not closed, i.e. the bracket of two functionals with this property does not necessarily produce a functional with this property. A method that circumvents this complication is to build the boundary condition into the Hamiltonian by a suitable potential energy functional.

It is evident that the Poisson bracket of (III.86) is not of Lie-Poisson from. However, if a transformation form the variables v, ρ, and s to the conserved variables $M := \rho v$, ρ,

*P. J. Morrison and J. M. Greene, Phys. Rev. Lett. **45**, 790 (1980); *ibid.* **48**, 569 (1982).

†See, for three-dimensional vortex dynamics, E. A. Kuznetsov and A. Mikhailov, Phys. Lett. **77A**, 37 (1980).

and $\sigma := \rho s$, which were introduced in Lecture I (and alluded to above), is made, then the bracket becomes[‡]

$$\{F,G\} = -\int_D \left[M_i \left(\frac{\delta F}{\delta M_j} \frac{\partial}{\partial x_j} \frac{\delta G}{\delta M_i} - \frac{\delta G}{\delta M_j} \frac{\partial}{\partial x_j} \frac{\delta F}{\delta M_i} \right) + \rho \left(\frac{\delta F}{\delta M} \cdot \nabla \frac{\delta G}{\delta \rho} - \frac{\delta G}{\delta M} \cdot \nabla \frac{\delta F}{\delta \rho} \right) \right.$$
$$\left. + \sigma \left(\frac{\delta F}{\delta M} \cdot \nabla \frac{\delta G}{\delta \sigma} - \frac{\delta G}{\delta M} \cdot \nabla \frac{\delta F}{\delta \sigma} \right) \right] d^3r \,. \qquad \text{(III.89)}$$

This transformation requires the use of the chain rule for functional derivatives, which gives formulas like the following:

$$\left. \frac{\delta F}{\delta \rho} \right|_{v,s} = \left. \frac{\delta F}{\delta \rho} \right|_{M,s} + \frac{M}{\rho} \cdot \frac{\delta F}{\delta M} + \frac{\sigma}{\rho} \frac{\delta F}{\delta \sigma} \,. \qquad \text{(III.90)}$$

It is straight forward to show that (III.89) together with the Hamiltonian

$$H[M,\rho,\sigma] = \int_D \left(\tfrac{1}{2} \frac{M^2}{\rho} + \rho U(\rho, \sigma/\rho) \right) d^3r \,, \qquad \text{(III.91)}$$

produces the fluid equations of motion in conservation form as follows:

$$\frac{\partial M}{\partial t} = \{M,H\} \,, \qquad \frac{\partial \rho}{\partial t} = \{\rho,H\} \,, \qquad \frac{\partial \sigma}{\partial t} = \{\sigma,H\} \,. \qquad \text{(III.92)}$$

Now consider the condition for the Casimir invariants, $\{F,C\} = 0$ for all F. From (III.86) it is seen that this implies

$$\nabla \cdot \frac{\delta C}{\delta v} = 0 \,, \qquad \frac{1}{\rho} \nabla s \cdot \frac{\delta C}{\delta v} = 0$$
$$\nabla \frac{\delta C}{\delta \rho} + \frac{(\nabla \times v)}{\rho} \times \frac{\delta C}{\delta v} - \frac{\nabla s}{\rho} \frac{\delta C}{\delta s} = 0 \,. \qquad \text{(III.93)}$$

One solution of these equations is

$$C_1[\rho,s] = \int_D \rho f(s) \, d^3r \,, \qquad \text{(III.94)}$$

where f is an arbitrary function. If we eliminate the entropy variable, s, from the theory, then another solution is the helicity

$$C_2[v] = \int_D v \cdot \nabla \times v \, d^3r \,. \qquad \text{(III.95)}$$

It will be left to you to investigate the general solution.

[‡]Morrison and Greene, *l.c.*; I. E. Dzyaloshinskii and G. E. Volovick, Ann. Phys. **125**, 67 (1980).

7. General Comments

Above we presented a variety of noncanonical Poisson brackets, of one, two and three spatial dimensions and of one or more field variables, culminating in that of the three-dimensional fluid with the field variables (v, ρ, s) or (M, ρ, σ). In closing this lecture we make some brief comments about the classification of the various brackets.

Consider the cases where there is only a single field variable. We presented two such $1+1$ theories, that for the KdV equation and that for the pressureless fluid. It is natural to ask whether or not these brackets are in some sense equivalent. Is it possible by a coordinate change to map one into the other? A simple scaling analysis suggests that a quadratic transformation might do this. An invertible transformation of this kind is given by

$$\tilde{u} = \tfrac{1}{6}u^2 \operatorname{sgn}(u)\,, \tag{III.96}$$

with the inverse

$$u = \operatorname{sgn}(\tilde{u})\sqrt{6\tilde{u}}\,. \tag{III.97}$$

Inserting

$$\frac{\delta F}{\delta u} = 2 \operatorname{sgn}(\tilde{u})\sqrt{6\tilde{u}}\,\frac{\delta F}{\delta \tilde{u}} \tag{III.98}$$

into the KdV bracket yields

$$\{F,G\} = -\int_D \frac{\delta F}{\delta u}\frac{\partial}{\partial x}\frac{\delta G}{\delta u}\,dx = -\tfrac{1}{3}\int_D \tilde{u}\left[\frac{\delta F}{\delta \tilde{u}}\frac{\partial}{\partial x}\frac{\delta G}{\delta \tilde{u}} - \frac{\delta G}{\delta \tilde{u}}\frac{\partial}{\partial x}\frac{\delta F}{\delta \tilde{u}}\right]\,dx\,. \tag{III.99}$$

Now it is evident from (III.99) and from above, where we changed fluid variables form (v, ρ, s) to (M, ρ, σ), that sometimes brackets can be mapped into the Lie-Poisson form by an invertible transformation. The study of when this can be done is an interesting area that we will not address here. However, since typically for fluid theories this can be done, this suggests a classification of such theories by their Lie-Poisson bracket, which in turn are classified by the Lie group corresponding to the structure operators. Thus theories can be classified by a Lie group* and the corresponding Casimir invariants are determined. In the case of $1+1$ theories discussed above, the group is that of coordinate changes and the algebra is in essence the infinitesimal generator $\partial/\partial x$. In the case of the $2+1$ theory of Euler's fluid equations the group is the group of canonical transformations of the plane, or equivalently area preserving transformations. When one increases the number of spatial dimensions the possibilities increase. When more than one field variable is considered the groups become more complicated. They are groups by extension, such as the direct product or semidirect product. Treatment of this area is beyond the scope of these lectures, although we will briefly comment on this in the context of Clebsch variables in Lecture IV.

*This idea is an old one. It in essence was developed in the work of Sudarshan (1963), *Ref. IV B*. See also Sudarshan and Mukunda (1974), *Ref. III A*. Further development in the geometrical setting was given by V. I. Arnold, Ann. Inst. Four. **16**, 319 (1966) and Usp. Mat. Nauk. **24**, 225 (1969), although unlike here the (cumbersome) Lagrange bracket is emphasized.

IV. Tutorial on Lie Groups and Algebras, Reduction—Realization, and Clebsch Variables

A. Tutorial on Lie Groups and Lie Algebras

This section, which was in fact a lecture, was given after all the others. However in retrospect it appears for continuity better placed here. It can be skipped by the cognoscenti.

A Lie group $\mathcal{G}$ is both a group and a differentiable manifold. The elements of the group, which are uncountaby infinite in number, correspond to points of the manifold. To be concrete we will consider a realization where elements of $\mathcal{G}$ correspond to functions that define transformations (coordinate changes) on some manifold $\mathcal{Z}$.

Suppose the manifold $\mathcal{Z}$ has coordinates z^i, $i = 1, 2, \ldots, M$, and a family of transformations is given by

$$z'^i = f^i(z, a) \qquad i = 1, 2, \ldots, M\,, \tag{IV.1}$$

where $z = (z^1, z^2, \ldots, z^M) \in \mathcal{Z}$ and $a = (a^1, a^2, \ldots, a^N) \in \mathcal{G}$ denotes a parameterization of the family. For each value of a the functions f constitute a one-one, onto transformation of $\mathcal{Z}$ to itself. For convenience we denote this by T_a. Thus $T_a{:}\mathcal{Z} \to \mathcal{Z}$ and $z' = T_a z$. The set of T_a's form a group under composition of functions.

It is important to distinguish between the M-dimensional manifold $\mathcal{Z}$ and the N-dimensional group manifold $\mathcal{G}$. The latter is called either the *parameter space*, *group space*, or the *group manifold*. We are introducing $\mathcal{Z}$ now so that you have something concrete to visualize, but this is really unnecessary—it could be done completely in the abstract.

Another distinction to be made is between the *passive* and *active* viewpoints of the transformation T_a. In the passive viewpoint (adopted above) the point of $\mathcal{Z}$ remains fixed and T_a represents a change in the coordinates used to identify the point. In the active viewpoint there is dynamics of a sort; a point of $\mathcal{Z}$ is mapped into a new point. Below you are, for the most part, free to think in terms of either viewpoint.

The group product, as noted above, is composition. *Closure* requires the existence of a group element T_c such that

$$T_c z = T_b T_a z \tag{IV.2}$$

for all T_b and T_c. Hence, there must be a function $\phi(b, a) = c$. It is this function that really defines the group. If one assumes that ϕ possesses three derivatives in each of its arguments, it is a wonderful thing that this guarantees the existence of all derivatives. We will see how this goes, but not work it out in detail. In terms of the function of (IV.1) closure can be stated as follows:

$$f(z, c) = f(f(z, a), b) = f(z, \phi(b, a))\,. \tag{IV.3}$$

A simple example of a Lie group is that of $SO(2)$, rotations of the plane. These are linear transformations given by

$$\begin{bmatrix} z'^1 \\ z'^2 \end{bmatrix} = \begin{bmatrix} \cos\theta & \sin\theta \\ -\sin\theta & \cos\theta \end{bmatrix} \begin{bmatrix} z^1 \\ z^2 \end{bmatrix}\,, \tag{IV.4}$$

or equivalently

$$z' = T_\theta z\,. \tag{IV.5}$$

This a one parameter group with $\theta \in [0, 2\pi]$. Closure requires that a rotation through an angle θ followed by a rotation through an angle ψ must be equivalent to a rotation through some angle χ:

$$T_\psi T_\theta = \begin{bmatrix} \cos\psi & \sin\psi \\ -\sin\psi & \cos\psi \end{bmatrix} \begin{bmatrix} \cos\theta & \sin\theta \\ -\sin\theta & \cos\theta \end{bmatrix} = \begin{bmatrix} \cos(\psi+\theta) & \sin(\psi+\theta) \\ -\sin(\psi+\theta) & \cos(\psi+\theta) \end{bmatrix} =: T_\chi\,. \tag{IV.6}$$

Evidently, the analogue of $c = \phi(b, a)$ is $\chi = \phi(\psi, \theta) = \psi + \theta$, mod 2π.

You may know that in addition to closure, groups have three other properties: associativity, the existence of an identity, and the existence of an inverse. These properties are natural if you think about elements of the group corresponding to coordinate changes.

Associativity requires

$$T_a(T_bT_c) = (T_aT_b)T_c\,. \tag{IV.7}$$

Since $T_aT_b = f(f(z, b), a)$, the right hand side is

$$(T_aT_b)T_c = f(f(f(z, c), b), a) = f(f(z, c), \phi(a, b)) = f(z, \phi(\phi(a, b), c))\,. \tag{IV.8}$$

Since $T_bT_c = T_{\phi(b,c)}$, the left hand side is

$$T_a(T_bT_c) = T_{\phi(a,\phi(b,c))}\,. \tag{IV.9}$$

Upon comparing (IV.8) and (IV.9) we see that associativity implies

$$\phi(a, \phi(b, c)) = \phi(\phi(a, b), c)\,. \tag{IV.10}$$

This relation is clearly not satisfied for all ϕ; it in fact places a strict restriction on the functions that define a group, as we shall see.

The *identity* element of the group is denoted by T_0. It must satisfy

$$T_0T_a = T_aT_0 = T_a \tag{IV.11}$$

or

$$f(f(z, a), 0) = f(f(z, 0), a) = f(z, a)\,. \tag{IV.12}$$

Therefore,

$$\phi(0, a) = \phi(a, 0) = a\,. \tag{IV.13}$$

For every element a of a group $\mathfrak{G}$ there must exist an inverse, which we denote by a^{-1}, such that

$$T_aT_{a^{-1}} = T_{a^{-1}}T_a = T_0\,. \tag{IV.14}$$

Evidently,

$$\phi(a, a^{-1}) = \phi(a^{-1}, a) = 0 \tag{IV.15}$$

In order for these equations to have a unique solution for a^{-1}, given a,

$$\det\left(\frac{\partial\phi(a,b)}{\partial a}\right) \neq 0\,; \qquad \det\left(\frac{\partial\phi(a,b)}{\partial b}\right) \neq 0\,. \tag{IV.16}$$

It is easy to verify the above properties for the example of $SO(2)$; it is recommend that you do this.

A *Lie algebra*, $\mathfrak{g}$, arises in studying the group manifold in a neighborhood of the identity. Such a study yields ordinary differential equations for ϕ.

Suppose δa is small and consider

$$T_{\tilde{a}} := T_a T_{\delta a} \tag{IV.17}$$

or

$$\tilde{a} = \phi(a, \delta a)\,. \tag{IV.18}$$

Since ϕ was assumed to be continuous $\tilde{a}$ must be near a, so we write

$$\tilde{a} = a + da = \phi(a, \delta a) \tag{IV.19}$$

or in terms of the transformations

$$T_{a+da} z = T_a T_{\delta a} z\,. \tag{IV.20}$$

This is depicted in Figure 1.

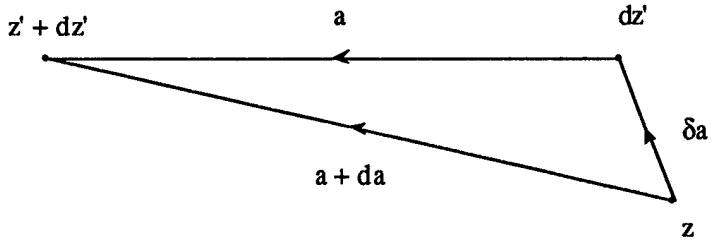

Figure 1:

Taylor expanding (IV.18) about $a = b = 0$ yields

$$a^\alpha + da^\alpha = \phi^\alpha(a, 0) + \left.\frac{\partial \phi^\alpha(a,b)}{\partial b^\beta}\right|_{b=0} \delta a^\beta + \dots\,, \tag{IV.21}$$

where the greek indicies α, β etc., which we will use to denote coordinates of the group manifold, run over $1, 2, \dots, N$. From (IV.21),

$$da^\alpha = L^\alpha_\beta(a) \delta a^\beta \tag{IV.22}$$

where

$$L^\alpha_\beta(a) := \left.\frac{\partial \phi^\alpha(a,b)}{\partial b^\beta}\right|_{b=0}\,. \tag{IV.23}$$

Consider now a function defined on the group manifold $F:\mathfrak{G} \to \mathbb{R}$. How does $F(a)$ differ from $F(\tilde{a})$?

$$\begin{aligned} dF(a) &:= F(\tilde{a}) - F(a) = F(a + da) - F(a) \\ &\approx \frac{\partial F}{\partial a^\alpha} da^\alpha = \frac{\partial F}{\partial a^\alpha} L^\alpha_\beta(a) \delta a^\beta \\ &=: \delta a^\beta X_\beta F(a) \,. \end{aligned} \tag{IV.24}$$

The quantities X_β defined by

$$X_\beta := L^\alpha_\beta(a) \frac{\partial}{\partial a^\alpha} \,, \tag{IV.25}$$

are called the *infinitesimal generators* of the Lie group. They are in fact elements of the *Lie algebra*, $\mathfrak{g}$, associated with $\mathfrak{G}$. The quantities X_β are to be thought of as vectors with components $\{L^\alpha_\beta\}$ and basis vectors $\{\partial/\partial a^\alpha\}$. Evidently, if we choose $F(a) = a$, (IV.24) implies

$$da^\gamma = \delta a^\beta X_\beta a^\gamma = L^\gamma_\beta \delta a^\beta \,. \tag{IV.26}$$

We will use this later.

Now let us return to our quest of determining what the group properties say about ϕ. Taylor expanding ϕ about $a = b = 0$ through third order yields

$$\begin{aligned} \phi^\nu(a,b) = \phi^\nu(0,0) &+ \frac{\partial \phi^\nu(0,0)}{\partial a^\kappa} a^\kappa + \frac{\partial \phi^\nu(0,0)}{\partial b^\kappa} b^\kappa + \frac{1}{2} \frac{\partial^2 \phi^\nu(0,0)}{\partial a^\kappa \partial a^\lambda} a^\kappa a^\lambda \\ &+ \frac{\partial^2 \phi^\nu(0,0)}{\partial a^\kappa \partial b^\lambda} a^\kappa b^\lambda + \frac{1}{2} \frac{\partial^2 \phi^\nu(0,0)}{\partial b^\kappa \partial b^\lambda} b^\kappa b^\lambda + \frac{1}{3!} \frac{\partial^3 \phi^\nu(0,0)}{\partial a^\kappa \partial a^\lambda \partial a^\mu} a^\kappa a^\lambda a^\mu \\ &+ \frac{1}{2} \frac{\partial^3 \phi^\nu(0,0)}{\partial a^\kappa \partial a^\lambda \partial b^\mu} a^\kappa a^\lambda b^\mu + \frac{1}{2} \frac{\partial^3 \phi^\nu(0,0)}{\partial a^\kappa \partial b^\lambda \partial b^\mu} a^\kappa b^\lambda b^\mu + \frac{1}{3!} \frac{\partial^3 \phi^\nu(0,0)}{\partial b^\kappa \partial b^\lambda \partial b^\mu} b^\kappa b^\lambda b^\mu \\ &+ \mathcal{O}(4) \,, \end{aligned} \tag{IV.27}$$

where derivatives with respect to a are taken in the first slot of ϕ^ν and those with respect to b in the second. Since

$$\phi(a,0) = \phi(0,a) = a \tag{IV.28}$$

for all a, it is clear that $\phi(0,0) = 0$, and upon differentiating (IV.28)

$$\begin{aligned} \frac{\partial \phi^\nu(0,0)}{\partial a^\kappa} &= R^\nu_\kappa(0) = \delta^\nu_\kappa \\ \frac{\partial \phi^\nu(0,0)}{\partial b^\kappa} &= L^\nu_\kappa(0) = \delta^\nu_\kappa \,. \end{aligned} \tag{IV.29}$$

Differentiating (IV.28) twice and then thrice in the nonzero argument implies

$$\frac{\partial^2 \phi^\nu(0,0)}{\partial a^\kappa \partial a^\lambda} = \frac{\partial^2 \phi^\nu(0,0)}{\partial b^\kappa \partial b^\lambda} = \frac{\partial^3 \phi^\nu(0,0)}{\partial a^\kappa \partial a^\lambda \partial a^\mu} = \frac{\partial^3 \phi^\nu(0,0)}{\partial b^\kappa \partial b^\lambda \partial b^\mu} = 0 \,. \tag{IV.30}$$

However, (IV.28) does not contain information about mixed derivatives; viz.

$$\frac{\partial^2\phi^\nu(0,0)}{\partial a^\kappa \partial b^\lambda}, \qquad \frac{\partial^3\phi^\nu(0,0)}{\partial a^\kappa \partial a^\lambda \partial b^\mu}, \qquad \frac{\partial^3\phi^\nu(0,0)}{\partial a^\kappa \partial b^\lambda \partial b^\mu}. \tag{IV.31}$$

Thus far we have reduced (IV.27) to

$$\phi^\nu(a,b) = a^\nu + b^\nu + \frac{\partial^2\phi^\nu(0,0)}{\partial a^\kappa \partial b^\lambda} a^\kappa b^\lambda + \frac{1}{2}\frac{\partial^3\phi^\nu(0,0)}{\partial a^\kappa \partial a^\lambda \partial b^\mu} a^\kappa a^\lambda b^\mu + \frac{1}{2}\frac{\partial^3\phi^\nu(0,0)}{\partial a^\kappa \partial b^\lambda \partial b^\mu} a^\kappa b^\lambda b^\mu + \mathcal{O}(4), \tag{IV.32}$$

To go farther the associativity condition (IV.10) is imposed. If you expand through second order, in anticipation of a result, you will be disappointed. Associativity places no constraint to this order. If you attempt to expand through third order you will also be dissapointed because you will generate a tedious mess. Nevertheless, perseverance and a tad of cleverness results in a condition on ϕ. If we define

$$c^\nu_{\kappa\lambda} := \frac{\partial^2\phi^\nu(0,0)}{\partial a^\kappa \partial b^\lambda} - \frac{\partial^2\phi^\nu(0,0)}{\partial a^\lambda \partial b^\kappa}, \tag{IV.33}$$

which obviously satisfies

$$c^\nu_{\kappa\lambda} = -c^\nu_{\lambda\kappa}, \tag{IV.34}$$

the condition obtained is

$$c^\nu_{\kappa\lambda}c^\lambda_{\delta\gamma} + c^\nu_{\gamma\lambda}c^\lambda_{\kappa\delta} + c^\nu_{\delta\lambda}c^\lambda_{\gamma\kappa} = 0. \tag{IV.35}$$

The numbers $c^\nu_{\kappa\lambda}$ were called *structure constants* by Sophus Lie. They are the heart of the matter.

You might wonder what happens to next order. It turns out that (IV.34) and (IV.35) are enough to determine ϕ—the structure of the group (that is connected to the identity).

Now we will obtain a differential equation for the group and then discuss briefly some important theorems proved by Lie. Recall Eq.(IV.26)

$$da^\gamma = \delta a^\beta X_\beta a^\gamma = L^\gamma_\beta \delta a^\beta, \tag{IV.36}$$

which we derived by expanding $T_{a+da} = T_a T_{\delta a}$. Since $\phi(a, a^{-1})$ must have a solution, this implies $L^\alpha_\beta(a)$ has an inverse for all a. We call this $L^{-1\beta}_\gamma$; i.e.

$$L^\alpha_\beta L^{-1\beta}_\gamma = \delta^\alpha_\gamma \tag{IV.37}$$

and (IV.26) can be inverted

$$\delta a^\beta = L^{-1\beta}_\alpha \, da^\alpha. \tag{IV.38}$$

Now suppose

$$T_{c+dc} = T_a T_{b+db} = T_a T_b T_{\delta b}, \tag{IV.39}$$

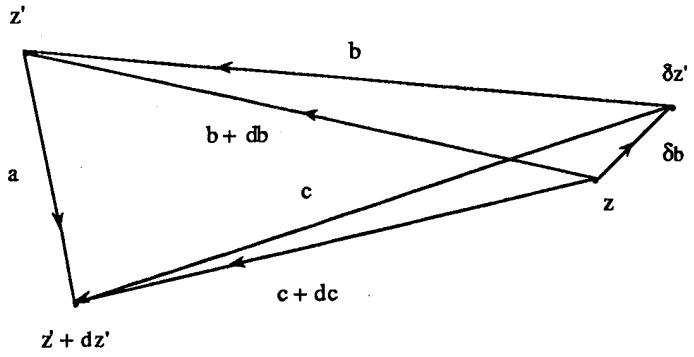

Figure 2:

which is depicted below in Figure 2.

Equation (IV.39) implies

$$c + dc = \phi(a, b + db) = \phi(a, \phi(b, \delta b))\,. \tag{IV.40}$$

If $dc = db = \delta b = 0$, then $c = \phi(a, b)$; thus (IV.40) becomes by associativity,

$$c + dc = \phi(\phi(a, b), \delta b) = \phi(c, \delta b)\,. \tag{IV.41}$$

Therefore,

$$c^\alpha + dc^\alpha = \phi^\alpha(c, \delta b) = \phi^\alpha(c, 0) + L^\alpha_\beta(c)\,\delta b^\beta + \dots\,, \tag{IV.42}$$

and

$$dc^\alpha = L^\alpha_\beta(c)\,\delta b^\beta = L^\alpha_\beta(c) L^{-1\beta}_\gamma(b)\,db^\gamma\,, \tag{IV.43}$$

where the second equality follows from (IV.38). Evidently,

$$\frac{\partial c^\alpha}{\partial b^\gamma} = L^\alpha_\beta(c) L^{-1\beta}_\gamma(b)\,, \tag{IV.44}$$

but since $c = \phi(a, b)$

$$\frac{\partial \phi^\alpha(a, b)}{\partial b^\gamma} = L^\alpha_\beta(\phi(a, b)) L^{-1\beta}_\gamma(b)\,. \tag{IV.45}$$

Equation (IV.45) is a system of partial differential equations of Mayer-Lie type. Here $\phi(a, b)$ is the unknown and a is a fixed parameter. A similar equation holds where the roles of a and b are reversed. In order for a system of equations of this type to possess a solution, they must satisfy an integrability condition, *viz*

$$\frac{\partial^2 \phi^\alpha(a, b)}{\partial b^\mu \partial b^\gamma} = \frac{\partial^2 \phi^\alpha(a, b)}{\partial b^\gamma \partial b^\mu}\,, \tag{IV.46}$$

which implies

$$\frac{\partial}{\partial b^\mu}\left[L^\alpha_\beta(\phi(a, b)) L^{-1\beta}_\gamma(b)\right] = \frac{\partial}{\partial b^\gamma}\left[L^\alpha_\beta(\phi(a, b)) L^{-1\beta}_\mu(b)\right]\,. \tag{IV.47}$$

Performing the differentiation in (IV.41)

$$\frac{\partial L^{\alpha}_{\beta}(c)}{\partial c^{\nu}}\frac{\partial \phi^{\nu}(a,b)}{\partial b^{\mu}}L^{-1\beta}_{\gamma}(b) + L^{\alpha}_{\beta}(c)\frac{\partial L^{-1\beta}_{\gamma}(b)}{\partial b^{\mu}}$$

$$= \frac{\partial L^{\alpha}_{\beta}(c)}{\partial c^{\nu}}\frac{\partial \phi^{\nu}(a,b)}{\partial b^{\gamma}}L^{-1\beta}_{\mu}(b) + L^{\alpha}_{\beta}(c)\frac{\partial L^{-1\beta}_{\mu}(b)}{\partial b^{\gamma}}, \qquad \text{(IV.48)}$$

and then using (IV.44) yields

$$\frac{\partial L^{\alpha}_{\beta}(c)}{\partial c^{\nu}}\left[L^{\nu}_{\delta}(c)L^{-1\delta}_{\mu}(b)L^{-1\beta}_{\gamma}(b) - L^{\nu}_{\delta}(c)L^{-1\delta}_{\gamma}(b)L^{-1\beta}_{\mu}(b)\right]$$

$$= L^{\alpha}_{\beta}(c)\left[\frac{\partial L^{-1\beta}_{\mu}(b)}{\partial b^{\gamma}} - \frac{\partial L^{-1\beta}_{\gamma}(b)}{\partial b^{\mu}}\right], \qquad \text{(IV.49)}$$

Now the left hand side can be made a function of c alone and the right hand side can be made a function of b alone, by multiplying by "$L(b)L(b)L^{-1}(c)$" with the appropriate indices. We obtain

$$L^{-1\gamma}_{\alpha}(c)\left[\frac{\partial L^{\alpha}_{\beta}(c)}{\partial c^{\nu}}L^{\nu}_{\delta}(c) - \frac{\partial L^{\alpha}_{\delta}(c)}{\partial c^{\nu}}L^{\nu}_{\beta}(c)\right]$$

$$= L^{\nu}_{\delta}(b)L^{\alpha}_{\beta}(b)\left[\frac{\partial L^{-1\gamma}_{\nu}(b)}{\partial b^{\alpha}} - \frac{\partial L^{-1\gamma}_{\alpha}(b)}{\partial b^{\nu}}\right], \qquad \text{(IV.50)}$$

Since the points b and c were arbitrary, the two sides of (IV.50) must equal the same constant, which is determined by setting $c = 0$. Using

$$L^{\nu}_{\delta}(0) = L^{-1\nu}_{\delta}(0) = \delta^{\nu}_{\delta} \qquad \text{(IV.51)}$$

and

$$\frac{\partial L^{\alpha}_{\beta}(0)}{\partial c^{\nu}} = \frac{\partial^2 \phi^{\alpha}(0,0)}{\partial c^{\nu}\partial b^{\beta}} \qquad \text{(IV.52)}$$

yields for the two sides

$$\frac{\partial L^{\alpha}_{\beta}(c)}{\partial c^{\nu}}L^{\nu}_{\gamma}(c) - \frac{\partial L^{\alpha}_{\gamma}(c)}{\partial c^{\nu}}L^{\nu}_{\beta}(c) = c^{\delta}_{\gamma\beta}\,L^{\alpha}_{\delta}(c)\,, \qquad \text{(IV.53)}$$

$$\frac{\partial L^{-1\delta}_{\nu}(b)}{\partial b^{\gamma}} - \frac{\partial L^{-1\delta}_{\gamma}(b)}{\partial b^{\nu}} = c^{\delta}_{\alpha\beta}\,L^{-1\alpha}_{\nu}(b)L^{-1\beta}_{\gamma}(b)\,. \qquad \text{(IV.54)}$$

Equation (IV.54) is an important equation known as the Maurer-Cartan equation. Since its left hand side is a "curl", the divergence of its right hand side must vanish. This is true provided the structure constants satisfy (IV.35). Therefore (IV.54) can be solved for $L^{-1}(b)$. With this value of L^{-1} (IV.44) is solved for ϕ.

Above we have described the connection between Lie groups and the Lie algebra of generators. It needs to be emphasized that Lie proved a remarkable theorem: given the Lie algebra of generators

$$[X_\alpha, X_\beta] = c^\gamma_{\alpha\beta} X_\gamma \tag{IV.55}$$

where the structure constants $c^\gamma_{\alpha\beta}$ satisfy (IV.34) and (IV.35), or equivalently

$$[X_\alpha, X_\beta] = -[X_\beta, X_\alpha]\,, \tag{IV.56}$$

$$\big[X_\alpha, [X_\beta, X_\gamma]\big] + [X_\beta, [X_\gamma, X_\alpha]] + [X_\gamma, [X_\alpha, X_\beta]] = 0\,, \tag{IV.57}$$

then there exists some Lie group for which the "c's" are the structure constants. Moreover, in the vicinity of the identity this group is unique. The proof of this theorem in the general case is difficult. It requires a deep understanding of the structure of Lie algebras; namely, that any Lie algebra can be decomposed into the sum of two kinds of algebras—a semi-simple algebra and a solvable algebra. It is not possible to pursue this within the confines of a single lecture like this.

References

[1] L. P. Eisenhart, *Continuous Groups of Transformations*, (Dover, New York, 1961).

[2] F. Gürsey, "Introduction to Group Theory," in *Relativity, Groups and Topology*, eds. C. DeWitt and B. DeWitt (Gordon-Breach, New York, 1963) pp. 91-161.

[3] M. Hammermesh,*Group Theory and its Applications to Physical Problems*, (Addison-Wesley, Reading, MA, 1962).

[4] C. Loewner, *Theory of Continuous Groups*, notes by H. Flanders and M. Protter, (MIT Press, Cambridge, MA, 1971).

[5] R. Salmon, "Proceedings of the 1990 Geophysical Fluid Dynamics Summer School," Woods Hole Oceanographic Institution, WHOI report (1990).

B. Reduction—Realization

Reduction is a procedure for obtaining from a given Hamiltonian system one of smaller dimension. The idea dates to Poincaré and Cartan. It is an example of generating dynamics via a canonical realization of a Lie group, which is a subgroup associated with a Lie algebra composed of the ordinary Poisson bracket and a selected collection of functions defined on phase space*. There are two parts to reduction: kinematics and dynamics. The kinematic

*See again Sudarshan (1963) and Sudarshan and Mukunda (1974), *l.c.*

part is concerned with the use of special variables that have a certain closure property, while the dynamic part refers to a symmetry of the Hamiltonian, viz. that the Hamiltonian be expressible in terms of the special variables. The symmetry gives rise to one or more constants of motion (Casimirs) that can, in principle, be used to reduce the order of the system. However, the term reduction is, in a sense, a misnomer since in practice the procedure does not reduce the order of a system, but splits the system in such a way that it can be integrated in stages.

In this section we discuss reduction in general terms for finite systems, and then consider a reduction that we term *standard reduction*, where the new variables are linear in the momenta. This is followed by two examples, the free rigid body and the ideal fluid, both of which are standard reductions. In the next section we discuss Clebsch variables, a reduction that is bilinear in canonical coordinates and momenta.

1. Reduction of Finite Dimensional Systems

In the first part of reduction, that which pertains to kinematics, the system is transformed into a useful set of (generally) noncanonical coordinates. To see how this goes, we begin with the canonical Poisson bracket

$$[f,g] = \frac{\partial f}{\partial z^i} J_c^{ij} \frac{\partial g}{\partial z^j} \qquad i,j = 1,2,\cdots,2N\,, \tag{IV.58}$$

where recall

$$(J_c^{ij}) = \begin{bmatrix} 0_N & I_N \\ -I_N & 0_N \end{bmatrix}, \tag{IV.59}$$

and

$$z = (q,p)\,, \tag{IV.60}$$

and suppose we have a set of functions $w^\alpha(z)$, with $\alpha = 1,\cdots,M$, where in general, these functions are noninvertible functions of z and $M < 2N$. Also suppose f and g obtain their z-dependence through the functions w, i.e.

$$f(z) = \bar{f}(w(z))\,. \tag{IV.61}$$

Differentiation of (IV.61) yields,

$$\frac{\partial f}{\partial z^i} = \frac{\partial \bar{f}}{\partial w^\alpha} \frac{\partial w^\alpha}{\partial z^i}\,, \tag{IV.62}$$

which upon insertion into (IV.58) gives

$$[f,g] = \frac{\partial f}{\partial w^\alpha} \frac{\partial g}{\partial w^\beta} \left(\frac{\partial w^\alpha}{\partial z^i} J_c^{ij} \frac{\partial w^\beta}{\partial z^j} \right), \tag{IV.63}$$

where we have dropped the "overbar." The quantity

$$J^{\alpha\beta} := \frac{\partial w^\alpha}{\partial z^i} J_c^{ij} \frac{\partial w^\beta}{\partial z^j} \tag{IV.64}$$

is in general a function of z. However, it is possible that $J^{\alpha\beta}$ can be written as a function of w only. When this closure condition occurs we have a reduction. Said another way, we have a Lie algebra realization composed of the functions w and the Poisson bracket.

In order for functions of w together with the bracket

$$[f,g] = \frac{\partial f}{\partial w^\alpha}\frac{\partial g}{\partial w^\beta}J^{\alpha\beta}(w)\,, \tag{IV.65}$$

to be a Lie algebra, in is necessary for [,] to satisfy the Jacobi identity for all such functions. This is equivalent to

$$S^{\alpha\beta\gamma}(w) := J^{\alpha\delta}\frac{\partial J^{\beta\gamma}}{\partial w^\delta} + J^{\gamma\delta}\frac{\partial J^{\alpha\beta}}{\partial w^\delta} + J^{\beta\delta}\frac{\partial J^{\gamma\alpha}}{\partial w^\delta} = 0\,. \tag{IV.66}$$

(Recall Lecture III.) Substituting (IV.64) into (IV.66) gives

$$S^{\alpha\beta\gamma}(w) = \frac{\partial w^\alpha}{\partial z^i}J^{ij}\frac{\partial w^\delta}{\partial z^j}\frac{\partial}{\partial w^\delta}\left(\frac{\partial w^\beta}{\partial z^k}J^{kl}\frac{\partial w^\gamma}{\partial z^l}\right) + \tag{IV.67}$$

$$= \frac{\partial w^\alpha}{\partial z^i}J^{ij}\frac{\partial}{\partial z^j}\left(\frac{\partial w^\beta}{\partial z^k}J^{kl}\frac{\partial w^\gamma}{\partial z^l}\right) + \tag{IV.68}$$

$$= [w^\alpha,[w^\beta,w^\gamma]] + [w^\beta,[w^\gamma,w^\alpha]] + [w^\gamma,[w^\alpha,w^\beta]] = 0\,, \tag{IV.69}$$

where the last equality follows from the original Jacobi identity applied to the functions w^α. Thus any reduction produces a bracket that satisfies the Jacobi identity.

Now consider briefly the second part of reduction, that which concerns the symmetry property of the Hamiltonian. In order to have a complete, reduced description of the dynamics, i.e. one entirely in terms of the w's, the original Hamiltonian $H(z)$ must be expressible solely in terms of these varibles, i.e. there must exist a function $\bar{H}(w)$ such that

$$H(z) = \bar{H}(w)\,. \tag{IV.70}$$

Equation (IV.70) is in fact a statement of symmetry. This is a condition that must be verified case by case, but it is not difficult if one knows the generators of the symmetry.

2. Standard Reduction

For standard reduction the functions w have the following special form:

$$w^\alpha = A^{\alpha i}(q)p_i\,. \tag{IV.71}$$

Writing out (IV.64)

$$J^{\alpha\beta} = \frac{\partial w^\alpha}{\partial p^i}\frac{\partial w^\beta}{\partial q^i} - \frac{\partial w^\beta}{\partial p^i}\frac{\partial w^\alpha}{\partial q^i}\,, \tag{IV.72}$$

and inserting (IV.72) into (IV.71) yields

$$J^{\alpha\beta} = A^{\alpha i}\frac{\partial A^{\beta j}}{\partial q^i}p_j - A^{\beta i}\frac{\partial A^{\alpha j}}{\partial q^i}p_j$$

$$= \left(A^{\alpha i}\frac{\partial A^{\beta j}}{\partial q^i} - A^{\beta i}\frac{\partial A^{\alpha j}}{\partial q^i}\right)p_j\,. \qquad \text{(IV.73)}$$

Closure occurs if constant numbers $c_\gamma^{\alpha\beta}$ can be found such that

$$\left(A^{\alpha i}\frac{\partial A^{\beta j}}{\partial q^i} - A^{\beta i}\frac{\partial A^{\alpha j}}{\partial q^i}\right)p_j = c_\gamma^{\alpha\beta}A^{\gamma j}p_j = c_\gamma^{\alpha\beta}w^\gamma\,. \qquad \text{(IV.74)}$$

The form of (IV.74) may ring a bell. Recall the discussion in Section A where we talked about integrability and obtained the Maurer-Cartan equation. From Eq.(IV.53) it is clear that if the A's are chosen to be the components of the infinitesimal generators of some Lie algebra, then Eq.(IV.74) holds, with the constant numbers $c_\gamma^{\alpha\beta}$ being the structure constants.

You may have noticed that above the structure constants have two covariant indices and one contravariant index, which is the opposite of that of Section A. Technically, above we have considered the dual of the algebra—the algebra of linear functionals. Evidently there is more to this story than we are telling you. For now, we emphasize that the important thing is that (IV.53) have a solution.

Since reduction involves a symmetry and symmetries are related to constants of motion, it should come as no surprise that a general expression for constants of motion, which are, of course the Casimir invariants, comes along with the reduction framework. A clean way of seeing this is afforded by *triple bracket* dynamics*.

This construction begins by considering a semisimple Lie algebra with structure constants c_{ij}^k and metric tensor† g_{ij} which is given by

$$g_{ij} = -c_{il}^k\, c_{jk}^l\,. \qquad \text{(IV.75)}$$

This quantity can be used to raise and lower indices. (Note the minus sign is introduced here to make g_{ij} positive for e.g. the rotation group.)

The fact that the structure constants have three indices hints at the existence of a geometric bracket operation on three functions, and it would be appealing if all three functions appeared on equal footing. This can be achieved by using the fully antisymmetric form of the structure constants,

$$c^{ijk} = g^{im}\,g^{jn}\,c_{mn}^k\,, \qquad \text{(IV.76)}$$

from which the following triple bracket is constructed:

$$[A,B,C] = -c^{ijk}\frac{\partial A}{\partial w^i}\frac{\partial B}{\partial w^j}\frac{\partial C}{\partial w^k}\,. \qquad \text{(IV.77)}$$

*Bialynicki-Birula and Morrison, (1991), *Ref. IV C.* Triple bracket dynamics is a generalization of a formalism due to Y. Nambu, Phys. Rev. D **7**, 2405 (1973).

†This is also called either the trace form or Killing form. See e.g. Jacobson, *l.c.*

A simple relationship exists between $[f,g,h]$ and the Lie-Poisson bracket $[f,g]$. This is made manifest by inserting the Casimir of the Lie algebra, as given by

$$C := \frac{1}{2} g_{ij} w^i w^j \,, \tag{IV.78}$$

into one of the slots of the triple bracket, i.e.

$$[f,g,h] = [f,g] \,, \tag{IV.79}$$

Due to this relationship time evolution can be represented as follows:

$$\frac{df}{dt} = [f,H,C], \tag{IV.80}$$

where f is an arbitrary dynamical variable. In this formulation the dynamics is determined by two generating functions, the Hamiltonian H and the Casimir C and because of the complete antisymmetry the Casimir is necessarily conserved.

3. Reduction of the Free Rigid Body

The free rigid body, which is a sort of prototype for reduction, is a good example because it is finite dimensional and the computations are relatively easy. A free rigid body is a rigid body that is subject to no external forces, and thus a frame of reference can be assumed in which the center of mass is fixed. It takes three numbers to specify the state of the body: if a mark is placed on (or in) the body as a reference point, then two angles specify the orientation of the line from the center-of-mass to the mark, while another angle is needed to specify the orientation relative to the line; i.e. the location of another mark (not along the line) is determined by a rotation about the line. Thus the dimension of the configuration space $\mathcal{Q}$, for the free rigid body, is three. A traditional set of coordinates is provided by the Euler angles $\chi = (\chi_1, \chi_2, \chi_3)$, which are defined by Figure 3 below.

Evidently, the rotation matrix, $R(\chi)$, that takes the primed into the unprimed axes is the product of three rotations through the three Euler angles.

By imagining infinitesimal rotations, $\delta\chi$, or by consulting a mechanics book, you can obtain the following important formulae relating the angular velocites, relative to a set of cartesian coordinates fixed in the body, to the time rate of change of the Euler angles:

$$\begin{aligned}
\omega_1 &= \dot{\chi}_1 \cos\chi_3 + \dot{\chi}_2 \sin\chi_1 \sin\chi_3 \\
\omega_2 &= -\dot{\chi}_1 \sin\chi_3 + \dot{\chi}_2 \sin\chi_1 \cos\chi_3 \\
\omega_3 &= \dot{\chi}_3 + \dot{\chi}_2 \cos\chi_2 \,.
\end{aligned} \tag{IV.81}$$

The body axes are convenient since in these axes the moment of inertia tensor is constant in time and one can choose them so that the moment of inertial tensor is diagonal, the so-called principal axes. In these coordinates the Lagrangian is deceptively simple,

$$L(\chi,\dot{\chi}) = \tfrac{1}{2}\left(I_1\omega_1^2 + I_2\omega_2^2 + I_3\omega_3^2\right) \,, \tag{IV.82}$$

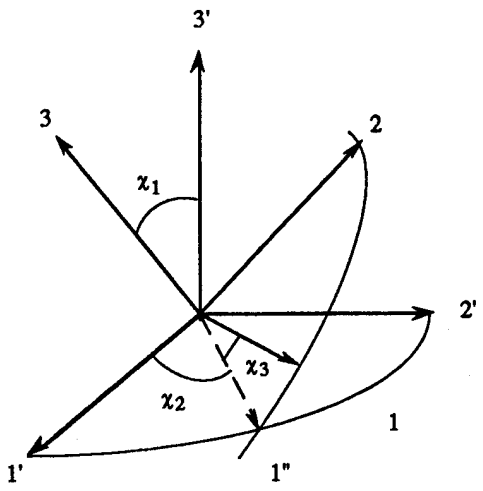

Figure 3:

it being merely the kinetic energy since there are no external forces. Note however, upon insertion of (IV.81) the Lagrangian becomes a complicated function of χ and $\dot{\chi}$. I will leave it as an exercise for you to calculate the equations of motion.

Since the Lagrangian is convex in $\dot{\chi}$ we can effect the Legendre transformation. The canonical momenta are given by

$$p_i = \frac{\partial L}{\partial \dot{\chi}_i} = \frac{\partial L}{\partial \omega_j}\frac{\partial \omega_j}{\partial \dot{\chi}_i} = \ell_j \frac{\partial \omega_j}{\partial \dot{\chi}_i}\,, \tag{IV.83}$$

i.e.

$$p_i = A^{-1}_{ij}(\chi)\,\ell_j\,, \tag{IV.84}$$

where

$$(A^{-1}) = \begin{pmatrix} \cos\chi_3 & -\sin\chi_3 & 0 \\ \sin\chi_1 \sin\chi_3 & \sin\chi_1 \cos\chi_3 & 0 \\ 0 & 0 & 1 \end{pmatrix}, \tag{IV.85}$$

and the angular momentum $\ell_i := I_i\omega_i$ (not summed). Comparing (IV.81) with (IV.84) reveals that

$$\omega_i = D_{ij}\dot{\chi}_j\,, \tag{IV.86}$$

where $D^T = A^{-1}$ with "T" indicating transpose. If Ω is defined to be the antisymmetric matrix composed of the three components of ω, then an important way to write (IV.85) is as follows:

$$\Omega = R^T\dot{R}\,. \tag{IV.87}$$

This form is analogous to that of the map from Lagrange to Euler variables. I will leave it for you to work this out.

The inverse of (IV.84) is given by

$$\ell_j = A_{ji}(\chi)\,p_i\,, \tag{IV.88}$$

where

$$(A) = \frac{1}{\sin\chi_1}\begin{pmatrix} \sin\chi_1\cos\chi_3 & \sin\chi_3 & -\sin\chi_3\cos\chi_1 \\ -\sin\chi_1\sin\chi_3 & \cos\chi_3 & -\cos\chi_3\cos\chi_1 \\ 0 & 0 & \sin\chi_1 \end{pmatrix} . \tag{IV.89}$$

This is the standard reduction formula of the form of (IV.71).

Upon effecting the Legendre transform, the Hamiltonian is obtained:

$$H(p,\chi) = p_i\dot{\chi}_i - L = \tfrac{1}{2}\ell_k\omega_k = \tfrac{1}{2}\sum_k \frac{\ell_k^2}{I_k} = \tfrac{1}{2}\sum_k \frac{1}{I_k} A_{ki}A_{kj}\, p_i p_j \,, \tag{IV.90}$$

which obviously possesses the necessary symmetry of (IV.70).

It remains to show whether or not the variables ℓ_i allow a reduction. To see if this is the case consider $[\ell_i, \ell_j]$, which upon insertion of (IV.88) becomes

$$[\ell_i,\ell_j] = A^{-1}_{rs}\ell_s\left(\frac{\partial A_{ir}}{\partial\chi_k}A_{jk} - \frac{\partial A_{jr}}{\partial\chi_k}A_{ik}\right) , \tag{IV.91}$$

as expected from the results of the previous subsection. Since the left hand side of (IV.91) is difficult to evaluate, we make use of

$$\frac{\partial A_{ir}}{\partial\chi_k}A^{-1}_{rs} = -A_{ir}\frac{\partial A^{-1}_{rs}}{\partial\chi_k} , \tag{IV.92}$$

which follows upon differentiating

$$A_{ir}A^{-1}_{rs} = \delta_{is} \,, \tag{IV.93}$$

to obtain

$$[\ell_i,\ell_j] = \left(\ell_s\frac{\partial A^{-1}_{rs}}{\partial\chi_k}\right)(A_{jr}A_{ik} - A_{ir}A_{jk}) \,. \tag{IV.94}$$

The matrix in the first parentheses is not too difficult to calculate. The evaluation of the second parenthesis amounts to the determination of three matrices; since $[\ell_i, \ell_j]$ is antisymmetric only $[\ell_1, \ell_2]$, $[\ell_1, \ell_3]$, and $[\ell_2, \ell_3]$ must be obtained. Multiplying out the matrices of the two parentheses (three times) yields the following compact and expected result:

$$[\ell_i,\ell_j] = -\epsilon_{ijk}\,\ell_k \,. \tag{IV.95}$$

4. Reduction for the Ideal Fluid: Lagrangian → Eulerian Variables

Now consider reduction for the ideal fluid, which amounts to the transformation from Lagrangian to Eulerian variables. In the Lagrangian variable description of Lecture II we had the Hamiltonian

$$H[\pi,q] = \int_D \left[\frac{\pi^2}{2\rho_0} + \rho_0 U(s_0, \rho_0/\mathcal{J})\right] d^3a \tag{IV.96}$$

which together with the canonical Poisson bracket,

$$[F,G] = \int_D \left[\frac{\delta F}{\delta q}\cdot\frac{\delta G}{\delta\pi} - \frac{\delta G}{\delta q}\cdot\frac{\delta F}{\delta\pi}\right] d^3a \,. \tag{IV.97}$$

produces the ideal fluid equations of motion. For the moment, let us forget about the Hamiltonian structure and just consider the change from (q, π), the Lagrangian canonically conjugate pair, to (ρ, σ, M), the Eulerian non-canonical variables. Recall from Lecture II that

$$\rho(r,t) = \int_D \rho_0(a)\, \delta(r - q(a,t))\, d^3a\,,$$

$$\sigma(r,t) = \int_D \sigma_0(a)\, \delta(r - q(a,t))\, d^3a\,,$$

$$M(r,t) = \int_D \pi\, \delta(r - q(a,t))\, d^3a\,. \tag{IV.98}$$

Clearly, from the above three relations, we can calculate (ρ, σ, M) for a given displacement field q and a given momentum field π. The chain rule thus goes the way we need it to calculate variations of

$$F[q,\pi] = \bar{F}[\rho, \sigma, M]\,. \tag{IV.99}$$

In (IV.99) we are supposing that F obtains its q and π dependence through some functional $\bar{F}$ of (ρ, σ, M). The functionals F and $\bar{F}$ are defined on different functions, which are themselves defined on different (space-like) domains, a and x, respectively.

Consider the variation of F,

$$\delta F = \int_D \left[\frac{\delta F}{\delta q}\cdot\delta q + \frac{\delta F}{\delta \pi}\cdot\delta\pi\right]\, d^3a$$

$$= \int_D \left[\frac{\delta \bar{F}}{\delta \rho}\delta\rho + \frac{\delta \bar{F}}{\delta \sigma}\delta\sigma + \frac{\delta \bar{F}}{\delta M}\cdot\delta M\right]\, d^3r\,. \tag{IV.100}$$

Note that the two domains of integration coincide, although the variables of integration have different names. We will now try to find the functional derivatives with respect to the Lagrangian fields in terms of the Eulerian fields. This will allow us to express the bracket in Eulerian fields. The variations of the Eulerian fields induced by a variation of the Lagrangian fields are

$$\delta\rho = -\int_D \rho_0(a)\, \nabla\delta(r-q)\cdot\delta q\; d^3a\,,$$

$$\delta\sigma = -\int_D \sigma_0(a)\, \nabla\delta(r-q)\cdot\delta q\; d^3a\,,$$

$$\delta M = \int_D \left[\delta\pi\, \delta(r-q) - \pi\nabla\delta(r-q)\cdot\delta q\right]\; d^3a\,. \tag{IV.101}$$

Above (and below) the ∇-operator operates on the r-dependence. Inserting (IV.101) into (IV.100), interchanging the order of integration, and equating the coefficients of δq and $\delta\pi$ implies

$$\frac{\delta F}{\delta q} = -\int_D \left[\rho_0\frac{\delta \bar{F}}{\delta \rho} + \sigma_0\frac{\delta \bar{F}}{\delta \sigma} + \pi\cdot\frac{\delta \bar{F}}{\delta M}\right]\, \nabla\delta(r-q)\; d^3r$$

$$= \int_D \left[\rho_0 \nabla \frac{\delta \bar{F}}{\delta \rho} + \sigma_0 \nabla \frac{\delta \bar{F}}{\delta \sigma} + \pi_i \nabla \frac{\delta \bar{F}}{\delta M_i} \right] \delta(r-q)\, d^3r \qquad \text{(IV.102)}$$

$$\frac{\delta F}{\delta \pi} = \int_D \frac{\delta \bar{F}}{\delta M} \delta(r-q)\, d^3r = \left. \frac{\delta \bar{F}}{\delta M} \right|_{r=q} d^3r =: \frac{\delta \bar{F}}{\delta M'}, \qquad \text{(IV.103)}$$

where the second formula is obtained after integration by parts, assuming the boundary terms vanish. Inserting (IV.102) and (IV.103), for both F and G, into (IV.98), yields

$$\{\bar{F}, \bar{G}\} = \int_D \delta(r-q) \left\{ \rho_0 \nabla \frac{\delta \bar{F}}{\delta \rho} \cdot \frac{\delta \bar{G}}{\delta M'} + \sigma_0 \nabla \frac{\delta \bar{F}}{\delta \sigma} \cdot \frac{\delta \bar{G}}{\delta M'} + \frac{\delta \bar{G}}{\delta M'_j} \pi_i \frac{\partial}{\partial x_j} \frac{\delta \bar{F}}{\delta M_i} \right.$$

$$\left. - \rho_0 \nabla \frac{\delta \bar{G}}{\delta \rho} \cdot \frac{\delta \bar{F}}{\delta M'} - \sigma_0 \nabla \frac{\delta \bar{G}}{\delta \sigma} \cdot \frac{\delta \bar{F}}{\delta M'} - \frac{\delta \bar{F}}{\delta M_j} \pi_i \frac{\partial}{\partial_j} \frac{\delta \bar{G}}{\delta M_i} \right\} d^3a\,. \qquad \text{(IV.104)}$$

After interchanging the order of integration, the integral over d^3a can be carried out,

$$\{F, G\} = -\int_D \left[M_i \left(\frac{\delta F}{\delta M_j} \frac{\partial}{\partial x_j} \frac{\delta G}{\delta M_i} - \frac{\delta G}{\delta M_j} \frac{\partial}{\partial x_j} \frac{\delta F}{\delta M_i} \right) + \rho \left(\frac{\delta F}{\delta M} \cdot \nabla \frac{\delta G}{\delta \rho} - \frac{\delta G}{\delta M} \cdot \nabla \frac{\delta F}{\delta \rho} \right) \right.$$

$$\left. + \sigma \left(\frac{\delta F}{\delta M} \cdot \nabla \frac{\delta G}{\delta \sigma} - \frac{\delta G}{\delta M} \cdot \nabla \frac{\delta F}{\delta \sigma} \right) \right] d^3r\,. \qquad \text{(IV.105)}$$

Equation(IV.105) is the noncanonical bracket that was given in Lecture III. It is a bracket expression in terms of Eulerian functionals, that is ones that depend on Eulerian fields, integrated over the Eulerian spatial domain.

Above we have considered the transformation of variables only. This can be viewed as kinematics. To complete the Hamiltonian description in terms of Eulerian variables we must obtain the Hamiltonian in terms of ρ, σ, and M. The reduction we have performed can only yield dynamics if we can find a Hamiltonian, $\bar{H}$ that satisfies

$$H[q, \pi] = \bar{H}[\rho, \sigma, M]\,, \qquad \text{(IV.106)}$$

upon substitution of Eqs. (IV.98). In general this is not possible, but for the ideal fluid the one that does the trick is of course

$$\bar{H}[\rho, \sigma M] = \int_D \left[\tfrac{1}{2} \frac{M^2}{\rho} + \rho U(\rho, \frac{\sigma}{\rho}) \right] d^3r\,. \qquad \text{(IV.107)}$$

Note that while the reduction of the bracket only depends upon the definitions of ρ, σ, and M, the corresponding reduction of the Hamiltonian involves a symmetry, namely the independence of the Hamiltonian under fluid particle relabelling.

References

[1] E. Sudarshan, "Principles of Classical Dynamics," Report NYO 10250, University of Rochester, Department of Physics and Astronomy (1963).

[2] E. Sudarshan and N. Mukunda, *Classical Dynamics: a Modern Perspective* (John Wiley, New York, 1974).

[3] P. J. Morrison,"Hamiltonian field description of two-dimensional vortex fluids an guiding center plasmas," Princeton University Plasma Physics Laboratory Report, PPPL-1783 (1981). Available as American Institute of Physics Document No. PAPS-PFBPE-04-771, AIP Auxiliary Publication Service, 335 East 45th Street, New York, NY 10017.

[4] J. E. Marsden, A. Weinstein, T. Ratiu, R. Schmid, and R. Spencer, Proc. IUTAM-ISIMM Symposium on Modern Developments in Analytical Mechanics, Actti della Acad. della Sc. di Torino **117**, 289 (1983).

[5] J. E. Marsden and A. Weinstein, Rep. Math. Phys. **5**, 121-130 (1974).

[6] V. I. Arnold, V. V. Kozlov, and A. I. Neishtadt, *Dynamics III: Mathematical Aspects of Classical and Celestial Mechanics* (Springer-Verlag, Berlin, 1980).

C. Clebsch Variables

In this section we consider *Clebsch variables.* These are canonical variables that reduce to noncanonical variables where, as mentioned above, the noncanonical variables are bilinear in the momenta and configuration space coordinates. We will use the term Clebsch to describe all such bilinear transformations for which there is a reduction, however, particular forms are of special interest. Below we consider finite systems, infinite systems, the semidirect product, and several examples of each, notably the Clebsch representation for the ideal fluid, whence the name Clebsch orignates*.

1. Clebsch Variables for Finite Systems

It is well known that the three components of the angular momentum, $q \times p$, form a canonical realization; if one restricts phase space functions to be functions of only these three variables, then the canonical Poisson bracket of two such functions produces another such function. This is just the closure condition discussed in the previous section. The resulting noncanoical Poisson bracket in this case, like that for the free rigid body, is that corresponding to $SO(3)$.

We will present the Clebsch reduction from an historical, if not logical, point of view. Suppose we have a noncanonical Lie-Poisson bracket of the following form:

$$[f,g] = -w^k c_k^{ij} \frac{\partial f}{\partial w^i} \frac{\partial f}{\partial w^j}, \qquad \text{(IV.108)}$$

*A. Clebsch, J. Reine Angew. Math. **54**, 293 (1857); *ibid.* **56**, 1 (1859).

where c_k^{ij} are the structure constants for an arbitrary Lie algebra. We know from the previous section that a canonical Poisson bracket, with a transformation of the form of (IV.71), reduces to this form. Now we turn things around and ask the question, can we inflate (IV.108) and obtain other canonical descriptions. Here we have used the word inflation, since we are not talking about the canonical description on the symplectic leaves of Lecture III, which would be a further "reduction." This inflation is in essence what Clebsch did for the ideal fluid: he found a set of variables that uniquely determines the usual physical fluid variables, but the inverse of his transformation does not exist. For this reason we say there are "gauge" conditions analogous to those for the vector potential in electromagnetism.

The following transformation, which is motivated by the angular momentum reduction described above, is a finite dimensional generalization of Clebsch's transformation:

$$w^i = c_k^{ij} q^k p_j \,, \tag{IV.109}$$

where all indices are summed on $1, 2, \ldots, N$. The quantities w^i could be thought of as components of a generalized angular momentum. Given a canonical description in terms of the q_i and p_i,

$$\{f, g\} = \frac{\partial f}{\partial q^i}\frac{\partial g}{\partial p_i} - \frac{\partial f}{\partial p_i}\frac{\partial g}{\partial q^i} \,, \tag{IV.110}$$

the bracket in terms of w is obtained by a reduction. This is seen upon substituting

$$\begin{aligned} \frac{\partial f}{\partial p_i} &= \frac{\partial f}{\partial w^j} c_k^{ji} q^k \\ \frac{\partial f}{\partial q^i} &= \frac{\partial f}{\partial w^j} c_i^{jk} p_k \,, \end{aligned} \tag{IV.111}$$

into (IV.110)

$$\begin{aligned} \frac{\partial f}{\partial q^i}\frac{\partial g}{\partial p_i} - \frac{\partial f}{\partial p_i}\frac{\partial g}{\partial q^i} &= p_t q^r \left(c_k^{it} c_r^{jk} - c_k^{jt} c_r^{ik} \right) \frac{\partial f}{\partial w^i}\frac{\partial g}{\partial w^j} \\ &= -w^k c_k^{ij} \frac{\partial f}{\partial w^i}\frac{\partial g}{\partial w^j} \,, \end{aligned} \tag{IV.112}$$

where the last equality follows upon making use of the Jacobi identity for the structure constants, (IV.35).

Given any noncanonical system in terms of the w's one can obtain a canonical system of equations in terms of the Clebsch q and p; when these are solved for $q(t)$ and $p(t)$ then the w constructed according to (IV.109) is a solution of the noncanonical system.

2. Clebsch Variables for Infinite Systems

Here we will be a bit formal and define things in somewhat general terms. First we will denote by $\langle \, , \, \rangle$ a pairing between a vector space and its dual. We will, for now, leave the particular form of this unspecified, but we have in the back of our mind an integration like

that in (III.36). The first slot of $\langle\ ,\ \rangle$ can be thought of as an infinite dimensional analogue of the finite dimensional "up" indices, while the second slot is the analogue of the "down" indices. We will refer to elements of the first slot as belonging to $\mathfrak{g}$ and those of the second slot, the dual, as belonging to $\mathfrak{g}^*$. In general the pairing is not symmetric.

In terms of the pairing, noncanonical Lie-Poisson brackets have the following compact form:

$$\{F, G\} = -\langle \chi, [F_\chi, G_\chi] \rangle \ , \tag{IV.113}$$

where $[\ ,\ ]$ is a Lie algebra product, which takes $\mathfrak{g}^* \times \mathfrak{g}^* \to \mathfrak{g}^*$, and we have introduced the shorthand

$$F_\chi := \frac{\delta F}{\delta \chi}, \qquad G_\chi := \frac{\delta G}{\delta \chi}, \tag{IV.114}$$

which are, of course, in $\mathfrak{g}^*$. We refer to $\{\ ,\ \}$ as the "outer" bracket and $[\ ,\ ]$ as the "inner" bracket.

Now we define the binary operator $[\ ,\ ]^\dagger$ as follows:

$$\langle \chi, [f, g] \rangle =: \left\langle [\chi, g]^\dagger, f \right\rangle \ , \tag{IV.115}$$

where evidently $\chi \in \mathfrak{g}$, $g, f \in \mathfrak{g}^*$, and $[\ ,\ ]^\dagger : \mathfrak{g} \times \mathfrak{g}^* \to \mathfrak{g}$. The operator $[\ ,\ ]^\dagger$ is necessary for obtaining the equations of motion from a Lie-Poisson bracket. The bilinear Clebsch transformation analogous to (IV.109) is given by

$$\chi = [Q, \Pi]^\dagger . \tag{IV.116}$$

In order to effect the reduction, consider a variation of (IV.116),

$$\delta\chi = [\delta Q, \Pi]^\dagger + [Q, \delta\Pi]^\dagger , \tag{IV.117}$$

which is used to relate functional derivatives as follows:

$$\begin{aligned} \delta F &= \langle \delta\chi, F_\chi \rangle \\ &= \left\langle [\delta Q, \Pi]^\dagger + [Q, \delta\Pi]^\dagger, F_\chi \right\rangle \\ &= \langle \delta Q, F_Q \rangle + \langle F_\Pi, \delta\Pi \rangle \ . \end{aligned} \tag{IV.118}$$

Manipulation of the second equality of (IV.118) yields

$$\begin{aligned} \delta F &= \langle \delta Q, [F_\chi, \Pi] \rangle + \langle Q, [F_\chi, \delta\Pi] \rangle \\ &= \langle \delta Q, [F_\chi, \Pi] \rangle - \langle Q, [\delta\Pi, F_\chi] \rangle \\ &= \langle \delta Q, [F_\chi, \Pi] \rangle - \left\langle [Q, F_\chi]^\dagger, \delta\Pi \right\rangle , \end{aligned} \tag{IV.119}$$

where the antisymmetry of $[\ ,\ ]$ and the definition of $[\ ,\ ]^\dagger$ have been used. Upon comparing the last equality of (IV.119) with the last equality of (IV.118) we obtain

$$F_Q = [F_\chi, \Pi] , \qquad F_\Pi = -[Q, F_\chi]^\dagger . \tag{IV.120}$$

The canonical bracket in terms of Q and Π can be written as

$$\{F,G\} = \langle G_\Pi, F_Q\rangle - \langle F_\Pi, G_Q\rangle \ . \tag{IV.121}$$

Inserting (IV.120), produces

$$\begin{aligned}\{F,G\} &= -\left\langle [Q,G_\chi]^\dagger, [F_\chi,\Pi]\right\rangle + \left\langle [Q,F_\chi]^\dagger, [G_\chi,\Pi]\right\rangle \\ &= \left\langle Q, \left[[G_\chi\Pi], F_\chi\right] + \left[[\Pi,F_\chi], G_\chi\right]\right\rangle \\ &= \left\langle Q, \left[[G_\chi,F_\chi],\Pi\right]\right\rangle = -\left\langle [Q,\Pi]^\dagger, [F_\chi,G_\chi]\right\rangle \\ &= -\langle \chi, [F_\chi,G_\chi]\rangle \ ,\end{aligned} \tag{IV.122}$$

where use has been made of the Jacobi identity of $[\ ,\ ]$.

3. Fluid Examples

Now consider two examples from fluid mechanics: the first is the two-dimensional Euler equation, while the second is related to the three-dimensional ideal fluid.

As observed above the structure constants for the free rigid body noncanonical bracket are ϵ_{ijk}, which is completely antisymmetric. The structure operator for the 2-D Euler noncanonical bracket, which was given in Lecture III, shares this property. This is clear from the "fgh" identity of (III.78), from which we also observe that

$$[f,g]^\dagger = -[f,g] \, . \tag{IV.123}$$

Here no distinction is made between the vector space and its dual. For this case

$$[f,g] = \frac{\partial f}{\partial x}\frac{\partial g}{\partial y} - \frac{\partial f}{\partial y}\frac{\partial g}{\partial x} \, , \tag{IV.124}$$

and

$$\langle\ ,\ \rangle = \int_D \ d^2r \, . \tag{IV.125}$$

The Clebsch variables $Q(r,t)$ and $\Pi(r,t)$ are related to the scalar vorticity via

$$\omega(r,t) = [\Pi, Q] \, , \tag{IV.126}$$

and the reduction from these canonical variables to the 2-D Euler bracket parallels exactly the calculation of the previous subsection*. There are two ways to obtain the equations of motion for $Q(r,t)$ and $\Pi(r,t)$. One way is to insert (IV.126) into the Hamiltonian $H[\omega]$ of (III.74) and then calculate

$$\frac{\partial Q}{\partial t} = \frac{\delta H}{\delta \Pi} \, , \qquad \frac{\partial \Pi}{\partial t} = -\frac{\delta H}{\delta Q} \, . \tag{IV.127}$$

*The careful reader will notice a sign discrepency. There is a story that goes with this sign, but unfortunately we are not able to tell it here.

The other way is to insert (IV.126) directly into the equation of motion for ω, viz.

$$\frac{\partial \omega}{\partial t} = -[\psi, \omega]\,, \tag{IV.128}$$

[cf. (III.72)] and then manipulate as follows:

$$\begin{aligned}\frac{\partial \omega}{\partial t} &= \left[\frac{\partial \Pi}{\partial t}, Q\right] + \left[\Pi, \frac{\partial Q}{\partial t}\right] \\ &= -\Big[\psi, [\Pi, Q]\Big] = \Big[\Pi, [Q, \psi] + [Q, [\psi, \Pi]\Big]\,,\end{aligned} \tag{IV.129}$$

where the Jacobi identity was used to obtain the last equality. From (IV.129) we obtain

$$\left[\frac{\partial \Pi}{\partial t} + [\psi, \Pi], Q\right] + \left[\Pi, \frac{\partial Q}{\partial t} + [\psi, Q]\right] = 0\,, \tag{IV.130}$$

which is satisfied if

$$\begin{aligned}\frac{\partial \Pi}{\partial t} &= -[\psi, \Pi] + \frac{\partial \Upsilon}{\partial \Pi} \\ \frac{\partial Q}{\partial t} &= -[\psi, Q] - \frac{\partial \Upsilon}{\partial Q}\,,\end{aligned} \tag{IV.131}$$

where the terms involving Υ point to the gauge ambiguity present in (IV.126), something that will not be discussed further here. If $Q(r,t)$ and $\Pi(r,t)$ are solutions of (IV.131), then the $\omega = [\Pi, Q]$ constructed from these solutions are solutions of (IV.128).

Turn now to the following bracket, which is a portion of the noncanonical bracket for the ideal fluid, [cf. (III.89)]:

$$\begin{aligned}\{F, G\} &= -\int_D M_i \left(\frac{\delta F}{\delta M_j}\frac{\partial}{\partial x_j}\frac{\delta G}{\delta M_i} - \frac{\delta G}{\delta M_j}\frac{\partial}{\partial x_j}\frac{\delta F}{\delta M_i}\right) d^3 r \\ &=: -\langle M, [F_M, G_M]\rangle\ .\end{aligned} \tag{IV.132}$$

It is obvious that this bracket will satisfy the Jacobi identity if (III.89) does. The inner bracket in this case is given by

$$[f, g]_i = f_j \frac{\partial g_i}{\partial x_j} - g_j \frac{\partial f_i}{\partial x_j}\,, \tag{IV.133}$$

where, evidently, f and g now have three components. Integration by parts and neglect of surface terms yields

$$[\chi, g]^\dagger_j = \chi_i \frac{\partial g_i}{\partial x_j} + \frac{\partial (\chi_j g_i)}{\partial x_i}\,, \tag{IV.134}$$

whence the Clebsch variables are seen to be related to M by

$$M_j = Q_i \frac{\partial \Pi_i}{\partial x_j} + \frac{\partial (Q_j \Pi_i)}{\partial x_i} . \tag{IV.135}$$

In reality the decomposition above is not quite that due to Clebsch, whose transformation did not have the second term of (IV.135). However, it is closely related to that introduced for MHD*. In fact the reduction occurs without this last term; it also occurs with the last term with opposite sign. Also, it is not important that Q and Π have three components. Some of this will be discussed below in the last subsection of this lecture.

4. Semidirect Product Reductions

The semidirect product is an example of an extension, a group theoretic notion for making bigger groups out of a given group. We cannot discuss this is any kind of detail here so the interested reader is referred to the references*. However, this notion makes its way up to Lie algebras and thus to Lie-Poisson brackets, a case of which we will discuss (briefly) here.

Suppose the functional F in (IV.118), in addition to its χ dependence, depends upon Q, i.e., $\bar{F}[\chi, Q] = F[Q, \Pi]$. (We have included the overbar now, as in Lecture II, to avoid confusion.) Effecting the chain rule with this additional dependence yields

$$F_Q = [\bar{F}_\chi, \Pi] + \bar{F}_Q \, , \tag{IV.136}$$

which upon substitution into (IV.121) produces instead of (IV.122), the following:

$$\begin{aligned} \{\bar{F}, \bar{G}\} &= -\left\langle \chi, [\bar{F}_\chi, \bar{G}_\chi] \right\rangle - \left\langle [Q, \bar{G}_\chi]^\dagger, \bar{F}_Q \right\rangle + \left\langle [Q, \bar{F}_\chi]^\dagger, \bar{G}_Q \right\rangle \\ &= -\left\langle \chi, [\bar{F}_\chi, \bar{G}_\chi] \right\rangle + \left\langle Q, [\bar{G}_\chi, \bar{F}_Q] - [\bar{F}_\chi, \bar{G}_Q] \right\rangle \, , \end{aligned} \tag{IV.137}$$

where the second equality follows from manipulations simliar to those performed above.

Many systems possess brackets of this (and similar) form(s). The rigid body in a gravitational field is an example of finite dimension. An example of infinite dimension, which was first given in the context of reduced MHD†, but also occurs in fluid mechanics, is the semidirect product extension of the noncanonical bracket for the 2-D Euler fluid. For this example one simply interprets (IV.137) using (IV.124) and (IV.125).

5. Other Clebsch Reductions: That for the Ideal Fluid

In this final subsection we present some other forms of Clebsch reductions. The first is another way to reduce to the reduced MHD bracket of above. This emphasizes the fact that reductions are not unique. Following this we show another way to reduce to the portion

*P. J. Morrison and J. M. Greene, Phys. Rev. Lett. **48**, 569 (1982) and Morrison (1982), *Ref. IV C.*

*See e.g. Sudarshan and Mukunda (1974), *Ref. IV C*, J. E. Marsden and P. J. Morrison, Contemp. Math. **28**, 133 (1984).

†Morrison and Hazeltine (1984), *Ref. IV C.*

of the ideal fluid bracket, also treated above. Finally we reduce to the complete ideal fluid noncanonical bracket. This final transformation is the one actually due to Clebsch.

Suppose we have a system with canonical variables $(Q_i(r,t), \Pi_i(r,t))$, where $i = 1, 2$ and $r = (x, y)$. The canonical Poisson bracket is then

$$\{F, G\} = \int_D (F_Q \cdot G_\Pi - G_Q \cdot F_\Pi)\, d^2r\,. \tag{IV.138}$$

The following transformation is a reduction:

$$\chi = [Q_1, \Pi_1] + [Q_2, \Pi_2]$$

$$\psi = [Q_1, Q_2]\,, \tag{IV.139}$$

where $[\,,\,]$ is given by (IV.124). We leave it as an exercise to show via the chain rule that with (IV.139), (IV.138) reduces to a bracket of the form of (IV.137).

Now consider the portion of the fluid bracket discussed above in (IV.132), but now instead of (IV.135) we let

$$M = Q_i \nabla \Pi_i\,. \tag{IV.140}$$

where $i = 1, 2, ...N$ and N is arbitrary. We also leave it as an exercise to show via the chain rule that with (IV.140), a canonical bracket in terms of $(Q_i(r,t), \Pi_i(r,t))$, where now $r = (x, y, z)$, reduces to a bracket of the form of (IV.132).

Finally, suppose in addition to (IV-14-3) that

$$\rho = Q_1\,, \qquad\qquad \sigma = Q_2\,. \tag{IV.141}$$

We leave it as a *last* exercise to show via the chain rule that with (IV.140) and (IV.141), a canonical bracket in terms of $(Q_i(r,t), \Pi_i(r,t))$, reduces to the ideal 3-D fluid bracket of (III.89). One can chose N large enough to describe the velocity field of interest.

References

[1] H. Lamb, *Hydrodynamics* (Dover, New York, 1945) art. 167.

[2] P. J. Morrison,"Hamiltonian Field Description of Two-dimensional Vortex Fluids and Guiding Center Plasmas," Princeton University Plasma Physics Laboratory Report, PPPL-1783 (1981). Available as American Institute of Physics Document No. PAPS-PFBPE-04-771, AIP Auxiliary Pub. Service, 335 East 45th St., New York, NY 10017.

[3] P. J. Morrison, in *Mathematical Methods in Hydrodynamics and Integrability in Related Dynamical Systems*, eds. M. Tabor and Y. Treve, AIP Conference Proceedings **88**, La Jolla, 1982, p. 13.

[4] D. D. Holm and B. Kupershmidt, Physica D **6**, 347 (1983).

[5] P. J. Morrison and R. D. Hazeltine, Physics of Fluids, **27**, 886 (1984).

[6] I. Bialynicki-Birula and P. J. Morrison, Phys. Lett. A **158**, 453 (1991).

[7] E. Sudarshan and N. Mukunda, *Classical Dynamics: a Modern Perspective* (John Wiley, New York, 1974).

V. Stability and Hamiltonian Systems

This Lecture concerns notions of stability in Hamiltonian systems. In Section A canonical systems are considered. Here, basic definitions are reviewed, energy arguments for stability are discussed, and the notion of a *negative energy mode* (NEM) is introduced. An example that illustrates properties of NEM's is given, in which context simple Hamiltonian bifurcation theory is reviewed. Finally in this section, these ideas are applied to the ideal fluid in the Lagrangian variable description. Section B is concerned with stability in noncanonical Hamiltonian systems. The energy-Casimir method is described and two examples are given: a charged rigid body in an external magnetic field and the 2-D Euler equation. The examples exhibit a pathology related to the rank changing behavior of the cosymplectic form, that is discussed. In Section C the notion of *dynamical accessibility*, which can be used to make statements about stability, in spite of the rank changing behavior, is introduced. Finally, it is shown how Eulerian variations, constrained by the condition of dynamical accessibility, lead to the same expression for the potential energy, $\delta^2 W$, as Lagrangian variations.

A. Stability and Canonical Hamiltonian Systems

Consider a dynamical system of the form

$$\dot{z}^i = V^i(z), \qquad i = 1, 2, \ldots, M, \tag{V.1}$$

where, as in Lecture III, we will not get into what is required of $V(z)$ for existence and uniqueness of solutions, but just assume everything is alright. An *equilibrium point*, z_e, is a type of solution of (V.1) that satisfies $V(z_e) = 0$. Stability concerns the behavior of solutions near such equilibrium points. Roughly speaking, z_e is *stable* if solutions starting "close" to z_e at $t = 0$ remain close to z_e for all later times. This idea is formalized by the following:

> *The equilibrium point z_e is said to be stable if, for any neighborhood N of z_e there exists a subneighborhood $S \subset N$ of z_e such that if $z(t = 0) \in S$ then $z(t) \in N$ for all time $t > 0$.*

At first one might wonder why such a fancy definition is needed. Why introduce the subneighborhood? Why don't we just say, if it starts in a set and stays in the set, then it is stable? The answer to this is illustrated in Figure 1, which is the phase portrait for the simple harmonic oscillator. In this figure the circles are surfaces of constant energy. Here we have chosen as a neighborhood N the rectangular region in which we have marked an initial condition by the symbol "$\times$". Since trajectories move round and round on the circles of constant H, it is clear that in a short time the trajectory starting at $\times$ will leave N, in spite of the fact that the equilibrium point at the origin is stable. However, if we choose initial conditions inside the subneighborhood S, which is defined as the region bounded by an H = constant surface contained in N, then the trajectory will remain in N for all time. Thus, H = constant surfaces serve as a handy means of defining subneighborhoods.

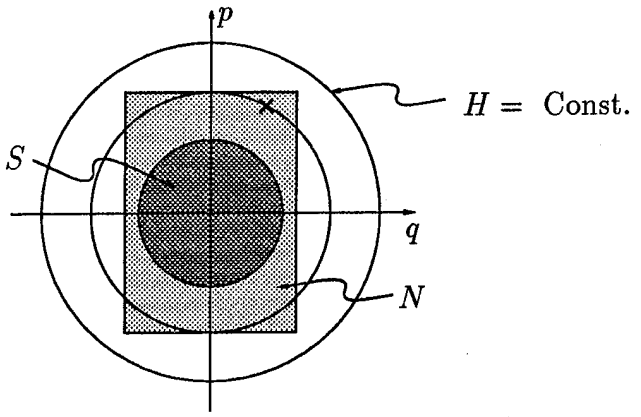

Figure 1:

Observe that the neighborhood N can be chosen to be *any* neighborhood N of z_e. We can make them smaller and smaller, and in this way, probe the stability property of the point z_e. In the example above we can always find tiny circular energy surfaces inside any N, no matter how small.

When $z(t)$ is determined from the linearized dynamics,

$$\delta \dot{z}^i = \frac{\partial V^i}{\partial z^j}(z_e)\, \delta z^j\,, \tag{V.2}$$

where now $z(t) := z_e + \delta z$, and this dynamics is stable according to the above definition, we say that (V.2) or z_e is *linearly stable.*

One might think, since N can be made as small as we like, that these types of stability are equivalent, but this is not the case, as we shall see below. To distinguish, we sometimes call stability under the full nonlinear dynamics, $V(z)$, *nonlinear stability.* Equilibria that are unstable under nonlinear dynamics, yet stable under linear dynamics are said to be *nonlinearly unstable.* This is different from *finite amplitude instability,* where the equilibrium point is nonlinearly stable until it is pushed hard enough. In a sense (almost) all physical systems are finite amplitude unstable; for example, any laboratory experiment is unstable to a perturbation caused by a large enough earthquake.

One last definition is that of *spectral stability.* A linear system such as (V.2) has this type of stability if upon substituting $\delta z = \delta \hat{z}\ e^{i\omega t}$, and solving the resulting linear algebra problem for $\omega := \omega_R + i\gamma$, there exist no solutions with $\gamma < 0$. Clearly, linear stability implies spectral stability, but beware, the converse is not true.

A nice thing about Hamiltonian systems is that they have a built in method for proving nonlinear stability. In the case where the Hamiltonian has a *separable* form, $H = p^2/2 + V(q)$, an old theorem due to Lagrange states that an equilibrium point with $p_e = 0$ and q_e being a local minimum of V is stable. It is tempting to think that the converse should be true, but

a counterexample from the book of A. Wintner* shows this not to be the case. Consider

$$V(q) = \begin{cases} e^{-1/q^2}\cos(1/q) & q \neq 0 \\ 0 & q = 0\,. \end{cases} \tag{V.3}$$

The equilibrium position $q_e = 0$ is stable, but due to the wild oscillation that occurs as $q \to 0$, the origin is not a local minimum. However, with some relatively mild restrictions on V, *Lagrange's theorem* is both necessary and sufficient for Hamiltonians of this restricted form. Sufficiency follows since surfaces of constant H serve to define subneighborhoods, as in the example of the simple harmonic oscillator above. Necessity is more difficult to see, but rests upon the idea that there exists a direction where the trajectory can fall down to a state of lower potential energy.

For "well-behaved" $V(q)$, stability can be determined by analyzing the potential energy matrix, $\partial^2 V(q_e)/\partial q_i \partial q_j$. If all the eigenvalues are greater than zero, the equilibrium point H defines good subneighborhoods (topological 2N-spheres) and the equilibrium is stable—in fact nonlinearly stable. If there exists a negative eigenvalue the system is unstable.

One might be fooled into thinking that nonlinear stability implies linear stability; however, with a little thought you can see that this is not true. The one degree-of-freedom system with potential

$$V(q) = \frac{q^4}{4} \tag{V.4}$$

has an equilibrium point $q_e = 0$, and it is clear that this is nonlinearly stable since H defines good subneighborhoods. However, the linear dynamics satisfy

$$\delta\dot{p} = 0\,, \qquad \delta\dot{q} = \delta p \tag{V.5}$$

and thus

$$\delta p = \text{constant}\,, \qquad \delta q = \delta q_0 + \delta p t\,. \tag{V.6}$$

Obviously, trajectories leave any neighborhood of the equilibrium point provided $\delta p \neq 0$. This example also reveals why spectral stability does not imply linear stability. Adding another degree of freedom, (q', p') and defining the potential $V(q, q') = q^4/4 + q'^2/2$, produces a linearly unstable, yet spectrally stable, system.

In the 1950's, project Matterhorn was begun at Princeton for the purpose of investigating controlled fusion reactions as a source of energy. The idea was (and still is) to confine hot plasmas by means of magnetic fields. Since the dominant force balance is governed by MHD, a great deal of stability analyses using this model were undertaken in a variety of confinement configurations invoking different magnetic field geometries. What is in essence the infinite degree-of-freedom version of Lagrange's theorem was worked out for MHD*. This goes by the name of the energy principle or "δW" (which is in fact the second variation of the potential energy). Extremization techniques applied to this quantity have been used

*A. Wintner, *The Analytical Foundations of Celestial Mechanics* (Princeton University, Princeton, New Jersey, 1947).

*I. Bernstein, E. A. Frieman, M. D. Kruskal, and R. M. Kulsrud, Proc. Roy. Soc. A **244**, 17-40 (1958); Von K. Hain, R. Lüst, and A. Schlüter, Zeitschrift für Naturforschung A **12**, 833-841 (1957); G. Laval, C. Mercier, and R. Pellat, Nuc. Fusion **5**, 156-158 (1965).

to determine stability and instability, and such procedures were automated in PEST, the Princeton Equilibrium and Stability code, and elsewhere. Early MHD calculations were successful in explaining and eliminating the fastest plasma instabilities.

Often, (as we shall see) Hamiltonian systems are not of the separable form $H(q,p) = p^2/2 + V(q)$, but are instead general functions of q and p. When this is the case another old theorem, which is sometimes called *Dirichlet's theorem*, gives a sufficient condition for stability. It should be no surprise to you now that if in the vicinity of an equilibrium point surfaces of $H =$ constant define a family of good neighborhoods, then the equilibrium is nonlinearly stable. For well-behaved Hamiltonians one need only analyze the matrix $\partial^2 H(z_e)/\partial z^i \partial z^j$, where $z := (q,p)$. If this quantity is definite, i.e., there are no zero eigenvalues and they all have the same sign, then we have stability. Observe that H could in fact be an energy maximum. This can occur for rigid body dynamics and is typically the case for a localized vortex in fluid mechanics.

There is an important example due to Cherry* that illustrates two things: that Dirichlet's theorem is not necessary and sufficient and that linear stability does not imply nonlinear stability. Cherry's Hamiltonian is

$$H = \tfrac{1}{2}\omega_2(p_2^2 + q_2^2) - \tfrac{1}{2}\omega_1(p_1^2 + q_1^2) + \tfrac{1}{2}\alpha\left[2q_1p_1p_2 - q_2(q_1^2 - p_1^2)\right], \qquad \text{(V.7)}$$

where $\omega_{1,2} > 0$ and α are constants. If α is set to zero Cherry's system reduces to a linear system of two stable simple harmonic oscillators. However, because of the minus sign, $\partial^2 H/\partial z_i \partial z_j$ is not definite. Observe that this minus sign cannot be removed by a time independent canonical transformation and in the generic case cannot be removed by any canonical transformation. Oscillator "1" of this system is a *negative energy mode* (NEM).

Negative energy modes are important because when dissipation is added, they tend to become linearly unstable: If energy is removed from an NEM its amplitude increases†. Also, with the inclusion of nonlinearity NEM's can be driven unstable. The example of Cherry demonstrates this; assuming $\alpha \neq 0$ and $\omega_2 = 2\omega_1$, (V.7) possesses a solution‡ of the form

$$q_1 = \frac{\sqrt{2}}{\epsilon - \alpha t}\sin(\omega_1 t + \gamma), \qquad p_1 = -\frac{\sqrt{2}}{\epsilon - \alpha t}\cos(\omega_1 t + \gamma)$$

$$q_2 = -\frac{\sqrt{2}}{\epsilon - \alpha t}\sin(2\omega_1 t + 2\gamma), \qquad p_2 = -\frac{\sqrt{2}}{\epsilon - \alpha t}\cos(2\omega_1 t + 2\gamma). \qquad \text{(V.8)}$$

This is a two parameter, (α, γ), subfamily of the general four parameter solution set of Cherry's system. These solutions are of interest since they can diverge in finite time. In fact, in any neighborhood of the equilibrium point $q_1 = q_2 = p_1 = p_2 = 0$ there exist initial conditions for solutions that diverge in finite time. Such behavior is referred to as

*T. M. Cherry, Trans. Cambridge Philos. Soc. **23**, 199 (1925)

†This is a fairly old idea that is sometimes called the Kelvin-Tait theorem. See W. Thompson and P. G. Tait, *Treatise on Natural Philosophy* (Cambridge University Press, Cambridge, 1921), part 1, p. 388.

‡See E. T. Whittaker, *Analytical Dynamics* (Cambridge University Press, London, 1937), Sec. 136, p. 101, but be careful because there are typographical errors.

explosive growth and is characteristic of systems that possess both NEM's and resonance. Another example is the well-known "three-wave" problem[§]. The three-wave problem and Cherry's "two-wave" problem are examples of systems with order three resonances that are driven unstable by cubic terms in the Hamiltonian. These are in fact normal forms that are obtained upon averaging a general class of Hamiltonians. Thus explosive behavior is to be expected when there is resonance. When the resonance is detuned these systems generally are finite amplitude unstable and systems with three or more degrees of freedom may in fact be unstable, although with very small growth.

One might think that systems with NEM's are artifacts or unphysical, purely mathematical, oddities; this, however, is not the case. They occur in fluid and plasma systems* for a reason that will become clear below. Generally, they occur in mechanical systems with gyroscopic forces, like the Coriolis force, and they occur in the dynamics of particles in magnetic fields. An example that exhibits both of these is described by a Lagrangian of the form

$$L = \tfrac{1}{2}m(\dot{x}^2 + \dot{y}^2) + G(\dot{y}x - \dot{x}y) + \tfrac{1}{2}k(x^2 + y^2)\,, \tag{V.9}$$

where G is a constant that is either proportional to the constant angular speed of a rotating coordinate system or to a constant magnetic field. Note that for $k > 0$ the potential energy term corresponds to a hill and thus without the gyroscopic term the system would be unstable. Upon Legendre transforming and scaling, the following Hamiltonian is obtained:

$$H = \tfrac{1}{2}(p_1^2 + p_2^2) + \omega_G(q_2p_1 - q_1p_2) + \tfrac{1}{2}(\omega_G^2 - \omega_k^2)(q_1^2 + q_2^2)\,, \tag{V.10}$$

where the two time scales of the problem are determined by the frequencies

$$\omega_G := \frac{G}{m}\,, \qquad \omega_k := \sqrt{\frac{k}{m}}\,. \tag{V.11}$$

Assuming $q_{1,2},\ p_{1,2} \sim e^{i\omega t}$, it is easy to solve for eigenvalues,

$$\omega = \pm\omega_k(\sqrt{\varepsilon - 1} \pm \sqrt{\varepsilon})\,, \tag{V.12}$$

where $\varepsilon := \omega_G^2/\omega_k^2$. This system possesses the three types of Hamiltonian spectra:

1. $\omega = \pm\omega_R$ stable
2. $\omega = \pm i\gamma$ unstable
3. $\omega = \pm\omega_R \pm i\omega_I$ unstable

[§]See e.g. C. Kueny, "Nonlinear Instability and Chaos in Plasma Wave-Wave Interactions," Ph.D. Thesis, University of Texas at Austin (1993) and many references cited therein; See also D. Pfirsch, Phys. Rev. D **48**, 1428 (1993).

*In the context of MHD see J. M. Greene and B. Coppi, Phys. Fluids **8**, 1745 (1965); of fluids see R. A. Cairns, J. Fluid Mech. **92** 1 (1979), R. S. MacKay and P. G. Saffman, Proc. Roy. Soc. A **406**, 115 (1986), P. Ripa, Geophys. Astrophys. Fluid Dyn. 70, 85 (1993); and of Vlasov theory see P. J. Morrison and D. Pfirsch, Phys. Rev. A **40**, 3998 (1989), Phys. Fluids B **2**, 1105 (1990) and *ibid.* **4**, 3038 (1992).

In Hamiltonian systems eigenvalues occur in doublets or quartets. Case (1) is the only stable case. It occurs in the example when $\varepsilon = \omega_G^2/\omega_k^2 > 1$, which means the rotation or magnetic field is large enough to make the system stable in spite of the destabilizing potential energy. In this case we have two stable doublets, a fast one and a slow one. The slow one is an NEM. For $\varepsilon > 1$ there exists a canonical transformation $(q,p) \to (Q,P)$ that takes H into

$$H(Q,P) = -\tfrac{1}{2}\omega_s(P_s^2 + Q_s^2) + \tfrac{1}{2}\omega_f(P_f^2 + Q_f^2)\,, \tag{V.13}$$

which is the linear part of Cherry's Hamiltonian. The canonical transformation is effected by the following mixed variable generating function:

$$F_2(q_1, q_2, P_f, P_s) = c(q_1 P_s + q_2 P_f) + P_f P_s + \tfrac{1}{2}c^2 q_1 q_2\,, \tag{V.14}$$

where $c := [4(\omega_G^2 - \omega_k^2)]^{1/4}$.

Case (2) occurs if G is set to zero. There exist two unstable doublets, corresponding to the two directions for falling off the hill.

Case (3) occurs when $\varepsilon < 1$. This case of the quartet obviously requires two degrees of freedom, and is obviously unstable.

A nice feature of the above example is that it displays the two kinds of bifurcations that are generic to Hamiltonian systems. The first is when a doublet makes a transition between cases (1) and (2). There is a steady state bifurcation where the frequencies go through the origin of the ω-plane as shown in Figure 2. Here the stable pair is indicated by $\times$ while the

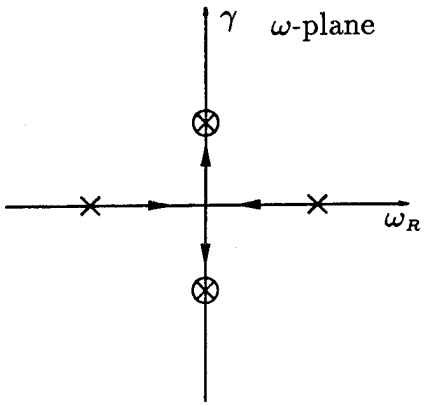

Figure 2:

unstable pair by the $\otimes$. This bifurcation generally occurs in systems where the Hamiltonian is separable, i.e. $H = p^2/2 + V(q)$, i.e. those for which Lagrange's theorem applies. It occurs in one degree-of-freedom systems where the potential goes from concave up to concave down. The arrows of the figure correspond to this case. For the system of (V.10) it occurs when $G = 0$ and $\omega_k^2 \to -\omega_k^2$.

The other bifurcation, which is something called a *Krein crash*, is illustrated in Figure 3. The arrows indicate the path followed by the eigenvalues of system (V.10) as ε is decreased from some value greater than unity. At $\varepsilon = 1$ the fast and slow modes coalesce at a value $|\omega_k| \neq 0$. Two possibilities exist: either the modes go through each other and remain on the

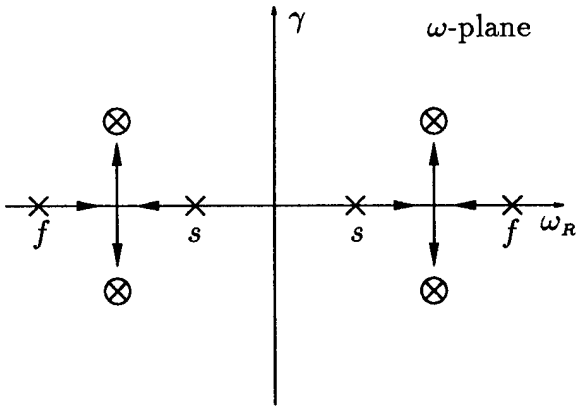

Figure 3:

real axis or they can migrate off the real axis as shown in the figure. *Krein's theorem** states that a necessary condition for this latter case is that the signature of the colliding modes must be different, i.e. one of them must be an NEM. The proof of Krein's theorem is not difficult; it relies on the fact that definite Hamiltonians cannot have instabilities.

Krein's theorem provides a means for detecting the occurrence of NEM's. If you have performed an eigenanalysis in some nondissipative system, one that you believe is Hamiltonian, and you observe the bifurcation described above, there must exist an NEM. This bifurcation is very common in fluid and plasma models. Why?

To answer this question we return to the Hamiltonian formulation of the ideal fluid in terms of the Lagrangian variables q and π that we discussed in Lecture II. Since we have defined an equilibrium point of a dynamical system to be a solution obtained by setting time derivatives to zero, it is evident that the sets of Lagrangian and Eulerian equilibria are not equivalent. Although static Eulerian equilibria, i.e. ones for which $v = 0$ for all r, certainly correspond to Lagrangian equilibria with $\pi = 0$ and $q =$ constant, stationary Eulerian equilibria, i.e. ones for which $v = v(r)$, do not correspond to Lagrangian equilibria, but to a particular kind of time dependent orbit, which we denote by

$$q_e = q_e(a,t), \qquad \pi_e = \pi_e(a,t)\,. \tag{V.15}$$

The functions above are particular in that they have the properties

$$\left.\frac{\rho_0(a)}{\mathcal{J}(a,t)}\right|_{a=q_e^{-1}(r,t)} = \rho_e(r) \tag{V.16}$$

$$s_0(a)|_{a=q_e^{-1}(r,t)} = s_e(r) \tag{V.17}$$

$$\left.\frac{\pi_e(a,t)}{\rho_0}\right|_{a=q_e^{-1}(r,t)} = \dot{q}_e(a,t)|_{a=q_e^{-1}(r,t)} = v_e(r)\,, \tag{V.18}$$

*Moser (1958) and (1968), *Ref. V A.*

where we emphasize that, upon doing the substitutions indicated on the right hand sides of the above equations, the resulting functions ρ_e, s_e and v_e are independent of time.

Although (q_e, π_e) does not constitute a Lagrangian equilibrium state, it is a reference state about which we could linearize. We could set

$$q(a,t) = q_e(a,t) + \xi(a,t), \qquad \pi = \pi_e(a,t) + p(a,t) \tag{V.19}$$

and expand (II.88); however, the resulting equation would have explicit time dependence due to that in (q_e, π_e). Even when the time dependence is periodic, analysis of such linear equations is not trivial (recall Mathieu's equation).

We can get out of this bind by an old trick. To see this we turn to the action principle of (II.72), insert (V.19), and expand

$$S[q] = S[q_e] + \delta S[q_e;\xi] + \delta^2 S[q_e;\xi] + \dots . \tag{V.20}$$

The first term of (V.20) is merely a number, while the second term vanishes since the reference trajectory q_e is assumed to be a solution and is thus an extremal point. The third term, upon variation with respect to ξ, generates the linear dynamics relative to the reference state q_e. It is given by

$$\delta^2 S[q_e;\xi] = \int_{t_0}^{t_1} dt \int_D d^3a \left(\tfrac{1}{2}\,\rho_0 \dot{\xi}^2 - \left[\frac{\rho_0^2 U_\rho}{2\mathcal{J}}\right]_{q_e} \left[(\xi_{i,i})^2 + \xi_{j,i}\,\xi_{i,j}\right] - \left[\frac{\rho_0^3}{2\mathcal{J}^2} U_{\rho\rho}\right]_{q_e} (\xi_{i,i})^2 \right) . \tag{V.21}$$

It is important to observe that in (V.21) the term involving U_ρ and $U_{\rho\rho}$ possesses the explicit time dependence arising from $q_e(a,t)$. The old trick is to view the perturbation of a trajectory in a frame of reference moving with the reference trajectory. This can be done since $q_e = q_e(a,t)$ is invertible. Thus we define

$$\eta(r,t) := \xi(a,t)|_{a=q_e^{-1}(r,t)} . \tag{V.22}$$

The quantity $\eta(r,t)$ is a sort of Eulerian field for the Lagrangian displacement variable. A time derivative of (V.22) yields

$$\dot{\xi}(a,t) = \frac{\partial \eta(r,t)}{\partial t} + \frac{\partial \eta(r,t)}{\partial r} \cdot \dot{q}_e|_{a=q_e^{-1}(r,t)} \tag{V.23}$$

or in light of (V.18)

$$\dot{\xi}(a,t) = \frac{\partial \eta(r,t)}{\partial t} + v_e(r) \cdot \nabla \eta(r,t) . \tag{V.24}$$

Note that we have used "$\cdot$" for time derivatives at constant a and $\partial/\partial t$ for time derivatives at constant r. Since in (V.24) $v_e(r)$, the equilibrium velocity, is time independent, no explicit time dependence is introduced by this transformation.

It is interesting and revealing to compare (V.24) with the transformation for time derivatives when going into a rotating frame of reference

$$\left.\frac{\partial}{\partial t}\right|_{\text{fixed}} = \left.\frac{\partial}{\partial t}\right|_{\text{rot}} + \Omega \times . \tag{V.25}$$

Just as the second term of (V.25) gives rise to noninertial (or fictional) forces, notably the Coriolis force that gives rise to the gyroscopic term in the Hamiltonian of (V.10), the second term of (V.24) will give rise to a noninertial type force in the fluid Hamiltonian. Transforming (V.21), using (V.22) and (V.24) yields

$$\delta^2 S[\eta] = \tfrac{1}{2}\int_{t_0}^{t_1} dt \int_D d^3r \left(\rho_e \, |\dot{\eta} + v_e \cdot \nabla\eta|^2 - \eta \cdot \mathfrak{V}_e \cdot \eta\right) \tag{V.26}$$

where $\mathfrak{V}_e$ is an operator, although one without explicit time dependence because it is now a function of the equilibrium quantities ρ_e and s_e. The second term, the potential energy, can be written as

$$\begin{aligned}\delta^2 W &:= \tfrac{1}{2}\int_D d^3r \, \eta \cdot \mathfrak{V}_e \cdot \eta \\ &= \tfrac{1}{2}\int_D d^3r \left((\nabla\cdot\eta)^2 \, \rho_e \frac{\partial p_e}{\partial \rho_e} + (\nabla\cdot\eta)(\eta\cdot\nabla p_e)\right),\end{aligned} \tag{V.27}$$

where $p_e(\rho_e, s_e)$ is the equilibrium pressure expressed as a function of the equilibrium density and entropy.

We can now obtain the (time independent) Hamiltonian by Legendre transformation. The canonical momentum is given by

$$p = \frac{\delta L}{\delta \dot{\eta}} = \rho_e(\dot{\eta} + v_e \cdot \nabla\eta)\,, \tag{V.28}$$

whence the Hamiltonian is seen to be

$$\delta^2 H[p,\eta] = \tfrac{1}{2}\int_D d^3r \left(\frac{p^2}{\rho_e} - 2p\cdot(v_e\cdot\nabla\eta) + \eta\cdot\mathfrak{V}_e\cdot\eta\right), \tag{V.29}$$

which has the "noninertial" term $-p_i \, v_{ej} \, \partial\eta_i/\partial r_j$ that is reminiscent of the gyroscopic term of (V.10).

Now, it should come as no surprise that ideal fluids typically have negative energy modes, and generally $\delta^2 H$ is not positive definite as required for Dirichlet's theorem. In spite of the indefiniteness of $\delta^2 H$ the system can be spectrally stable; Lagrange's theorem, which is a necessary and sufficient condition for stability, is not possible since the Hamiltonian is not of the separable form.

References

[1] N. G. Van Kampen and B. U. Felderhof, *Theoretical Methods in Plasma Physics* (North Holland, Amsterdam, 1967).

[2] W.A. Newcomb, "Lagrangian and Hamiltonian Methods in Magnetohydrodynamics," Nuclear Fusion: Supplement, pt. 2, 451-463 (1962).

[3] J.K. Moser, Comm. Pure Appl. Math. **11**, 81 (1958); Mem.Am. Math. Soc.**81**, 1 (1968).

[4] P. J. Morrison and M. Kotschenreuther, "The Free Energy Principle, Negative Energy Modes, and Stability," in *Nonlinear World: IV International Workshop on Nonlinear and Turbulent Processes in Physics* eds. V.G. Bar'yakhtar, V.M. Chernousenko, N.S. Erokhin, A.B. Sitenko, and V.E. Zakharov (World Scientific, Singapore, 1990).

[5] D. Pfirsch and R. N. Sudan, Phys. Fluids B **5**, 2052 (1993).

B. Stability and Noncanonical Hamiltonian Systems

In noncanonical Hamiltonian systems it is still the case that equilibria occur at extremal points of the Hamiltonian,

$$\dot{z}^i = J^{ij}\frac{\partial H}{\partial z^j} = [z^i, H] = 0\,, \tag{V.30}$$

but the situation is more complicated. To see that something is amiss, consider the variation of the energy for a barotropic fluid, where

$$H[p,v] = \int_D \left[\tfrac{1}{2}\rho v^2 + \rho U(\rho)\right] d^3r\,; \tag{V.31}$$

namely,

$$\begin{aligned}\frac{\delta H}{\delta v} &= \rho v \\ \frac{\delta H}{\delta \rho} &= \frac{v^2}{2} + U(\rho) + \rho U(\rho)\,.\end{aligned} \tag{V.32}$$

Setting the right hand side of (V.32) to zero results in the trivial equilibrium state with $v = 0$ and $\rho =$ constant (which is generally zero). If this were the only equilibrium state, fluid mechanics would not be a very interesting discipline. Where are the other equilibria? Why are they not extremal points of the Hamiltonian?

To answer these questions, compare (V.30) with its counterpart for the canonical case:

$$\dot{z}^i = J_c^{ij}\frac{\partial H}{\partial z^j} = 0\,. \tag{V.33}$$

Since $\det J_c = 1$, it is evident that $\dot{z} = 0$ implies $\partial H/\partial z^j = 0$. Thus all equilibria are extremal points. However, in the noncanonical case this is not so when $\det J = 0$. In the vicinity of points where the rank of J does not change, the null space of J is spanned by $\partial C^\alpha/\partial z^i$, $\alpha = 1, 2, \ldots \nu$, where ν is the corank of J. In this case the general solution to (V.33) is given by

$$\left.\frac{\partial F}{\partial z^i}\right|_{z_e} = \left.\frac{\partial H}{\partial \lambda^i}\right|_{z_e} + \lambda_\alpha \left.\frac{\partial C^\alpha}{\partial z^i}\right|_{z_e} = 0\,. \tag{V.34}$$

Here λ_α are Lagrange multipliers, which are determined by choosing the values of the constants C^α. Thus (V.34) gives those equilibria that lie on the symplectic leaf with the chosen values.

Not surprisingly, the linear dynamics obtained by setting $z = z_e + \delta z$ and expanding to first order, exhibits behavior arising from $\det J = 0$, namely, the existence of zero frequency modes. The equation for the linear dynamics is easily seen to be

$$\delta \dot{z} = A^i_k(z_e)\delta z^k\,, \tag{V.35}$$

where

$$A^i_k(z_e) := J^{ij}(z_e)\frac{\partial^2 F(z_e)}{\partial z^i \partial z^k} =: J^{ij}_e F_{,jk}\,. \tag{V.36}$$

[Note, this linear dynamics has a Hamiltonian structure with the Poisson bracket defined by J_e (which is constant) and the Hamiltonian given by $\delta^2 F := 1/2\ F_{,jk}\ \delta z^i \delta z^j$.] Assuming $\delta z \sim e^{i\omega t}$ yields an eigenvalue problem with a characteristic equation given by

$$\det(i\omega I - A) = 0\,, \tag{V.37}$$

where zero frequency modes satisfy

$$\det A = 0\,. \tag{V.38}$$

In the canonical case, A is given by

$$A^i_{c\,k} = J^{ij}_c H_{,jk} \tag{V.39}$$

and

$$\det(A^i_{c\,k}) = \det(J^{ij}_c)\det(H_{,jk}) = \det(H_{,jk})\,. \tag{V.40}$$

Thus all the zero eigenvalues of A_c arise from $\det(H_{,jk}) = 0$. These zero eigenvalues correspond to (local) troughs in the energy surface.

In the noncanonical case zero eigenvalues can arise from two places, namely, $\det(J^{ij}) = 0$ and $\det(F_{,ij}) = 0$. An accounting of these zero eigenvalues is given by

$$\mathrm{Rank}(A^i_k) \le \min\{\mathrm{Rank}(J^{ij}), \mathrm{Rank}(F_{,jk})\}. \tag{V.41}$$

Thus for every Casimir there exists a null eigenvector, δz^k_0. To avoid complication suppose $\det(F_{,jk}) \neq 0$, i.e. that there are no local troughs in F, then all the null eigenvectors come from degeneracy in the bracket and they are given by

$$\delta z^0_k = (F^{-1})^{kj}\frac{\partial C(z_e)}{\partial z^j}, \tag{V.42}$$

where $(F^{-1})^{kj}F_{,jl} = \delta^k_l$. Evidently, with δz_0 given by (V.42),

$$A^j_k \delta z^0_k = J^{ij}F_{jk}F^{-1}_{kl}\frac{\partial C}{\partial z_l} = J^{ij}\frac{\partial C}{\partial z_l} = 0. \tag{V.43}$$

In spite of the existence of null eigenvalues, a version of Dirichlet's theorem goes through in the noncanonical case. Since F is a constant of motion it can be used to define the

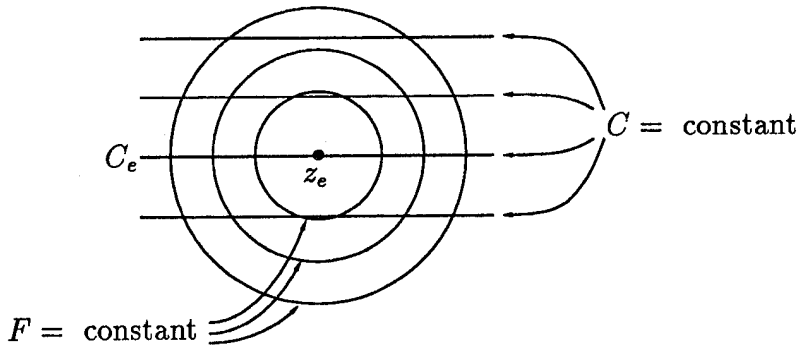

Figure 4:

subneighborhoods in the definition of stability given above, provided $\delta^2 F = 1/2 F_{,jk} \delta z^j \delta z^k =$ constant defines compact (as depicted in Figure 4) surfaces in the vicinity of z_e. This will be the case if $F_{,jk}(z_e)$ is definite.

It is of interest to note that this prescription for stability places no restrictions on δz, even though dynamically δz is confined to surfaces of constant C^α (as depicted Figure 4). We will see in the next section that sometimes it is useful to take advantage of this information.

Although the picture described above for equilibrium and stability of noncanonical Hamiltonian systems may seem nice and tidy, there is a complication that occurs at places where the rank of J changes. Generally, this happens at isolated points but it can happen on curves or surfaces. When the rank changes it is no longer true that setting $\dot{z}^i = 0$ and solving for z_e is equivalent to solving (V.34) for all choices of λ_α. When the rank decreases on an open set, there is no problem in obtaining new Casimirs whose gradients span the null space of J. However, when the rank changes at (for example) a point, a new null eigenvector of J appears, an eigenvector that cannot be written as a gradient in the normal way.

The above pathology is perhaps best illustrated by an example. Consider the free rigid body of Lecture III, but modified so that the Hamiltonian has the form

$$H = \sum_{i=1}^{3} \left(\frac{\ell_i^2}{2I_i} + B_i \ell_i \right) . \tag{V.44}$$

Here, we have added the linear term with B_i constant and nonzero for $i = 1, 2, 3$. This Hamiltonian is a sort of mixture between that of a spin system and a free rigid body. This form serves our purpose and we won't dwell on the physics, although it isn't hard to imagine a physical system where Hamiltonians of this form might arise. The equations of motion are now

$$\dot{\ell}_i = -\epsilon_{ijk} \ell_k \frac{\partial H}{\partial \ell_j} = -\epsilon_{ijk} \ell_k \left(\frac{\ell_j}{I_j} + B_j \right) \tag{V.45}$$

and it is clear that equilibria must satisfy

$$\begin{aligned} \ell_1 (I_2^{-1} \ell_2 + B_2) - \ell_2 (I_1^{-1} \ell_1 + B_1) = 0 \\ \ell_1 (I_3^{-1} \ell_3 + B_3) - \ell_3 (I_1^{-1} \ell_1 + B_1) = 0 \end{aligned} \tag{V.46}$$

$$\ell_2(I_3^{-1}\ell_3 + B_3) - \ell_3(I_2^{-1}\ell_2 + B_2) = 0\,.$$

From (V.47) it is clear that a nonrotating configuration with $\ell_1 = \ell_2 = \ell_3 = 0$ is an equilibrium point, but there are other, uniformly rotating equilibria as well.

Now, consider the equilibria that arise upon extremizing $F = H + \lambda C$, where C is given by (III.45). (Note the Casimirs remain the same as in Lecture III since we have not altered the bracket—only the Hamiltonian.) From $\partial F/\partial \ell_i = 0$ for $i = 1, 2, 3$, respectively, we obtain

$$\begin{aligned} \ell_1(I_1^{-1} + \lambda) &= -B_1 \\ \ell_2(I_2^{-1} + \lambda) &= -B_2 \\ \ell_3(I_3^{-1} + \lambda) &= -B_3\,. \end{aligned} \tag{V.47}$$

It is evident from (V.47) that there exists no choice of λ for which the equilibrium point

$$\ell_1 = \ell_2 = \ell_3 = 0 \tag{V.48}$$

extremizes F. Observe, also, that the inequivalence of (V.47) and (V.44) occurs for an equilibrium, namely (V.48), that corresponds to a point where $J^{ij} = -\epsilon_{ijk}\ell_k$ changes from rank 2 to rank 0.

Another example* where $\delta F = 0$ does not yield all equilibria, is that of the 2-D Euler's equations for fluid motion (cf. Lecture III). Here the equation of motion yields the equilibrium relation

$$\frac{\partial \omega}{\partial t} = [\omega, \psi] = 0\,, \tag{V.49}$$

which is satisfied if ω and ψ are functionally dependent. Suppose $S = S(x, y)$ defines a locus of points, then the equilibrium relation is satisfied if $\omega_e = \omega_e(S)$ and $\psi_e = \psi_e(S)$. Note that ω_e need not be the graph of ψ_e and vice versa. Thus we can write, e.g.

$$\nabla^2\psi_e = G(\psi_e)\,, \tag{V.50}$$

where $G(\psi_e)$ is an arbitrary function of ψ_e.

Let us contrast this with the equation obtained upon varying the functional $F = H + C$, which for the 2-D Euler equations, is given by

$$F[\omega] = -\frac{1}{2}\int_D \psi\,\omega\,d^2r + \int_D \mathcal{C}(\omega)\,d^2r\,. \tag{V.51}$$

The functional derivative $\delta F/\delta\omega = 0$ implies

$$\psi_e = \mathcal{C}'(\omega_e)\,. \tag{V.52}$$

*This example is credited to V. Arnold, Izv. Vyssh. Uchebn. Zaved. Mat. **5** (54), 3 (1966) and (1966), *l.c.* Lecture III, which is the origin of the popular terminology "Arnold's method" or "Arnold's theorem" for the application of these ideas to other situations. This terminology is erroneous since the method was used in earlier papers: R. Fjortoft, Geofy. Pub. **17**, 1 (1950), W. Newcomb, in Appendix of I. Bernstein, Phys. Rev. **109**, 10 (1958), M. D. Kruskal and C. Oberman, Phys. Fluids **1**, 275 (1958), C. S. Gardner quoted in K. Fowler, J. Math. Phys. **4**, 559 (1963) and Phys. Fluids **6**, 839 (1963), and K. Fowler, *ibid.*

Assuming $\mathcal{C}'(\omega)$ is monotonic we can solve for ω as follows:

$$\omega_e = \nabla^2\psi_e = \mathcal{C}'^{-1}(\psi_e)\,. \tag{V.53}$$

Thus here, in contrast to (V.50), the vorticity must be a monotonic function of the stream function—if it is not, then it does not satisfy (V.52) and hence is not extremal. (Suppose $\psi_0 \neq \psi_1$ and $\omega(\psi_0) = \omega(\psi_1) = \omega_*$. Then (V.52) implies $\psi_0 = \mathcal{C}'(\omega_*) = \psi_1$, which is a contradiction.)

In stability analyses it is important for the equilibrium to be extremal. When this is the case, as for the monotonic equilibria above, one can calculate the second variation

$$\begin{aligned}\delta^2 F[\omega_e;\delta\omega] &= \tfrac{1}{2}\int_D \left(|\nabla\psi|^2 + \mathcal{C}''(\delta\omega)^2\right)\, d^2r \\ &= \tfrac{1}{2}\int_D \left(|\nabla\psi|^2 + (\delta\omega)^2\left(\frac{\partial\omega_e(\psi_e)}{\partial\psi_e}\right)^{-1}\right)\, d^2r\,,\end{aligned} \tag{V.54}$$

where the second equality follows upon differentiation of (V.52) with respect to ψ_e. Formally, if we have an equilibrium for which $\partial\omega_e(\psi_e)/\partial\psi_e > 0$, then $\delta^2 F$ is positive definite and in analogy with finite degree-of-freedom systems we could claim stability, in a "norm" defined by $\delta^2 F$. This would also be the case if $\partial\omega_e(\psi_e)/\partial\psi_e < 0$ and the second term of (V.54) could be shown to always dominate the first when $\delta\omega$ is in some space. This case, which is typical of localized vortices, corresponds to an energy maximum. In either case the situation would be pretty good, but in infinite dimensions things can still be slippery. Recall in Lecture II we gave an example of a functional with positive second variation at a point that was not a minimum. The condition of strong positivity is needed to show convexity. A rigorous stability analysis requires the definition of a Banach space in which the solution must be shown to exist. Convexity is one technical piece that is needed in a complete proof of stability.

If the first variation exists and does not vanish on the equilibrium of interest, then it is impossible for $F[\omega_e]$ to be convex and thus impossible to obtain a norm as discussed above. It can turn out that the functional is not differentiable at the equilibrium of interest but still can be proven to be stable by obtaining appropriate bounds*. Another technique is to restrict the class of variations so that they lie within symplectic leaves. In the next section we will see how this removes problems related to the rank changing behavior of J.

References

[1] D. D. Holm, J. E. Marsden, T. Ratiu, A. Weinstein, "Nonlinear Stability of Fluid and Plasma Equilibria," Physics Reports **123**, 1-116 (1985).

[2] P. J. Morrison and S. Eliezer, "Spontaneous Symmetry Breaking and Neutral Stability in the Noncanonical Hamiltonian Formalism," Physical Rev. A **33**, 4205-4214 (1986).

*G. Rein, preprint (1993).

[3] P. J. Morrison and M. Kotschenreuther, "The Free Energy Principle, Negative Energy Modes, and Stability," in *Nonlinear World: IV International Workshop on Nonlinear and Turbulent Processes in Physics* eds. V.G. Bar'yakhtar, V.M. Chernousenko, N.S. Erokhin, A.B. Sitenko, and V.E. Zakharov (World Scientific, Singapore, 1990).

[4] M. E. McIntyre and T. G. Shepherd and , J. Fluid Mech. **181**, 527-565 (1987).

[5] T. G. Shepherd, "Extremal Properties and Hamiltonian Structure of the Euler Equations," in, *Topological Aspects of the Dynamics of Fluids and Plasmas*, eds. H. K. Moffatt et al. (Kluwer Academic, 1992), 275-283.

C. Dynamical Accessibility

Dynamically accessible perturbations are ones for which *all* the Casimir invariants are unchanged. As depicted in Figure 5, these perturbations lie in the surfaces defined by $C^\alpha =$ constant for all α. In the prescription described above for obtaining equilibria of noncanonical systems from a variational principle, the energy was extremized subject to a selection of Casimir invariants. The values of these invariants are determined by the Lagrange multipliers (and vice versa). In contrast, dynamically accessible perturbations are "direct" variations that automatically satisfy the constraints without choosing their particular values. The particular constraint surface is selected after the fact by the equilibrium point, rather than by Lagrange multipliers. Since the cosymplectic form, J^{ij}, projects (co)vectors onto the symplectic leaves, it is natural to consider a first order variation of the form

$$\delta z^i_{da} = [\mathcal{G}, z^i] = J^{ji}(z) g_j \,, \tag{V.55}$$

where $\mathcal{G} := z^i g_i$. Here the arbitrariness in the variation is embodied in the arbitrariness in the generating function g_j, but because of the presence of J^{ij} the variation $\delta^{(1)} z_{da}$ is arbitrary only within the symplectic leaf. Observe that J^{ij} is evaluated at any point z, in practice this will be a candidate equilibrium point that is determined after setting the first variation to zero.

Whether or not one wants to restrict to dynamically accessible variations, as described above, is a question of physics that likely must be determined on a case by case basis. In some systems the constraint is quite robust, while in others it is not. However, we will make the comment that if there exist mechanisms for creating perturbations that are not dynamically accessible, then it would seem appropriate to reexamine the model equation to see if such a mechanism should be incorporated into the dynamics.

Before considering equilibria and stability with this kind of variation, let us show explicitly that $\delta^{(1)} z_{da}$ preserves the constraints to first order:

$$\delta C(z) = \frac{\partial C}{\partial z^i}\, \delta^{(1)} z^i = \frac{\partial C}{\partial z^i}\, J^{ji} g^{(1)}_j = 0 \,. \tag{V.56}$$

An expression that preserves the constraint to second order is given by

$$\delta^{(2)} z^i_{da} = J^{ij} g^{(2)}_j + \tfrac{1}{2} J^{jl}\, \frac{\partial J^{ti}}{\partial z^l}\, g^{(1)}_t g^{(1)}_j \,. \tag{V.57}$$

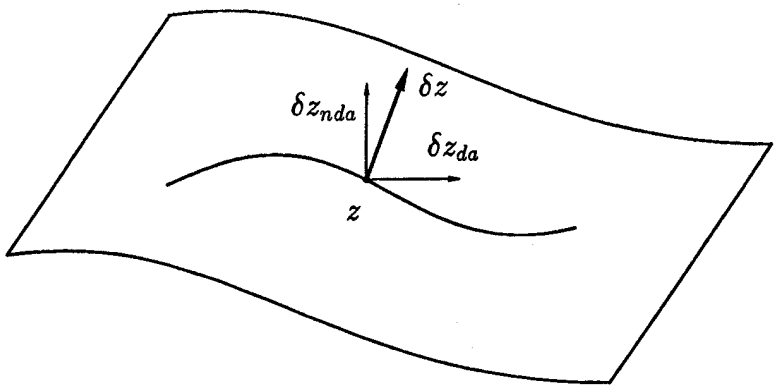

Figure 5:

Here we have added the superscripts (1) and (2) to distinguish the first order from the second order generating functions. Inserting (V.57) into $\delta^2 C$ and using the fact that $J^{ij}\partial C/\partial z^i = 0$ (in at least an open set) verifies the assertion.

In the case where $J^{ij} = c_k^{ij} z^k$, the first and second order variations have the form

$$\delta^{(1)} z_{da}^i = = c_k^{ji} z^k g_j^{(1)}$$

$$\delta^{(2)} z_{da}^i = c_k^{ji} z^k g_j^{(2)} + \tfrac{1}{2} c_l^{ti} c_k^{jl} z^k g_t^{(1)} g_j^{(1)} \,. \tag{V.58}$$

A convenient form to all orders is given by

$$\hat{z}^i = e^{g_j c_k^{ji}} z^k \,. \tag{V.59}$$

where $\Delta z := \hat{z} - z$ is a finite variation. The infinite dimensional analogue of (V.59) can be used to construct finite leaf variations, which are important for proving convexity in infinite dimensional systems. Expanding $g = g^{(1)} + g^{(2)} + \ldots$ and the exponential of (V.59), yields Eq. (V.58) to second order.

Return now to the example of the rigid body with the modified Hamiltonian. Using

$$\delta \ell_i^{da} = \epsilon_{ijk} \ell_k g_j \,, \tag{V.60}$$

we obtain

$$\delta F = \frac{\partial F}{\partial \ell_i} \delta \ell_i^{da} = \frac{\partial H}{\partial \ell_i} \delta \ell_i^{da} = (I_i^{-1} \ell_i + B_i) \epsilon_{ijk} \ell_k g_j^{(1)} = 0 \,, \tag{V.61}$$

for the extremal equilibrium condition. Equation (V.61) yields a result that is identical to (V.47), the equilibrium condition obtained upon setting $\dot{\ell}_i = 0$ in the equation of motion.

In the case of the 2-D Euler fluid

$$\delta \omega_{da} = \{\mathcal{G}, \omega\} = -[g, \omega] \,, \tag{V.62}$$

where $\mathcal{G} := \int_D \omega g \, d^2r$ with g arbitrary, and

$$\delta F_{da} := \delta F[\omega; \delta\omega_{da}] = -\int_D \psi \, \delta\omega_{da} \, d^2r$$

$$= \int_D \psi[g,\omega] \, d^2r = -\int_D g[\psi,\omega] \, d^2r = 0\,, \tag{V.63}$$

which implies $[\psi,\omega] = 0$—the condition obtained upon setting $\partial\omega/\partial t = 0$ in (V.49).

Proceeding now to the second variation, it is clear that stability can depend upon the class of variations allowed. Decomposing a general perturbation as

$$\delta z = \delta z_{da} + \delta z_{nda} \tag{V.64}$$

and inserting into $\delta^2 F$ yields

$$\delta^2 F = \delta^2 F_{da} + \delta^2 F_{nda}\,, \tag{V.65}$$

where

$$\delta^2 F_{da} = \tfrac{1}{2}\left(\frac{\partial^2 H(z_e)}{\partial z^i \partial z^j} + \lambda_\alpha \frac{\partial^2 C^\alpha(z_e)}{\partial z^i \partial z^j}\right) J^{li}(z_e) g_l^{(1)} J^{kj}(z_e) g_k^{(1)}\,. \tag{V.66}$$

Note, it is always the case that $\delta^2 F_{nda}$ depends only on the first order g's. It is evident that $\delta^2 F$ can be indefinite because of the presence of $\delta^2 F_{nda}$, even if $\delta^2 F_{da}$, which involves only perturbations of the form $J^{ij}(z_e) g_i^{(1)}$, is of definite sign. An example is given by the free rigid body with the equilibrium

$$\ell_1^e = -\frac{BI_1}{\lambda I_1 + 1}\,, \qquad \ell_2^e = \ell_3^e = 0\,, \tag{V.67}$$

where we set $B_1 = B$ and $B_2 = B_3 = 0$. In this case

$$\delta^2 F = -\frac{B}{2\ell_1^e}(\delta\ell_1)^2 + \frac{1}{2}\left(\frac{1}{I_2} - \frac{1}{I_1}\right)(\delta\ell_2)^2 + \frac{1}{2}\left(\frac{1}{I_3} - \frac{1}{I_1}\right)(\delta\ell_3)^2\,. \tag{V.68}$$

If $I_1 < I_2 < I_3$, the last two terms are positive; however, the first term can have either sign. Dynamically accessible perturbations satisfy

$$\delta\ell_i^{da} = \epsilon_{ijk}\ell_j^e g_k = \epsilon_{ijk}\ell_j^e g_k\,; \tag{V.69}$$

hence $\delta\ell_1^{da} = 0$. Therefore, $\delta^2 F_{da}$ is definite, even though $\delta^2 F$ need not be. Observe that the nondynamically accessible perturbation corresponds to the null eigenvector described above.

In this example, and above, we substituted the first order dynamically accessible variation into the second order quantity $\delta^2 F$. To some of you it may not be clear that $\delta^2 F_{da}$ is identical to $\delta^2 H_{da}$, which is obtained by expanding H to second order and then inserting (V.55) and (V.57). It is, however, straightforward to show that these are in fact identical. Expanding some Casimir C^α to second order about the equilibrium yields

$$\Delta^{(2)} C^\alpha = \frac{\partial C^\alpha}{\partial z^i}\delta^{(2)} z^i + \tfrac{1}{2}\frac{\partial^2 C^\alpha}{\partial z^i \partial z^j}\delta^{(1)} z^i \delta^{(1)} z^j\,, \tag{V.70}$$

but, when restricted to the constraint surface, (V.70) reduces to

$$\Delta^{(2)}C^{\alpha}_{da} = \frac{\partial C^{\alpha}}{\partial z^i} J^{li}_e g^{(1)}_l + \frac{\partial C^{\alpha}}{\partial z^i} J^{li}_e g^{(2)}_l$$

$$+ \tfrac{1}{2}\frac{\partial C^{\alpha}}{\partial z^i}\frac{\partial J^{ti}_e}{\partial z^l_0} J^{jl}_e g^{(1)}_t g^{(1)}_j + \tfrac{1}{2}\frac{\partial^2 C^{\alpha}}{\partial z^i \partial z^j} J^{li}_e g^{(1)}_l J^{kj}_e g^{(1)}_k \,. \tag{V.71}$$

The first and second terms in (V.71) clearly vanish because

$$J^{ij}\frac{\partial C}{\partial z^j} = 0 \,. \tag{V.72}$$

However, by exploiting the local nature of the constraint surface, it is also possible to show that the last two terms cancel, so that, to second order, $\Delta^{(2)}C^{\alpha}_{da}$ vanishes identically. Indeed, one can realize (V.72) as a Taylor series about the equilibrium point z_e and observe that, since this equation holds for all z (at least in a neighborhood of z_e), each power of δz in the expansion

$$0 = J^{ij}\frac{\partial C}{\partial z^j} = J^{ij}_e \frac{\partial C}{\partial z^j_e} + \delta z^l \left(\frac{\partial J^{ij}_e}{\partial z^l_e}\frac{\partial C^{\alpha}}{\partial z^j_e} + J^{ij}_e \frac{\partial^2 C^{\alpha}}{\partial z^l_e \partial z^j_e} \right) + \ldots \tag{V.73}$$

must vanish identically. The first term in (V.73) is clearly zero, while the vanishing of the second term, the one linear in δz^l, yields the desired relation

$$\frac{\partial J^{ij}_e}{\partial z^l_e}\frac{\partial C^{\alpha}}{\partial z^j_e} = -J^{ij}_e \frac{\partial^2 C^{\alpha}}{\partial z^l_e \partial z^j_e} \,, \tag{V.74}$$

between the first and second partial derivatives of C^{α}. It follows immediately that the second variation $\Delta^2 C_{da} = 0$.

Similarly, expanding H to second order yields

$$\Delta^{(2)}H = \frac{\partial H}{\partial z^i}\delta^{(1)}z^i + \frac{\partial H}{\partial z^i}\delta^{(2)}z^i + \tfrac{1}{2}\frac{\partial^2 H}{\partial z^i \partial z^j}\delta^{(1)}z^i \delta^{(1)}z^j \,, \tag{V.75}$$

which, when restricted to lie within the constraint surface, takes the form

$$\Delta^{(2)}H_{da} = \delta^{(2)}H_{da} = \tfrac{1}{2}\frac{\partial^2 H}{\partial z^i \partial z^j} J^{li}_e g^{(1)}_l J^{kj}_e g^{(1)}_k + \tfrac{1}{2}\frac{\partial H}{\partial z^i}\frac{\partial J^{ti}_e}{\partial z^l_e} J^{jl}_e g^{(1)}_t g^{(1)}_j \,. \tag{V.76}$$

It is evident that the first term of (V.76) is the same as the first term of the free energy $\delta^{(2)}F_{da}$, but in order to compare the second terms in these relations, one must again use (V.74) and the equilibrium condition (V.34) involving the Lagrange multipliers. Indeed, by summing (V.74) over λ_{α} and then exploiting (V.34), one concludes that

$$\lambda_{\alpha} J^{ij}_e \frac{\partial^2 C^{\alpha}}{\partial z^l_e \partial z^j_e} = -\lambda_{\alpha}\frac{\partial J^{ij}_e}{\partial z^l_e}\frac{\partial C^{\alpha}}{\partial z^j_e} = \frac{\partial J^{ij}_e}{\partial z^l_e}\frac{\partial H}{\partial z^j_e} \,. \tag{V.77}$$

It thus follows that, as was asserted, the constrained variation $\delta^{(2)}H_{da} = \delta^{(2)}F_{da}$.

Now we show how dynamically accessible variations are related to Lagrangian variations, in the context of the ideal fluid. In particular we will relate the Lagrangian and Eulerian potential energy functional.

To obtain dynamically accessible variations for the fluid, the following functional:

$$\mathcal{G} := \int_D (M \cdot \eta + h\rho + k\sigma)\ d^3r\,, \tag{V.78}$$

can be inserted into the bracket of (III.89). Here the arbitrariness of variation within the symplectic leaf is described by the free functions of r: η, h, and k. We will only need the expressions for the first and second variations of the density and entropy per unit mass

$$\begin{aligned}
\delta^{(1)}\rho_{da} &= \{\mathcal{G},\rho\} = \nabla\cdot\left(\rho\frac{\delta\mathcal{G}}{\delta M}\right) = \nabla\cdot(\rho\eta)\\
\delta^{(1)}\sigma_{da} &= \{\mathcal{G},\sigma\} = \nabla\cdot\left(\sigma\frac{\delta\mathcal{G}}{\delta M}\right) = \nabla\cdot(\sigma\eta)
\end{aligned} \tag{V.79}$$

$$\begin{aligned}
\delta^{(2)}\rho_{da} &= \tfrac{1}{2}\{\mathcal{G},\{\mathcal{G},\rho\}\} = \tfrac{1}{2}\nabla\cdot[\eta\nabla\cdot(\rho\eta)]\\
\delta^{(2)}\sigma_{da} &= \tfrac{1}{2}\{\{\mathcal{G},\mathcal{G},\sigma\}\} = \tfrac{1}{2}\nabla\cdot[\eta\nabla\cdot(\sigma\eta)]\,.
\end{aligned} \tag{V.80}$$

(Note we are not expanding $\mathcal{G}$ since we already know only the first order part contributes.) Observe that the variations of (V.79) are compatible with those of (IV.101), which are induced by variation of the Lagrangian coordinates.

The potential energy functional for the ideal fluid is

$$W[\rho,\sigma] = \int_D \rho\tilde{U}(\rho,\sigma)\ d^3r\,, \tag{V.81}$$

where recall $\tilde{U}$ is the internal energy per unit mass and $\sigma = \rho s$. In terms of the function $\tilde{U}(\rho,\sigma)$ the equation of state for the pressure is given by

$$\tilde{p}(\rho,\sigma) = \rho^2\left(\frac{\partial\tilde{U}}{\partial\rho} + \frac{\sigma}{\rho}\frac{\partial\tilde{U}}{\partial\sigma}\right). \tag{V.82}$$

Here we have used the tilde to indicate that the dependence is upon ρ and σ instead of ρ and s. Upon Taylor expansion, the second order potential energy functional is seen to be

$$\begin{aligned}
\delta^2W = \tfrac{1}{2}\int_D \Big(&\left(\delta^{(1)}\rho\right)^2\left(\rho\tilde{U}_{\rho\rho} + 2\tilde{U}_\rho\right) + \left(\delta^{(1)}\sigma\right)^2\left(\rho\tilde{U}_{\sigma\sigma}\right) + 2\left(\delta^{(1)}\sigma\ \delta^{(1)}\rho\right)\left(\rho\tilde{U}_{\rho\sigma} + \tilde{U}_\sigma\right)\\
&+ 2\left(\delta^{(2)}\rho\right)\left(\rho\tilde{U}_\rho + \tilde{U}\right) + 2\left(\delta^{(2)}\sigma\right)\left(\rho\tilde{U}_\sigma\right)\Big)\ d^3r\,,
\end{aligned} \tag{V.83}$$

where subscripts denote partial differentiation. Inserting (V.79) and (V.80) into (V.83) creates a relatively complicated formula, one with terms that are similar but with no immediate

simplification. What we have is in reality a sort of integration by parts puzzle. We will not give all the details here of a calculation that gets us to the desired end, but only a few "landmarks." The first move is to integrate the second order variations by parts. Next, the terms are grouped as follows:

$$\delta^2 W_{da} = \tfrac{1}{2}\int_D \Big((\nabla\cdot\eta)^2 \left(\rho^3\tilde{U}_{\rho\rho} + 2\rho^2\tilde{U}_\rho + \sigma^2\rho\tilde{U}_{\sigma\sigma} + 2\sigma\rho^2\tilde{U}_{\sigma\rho} + 2\sigma\rho\tilde{U}_\sigma\right)$$
$$+ (\nabla\cdot\eta)(\eta\cdot\nabla\sigma)\left(\sigma\rho\tilde{U}_{\sigma\sigma} + \rho^2\tilde{U}_{\rho\sigma} + \rho\tilde{U}_\rho\right)$$
$$+ (\nabla\cdot\eta)(\eta\cdot\nabla\rho)\left(\rho^2\tilde{U}_{\rho\rho} + 2\rho\tilde{U}_\rho + \sigma\rho\tilde{U}_{\rho\sigma} + \sigma\tilde{U}_\sigma\right)\Big)\, d^3r\,, \tag{V.84}$$

which upon making use of (V.82) can be put into the form

$$\delta^2 W_{da} = \tfrac{1}{2}\int_D \left((\nabla\cdot\eta)^2(\rho\tilde{p}_\rho + \sigma\tilde{p}_\sigma) + (\nabla\cdot\eta)(\eta\cdot\nabla\tilde{p})\right)\, d^3r\,. \tag{V.85}$$

The definition $p(\rho,s) := \tilde{p}(\rho,\sigma)$ and the chain rule imply $\rho\tilde{p}_\rho + \sigma\tilde{p}_\sigma = \rho p_\rho$, which when used in (V.85) yields, finally,

$$\delta^2 W_{da} = \tfrac{1}{2}\int_D \left((\nabla\cdot\eta)^2(\rho p_\rho) + (\nabla\cdot\eta)(\eta\cdot\nabla\tilde{p})\right)\, d^3r\,. \tag{V.86}$$

This expression, when evaluated on $\rho = \rho_e$ and $\sigma = \sigma_e$, is precisely that of (V.27), which was obtained in the strictly Lagrangian variable context. We have thus, in a sense, gone full circle!

References

[1] V. I. Arnold, "The Hamiltonian Nature of the Euler Equations in the Dynamics of a Rigid Body and of an Ideal Fluid," Usp. Mat. Nauk. **24**, 225 (1969).

[2] H. E. Kandrup and P. J. Morrison, "Hamiltonian Structure of the Vlasov-Einstein System and the Problem of Stability for Spherical Relativistic Star Clusters," Annals of Phys. **225**, 114-166 (1993).

[3] P. J. Morrison and M. Kotschenreuther, "The Free Energy Principle, Negative Energy Modes, and Stability," in *Nonlinear World: IV International Workshop on Nonlinear and Turbulent Processes in Physics* eds. V.G. Bar'yakhtar, V.M. Chernousenko, N.S. Erokhin, A.B. Sitenko, and V.E. Zakharov (World Scientific, Singapore, 1990).

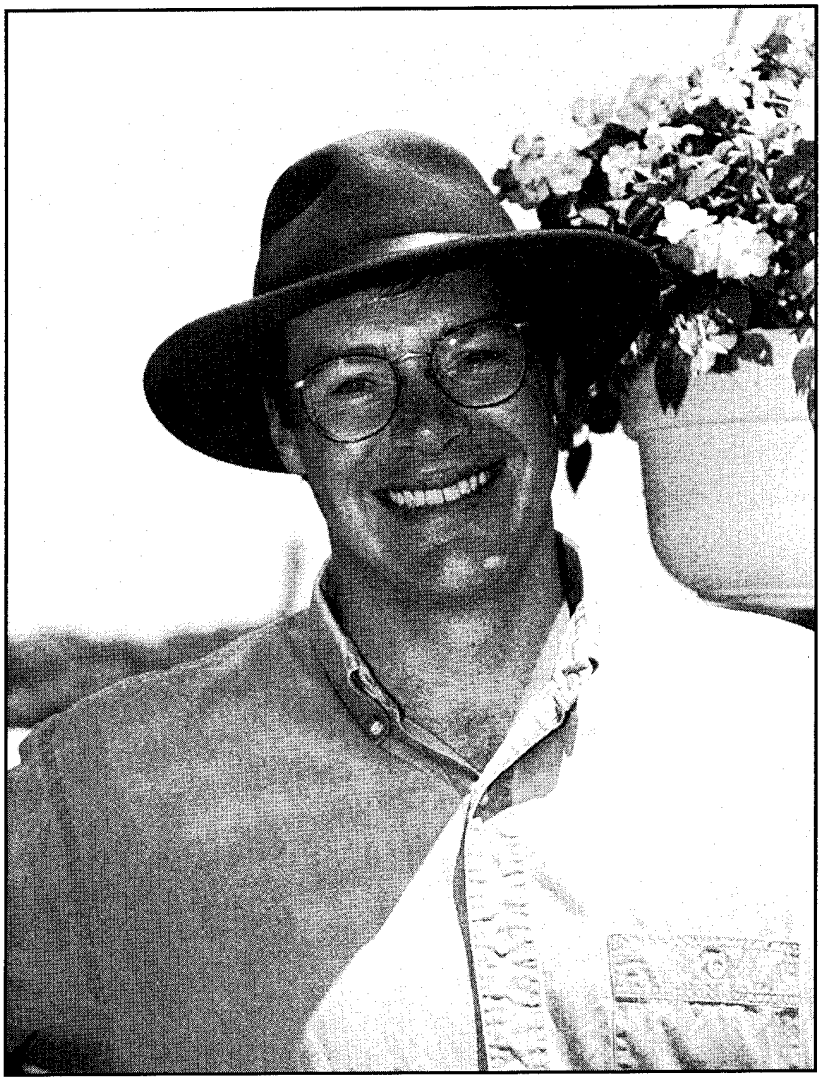

Principal Lecturer Ted Shepherd

Applications of Hamiltonian theory to GFD

Theodore G. Shepherd

Department of Physics, University of Toronto

1 Generalized Hamiltonian dynamics

1.1 Introduction

Virtually every model used in Geophysical Fluid Dynamics (GFD) is, in its conservative form, Hamiltonian. This is not too surprising since the fundamental equations from which every model is derived are themselves Hamiltonian: namely the three-dimensional Euler equations for compressible, stratified flow (Morrison & Greene 1980; Morrison 1982).

The Hamiltonian formulation of dynamics is relevant to the description of many different phenomena. In the field of theoretical physics, it provides a general foundation for quantum mechanics, quantum field theory, statistical mechanics, relativity, optics and celestial mechanics. Hamiltonian structure constitutes a unifying framework, wherein symmetry properties are readily apparent which may be connected to conservation laws by Noether's theorem. One therefore expects some of the same advantages to hold in GFD.

In these lectures we will consider particularly the application of Hamiltonian structure to problems involving disturbances to basic states. As we shall see, such diverse topics as available potential energy, wave action, and most of the well-known hydrodynamical stability theorems (static stability, symmetric stability, centrifugal stability, and the Rayleigh-Kuo and Charney-Stern theorems) may all be understood — and in some cases significantly generalized — within the Hamiltonian framework.

It is sometimes objected that Hamiltonian structure is irrelevant to GFD because real fluids are viscous. Against this, we note simply that many phenomena in GFD are essentially conservative (inviscid, adiabatic) since they occur at high Reynolds numbers, $Re \gg 1$. For example, in the free atmosphere $Re \sim 10^{15}$. Thus many GFD phenomena (instabilities, wave propagation, and wave, mean-flow interaction) are traditionally studied within the framework of a conservative model. Even if non-conservative effects arise, these may often be understood as localized effects on otherwise conserved quantities: examples include fronts, shocks, and gravity-wave drag (cf. Benjamin & Bowman 1987).

Moreover, many of the most interesting phenomena in GFD arise from the *nonlinear* (usually advective) terms in the relevant equations. Examples include wave, mean-flow interaction, energy budgets and conversions, and spectral transfers in turbulent flow. These nonlinear terms are conservative, and are therefore part of the Hamiltonian structure of the problem. It follows that the nonlinear interactions are constrained by preservation of invariant quantities (e.g. energy, enstrophy) which are connected to the underlying Hamiltonian

structure of the model: one cannot deduce the correct spectral transfers in a problem unless one imposes the correct invariants on the nonlinear dynamics.

Hamiltonian structure also provides a natural framework within which to derive approximate models. It is well known that in making approximations one should attempt to maintain fundamental conserved quantities. A good example of this is provided by the hydrostatic primitive equations on the sphere (Lorenz 1967), where energy and angular momentum conservation are lost under the hydrostatic approximation, and certain manipulations must be made to the equations in order to restore them. Rather than such trial-and-error methods, it is preferable to ensure maintenance of invariance properties by making the approximations within a Hamiltonian framework (Salmon 1983, 1985, 1988*a*).

The approach followed in these lectures is to use the Hamiltonian structure of GFD in a very practical way. In particular, there is no need to use the Poisson bracket itself, or even to know it, if one knows the invariants. One needs merely to know that the bracket is there! All the manipulations required here can be expressed in terms of standard variational calculus: one has merely to vary all dependent variables, integrate by parts, and check the boundary conditions. Finally, everything derived from Hamiltonian theory may always be verified afterwards by direct use of the equations of motion.

1.2 Dynamics

We consider the generalized Hamiltonian dynamical system

$$\frac{\partial \boldsymbol{u}}{\partial t} = J\frac{\delta \mathcal{H}}{\delta \boldsymbol{u}}, \tag{1}$$

where $\boldsymbol{u}(\boldsymbol{x},t)$ are the dynamical fields, $\mathcal{H}$ is the Hamiltonian, and J is a skew-symmetric operator (called the *cosymplectic form*) having the required algebraic properties (see Morrison's lectures). The equivalent formulation in terms of Poisson brackets is

$$\frac{d\mathcal{F}}{dt} = [\mathcal{F},\mathcal{H}], \tag{2}$$

where $\mathcal{F}[\boldsymbol{u}]$ is an admissible functional. The Poisson bracket is defined by

$$[\mathcal{F},\mathcal{G}] = \Big\langle \frac{\delta \mathcal{F}}{\delta \boldsymbol{u}}, J\frac{\delta \mathcal{G}}{\delta \boldsymbol{u}} \Big\rangle \tag{3}$$

(the angle brackets denoting an appropriate inner product), and the bracket satisfies properties analogous to those of J. Typically

$$\Big\langle \frac{\delta \mathcal{F}}{\delta \boldsymbol{u}}, J\frac{\delta \mathcal{G}}{\delta \boldsymbol{u}} \Big\rangle = \int \delta \boldsymbol{x} \sum_{i,j} \frac{\delta \mathcal{F}}{\delta \boldsymbol{u}_i} J_{ij} \frac{\delta \mathcal{G}}{\delta \boldsymbol{u}_j}; \tag{4}$$

i.e. the inner product is the spatial integral of the dot product of the two vectors. Further discussion of the forms (1) and (2) as applied to fluid dynamics may be found in Morrison (1982), Benjamin (1984), Salmon (1988*b*), and Shepherd (1990, 1992*a*).

Let us verify the equivalence of the above two formulations, (1) and (2). Assuming first that (1) holds, we note from (3) that

$$[\mathcal{F},\mathcal{H}] = \Big\langle \frac{\delta \mathcal{F}}{\delta \boldsymbol{u}}, J\frac{\delta \mathcal{H}}{\delta \boldsymbol{u}} \Big\rangle = \Big\langle \frac{\delta \mathcal{F}}{\delta \boldsymbol{u}}, \frac{\partial \boldsymbol{u}}{\partial t} \Big\rangle = \frac{d\mathcal{F}}{dt} \tag{5}$$

(the last step invoking the chain rule for functionals), and hence (2) is verified. Now assuming that (2) holds, let us take

$$\mathcal{F}[\boldsymbol{u}] = \boldsymbol{u}_i(\boldsymbol{x}_o) = \int \delta(\boldsymbol{x} - \boldsymbol{x}_o)\, \boldsymbol{u}_i(\boldsymbol{x})\, d\boldsymbol{x} \tag{6}$$

for some i and some $\boldsymbol{x}_o$, where $\delta(\boldsymbol{x} - \boldsymbol{x}_o)$ is the Dirac delta-function; thus

$$\delta\mathcal{F} = \int \delta(\boldsymbol{x} - \boldsymbol{x}_o)\delta\boldsymbol{u}_i(\boldsymbol{x})\, d\boldsymbol{x}, \qquad \frac{\delta\mathcal{F}}{\delta\boldsymbol{u}_j} = \delta(\boldsymbol{x} - \boldsymbol{x}_o)\, \delta_{ij}, \tag{7}$$

where δ_{ij} is the Kronecker delta. Then using (2), (6) and (7), we have

$$\frac{\partial \boldsymbol{u}_i}{\partial t}(\boldsymbol{x}_o) = \frac{d\mathcal{F}}{dt} = \left\langle \frac{\delta\mathcal{F}}{\delta\boldsymbol{u}}, J\frac{\delta\mathcal{H}}{\delta\boldsymbol{u}} \right\rangle = \left\langle \delta(\boldsymbol{x} - \boldsymbol{x}_o)\delta_{ij}, \left(J\frac{\delta\mathcal{H}}{\delta\boldsymbol{u}}\right)_j \right\rangle = \left(J\frac{\delta\mathcal{H}}{\delta\boldsymbol{u}}\right)_i(\boldsymbol{x}_o). \tag{8}$$

Thus (1) is verified, component by component.

1.3 Steady states and conditional extrema

Let $\boldsymbol{u} = \boldsymbol{U}$ be a steady solution of the dynamics (1). If J is invertible, then

$$J\frac{\delta\mathcal{H}}{\delta\boldsymbol{u}}\bigg|_{\boldsymbol{u}=\boldsymbol{U}} = \frac{\partial \boldsymbol{U}}{\partial t} = 0 \tag{9}$$

leads to

$$\frac{\delta\mathcal{H}}{\delta\boldsymbol{u}}\bigg|_{\boldsymbol{u}=\boldsymbol{U}} = 0. \tag{10}$$

Hence steady solutions are extrema of $\mathcal{H}$.

But suppose now that the dynamics of the system is non-canonical, in the sense that J is non-invertible (cf. Morrison's lectures). Then (9) does *not* imply (10). However, Casimirs $\mathcal{C}$ may be defined such that

$$J\frac{\delta\mathcal{C}}{\delta\boldsymbol{u}} = 0 \qquad \text{(equivalently, } [\mathcal{C}, \mathcal{F}] = 0\ \forall\ \mathcal{F}\text{)}, \tag{11}$$

and the set of all vectors $\delta\mathcal{C}/\delta\boldsymbol{u}$ spans the kernel of J. At $\boldsymbol{u} = \boldsymbol{U}$, therefore, $\delta\mathcal{H}/\delta\boldsymbol{u}$ is locally parallel to $\delta\mathcal{C}/\delta\boldsymbol{u}$ for some $\mathcal{C}$ (a different $\mathcal{C}$ for each choice of $\boldsymbol{U}$); equivalently, there generically exists a Casimir $\mathcal{C}$ such that

$$\frac{\delta\mathcal{H}}{\delta\boldsymbol{u}}\bigg|_{\boldsymbol{u}=\boldsymbol{U}} = -\frac{\delta\mathcal{C}}{\delta\boldsymbol{u}}\bigg|_{\boldsymbol{u}=\boldsymbol{U}}. \tag{12}$$

One must be careful here with classes of admissible variations; this point will come up again when we consider nonlinear stability. Note that Casimirs are always invariants of the motion, since

$$\frac{d\mathcal{C}}{dt} = [\mathcal{C}, \mathcal{H}] = \left\langle \frac{\delta\mathcal{C}}{\delta\boldsymbol{u}}, J\frac{\delta\mathcal{H}}{\delta\boldsymbol{u}} \right\rangle = -\left\langle J\frac{\delta\mathcal{C}}{\delta\boldsymbol{u}}, \frac{\delta\mathcal{H}}{\delta\boldsymbol{u}} \right\rangle = 0. \tag{13}$$

From (12), we have that

$$\frac{\delta}{\delta \boldsymbol{u}}(\mathcal{H}+\mathcal{C})\Big|_{\boldsymbol{u}=\boldsymbol{U}} = 0. \tag{14}$$

This statement has two interpretations: (i) $\boldsymbol{U}$ is an extremum of the invariant $\mathcal{H}+\mathcal{C}$; and (ii) $\boldsymbol{U}$ is a conditional extremum of $\mathcal{H}$, subject to the constraint $\mathcal{C}$ = const. (as with Lagrange multipliers). An example of an elliptic fixed point, representing a maximum or minimum, is sketched below; the curves are lines of constant $\mathcal{H}$, and the constraint surface is the "symplectic leaf" $\mathcal{C}$ = const.

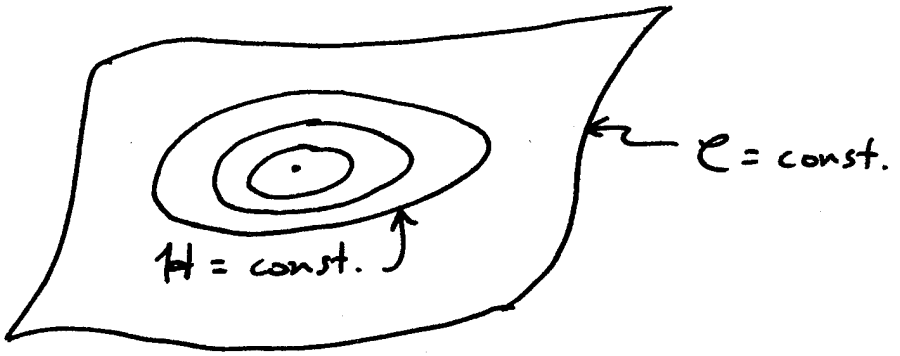

1.4 Example: barotropic vorticity equation

This model is discussed in Morrison's lectures, but it is useful to consider it in the present context. The discussion will also illustrate some of the complications that are introduced by boundaries. The governing equation is the (2-D) vorticity equation

$$\frac{\partial \omega}{\partial t} + \partial(\psi, \omega) = 0\,, \tag{15}$$

where ψ is the stream function, the velocity is given by $\boldsymbol{v} = \hat{\mathbf{z}} \times \boldsymbol{\nabla}\psi$, $\omega = \nabla^2\psi$ is the vorticity, and $\partial(a,b) \equiv a_x b_y - a_y b_x$ is the two-dimensional Jacobian operator. With this choice of ω, the system is identical to the 2-D Euler equations. We consider a closed, multiply-connected domain D with N connected boundaries ∂D_i $(i = 1, \ldots, N)$ on which $\boldsymbol{v}\cdot\hat{\mathbf{n}} = 0$ (or $\partial\psi/\partial s = 0$, where s is arclength along ∂D_i), where $\hat{\mathbf{n}}$ is the unit outward normal vector.

This system is Hamiltonian with

$$\mathcal{H} = \iint_D \frac{1}{2}|\boldsymbol{\nabla}\psi|^2\, dxdy. \tag{16}$$

The first variation of $\mathcal{H}$ is given by

$$\begin{aligned}
\delta\mathcal{H} &= \iint_D \boldsymbol{\nabla}\psi \cdot \delta\boldsymbol{\nabla}\psi\, dxdy \\
&= \iint_D \left[\boldsymbol{\nabla}\cdot(\psi\delta\boldsymbol{\nabla}\psi) - \psi\,\delta\nabla^2\psi\right] dxdy \\
&= \sum_i \psi\,\delta \oint_{\partial D_i} \boldsymbol{\nabla}\psi\cdot\hat{\mathbf{n}}\, ds - \iint_D \psi\delta\omega\, dxdy,
\end{aligned} \tag{17}$$

where the last step follows from the fact that ψ is constant on the boundaries. This means that one cannot write $\delta\mathcal{H} = \langle(\delta\mathcal{H}/\delta\omega), \delta\omega\rangle$ alone. Stated otherwise, ω is not enough to determine the dynamics; we need boundary terms as well, as follows.

Defining $\gamma_i \equiv \oint_{\partial D_i} \nabla\psi \cdot \hat{\mathbf{n}}\, ds$ to be the circulation on each connected piece ∂D_i of ∂D, recall that $d\gamma_i/dt = 0$. (This is the usual boundary condition on the tangential velocity; it follows from consideration of the momentum equations underlying (15).) The boundary circulations can therefore be considered dynamical variables, and one may rewrite $\delta\mathcal{H}$ in terms of $\delta\gamma_i$ in addition to $\delta\omega$: from (17),

$$\delta\mathcal{H} = \sum_i \psi\, \delta\gamma_i - \iint_D \psi\delta\omega\, dxdy\,, \tag{18}$$

which implies

$$\frac{\delta\mathcal{H}}{\delta\omega} = -\psi, \qquad \frac{\delta\mathcal{H}}{\delta\gamma_i} = \psi\big|_{\partial D_i}. \tag{19}$$

Note that in the first equation of (19), one cannot think in terms of partial derivatives: in particular, $\partial|\boldsymbol{v}|^2/\partial\omega$ makes no sense. Instead, it is clear that variational derivatives are required.

Relative to ω alone, the γ_i's extend the phase space in the following way: there are now $N+1$ dynamical variables $\boldsymbol{u} = (\omega, \gamma_1, \ldots, \gamma_N)^T$, and the cosymplectic form J is an $(N+1)\times(N+1)$ matrix operator:

$$J = \begin{pmatrix} -\partial(\omega,\cdot) & 0 & \ldots & 0 \\ 0 & 0 & & 0 \\ \vdots & & \ddots & \vdots \\ 0 & \ldots & \ldots & 0 \end{pmatrix}. \tag{20}$$

Substituting (19) and (20) into (1) yields, as expected, the equations of motion

$$\Big(\frac{\partial\omega}{\partial t}, \frac{d\gamma_1}{dt}, \ldots, \frac{d\gamma_N}{dt}\Big)^T = \frac{\partial\boldsymbol{u}}{\partial t} = J\frac{\delta\mathcal{H}}{\delta\boldsymbol{u}} = \Big(-\partial(\omega,-\psi), 0, \ldots, 0\Big)^T. \tag{21}$$

Having seen that arbitrary disturbances can be incorporated into the Hamiltonian description, let us now, for simplicity, restrict our attention to circulation-preserving disturbances: namely those with $\delta\gamma_i = 0$ for all i. (If this condition holds at one time, it will hold at all subsequent times.) For this special case, ω is the sole dynamical variable and $J = -\partial(\omega,\cdot)$. Let us find the Casimirs. Solving (11) in this case, we obtain

$$\partial(\omega, \frac{\delta\mathcal{C}}{\delta\omega}) = 0\,; \tag{22}$$

in other words, lines of constant ω and constant $\delta\mathcal{C}/\delta\omega$ coincide. Locally, at least, this means that $\delta\mathcal{C}/\delta\omega = f(\omega)$ for some function f. Such a function may not be defined over the entire domain D, however. A sub-class of these Casimirs which is useful for applications (see the later sections on stability) consists of those for which the functional relation is global: these may be written as

$$\mathcal{C}[\omega] = \iint_D C(\omega)\, dxdy \tag{23}$$

for some function C. Since Casimirs are always invariants of the motion, this demonstrates that

$$\frac{d}{dt}\iint_D C(\omega)\, dxdy = 0 \tag{24}$$

for *any* function $C(\omega)$. The set of conservation laws described by (24) reflects the fact that ω is a Lagrangian or material invariant of the dynamics (15), given that the flow is non-divergent. Since the dynamical evolution takes place on the symplectic leaf $\mathcal{C}$ =const., where the constraint refers to *all* Casimirs simultaneously, we see that the Casimirs provide a severe restriction on dynamically possible behaviour. This is intuitively obvious for piecewise-constant vorticity profiles. The calculation also demonstrates that there is nothing esoteric about Casimirs: they have real physical meaning.

We should be able to show that steady solutions of (15) are conditional extrema of $\mathcal{H}$, subject to the constraint that the variations preserve $\mathcal{C}$. First consider the extremal condition (12), which takes the form $\psi = C'(\omega)$ in this case for $\mathcal{C}$ given by (23). If, therefore, (12) holds, it follows that

$$\omega_t = -\partial(\psi, \omega) = -\partial(C'(\omega), \omega) = 0, \tag{25}$$

and the flow is steady. One may also build in the constraint imposed by conservation of $\mathcal{C}$ directly on the variations. To do this, set $\delta\omega = \partial(\varphi, \omega)$ for some arbitrary φ which is constant on the boundaries. Such variations $\delta\omega$ are clearly just non-divergent (area-preserving) rearrangements of the vorticity field ω, for which

$$\delta\mathcal{C} = \iint_D \frac{\delta\mathcal{C}}{\delta\omega}\,\delta\omega\,dxdy = \iint_D C'(\omega)\partial(\varphi,\omega)\,dxdy = \iint_D \partial(\varphi, C(\omega))\,dxdy = 0. \tag{26}$$

For steady states with $\partial(\psi, \omega) = 0$, the variation of $\mathcal{H}$ is then

$$\delta\mathcal{H} = \iint_D \frac{\delta\mathcal{H}}{\delta\omega}\,\delta\omega\,dxdy = -\iint_D \psi\partial(\varphi,\omega)\,dxdy = \iint_D \varphi\partial(\psi,\omega)\,dxdy = 0 \tag{27}$$

(using the fact that both ψ and φ are constant on the boundary); hence steady solutions of (15) are seen to be unconditional extrema of $\mathcal{H}$ for vorticity-preserving variations, as expected on general grounds.

The variations $\delta\omega = \partial(\varphi, \omega)$ considered above may be written in the form $\delta\omega = J\varphi$, which suggests the general form $\delta\boldsymbol{u} = J\varphi$ for a vector φ. Evidently such variations are guaranteed to be Casimir-preserving, since

$$\delta\mathcal{C} = \left\langle \frac{\delta\mathcal{C}}{\delta\boldsymbol{u}}, \delta\boldsymbol{u} \right\rangle = \left\langle \frac{\delta\mathcal{C}}{\delta\boldsymbol{u}}, J\varphi \right\rangle = -\left\langle J\frac{\delta\mathcal{C}}{\delta\boldsymbol{u}}, \varphi \right\rangle = 0. \tag{28}$$

The reader is referred to Morrison's notes for a more detailed description of such variations, which he refers to as being "dynamically accessible".

1.5 Symmetries and conservation laws

As in textbook classical mechanics (e.g. Goldstein 1980), for any functional $\mathcal{F}$ we can define a one-parameter family of infinitesimal variations $\delta_{\mathcal{F}}\boldsymbol{u}$ induced by $\mathcal{F}$ by

$$\delta_{\mathcal{F}}\boldsymbol{u} = \epsilon J\frac{\delta\mathcal{F}}{\delta\boldsymbol{u}}, \tag{29}$$

where ϵ is the infinitesimal parameter. The change in another functional $\mathcal{G}$ induced by this variation is

$$\Delta_{\mathcal{F}}\mathcal{G} \equiv \mathcal{G}[\boldsymbol{u} + \delta_{\mathcal{F}}\boldsymbol{u}] - \mathcal{G}[\boldsymbol{u}] = \left\langle \frac{\delta\mathcal{G}}{\delta\boldsymbol{u}}, \delta_{\mathcal{F}}\boldsymbol{u} \right\rangle + \mathcal{O}((\delta_{\mathcal{F}}\boldsymbol{u})^2) = \epsilon[\mathcal{G}, \mathcal{F}] + \mathcal{O}(\epsilon^2), \tag{30}$$

where the second step follows from the definition of the functional derivative, and the third step from the definition of the bracket together with (29). This proves

Noether's Theorem: The Hamiltonian is invariant under infinitesimal variations generated by a functional $\mathcal{F}$, in the sense that $\Delta_{\mathcal{F}}\mathcal{H} = 0$, if and only if $\mathcal{F}$ is a constant of the motion.

Therefore, given a symmetry of the Hamiltonian (a variation $\delta\boldsymbol{u}$ under which the Hamiltonian is invariant), one can attempt to solve (29) to find the corresponding invariant (modulo a Casimir). Equally, given a known invariant $\mathcal{F}$, one can use (29) to determine the corresponding symmetry.

Exercise: Cyclic coordinates in a finite-dimensional canonical system. If $\mathcal{H}$ is invariant under translations in q_i (i.e. $\partial\mathcal{H}/\partial q_i = 0$ for some i), use (29) to show that the corresponding p_i is a constant of the motion.

As is well known, the KdV equation possesses more than one (non-trivially related) Hamiltonian representation. Consider two representations with cosymplectic forms J_1 and J_2. Suppose that δu_1 is a symmetry of the system; using J_1 with (29) then defines an invariant I_1. But knowing I_1, (29) may now be used with J_2 to find a new symmetry, δu_2. Then substituting δu_2 back into (29) with J_1 produces a new invariant I_2, and so on. This procedure will continue indefinitely as long as we keep generating new invariants; in the case of the KdV equation this turns out to be true, and leads to exact integrability. See Olver (1986) for a more thorough, and highly readable, discussion of this topic.

Returning to the relation (29), we see that Casimirs correspond to *invisible* symmetries since

$$\delta_{\mathcal{C}}\boldsymbol{u} = \epsilon J\frac{\delta\mathcal{C}}{\delta\boldsymbol{u}} = 0 : \tag{31}$$

Casimirs induce no change whatsoever in the dynamical variables.

Let us now consider some examples of symmetries and conservation laws. First suppose that the Hamiltonian $\mathcal{H}$ is invariant under translation in time. We can set $\delta_{\mathcal{F}}\boldsymbol{u} = -\epsilon(\partial\boldsymbol{u}/\partial t)$ as the variation in $\boldsymbol{u}$ induced by a shift in time, $\epsilon = \delta t$. (The minus sign is indeed correct: think about it!) To find the corresponding invariant $\mathcal{F}$ we must therefore solve $-(\partial\boldsymbol{u}/\partial t) = J(\delta\mathcal{F}/\delta\boldsymbol{u})$, which implies $\mathcal{F} = -\mathcal{H}$ (to within a Casimir). This shows that $\mathcal{H}$ is the invariant corresponding to time-translation invariance. (This statement is not trivial. In particular, recall the relation $d\mathcal{H}/dt = \partial\mathcal{H}/\partial t$ in classical mechanics; the former corresponds to a conservation law, the latter to a symmetry-invariance.)

As another example, suppose that the Hamiltonian $\mathcal{H}$ is invariant under translation in space: x_j, say, for some j. We can set $\delta_{\mathcal{F}}\boldsymbol{u} = -\epsilon(\partial\boldsymbol{u}/\partial x_j)$, and to find the corresponding invariant we must solve $-(\partial\boldsymbol{u}/\partial x_j) = J(\delta\mathcal{F}/\delta\boldsymbol{u})$. In the case of the barotropic vorticity equation, for example, with $j = 1$ this becomes

$$\begin{aligned} \frac{\partial\omega}{\partial x} &= \partial\Big(\omega, \frac{\delta\mathcal{F}}{\delta\omega}\Big) \qquad \Longrightarrow \qquad \frac{\delta\mathcal{F}}{\delta\omega} = y \\ \Longrightarrow \qquad \mathcal{F} &= \iint_D y\omega\, dxdy = \iint_D y\Big(\frac{\partial v}{\partial x} - \frac{\partial u}{\partial y}\Big)\, dxdy = \int\!\!\int_D u\, dxdy \end{aligned} \tag{32}$$

(to within a Casimir). Therefore the invariant corresponding to x-translation invariance of the dynamics is seen to be the zonal momentum, as expected.

For $j = 2$, similar considerations lead to

$$\frac{\partial \omega}{\partial y} = \partial(\omega, \frac{\delta \mathcal{F}}{\delta \omega}) \qquad \Longrightarrow \qquad \frac{\delta \mathcal{F}}{\delta \omega} = -x$$

$$\Longrightarrow \qquad \mathcal{F} = -\iint_D x\omega \, dxdy = \iint_D x(\frac{\partial u}{\partial y} - \frac{\partial v}{\partial x}) \, dxdy = \iint_D v \, dxdy \tag{33}$$

(also to within a Casimir). Therefore the invariant corresponding to y-translation invariance of the dynamics is seen to be the meridional momentum.

By Noether's theorem, the same construction is guaranteed to work for *any* continuous symmetry. Let us show it for a rotation. We take the variation to be $\delta r = 0$, $\delta\theta = \epsilon$, where r and θ are polar coordinates defined by $x = r\cos\theta$ and $y = r\sin\theta$. The corresponding variations in x and y are given by

$$\delta x = -r\sin\theta \, \delta\theta = -y\epsilon, \qquad \delta y = r\cos\theta \, \delta\theta = x\epsilon. \tag{34}$$

It follows that the variation in the dynamical variable ω is

$$\delta\omega = -\frac{\partial \omega}{\partial x}\delta x - \frac{\partial \omega}{\partial y}\delta y = \big(y\frac{\partial \omega}{\partial x} - x\frac{\partial \omega}{\partial y}\big)\epsilon. \tag{35}$$

Then to determine the invariant corresponding to this symmetry we must solve (29), which takes the form

$$x\frac{\partial \omega}{\partial y} - y\frac{\partial \omega}{\partial x} = \partial(\omega, \frac{\delta \mathcal{F}}{\delta \omega}) \qquad \Longrightarrow \qquad \frac{\delta \mathcal{F}}{\delta \omega} = -\frac{1}{2}(x^2 + y^2) = -\frac{r^2}{2}$$

$$\Longrightarrow \qquad \mathcal{F} = -\iint_D \frac{r^2}{2}\omega \, dxdy = \iint_D \hat{\mathbf{z}} \cdot (\boldsymbol{r} \times \boldsymbol{v}) dxdy \tag{36}$$

(to within a Casimir). The last computation is obtained after integrating by parts. As expected, we obtain the angular momentum.

1.6 Steadily-translating solutions

Suppose there exists a solution to the system (1) translating steadily in x at a speed c, i.e. $\boldsymbol{u}(x, y, z, t) = \boldsymbol{U}(x - ct, y, z)$. Then clearly

$$\frac{\partial \boldsymbol{U}}{\partial t} = -c\frac{\partial \boldsymbol{U}}{\partial x}. \tag{37}$$

The fact that the solution is translating in x implies that there is a symmetry in x; if $\mathcal{M}$ is the invariant corresponding to this symmetry, then by (29)

$$-\frac{\partial \boldsymbol{U}}{\partial x} = J\frac{\delta \mathcal{M}}{\delta \boldsymbol{u}}\bigg|_{\boldsymbol{u}=\boldsymbol{U}}. \tag{38}$$

On the other hand, we have

$$\frac{\partial \boldsymbol{U}}{\partial t} = J\frac{\delta \mathcal{H}}{\delta \boldsymbol{u}}\bigg|_{\boldsymbol{u}=\boldsymbol{U}}. \tag{39}$$

It follows from (37), (38), and (39) that

$$J\frac{\delta\mathcal{H}}{\delta \boldsymbol{u}}\bigg|_{\boldsymbol{u}=\boldsymbol{U}} = cJ\frac{\delta\mathcal{M}}{\delta \boldsymbol{u}}\bigg|_{\boldsymbol{u}=\boldsymbol{U}} \quad \Longrightarrow \quad J\frac{\delta(\mathcal{H}-c\mathcal{M})}{\delta \boldsymbol{u}}\bigg|_{\boldsymbol{u}=\boldsymbol{U}} = 0$$

$$\Longrightarrow \quad \frac{\delta(\mathcal{H}-c\mathcal{M}+\mathcal{C})}{\delta \boldsymbol{u}}\bigg|_{\boldsymbol{u}=\boldsymbol{U}} = 0 \tag{40}$$

for some Casimir $\mathcal{C}$. Thus $\boldsymbol{U}$ is seen to be a conditional (or constrained) extremum of the invariant $\mathcal{H} - c\mathcal{M}$. We note that (40) provides a variational principle for travelling-wave solutions (cf. Benjamin 1984).

2 Hamiltonian structure of quasi-geostrophic flow

In order to illustrate the general theory of the previous section, we describe in some detail the Hamiltonian structure of what is probably the most widely-used model in theoretical geophysical fluid dynamics: quasi-geostrophic flow. Two specific such models are considered: the two-layer model in a periodic zonal β-plane channel, and continuously stratified flow over topography.

2.1 The two-layer model

The governing equations may be written (e.g. Pedlosky 1987) as

$$\frac{\partial q_i}{\partial t} + \boldsymbol{v}_i \cdot \boldsymbol{\nabla} q_i = 0 \quad [i = 1,2], \tag{41}$$

where the velocity in each layer is given by $\boldsymbol{v}_i = \hat{\mathbf{z}} \times \boldsymbol{\nabla}\psi_i$, and the potential vorticity by

$$q_i = \nabla^2\psi_i + (-1)^i F_i(\psi_1 - \psi_2) + f + \beta y \quad [i = 1,2]. \tag{42}$$

The parameter F_i is a measure of the stratification; if the layer depths are denoted D_i, then we have the geometric constraint $D_1F_1 = D_2F_2$. All fields are assumed to be periodic in x. The boundary conditions at the channel walls $y = 0, 1$ are the usual ones of no normal flow,

$$\frac{\partial\psi_i}{\partial x} = 0 \qquad \text{at } y = 0,1 \quad [i = 1,2]; \tag{43}$$

and conservation of circulation,

$$\frac{d}{dt}\int \frac{\partial\psi_i}{\partial y}\,dx\bigg|_{y=0} \equiv -\frac{d}{dt}\gamma_i^0 = 0, \qquad \frac{d}{dt}\int \frac{\partial\psi_i}{\partial y}\,dx\bigg|_{y=1} \equiv \frac{d}{dt}\gamma_i^1 = 0 \qquad [i = 1,2]. \tag{44}$$

The dynamical variables are q_1, q_2, γ_1^0, γ_1^1, γ_2^0, and γ_2^1. We can write the Hamiltonian as

$$\mathcal{H} = \iint_D \frac{1}{2}\Big\{D_1|\boldsymbol{\nabla}\psi_1|^2 + D_2|\boldsymbol{\nabla}\psi_2|^2 + D_1F_1(\psi_1 - \psi_2)^2\Big\}\,dxdy, \tag{45}$$

in which case

$$\begin{aligned}\delta\mathcal{H} &= \iint_D \Big\{ D_1 \boldsymbol{\nabla}\psi_1 \cdot \boldsymbol{\nabla}\delta\psi_1 + D_2 \boldsymbol{\nabla}\psi_2 \cdot \boldsymbol{\nabla}\delta\psi_2 + D_1 F_1 (\psi_1 - \psi_2)\delta(\psi_1 - \psi_2) \Big\}\, dxdy \\ &= \iint_D \Big\{ D_1 \boldsymbol{\nabla}\cdot(\psi_1 \boldsymbol{\nabla}\delta\psi_1) - D_1\psi_1\delta\nabla^2\psi_1 + D_2\boldsymbol{\nabla}\cdot(\psi_2\boldsymbol{\nabla}\delta\psi_2) - D_2\psi_2\delta\nabla^2\psi_2 \\ &\qquad + D_1 F_1\,\psi_1\delta(\psi_1-\psi_2) - D_2F_2\,\psi_2\delta(\psi_1-\psi_2)\Big\}\, dxdy. \end{aligned} \tag{46}$$

To obtain the last line, the relation $D_1F_1 = D_2F_2$ has been used. This gives

$$\begin{aligned}\delta\mathcal{H} &= D_1\psi_1\Big|_{y=1}\delta\gamma_1^1 + D_1\psi_1\Big|_{y=0}\delta\gamma_1^0 + D_2\psi_2\Big|_{y=1}\delta\gamma_2^1 + D_2\psi_2\Big|_{y=0}\delta\gamma_2^0 \\ &\quad - \iint_D \Big\{ D_1\psi_1\,\delta[\nabla^2\psi_1 - F_1(\psi_1-\psi_2)] + D_2\psi_2\,\delta[\nabla^2\psi_2 + F_2(\psi_1-\psi_2)]\Big\}\, dxdy, \end{aligned} \tag{47}$$

from which we may infer

$$\frac{\delta\mathcal{H}}{\delta q_i} = -D_i\psi_i \qquad \text{and} \qquad \frac{\delta\mathcal{H}}{\delta\gamma_i^{0,1}} = D_i\psi_i\Big|_{y=0,1} \quad [i=1,2]. \tag{48}$$

The functional derivatives in this system are evidently analogous to those of the barotropic system, as described in Section 1.4. Taking the dynamical variable $\boldsymbol{u}$ to be

$$\boldsymbol{u} = (q_1, q_2, \gamma_1^0, \gamma_1^1, \gamma_2^0, \gamma_2^1)^T, \tag{49}$$

the cosymplectic form J is clearly

$$J = \begin{pmatrix} -\frac{1}{D_1}\partial(q_1,\cdot) & 0 & 0&0&0&0 \\ 0 & -\frac{1}{D_2}\partial(q_2,\cdot) & 0&0&0&0 \\ 0&0&0&0&0&0 \\ 0&0&0&0&0&0 \\ 0&0&0&0&0&0 \\ 0&0&0&0&0&0 \end{pmatrix}. \tag{50}$$

The Casimirs are of the form

$$\mathcal{C}[q_1,q_2,\gamma_1^0,\gamma_1^1,\gamma_2^0,\gamma_2^1] = \iint_D \Big\{ C_1(q_1) + C_2(q_2)\Big\}\, dxdy + \sum_{i=1,2}^{j=0,1} C_i^j\,\gamma_i^j, \tag{51}$$

where the C_i's are arbitrary functions of one argument, and the C_i^j's are arbitrary scalars. It is easy to see that

$$\frac{\delta\mathcal{C}}{\delta q_i} = C_i'(q_i), \qquad \frac{\delta\mathcal{C}}{\delta\gamma_i^j} = C_i^j, \tag{52}$$

whence the condition (11) is verified. To find the steady states, we must solve the following extremal equations: for q_i,

$$\frac{\delta\mathcal{H}}{\delta q_i} = -\frac{\delta\mathcal{C}}{\delta q_i} \qquad \Longrightarrow \qquad D_i\psi_i = C_i'(q_i), \tag{53}$$

which implies $\psi_i = \psi_i(q_i)$; and for γ_i^j,

$$\frac{\delta \mathcal{H}}{\delta \gamma_i^j} = -\frac{\delta \mathcal{C}}{\delta \gamma_i^j} \qquad \Longrightarrow \qquad D_i \psi_i \Big|_{y=j} = -C_i^j, \tag{54}$$

which implies that ψ_i is constant along the boundaries.

To find the zonal momentum invariant $\mathcal{M}$, we must solve the equations

$$\frac{\partial q_1}{\partial x} = \frac{1}{D_1}\partial(q_1, \frac{\delta \mathcal{M}}{\delta q_1}), \qquad \frac{\partial q_2}{\partial x} = \frac{1}{D_2}\partial(q_2, \frac{\delta \mathcal{M}}{\delta q_2}) \tag{55}$$

simultaneously. Note that there is no continuous symmetry for γ_i^j. The solution (to within a Casimir) of (55) is evidently

$$\frac{\delta \mathcal{M}}{\delta q_i} = D_i y \qquad \Longrightarrow \qquad \mathcal{M} = \iint_D \left\{ D_1 y q_1 + D_2 y q_2 \right\} dxdy, \tag{56}$$

again analogous to the barotropic case. Using the definition of q_i,

$$\begin{aligned} \mathcal{M} &= \iint_D y\Big\{ D_1\big(\frac{\partial^2 \psi_1}{\partial x^2} + \frac{\partial^2 \psi_1}{\partial y^2}\big) + D_2\big(\frac{\partial^2 \psi_2}{\partial x^2} + \frac{\partial^2 \psi_2}{\partial y^2}\big) + (D_1 + D_2)(f + \beta y)\Big\}\, dxdy \\ &= \Big[y \int \big(D_1 \frac{\partial \psi_1}{\partial y} + D_2 \frac{\partial \psi_2}{\partial y} \big) dx \Big]_{y=0}^{y=1} - \iint_D \Big\{ D_1 \frac{\partial \psi_1}{\partial y} + D_2 \frac{\partial \psi_2}{\partial y} \Big\}\, dxdy + \text{const.} \\ &= D_1 \gamma_1^1 + D_2 \gamma_2^1 + \iint_D (D_1 u_1 + D_2 u_2)\, dxdy + \text{const.} \end{aligned} \tag{57}$$

The first two terms of the above expression are Casimirs, while the spatial integral represents the zonal momentum.

2.2 Continuously stratified flow over topography

In the above sub-section we have shown how to handle the circulation terms on the side walls, so to simplify the following manipulations we now restrict our attention to the case where the circulation is held fixed when performing the variations. We again consider a periodic zonal channel, bounded top and bottom by rigid lids, with $0 \le z \le 1$. The dynamics is given by (e.g. Pedlosky 1987)

$$\frac{Dq}{Dt} \equiv \frac{\partial q}{\partial t} + \partial(\psi, q) = 0 \quad [0 < z < 1], \tag{58}$$

$$\frac{D}{Dt}(\psi_z + fSh) = 0 \quad [z = 0], \qquad \frac{D}{Dt}(\psi_z) = 0 \quad [z = 1], \tag{59}$$

where the potential vorticity q is defined by

$$q = \psi_{xx} + \psi_{yy} + \frac{1}{\rho_s}\Big(\frac{\rho_s}{S}\psi_z\Big)_z + f + \beta y. \tag{60}$$

The density $\rho_s(z)$ and stratification function $S(z) = N^2/f^2$ (where $N(z)$ is the buoyancy frequency) are both prescribed, $h(x, y)$ is the topography at the lower surface, and ψ_z is proportional to the temperature.

The dynamical boundary conditions (59) on the lids $z = 0, 1$ are necessary, and represent true degrees of freedom. This can be seen by varying $\mathcal{H}$:

$$\mathcal{H} = \iiint_D \frac{\rho_s}{2}\Big\{|\nabla\psi|^2 + \frac{1}{S}\psi_z^2\Big\}\,dxdydz \tag{61}$$

implies

$$\begin{aligned}
\delta\mathcal{H} &= \iiint_D \rho_s\Big\{\nabla\psi\cdot\nabla\delta\psi + \frac{1}{S}\psi_z\delta\psi_z\Big\}\,dxdydz \\
&= \iiint_D \Big\{-\rho_s\psi\delta\nabla^2\psi + \frac{\partial}{\partial z}\Big(\frac{\rho_s}{S}\psi\delta\psi_z\Big) - \psi\frac{\partial}{\partial z}\Big(\frac{\rho_s}{S}\delta\psi_z\Big)\Big\}\,dxdydz \\
&= \Big[\iint \frac{\rho_s}{S}\,\psi\delta\psi_z\,dxdy\Big]_{z=0}^{z=1} - \iiint_D \rho_s\psi\delta q\,dxdydz
\end{aligned} \tag{62}$$

(noting that the variations in the side-wall circulations have been taken to vanish). In particular, we cannot write $\delta\mathcal{H} = \langle(\delta\mathcal{H}/\delta q), \delta q\rangle$ unless we treat the terms in (62) involving the spatial integrals over the lids.

One option is to make the lids isentropic: $\psi_z =$ constant. Then in a completely analogous fashion to the way in which one may eliminate the circulation terms, one may restrict attention to variations with $\delta\psi_z = 0$ on $z = 0, 1$, in which case the integrals over the lids in (62) disappear. Note that this is dynamically self-consistent: from the governing equations, it follows that isentropic lids remain isentropic under the dynamics. Pursuing this option leaves us with a dynamical structure very similar to that of the barotropic system, but this is very restrictive indeed. For example, it eliminates the meridional temperature gradient at the lower surface which is so crucial in driving the atmospheric circulation.

A better option is to incorporate the terms in question into $\delta\mathcal{H}$. This can be done by introducing additional dynamical variables, just as one may introduce the side-wall circulations as dynamical variables (see previous sub-section). It is natural to define

$$\lambda_0 = \frac{\rho_s}{S}(\psi_z + fSh)\Big|_{z=0}, \qquad \lambda_1 = \frac{\rho_s}{S}\psi_z\Big|_{z=1}, \tag{63}$$

in which case (59) take the form

$$\frac{D\lambda_0}{Dt} = 0, \qquad \frac{D\lambda_1}{Dt} = 0. \tag{64}$$

Then (62) can be written

$$\delta\mathcal{H} = \iint \psi\,\delta\lambda_1\,dxdy\Big|_{z=1} - \iint \psi\,\delta\lambda_0\,dxdy\Big|_{z=0} - \iiint_D \rho_s\psi\,\delta q\,dxdydz; \tag{65}$$

the entire variation of $\mathcal{H}$ is now captured, with the functional derivatives

$$\frac{\delta\mathcal{H}}{\delta q} = -\rho_s\psi, \qquad \frac{\delta\mathcal{H}}{\delta\lambda_0} = -\psi\Big|_{z=0}, \qquad \frac{\delta\mathcal{H}}{\delta\lambda_1} = \psi\Big|_{z=1}. \tag{66}$$

Taking the dynamical variable to be $\boldsymbol{u} = (q, \lambda_0, \lambda_1)^T$, the cosymplectic form is evidently

$$J = \begin{pmatrix} -\frac{1}{\rho_s}\partial(q,\cdot) & 0 & 0 \\ 0 & -\partial(\lambda_0,\cdot) & 0 \\ 0 & 0 & \partial(\lambda_1,\cdot) \end{pmatrix}. \tag{67}$$

The Casimirs are clearly of the form

$$\mathcal{C}[q,\lambda_0,\lambda_1] = \iiint_D \rho_s C(q)\,dxdydz + \iint C_0(\lambda_0)\,dxdy\Big|_{z=0} + \iint C_1(\lambda_1)\,dxdy\Big|_{z=1} \tag{68}$$

for arbitrary functions C, C_0, and C_1, with

$$\frac{\delta\mathcal{C}}{\delta q} = \rho_s C'(q), \qquad \frac{\delta\mathcal{C}}{\delta\lambda_0} = C_0'(\lambda_0), \qquad \frac{\delta\mathcal{C}}{\delta\lambda_1} = C_1'(\lambda_1), \tag{69}$$

which when combined with (67) may be seen to satisfy (11).

The steady-state solutions satisfy

$$\frac{\delta\mathcal{H}}{\delta q} = -\frac{\delta\mathcal{C}}{\delta q}, \tag{70}$$

which implies $\rho_s\psi = \rho_s C'(q)$ and thus $\psi = \psi(q)$; and

$$\frac{\delta\mathcal{H}}{\delta\lambda_i} = -\frac{\delta\mathcal{C}}{\delta\lambda_i} \quad [i=0,1], \tag{71}$$

which implies $(-1)^i\psi = C_i'(\lambda_i)$ and thus $\psi = \psi(\lambda_i)$ on $z = i$.

To find the zonal momentum invariant $\mathcal{M}$, we must solve the equations

$$\frac{\partial q}{\partial x} = \frac{1}{\rho_s}\partial\Big(q, \frac{\delta\mathcal{M}}{\delta q}\Big), \qquad \frac{\partial\lambda_0}{\partial x} = \partial\Big(\lambda_0, \frac{\delta\mathcal{M}}{\delta\lambda_0}\Big), \qquad \frac{\partial\lambda_1}{\partial x} = -\partial\Big(\lambda_1, \frac{\delta\mathcal{M}}{\delta\lambda_1}\Big) \tag{72}$$

simultaneously; the solution (to within a Casimir) is

$$\mathcal{M} = \iiint_D \rho_s yq\,dxdydz + \iint y\lambda_0\,dxdy\Big|_{z=0} - \iint y\lambda_1\,dxdy\Big|_{z=1}. \tag{73}$$

Exercise: Show that (to within a Casimir) $\mathcal{M} = \iiint_D \rho_s u\,dxdydz$.

3 Pseudoenergy and available potential energy

3.1 Disturbances to basic states

Very often one is interested in flows that are close to some given basic state. Examples include the energetics of waves, stability and instability of basic flows, wave propagation in inhomogeneous media, and wave, mean-flow interaction. We would therefore like a Hamiltonian description of the *disturbance* problem. Ideally it should be exact, i.e. nonlinear. Two questions immediately arise: What is the correct Hamiltonian? What is the energy? The answer to these questions involves a new quantity, often referred to as the *pseudoenergy*. One of the simplest contexts in which the relevant issues arise is the familiar and classical one of available potential energy (APE), so we shall discuss it at some length. Further details may be found in Shepherd (1993*a*).

3.2 APE of internal gravity waves

Consider the energy of internal gravity waves in an incompressible, Boussinesq fluid, governed by the equations

$$\boldsymbol{v}_t + (\boldsymbol{v}\cdot\boldsymbol{\nabla})\boldsymbol{v} + f\hat{\mathbf{z}}\times\boldsymbol{v} = -\frac{\boldsymbol{\nabla}p}{\rho_{00}} - \frac{\rho}{\rho_{00}}g\hat{\mathbf{z}}, \tag{74}$$

$$\rho_t + \boldsymbol{v}\cdot\boldsymbol{\nabla}\rho = 0, \qquad \boldsymbol{\nabla}\cdot\boldsymbol{v} = 0, \tag{75}$$

where ρ_{00} is a constant reference density. The notation is standard. The resting basic state on which the waves exist is assumed to have a horizontally uniform density $\rho = \rho_0(z)$, with stable stratification: $g(d\rho_0/dz) < 0$. The kinetic and the potential energy per unit volume are given by

$$E_K = \frac{1}{2}\rho_{00}|\boldsymbol{v}|^2, \qquad E_P = \rho g z. \tag{76}$$

Since it integrates to a constant, we might as well remove $\rho_0 gz$ from the potential energy. This leaves

$$E_P = (\rho - \rho_0)gz. \tag{77}$$

Now, for small-amplitude waves, $E_K = \mathcal{O}(a^2)$ but $E_P = \mathcal{O}(a)$, where $a \ll 1$ is the wave amplitude. This is odd, for a number of reasons. First, $E_K \ll E_P$, which is counter-intuitive (one expects the two forms of energy to be of the same order); second, E_P is not sign-definite; and third, the disturbance energy cannot be calculated to leading order from linear theory. To see this, consider a solution involving a perturbation expansion in some small parameter ε:

$$\rho - \rho_0 = \varepsilon\rho_1 + \varepsilon^2\rho_2 + \ldots, \qquad \boldsymbol{v} = \varepsilon\boldsymbol{v}_1 + \varepsilon^2\boldsymbol{v}_2 + \ldots. \tag{78}$$

The subscript 1 variables would be determined from linear theory, the subscript 2 variables from second-order nonlinear theory, and so on. Expanding the energies in terms of ε yields

$$E_K = \frac{1}{2}\rho_{00}|\boldsymbol{v}_1|^2\varepsilon^2 + \mathcal{O}(\varepsilon^3), \qquad E_P = \rho_1 gz\varepsilon + \rho_2 gz\varepsilon^2 + \mathcal{O}(\varepsilon^3). \tag{79}$$

If we are considering sinusoidal waves then $\overline{\rho_1} = 0$ but $\overline{\rho_2} \neq 0$ in general, where the overbar denotes an average over phase. Therefore to determine E_P at leading order, $\overline{\rho_2}$ must be determined; but this requires a solution of the nonlinear problem.

All these difficulties arise from the fact that the expression for E_P is formally $\mathcal{O}(a)$. Fortunately, however, there is a remedy. Traditionally (e.g. Holliday & McIntyre 1981) it is presented as a trick. For incompressible fluids, (75) implies that $\iiint_D F(\rho)\,dxdydz$ is conserved for any function $F(\cdot)$. For a statically stable basic state $\rho_0(z)$, the inverse function $z = Z(\rho_0(z))$ is well defined. We may then take

$$F(\rho) = -\int^{\rho} gZ(\tilde{\rho})\,d\tilde{\rho}, \tag{80}$$

and note that

$$\iiint_D \left\{E_K + E_P + F(\rho) - F(\rho_0)\right\} dxdydz \tag{81}$$

is conserved. That is, we combine energy conservation with mass conservation, to obtain a new conserved quantity with density per unit volume given by

$$\begin{aligned} A &= E_K + E_P + F(\rho) - F(\rho_0) \\ &= \frac{1}{2}\rho_{00}|\boldsymbol{v}|^2 + (\rho-\rho_0)gz - \int_{\rho_0}^{\rho} gZ(\tilde{\rho})\,d\tilde{\rho} \\ &= \frac{1}{2}\rho_{00}|\boldsymbol{v}|^2 + (\rho-\rho_0)gz - \int_{0}^{\rho-\rho_0} gZ(\rho_0+\tilde{\rho})\,d\tilde{\rho} \\ &= \frac{1}{2}\rho_{00}|\boldsymbol{v}|^2 - \int_{0}^{\rho-\rho_0} g\left[Z(\rho_0+\tilde{\rho}) - Z(\rho_0)\right]\,d\tilde{\rho}. \end{aligned} \tag{82}$$

The small-amplitude approximation to A (appropriate for waves, say) is

$$A \approx \frac{1}{2}\rho_{00}|\boldsymbol{v}|^2 - \frac{1}{2}gZ'(\rho_0)(\rho-\rho_0)^2 = \frac{1}{2}\rho_{00}|\boldsymbol{v}|^2 - \frac{1}{2}\frac{g}{\rho_0'(z)}(\rho-\rho_0)^2. \tag{83}$$

The second term in (83) is the familiar expression for the APE of internal gravity waves (see e.g. Gill 1982, §6.7 or Lighthill 1978, §4.1). The conserved quantity A has the properties we would expect from a disturbance energy: $A = \mathcal{O}(a^2)$; $A > 0$ if the background is stably stratified (this is also true at finite amplitude); and A is calculable to leading order from the linearized solution. In textbooks, the small-amplitude form is derived by direct manipulation of the linearized equations — thereby obscuring the fact that mass conservation has been used.

Other cases where a similar situation arises include the energy of acoustic waves (Lighthill 1978, §1.3) and the APE of a hydrostatic compressible ideal gas (Lorenz 1955).

3.3 Pseudoenergy

When one considers the wide variety of situations in which the concept of APE arises, certain questions naturally arise. In particular: Why do other conservation laws (like mass conservation) need to be brought in? Which conservation laws are needed? Is there a systematic way to construct the APE? Does the concept extend to arbitrary fluid systems? And does it extend to non-resting basic states?

It turns out that these questions can all be answered by considering things within the Hamiltonian framework. Since fluid systems are generally non-canonical, perturbing a steady state $\boldsymbol{U}$ with a variation $\delta\boldsymbol{u}$ will give rise to a change in the Hamiltonian

$$\Delta\mathcal{H}[\boldsymbol{U};\delta\boldsymbol{u}] = \mathcal{H}[\boldsymbol{U}+\delta\boldsymbol{u}] - \mathcal{H}[\boldsymbol{U}] = \Big\langle \underbrace{\left.\frac{\delta\mathcal{H}}{\delta\boldsymbol{u}}\right|_{\boldsymbol{u}=\boldsymbol{U}}}_{\neq 0}, \delta\boldsymbol{u}\Big\rangle + \mathcal{O}((\delta\boldsymbol{u})^2). \tag{84}$$

This is the reason why there is an $\mathcal{O}(\delta\boldsymbol{u}) = \mathcal{O}(a)$ term in the expression for potential energy. For canonical systems, the underbraced term would vanish and the change in the Hamiltonian would automatically be quadratic in the disturbance amplitude. This is not the case here, but we know that generically there exists some Casimir $\mathcal{C}$ such that

$$\left.\frac{\delta\mathcal{H}}{\delta\boldsymbol{u}}\right|_{\boldsymbol{u}=\boldsymbol{U}} = -\left.\frac{\delta\mathcal{C}}{\delta\boldsymbol{u}}\right|_{\boldsymbol{u}=\boldsymbol{U}}. \tag{85}$$

So if we choose

$$\mathcal{A}[\boldsymbol{U};\delta\boldsymbol{u}] = \mathcal{H}[\boldsymbol{U}+\delta\boldsymbol{u}] - \mathcal{H}[\boldsymbol{U}] + \mathcal{C}[\boldsymbol{U}+\delta\boldsymbol{u}] - \mathcal{C}[\boldsymbol{U}], \tag{86}$$

with $\mathcal{C}$ determined by (85), then we will have a quantity which by construction satisfies

$$\mathcal{A}[\boldsymbol{U};\boldsymbol{0}] = 0 \qquad \text{and} \qquad \left.\frac{\delta\mathcal{A}}{\delta\boldsymbol{u}}\right|_{\boldsymbol{u}=\boldsymbol{U}} = \left.\left(\frac{\delta\mathcal{H}}{\delta\boldsymbol{u}} + \frac{\delta\mathcal{C}}{\delta\boldsymbol{u}}\right)\right|_{\boldsymbol{u}=\boldsymbol{U}} = 0. \tag{87}$$

Hence $\mathcal{A}[\boldsymbol{U};\delta\boldsymbol{u}] = \mathcal{O}((\delta\boldsymbol{u})^2)$, and we have what we want.

This quantity $\mathcal{A}$ is the pseudoenergy (e.g. McIntyre & Shepherd 1987). It is an exact nonlinear invariant of the equations of motion. Its construction involves a combination of energy *and* a suitable Casimir. For disturbances to resting basic states, these Casimirs invariably involve mass conservation. The available potential energy is evidently the non-kinetic part of the pseudoenergy. To construct the available potential energy, therefore, we need only know the Hamiltonian $\mathcal{H}$; the dynamic variables, i.e. the fields $\boldsymbol{u}$; and suitable Casimirs $\mathcal{C}$ such that (85) is satisfied. One may well know these things without knowing J, in which case the Hamiltonian structure underlies the method without appearing explicitly.

Prescient adumbrations of the above realization can be found in the classical GFD literature. In a brilliant and now largely forgotten paper, Fjørtoft (1950) noted that (stably) stratified, resting basic states were energy extrema for adiabatic disturbances; this variational principle corresponds to the Hamiltonian statement that resting steady states are conditional extrema of the Hamiltonian, with the relevant Casimirs being those arising from the material conservation of entropy. Building on Fjørtoft's work, Van Mieghem (1956) used this variational principle to construct a small-amplitude expression for APE, thereby recovering the formula of Lorenz (1955). This can now be seen as the non-kinetic part of the small-amplitude (or quadratic) pseudoenergy.

Having examined this problem from the Hamiltonian standpoint, the questions raised at the beginning of this sub-section may be answered immediately.

Question: Why is energy not good enough? Why do other conservation laws (like mass conservation) need to be brought in?

Answer: Because the Eulerian descriptions of fluid motion are generally non-canonical, which means that steady states are not necessarily energy extrema.

Question: Which conservation laws are needed?

Answer: Those associated with the non-canonical nature of the dynamics: the Casimir invariants.

Question: Is there a systematic way to construct the APE?

Answer: The APE is the non-kinetic part of the pseudoenergy relative to a resting basic state.

Question: Does the concept extend to arbitrary fluid systems?

Answer: Yes, provided the system is Hamiltonian.

Question: And does it extend to non-resting basic states?

Answer: In principle, yes — provided the pseudoenergy is sign-definite. See Section 4.3 for further discussion.

3.4 Example: stratified Boussinesq flow

The algorithm described above for constructing the APE will now be demonstrated in the context of 3-D, incompressible, stratified, Boussinesq flow, governed by (74,75). The dynamical variables are evidently ρ and $\boldsymbol{v}$. The Hamiltonian is given by

$$\mathcal{H} = \iiint_D \left\{ \frac{1}{2}\rho_{00}|\boldsymbol{v}|^2 + \rho g z \right\} dxdydz, \tag{88}$$

with functional derivatives

$$\frac{\delta \mathcal{H}}{\delta \boldsymbol{v}} = \rho_{00}\boldsymbol{v}, \qquad \frac{\delta \mathcal{H}}{\delta \rho} = gz. \tag{89}$$

The determination of an appropriate J gets us into the issue of constrained dynamics (see Abarbanel *et al.* 1986; also Salmon 1988*a*), but for our purposes only the invariants $\mathcal{H}$ and $\mathcal{C}$ are required. An unconstrained Hamiltonian representation of this system, in the form (1), can be obtained by working in isentropic — or, in this case, isopycnal — coordinates (Holm & Long 1989), but for applications it is desirable to have an expression for APE in physical coordinates.

What are the Casimirs for this system? It can be verified that the potential vorticity $q = \boldsymbol{\omega} \cdot \boldsymbol{\nabla}\rho$, where $\boldsymbol{\omega} = \boldsymbol{\nabla} \times \boldsymbol{v}$, satisfies

$$q_t + \boldsymbol{v} \cdot \boldsymbol{\nabla} q = 0. \tag{90}$$

Putting (90) together with (75) implies that

$$\mathcal{C}[\boldsymbol{v}, \rho] = \iiint_D C(\rho, q)\, dxdydz \tag{91}$$

is a class of conserved quantities for arbitrary functions C. These are in fact the Casimirs, as can be verified by examining the system in isopycnal coordinates. However, such verification is not actually necessary: usually one can guess the Casimirs based on knowledge of the materially conserved quantities; if one cannot satisfy the condition (85), then one must consider a broader class of conserved functionals.

Taking the first variation of $\mathcal{C}$ gives

$$\begin{aligned} \delta \mathcal{C} &= \iiint_D \left\{ C_\rho \delta\rho + C_q \delta q \right\} dxdydz \\ &= \iiint_D \left\{ C_\rho \delta\rho + C_q [(\boldsymbol{\nabla} \times \delta\boldsymbol{v}) \cdot \nabla\rho + \boldsymbol{\omega} \cdot \boldsymbol{\nabla}\delta\rho] \right\} dxdydz. \end{aligned} \tag{92}$$

After integration by parts, one obtains

$$\frac{\delta \mathcal{C}}{\delta \rho} = C_\rho - \boldsymbol{\nabla} \cdot (C_q \boldsymbol{\omega}), \qquad \frac{\delta \mathcal{C}}{\delta \boldsymbol{v}} = \boldsymbol{\nabla} \times (C_q \boldsymbol{\nabla}\rho). \tag{93}$$

We may now follow the recipe set forth earlier. Given a steady state $\boldsymbol{U} = (\boldsymbol{0}, \rho_0(z))$, $\mathcal{C}$ is determined from the condition

$$\begin{aligned} \left.\frac{\delta \mathcal{H}}{\delta \boldsymbol{v}}\right|_{\boldsymbol{u}=\boldsymbol{U}} = -\left.\frac{\delta \mathcal{C}}{\delta \boldsymbol{v}}\right|_{\boldsymbol{u}=\boldsymbol{U}} &\iff \rho_{00}\boldsymbol{v} = -\boldsymbol{\nabla} \times (C_q \boldsymbol{\nabla}\rho) \quad \text{at} \quad \rho = \rho_0,\ \boldsymbol{v} = \boldsymbol{0} \\ &\iff \boldsymbol{0} = \boldsymbol{\nabla} \times (C_q \boldsymbol{\nabla}\rho_0), \end{aligned} \tag{94}$$

which will be satisfied if we take $C = C(\rho)$, in conjunction with the condition

$$\left.\frac{\delta \mathcal{H}}{\delta \rho}\right|_{\boldsymbol{u}=\boldsymbol{U}} = -\left.\frac{\delta \mathcal{C}}{\delta \rho}\right|_{\boldsymbol{u}=\boldsymbol{U}} \quad \Longleftrightarrow \quad gz = -C_\rho + \boldsymbol{\nabla}\cdot(C_q\boldsymbol{\omega}) \quad \text{at} \quad \rho = \rho_0, \boldsymbol{v} = \boldsymbol{0}$$
$$\Longleftrightarrow \quad gz = -C_\rho \quad \text{at} \quad \rho = \rho_0. \tag{95}$$

Now $\rho_0(z)$, being monotonic by hypothesis, has a well-defined inverse, Z: i.e. $z = Z(\rho_0(z))$. It can be easily seen that

$$C(\rho) = -\int^\rho gZ(\tilde{\rho})\, d\tilde{\rho} \tag{96}$$

satisfies the required condition (95):

$$C_\rho\big|_{\rho=\rho_0} = -gZ(\rho_0) = -gz. \tag{97}$$

(It is in fact a general result that when the basic state is at rest, only that part of the Casimir depending on the density (or more generally, the entropy) needs to be considered; possible dependence on the potential vorticity is not required (see Shepherd 1993*a*). This is why Fjørtoft's (1950) variational principle could describe all resting steady states.)

With this choice of C, the pseudoenergy takes the form

$$\begin{aligned}
\mathcal{A} &= \mathcal{H}[\boldsymbol{v},\rho] - \mathcal{H}[\boldsymbol{0},\rho_0] + \mathcal{C}[\boldsymbol{v},\rho] - \mathcal{C}[\boldsymbol{0},\rho_0] \\
&= \iiint_D \Big\{\tfrac{1}{2}\rho_{00}|\boldsymbol{v}|^2 + (\rho-\rho_0)gz - \int_{\rho_0}^{\rho} gZ(\tilde{\rho})\, d\tilde{\rho}\Big\}\, dxdydz \\
&= \iiint_D \Big\{\tfrac{1}{2}\rho_{00}|\boldsymbol{v}|^2 + (\rho-\rho_0)gZ(\rho_0) - \int_0^{\rho-\rho_0} gZ(\rho_0+\tilde{\rho})\, d\tilde{\rho}\Big\}\, dxdydz \\
&= \iiint_D \Big\{\tfrac{1}{2}\rho_{00}|\boldsymbol{v}|^2 \underbrace{- \int_0^{\rho-\rho_0} g[Z(\rho_0+\tilde{\rho}) - Z(\rho_0)]\, d\tilde{\rho}}_{\text{APE}}\Big\}\, dxdydz.
\end{aligned} \tag{98}$$

This recovers the expression (82) obtained earlier by direct methods. Note that provided $g(d\rho_0/dz) < 0$, then $g(dZ/d\rho_0) < 0$; thus the APE, and in consequence $\mathcal{A}$ itself, will necessarily be positive definite for $\rho - \rho_0 \neq 0$.

The finite-amplitude expression for APE provided above has a simple geometrical interpretation: the APE is g times the area under the curve $Z(\rho)$ (see below).

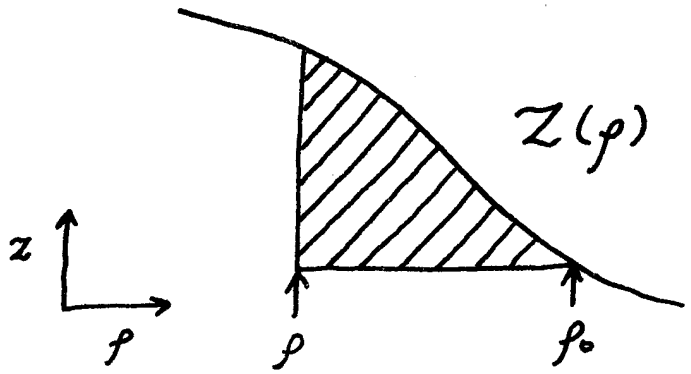

3.5 Nonlinear static stability

The existence of a positive definite conserved quantity suggests stability. Of course, the condition $g(d\rho_0/dz) < 0$ is precisely the condition for static stability. Note that $\delta\mathcal{A} = 0$ by construction while the second variation of $\mathcal{A}$ is

$$\delta^2\mathcal{A} = \iiint_D \frac{1}{2}\Big\{\rho_{00}|\delta\boldsymbol{v}|^2 - \frac{g}{\rho_0'(z)}(\delta\rho)^2\Big\}\,dxdydz \;>\; 0. \tag{99}$$

Thus by analogy with finite-dimensional systems, statically stable equilibria are elliptic fixed points. This is what is usually referred to as *formal stability* (e.g. Holm *et al.* 1985; see also Morrison's lectures). However, for infinite-dimensional (or continuous) dynamical systems, such as fluids, mere positivity of the second variation does not, in itself, establish anything about stability. Instead, one must attempt to obtain explicit bounds on the growth of disturbance norms. One might think it wise to begin with the linearized equations; however, if stability is established in the linear dynamics this proves nothing for the actual dynamics, since the system is Hamiltonian. (Stability can never be asymptotic for Hamiltonian systems.) Thus one is forced to consider the full nonlinear dynamics right from the start.

Definition: (Normed Stability) If we measure the deviation from a particular steady field $\boldsymbol{U}$ by the norm $||\boldsymbol{u}'||$, where $\boldsymbol{u} = \boldsymbol{U} + \boldsymbol{u}'$, then $\boldsymbol{U}$ is *stable* in that norm if for any $\epsilon > 0$ there exists a $\delta(\epsilon) > 0$ such that

$$||\boldsymbol{u}'(0)|| < \delta \quad \Longrightarrow \quad ||\boldsymbol{u}'(t)|| < \epsilon\,, \qquad \forall t \geq 0. \tag{100}$$

This is also called *Liapunov stability*.

In the present context we may define our norm by

$$||(\boldsymbol{v}, \rho - \rho_0)||^2 = \iiint_D \frac{1}{2}\Big\{\rho_{00}|\boldsymbol{v}|^2 + \lambda(\rho - \rho_0)^2\Big\}\,dxdydz, \tag{101}$$

$$\text{with} \quad c_1 \leq \lambda \leq c_2 \quad \text{where} \quad \begin{cases} c_1 &= \min\{-gZ'(\rho_0)\} > 0 \\ c_2 &= \max\{-gZ'(\rho_0)\} < \infty. \end{cases} \tag{102}$$

The existence of such constants c_1, c_2 will be referred to as the *convexity condition*. Under these circumstances it can be shown that the available potential energy,

$$\text{APE} = -\int_0^{\rho-\rho_0} g[Z(\rho_0 + \tilde{\rho}) - Z(\rho_0)]\,d\tilde{\rho}, \tag{103}$$

is bounded from both above and below:

$$\frac{1}{2}c_1(\rho - \rho_0)^2 \leq \text{ APE } \leq \frac{1}{2}c_2(\rho - \rho_0)^2. \tag{104}$$

If $Z(\rho_0)$ is smooth then this result follows immediately from Taylor's remainder theorem. However, it is true for $Z(\rho_0)$ that are only piecewise differentiable. This bound on the APE,

coupled with the fact that the pseudoenergy $\mathcal{A}$ is conserved, leads to the following chain of inequalities for basic flows satisfying the convexity condition (102):

$$\begin{aligned} ||(\boldsymbol{v}, \rho - \rho_0)(t)||^2 &= \iiint_D \frac{1}{2}\Big\{\rho_{00}|\boldsymbol{v}|^2 + \lambda(\rho - \rho_0)^2\Big\}(t)\, dxdydz \\ &\leq \frac{\lambda}{c_1}\mathcal{A}(t) = \frac{\lambda}{c_1}\mathcal{A}(0) \leq \frac{c_2}{c_1}||(\boldsymbol{v}, \rho - \rho_0)(0)||^2. \end{aligned} \tag{105}$$

By taking $\delta = \sqrt{c_1/c_2}\epsilon$, (105) proves nonlinear normed stability in the norm defined by (101).

It is well known that the small-amplitude definition of APE is closely connected to linearized static stability. The above results show that the definition of *finite-amplitude* APE is closely connected to *finite-amplitude* static stability.

A comment should be made concerning the definition of the function $Z(\cdot)$ used to calculate the pseudoenergy, which appears in the integrand of expression (103) for the APE. What if ρ lies outside the range of ρ_0? How do we evaluate $Z(\rho)$ in that case? First note that if a disturbance is "dynamically accessible" (see Morrison's lectures) then ρ always lies within the range of ρ_0. However if one is interested in a larger class of disturbances, then the definition of $Z(\rho)$ can be extended outside the range of ρ_0 while still keeping $\mathcal{A}$ as a conserved quantity. This is because *any* function $C(\rho)$ can be used to obtain a Casimir. In fact, it is only the condition that $\mathcal{A} = \mathcal{O}(a^2)$ in the small-amplitude limit that determined the particular choice of C involving Z, and this constraint only determines C for values of its argument lying within the range of ρ_0. So to allow the possibility of arbitrary disturbances, the expression (103) can still be used provided we extend the function $Z(\rho)$ outside the range of ρ_0 in some arbitrary way, subject only to

$$c_1 \leq -gZ'(\rho) \leq c_2 \tag{106}$$

in order not to weaken our bounds. Clearly, this extension can always be made.

3.6 Nonlinear saturation of instabilities

The APE provides a rigorous upper bound on the saturation of static instabilities. In a way, this is a more robust definition of static stability than the concept of normed stability presented in the previous sub-section.

To see this, consider the case of a fluid that is initially at rest but statically unstable. We may consider this initial state to be a (finite-amplitude) disturbance to some statically stable, resting basic state. Using conservation of the pseudoenergy relative to this basic state, and noting that $\boldsymbol{v}(t=0) = \mathbf{0}$ by hypothesis, yields

$$\iiint_D \frac{1}{2}\rho_{00}|\boldsymbol{v}|^2(t)\, dxdydz \leq \mathcal{A}(t) = \mathcal{A}(0) = \iiint_D APE(0)\, dxdydz. \tag{107}$$

Thus the kinetic energy at any time t is bounded from above by the initial APE: this is, after all, why it was called "available" by Lorenz. For example, consider the situation sketched below.

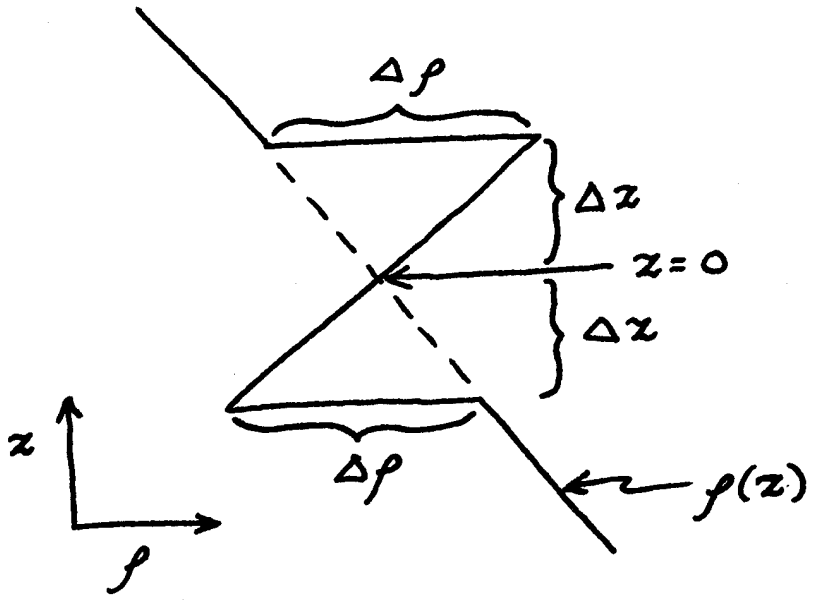

The initial density profile $\rho(z)$ is shown by the solid line, and consists of a statically unstable inversion layer $-\Delta z \le z \le \Delta z$ located within a stably stratified region with $d\rho/dz = -r$. Suppose for definiteness that $\rho(z=0) = 0$. (Recall that ρ is the departure from the reference state ρ_{00}, and therefore may be negative.) One may choose as the basic state $\rho_0(z) = -rz$, which is stable and which satisfies (102) with $c_1 = c_2 = g/r$. The initial disturbance is then

$$\rho' = \rho - \rho_0 = \begin{cases} \dfrac{\Delta\rho}{\Delta z} z, & \text{if } -\Delta z \le z \le \Delta z \\ 0, & \text{otherwise .} \end{cases} \tag{108}$$

The integrated APE (averaged in x and y) is then easily computed, yielding the saturation bound

$$\iiint_D \frac{1}{2}\rho_{00}|\boldsymbol{v}|^2(t)\, dxdydz \le \frac{g}{3r}(\Delta\rho)^2\Delta z. \tag{109}$$

It is interesting to note here that the disturbance ρ' is not, in general, dynamically accessible; or, rather, the initial condition $\rho(t=0)$ is not dynamically accessible from the basic state $\rho_0(z)$. It would only be so in the special case $\Delta\rho/\Delta z = r$. The bound represented by (109) therefore highlights the fact that pseudoenergy conservation holds for *arbitrary* disturbances, not just dynamically accessible ones. It also demonstrates that, in many practical cases of interest, the freedom to consider disturbances that are not dynamically accessible is quite useful. The original, physical definition of APE proposed by Margules (1903) and formalized by Lorenz (1955) was keyed around the idea of dynamically accessible perturbations: the APE was defined to be the amount of energy released in an adiabatic rearrangement of the mass into a statically stable state. The variational approach of Fjørtoft (1950) and Van Mieghem (1956) likewise builds dynamical accessibility directly into the theory. In contrast, the use of integral invariants, in particular the pseudoenergy, goes beyond this in a powerful

way: the basic state may be *any* statically stable state, not just the dynamically accessible one. This insight was first noted by Holliday & McIntyre (1981) and Andrews (1981), and is vividly demonstrated by the above example.

One may logically define the APE in (107) to be the minimum APE over all possible choices of the stable basic state. This extremization problem is highly non-trivial, and would make a good topic for further study from a mathematical perspective. In the above example, for instance, the expression (109) is merely one bound, not necessarily the minimum one.

Exercise: Calculate the amount of APE in the initial condition of the above example, taking the basic state $\rho_0(z)$ to be the unique, dynamically accessible state obtained through an adiabatic rearrangement of the mass.

There is a well-known analogy between static stability and so-called *symmetric stability*: namely the stability of a baroclinic flow to disturbances that do not vary in the downstream direction (also known as "slantwise convection"). This analogy has recently been exploited by Cho, Shepherd & Vladimirov (1993), who prove a nonlinear stability theorem and use it to determine a finite-amplitude APE for such motion.

4 Pseudoenergy and Arnol'd's stability theorems

4.1 Arnol'd's stability theorems

In the previous section the steady basic state was at rest, so the kinetic energy contribution to the pseudoenergy was solely the disturbance kinetic energy. But what happens when the kinetic energy of the steady state is nonzero? To explore this question, we study the barotropic vorticity equation on the β-plane (cf. §1.4)

$$P_t + \partial(\Phi, P) = 0, \tag{110}$$

where Φ is the stream function, P is the potential vorticity

$$P = \nabla^2\Phi + f + \beta y + h(x,y), \tag{111}$$

and h is the topographic height. Three possible geometries are considered: (i) periodic in x and y; (ii) unbounded, with decay conditions at infinity; and (iii) multiple boundaries (as with a zonal channel). The last case is the most complicated, since the boundary terms enter the equations directly, so we choose to analyze it.

Suppose there exists a steady solution, $\Phi = \Psi$, $P = Q$ with $\Psi = \Psi(Q)$ a monotonic function. We seek Casimirs such that $\delta\mathcal{A} = 0$. We have

$$\mathcal{H} = \iint_D \frac{1}{2}|\nabla\Phi|^2\, dxdy, \tag{112}$$

$$\mathcal{C} = \iint_D C(P)\, dxdy + \sum_i a_i\mu_i, \tag{113}$$

where $\mu_i \equiv \oint_{\partial D_i} \nabla\Phi \cdot \hat{\mathbf{n}}\, ds$ is the circulation on each connected piece, ∂D_i, of the boundary ∂D. To determine the pseudoenergy, we must solve the equations

$$\left.\frac{\delta\mathcal{H}}{\delta P}\right|_{P=Q} = -\left.\frac{\delta\mathcal{C}}{\delta P}\right|_{P=Q}, \qquad \left.\frac{\delta\mathcal{H}}{\delta\mu_i}\right|_{P=Q} = -\left.\frac{\delta\mathcal{C}}{\delta\mu_i}\right|_{P=Q}. \tag{114}$$

The left half of (114) gives (see §1.4)

$$\Psi = C'(Q), \tag{115}$$

which integrates to

$$C(Q) = \int^Q \Psi(\eta)d\eta, \tag{116}$$

while the right half of (114) gives

$$\Psi\big|_{\partial D_i} = -a_i. \tag{117}$$

If we consider the disturbance problem

$$P = Q + q, \quad \Phi = \Psi + \psi, \quad \mu_i = \Gamma_i + \gamma_i, \tag{118}$$

then noting that $q = \nabla^2\psi$ we construct the finite-amplitude pseudoenergy as follows:

$$\begin{aligned}
\mathcal{A} &= \mathcal{H}[Q+q, \Gamma_i+\gamma_i] - \mathcal{H}[Q,\Gamma_i] + \mathcal{C}[Q+q,\Gamma_i+\gamma_i] - \mathcal{C}[Q,\Gamma_i] \\
&= \iint_D \Big\{ \nabla\Psi\cdot\nabla\psi + \frac{1}{2}|\nabla\psi|^2 + \int_Q^{Q+q} \Psi(\tilde{q})\, d\tilde{q} \Big\}\, dxdy + \sum_i a_i\gamma_i \\
&= \iint_D \Big\{ \nabla\cdot(\Psi\nabla\psi) - \Psi\nabla^2\psi + \frac{1}{2}|\nabla\psi|^2 + \int_0^q \Psi(Q+\tilde{q})\, d\tilde{q} \Big\}\, dxdy - \sum_i \Psi\big|_{\partial D_i}\gamma_i
\end{aligned} \tag{119}$$

In the last line, the first term can be directly integrated and found to cancel the boundary circulation terms. Furthermore, noting that

$$-\Psi\nabla^2\psi = -\Psi q = -\int_0^q \Psi(Q), \tag{120}$$

the pseudoenergy can be written simply as

$$\mathcal{A} = \iint_D \Big\{ \frac{1}{2}|\nabla\psi|^2 + \int_0^q [\Psi(Q+\tilde{q}) - \Psi(Q)]\, d\tilde{q} \Big\}\, dxdy \tag{121}$$

(McIntyre & Shepherd 1987). The pseudoenergy is an exact, nonlinear invariant, as may be checked by direct substitution into the equations of motion. It is valid for *arbitrary* disturbances (not necessarily dynamically accessible ones). If there exist values of $Q+q$ outside the range of Q, one can extend the definition of $\Psi(Q)$ arbitrarily to cover those values, as discussed in §3.5. $\mathcal{A}$ is evidently sign-definite when

$$\frac{d\Psi}{dQ} > 0. \tag{122}$$

Essentially, this is Arnol'd's (1966) first stability theorem.

Suppose that

$$c_1 = \min_Q \left\{ \frac{d\Psi}{dQ} \right\} > 0, \qquad c_2 = \max_Q \left\{ \frac{d\Psi}{dQ} \right\} < \infty. \tag{123}$$

In this case we can establish normed stability of the basic state. The "convexity" condition provides

$$\frac{1}{2} c_1 q^2 \leq \int_0^q \left[\Psi(Q+\tilde{q}) - \Psi(Q) \right] d\tilde{q} \leq \frac{1}{2} c_2 q^2, \tag{124}$$

which is valid for continuous (possibly non-smooth) $\Psi(Q)$. In particular, let us choose the norm defined by

$$||q||^2 = \iint_D \frac{1}{2} \left\{ |\nabla \psi|^2 + \lambda q^2 \right\} dxdy, \tag{125}$$

with $c_1 \leq \lambda \leq c_2$. Then

$$||q(t)||^2 \leq \frac{\lambda}{c_1} \mathcal{A}(t) = \frac{\lambda}{c_1} \mathcal{A}(0) \leq \frac{c_2}{c_1} ||q(0)||^2. \tag{126}$$

So given $\epsilon > 0$, choose $\delta = \sqrt{c_1/c_2}\epsilon$ to prove nonlinear normed stability. As with static stability, this holds for *arbitrarily* large disturbances.

It is important to emphasize that the demonstration of normed stability provided above depends on the choice of norm. For normed stability, it is *always* essential to specify the norm; this is because in infinite-dimensional spaces, all norms are not equivalent. This point is highlighted by the following example.

Consider (110) in the special case $P = \nabla^2 \Phi$, and introduce a basic state $U(y) = \lambda y$. The disturbance (q, ψ) is given by

$$P = Q + q = -\lambda + q, \qquad \Phi = \Psi + \psi = -\frac{1}{2}\lambda y^2 + \psi, \tag{127}$$

and the exact equation for the disturbance vorticity $q = \nabla^2 \psi$ is

$$q_t = -\partial(\Psi, q) - \partial(\psi, Q) - \partial(\psi, q) = -\lambda y q_x - \partial(\psi, q). \tag{128}$$

Multiplying (128) by q and integrating over the domain yields

$$\begin{aligned} \frac{d}{dt} \iint_D \frac{1}{2} q^2 \, dxdy &= -\iint_D \lambda y q q_x \, dxdy - \iint_D q \partial(\psi, q) \, dxdy \\ &= -\iint_D \frac{\partial}{\partial x} \left(\frac{1}{2} \lambda y q^2 \right) dxdy - \iint_D \partial(\psi, \frac{1}{2} q^2) \, dxdy \\ &= 0. \end{aligned} \tag{129}$$

This proves that 2-D linear shear flow is stable in the *enstrophy* norm. However, consider an initial condition consisting of a plane wave $q(t=0) = \Re\{e^{i(kx+l_0 y)}\}$. Then the disturbance energy is given by (e.g. Shepherd 1985)

$$\mathcal{E}(t) = \iint_D \frac{1}{2} |\nabla \psi|^2(t) \, dxdy = \frac{\iint_D \frac{1}{2} q^2(t) \, dxdy}{k^2 + l^2} = \frac{\iint_D \frac{1}{2} q^2(0) \, dxdy}{k^2 + l^2}. \tag{130}$$

It can be shown that l evolves with time according to $l = l_0 + \lambda k t$, while k is constant. So for $l_0 < 0$ and $\lambda k > 0$, the energy will attain its maximum amplification

$$\frac{\mathcal{E}(t)}{\mathcal{E}(0)} = \frac{k^2 + l_0^2}{k^2} \qquad \text{at} \qquad t = \frac{-l_0}{k\lambda}. \tag{131}$$

Clearly, the amplification described by (131) becomes arbitrarily large in the limit $|l_0| \to \infty$. This example demonstrates the point that stability in one norm (here the enstrophy) does not imply stability in another (here the energy).

Returning to the general form of (110), consider the special case of zonal (x-invariant) flow, with $h = 0$. Then the condition

$$\frac{d\Psi}{dQ} = \frac{\nabla\Psi}{\nabla Q} = \frac{\Psi_y}{Q_y} = \frac{-U}{Q_y} > 0 \tag{132}$$

is sufficient for stability of the flow. This is the nonlinear generalization of the result of Fjørtoft (1950).

There is an interesting possibility in this barotropic case which did not arise in the previously discussed case of static stability. Recall from §3.5 that in that case the pseudoenergy was given by

$$\mathcal{A} = \iiint_D \left\{ \frac{1}{2}\rho_{00}|\boldsymbol{v}|^2 + \mathrm{APE}(\rho - \rho_0) \right\} dxdydz. \tag{133}$$

Since ρ and $\boldsymbol{v}$ are independent variables, $\mathcal{A}$ can never be negative definite. This is like the case of "natural systems" discussed in traditional classical mechanics. In the present case, however, there is only one dynamical variable, and in principle $\mathcal{A}$ *could* be negative definite. This gives what is called Arnol'd's (1966) second stability theorem.

How does this happen? Suppose

$$\frac{d\Psi}{dQ} < 0 \quad \text{and} \quad c_1 = \min\left\{ -\frac{d\Psi}{dQ} \right\} > 0, \quad c_2 = \max\left\{ -\frac{d\Psi}{dQ} \right\} < \infty. \tag{134}$$

Then

$$\int_0^q \left[\Psi(Q + \tilde{q}) - \Psi(Q) \right] d\tilde{q} \le -\frac{1}{2} c_1 q^2, \tag{135}$$

so this quantity has the potential for being more negative than $\frac{1}{2}|\nabla\psi|^2$ is positive, when integrated over the domain. In fact, for bounded domains this is possible. A detailed discussion is provided in McIntyre & Shepherd (1987, §6).

4.2 Andrews' theorem

The appearance of Arnol'd-type stability arguments created considerable interest in the meteorological community, for it appeared that they could be used to examine the stability of non-parallel flow profiles $\Psi = \Psi(Q)$. However, Arnol'd's theorems turn out to be not as powerful as they might seem in this regard. A theorem proved by Andrews (1984) shows this quite succinctly, as follows.

Suppose we are given a basic flow profile $\Psi = \Psi(Q)$, and suppose that the given problem is zonally symmetric: i.e. $h = h(y)$, and the boundaries (if any) are independent of x. A zonal channel would be the most common such geometry.

Claim: If $\dfrac{d\Psi}{dQ} > 0$, then $Q_x = 0$ and $\Psi_x = 0$.

Proof: The chain rule of differentiation implies

$$\Psi_x = \Psi'(Q) Q_x. \tag{136}$$

Multiplying this expression by Q_x and integrating over the domain yields

$$\begin{aligned} \iint_D \Psi_x Q_x \, dxdy &= \iint_D \Psi'(Q) \, (Q_x)^2 \, dxdy \\ \iff \iint_D \Psi_x \nabla^2 \Psi_x \, dxdy &= \iint_D \Psi'(Q) \, (Q_x)^2 \, dxdy \\ \iff \iint_D \boldsymbol{\nabla} \cdot (\Psi_x \boldsymbol{\nabla} \Psi_x) \, dxdy &= \iint_D \left\{ |\boldsymbol{\nabla} \Psi_x|^2 + \Psi'(Q) \, (Q_x)^2 \right\} dxdy. \end{aligned} \tag{137}$$

The integral on the left-hand side vanishes if the boundaries are zonally symmetric, which implies that $\Psi_x = 0 = Q_x$ everywhere.

Therefore, any flow in a zonally symmetric domain that is stable by Arnol'd's first theorem must itself be zonally symmetric! The argument can also be shown to apply to Arnol'd's second theorem (Carnevale & Shepherd 1990). These results help explain the conspicuous lack of non-zonal Arnol'd-stable flows in the literature.

There is a simple heuristic explanation of Andrews' theorem. If a problem is zonally symmetric, but the basic state is non-zonal, then a possible disturbance is the simple one generated by a zonal translation of the basic state. This zonal translation cannot change the pseudoenergy. Therefore, such basic states cannot be true extrema of the pseudoenergy — equivalently, $\mathcal{A}$ is not sign-definite — which implies that they cannot be Arnol'd stable.

However, it should be noted that Andrews' theorem may not apply to certain zonally symmetric problems in unbounded domains because of the boundary conditions at infinity (Carnevale & Shepherd 1990). Otherwise one could deduce, for example, that circular vortices were not Arnol'd stable — something which is demonstrably untrue.

4.3 Available energy

Can we regard the quantity

$$\int_0^q [\Psi(Q + \tilde{q}) - \Psi(Q)] \, d\tilde{q} \tag{138}$$

as a generalization of APE? In a sense, yes. For any stable flow (Ψ, Q) with $d\Psi/dQ > 0$, we have

$$\iint_D \frac{1}{2} |\boldsymbol{\nabla} \psi|^2(t) \, dxdy \leq \mathcal{A}(t) = \mathcal{A}(0) = \mathcal{A}[Q; q(0)]. \tag{139}$$

For a given initial condition, $P(0)$, one can vary the right-hand side of (139) over various stable Q to seek the tightest possible bound on the disturbance energy.

In the case of static stability, the variations were over ρ_0 and didn't affect $\frac{1}{2}|\boldsymbol{v}|^2$. Here $\psi = \Phi - \Psi$, so when one changes the basic flow, one also changes the definition of the disturbance. This is not a satisfactory situation.

Suppose, however, that the problem is zonally symmetric and that one is interested in the eddy energy. We may write

$$\Phi = \overline{\Phi} + \Phi' \text{ where } \overline{(\,)} \equiv x\text{-average and } \overline{\Phi'} = 0. \tag{140}$$

Then, if we choose a zonally symmetric flow (as required by Andrews' theorem), i.e.

$$\Psi' = 0, \qquad Q' = 0, \tag{141}$$

this implies

$$\Phi' = \psi', \qquad P' = q'. \tag{142}$$

Hence (q', ψ') are independent of the choice of the basic state. Then, for the eddy energy we have the upper bound

$$\begin{aligned} \mathcal{E}' \equiv \iint_D \frac{1}{2}|\nabla\Phi'|^2(t)\,dxdy = \iint_D \frac{1}{2}|\nabla\psi'|^2(t)\,dxdy &\leq \iint_D \frac{1}{2}|\nabla\psi|^2(t)\,dxdy \\ &\leq \mathcal{A}[Q; q(0)]. \end{aligned} \tag{143}$$

Now one can vary the right-hand side of (143) to seek the tightest possible bound on the eddy energy.

We now illustrate the general method by applying it to the case of baroclinic flow.

4.4 Nonlinear saturation of baroclinic instability

The two-layer model was presented in §2.1. The notation has been changed somewhat for convenience; q there corresponds to P here, while ψ there corresponds to Φ here. Further details of the following analysis may be found in Shepherd (1993*b*).

Suppose $F_1 = F_2 = F$ in the domain $0 \leq y \leq 1$, periodic in x. The potential vorticity in each layer is given by

$$P_i = \nabla^2\Phi_i + (-1)^i F(\Phi_1 - \Phi_2) + f + \beta y \quad [i = 1, 2]. \tag{144}$$

Consider the basic-state stream function $\Psi_i = \Psi_i(Q_i)$ corresponding to the purely zonal flow

$$U_i(y) = -d\Psi_i/dy \quad [i = 1, 2], \tag{145}$$

with potential vorticity

$$Q_i(y) = \nabla^2\Psi_i + (-1)^i F(\Psi_1 - \Psi_2) + f + \beta y \quad [i = 1, 2]. \tag{146}$$

Let ψ_i be the disturbance stream function, so that

$$\Phi_i = \Psi_i(y) + \psi_i(x, y, t) \quad [i = 1, 2]. \tag{147}$$

This allows the pseudoenergy to be written

$$\begin{aligned} \mathcal{A} \;=\; \iint_D \Big\{ &\frac{1}{2}\big[|\nabla\psi_1|^2 + |\nabla\psi_2|^2 + F(\psi_1 - \psi_2)^2\big] \\ &+ \int_0^{q_1} [\Psi_1(Q_1 + \tilde{q}) - \Psi_1(Q_1)]\,d\tilde{q} + \int_0^{q_2} [\Psi_2(Q_2 + \tilde{q}) - \Psi_2(Q_2)]\,d\tilde{q} \Big\}\, dxdy, \end{aligned} \tag{148}$$

where q_i is the disturbance potential vorticity

$$q_i = \nabla^2\psi_i + (-1)^i F(\psi_1 - \psi_2) \quad [i = 1,2]. \tag{149}$$

It is clear from (148) that if

$$\frac{d\Psi_1}{dQ_1} > 0 \qquad \text{and} \qquad \frac{d\Psi_2}{dQ_2} > 0, \tag{150}$$

then $\mathcal{A} > 0$. This is Arnol'd's first stability theorem applied to quasi-geostrophic flow (Holm *et al.* 1985). Since we are considering the zonally symmetric case, these conditions are satisfied if

$$\frac{U_i}{dQ_i/dy} < 0 \quad [i = 1,2]; \tag{151}$$

put this way, the theorem represents the nonlinear version of the Fjørtoft-Pedlosky theorem.

Suppose our initial condition consists of an infinitesimal disturbance to the Phillips zonal flow

$$-\frac{\partial\overline{\Phi}_1}{\partial y} = \hat{U}_1 = \frac{\beta}{F}(1+\epsilon) + u_0, \qquad -\frac{\partial\overline{\Phi}_2}{\partial y} = \hat{U}_2 = u_0, \tag{152}$$

where u_0 is an arbitrary constant. The flow (152) is known to be unstable if $\epsilon > 0$, provided the domain is sufficiently wide in an appropriate sense (e.g. Pedlosky 1987, §7.11).

Now choose a one-parameter family of stable basic flows

$$-\frac{\partial\Psi_1}{\partial y} = U_1 = \frac{\beta}{F}(1-\delta) + u_0, \qquad -\frac{\partial\Psi_2}{\partial y} = U_2 = u_0, \tag{153}$$

with associated potential vorticity

$$Q_1 = \beta(2-\delta)(y-\lambda) + f + \beta\lambda, \qquad Q_2 = \beta\delta(y-\lambda) + f + \beta\lambda, \tag{154}$$

where λ is a constant of integration. We have three free parameters: λ, u_0, and δ. For all λ, u_0, and δ such that $d\Psi_i/dQ_i > 0$ we then have the rigorous upper bound on the eddy energy

$$\begin{aligned}
\mathcal{E}' &\equiv \iint_D \frac{1}{2}\Big\{|\nabla\Phi_1'|^2 + |\nabla\Phi_2'|^2 + F(\Phi_1' - \Phi_2')^2\Big\}\,dxdy \\
&\le \iint_D \frac{1}{2}\Big\{|\nabla\psi_1|^2 + |\nabla\psi_2|^2 + F(\psi_1 - \psi_2)^2\Big\}\,dxdy \\
&\le \mathcal{A}(t) \\
&= \mathcal{A}(0) \\
&= \frac{\beta^2(\epsilon+\delta)^2}{F^2}\Big\{\frac{1}{2}\Big[1 + F\int_0^1 (y-\lambda)^2 dy\Big] \\
&\quad -\frac{1}{2}\Big[\frac{\beta(1-\delta)+u_0F}{\beta F(2-\delta)} + \frac{u_0}{\beta\delta}\Big]F^2\int_0^1 (y-\lambda)^2 dy\Big\} \\
&\quad + \text{terms involving the initial non-zonal disturbance.}
\end{aligned} \tag{155}$$

The contribution to the initial pseudoenergy associated with the initial non-zonal disturbance can, of course, be included in the above bound. However, in the situation we are considering

here of an infinitesimal initial disturbance to the Phillips initial condition, this contribution is negligible compared with the pseudoenergy arising from the zonal-mean part of the initial disturbance to the stable basic flow, which is the part written out explicitly in the last line of (155).

Now, choosing $\lambda = \frac{1}{2}$ so that

$$\int_0^1 (y-\lambda)^2 dy = \frac{1}{12}, \tag{156}$$

which is the best choice, and setting

$$\beta(1-\delta) + u_0 F = 0 \qquad \Longrightarrow \qquad u_0 = -\frac{\beta(1-\delta)}{F}, \tag{157}$$

leaves

$$\mathcal{A}(0) = \frac{\beta^2(\epsilon+\delta)^2}{2F^2}\Big[1 + \frac{F}{12} + \frac{(1-\delta)F}{12\delta}\Big] = \frac{\beta^2(\epsilon+\delta)^2}{24F^2}\Big[12 + \frac{F}{\delta}\Big]. \tag{158}$$

Setting $\partial A(0)/\partial\delta = 0$ yields a minimum at

$$\delta = \frac{F}{48}\Big[-1 + \sqrt{1 + (96\epsilon/F)}\Big] \simeq \epsilon \qquad \text{for} \qquad \epsilon \ll 1. \tag{159}$$

One could, of course, use the optimal value of δ, but the simple choice $\delta = \epsilon$ certainly gives a valid saturation bound too, which is

$$\mathcal{E}' \le \mathcal{A}(0) = \frac{\beta^2}{6F}\Big(1 + \frac{12\epsilon}{F}\Big)\epsilon. \tag{160}$$

Now the eddy energy is also bounded by the total energy of the system, namely

$$\mathcal{E}' \le \mathcal{E}_{\text{total}} = \frac{\beta^2}{24F}\Big(1 + \frac{6}{F}\Big)(1+\epsilon)^2. \tag{161}$$

However it is clear that $\mathcal{E}_{\text{total}} \gg \mathcal{A}(0)$ for $\epsilon \ll 1$, so the bound (160) is providing a non-trivial constraint on the dynamics.

This gives a bound on the scaling of the saturation amplitude of the instability. But is it any good? Weakly-nonlinear theory (Pedlosky 1970; Warn & Gauthier 1989) gives

$$\mathcal{E}'_{\max} \sim \frac{\beta^2\epsilon}{F} \tag{162}$$

for $\epsilon \ll 1$, which is the *same* scaling as (160); the numerical factors in (162) are $1/\pi^2$ for the non-resonant case, and $1/8$ for the resonant case. This is to be compared with a coefficient of $1/6$ for the stability-based bound. So the bound is, in fact, not too bad as an estimate of the saturation amplitude.

An important generalization of these saturation bounds is to forced-dissipative systems. If

$$\frac{DP}{Dt} = -r(P - P_e) \tag{163}$$

(potential vorticity relaxation), where $P_e = \overline{P}(t=0)$, then these bounds on the eddy energy remain valid (see Shepherd 1988*b*).

5 Pseudomomentum

5.1 General construction

We have seen how one can construct the pseudoenergy, a second-order invariant, for disturbances to a *steady* basic state under *time-invariant* dynamics. Similarly, if the dynamics under consideration is invariant to translations in the x direction, we may construct a second-order invariant for disturbances to *x-invariant* basic states.

Recall how we constructed the pseudoenergy from the Hamiltonian, $\mathcal{H}$, and the Casimirs, $\mathcal{C}$: since the basic state $\boldsymbol{U}$ in that case is a steady solution of the dynamics,

$$J\left.\frac{\delta\mathcal{H}}{\delta\boldsymbol{u}}\right|_{\boldsymbol{u}=\boldsymbol{U}}=0. \tag{164}$$

It follows that for some Casimir $\mathcal{C}$,

$$\left.\frac{\delta\mathcal{H}}{\delta\boldsymbol{u}}\right|_{\boldsymbol{u}=\boldsymbol{U}}=-\left.\frac{\delta\mathcal{C}}{\delta\boldsymbol{u}}\right|_{\boldsymbol{u}=\boldsymbol{U}}. \tag{165}$$

The pseudoenergy is then

$$\mathcal{A}[\boldsymbol{U};\delta\boldsymbol{u}]=\mathcal{H}[\boldsymbol{U}+\delta\boldsymbol{u}]-\mathcal{H}[\boldsymbol{U}]+\mathcal{C}[\boldsymbol{U}+\delta\boldsymbol{u}]-\mathcal{C}[\boldsymbol{U}], \tag{166}$$

where $\mathcal{C}$ is defined by (165).

In the very same way, we may construct the *pseudomomentum* from the momentum invariant, $\mathcal{M}$. By definition of $\mathcal{M}$ (see §1.5), $J(\delta\mathcal{M}/\delta\boldsymbol{u})=-\boldsymbol{u}_x$. Now, since the Hamiltonian is presumed to be invariant under translations in the x direction, it follows from Noether's theorem that $\mathcal{M}$ is an integral of the motion. If the basic state $\boldsymbol{U}$ is also invariant with respect to x translations, then

$$J\left.\frac{\delta\mathcal{M}}{\delta\boldsymbol{u}}\right|_{\boldsymbol{u}=\boldsymbol{U}}=-\boldsymbol{U}_x=0. \tag{167}$$

It follows that there exists a $\mathcal{C}$ such that

$$\left.\frac{\delta\mathcal{M}}{\delta\boldsymbol{u}}\right|_{\boldsymbol{u}=\boldsymbol{U}}=-\left.\frac{\delta\mathcal{C}}{\delta\boldsymbol{u}}\right|_{\boldsymbol{u}=\boldsymbol{U}}. \tag{168}$$

Finally we define the pseudomomentum by

$$\mathcal{A}[\boldsymbol{U};\delta\boldsymbol{u}]=\mathcal{M}[\boldsymbol{U}+\delta\boldsymbol{u}]-\mathcal{M}[\boldsymbol{U}]+\mathcal{C}[\boldsymbol{U}+\delta\boldsymbol{u}]-\mathcal{C}[\boldsymbol{U}], \tag{169}$$

where $\mathcal{C}$ is defined by (168) so that $(\delta\mathcal{A}/\delta\boldsymbol{u})|_{\boldsymbol{u}=\boldsymbol{U}}=0$. In fact, it is clear from Noether's theorem that we may generate a similar functional for *any* continuous symmetry of the dynamics.

The pseudomomentum, like the pseudoenergy, is guaranteed to have the following nice properties: (i) it is calculable to leading order from linear theory; (ii) it may be sign-definite under certain conditions. If we find some zonal basic states for which the pseudomomentum

is sign definite, then it is clear that we are in a position to generate more nonlinear stability theorems.

If the basic flow is both zonally symmetric and steady (as zonally symmetric flows often are), we may combine the pseudoenergy and the pseudomomentum to generate still more quadratic invariants, according to

$$\mathcal{A} = (\mathcal{H} + \alpha\mathcal{M} + \mathcal{C})[\boldsymbol{u}] - (\mathcal{H} + \alpha\mathcal{M} + \mathcal{C})[\boldsymbol{U}]. \tag{170}$$

Here we may choose α arbitrarily and, again, $\mathcal{C}$ is chosen so that $(\delta\mathcal{A}/\delta\boldsymbol{u})|_{\boldsymbol{u}=\boldsymbol{U}} = 0$.

5.2 Example: Barotropic vorticity equation

In this section we will develop an expression for the pseudomomentum of the barotropic model in a β-plane zonal channel. The flows we will consider are governed by the vorticity equation

$$P_t + \partial(\Phi, P) = 0 \tag{171}$$

where Φ is the stream function, and P is the absolute vorticity

$$P = \nabla^2\Phi + f + \beta y. \tag{172}$$

For definiteness, we consider flows that are periodic in the x (zonal) direction, and bounded by rigid walls in the y direction.

We take as the state variable the absolute vorticity, P, and the boundary circulations, $\mu_i \equiv \oint_{\partial D_i} \nabla\Phi \cdot \hat{\mathbf{n}}\, ds$. Recall that in this formulation, the Hamiltonian is given by

$$\mathcal{H} = \iint_D \frac{1}{2}|\nabla\Phi|^2\, dxdy. \tag{173}$$

The cosymplectic operator, J, acting on the basis (P, μ_1, μ_2), is given by

$$J = \begin{pmatrix} -\partial(P,\cdot) & 0 & 0 \\ 0 & 0 & 0 \\ 0 & 0 & 0 \end{pmatrix}. \tag{174}$$

The Casimirs associated with J are functionals of the form

$$\mathcal{C} = \iint_D C(P)\, dxdy + \sum_{i=1}^{2} a_i\mu_i \tag{175}$$

for arbitrary functions $C(\cdot)$ and scalars a_i. The momentum invariant $\mathcal{M}$ is found by solving

$$-\Big(\frac{\partial P}{\partial x}, 0, 0\Big)^T = J\Big(\frac{\delta\mathcal{M}}{\delta P}, \frac{\delta\mathcal{M}}{\delta\mu_1}, \frac{\delta\mathcal{M}}{\delta\mu_2}\Big)^T \quad \Longrightarrow \quad \frac{\partial P}{\partial x} = \partial\Big(P, \frac{\delta\mathcal{M}}{\delta P}\Big). \tag{176}$$

The solution (to within a Casimir) of (176) is given by

$$\frac{\delta\mathcal{M}}{\delta P} = y \quad \Longrightarrow \quad \mathcal{M} = \iint_D yP\, dxdy. \tag{177}$$

This expression differs from the usual definition of momentum, which is $\iint_D u\,dxdy$. The reader may verify (cf. §1.5) that the difference between these two expressions can be written solely as a function of the boundary circulations μ_1 and μ_2 — in other words, the difference is a Casimir.

If the basic state is given by $\Phi = \Psi$, $P = Q$, then to find the pseudomomentum we must solve

$$\left.\frac{\delta \mathcal{M}}{\delta P}\right|_{P=Q} = -\left.\frac{\delta \mathcal{C}}{\delta P}\right|_{P=Q} \qquad \Longrightarrow \qquad y = -C'(Q). \tag{178}$$

Note that this requires Q to be independent of x, i.e. $Q = Q(y)$. Thus zonally symmetric states are seen to be constrained extrema of $\mathcal{M}$, just as steady states are constrained extrema of $\mathcal{H}$. Solving (178) for C yields

$$C(Q) = -\int^{Q} Y(\tilde{q})\,d\tilde{q}, \tag{179}$$

where $Y(\cdot)$ is the inverse of $Q(y)$: that is, $y = Y(Q(y))$.

Note that since the disturbance need not be dynamically accessible, we may (as before) extend the definition of $Y(\cdot)$, if required, to cover values of its argument outside the range of the basic state Q.

The pseudomomentum, $\mathcal{A}$, is given by

$$\mathcal{A} = \iint_D y(P-Q)\,dxdy + \mathcal{C}[P] - \mathcal{C}[Q]. \tag{180}$$

Setting $P = Q + q$, and substituting (179) for C, yields

$$\mathcal{A} = \iint_D \left\{ yq - \int_Q^{Q+q} Y(\tilde{q})\,d\tilde{q} \right\} dxdy. \tag{181}$$

Finally, since $y = Y(Q)$, we may write

$$\mathcal{A} \equiv \iint_D A\,dxdy = \iint_D \left\{ -\int_0^{q} [Y(Q+\tilde{q}) - Y(Q)]\,d\tilde{q} \right\} dxdy \tag{182}$$

(Killworth & McIntyre 1985). Note the similarity between the pseudomomentum (182) and the expression in (98) for the APE. As a consequence, (182) has the same geometrical interpretation as the APE (see the sketch in §3.4).

If dQ/dy (and thus dY/dQ) is sign-definite, then so is $\mathcal{A}$. In particular if $dY/dQ \neq 0$ and

$$0 < c_1 \leq \left|\frac{dY}{dQ}\right| \leq c_2 < \infty, \tag{183}$$

then

$$\frac{1}{2}c_1 q^2 \leq |A| \leq \frac{1}{2}c_2 q^2. \tag{184}$$

This is the convexity condition for this problem. We then have normed stability under the enstrophy norm. In particular, if we define our norm according to

$$\|q\|^2 = \iint_D \frac{1}{2}q^2\,dxdy, \tag{185}$$

then we have

$$\|q(t)\|^2 \leq \frac{1}{c_1}\mathcal{A}(t) = \frac{1}{c_1}\mathcal{A}(0) \leq \frac{c_2}{c_1}\|q(0)\|^2, \tag{186}$$

which proves normed stability.

As with the previous stability criteria, this stability criterion applies to arbitrarily large disturbances. It is the finite-amplitude version of the Rayleigh-Kuo theorem (Shepherd 1988*b*). The same procedure applied to the quasi-geostrophic equations yields a finite-amplitude Charney-Stern theorem (Shepherd 1988*a*, 1989).

In §3.6 and §4.4, pseudoenergy-based finite-amplitude stability theorems were used to obtain rigorous upper bounds on the nonlinear saturation of instabilities. The same procedure is of course possible with the pseudomomentum. For a general discussion and applications to parallel flows on the barotropic β-plane, see Shepherd (1988*b*). Further applications are provided in Shepherd (1988*a*, 1989, 1991).

5.3 Wave, mean-flow interaction

In this section we shed some light on why $\mathcal{A}$ is called the pseudomomentum. Still considering the barotropic vorticity equation, if we take the x-average of the zonal momentum equation we get

$$\frac{\partial \overline{u}}{\partial t} = -\overline{\frac{\partial\,(u^2)}{\partial x}} - \overline{\frac{\partial\,(uv)}{\partial y}} + f\overline{v} - \overline{\frac{\partial p}{\partial x}}. \tag{187}$$

The first and last two terms on the right-hand side vanish due to the presumed periodicity in x, together with the fact that $v = -\psi_x$ so $\overline{v} = 0$. This leaves

$$\frac{\partial \overline{u}}{\partial t} = -\overline{\frac{\partial\,(u'v')}{\partial y}}, \tag{188}$$

where the primes indicate departures from the x-average flow. Using the fact that the flow is non-divergent, we can rewrite the previous equation as

$$\frac{\partial \overline{u}}{\partial t} = -\overline{v'\Big(\frac{\partial u'}{\partial y} - \frac{\partial v'}{\partial x}\Big)} + \frac{\partial}{\partial x}\overline{\Big[\frac{1}{2}\big(u'^2 - v'^2\big)\Big]}. \tag{189}$$

The second term on the right-hand side vanishes under the zonal average, while the first term represents the meridional flux of potential vorticity, q', hence

$$\frac{\partial \overline{u}}{\partial t} = \overline{v'q'}. \tag{190}$$

On the other hand, from the linearized potential vorticity equation

$$q'_t + Uq'_x + v'Q_y = 0 \tag{191}$$

we get

$$v' = -\frac{1}{Q_y}\left(q'_t + Uq'_x\right). \tag{192}$$

Substituting this expression for v' into (190) then leads to

$$\frac{\partial \overline{u}}{\partial t} = -\frac{\partial}{\partial t}\Big(\frac{1}{2}\frac{\overline{q'^2}}{Q_y}\Big). \tag{193}$$

This is the well-known relation of Taylor (1915), describing how disturbance growth or decay induces mean-flow changes. But note that the small-amplitude limit of the pseudomomentum density (182) is

$$A \approx -\frac{1}{2}\frac{q'^2}{Q_y}. \tag{194}$$

Combining this with the previous equation then yields the small-amplitude relation

$$\frac{\partial \overline{u}}{\partial t} = \frac{\partial \overline{A}}{\partial t}, \tag{195}$$

which justifies the interpretation of $\mathcal{A}$ as a pseudomomentum. (The prefix "pseudo" has led to some confusion. However, to discuss the "momentum" of waves has historically been a source of profound confusion! For background on this issue, as well as a defense of the current nomenclature, the reader is referred to the spirited article of McIntyre (1981).)

In the continuously stratified quasi-geostrophic case, (190) generalizes to (see e.g. Pedlosky 1987, §6.14)

$$\mathcal{L}\Big(\frac{\partial \overline{u}}{\partial t}\Big) = \frac{\partial^2}{\partial y^2}\overline{(v'q')}, \tag{196}$$

where $\mathcal{L}$ is the linear elliptic operator

$$\mathcal{L} = \frac{\partial^2}{\partial y^2} + \frac{1}{\rho_s}\frac{\partial}{\partial z}\frac{\rho_s}{S}\frac{\partial}{\partial z}. \tag{197}$$

The pseudomomentum conservation relation may be written in local form, *including non-conservative effects*, as

$$\frac{\partial A}{\partial t} + \boldsymbol{\nabla}\cdot\mathbf{F} = D, \tag{198}$$

where D represents the non-conservative effects and $-\mathbf{F}$ is the so-called Eliassen-Palm flux (Andrews & McIntyre 1976), satisfying

$$\boldsymbol{\nabla}\cdot\overline{\mathbf{F}} = -\overline{v'q'}. \tag{199}$$

(The minus sign in the definition of the E-P flux is for historical reasons: the introduction of the E-P flux predated its understanding in terms of pseudomomentum.) From these relations we get the following equation for the mean-flow tendency:

$$\mathcal{L}\Big(\frac{\partial \overline{u}}{\partial t}\Big) = \frac{\partial^2}{\partial y^2}\overline{(v'q')} = -\frac{\partial^2}{\partial y^2}\big(\boldsymbol{\nabla}\cdot\overline{\mathbf{F}}\big) = \frac{\partial^2}{\partial y^2}\Big(\frac{\partial \overline{A}}{\partial t} - \overline{D}\Big). \tag{200}$$

Relation (200) generalizes (195) in two distinct ways: first, by including non-conservative effects; and second, by extending the relation to quasi-geostrophic flow. Integrating (200) in

time over some finite time interval then gives the following expression for the net change in the zonal flow, $\Delta\overline{u}$:

$$\Delta\overline{u} = \mathcal{L}^{-1}\Big\{\frac{\partial^2}{\partial y^2}\Big(\Delta\overline{A} - \int \overline{D}\,dt\Big)\Big\}. \tag{201}$$

That is, to have a change in $\overline{u}$, we need either transience in the wave activity, $\Delta\overline{A} \neq 0$, or wave-activity dissipation, $\overline{D} \neq 0$; this is the "non-acceleration theorem" (Andrews & McIntyre 1976). The insight provided by this theoretical framework has recently led to profound advances in our understanding of some classical questions in large-scale atmospheric dynamics, including the maintenance of the westerlies (see the discussion in Shepherd 1992*b*).

The beauty of the Hamiltonian framework is that it provides insight into which aspects of a particular derivation may be generalizable to other systems. For example, the wave, mean-flow interaction theory exemplified by the relation (200) is clearly generalizable through the unifying concept of pseudomomentum (e.g. Scinocca & Shepherd 1992; Kushner & Shepherd 1993).

5.4 Wave action

There is a classical literature in fluid mechanics that is relevant to wave propagation in inhomogeneous, moving media. For WKB conditions — namely, a nearly monochromatic wave packet propagating in a slowly varying background state — there is a conservation law for the so-called "wave action" (Whitham 1965; Bretherton & Garrett 1968). The wave action is given by $E'/\hat{\omega}$, where E' is the wave energy (as measured in the local frame of reference, moving with the mean flow) and $\hat{\omega}$ is the intrinsic frequency of the waves (i.e. the frequency in the local frame of reference). In the case of the barotropic vorticity equation with a zonal basic state, for example,

$$E' = \frac{1}{2}\overline{|\nabla\psi'|^2} \qquad \text{and} \qquad \hat{\omega} = -\frac{kQ_y}{k^2+l^2}, \tag{202}$$

where k and l are the x and y wavenumbers, respectively, Q_y is the basic-state potential-vorticity gradient, and the overbar now represents an average over the phase of the waves. Thus the wave action for Rossby waves is given by

$$\frac{E'}{\hat{\omega}} = -\frac{1}{2k}\frac{(k^2+l^2)\overline{|\nabla\psi'|^2}}{Q_y} = -\frac{1}{2k}\frac{\overline{q'^2}}{Q_y}. \tag{203}$$

Referring to (194), we conclude that the wave action is the pseudomomentum divided by the zonal wavenumber,

$$\frac{E'}{\hat{\omega}} = \frac{A}{k}. \tag{204}$$

Of course, wave action is a local concept which may be defined even when there is no global symmetry in the problem (provided the WKB conditions are satisfied). However, when the basic state *has* a zonal symmetry, the pseudomomentum may be defined and is related to the wave action in the above fashion; the factor of k is then irrelevant since it is constant. Under such conditions, the pseudomomentum may be regarded as a generalization of wave action insofar as it is not restricted to WKB (slowly varying) conditions, neither is it restricted to

small amplitude. This connection has already been made by Andrews & McIntyre (1978) within the context of Generalized Lagrangian Mean theory; the present treatment illustrates how it holds for the Eulerian formulation of fluid dynamics.

5.5 Instabilities

Analysis of normal-mode instabilities is often facilitated by the use of quadratic invariants such as pseudomomentum and pseudoenergy. This is because for a normal mode,

$$\mathcal{A} = \mathcal{A}_0 e^{2\sigma t} \tag{205}$$

where $\mathcal{A}_0 \equiv \mathcal{A}(t=0)$ and σ is the real part of the growth rate. However, $\mathcal{A}$ is conserved in time, which implies that $\sigma\mathcal{A} = 0$. Therefore, we conclude that growing or decaying normal modes (with $\sigma \neq 0$) must have $\mathcal{A} = 0$. [In fact, many of the well-known derivations of linear stability criteria involve the implicit use of this relation $\sigma\mathcal{A} = 0$: an example is Pedlosky (1987, Eq.(7.4.22))].

The constraint $\mathcal{A} = 0$ on normal-mode instabilities means that such instabilities consist of regions of positive and negative A. This is a generalization of the notion of positive and negative energy modes discussed in Morrison's lectures. It is clear from the Hamiltonian perspective that one may speak of positive and negative pseudoenergy, or positive and negative pseudomomentum, or even some combination of the two, depending on which invariant quantity is most appropriate for the problem at hand.

This concept is most useful when the wave-activity invariant being considered is sign-definite in certain parts of the flow, and can be associated (in an appropriate limiting sense) with certain wave modes. Typically in the short-wave limit these modes decouple and are neutral.

As an example, consider baroclinic instability in the continuously stratified quasi-geostrophic model, with $z_0 \leq z \leq z_1$. In this case the small-amplitude expansion of the pseudomomentum gives (Shepherd 1989)

$$\mathcal{A} = \mathcal{A}_1 + \mathcal{A}_2 + \mathcal{A}_3 \tag{206}$$

where

$$\mathcal{A}_1 = -\iiint_D \frac{\rho_s}{2}\frac{q^2}{dQ/dy}\,dxdydz, \tag{207}$$

$$\mathcal{A}_2 = \iint \frac{1}{2}\frac{\lambda_1^2}{d\Lambda_1/dy}\,dxdy\bigg|_{z=z_1}, \qquad \mathcal{A}_3 = -\iint \frac{1}{2}\frac{\lambda_0^2}{d\Lambda_0/dy}\,dxdy\bigg|_{z=z_0}. \tag{208}$$

Here Q and q are the basic-state and disturbance potential vorticity fields, while $\Lambda_i = \frac{\rho_s}{S}\Psi_z\big|_{z=z_i}$ and $\lambda_i = \frac{\rho_s}{S}\psi_z\big|_{z=z_i}$ where Ψ and ψ are the basic-state and disturbance stream function fields. All known (inviscid) quasi-geostrophic baroclinic instabilities may be understood within this framework. In the case of the Eady model, we have

$$\frac{dQ}{dy} = 0, \quad q = 0, \quad \text{and} \quad \frac{d\Lambda_i}{dy} < 0. \tag{209}$$

Therefore, in this model instability is possible with $\mathcal{A}_1 = 0$, $\mathcal{A}_2 < 0$, and $\mathcal{A}_3 > 0$. In the case of the Charney model there is no upper lid so the contribution to $\mathcal{A}_2$ vanishes, while

$$\frac{dQ}{dy} > 0 \quad \text{and} \quad \frac{d\Lambda_0}{dy} < 0. \tag{210}$$

Thus in this case $\mathcal{A}_1 < 0$, $\mathcal{A}_2 = 0$, and $\mathcal{A}_3 > 0$. For internal baroclinic instability (like in the Phillips model), $\mathcal{A}_2 = 0$ and $\mathcal{A}_3 = 0$ so we must have $\mathcal{A}_1 = 0$, but characteristically

$$\frac{dQ}{dy} > 0 \quad \text{for} \quad z > z_c \quad \text{and} \quad \frac{dQ}{dy} < 0 \quad \text{for} \quad z < z_c \tag{211}$$

for some z_c, so $\mathcal{A}_1$ consists of a negative-A mode above a positive-A mode.

A very important feature of these wave-activity invariants is that their finite-amplitude forms are meaningful even for discontinuous basic-state profiles. Indeed, the understanding of instabilities in terms of interacting modes is clearest when the modes are spatially localized on material interfaces. For example, consider the barotropic system with a basic state

$$Q(y) = \begin{cases} Q_2, & y > 0 \\ Q_1, & y < 0 \end{cases} \tag{212}$$

where $Q_1 < Q_2$. We can study the stability of this profile by looking at the regions where $A \neq 0$. In this case the pseudomomentum is given by

$$A = -\int_0^q [Y(Q + \tilde{q}) - Y(Q)]\, d\tilde{q}. \tag{213}$$

Note that $A = 0$ except in the hatched regions (see figure below).

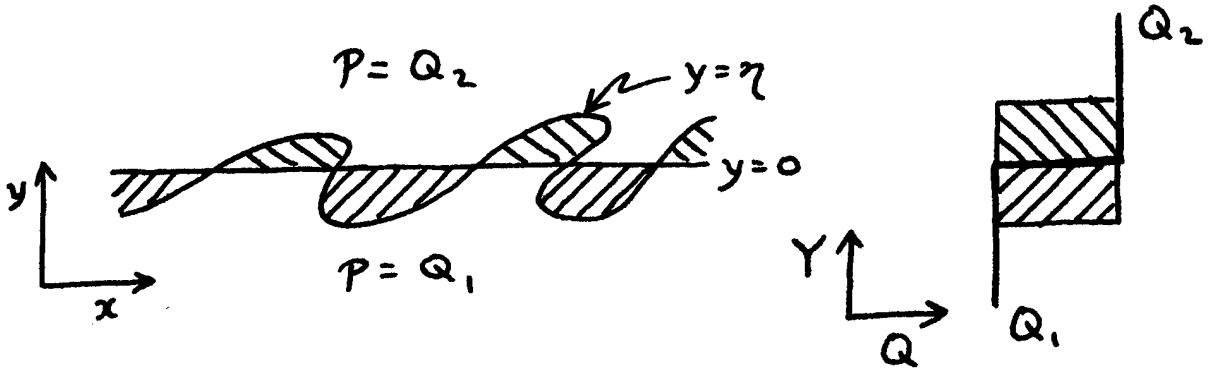

It turns out (see Shepherd 1988*b*, Appendix A) that

$$\mathcal{A} = \iint_D A\, dxdy = -\frac{1}{2}(Q_2 - Q_1) \oint \eta^2\, dx, \tag{214}$$

where η is the meridional displacement of the material contour where the vorticity jump occurs. Evidently in this case $\mathcal{A} < 0$, and the basic state (212) is stable. The above formula can be generalized for N contours (denoted by C_i) as follows:

$$\mathcal{A} = \iint_D A\, dxdy = -\frac{1}{2}\sum_{i=1}^{N} \oint_{C_i} \eta^2\, dx. \tag{215}$$

So we see that the pseudomomentum resides in each contour, and has a sign opposite to that of the vorticity jump. This is in contrast to the pseudoenergy, which is not so localized.

REFERENCES

Abarbanel, H.D.I., Holm, D.D., Marsden, J.E. & Ratiu, T. 1986 Nonlinear stability analysis of stratified fluid equilibria. *Phil.Trans.Roy.Soc.Lond.A* **318**, 349–409.

Andrews, D.G. 1981 A note on potential energy density in a stratified compressible fluid. *J.Fluid Mech.* **107**, 227–236.

Andrews, D.G. 1984 On the existence of nonzonal flows satisfying sufficient conditions for stability. *Geophys.Astrophys.Fluid Dyn.* **28**, 243–256.

Andrews, D.G. & McIntyre, M.E. 1976 Planetary waves in horizontal and vertical shear: The generalized Eliassen-Palm relation and the mean zonal acceleration. *J.Atmos.Sci.* **33**, 2031–2048.

Andrews, D.G. & McIntyre, M.E. 1978 On wave-action and its relatives. *J.Fluid Mech.* **89**, 647–664. (*Corrigenda*, **95**, 796.)

Arnol'd, V.I. 1966 On an a priori estimate in the theory of hydrodynamical stability. *Izv.Vyssh. Uchebn.Zaved.Matematika* **54**, no.5, 3–5. (English translation: *Amer.Math.Soc.Transl., Series 2* **79**, 267–269 (1969).)

Benjamin, T.B. 1984 Impulse, flow force and variational principles. *IMA J.Appl.Math.* **32**, 3–68.

Benjamin, T.B. & Bowman, S. 1987 Discontinuous solutions of one-dimensional hamiltonian systems. *Proc.Roy.Soc.Lond.A* **413**, 263–295.

Bretherton, F.P. & Garrett, C.J.R. 1968 Wavetrains in inhomogeneous moving media. *Proc. Roy.Soc.Lond.A* **302**, 529–554.

Carnevale, G.F. & Shepherd, T.G. 1990 On the interpretation of Andrews' theorem. *Geophys.Astrophys.Fluid Dyn.* **51**, 1–17.

Cho, H.-R., Shepherd, T.G. & Vladimirov, V.A. 1993 Application of the direct Liapunov method to the problem of symmetric stability in the atmosphere. *J.Atmos.Sci.* **50**, 822–836.

Fjørtoft, R. 1950 Application of integral theorems in deriving criteria of stability for laminar flows and for the baroclinic circular vortex. *Geofys.Publ.* **17**, no.6, 1–52.

Gill, A.E. 1982 *Atmosphere–Ocean Dynamics.* Academic Press, 662 pp.

Goldstein, H. 1980 *Classical Mechanics*, 2nd edn. Addison-Wesley, 672 pp.

Holliday, D. & McIntyre, M.E. 1981 On potential energy density in an incompressible, stratified fluid. *J.Fluid Mech.* **107**, 221–225.

Holm, D.D., Marsden, J.E., Ratiu, T. & Weinstein, A. 1985 Nonlinear stability of fluid and plasma equilibria. *Phys.Reports* **123**, 1–116.

Holm, D.D. & Long, B. 1989 Lyapunov stability of ideal stratified fluid equilibria in hydrostatic balance. *Nonlinearity* **2**, 23–35.

Killworth, P.D. & McIntyre, M.E. 1985 Do Rossby-wave critical layers absorb, reflect, or over-reflect? *J.Fluid Mech.* **161**, 449–492.

Kushner, P.J. & Shepherd, T.G. 1993 Wave-activity conservation laws and stability theorems for semi-geostrophic dynamics. *J.Fluid Mech.*, to be submitted.

Lighthill, M.J. 1978 *Waves in Fluids.* Cambridge University Press, 504 pp.

Lorenz, E.N. 1955 Available potential energy and the maintenance of the general circulation. *Tellus* **7**, 157–167.

Lorenz, E.N. 1967 *The Nature and Theory of the General Circulation of the Atmosphere.* World Meteorological Organization, Geneva, 161 pp.

Margules, M. 1903 Über die energie der stürme. *Jahrb.Zentralanst.Meteorol.Wien* **40**, 1–26. (English translation by C. Abbe in Smithsonian Misc.Coll., 1910, **51.**)

McIntyre, M.E. 1981 On the 'wave momentum' myth. *J.Fluid Mech.* **106**, 331–347.

McIntyre, M.E. & Shepherd, T.G. 1987 An exact local conservation theorem for finite-amplitude disturbances to non-parallel shear flows, with remarks on Hamiltonian structure and on Arnol'd's stability theorems. *J.Fluid Mech.* **181**, 527–565.

Morrison, P.J. 1982 Poisson brackets for fluids and plasmas. In *Mathematical Methods in Hydrodynamics and Integrability in Dynamical Systems* (M. Tabor and Y.M. Treve, eds.), Amer.Inst.Phys.Conf.Proc., vol.88, 13–46.

Morrison, P.J. & Greene, J.M. 1980 Noncanonical Hamiltonian density formulation of hydrodynamics and ideal magnetohydrodynamics. *Phys.Rev.Lett.* **45**, 790–794. (*Errata*, **48**, 569.)

Olver, P.J. 1986 *Applications of Lie Groups to Differential Equations.* Springer-Verlag, 497 pp.

Pedlosky, J. 1970 Finite-amplitude baroclinic waves. *J.Atmos.Sci.* **27**, 15–30.

Pedlosky, J. 1987 *Geophysical Fluid Dynamics*, 2nd edn. Springer-Verlag, 710 pp.

Salmon, R. 1983 Practical use of Hamilton's principle. *J.Fluid Mech.* **132**, 431–444.

Salmon, R. 1985 New equations for nearly geostrophic flow. *J.Fluid Mech.* **153**, 461–477.

Salmon, R. 1988*a* Semigeostrophic theory as a Dirac-bracket projection. *J.Fluid Mech.* **196**, 345–358.

Salmon, R. 1988*b* Hamiltonian fluid mechanics. *Ann.Rev.Fluid Mech.* **20**, 225–256.

Scinocca, J.F. & Shepherd, T.G. 1992 Nonlinear wave-activity conservation laws and Hamiltonian structure for the two-dimensional anelastic equations. *J.Atmos.Sci.* **49**, 5–27.

Shepherd, T.G. 1985 Time development of small disturbances to plane Couette flow. *J.Atmos. Sci.* **42**, 1868–1871.

Shepherd, T.G. 1988*a* Nonlinear saturation of baroclinic instability. Part I: The two-layer model. *J.Atmos.Sci.* **45**, 2014–2025.

Shepherd, T.G. 1988*b* Rigorous bounds on the nonlinear saturation of instabilities to parallel shear flows. *J.Fluid Mech.* **196**, 291–322.

Shepherd, T.G. 1989 Nonlinear saturation of baroclinic instability. Part II: Continuously stratified fluid. *J.Atmos.Sci.* **46**, 888–907.

Shepherd, T.G. 1990 Symmetries, conservation laws, and Hamiltonian structure in geophysical fluid dynamics. *Adv.Geophys.* **32**, 287–338.

Shepherd, T.G. 1991 Nonlinear stability and the saturation of instabilities to axisymmetric vortices. *Eur.J.Mech.B/Fluids* **10**, N° 2–Suppl., 93–98.

Shepherd, T.G. 1992*a* Extremal properties and Hamiltonian structure of the Euler equations. In *Topological Aspects of the Dynamics of Fluids and Plasmas* (ed. H.K. Moffatt *et al.*), pp. 275–292, Kluwer Academic.

Shepherd, T.G. 1992*b* On the maintenance of the westerlies. *Woods Hole 1992 GFD Summer School*, pp. 186–189. (Woods Hole Oceanog. Inst. Technical Report, WHOI–93–24.)

Shepherd, T.G. 1993*a* A unified theory of available potential energy. *Atmosphere-Ocean* **31**, 1–26.

Shepherd, T.G. 1993*b* Nonlinear saturation of baroclinic instability. Part III: Bounds on the energy. *J.Atmos.Sci.* **50**, 2697–2709.

Taylor, G.I. 1915 Eddy motion in the atmosphere. *Phil.Trans.Roy.Soc.Lond.A* **240**, 1–26.

Van Mieghem, J. 1956 The energy available in the atmosphere for conversion into kinetic energy. *Beit.Phys.Atmos.* **29**, no.2, 129–142.

Warn, T. & Gauthier, P. 1989 Potential vorticity mixing by marginally unstable baroclinic disturbances. *Tellus* **41A**, 115–131.

Whitham, G.B. 1965 A general approach to linear and non-linear dispersive waves using a Lagrangian. *J.Fluid Mech.* **22**, 273–283.

A Nonlinear Wave in Rotating Shallow Water

Oliver Bühler
Department of Applied Mathematics and Theoretical Physics, Cambridge, U.K.

Introduction

In this project the one-dimensional shallow-water equations on an f-plane have been studied. One equation describing all possible dynamics has been derived. The potential vorticity structure appears explicitly in that equation. A nonlinear steadily translating periodic wave has been found and its limiting amplitude behaviour studied. There exists no solitary wave in this system. The Lagrangian description of fluid motion has been used, taking particle displacements as dependent variables.

The Lagrangian Description of Fluid Motion

The Lagrangian description of fluid motion is a formalism which is not very often put to work. Both the Eulerian equations and the Lagrangian equations appear on equal footing in the introductory chapter of Lamb's *Hydrodynamics*, but the latter are almost completely neglected in the following chapters. Only once do they appear explicitly in the book, in paragraph 251 when Gerstner's (1802) rotational deep-water surface wave is described. That wave is a fully nonlinear solution to the free-surface problem on a homogeneous and infinitely deep fluid. It is easily written down using Lagrangian coordinates but it is very difficult to solve for it in Eulerian coordinates. As Stokes describes it in the appendix to his paper on Oscillatory Waves (Collected Papers, vol. I, page 219ff), the wave is derived assuming that material surfaces coincide with surfaces of constant pressure throughout the fluid body. (It has not been stated in Lamb's book, nor in Stokes's or Rankine's papers—who found the same wave independently fifty years after Gerstner—, that the same assumption allows the wave to exist in a *stratified* fluid as well. This is because the baroclinic term in the vorticity equation $\nabla\rho \times \nabla p \equiv 0$ by the assumption.) This assumption is true at the free-surface, and at great depth, where the motion ceases, but not necessarily in-between. Indeed, the classical irrotational water wave does not have this property.

Why is this almost the only example of a practically successful Lagrangian solution ? Probably because asking for a solution to the Lagrangian equations is often asking for too much information, namely the complete displacement history of each fluid particle. It appears reasonable to assume that only very special flows will produce displacement fields which are describable with a couple of known functions (in Gerstner's case particle paths are perfect circles). From a more problem-oriented perspective, incompressible and irrotational two-dimensional motions are much more easily described in the Eulerian formalism where the mathematical task is reduced to solving Laplace's equation. Posing the same problem in the Lagrangian description leads to no simplification of the original equations at all.

In the extreme case of one-dimensional motion, however, the Lagrangian description can be used to some advantage, because particles cannot interchange their positions and this simplifies the problem in terms of particle locations.

Shallow-Water Equations in Lagrangian Form

The familiar shallow-water equations on an f-plane in Eulerian form are three partial differential equations for the fields of the horizontal velocity (u, v) and the layer depth h in terms of the three independent variables x, y and t:

$$\frac{\mathrm{D}u}{\mathrm{D}t} - fv = -g\frac{\partial h}{\partial x} \tag{1}$$

$$\frac{\mathrm{D}v}{\mathrm{D}t} + fu = -g\frac{\partial h}{\partial y} \tag{2}$$

$$\frac{\mathrm{D}h}{\mathrm{D}t} + h\boldsymbol{\nabla}\cdot\mathbf{u} = 0. \tag{3}$$

The equations in Lagrangian form look quite different, and they are the result of changing both dependent and independent variables. The dependent variables are taken to be the particle displacements vector (X, Y), and the independent variables are particle labels (a, b) and time t. The particle labels will be chosen arbitrarily up to the constraint that the Jacobian of the displacement fields with respect to the labels must equal the inverse layer depth:

$$\mathcal{J} \equiv \frac{\partial(X,Y)}{\partial(a,b)} = 1/h. \tag{4}$$

This requirement satisfies the continuity equation identically for *any* choice of $X(a, b, t)$ and $Y(a, b, t)$, thus reducing the number of equations from three to two. The material time derivative becomes an ordinary partial time derivative, denoted by a simple dot, and the spatial derivatives transform as:

$$\begin{aligned}\frac{\partial h}{\partial x} &= \frac{\partial(h,y)}{\partial(x,y)} = \frac{\partial(a,b)}{\partial(X,Y)}\frac{\partial(h,Y)}{\partial(a,b)} \\ &= \frac{1}{\mathcal{J}}\frac{\partial(1/\mathcal{J},Y)}{\partial(a,b)} = -\frac{1}{\mathcal{J}^3}\frac{\partial(\mathcal{J},Y)}{\partial(a,b)}.\end{aligned} \tag{5}$$

The resulting equations read

$$\begin{aligned}\mathcal{J}^3\left\{\ddot{X} - f\dot{Y}\right\} &= g\frac{\partial(\mathcal{J},Y)}{\partial(a,b)} \\ \mathcal{J}^3\left\{\ddot{Y} + f\dot{X}\right\} &= g\frac{\partial(X,\mathcal{J})}{\partial(a,b)},\end{aligned} \tag{6}$$

where $\mathcal{J}$ is given by (4).

Restriction to one-dimensional motion

If the velocity and the layer depth at each instant are independent of one space coordinate (y, say), then the motion is one-dimensional. To get anywhere in the new variables, we have to align one of the particle label coordinates with the Y-axis. If this holds true initially, then it will be true at later times as well. Let's assign the labels such that the lines of constant a are parallel to the Y-axis. For any Y-independent initial depth field we can then find a b to fulfill (4). This translates into the restrictions

$$X = X(a,t), \qquad \mathcal{J} = \mathcal{J}(a,t) \text{ and } \dot{Y} = \dot{Y}(a,t) \tag{7}$$

which can be used to simplify (6) as far as possible.

The right hand side of the second equation of (6) is zero, therefore one can integrate once with respect to time and get

$$\dot{Y} + fX = K(a,b), \tag{8}$$

the left hand side of which is independent of b, therefore

$$K = K(a). \tag{9}$$

Since $\dot{Y}$ is independent of b, the most general form for Y,

$$Y = P(a,t) + Q(a,b) \tag{10}$$

is obtained. Plugging this form into the requirement for $\mathcal{J}$, (7), one gets

$$\begin{aligned} \mathcal{J}_b(a,t) = 0 = X_a Y_{bb} &= X_a Q_{bb} \quad \text{and hence} \\ Q(a,b) &= A(a)b + B(a). \end{aligned} \tag{11}$$

The first equation of (6) now takes the preliminary form

$$(X_a A(a))^3 \left\{ \ddot{X} + f^2 X - fK(a) \right\} = g(X_a A(a))_a A(a). \tag{12}$$

The a-derivatives only appear in conjunction with the function $A(a)$, hence for any choice of $A(a)$, a can be rescaled such that $A\,d\tilde{a} = da$. The long and the short is, that one can conveniently set $A(a) \equiv 1/H$, where H is the undisturbed layer depth, without loss of generality. This gives a the dimension of length.

The end result is this equation:

$$\boxed{\ddot{X} + f^2 X = fK(a) + gH \frac{X_{aa}}{X_a^3} \quad \text{for } X = X(a,t),} \tag{13}$$

which describes all possible Y-independent motions on an f-plane. After this equation has been solved for the X-displacement field, the Y-field can be found by time-integrating (8) and finding the functions $P(a,t)$ and $Q(a,b)$. The depth field is given by (4) as

$$1/h = X_a/H. \tag{14}$$

Significance of $K(a)$

The shallow-water potential vorticity is defined as

$$PV \equiv (v_x - u_y + f)/h, \tag{15}$$

which in our case becomes (using (8) and the transform rule (5))

$$PV = \frac{1}{H}\frac{\mathrm{d}K}{\mathrm{d}a} \equiv K'(a)/H. \tag{16}$$

From the assumption of one-dimensional motion, the potential vorticity is independent of Y *and* independent of time, which must be the case because PV is a materially conserved quantity, i.e., constant following particles.

The potential-vorticity structure thus takes a prominent and explicit place in the equation of motion and mediates the dynamics.

Steadily Translating Patterns

The shallow-water f-plane has both nonlinear and dispersive properties. The nonlinear effects try to steepen wave fronts by moving crests faster than troughs, the dispersive effects can counter this, and there might be a finite-amplitude balance where a wave-like shape translates without further distortion. To find out whether that's possible here,

$$\frac{\partial(\dot{X}, X - \hat{c}t)}{\partial(a,t)} = \frac{\partial(X_a, X - \hat{c}t)}{\partial(a,t)} \equiv 0 \tag{17}$$

is assumed, with $\hat{c}$ being an unknown constant wave speed. Using (13) and (17)[1] the requirement on $K(a)$ is found to be that it is a linear function of a, making the potential vorticity *uniform*.

The Simple Wave

Taking the PV uniform and equal to f/H throughout the plane and using the *ansatz*[2]

$$X = a + \xi(s) \quad \text{with } s = a - \hat{c}t \tag{18}$$

(13) becomes

$$\hat{c}^2\xi'' + f^2\xi = gH\frac{\xi''}{(1+\xi')^3}. \tag{19}$$

To non-dimensionalize this equation the Rossby-deformation length

$$L_R \equiv \sqrt{gH/f^2} \tag{20}$$

is defined and

$$\xi(s) = L_R\Phi(\tau) \text{ with } \tau \equiv s/L_R \tag{21}$$

is substituted. This yields

$$\boxed{\Phi''\left\{c^2 - \frac{1}{(1+\Phi')^3}\right\} + \Phi = 0,} \tag{22}$$

where $c^2 \equiv \hat{c}^2/gH$. A solution to this equation gives both X (through (18)) and the fields of u and h in a parametric representation; to find out what the wave looks like in physical space one has to plot it on a computer. After the scaling, the only parameter left is the wave speed c. The rotation rate f only sets the length scale through (20), such that for weaker rotation a longer wavelength is necessary to produce the same wave speed.

The equation resembles a nonlinear oscillator. For small amplitudes the bracket is almost constant and the wave-form is sinusoidal, for larger amplitudes it is varying through a period and the wave-form becomes distorted with peaky crests and wide troughs. Finally, there exists a critical amplitude where the bracket becomes zero at one point of the cycle. No physical meaningful solution exists with larger amplitude.

The study of the equation is greatly simplified by the existence of an exactly conserved quantity

$$\mathcal{H}(\Phi', \Phi) \equiv \frac{\Phi'^2}{2}\left\{c^2 - \frac{1}{(1+\Phi')^2}\right\} + \frac{\Phi^2}{2}. \tag{23}$$

[1]To really do that, you must take the Jacobian of (13) with $X - \hat{c}t$ and use $X \equiv K/f + \Delta(a,t)$ to find that necessarily $\Delta = \Delta(K/f - \hat{c}t)$. You plug that back into (17) and it only works if K' is *constant*.

[2]Which can be checked to satisfy (17).

The critical amplitude corresponds to a trajectory with

$$\mathcal{H}_c = (c^{2/3} - 1)^3/2. \tag{24}$$

Indeed, (22) can be written fully in Hamiltonian form, but with a singular bracket which goes to infinity at the saddle point of $\mathcal{H}(\Phi', \Phi)$ coinciding with the critical amplitude of the wave. Thus the saddle point is *not* a stationary point of the evolution, although the gradient of $\mathcal{H}$ vanishes there. This makes the contour plot of $\mathcal{H}$ over the phase space somewhat deceptive. In particular, the existence of a saddle point often signals the possibility of a soliton solution, but here the trajectory passes right through the saddle point in finite time and thus there exists no soliton for the shallow-water model on an f-plane.

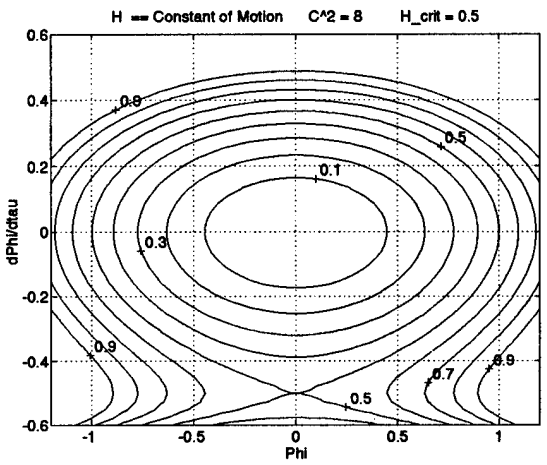

Figure 1: Trajectories of the nonlinear oscillator. Critical amplitude has a saddle point.

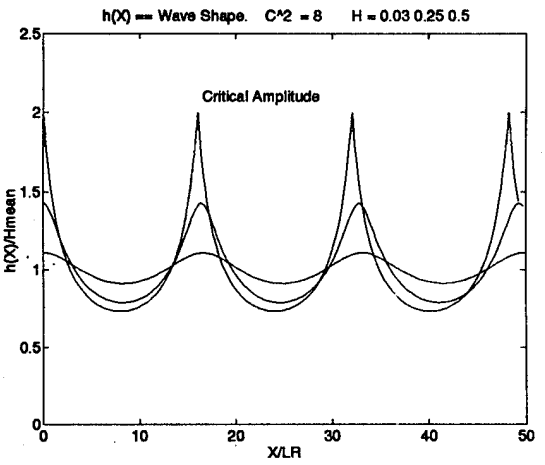

Figure 2: Wave Shape for different amplitudes. Critical amplitude $\mathcal{H} = 0.5$ has a sharp corner.

Relation between Velocity and Depth

From (18) and the identity (14) it follows that there exists a fixed relation between u and h, namely

$$u \equiv \sqrt{gH}c\frac{h - H}{h}. \tag{25}$$

This is the nonlinear extension of the familiar relation between the velocity and depth amplitudes for the linear wave. Presumably, this relation could be used to deduce the wave in an Eulerian frame as well.

Stokes Drift

The waves have periodic X-displacement fields, indicating at first sight a surprising absence of Stokes drift. But Stokes drift is defined as the difference between the Lagrangian mean velocity and the Eulerian mean velocity and thus everything works out, because the velocity over one wave period at a fixed point in space is not zero, but negative if c is positive. Therefore c actually gives the wave phase speed in a frame moving with the Stokes drift velocity:

$$c_{Ph} = u_{SD} + c. \tag{26}$$

This is an example of how understanding a solution to the Lagrangian equations in ordinary space-time pictures requires some work and might lead to unexpected results.

To find out how big the Stokes drift is (or rather how *small*, since we want to neglect it!) the velocity is averaged over one wavelength:

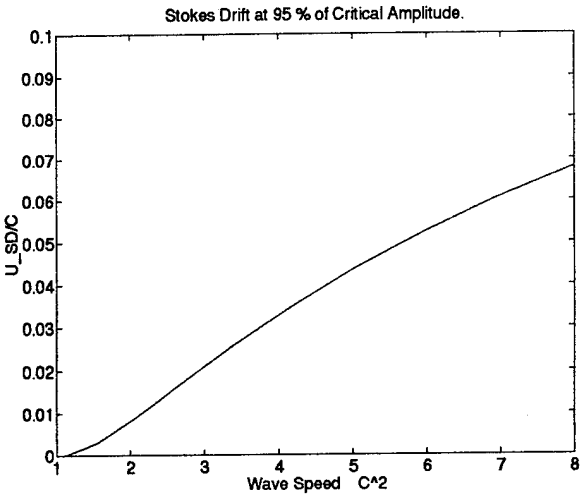

Figure 3: Stokes drift at 95 % of the critical amplitude.

Again, u_{SD} is the average velocity of a fixed particle as seen from a frame in which the average velocity at a fixed point is zero. It is below ten percent of the phase speed for the case considered in the wave shape picture (Fig.: 2). The drift speed increases more than linearly with c and comparing this with the general result from linear wave theory

$$u_{SD}/c \sim \frac{1}{2}\frac{u_{max}^2}{c^2} + O(\frac{u_{max}^4}{c^4})$$

indicates that u_{max}/c increases with increasing c.

Nonlinear Breaking Amplitudes

The sufficient breaking criterion $u_{\max}/c = 1$ comes from the following argument: for $f = 0$, surface waves are longitudinal, i.e., the particle displacement vector is parallel to the phase propagation direction of the wave. For $f \neq 0$, surface waves have an additional particle displacement component transverse to the propagation direction.

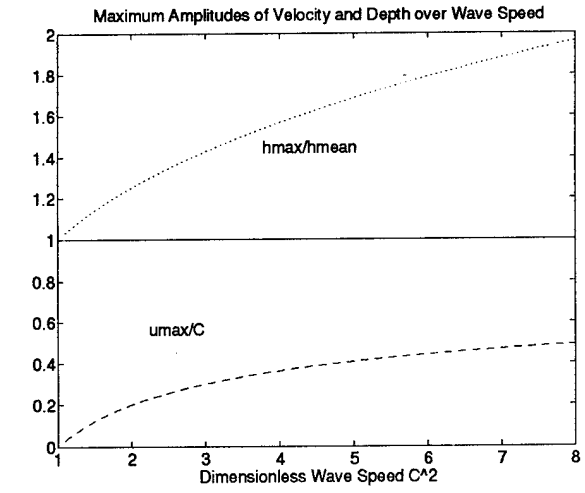

Figure 4: Breaking amplitudes of velocity and depth over wave speed squared.

But in both cases the wave can only exist if the phase speed exceeds the maximum particle velocity in direction of the phase propagation. Otherwise particles would surf on wave crests and never come back. Therefore the wave *must* break unless $u_{\max}/c < 1$. But the wave might already break nonlinearly at lower amplitudes. From (24) we can deduce the maximum particle velocity for each value of c as well as the maximum depth h. The lower half shows that the breaking velocity amplitude is much smaller than c, therefore breaking occurs much earlier than estimated from the sufficient criterion $u_{\max}/c = 1$. The upper half shows that the maximum layer depth is smaller than twice the mean layer depth for phase speeds smaller than $\sqrt{8}$.

Summary

Associated with every linear inertio-gravity wave in shallow water there is a nonlinear family of finite-amplitude waves with the same phase speed but varying amplitude. For each phase speed there exists a maximal amplitude for the waves. For bigger waves the nonlinear effects cannot be balanced any more by the dispersion, and the waves will break. This breaking criterion (see Fig.: 4) is much more restrictive than the sufficient criterion of maximal particle speed equals phase speed. Waves with equal phase speed but increasing amplitude have decreasing wavelengths.

Uniform potential vorticity is necessary for any steadily translating solution and then the derived wave family is the unique solution to that problem.

Acknowledgements

My greatest thanks go to Rick Salmon, firstly because without him I would have never made it to Woods Hole and secondly because he hit on the nonlinear wave effortlessly one night and together we could spend the rest of the summer trying to understand why it had worked! In addition, I would like to thank Joe Keller and Phil Morrison for encouraging and fruitful discussions about this work. Dean Petrich and Geoff Dairiki offered additional time and brain power and I fear that they have not been paid back adequately – but isn't that what good fellows are for ? I wish to thank the staff and all the people who populated Walsh Cottage over the summer for the wonderful time I had there, especially Ed Spiegel, whose sporting spirit and moral integrity turned the Fellow-Staff Softball game into an unforgettable event.

Finally, I wish to thank Trinity Hall, the Department of Applied Mathematics and Theoretical Physics in Cambridge, U.K. and the Gottlieb Daimler-und Karl Benz-Stiftung in Germany for their generous contribution to my travelling expenses and maintenance.

Drop formation from viscous fingering

Silvana S. S. Cardoso

Institute of Theoretical Geophysics, Department of Applied Mathematics and Theoretical Physics, Silver Street, Cambridge CB3 9EW, England

Abstract

The stability of the horizontal displacement of an intermediate layer of fluid bounded by two other fluids of different viscosities is analysed. We consider the flow of immiscible fluids in a porous medium; the results are also valid for the analog Hele-Shaw cell displacement. Linear stability analysis for both one-dimensional rectilinear and radial flows are presented. It is found that in a rectilinear displacement, the presence of a nearby stable interface cannot lead to the stabilisation of the other interface. The intermediate layer will then eventually breakup into drops. However, in the case of radial flow, the continuous thinning of the intermediate layer as it moves outward, results in the stabilisation of the system.

1. Introduction

When a fluid is horizontally displaced by another in a porous medium, the interface between them may be either stable or unstable, depending on the relative viscosities of the fluids and on their miscibility. The basic mechanism of this instability was first described by Hill (1952) and later by Saffman and Taylor (1958). Consider the rectilinear displacement of a fluid of viscosity μ_2 by a another fluid of viscosity μ_1 in a homogeneous porous medium (figure 1).

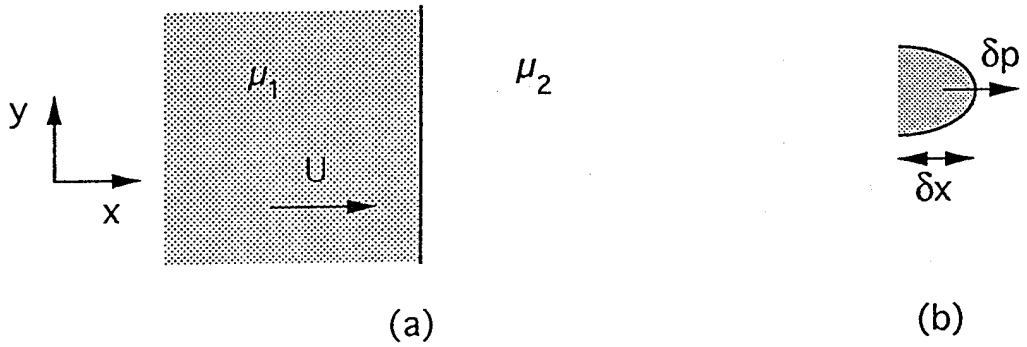

Figure 1. Rectilinear displacement of a fluid by another fluid of different viscosity.

The motion of the fluids through the porous medium is governed by Darcy's law, which for steady flow may be written as

$$\mathrm{u} = -\frac{\kappa}{\mu}\nabla p = -M\nabla p \tag{1}$$

where u denotes velocity, κ is the permeability of the medium and p is pressure. M is the mobility of the fluid. Suppose the interface between the two fluids is deformed slightly

such that there is a virtual displacement δx from its convected location (figure 1b). Then, from (1), the pressure force on the displaced fluid is $\delta p = p_1 - p_2 = (1/M_2 - 1/M_1)U\delta x$ where U is the steady state velocity. If the net pressure difference is positive, then any small perturbation to the interface will grow, leading to an instability. Hence, the interface will be unstable when a less viscous fluid displaces a more viscous fluid. Long 'fingers' of the displacing fluid will penetrate into the more viscous fluid ahead.

We have assumed above that the interface between the two fluids is sharp, i.e. that the fluids are immiscible. A detailed stability analysis should therefore take into account the effect of surface tension (Chouke *et al.*,). For disturbances in the form of normal modes proportional to $exp(\sigma t + iky)$, the general growth rate of the instability is given by

$$\sigma = \frac{M_1 - M_2}{M_1 + M_2} Uk - \frac{M_1 M_2}{M_1 + M_2} Tk^3 \qquad (2)$$

Here T denotes the surface tension coefficient and k is the wavenumber of the instability. The dispersion relation (2) shows that the effect of surface tension (second term) is to damp short waves, whereas the basic mechanism (first term) favours them. The competition of these two opposing effects leads to the occurence of a preffered mode (figure 2).

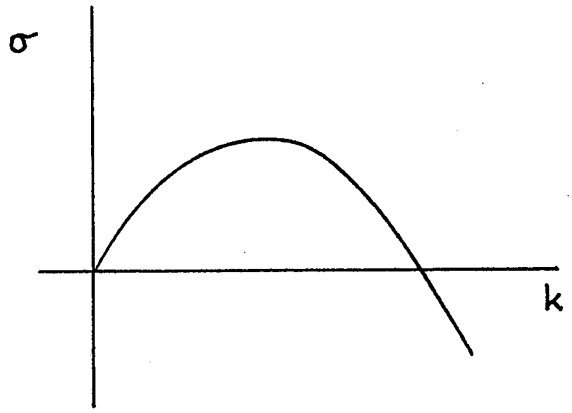

Figure 2. Dispersion relation for the rectilinear displacement of two immiscible fluids.

Many recent investigations (Homsy, 1987) on the Saffman-Taylor instability have been directed mainly at exploring different possibilities of surpressing the instability. This problem has been motivated by its relevance in oil recovery processes which attempt to produce oil by displacement with air or water; this is often accompanied by the addition of polymer to reduce the instability at the boundary between the oil and the displacing fluid (Mungan, 1971, Gorell and Homsy, 1983 and Paterson, 1984).

In the present study, we extend the work described above. We investigate the stability of the displacement of an intermediate layer of fluid bounded by two other fluids of different viscosities. The dynamics of the two interfaces and their interaction is studied; the possibility of stabilising an interface with the presence of another nearby interface is analysed. In section 2, we model the flow in a rectilinear geometry. In section 3, radial source flow is considered. Finally, in section 4, we draw some conclusions and give suggestions for future work.

2. Rectilinear displacement

Consider the displacement in a porous medium of an intermediate layer of fluid, bounded by two other fluids, as sketched in figure 3. The three fluids are assumed to have different viscosities and to be immiscible.

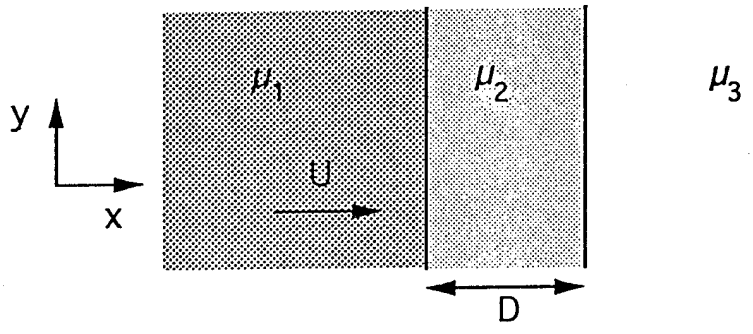

Figure 3. Displacement of an intermediate layer of fluid.

The equations describing the motion of the fluids are Darcy's law (c.f. (1)), which may be written in terms of a velocity potential $\phi = Mp$ as

$$\mathbf{u} = -\nabla\phi \tag{3}$$

and the continuity condition for incompressible fluids

$$\nabla.\mathbf{u} = 0 \tag{4}$$

The velocity potential therefore satisfies Laplace's equation $\nabla^2\phi = 0$. The boundary conditions for the problem specify the continuity of velocity and the pressure drop due surface tension at each interface. These equations admit the steady state solution

$$\phi_j^o = -Ux + c_j \qquad j = 1,2,3 \tag{5}$$

where the subscripts 1, 2 and 3 refer to the inner, intermediate and outer fluids respectively. The constants c_j may be detemined by specifying the magnitude of the pressure at some point in the flow.

As the interface moves, it experiences perturbations due to inhomogeneities. Consider a wavelike perturbation $a = Aexp(iky + \sigma t)$ at the interface between fluids 1 and 2, and a similar perturbation $b = Bexp(iky + \sigma t)$ at the interface between fluids 2 and 3, where σ is the growth rate of the instability and k its wavenumber. The required solution of (3) and (4) has the form $\phi_j = \phi_j^o + \phi_j^1$, with

$$\begin{aligned}
\phi_1^1 &= \alpha e^{iky+kx+\sigma t} \\
\phi_2^1 &= \beta e^{iky-kx+\sigma t} + \gamma e^{iky+kx+\sigma t} \\
\phi_3^1 &= \delta e^{iky-k(x-D)+\sigma t}
\end{aligned} \tag{6a,b,c}$$

where α, β, γ and δ are constants to be determined. We consider here a moving frame of reference in which the instant positions of the interfaces coincide with the planes $x = 0$ and $x = D$ (to first order). The continuity of velocity across the interface between fluids 1 and 2 (at x=a) is given by

$$u_1^o + u_{1x}^o a + u_1^1 = u_2^o + u_{2x}^o a + u_2^1 = a_t \tag{7}$$

The pressure condition at this interface is

$$\frac{\phi_1^o}{M_1} + (\frac{\phi_1^o}{M_1})_x a + \frac{\phi_1^1}{M_1} = \frac{\phi_2^o}{M_2} + (\frac{\phi_2^o}{M_2})_x a + \frac{\phi_2^1}{M_2} - T a_{yy} \tag{8}$$

Similar velocity and pressure conditions may be written for the interface between fluids 2 and 3. The resulting system of equations may be solved for the growth rate of the instability, σ, and for the ratio of the amplitudes of the perturbations at the two interfaces, A/B. The solution is

$$a_0 \left(\frac{\sigma}{Uk}\right)^2 + a_1 \left(\frac{\sigma}{Uk}\right) + a_2 = 0 \tag{9}$$

where a_0, a_1 and a_2 are given by

$$a_0 = \left(1 + \frac{M_2}{M_1}\frac{M_2}{M_3}\right) sinh(kD) + \left(\frac{M_2}{M_1} + \frac{M_2}{M_3}\right) cosh(kD)$$

$$a_1 = \left(\left(\frac{M_2}{M_1} - \frac{M_2}{M_3}\right) + \left(\frac{M_2}{M_1} + \frac{M_2}{M_3}\right)\frac{TM_2}{UD^2}(kD)^2\right) sinh(kD)$$
$$+ \left(\left(\frac{M_2}{M_1} - \frac{M_2}{M_3}\right) + \frac{2TM_2}{UD^2}(kD)^3\right) cosh(kD)$$

$$a_2 = \left(-\left(1 - \frac{M_2}{M_1}\right) + \frac{TM_2}{UD^2}(kD)^2\right)\left(\left(1 - \frac{M_2}{M_3}\right) + \frac{TM_2}{UD^2}(kD)^2\right) sinh(kD)$$

and

$$\frac{A}{B} = \frac{\sigma}{Uk} \Big/ \left(-\left(1 - \frac{M_2}{M_1}\right) sinh(kD) + \frac{\sigma}{Uk}\left(\frac{M_2}{M_1} sinh(kD) + cosh(kD)\right)\right.$$
$$\left. + \frac{TM_2}{UD^2}(kD)^2 sinh(kD)\right) \tag{10}$$

We have assumed here that the surface tension coefficient is the same at both interfaces.

Figure 4 shows a plot of the dispersion relation for a case in which both interfaces are unstable. The configuration of the intermediate layer, obtained from the ratio of amplitudes A/B, has been sketched beside each curve. It may be seen that there are two different modes. One in which the interfaces grow in phase , and another in which the interfaces grow in antiphase. Both modes are unstable for long wavelengths. Short wavelengths are stabilised by surface tension, as expected.

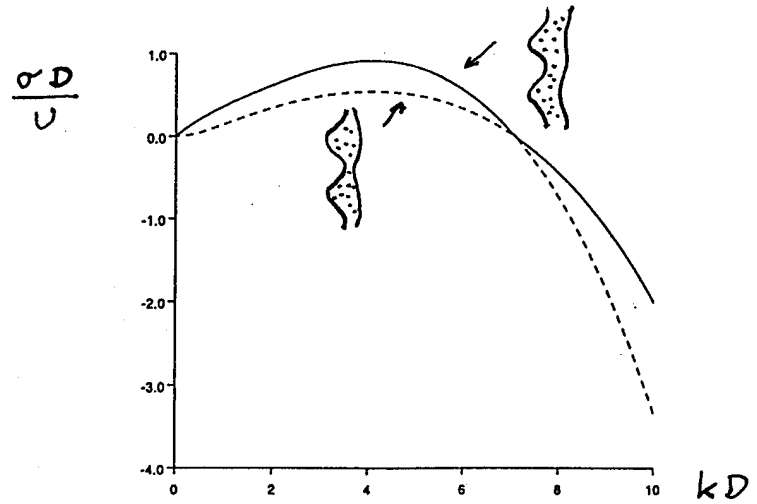

Figure 4. Dispersion relation when the two interfaces are unstable.

In figure 5, the dispersion relation for a case in which only one of the interfaces is unstable is represented. One of the modes is now stable for all wavelengths. The other mode is unstable for long wavelengths, but stabilised by surface tension for short wavelengths.

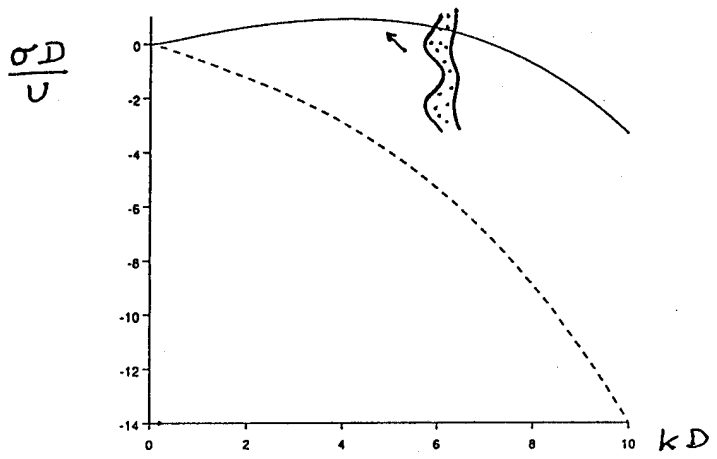

Figure 5. Dispersion relation when only one interface is unstable.

The limit of a thin intermediate layer

Let us consider the limit in which the thickness of the intermediate layer is small compared with the length scale of the motion, i.e. $kD \ll 1$. From equations (9) and (10), we have

$$\left(\frac{\sigma D}{U}\right)_1 = \frac{M_1 - M_2}{M_1 + M_3} kD - \frac{2T}{UD^2}\frac{M_1 M_3}{M_1 + M_3}(kD)^3$$

$$\left(\frac{\sigma D}{U}\right)_2 = \frac{\left(1 - \frac{M_2}{M_1}\right)\left(\frac{M_2}{M_3} - 1\right)}{\frac{M_2}{M_3} - \frac{M_2}{M_1}}(kD)^2 - \frac{\left(1 - \frac{M_2}{M_1}\right)^2 + \left(\frac{M_2}{M_3} - 1\right)^2}{\left(\frac{M_2}{M_3} - \frac{M_2}{M_1}\right)^2}\frac{M_2 T}{UD^2}(kD)^4 \qquad (11a, b)$$

and

$$\left(\frac{A}{B}\right)_1 = 1 - \left(\frac{2T}{UD^2}\frac{M_1M_2}{M_1 - M_3}\right)^2 (kD)^4$$

$$\left(\frac{A}{B}\right)_2 = -\frac{\frac{M_2}{M_3} - 1}{1 - \frac{M_2}{M_1}} \left(1 - \frac{\left(1 - \frac{M_2}{M_1}\right)^2 + \left(\frac{M_2}{M_3} - 1\right)^2}{\left(\frac{M_2}{M_3} - \frac{M_2}{M_1}\right)\left(1 - \frac{M_2}{M_1}\right)} \left(\frac{M_2}{M_3} - 1\right) \frac{M_2T}{UD^2}(kD)^2 \right. \qquad (12a, b)$$

$$\left. \left(1 + 2\frac{\frac{M_2}{M_3} - 1}{\left(1 - \frac{M_2}{M_1}\right)\left(\frac{M_2}{M_3} - \frac{M_2}{M_1}\right)} \frac{M_2T}{UD^2}(kD)^2 \right) \right)$$

Equation (11a) describes the stability of a mode similar to the Saffman-Taylor mode (compare with (2)). It is an overall mode since it is determined by the properties of only fluids 1 and 3. The other solution, given by (11b), represents a slower growing, internal mode. The results in figure 5 suggest that the Saffman-Taylor mode is unable to stabilise the internal mode. This result represents physically an important initial step for the eventual breakup of the intermediate layer into drops. A sketch of the expected evolution of this layer is shown in figure 6. This behaviour should be verified experimentally in future work.

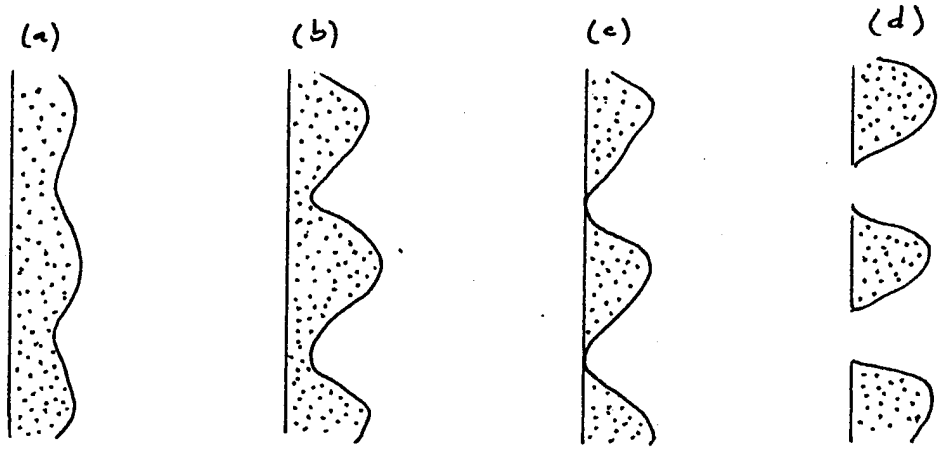

Figure 6. Breakup of the intermediate layer into drops.

3. Radial displacement

Consider the radial displacement of an annulus of fluid in a porous medium, as shown in figure 7.

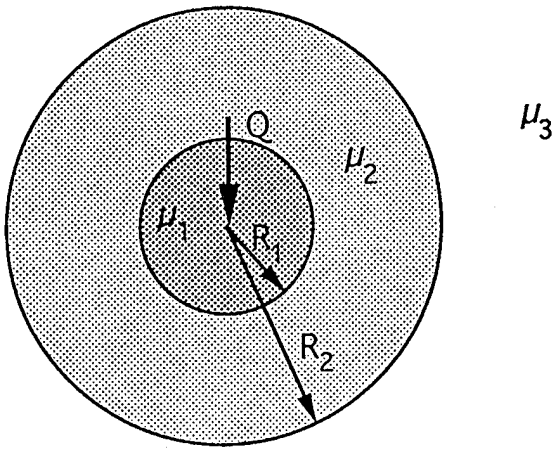

Figure 7. Radial displacement of an annulus of fluid.

The flow is described by Laplace's equation (c.f. (3) and (4)), which in polar coordinates reads

$$\phi_{rr} + \frac{1}{r}\phi_r + \frac{1}{r^2}\phi_{\theta\theta} = 0 \tag{13}$$

For a point source with volume flow rate per unit depth Q, the velocity potential of the steady flow satisfying (13) is

$$\phi_j^o = -\frac{Q}{2\pi} lnr + c_j \qquad j = 1,2,3 \tag{14}$$

This solution satisfies the continuity of velocity at each interface. The constants c_j may be determined by prescribing both the pressure drop due to surface tension at each interface and the magnitude of the pressure at some point in the flow.

Suppose that at some time the positions of the interfaces are $r = R_1$ and $r = R_2$ (figure 7) and that both interfaces are perturbed from the steady state circular configuration. The interface at $r = R_1$ undergoes a wavelike perturbation $a = A(t)exp(in\theta)$ and the interface at $r = R_2$ a perturbation $b = B(t)exp(in\theta)$, where both amplitudes are functions of time t.

The required solution of (13) is of the form $\phi_j = \phi_j^o + \phi_j^1$ with

$$\begin{aligned}
\phi_1^1 &= \alpha(t)(\frac{r}{R_1})^n e^{in\theta} \\
\phi_2^1 &= \beta(t)(\frac{r}{R_1})^{-n} e^{in\theta} + \gamma(t)(\frac{r}{R_2})^n e^{in\theta} \\
\phi_3^1 &= \delta(t)(\frac{r}{R_2})^{-n} e^{in\theta}
\end{aligned} \tag{15a,b,c}$$

The functions of time in the equations above may be determined by the boundary conditions at each interface. The continuity of velocity at the interface between fluids 1 and 2 ($r = R_1 + a$) requires that

$$v_1^o + v_{1r}^o a + v_1^1 = v_2^o + v_{2r}^o a + v_2^1 = v^o + a_t \tag{16}$$

The pressure condition at this interface is expressed by

$$\frac{\phi_1^o}{M_1} + (\frac{\phi_1^o}{M_1})_r a + \frac{\phi_1^1}{M_1} = \frac{\phi_2^o}{M_2} + (\frac{\phi_2^o}{M_2})_r a + \frac{\phi_2^1}{M_2} + T(\frac{1}{R_1} - \frac{a + a_{\theta\theta}}{R_1^2}) \tag{17}$$

Similar continuity conditions may be written for the interface at $r = R_2 + b$. The resulting system of equations may be solved for the growth rate of the instabilities of the two interfaces, A_t and B_t. The general solution is complicated and we shall therefore focus upon a more simple, limit situation.

If the viscosity of the displacing fluid (fluid 1) is very large, then $M_1 \to 0$ and therefore $A, A_t \to 0$. Physically, this means that the inner interface is rigid to any perturbation, and hence it remains circular as it moves outward with time. If we assume further that $M_2 \gg M_3$ and also that the annulus of fluid 2 is thin compared to the wavelength of the instability ($n\delta \ll 1$), we find

$$\frac{B_t}{B} = \frac{\frac{n-1}{R_2^2}\left(\frac{Q}{2\pi} - \frac{n(n+1)TM_3}{R_2}\right)}{1 + \frac{M_3}{M_2 n\delta}} - \frac{Q}{2\pi R_2^2}\frac{\frac{M_3}{M_2 n\delta}}{1 + \frac{M_3}{M_2 n\delta}} \tag{18}$$

where $\delta = (R_2 - R_1)/R_1$ is a non-dimensional thickness of the annulus. The first term in the expression above represents the opposing effects of the viscosity difference between fluids 2 and 3 (destabilising effect) and of the surface tension (stabilising effect). The numerator of this term is similar to that found by Paterson (1981) in his work on the stability of a single interface in radial source flow. The second term in (18) represents a new effect, that of the thickness of the annulus becoming smaller with time. This thinning of the intermediate layer tends to stabilise any perturbation to the interface between fluids 2 and 3. We may see that there is some interaction between the effects described above, since the denominator of the first term contains $n\delta$.

We are interested in finding the radius at which the interface first becomes unstable, for prescribed input conditions, that is the solution of the equation

$$\frac{B_t}{B} = 0 \tag{19}$$

It is possible to show that the mode that first becomes unstable depends on the radius of the interface, R_2. We must thus combine (19) with the condition

$$\left(\frac{B_t}{B}\right)_t = 0 \tag{20}$$

in order to determine the critical minimum radius and the corresponding wavelength for a perturbation to be maintained. Let us define the non-dimensional variable

$$\upsilon = \frac{M_3}{M_2}\frac{2\pi R_2^2}{V} \tag{21}$$

where $V = 2\pi R_2^2 \delta$ is the volume per unit depth of the annulus fluid and $R_c = (12T\pi M_3)/Q$ is the radius at which a circular interface first becomes unstable when only two fluids are present (see Paterson, 1981); v is thus a volume fraction.

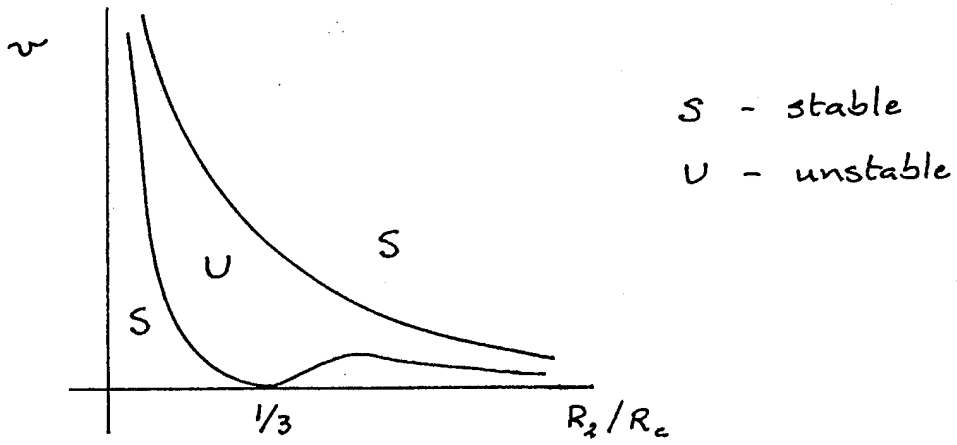

Figure 8. Stability diagram for the radial displacement.

The solution of equations (19) and (20) in (v)-(R_2/R_c) space is shown in figure 8. It may be seen that for a fixed volume of annulus fluid, the interface is stable at small radii; this is a result of the effect of surface tension. At larger radii, the interface becomes unstable due to the unfavourable viscosity difference. However, surprisingly, at still larger radii the interface is again stable. This stabilisation at large radii is a result of the thinning of the annulus during the outward flow in radial geometry, as seen above.

In the asymptotic limit of a relatively large volume of the annulus fluid, i.e. when $v \to 0$, the minimum wavenumber at which instability occurs is given by

$$n = (\frac{3}{2v})^{1/2} \tag{22}$$

4. Conclusions

The linear stability analysis of the one-dimensional displacement of an intermediate layer of fluid, bounded by two other fluids of different viscosities shows that there are two different modes. One of the modes is determined only by the properties of the bounding fluids; it is an overall mode, analogous to the Saffman-Taylor mode. The other mode depends on on the properties of the three fluids; this internal mode has a smaller growth rate than the Saffman-Taylor mode. The presence of one stable interface results in the stabilisation of one of the modes. In a rectilinear displacement, this stable mode is unable to stabilise the other mode. The intermediate layer is therefore unstable and will eventually breakup into drops. However, in a radial displacement the system can be totally stable owing to the continuous thinning of the intermediate layer during the outward flow.

At this stage it would be interesting to compare our theoretical predictions with experimental observations. Qualitative verification of the behaviour described above and, eventually,

measurement of the wavelength of the instability at its inception are significant points. A deeper mathematical analysis of the radial flow problem should also be carried out. In particular, the growth rate of the instability should be compared with the rate of change of the position of the intermediate layer. If the latter is non-negligible, integration of the growth rate of the instability over time should allow a more realistic modelling of the incipient instability.

Acknowledgements

I would like to thank Andy Woods for all his encouragement and help with the work presented here. I also thank Joe Keller for his helpful suggestions and Jack Whitehead for providing me with the facilities in the GFD laboratory. I am grateful to all GFD staff and particularly the fellows for making this a very enjoyable summer. Finally, I would like to acknowledge the financial support of the EEC Science Program.

References

Chouke, R. L., van Meurs, P., van der Poel, C. 1959 The instability of slow immiscible, viscous liquid-liquid displacements in permeable media. *Trans. AIME* **216** 188-94

Gorell, S., Homsy, G. M. 1983 A theory of optimal policy of oil recovery by secondary displacement processes. *SIAM J. Appl. Math.* **43** 79-98

Hill, S. 1952 Channelling in packed columns. *Chem. Eng. Sci.* **1** 247-53

Homsy, G.M. 1987 Viscous fingering in porous media. *Ann. Rev. Fluid Mech.* **19** 271-311

Mungan, N. 1971 Improved waterflooding through mobility control, *Canad. J. Chem. Engr.* **49** 32-37

Paterson, L. 1981 Radial fingering in a Hele-Shaw cell. *J. Fluid Mech.* **11** 513-29

Paterson, L. 1985 Fingering with miscible fluids in a Hele-Shaw cell, *Phys. Fluids* **28** (1) 26-30

Saffman,P. G., Taylor, G. I. 1958 The penetration of a fluid into a porous medium or Hele-Shaw cell containing a more viscous liquid. *Proc. R. Soc. London Ser. A* **245** 312-29

A Study of a Shell Model of Fully Developed Turbulence

Diego del-Castillo-Negrete

1 Introduction

The study of turbulence is one of the most challenging problems of science. At sufficiently high Reynolds numbers fluids exhibit fully developed turbulence. This state is characterized by extremely irregular variations of the velocity field both in space and in time due to strong nonlinear interactions between many degrees of freedom and scales. A landmark in the understanding of fully developed turbulence is the Kolmogorov scaling theory [1]. According to this theory, in a turbulent flow there is a local transfer of energy from large scales, where the system is driven, to small scales, where viscous dissipation dominates due to large velocity gradients. In an intermediate range of scales, called the inertial range, the fluid behaves like an inviscid unforced system and it exhibits scaling behavior. Assuming that the rate of energy transfer is constant and homogeneous in space one obtains, using dimensional arguments, the Kolmogorov scaling law for the energy spectrum $E(k) \sim k^{-5/3}$. This theory gives a good overall description of the energy spectrum of turbulent flows but fails to account for fluctuations in the energy transfer and dissipation seen experimentally [2,3] and numerically [4]. The deviations from Kolmogorov theory are more evident in the higher order moments statistics. It turns out that the energy transfer is not homogeneous but intermittent and that the majority of energy dissipation concentrates on a fractal-like structure rather than being spatially uniform. At present, there is not a satisfactory theory to explain the intermittency and high order statistics of fully developed turbulence based on the Navier-Stokes equation.

Early attempts to correct Kolmogorov's original idea were made by Landau [5] and by Kolmogorov [6]. Later on Mandelbrot [7] introduced a fractal model for the energy dissipation. Following this model, Frisch, Sulem and Nelkin [8] introduced the β-model in which the flux of energy is transferred to only a fixed fraction β of the eddies. To correct some of the discrepancies between the β-model and experimental results [2], Benzi, Paladin, Parisi and Vulpiani [12] presented the multifractal random β-model.

The main criticism of these models is that they are based on general scaling arguments that use Navier-Stokes equation only marginally. One would like to explain the intermittency directly from the dynamics of the Navier-Stokes equation. Unfortunately, this approach is not feasible since the number of relevant degrees of freedom increases rapidly with the Reynolds number. A scaling argument shows that the number of degrees of freedom required in

a numerical simulation is proportional to $Re^{9/4}$ where Re is the Reynolds number. An alternative is to consider few degrees of freedom models of Navier-Stokes equation. In recent years a class of models of this type, called shell models, has been successfully used in the study of fully developed turbulence. The objective of this report is to study the shell model proposed by Yamada and Ohkitani [9].

2 Shell Models

The basic idea of the shell models is to divide the Fourier space into N shells. Each shell, k_n, contains all the wave numbers $\vec{k}$ in the range $a^n \leq \mid \vec{k} \mid < a^{n+1}$, where a is a constant (usually $a = 2$). The velocity field is specified by N complex numbers u_n which represent the Fourier transform of the velocity field on the scale $1/k_n$. The Navier Stokes equation is then approximated by N complex, ordinary, nonlinearly coupled, first-order differential equations governing the time evolution of the Fourier amplitudes. Here we consider a shell model for three dimensional fully developed turbulence originally proposed by Yamada and Ohkitani [9]. The model takes into account only first and second neighbor interactions between the Fourier modes and is given by

$$\left(\frac{d}{dt} + \nu k_n^2\right) u_n = i(a_n u_{n+1}^* u_{n+2}^* + b_n u_{n-1}^* u_{n+1}^* + c_n u_{n-1}^* u_{n-2}^*) + f\delta_{n,n_0} \qquad (1)$$

for $n = 1, 2, \ldots, N$, where ν is the viscosity and f is the forcing acting at the scale $1/k_{n_0}$. The coupling constants are chosen to be $a_n = k_n, b_n = -k_{n-1}/2, c_n = -k_{n-2}/2, b_1 = b_N = c_1 = c_2 = a_{N-1} = a_N = 0$ in order to have energy and phase space volume conservation in the inviscid, unforced case ($\nu = f = 0$).

In the recent years this model has been studied extensively, see for example, [9-11]. In [9,10] it was shown that the model has positive Lyapunov exponents and that its dynamics is chaotic and confined to a strange attractor in the $2N$-dimensional phase space. It was also observed that on the average the chaotic solution exhibits Kolmogorov scaling in an inertial subrange of shells. Numerical simulations by Jensen, Paladin and Vulpiani [11] show that the model gives a correction to Kolmogorov scaling due to intermittency which is very close to the experimental value. More generally, they computed the velocity structure functions, $\delta u^Q = \mid u(t+\tau) - u(t) \mid^Q$, and showed that on the average there is scaling behavior $\langle \delta u^Q \rangle \sim \tau^{\xi_Q}$ with ξ_Q a nonlinear function of Q. These results represent a correction to the linear dependence between ξ_Q and Q predicted by Kolmogorov theory and were shown to be consistent with the multifractal random β-model. Also, in [11] a connection was established between the energy bursts and the instantaneous Lyapunov exponents. Shell models have also been proposed for the study of one dimensional turbulence (Burger's equation) [13], two dimensional turbulence [14,15] and for the study of turbulent advection of passive scalar fields [16].

3 Fixed Points Analysis and Linear Stability of the Shell Model

In this section we study the fixed points ($du_n/dt = 0$) of the shell model and their linear stability. Our objective is to understand the relationship between Kolmogorov scaling and the fixed points of the system. From a physical point of view, the relevant quantity is the amplitude of the velocity (i.e. the energy), therefore it is convenient to use polar coordinates $u_n = r_n(\cos\theta_n + i\sin\theta_n)$, $f = \eta(\cos\xi + i\sin\xi)$ and write the Eqs. (1) as

$$\frac{dr_n}{dt} = a_n r_{n+1} r_{n+2}\sin(\theta_n + \theta_{n+1} + \theta_{n+2}) + b_n r_{n-1} r_{n+1}\sin(\theta_{n-1} + \theta_n + \theta_{n+1}) + c_n r_{n-1} r_{n-2}\sin(\theta_{n-2} + \theta_{n-1} + \eta\cos(\xi - \theta_n)\delta_{n,n_0} + \theta_n) - \nu k_n^2 r_n \tag{2}$$

$$\frac{d\theta_n}{dt} = \frac{a_n r_{n+1} r_{n+2}}{r_n}\cos(\theta_n + \theta_{n+1} + \theta_{n+2}) + \frac{b_n r_{n-1} r_{n+1}}{r_n}\cos(\theta_{n-1} + \theta_n + \theta_{n+1}) + \frac{c_n r_{n-1} r_{n-2}}{r_n}\cos(\theta_{n-2} + \theta_{n-1} + \theta_n) + \frac{\eta}{r_n}\sin(\xi - \theta_n)\delta_{n,n_0} \tag{3}$$

Let us assume for the moment that the boundary shells are fixed (i.e. $du_n/dt = 0$ for $n = 1, 2, N-1$ and N) and that the inner shells ($n = 3, \ldots, N-2$) evolve according to Eqs.(2) and (3) with $\nu = 0$ and $f = 0$. In a sense, this corresponds to considering an "inertial range" in the shell model since we are neglecting the effects of viscosity, forcing and of the smallest and largest scale shells. For this case, since the wave numbers scale as $k_n \sim a^n$ there are an infinite number of fixed points (r_n^*, θ_n^*) defined by the conditions $\theta_{n+3}^* = \theta_n^*$ and $r_{n+3}^* = r_n^*/a$. In the phase space this set of fixed points forms a six-dimensional manifold $\mathcal{F}$ which we can parameterize by three angles and three radii (for example, using α_0, α_1 and α_2 we have $\theta_n^* = \alpha_{n\,\mathrm{mod}\,3}$ for all n and similarly for r_n^*). The set of fixed points having the Kolmogorov scaling $r_n^* = k_n^{-1/3}$ is a three-dimensional submanifold, $\mathcal{K}$, of $\mathcal{F}$ defined by the extra condition $r_i^* = k_i^{-1/3}$ for $i = 1, 2$ and 3. It is interesting to observe that the only fixed points which exhibit scaling $r_n^* = k_n^\alpha$ belong to $\mathcal{K}$; that is, the only scaling solution corresponds to the Kolmogorov scaling.

Having found the fixed points of the system, the next step is the study of their linear stability. The linearized equations for a perturbation $(\delta r_n, \delta\theta_n)$ are given by

$$\frac{d}{dt}\begin{pmatrix}\delta r\\ \delta\theta\end{pmatrix} = \begin{pmatrix}\mathcal{I}\sin(\psi) & \mathcal{I}\cos(\psi)\\ \mathcal{R}\cos(\psi) & -\mathcal{R}\sin(\psi)\end{pmatrix}\begin{pmatrix}\mathcal{L}_r & 0\\ 0 & \mathcal{L}_\theta\end{pmatrix}\begin{pmatrix}\delta r\\ \delta\theta\end{pmatrix} \tag{4}$$

where $\psi = \alpha_1 + \alpha_2 + \alpha_3$, $\mathcal{R}_{nm} = \delta_{n,m}/r_n^*$, $\mathcal{I}$ is the identity matrix and

$$\begin{aligned}\mathcal{L}_{\theta nm} &= k_n r_{n+1}^* r_{n+2}^*\left[\delta_{n+2,m} + \frac{1}{2}\delta_{n+1,m} - \delta_{n-1,m} - \frac{1}{2}\delta_{n-2,m}\right]\\ \mathcal{L}_{rnm} &= k_n r_{n+1}^*\delta_{n+2,m} + \left[k_n r_{n+2}^* - \frac{k_{n-1} r_{n-1}^*}{2}\right]\delta_{n+1,m} - \\ &\quad \left[\frac{k_{n-1} r_{n+1}^* + k_{n-2} r_{n-2}^*}{2}\right]\delta_{n-1,m} - \frac{k_{n-2} r_{n-1}^*}{2}\delta_{n-2,m}\end{aligned} \tag{5}$$

Note that $(\delta r_n, \delta\theta_n)$ with $\delta r_{n+3} = \delta r_n/a$, $\delta\theta_{n+3} = \delta\theta_n$ for $n = 1, 2, \ldots, N$ are six null eigenvectors which correspond to perturbations tangent to the $\mathcal{F}$ manifold. Also, for $\psi = \pi/2$ the equations for δr and $\delta\theta$ decouple and the stability problem reduces to finding the eigenvalues of the band diagonal matrices $\mathcal{R}\mathcal{L}_\theta$ and $\mathcal{L}_r$.

4 The 2-1/2 shell model

The general N shells model is hard to analyze and for that reason it is better to deal with a simplified version of it. Here we consider a truncation of the model in which only two shells, say the n and the $n+1$, are assumed to vary both in phase and amplitude and the rest of the shells are held fixed at the Kolmogorov scaling value with phases equal to zero except for the phases of the $n-1$ and $n+2$ shells which are assumed to evolve according to the shell dynamics. We refer to this model as a 2-1/2 model since it consists of 2 shells coupled to "1/2" (i.e. only through the phases) of the $n-1$, $n+2$ boundary shells. The resulting model (taking $a = 2$) is the following six degrees of freedom dynamical system

$$
\begin{aligned}
\frac{dR_1}{dt} &= 2^{(2n-3)/3}\left\{\left[\sin(\theta_1+\theta_2+\mu_2) - \frac{\sin(\theta_1+\theta_2+\mu_1)}{2}\right]R_2 - \frac{\sin(\theta_1+\mu_1)}{2}\right\} - \nu 2^{2n} R_1 \\
\frac{dR_2}{dt} &= -\frac{2^{(2n-1)/3}}{2}\left\{\left[\sin(\theta_1+\theta_2+\mu_2)+\sin(\theta_1+\theta_2+\mu_1)\right]R_1 + \sin(\theta_2+\mu_2)\right\} - \nu 2^{2(n+1)} R_2 \\
\frac{d\theta_1}{dt} &= 2^{(2n-3)/3}\left\{\left[\cos(\theta_1+\theta_2+\mu_2) - \frac{\cos(\theta_1+\theta_2+\mu_1)}{2}\right]\frac{R_2}{R_1} - \frac{1}{2R_1}\cos(\theta_1+\mu_1)\right\} \\
\frac{d\theta_2}{dt} &= -\frac{2^{(2n-1)/3}}{2}\left\{\left[\cos(\theta_1+\theta_2+\mu_2)+\cos(\theta_1+\theta_2+\mu_1)\right]\frac{R_1}{R_2} + \cos(\theta_2+\mu_2)\right\} \\
\frac{d\mu_1}{dt} &= 2^{(2n-5)/3}\epsilon\left[R_1 R_2\cos(\theta_1+\theta_2+\mu_1) - \frac{R_1}{2}\cos(\theta_1+\mu_1) - \frac{1}{2}\cos\mu_1\right] \\
\frac{d\mu_2}{dt} &= 2^{(2n+1)/3}\epsilon\left[\cos\mu_2 - \frac{R_2}{2}\cos(\theta_2+\mu_2) - \frac{R_1 R_2}{2}\cos(\theta_1+\theta_2+\mu_2)\right]
\end{aligned}
\tag{6}
$$

where $R_1 = k_n^{1/3} r_n, R_2 = k_{n+1}^{1/3} r_{n+1}, \theta_1 = \theta_n, \theta_2 = \theta_{n+1}, \mu_1 = \theta_{n-1}$ and $\mu_2 = \theta_{n+2}$. In these rescaled radial coordinates Kolmogorov scaling corresponds to $R_i = 1$. Note that we have introduced the parameter ϵ, which is not in the original shell equations, to control the rate of change of μ_1 and μ_2. For $\epsilon = 0$, μ_1 and μ_2 remain constant and the system reduces to the 2 shell model whereas for $\epsilon = 1$ we recover the 2-1/2 shell model.

The use of polar coordinates is not convenient for the numerical integration of the model because of the $1/R_i$ singularities in the phases equations. To avoid this problem we have done all the numerical integrations using cartesian coordinates $x_{i+1} = R_{n+i}\cos\theta_{n+i}$, $y_{i+1} = R_{n+i}\sin\theta_{n+i}$, $i = 0, 1$ for which the equations become

$$
\frac{d}{dt}\begin{pmatrix} x_1 \\ y_1 \\ x_2 \\ y_2 \end{pmatrix} = \begin{pmatrix} -\nu 2^{2n} & 0 & \alpha_1 & \beta_1 \\ 0 & -\nu 2^{2n} & \beta_1 & -\alpha_1 \\ -\alpha_2 & -\beta_2 & -\nu 2^{2(n+1)} & 0 \\ -\beta_2 & \alpha_2 & 0 & -\nu 2^{2(n+1)} \end{pmatrix}\begin{pmatrix} x_1 \\ y_1 \\ x_2 \\ y_2 \end{pmatrix} + \begin{pmatrix} -\gamma_1 \\ -\gamma_2 \\ \gamma_3 \\ \gamma_4 \end{pmatrix} \tag{7}
$$

$$\frac{d\mu_1}{dt} = 2^{(2n-5)/3}\epsilon\cos\mu_1\left(x_1x_2 - y_1y_2 - \frac{x_1}{2} - \frac{1}{2}\right) - 2^{(2n-5)/3}\epsilon\sin\mu_1\left(y_1x_2 + x_1y_2 - \frac{y_1}{2}\right)$$
$$\frac{d\mu_2}{dt} = -2^{(2n+1)/3}\epsilon\cos\mu_2\left(\frac{x_1x_2 - y_1y_2}{2} + \frac{x_2}{2} - 1\right) + 2^{(2n+1)/3}\epsilon\sin\mu_2\left(\frac{y_1x_2 + x_1y_2}{2} - \frac{y_2}{2}\right)$$

where

$$\alpha_1 = 2^{(2n-3)/3}\left(\sin\mu_2 - \frac{1}{2}\sin\mu_1\right) \quad \beta_1 = 2^{(2n-3)/3}\left(\cos\mu_2 - \tfrac{1}{2}\cos\mu_1\right)$$
$$\alpha_2 = 2^{2(n-2)/3}\left(\sin\mu_1 + \sin\mu_2\right) \quad \beta_2 = 2^{2(n-2)/3}\left(\cos\mu_1 + \cos\mu_2\right)$$

$$\gamma_1 = 2^{(2n-6)/3}\sin\mu_1 \quad \gamma_2 = 2^{(2n-3)/3}\cos\mu_1$$
$$\gamma_3 = 2^{(2n-1)/3}\sin\mu_2 \quad \gamma_4 = 2^{(2n-1)/3}\cos\mu_2$$

It is interesting to observe that we can interpret this six-dimensional system as a four-dimensional linear system in the x_i, y_i variables depending parametrically on μ_1 and μ_2. For $\nu = 0$ the four-dimensional system is Hamiltonian.

For each value of the viscosity the 2-1/2 shell model has four fixed points $\mathcal{P}_i$, $(i = 1\ldots4)$. Defining $\Phi_i = (\theta_1^*, \theta_2^*, \mu_1^*, \mu_2^*)$ and writing $\mathcal{P}_i = (R_1^*, R_2^*, \Phi_i)$ we have

$$R_1^* = \frac{g_2\omega_1 - 2^{2(n+1)}\nu g_1}{2^{2(2n+1)}\nu^2 + \omega_1\omega_2}$$
$$R_2^* = \frac{g_1\omega_2 + 2^{2n}\nu g_2}{2^{2(2n+1)}\nu^2 + \omega_1\omega_2} \tag{8}$$

where

$$\omega_1 = 2^{(2n-3)/3}\left[\sin(\theta_1^* + \theta_2^* + \mu_2^*) - \frac{1}{2}\sin(\theta_1^* + \theta_2^* + \mu_1^*)\right] \tag{9}$$

$$\omega_2 = \frac{2^{(2n-1)/3}}{2}\left[\sin(\theta_1^* + \theta_2^* + \mu_2^*) + \sin(\theta_1^* + \theta_2^* + \mu_1^*)\right] \tag{10}$$

$$g_1 = \frac{2^{(2n-3)/3}}{2}\sin(\theta_1^* + \mu_1^*) \quad g_2 = 2^{(2n-1)/3}\sin(\theta_2^* + \mu_2^*) \tag{11}$$

Defining $\nu^* = 2^{-(4n+7)/3}$ we have for the phases the following cases

- $\nu < \nu^*$:

$$\Phi_1 = (0, 0, -\pi/2, -\pi/2) \quad \Phi_2 = (0, 0, \pi/2, \pi/2)$$
$$\Phi_3 = (0, -\pi, \pi/2, -\pi/2) \quad \Phi_4 = (0, 0, -\pi/2, \pi/2)$$

- $\nu^* < \nu < 2^{1/3}\nu^*$:

$$\Phi_1 = (0, 0, -\pi/2, -\pi/2) \quad \Phi_2 = (-\pi, 0, \pi/2, \pi/2)$$
$$\Phi_3 = (0, -\pi, \pi/2, -\pi/2) \quad \Phi_4 = (0, 0, -\pi/2, \pi/2)$$

- $2^{1/3}\nu^* < \nu < 3\nu^*$:

$$\Phi_1 = (0, \pi, -\pi/2, -\pi/2) \quad \Phi_2 = (-\pi, 0, \pi/2, \pi/2)$$
$$\Phi_3 = (0, -\pi, \pi/2, -\pi/2) \quad \Phi_4 = (0, 0, -\pi/2, \pi/2)$$

- $3\nu^* < \nu$:

$$\Phi_1 = (0, \pi, -\pi/2, -\pi/2) \quad \Phi_2 = (-\pi, 0, \pi/2, \pi/2)$$
$$\Phi_3 = (-\pi, \pi, \pi/2, -\pi/2) \quad \Phi_4 = (0, 0, -\pi/2, \pi/2)$$

In the limit $\nu \to 0$, $\mathcal{P}_1 \to (1, 1, \Phi_1)$, $\mathcal{P}_2 \to (1, 1, \Phi_2)$, $\mathcal{P}_3 \to (\infty, \infty, \Phi_3)$ and $\mathcal{P}_4 \to (\infty, \infty, \Phi_4)$; that is, two of the fixed points merge in the (R_1, R_2) plane at the Kolmogorov scaling value and the other two diverge to infinity. For small viscosity $\nu \approx 0$ the radial distance between $\mathcal{P}_1$ and $\mathcal{P}_2$ increases linearly with ν and in the limit of large viscosity $R_1^*, R_2^* \to 0$ for all the fixed points.

In the polar coordinates $(R_1, R_2, \theta_1, \theta_2, \mu_1, \mu_2)$ the linear stability problem decouples into the the stability problem of the R_i variables and the stability problem of the phases. WFriting $\delta r = (\delta R_1, \delta R_2)$ and $\delta\theta = (\delta\theta_1, \delta\theta_2, \delta\mu_1, \delta\mu_2)$ the equations have the form

$$\frac{d\delta R}{dt} = \mathcal{M}_r \delta R$$
$$\frac{d\delta\theta}{dt} = \mathcal{M}_\theta \delta\theta$$

where the $n \times n$ matrices $\mathcal{M}_r$ and $\mathcal{M}_\theta$ are obtained by linearizing Eqs. (6) at the fixed points. If $\nu = 0$ the eigenvalues of $\mathcal{P}_1$ and $\mathcal{P}_2$ are pure imaginary and the ones for $\mathcal{P}_3$ and $\mathcal{P}_4$ are equal to zero. For $\nu \neq 0$ the real part of the eigenvalues of $\mathcal{M}_r$ is always negative and therefore the four fixed are stable with respect to radial perturbations. The eigenvalues of $\mathcal{P}_3$ and $\mathcal{P}_4$ are always real and those for $\mathcal{P}_1$ and $\mathcal{P}_2$ are complex if $0 < \nu < 2^{7/3}/3$.

The stability properties of the system with respect to perturbations in the phases is more complicated and interesting. As a general rule, there is always at least one eigenvalue with positive real part and therefore the fixed points are unstable to perturbations in the phases. The dependence of the eigenvalues of $\mathcal{M}_\theta$ on the viscosity for the fixed points $\mathcal{P}_1$, $\mathcal{P}_2$, $\mathcal{P}_3$ and $\mathcal{P}_4$, is shown if Figures 1a, 1b,1c and 1d respectively. R_i denotes the real part and I_i the imaginary part of the i-th eigenvalue. The values of ϵ and n were $\epsilon = 1$ and $n = 4$. Observe that as the viscosity varies the stability of the fixed points changes due to bifurcations. When a pure real eigenvalue changes sign we have a steady-state bifurcation and when a complex conjugate pair crosses the imaginary axis we have a Hopf bifurcation [17] . Another kind of bifurcation, called eigenvalue collision, occurs when two pure real eigenvalues approach and merge into a complex conjugate pair. Collision of eigenvalues gives rise to the "forks" observed in Figure 1. $\mathcal{P}_1$ (Fig.1a) always has one positive real and one negative real eigenvalue. For small viscosity the other two eigenvalues are complex conjugate. As viscosity increases, the complex eigenvalues transform into two negative real eigenvalues by means of an eigenvalue collision. $\mathcal{P}_2$ (Fig.1b) always has one positive real eigenvalue. As viscosity

increases, we observe a Hopf bifurcation and three eigenvalue collisions that eventually give rise to three negative real eigenvalues. For small viscosity, $\mathcal{P}_3$ and $\mathcal{P}_4$ (Fig.1c and Fig.1d) have very large positive real eigenvalues. For $\mathcal{P}_3$ (Fig.1c), as viscosity increases, two eigenvalue collisions yield at the end to two real positive and two real negative eigenvalues. Finally, $\mathcal{P}_4$ (Fig. 1d) exhibits a complicated sequence of bifurcations that eventually results into four negative real eigenvalues at high viscosity.

Associated with each real eigenvector and each complex conjugate pair of eigenvectors is an invariant manifold. If the real part of the associated eigenvalue is negative (positive) the manifold is called stable (unstable) since the dynamics on it approaches (diverges from) the fixed point as $t \to +\infty$ [17]. A homoclinic connection occurs when an unstable manifold of a fixed point joins one of the stable manifolds at the same point. If the two manifolds belong to different fixed points the connection is called heteroclinic. In Figure 5 we show an example of an homoclinic connection in a three-dimensional dynamical system with one positive real and two complex conjugate (with negative real part) eigenvalues. The stable and unstable manifolds are denoted by W^s and W^u.

The homo(hetero)clinic connections are important because in their vicinity the dynamics of the system exhibit intermittent and pulse-like behavior (see for example [18]). A theorem by Šilnikov [17] gives the conditions for having chaotic orbits in a three-dimensional dynamical system with a homoclinic orbit with one real and two complex conjugate eigenvalues (see Fig.5). In [19] some generalizations of Ŝilnikov's theory were presented for the study of heteroclinic connections in a six-dimensional model of turbulent convection. It would be interesting to try to apply these ideas to the 2-1/2 shell model.

In Figures 2 and 3 we present numerical integrations of the 2-1/2 shell model in cartesian representation (Eq. (7)) with $(n = 4, \nu = 10^{-3}, \epsilon = 10^{-3})$ and $(n = 4, \nu = 3 \times 10^{-3}, \epsilon = 10^{-2})$ respectively. In both cases, a homoclinic connection at $\mathcal{P}_1$ seems to be responsible for the observed behavior. In Fig. 2 the approach and departure from $\mathcal{P}_1$ show oscillatory behavior indicating that the stable and unstable manifolds have complex eigenvalues (i.e. near $\mathcal{P}_1$ the manifolds are spiral). On the other hand, the behavior observed in Fig. 3 seems to indicate that the unstable manifold has a real eigenvalue and the stable a complex one. At present we have not been able to observe homo(hetero)clinic connections for $\epsilon = 1$, however, we believe that changing ν and n may eventually lead to them. In Figure 4 we show the numerical integration of the 2-1/2 model with $(n = 10, \nu = 5.55 \times 10^{-6}, \epsilon = 1)$. As is typical for the cases with $\epsilon = 1$, the fluctuations are stronger than for smaller ϵ, the "laminar" regions show larger oscillations and the "bursts" are less well defined.

5 Conclusions

For the general N shell model (with $\nu = f = 0$ and the boundary shells fixed) we have found that there is an infinite number of fixed points which form a six-dimensional manifold $\mathcal{F}$ in the phase space. The fixed points corresponding to Kolmogorov scaling form a three-dimensional submanifold, $\mathcal{K}$, of $\mathcal{F}$. There are no fixed points with scaling behavior different from Kolmogorov scaling. We interpreted geometrically the fluctuations of Kolmogorov

scaling in the model by saying that the trajectories escape intermittently from $\mathcal{K}$ (since this surface has unstable directions) but return to it due to the existence of stable attracting directions. An open question is why in the numerical simulations [11] the dynamics fluctuates only around $\mathcal{K}$ and not around the whole $\mathcal{F}$ manifold. In order to gain some understanding of the general shell model we studied a 2-1/2 shell model which consists of two shells coupled to the boundary shells through the phases. We have shown how this six-dimensional system can be interpreted as a parametrically excited four-linear system. For $\nu = 0$ this four-dimensional system is Hamiltonian. The 2-1/2 shell model has four fixed points. As ν approaches zero two of them approach Kolmogorov scaling and the other two diverge to infinity. We have computed, as a function of viscosity, all the eigenvalues of the linearized system. We have found that the fixed points are stable with respect to perturbations in R_i but unstable along the phases directions. We have observed steady state bifurcations, Hopf bifurcations and eigenvalue collisions as the value of the viscosity changes. Numerical integrations of the 2-1/2 model with small ϵ show intermittent and pulse like behavior due to the presence of homoclinic connections. For $\epsilon = 1$ the fluctuations in the system are large and the intermittency is not as clear as it is for $\epsilon \ll 1$.

Acknowledgment

First of all I would like to thank Ed Spiegel for all his advice, help and encouragement during this project. His contagious infinite-dimensional interest in all sorts of ideas have made this work possible. Thanks are also due to Lou Howard for his many useful suggestions and ideas. Thanks to Rick Salmon for all his efforts in making the Summer Program work. Thanks to Neil Balmforth, Joe Keller, Norman Lebovitz, Phil Morrison, Rodney Worthing and Bill Young for interesting discussions. Thanks to all the staff members, the visitors and the Fellows for all the things I have learned from them. Thanks to Brad Shadwick for all his help with LaTeX. Finally, thanks to Rossy for all her support and encouragement.

References

[1] A.N. Kolmogorov, C. R. (Dokl.) Acad. Sci., USSR **30**, 301 (1941).

[2] F. Anselmet, Y. Gagne, E.J. Hopfinger and R. Antonia, J. Fluid Mech. **140**, 63 (1984).

[3] C.M. Meneveau, K.R. Sreenivasan, P. Kailasnath and M.S. Fan, Phys. Rev. A **41**, 894 (1990).

[4] E.D. Siggia, "Numerical study of small-scale intermittency in three dimensional turbulence", J. Fluid Mech **107**, (1981) 375-406.

[5] L. D. Landau and E.M. Lifshitz, *Fluid Mechanics*, Pergamon Press, New York 1980.

[6] A.N. Kolmogorov, J. Fluid Mech, **13**, 82 (1962).

[7] B. Mandelbrot, J. Fluid Mech. **62**, 331 (1974).

[8] U. Frisch, P-L. Sulem and M. Nelkin, "A Simple Dynamical Model of Intermittent Fully Developed Turbulence", J. Fluid Mech. **87**, part 4 (1978) 719-736.

[9] M. Yamada and K. Ohkitani, "Lyapunov Spectrum of a Chaotic Model of Three Dimensional Turbulence", J. Phys. Soc. Japan **56**,12 (1987) 4210-4213.

[10] K. Ohkitani and M. Yamada, "Temporal Intermittency in the Energy Cascade Process and Lyapunov Analysis in Fully Developed Model Turbulence", Prog. Theor. Phys. **81**, 22 (1989) 329-341.

[11] M.H. Jensen, G. Paladin and A. Vulpiani, "Intermittency in a Cascade Model for Three Dimensional Turbulence", Phys. Rev. A **43**, 2 (1991) 798-805.

[12] R. Benzi, G. Paladin, G. Parisi and A. Vulpiani, "On the multifractal nature of fully developed turbulence and chaotic systems", J. Phys. A: Math. Gen. **17** (1984) 3521-3531.

[13] R.M. Kerr and E.D. Siggia, "Cascade Model of Fully Developed Turbulence", J. Stat. Phys. **19**, 5 (1988), 543-552.

[14] M. Yamada and K. Ohkitani, 'The Inertial Subrange and Non-positive Lyapunov Exponents in Fully Developed Turbulence", Prog. Theor. Phys. **79**, 6, (1988) 1265-1268

[15] P. Frick and E. Aurell, "On Spectral Laws of 2-D Turbulence in Shell Models", preprint 1993.

[16] M.H. Jensen, G.Paladin and A. Vulpiani, "Shell Model for Turbulent Advection of Passive Scalar Fields", Phys. Rev. A **45**, 10 (1992), 7214-7221.

[17] J. Guckenheimer and P. Holmes, *Nonlinear Oscillations, Dynamical Systems and Bifurcations of Vector Fields* Applied Math. Sciences 42, Springer-Verlag, New York 1983.

[18] N.J.Balmforth, G.R. Ierley and E.A. Spiegel, "Chaotic Pulse Trains", preprint 1993.

[19] L.N. Howard and R. Krishnamurti, "Large Scale Flow in Turbulent Convection: a Mathematical Model", J. Fluid Mech. **170** (1986) 385-410.

Figure Captions

- **Figure 1.** Eigenvalues of $\mathcal{M}_\theta$ as function of viscosity. Figures a, b, c and d correspond to the fixed points $\mathcal{P}_1$, $\mathcal{P}_2$, $\mathcal{P}_3$ and $\mathcal{P}_4$ respectively. The values of ϵ and n were $\epsilon = 1$ and $n = 4$. R_i denotes the real part and I_i the imaginary part of the i-th eigenvalue.
- **Figure 2.** Numerical integration of the 2-1/2 shell model (Eq. 7) with $n = 4, \nu = 10^{-3}$ and $\epsilon = 10^{-3}$. Figure a shows the projection of the phase space trajectory onto the (R_1, R_2) plane. Figure b and c show the time series of R_1 and R_2.
- **Figure 3.** Same as Figure 2 but with $n = 4, \nu = 3 \times 10^{-3}$ and $\epsilon = 10^{-2}$
- **Figure 4.** R_1 time series obtained from the numerical integration of the 2-1/2 shell model (Eq. (7)) with $n = 10, \nu = 5.55 \times 10^{-6}$ and $\epsilon = 1$.
- **Figure 5.** Homoclinic trajectory in a three dimensional dynamical system with one positive real and two complex conjugate (with negative real part) eigenvalues.

FIGURE 1a

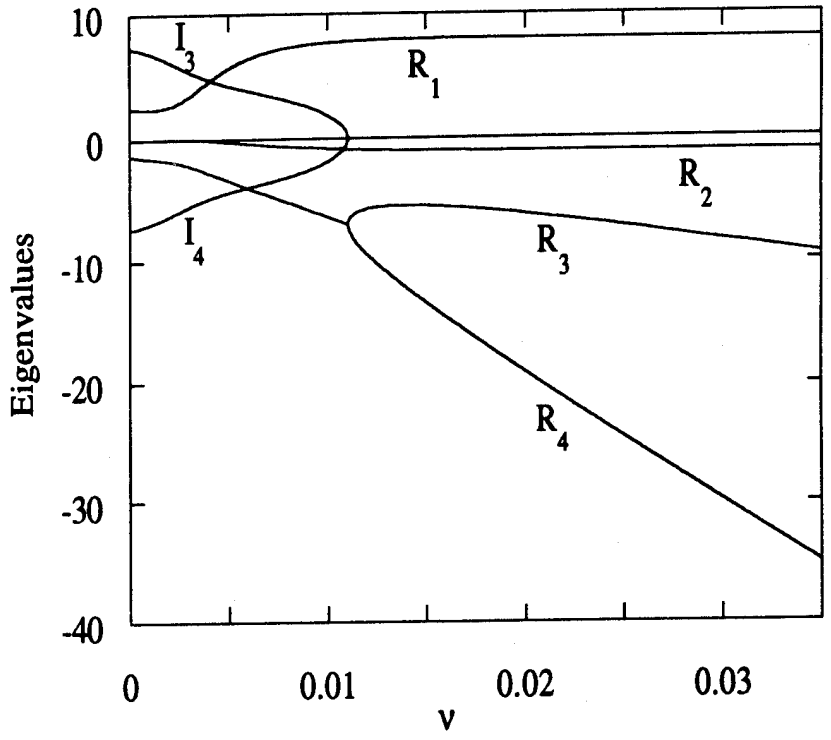

FIGURE 1b

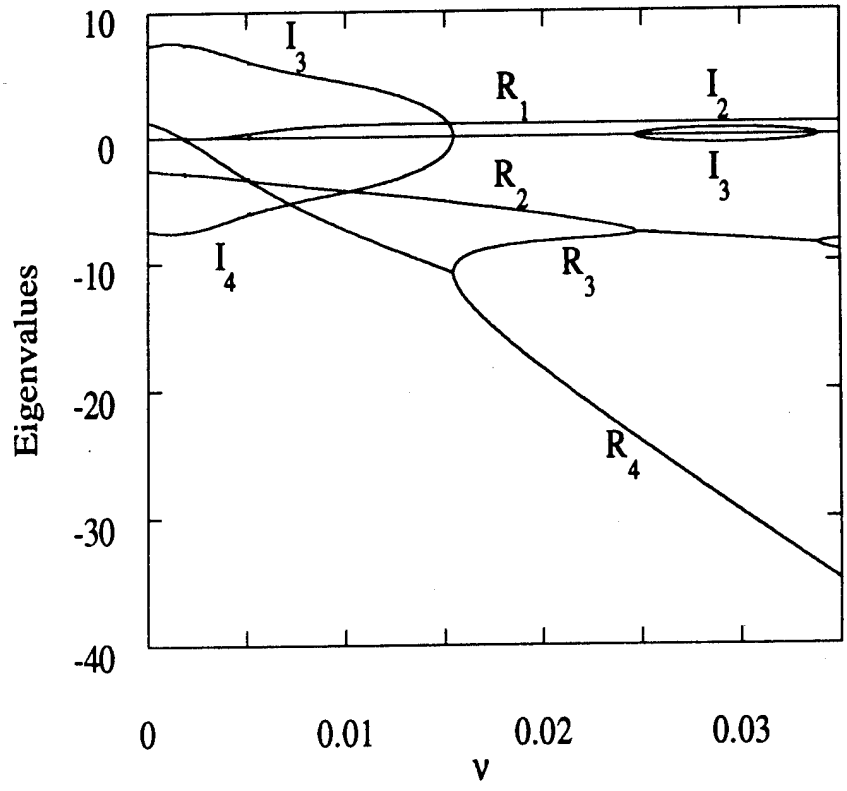

FIGURE 1c

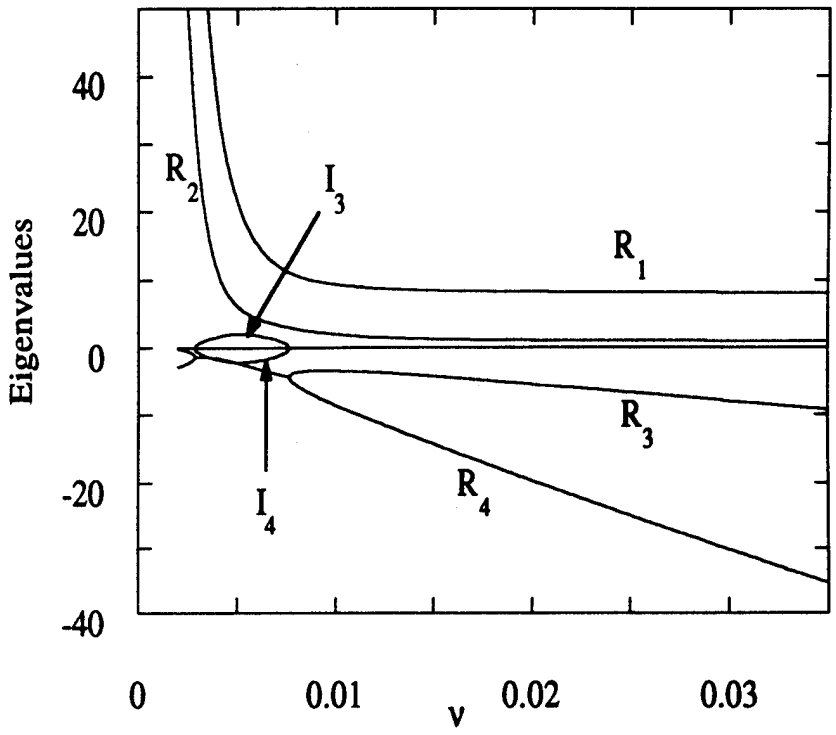

FIGURE 1d

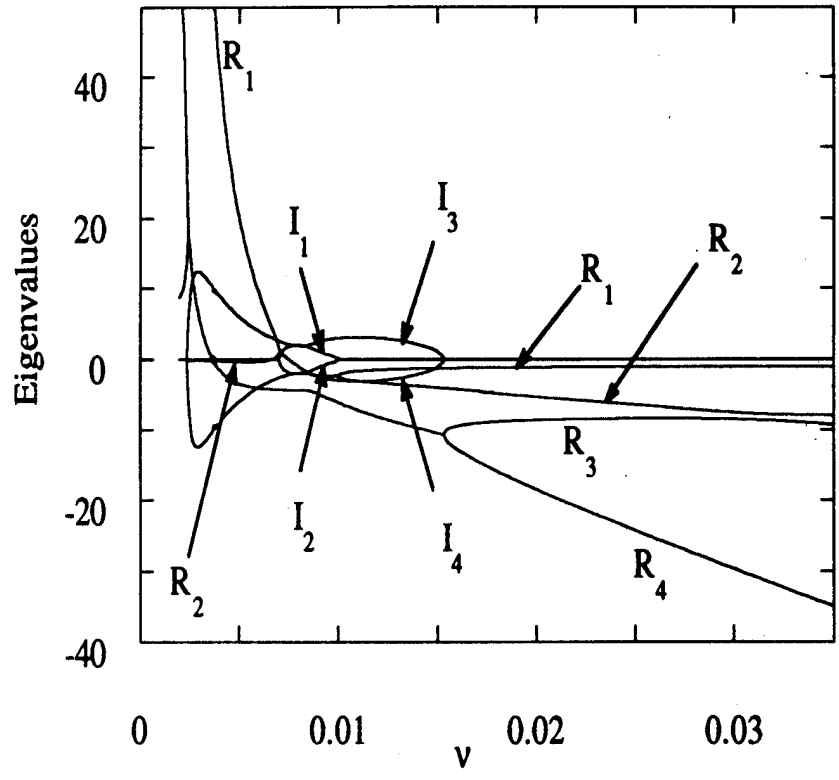

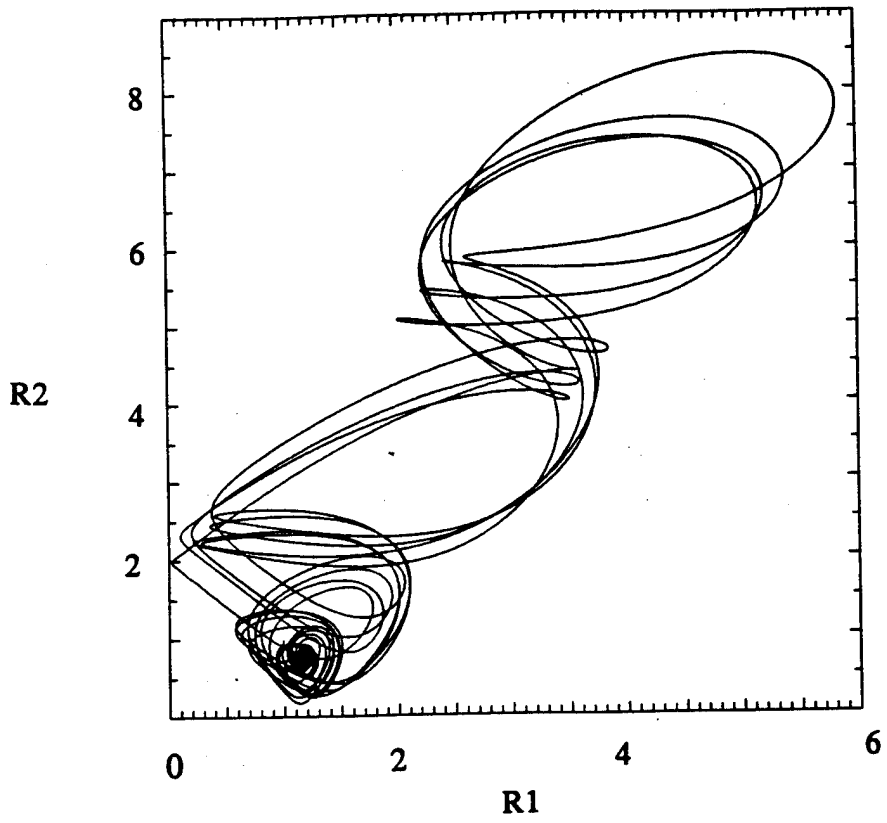

Figure 2a

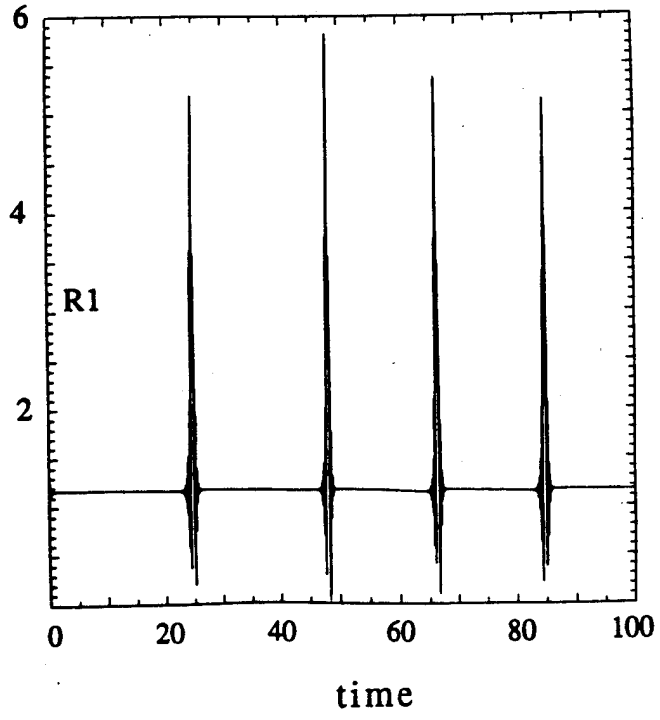

Figure 2b

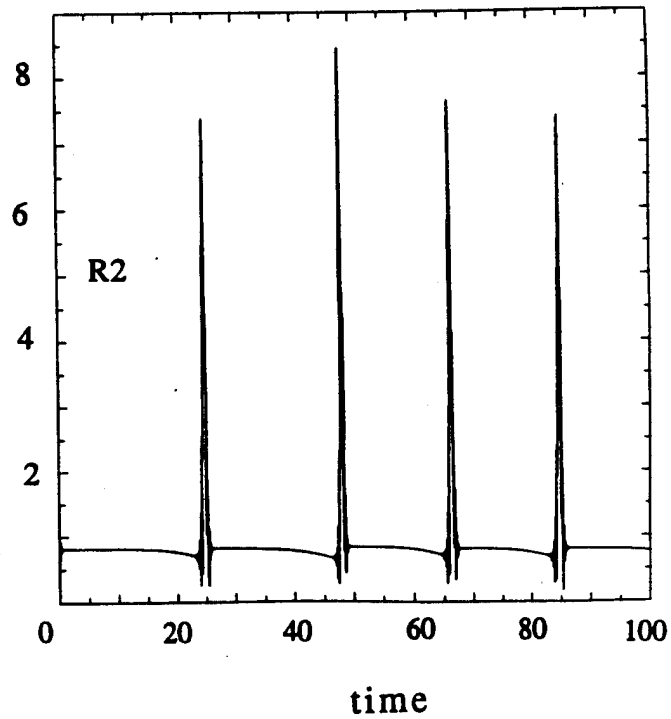

Figure 2c

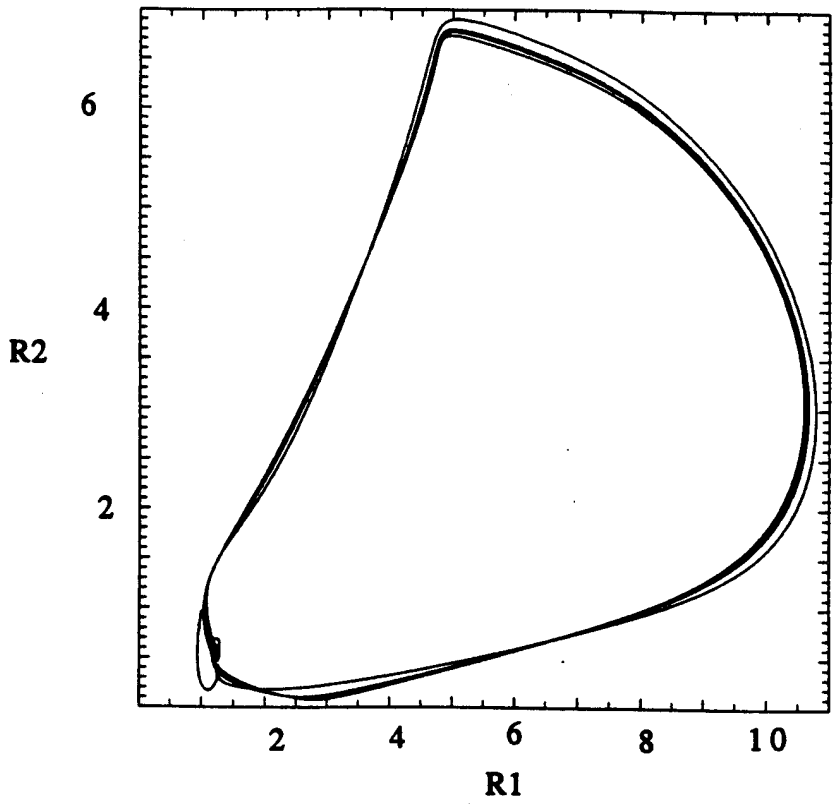

Figure 3a

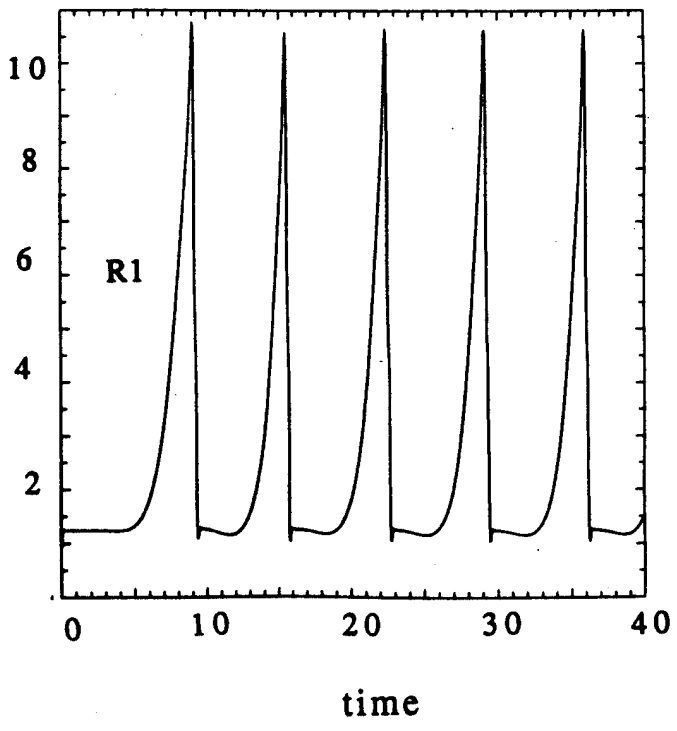

Figure 3b

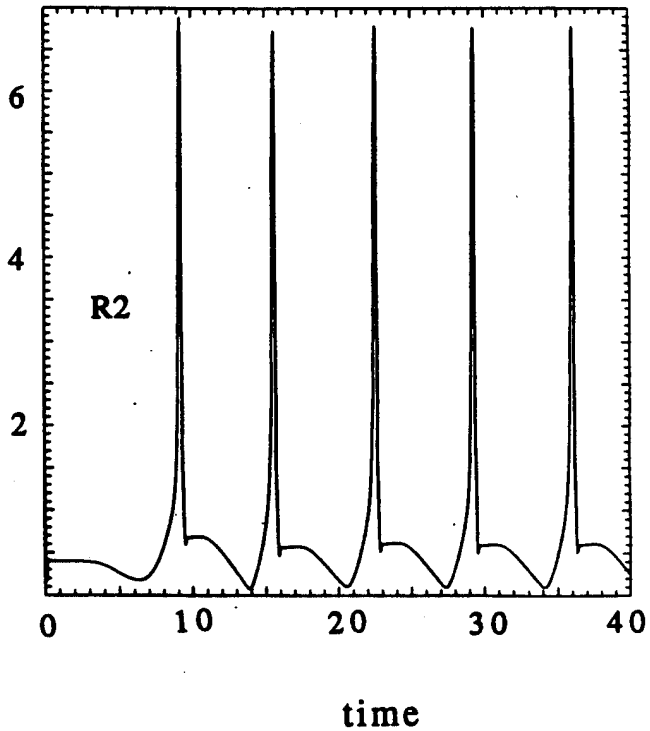

Figure 3c

Figure 4

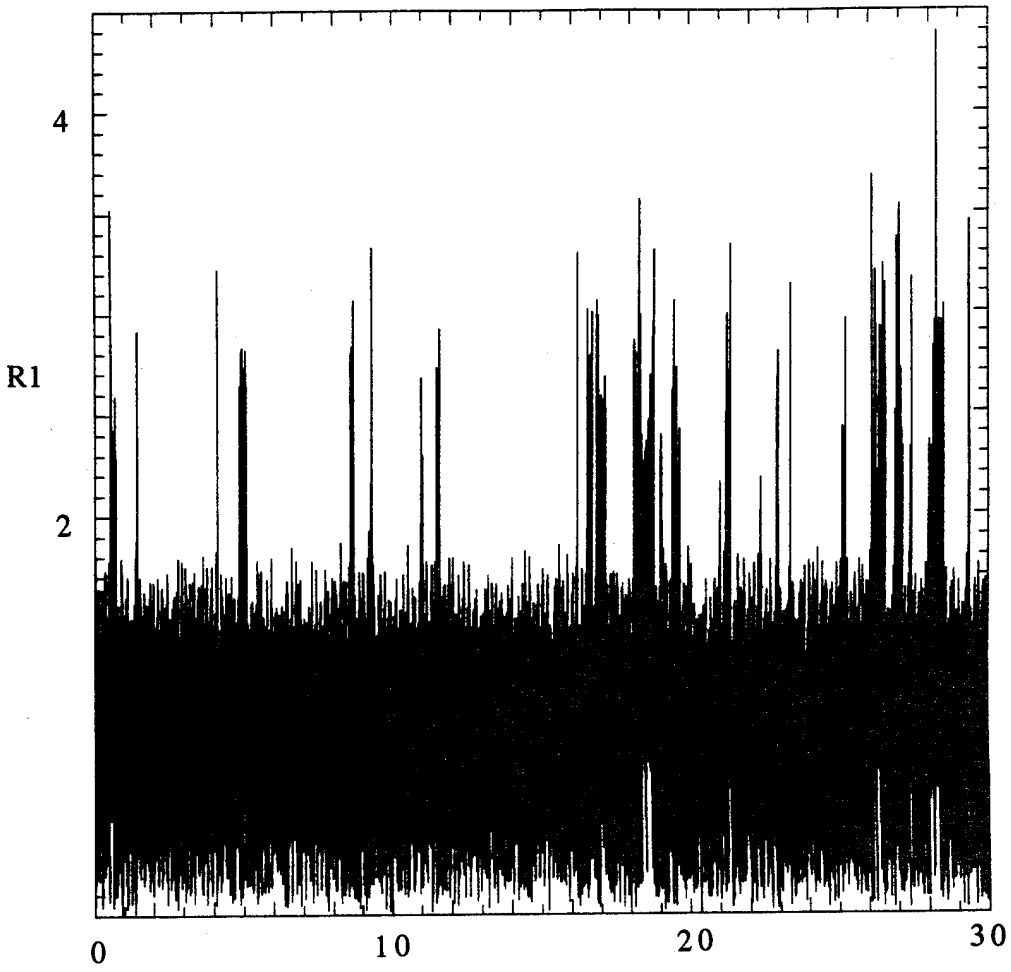

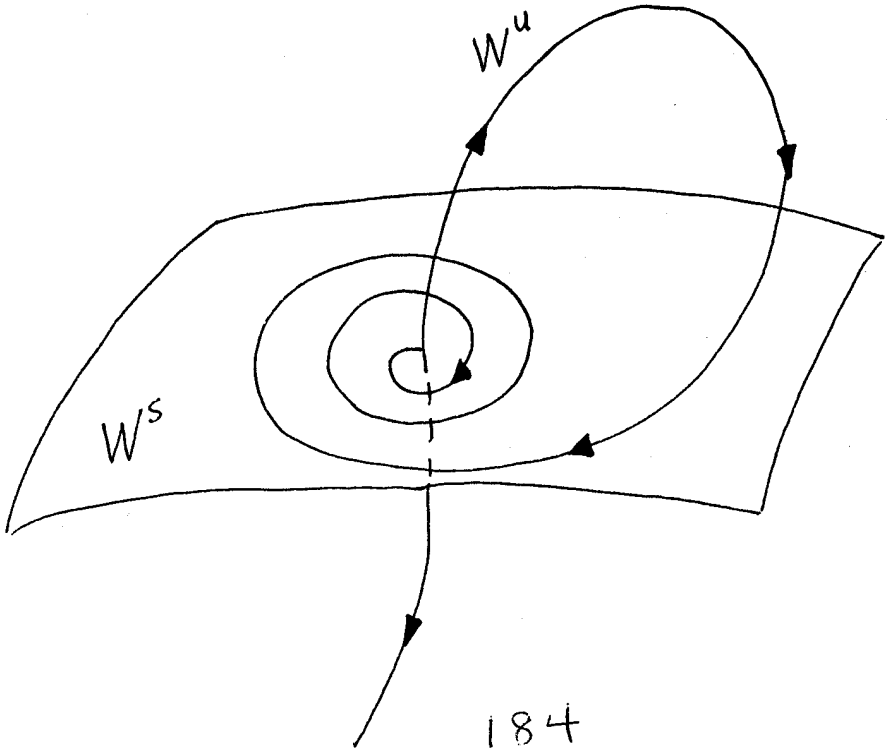

Figure 5

Gravity Wave Generation by Quasi-Geostrophic Point Vortices

Geoffrey T. Dairiki *

1 Introduction

Point vortex models have proven to be quite useful in improving our understanding of the behavior of the shallow water equations, particularly in the areas of two-dimensional and quasi-geostrophic turbulence.

The conventional point vortex models provide a class of *exact* solutions to either the two-dimensional Euler equations, or the quasi-geostrophic equations. These equations, however, are rather drastic approximations to the shallow water equations since they completely neglect any dynamics involving surface gravity waves. It is important to understand, then, how allowing for vortex-gravity wave interactions might change the the resulting vortex dynamics. Insight in this area could shed light not only on how the standard vortex models break down, but also on the limits of validity of the quasi-geostrophic and other similar "balance" models.

This report is concerned with the generation of weak gravity waves by rotating vortex pairs. Problems considered here include radiation by vortex pairs in an unbounded domain, both with and without background rotation. Also radiation by a vortices on a half-plane (i.e. near a coastline) will be considered. In each case, the far-field wave solution will be found, along with the radiated power. In all cases, it will be shown that wave radiation is weak; in some cases it is altogether negligible.

2 Standard Point Vortex Models

The development of two common vortex models will be reviewed in this section. First, the shallow water equations will be presented. Next, two approximations to the shallow water model are discussed. Finally, the point vortex models which correspond to these approximations will be introduced.

2.1 The Shallow Water Equations

The shallow water equations describe the dynamics of an inviscid, homogeneous and incompressible fluid, in which the horizontal scales of motion are much greater than the fluid depth. They consist of an equation expressing conservation of momentum,

$$\partial_t \boldsymbol{u} + (\boldsymbol{u}\cdot\nabla)\boldsymbol{u} + f\hat{\boldsymbol{z}}\times\boldsymbol{u} = -c^2\nabla\eta, \tag{1}$$

and an equation of mass conservation,

$$\partial_t \eta + (\boldsymbol{u}\cdot\nabla)\eta + (1+\eta)\nabla\cdot\boldsymbol{u}. \tag{2}$$

*The Applied Physics Laboratory, University of Washington; 1013 NE 40th Street; Seattle, WA 98105. (dairiki@u.washington.edu)

Where $\boldsymbol{u} = (u(x,y,t), v(x,y,t))$ is the horizontal component of the fluid velocity; $\eta(x,y,t)$ is the relative surface displacement (the fluid thickness is given by $h = H\{1+\eta\}$); f is the Coriolis parameter; c is the linear short gravity wave speed: $c^2 = gH$; g is the acceleration of gravity, and H the undisturbed fluid depth.

The shallow water equations comprise three coupled first-order ODE's. Upon linearization and fourier transformation one finds, for any given wavevector, $\boldsymbol{k}$, three linear eigenmodes. Two of these modes are termed *gravity modes* and are distinguished from the third *vortical mode* by their relatively high frequency.

Often, particularly in geophysical problems, one in interested primarily in the slow *geostrophic* (in the case $f \neq 0$) or *vortical* (in the case $f = 0$) dynamics. Lower order approximations to equations 1 and 2, which "filter out" the gravity modes are of interest. Two standard models which accomplish this are the *rigid lid* and the *quasi-geostrophic* models.

These models also lead naturally to point vortex formulations. It is these two models, and extensions of them, which will be considered for the remainder of the paper

2.2 The Rigid Lid Approximation

One obvious way to eliminate the gravity waves is to put a rigid lid over the ocean. In the shallow water equations this is roughly equivalent to taking the limit as $g \to \infty$; or more accurately the limit $\mathrm{Fr} \equiv ([\boldsymbol{u}]/c) \to 0$. Applying this limit to equations 1 and 2 with $f = 0$ (no rotation), one finds that $\eta \to$ constant, and thus $\nabla \cdot \boldsymbol{u} \to 0$. This allows $\boldsymbol{u}$ to be represented by a scalar stream-function ψ: $\boldsymbol{u} = \hat{\boldsymbol{z}} \times \nabla\psi$. Taking the curl of equation 1 to obtain a vorticity equation gives:

$$\partial_t \zeta + \partial(\psi, \zeta) = 0; \qquad \nabla^2 \psi = \zeta. \tag{3a,b}$$

Here, ζ is the vertical component of vorticity: $\zeta = \hat{\boldsymbol{z}} \cdot \nabla \times \boldsymbol{u} = \partial_x v - \partial_y u$, and $\partial(\cdot,\cdot)$ represents the two-dimensional Jacobian: $\partial(f,g) = \partial_x f\, \partial_y g - \partial_y f\, \partial_x g$. These equations are identical to the two-dimensional Euler equations for an incompressible, inviscid fluid.

Note that equation 3a is a prognostic equation which tells how vorticity is moved around. Equation 3b is a *diagnostic* equation which tells how to find the velocity field from the vorticity field. Also, the coupled set (3a, 3b) is first-order in time — the gravity modes are gone.

2.3 The Quasi-Geostrophic Approximation

The quasi-geostrophic model is the simplest in a series of *balance* models for nearly geostrophic flow. The derivation of the quasi-geostrophic equations is quite standard [Ped87, sec. 3.12]. One invokes a linearized version of potential vorticity conservation, and maintains that advection of potential vorticity by only the geostrophic component of velocity will yield a good enough answer. The quasi-geostrophic equations for a single layer f-plane ocean can be written

$$\partial_t q + \partial(\psi, q) = 0; \qquad \nabla^2 \psi - \lambda^{-2} \psi = q, \tag{4a,b}$$

where q is the quasi-geostrophic potential vorticity, $q \equiv \zeta - f\eta$; and $\lambda \equiv c/f$ is the Rossby radius of deformation.

2.4 Point Vortex Models

Both the 2-D Euler equations (eqs. 3a, 3b) and the quasi-geostrophic equations (eqs. 4a, 4b) have quite similar forms. Both models contain one *prognostic* equation which describes the advection of (potential-)vorticity by a scalar streamfunction, and one *diagnostic* equation which gives the streamfunction in terms of the vorticity distribution. It is this form which lends itself well to the development of a point-vortex model. This is done by approximating the (potential-)vorticity field by a sum of delta functions.

The point vortex models for the 2-D Euler and the quasi-geostrophic equations take very similar forms. The dynamics is summarized by a set of equations giving the velocities of the point vortices in terms of their positions:

$$\frac{d}{dt}\boldsymbol{x}_i = \sum_{j\neq i} \Gamma_j \hat{\boldsymbol{z}} \times \nabla \mathcal{G}(\boldsymbol{x}_i - \boldsymbol{x}_j). \tag{5}$$

Where $\boldsymbol{x}_i(t)$ are the locations of the point vortices, and $2\pi\Gamma_i$ are their circulations. $\mathcal{G}$ is the Green's function for either equation 3b or equation 4b. In an unbounded domain, for the Euler equations, $\mathcal{G}(\boldsymbol{x}) = \log|\boldsymbol{x}|$; for the QG equations, $\mathcal{G}(\boldsymbol{x}) = -\mathrm{K}_0(|\boldsymbol{x}|/\lambda)$ (where K_0 is a modified Bessel function.)

Solutions of equation 5 solve equations 3a and 3b or equations 4a and 4b exactly, with the vorticity distribution (ζ or q) $= \sum_i 2\pi\Gamma_i \delta_2(\boldsymbol{x} - \boldsymbol{x}_i)$.

3 Allowing for Weak Gravity Waves

It would be nice to generalize the rigid-lid (2-D Euler) model to allow for a weak gravity wave field — in other words, we would like a model valid for small but finite Froude number. One such model will be presented, somewhat informally, in this section. In later sections, this model will be more fully justified; and it will be applied to the problem of gravity wave generation by a rotating vortex pair.

Taking a time derivative of equation 1 and a gradient of equation 2, and then eliminating $\nabla\partial_t\eta$ between the two yields, after application of the vector identity $\nabla(\nabla\cdot\boldsymbol{u}) = \nabla^2\boldsymbol{u} - \hat{\boldsymbol{z}}\times\nabla\zeta$,

$$\partial_t^2\boldsymbol{u} - c^2\nabla^2\boldsymbol{u} = -c^2\hat{\boldsymbol{z}}\times\nabla\zeta \quad [+c^2\nabla\nabla\cdot(\eta\boldsymbol{u}) - \partial_t(\boldsymbol{u}\cdot\nabla)\boldsymbol{u}]. \tag{6}$$

Neglecting the last two terms on the right hand side — we will justify this approximation later — and introducing a vorticity equation obtained by taking the curl of equation 1 yields the pair of equations

$$\partial_t\zeta + \nabla\cdot(\boldsymbol{u}\zeta) = 0; \qquad \partial_t^2\boldsymbol{u} - c^2\nabla^2\boldsymbol{u} = -c^2\hat{\boldsymbol{z}}\times\nabla\zeta. \tag{7a,b}$$

These two equations present a picture somewhat similar to that given by the 2-D Euler model (equations 3a and 3b). The left equation describes advection of a conserved vorticity by a velocity field. The second relationship gives the velocity field in terms of the vorticity. In the case of the 2-D Euler equations, this second relation was completely diagnostic (no time derivatives). Now, in these new equations, the velocity is the solution of a linear wave equation which is forced by the vorticity field.

The vorticity field may be discretized, as in the previous section, to produce a point vortex model, roughly:

$$\frac{d}{dt}\boldsymbol{x}_i = \hat{\boldsymbol{z}}\times\nabla\psi|^r_{\boldsymbol{x}=\boldsymbol{x}_i}; \qquad \partial_t^2\psi - c^2\nabla^2\psi = -c^2\sum 2\pi\Gamma_i\delta_2(\boldsymbol{x}-\boldsymbol{x}_i).$$

(The ^{r} indicates that the streamfunction, ψ must by *regularized* — essentially, the singular part, which looks like $\Gamma_i \log|\boldsymbol{x} - \boldsymbol{x}_i|$, must be subtracted from ψ before the gradient may be taken at $\boldsymbol{x}_i$.) In this model, a rather satisfying picture emerges in which the vortices "communicate" with each other exclusively through the gravity wave field.

It is also encouraging that equations 7a and 7b, in the limit $c^2 \to \infty$, yield the 2-D Euler equations (eqs. 3a, 3b). (Since $\hat{\boldsymbol{z}} \times \nabla$ commutes with ∇^2, $\boldsymbol{u} = \hat{\boldsymbol{z}} \times \nabla\psi$ with $\nabla^2\psi = \zeta$ is a solution of $\nabla^2\boldsymbol{u} = \hat{\boldsymbol{z}} \times \nabla\zeta$.)

3.1 (Non)Existence of 'Steady' Vortex Pair Solutions

The two-vortex solutions of the 2-D Euler point vortex equations (eq. 5) are well known: two point vortices in an unbounded domain will exhibit steady, uniform rotation about their mutual center of vorticity [Bat67, sec. 7.3]. In the special case where the two vortices have circulations of identical magnitude, but opposite sign, the two vortices advect each other in steady linear translation (since their center of vorticity is at infinity).

It is interesting to investigate the existence of analogous steady solutions to equations 7a and 7b. It will be found that, in general, a vortex pair must *always* radiate gravity waves (albeit at a slow rate). This could set important constraints on the limits of validity of the 2-D Euler (and also the quasi-geostrophic) approximations to the shallow water equations.

3.1.1 Linearly Propagating Plus/Minus Pair

The special case of a linearly propagating plus/minus vortex pair is considered. Postulating the existence of a steadily translating vortex pair, and looking for solutions of equations 7a and 7b of the form

$$\zeta(x,y,t) = \hat{\zeta}(x - Ut, y) \equiv \hat{\zeta}(\hat{x}, \hat{y}), \qquad \boldsymbol{u}(x,y,t) = \hat{\boldsymbol{u}}(x - Ut, y) \equiv \hat{\boldsymbol{u}}(\hat{x}, \hat{y}),$$

gives the following equation for $\hat{\boldsymbol{u}}$

$$(1 - (U/c)^2)\hat{\partial}_x^2\hat{\boldsymbol{u}} + \hat{\partial}_y^2\hat{\boldsymbol{u}} = \hat{\boldsymbol{z}} \times \hat{\nabla}\hat{\zeta}.$$

As long as the Froude number, $\mathrm{Fr} \equiv U/c^2 < 1$, this equation is *elliptic*. It follows that there is indeed a solution of equations 7a and 7b which corresponds to a plus/minus vortex pair propagating along without loss of energy to gravity waves.

This problem is equivalent to that of steady, inviscid, sub-sonic flow around an obstacle — it is well know that no wake is generated as long as the upstream velocity is less than the phase speed of the slowest possible radiated wave. (This is known as D'Alembert's paradox [Bat67, sec. 5.11].)

3.1.2 Radiation by a Rotating Vortex Pair

When, however, one looks for steadily rotating solutions of the form

$$\boldsymbol{u}(r,\theta,t) = \tilde{\boldsymbol{u}}(r, \theta - \Omega t) \equiv \tilde{\boldsymbol{u}}(\tilde{r}, \tilde{\theta}),$$

the following equation arises

$$\{\tilde{r}^{-2} - (\Omega/c)^2\}\,\tilde{\partial}_\theta^2\tilde{\boldsymbol{u}} + \tilde{\partial}_r^2\tilde{\boldsymbol{u}} + \tilde{r}^{-1}\,\tilde{\partial}_r\tilde{\boldsymbol{u}} = \hat{\boldsymbol{z}} \times \tilde{\nabla}\tilde{\eta}. \tag{8}$$

This equation is elliptic in the region $\tilde{r} < R \equiv c/\Omega$, but it is *hyperbolic* for $\tilde{r} > R$. While this equation may still be solved, the resulting solution involves both outward and *inward* propagating waves at $\tilde{r} \rightsquigarrow \infty$. This solution does not satisfy radiation conditions, and it must be dismissed as non-physical.

Apparently, there are no (physically meaningful) steadily rotating solutions of equations 7a and 7b. Any rotating vortex pair must always radiate (and lose energy to) gravity waves. This is quite an important realization. It suggest that almost all non-trivial vortical or "balanced" solutions to the shallow water equations will constantly couple energy into the gravity wave field. One is left with a strong intuitive basis for doubting the existence of the sought-after "slow manifold".

4 Gravity Waves Radiated by a Vortex Pair

Now that we are convinced that a rotating vortex pair must radiate gravity waves, we proceed, in this section to calculate the radiated wave field and radiated wave energy flux from a rotating vortex pair. We will solve equation 6 and equation 7a asymptotically to lowest order for small Froude number. Since these equations are singular at Fr = 0 (the $\partial_t^2 \boldsymbol{u}$ term in equation 6 goes away) we will need to resort to matched asymptotics.

From the discussion in section 3.1 we expect an *inner solution* corresponding roughly to the elliptic region of equation 8, where $r < c/\Omega$. In this region the solution should look much like the familiar 2-D Euler (or rigid-lid) vortex solution.

The outer solution corresponds to the hyperbolic region of equation 8, and it is here that we expect to see propagating gravity waves. The wavelength of the radiated gravity waves should be on the order of $c/\Omega = R$. This is much greater than the inter-vortex spacing, so it is anticipated that the spatial coordinates will have to be rescaled in order to properly resolve the dynamics of this outer region.

4.1 Setup and Scaling

We consider two point vortices with circulations $2\pi\Gamma$, $2\pi\gamma\Gamma$, and initial separation d (we assume $|\gamma| < 1$ without loss of generality); c is the linear gravity wave speed: $c = gH$. The origin is taken to be at the center of vorticity of the vortex pair.

4.1.1 Inner Scaling

The appropriate length scale for the inner expansion is the inter-vortex spacing, d. Since it is expected that the length scale will have to be changed for the outer solution, the parameter α has been introduced. For now, it should be assumed that $\alpha = 1$, but it will be carried along as a convenient bookkeeping device, which will identify terms to be rescaled later on. The length scale is given by $L = d/\alpha$.

The velocity scale is given by $U = \alpha\Gamma/d$ — this is roughly the vortex advection velocity which would be expected from the standard 2-D Euler solution. Again, that darned α shows up — this is because velocities should fall off as r^{-1} for large r; when L is increased to look at large spatial scales, the velocity scale, U should be decreased accordingly. Vorticities, as is common, will be scaled by U/L.

Now the Froude number for this problem may be defined: $\varepsilon \equiv U/c = \Gamma/(cd)$.

The time scale, $T = d^2/\Gamma$, is the inverse of the angular rotational frequency which would be calculated for the equivalent incompressible 2-D Euler vortices.

Finally, applying these scalings to the shallow water momentum equation (eq. 1), reveals that that $\eta = O(\varepsilon^2)$.

The physical control parameters are taken to be c, d, and ε. Non-dimensional variables will be denoted with an overbar. (Barred operators like $\bar{\partial}_t$, and $\bar{\nabla}$ represent derivatives taken with respect to the appropriate non-dimensional independent variables.) The scalings are summarized:

$$\boldsymbol{u} = \varepsilon c \alpha \, \bar{\boldsymbol{u}}, \quad \boldsymbol{x} = (d/\alpha)\, \bar{\boldsymbol{x}}, \quad t = d(\varepsilon c)^{-1}\, \bar{t}, \quad \zeta = (\varepsilon c \alpha^2/d)\, \bar{\zeta}, \quad \eta = \varepsilon^2\, \bar{\eta}.$$

These scalings, when applied to equation 7a and equation 6 produce

$$\bar{\partial}_t \bar{\zeta} + \alpha^2\, \bar{\nabla} \cdot (\bar{\boldsymbol{u}} \bar{\zeta}) = 0, \tag{9}$$

and

$$(\varepsilon^2/\alpha^2)\, \bar{\partial}_t^2 \bar{\boldsymbol{u}} - \bar{\nabla}^2 \bar{\boldsymbol{u}} = -\hat{\boldsymbol{z}} \times \bar{\nabla} \bar{\zeta} + \varepsilon^2 \{\bar{\nabla}\bar{\nabla} \cdot (\bar{\eta} \bar{\boldsymbol{u}}) - \bar{\partial}_t (\bar{\boldsymbol{u}} \cdot \bar{\nabla}) \bar{\boldsymbol{u}}\}. \tag{10}$$

4.2 Solution

4.2.1 Inner Solution

In the inner region ($\alpha = 1$) equations 9 and 10 become

$$\bar{\partial}_t \bar{\zeta} + \bar{\nabla} \cdot (\bar{\boldsymbol{u}} \bar{\zeta}) = 0; \qquad \bar{\nabla}^2 \bar{\boldsymbol{u}} = \hat{\boldsymbol{z}} \times \bar{\nabla} \bar{\zeta} + O(\varepsilon^2).$$

The right hand equation is solved by $\bar{\boldsymbol{u}} = \hat{\boldsymbol{z}} \times \bar{\nabla} \bar{\psi}$, where $\bar{\psi}$ satisfies $\bar{\nabla}^2 \bar{\psi} = \bar{\zeta}$. The lowest order solution for the vortex motion, then, is given by plain old 2-D Euler vortex dynamics.

The positions of the vortices are given by

$$(\bar{x}_1, \bar{y}_1) = \frac{\gamma}{1+\gamma}(\cos \omega \bar{t}, \sin \omega \bar{t}), \quad (\bar{x}_2, \bar{y}_2) = -\frac{1}{1+\gamma}(\cos \omega \bar{t}, \sin \omega \bar{t}), \tag{11}$$

where $\omega = 1 + \gamma$ is the (non-dimensional) rotational frequency of the pair. (Dimensionally, $\Omega = (\Gamma/d^2)(1+\gamma)$.)

The velocity field associated with this inner solution may be written in terms of a (multiple-valued) velocity potential: $\bar{\boldsymbol{u}} = \bar{\nabla} \bar{\phi}$, where:

$$\bar{\phi} = \tan^{-1} \frac{\bar{y} - \bar{y}_1}{\bar{x} - \bar{x}_1} + \gamma \tan^{-1} \frac{\bar{y} - \bar{y}_2}{\bar{x} - \bar{x}_2}. \tag{12}$$

4.2.2 Outer Solution

It has already been mentioned, that in order be able to see gravity waves, lengths must be rescaled. This is because the wavelengths of the expected gravity waves ($\approx c/\Omega$) are much greater than than the inter-vortex spacing. Inspection of equation 10 also reveals that if lengths are rescaled by a factor of ε^{-1}, the singular $\bar{\partial}_t^2 \bar{\boldsymbol{u}}$ term will come into play. This rescaling is accomplished in equations equations 9 and 10 by setting the value of the place-keeper, α, to ε. The outer scalings (denoted by the subscript $_*$) are then

$$\boldsymbol{u}_* = \varepsilon^{-1}\, \bar{\boldsymbol{u}}, \quad \boldsymbol{x}_* = \varepsilon\, \bar{\boldsymbol{x}}, \quad t_* = \bar{t}, \quad \eta_* = \bar{\eta}.$$

Realizing that vorticity is non-zero only at the vortices themselves, we can safely set the vorticity, ζ_* to zero for the outer solution. Then $\boldsymbol{u}_*$ must satisfy

$$\partial_{t_*}^2 \boldsymbol{u}_* - \nabla_*^2 \boldsymbol{u}_* = \mathrm{O}(\varepsilon^2)$$

Writing $\boldsymbol{u}_*$ in terms of a velocity potential: $\boldsymbol{u}_* = \nabla_* \phi_*$ obtains to lowest order

$$\partial_{t_*}^2 \phi_* - \nabla_*^2 \phi_* = 0.$$

Since the inner solution, to the order that it has been resolved, is rotating at constant angular velocity, uniformly rotating outer solutions are sought. After decomposition into azimuthal modes, the solution is to be had in the terms of Hankel functions:

$$\phi_* = \mathrm{Re}\left\{ A_0 \tan^{-1}\frac{y_*}{x_*} + \sum_{m=1}^{\infty} A_m \mathrm{H}_m^{(1)}\left(m(1+\gamma) r_*\right) e^{im(\theta - \omega t_*)} \right\}. \tag{13}$$

4.2.3 Matching

The inner solution for the velocity potential, equation 12, may be Taylor expanded in terms of the $\bar{\boldsymbol{x}}_i$ for $(|\bar{\boldsymbol{x}}_i|/\bar{r}) \ll 1$. Then substituting for $\bar{\boldsymbol{x}}_i$ using equation 11 yields

$$\bar{\phi} \sim (1+\gamma)\tan^{-1}\frac{\bar{y}}{\bar{x}} + \sum_{m=2}^{\infty} \frac{\gamma^m + (-1)^m \gamma}{m(\gamma+1)^m} \bar{r}^{-m} \sin m(\theta - \omega \bar{t}), \qquad \bar{r} \gg 1. \tag{14}$$

The intriguing absence of azimuthal mode 1 from this expansion, is easily shown to be a consequence of linear momentum conservation for point vortices (which says: $\bar{\boldsymbol{x}}_1 + \gamma \bar{\boldsymbol{x}}_2 =$ *constant*). Lack of $m = 1$ radiation also follows from Lighthill's theory of sound generation, in which he proved, quite generally, that there can be no dipole acoustic radiation unless there is an *external* input of momentum [Lig78, sec. 1.10].

The outer solution, ϕ_* may be evaluated for $r_* \ll 1$ using the limiting form for a Hankel function of a small argument: $\mathrm{H}_m^{(1)}(z) \sim -(i/\pi)\Gamma(m)(z/2)^{-m}$. [AS70, eq. 9.1.9]

$$\phi_* \sim \mathrm{Re}\left\{ A_0 \tan^{-1}\frac{y_*}{x_*} + \sum_{m=1}^{\infty} A_m \frac{(m-1)!}{i\pi}\left(\frac{2}{m(1+\gamma)}\right)^m r_*^{-m} e^{im(\theta - \omega t_*)} \right\}, \quad r_* \ll 1. \tag{15}$$

Equating coefficients between equation 14 and equation 15 (keeping in mind that $r_* = \varepsilon \bar{r}$) gives

$$A_0 = 1+\gamma; \qquad A_1 = 0; \qquad A_m = \pi \frac{\gamma^m + (-1)^m \gamma}{m!}\left(\frac{m\varepsilon}{2}\right)^m, \quad m \geq 2. \tag{16}$$

This, along with equation 13 gives, to lowest order, the far-field solution for gravity waves radiated by a point vortex pair.

4.2.4 Energy Flux

Finally, we may calculate the rate of energy transfer to gravity waves from our rotating vortex pair.

The shallow water equations (eqs. 1, 2) may be combined to form an energy equation $\partial_t E + \nabla \cdot \boldsymbol{F} = 0$, where E, and $\boldsymbol{F}$ are the energy density and flux, respectively [Ped87, sec. 3.5]:

$$E \equiv \tfrac{1}{2}(1+\eta)|\boldsymbol{u}|^2 + \tfrac{1}{2}c^2(1+\eta)^2; \qquad \boldsymbol{F} \equiv \boldsymbol{u}(1+\eta)\{\tfrac{1}{2}|\boldsymbol{u}|^2 + c^2(1+\eta)\}. \tag{17a,b}$$

The rate of energy loss by the vortex pair to radiated gravity waves, is found by integrating the energy flux carried by the gravity wave of the outer solution at large r: $\dot{E} = \lim_{r\to\infty}\langle \oint \boldsymbol{F}\cdot\hat{\mathbf{n}}\, ds\rangle$, where $\langle\cdot\rangle$ denotes a time average. η may be calculated from $\boldsymbol{u}$ with the aid of the Bernoulli-type relation: $\frac{1}{2}|\boldsymbol{u}|^2 + c^2\eta - \Omega r u_\theta = constant$, valid for steadily rotating flows, in regions of zero vorticity.

Since the quantity of interest is really the rate of energy loss relative to the energy contained in the basic vortex solution, $\dot{E}$ is normalized using the inner scalings: $\dot{E} = (U^2d^2/T)\dot{\bar{E}} = (\varepsilon^3 c^3 d)\dot{\bar{E}}$. With this scaling, the inverse of $\dot{E}$ gives the ratio of the "spin-down" time to the orbital period for the vortex-pair. What emerges, after some algebra, is

$$\dot{\bar{E}} = \lim_{r_*\to\infty} 2r_* \int_0^{2\pi} \langle \boldsymbol{u}_*\eta_*\rangle\cdot\hat{\mathbf{n}}\, d\theta = \lim_{r_*\to\infty} 2\omega r_*^2 \int_0^{2\pi} \langle (u_*)_r (u_*)_\theta\rangle\, d\theta.$$

The solution for ϕ_*, (eq. 13) is approximated for large r_* using the asymptotic form $\mathrm{H}_m^{(1)}(z) \sim \sqrt{2/\pi z}e^{i(z-m\pi/2-\pi/4)}$, valid for $|z| \gg 1$ [AS70, eq. 9.2.3]. The radiated power is then given by

$$\boxed{\dot{\bar{E}} = \sum_{m=2}^{\infty} \frac{4\pi^2(1+\gamma)\left(\gamma^m + (-1)^m\gamma\right)^2}{m!(m-1)!}\left(\frac{m\varepsilon}{2}\right)^{2m}.} \tag{18}$$

For values of $\varepsilon = 0.1$, $\gamma = 1$, equation 18 gives a non-dimensional radiated power $\dot{\bar{E}} = 1.6\times10^{-2}$. Thus the time-scale for energy loss by a rotating vortex pair will be on the order of ten rotational periods. While this value seems quite significant, it should be kept in mind that $\dot{\bar{E}} = \mathrm{O}(\varepsilon^{-4})$, so that the radiated power decreases rapidly when the Froude number is decreased.

5 Wave Radiation by a Pseudo-Quasi-Geostrophic Vortex Pair

In this section, the analysis of the previous section will be repeated for the case $f \neq 0$. The problem of interest involves the generation of inertio-gravity waves by a vortex pair. The vortices are taken to be nearly geostrophic ($\mathrm{Ro} \ll 1$).

The imposition of background rotation imposes a lower cut-off frequency on the possible radiated waves: — (linear) free gravity waves do not exist at frequencies below f. By definition, the rotation rate for a "nearly geostrophic" vortex pair is $\ll f$. It is expected, then, that the relatively slow vortex motions will be very inefficient at exciting gravity waves. A simple back-of-the-envelope scaling argument indicates that free waves are only possible at azimuthal mode number of order Ro^{-1} or greater; and the results of the previous section show that radiated wave amplitude falls off rapidly as the mode number increases ($\propto \mathrm{Fr}^{-1}$). There is every reason to suspect that wave generation by geostrophic vortex pairs will be completely insignificant.

Nevertheless, we proceed.

5.1 Weak Gravity Wave Model

In order to develop a model, similar to equations 7a and 7b, which will be applicable to the case $f \neq 0$, first shallow water potential vorticity conservation is invoked:

$$\partial_t \varpi + (\boldsymbol{u} \cdot \nabla)\varpi = 0; \qquad \varpi \equiv \frac{\zeta - f\eta}{1+\eta}. \tag{19a,b}$$

(This equation follows exactly from the shallow water equations. The funny form for the potential vorticity, ϖ, differs from the more familiar form $\Pi = (f+\zeta)/(1+\eta)$ by a constant. Specifically, $\varpi = \Pi - f$.)

A time derivative of equation 2 combined with a gradient of equation 1 yields the wave equation for η:

$$\partial_t^2 \eta + f^2\eta - c^2\nabla^2\eta = -fq \quad [-\partial_t \nabla \cdot (\eta \boldsymbol{u}) + \nabla \cdot (\boldsymbol{u} \cdot \nabla)\boldsymbol{u}]. \tag{20}$$

This equation is exact with q being the quasi-geostrophic version of potential vorticity, $q \equiv \zeta - f\eta$.

If the last two terms on the right side of equation 20 are neglected, then we see the inertio-gravity wave field forced by the potential-vorticity field. (This equation should be compared with equation 7b.) Further, if q is substituted for ϖ in equation 19a, and $\boldsymbol{u}$ is found from the linear shallow water polarization relation:

$$\partial_t^2 \boldsymbol{u} + f^2 \boldsymbol{u} = -c^2(\partial_t \nabla\eta - f\hat{\boldsymbol{z}} \times \nabla\eta),$$

(all of these assumptions will be justified later), then once again the picture emerges of vorticity being advected by a wave field which is in turn forced by the vorticity field.

5.2 Setup and Scaling

As in section 4.1, the strengths of the two point vortices are $2\pi\Gamma$, and $2\pi\gamma\Gamma$. The inter-vortex separation is again taken to be d. This time, however, the vortices are on an f-plane.

The scalings used in the previous problem (section 4.1.1) will be adopted here with the following exceptions and additions. The Rossby number for the problem is defined $\delta \equiv U/(fL) = \Gamma/(d^2 f)$. Also, in anticipation of finding free waves only at high frequencies, a scale for the azimuthal mode number, μ, is introduced as a bookkeeping device in the scaling of time.

Since, with non-zero f, the momentum balance is primarily geostrophic, the scaling for η must also be changed. Examination and scaling of the shallow water momentum equation (eq. 1) indicates that $\eta = O(\varepsilon^2/\delta)$. Finally the potential vorticity is scaled by $\varepsilon c/d$.

In order that the quasi-geostrophic potential-vorticity, q be a decent approximation to the full shallow water potential-vorticity, ϖ, it must be that $[\eta] = (\varepsilon^2/\delta) \ll 1$. Therefore, it is assumed that $\varepsilon = O(\delta)$ (with $\delta \ll 1$). (Note that $\varepsilon/\delta = d/\lambda$, where $\lambda = c/f$ is the Rossby deformation radius. The situation considered here is one where the vortex spacing is of the same order as the Rossby radius.)

With the non-dimensionalizations:

$$\boldsymbol{u} = \varepsilon c\alpha\, \bar{\boldsymbol{u}}, \quad \boldsymbol{x} = (d/\alpha)\,\bar{\boldsymbol{x}}, \quad t = d(\varepsilon c\mu)^{-1}\,\bar{t}, \quad \eta = (\varepsilon^2/\delta)\,\bar{\eta}, \quad q = (\varepsilon c/d)\,\bar{q},$$

the shallow water momentum equation (eq. 1) becomes

$$\delta\mu\,\bar{\partial}_t \bar{\boldsymbol{u}} + \delta\alpha^2\,(\bar{\boldsymbol{u}} \cdot \bar{\nabla})\bar{\boldsymbol{u}} + \hat{\boldsymbol{z}} \times \bar{\boldsymbol{u}} = -\bar{\nabla}\bar{\eta}. \tag{21}$$

Equation 20 in non-dimensional form is

$$(\mu\delta)^2(\varepsilon/\delta)^2\,\bar{\partial}_t^2\bar{\eta} + (\varepsilon/\delta)^2\,\bar{\eta} - \alpha^2\,\bar{\nabla}^2\bar{\eta} = -\bar{q} - \mu\alpha^2\varepsilon^2\,\bar{\partial}_t\bar{\nabla}\cdot(\bar{\eta}\bar{\boldsymbol{u}}) + \alpha^4\delta\,\bar{\nabla}\cdot(\bar{\boldsymbol{u}}\cdot\bar{\nabla})\bar{\boldsymbol{u}}. \quad (22)$$

5.3 Vortex Motion

For the inner scaling, ($\mu = \alpha = 1$), the dominant terms of equations 19a, 21, and 22 give, respectively

$$\bar{\partial}_t\bar{q} + (\bar{\boldsymbol{u}}\cdot\bar{\nabla})\bar{q} = 0; \qquad \bar{\boldsymbol{u}} = \hat{\boldsymbol{z}}\times\bar{\nabla}\bar{\eta}; \qquad \bar{\nabla}^2\bar{\eta} - (\varepsilon/\delta)^2\,\bar{\eta} = \bar{q}. \quad (23a,b,c)$$

These turn out to be exactly the standard quasi-geostrophic equations! Maybe it is not too surprising that the (slow) vortex motions are given by plain old quasi-geostrophic dynamics.

In any case, the solution is straightforward. The (non-dimensional) orbital frequency of the vortex pair is given by $\omega = (1+\gamma)\Lambda$, where Λ is defined $\Lambda \equiv (\varepsilon/\delta)\mathrm{K}_1(\varepsilon/\delta)$. ($\mathrm{K}_1$ is a modified Bessel function.) The vortex positions are given by equation 11.

Equations 23a, 23b, and 23c are valid for all values of α (< 1), as long as $m = \mathrm{O}(1)$. Therefore, the quasi-geostrophic solution is uniformly valid ($0 \le r \le \infty$) for low mode number.

5.4 High Mode Gravity Wave Radiation

Once again, uniformly rotating solutions involving free (inertio-)gravity waves are sought. The (dimensional) frequency of the m^{th} mode is $m\Omega = m\delta\omega f$. Free waves are expected only for $m\Omega > f$, or $m \ge \mathrm{O}(\delta^{-1})$. Equation 22 corroborates this intuition, since $m \sim \delta^{-1}$ is just the scaling required to allow the $\bar{\partial}_t^2\bar{\eta}$ term to come into play. In this case the dominant terms of equation 22 are

$$(\varepsilon/\delta)^2(\delta^2\,\bar{\partial}_t^2\bar{\eta} + \bar{\eta}) - \bar{\nabla}^2\bar{\eta} = -\bar{q}. \quad (24)$$

The right hand side is known, since the motion of the vortices was found in the previous section. All that is left to do in order to find the radiated wave field is to solve this forced linear wave equation.

Written in cylindrical coordinates, and fourier transformed in both θ, and $\bar{t}$ (assuming solutions like $e^{im(\theta-\omega\bar{t})}$) this equation becomes:

$$\bar{r}^2\,\bar{\partial}_r^2\bar{\eta} + \bar{r}\,\bar{\partial}_r\bar{\eta} + \{\bar{r}^2(\varepsilon/\delta)^2(m^2\delta^2\omega^2 - 1) - m^2\}\bar{\eta} = 0.$$

Propagating wave solutions to this equation only exist for $m \ge m_c \equiv (\delta\omega)^{-1}$, as guessed above.

Also, for $r^2 \ll \varepsilon^{-2}$, the left term in the curly braces may be neglected in favor of m^2. So the near-field solution for $\bar{\eta}$, denoted by $\eta^\dagger$, is given simply by $\bar{\nabla}^2\eta^\dagger = \bar{q}$. The solution is

$$\eta^\dagger = \log|\bar{\boldsymbol{x}} - \bar{\boldsymbol{x}}_1| + \gamma\log|\bar{\boldsymbol{x}} - \bar{\boldsymbol{x}}_2|, \qquad |\bar{\boldsymbol{x}}| \ll \varepsilon^{-2}. \quad (25)$$

The far-field solution, $\eta^\ddagger$, is found by solving equation 24 with the right hand side set to zero (since for $\bar{r} > 1$, $\bar{q}$ is identically zero). The solution is found in terms of (the now familiar) Hankel functions.

$$\eta^\ddagger = \left[\begin{array}{c}\text{lower,}\\ \text{evanescent}\\ \text{modes}\end{array}\right] + \mathrm{Re}\left\{\sum_{m=m_c}^{\infty} A_m\mathrm{H}_m^{(1)}(\bar{k}_m\bar{r})e^{im(\theta-\omega\bar{t})}\right\}, \qquad \bar{r} \gg 1, \quad (26)$$

where

$$\bar{k}_m = \frac{\varepsilon}{\delta}\sqrt{m^2\delta^2\omega^2 - 1}.$$

Matching equation 26 in the limit $\bar{r} \to 0$ to equation 25 in the limit $\bar{r} \to \infty$, much like as was done in section 4.2.3, gives the amplitudes of the radiated modes

$$A_m = -i\pi\frac{\gamma^m + (-1)^m\gamma}{m!}\left(\Lambda^2 - \{m\delta(1+\gamma)\}^{-2}\right)^{\frac{m}{2}}\left(\frac{m\varepsilon}{2}\right)^m, \quad m \geq m_c.$$

5.5 Radiated Energy Flux

The outgoing energy flux, $\lim_{\bar{r}\to\infty}\langle \oint \bar{\boldsymbol{F}} \cdot \hat{\mathbf{n}}\, ds\rangle$, with $\bar{\boldsymbol{F}}$ given by equation 17b, is evaluated with help from the linear shallow water polarization relation

$$\delta^2\,\bar{\partial}_t^2\bar{\boldsymbol{u}} + \bar{\boldsymbol{u}} = -\delta\,\bar{\partial}_t\bar{\nabla}\bar{\eta} + \hat{\mathbf{z}} \times \bar{\nabla}\bar{\eta},$$

which may be derived from the dominant terms of a time derivative of equation 21 combined with $\hat{\mathbf{z}} \times (\cdot)$ of the same equation.

$\dot{E}$ is non-dimensionalized, as in section 4.2.4, by the appropriate scales for the basic vortex solution. In this case, $\dot{E} = (c^2[\eta]/T)\dot{\bar{E}} = c^3\varepsilon^3(d\delta)^{-1}\dot{\bar{E}}$. To lowest order, the non-dimensional power radiated by the vortex pair is given by

$$\dot{\bar{E}} = \lim_{\bar{r}\to\infty} 2\bar{r}\int_0^{2\pi}\langle\bar{\boldsymbol{u}}\bar{\eta}\rangle \cdot \hat{\mathbf{n}}\, d\theta.$$

After some authentic *Seattle grunge*, it is found that

$$\boxed{\dot{\bar{E}} = \sum_{m\geq m_c}\frac{4\pi^2}{(m!)^2\, m\delta}\left(\frac{\gamma^m + (-1)^m\gamma}{1+\gamma}\right)^2\left(\Lambda^2 - \{\delta m(1+\gamma)\}^{-2}\right)^{m-1}\left(\frac{m\varepsilon}{2}\right)^{2m}.}$$

The radiated power, $\dot{\bar{E}} = O(\varepsilon^{2m_c})$ — a small number. This finding supports Rupert Ford's linear stability analysis of shallow water vortex patches. He finds that axisymmetric vortex patches are always unstable to gravity wave generation. The growth rate of the most unstable mode is $O(\mathrm{Fr}^{2m_c})$. [For93]

For a Rossby number, $\delta = 0.1$, and $\gamma = 1$, $\dot{\bar{E}}$ attains a maximum value of 2×10^{-21} at $\varepsilon \approx 3 \times 10^{-2}$. Assuming that the orbital period of the vortex pair is on the order of a day, this gives a radiation time-scale of 100 million times the age of the universe! The effects of gravity wave radiation in this case are miserably negligible.

6 Quasi-Geostrophic Vortices Near a Wall

It was found in the previous section that, for quasi-geostrophic vortices on a constant depth, unbounded f-plane, there is practically no coupling from the quasi-geostrophic motions into the gravity wave field. In this section we will consider a quasi-geostrophic vortex pair near a wall. It will be shown that in this case, weak but conceivably significant radiation can occur.

The reason that the coupling was so weak in the previous case, was that there were no free wave modes with frequencies near that of the slow quasi-geostrophic motion. When the vortices are near a coastline, however, the possibility of exciting boundary trapped *Kelvin waves* exists [Ped87, sec. 3.9]. These remarkable waves exist at all frequencies, so the potential exists that the slow geostrophic motions might be able to excite gravity waves of non-negligible amplitude.

6.1 Setup & Scaling

Again a vortex pair is considered. This time though the vortices are confined to the semi-infinite half-plane, $y > 0$. For simplicity, it will be assumed that the two vortices have equal strengths, both equal to $2\pi\Gamma$. Their initial positions are taken to be $\boldsymbol{x}_1|_{t=0} = (d/2, y_0)$, and $\boldsymbol{x}_2|_{t=0} = (-d/2, y_0)$. A no flow condition: $v|_{y=0} = 0$ is imposed at the boundary.

6.2 Vortex Motion

The appropriate inner scalings ($\alpha = 1$) are the same as those in the previous problem (see section 5.3), namely

$$\boldsymbol{u} = \varepsilon c\,\boldsymbol{u}, \quad \boldsymbol{x} = d\,\boldsymbol{x}, \quad t = d(\varepsilon c)^{-1}\,t, \quad \eta = (\varepsilon^2/\delta)\,\eta, \quad q = (\varepsilon c/d)\,q.$$

As before, the vortex motion, to lowest order, is given by regular quasi-geostrophic theory.

The presence of the coastline, however, complicates the solution somewhat. The proper boundary condition may be seen upon consideration of the x-component of the shallow water momentum equation, (eq.1) which when non-dimensionalized becomes

$$\delta\,\partial_t u + \delta\,u\partial_x u + \delta\,v\partial_y u - v = -\partial_x \eta.$$

At the boundary, v is zero. So

$$\partial_x \eta|_{y=0} = -\delta(\partial_t u + u\partial_x u)|_{y=0} = \mathrm{O}(\delta). \tag{27}$$

To lowest order, then, the vortex motions are given by the solution of the quasi-geostrophic equations, with the boundary condition $\partial_x \eta|_{y=0} = 0$.

The point vortex solution which satisfies this boundary condition may be found using the *method of images*. The two-vortex problem turns into a four-vortex problem (with a certain amount of symmetry). While the problem is still integrable, the solution is quite a mess, and not very illuminating. It is straightforward to show, though, that the vortices will still always follow closed, periodic orbits.

For the sake of the calculations in the rest of this section, it will suffice to assume that the orbits are still roughly circular, with an orbital period which approximates that for an equivalent vortex pair in an unbounded domain.

6.3 Kelvin Wave Generation

Equation 27 verifies that $\partial_x \eta|_{y=0}$ is small enough that the inner solution (to lowest order) may be obtained by setting η to a constant on the boundary. At the same time, however, it shows that $\partial_x \eta|_{y=0}$ is not identically zero — there will be a *jump* in η across the region of the inner solution. This jump may be calculated as follows:

$$\lfloor \eta_0 \rceil \equiv \int_{-\infty}^{+\infty} \partial_x \eta|_{y=0}\,dx' = -\delta \int_{-\infty}^{+\infty} \{\partial_t u|_{y=0} + \tfrac{1}{2}\partial_x (u|_{y=0})^2\}\,dx' \approx \delta\,\partial_t \int_{-\infty}^{+\infty} (\partial_y \eta)|_{y=0}\,dx, \tag{28}$$

where u has been approximated by the geostrophic velocity, $u_g \equiv -\partial_y \eta$. Note that for the vortex pair solution under consideration, $\lfloor \eta_0 \rceil$ will be periodic in time with a period half that of the orbital vortex motion.

For the inner, quasi-geostrophic solution, η is given by

$$\eta = -\{\mathrm{K}_0(\varepsilon\delta^{-1}\,|\boldsymbol{x} - \boldsymbol{x}_1|) - \mathrm{K}_0(\varepsilon\delta^{-1}\,|\boldsymbol{x} - \boldsymbol{x}_1^i|) + \mathrm{K}_0(\varepsilon\delta^{-1}\,|\boldsymbol{x} - \boldsymbol{x}_2|) - \mathrm{K}_0(\varepsilon\delta^{-1}\,|\boldsymbol{x} - V\boldsymbol{x}_2^i|)\}.$$

Here, the locations of the "image" vortices has been noted by the superscript ^{i}: $\boldsymbol{x}_1^i = (x_1, -y_1)$. The last integral in equation 28 may be evaluated with help from a hefty table of integrals [GR80, eqs. 6.596.3, 8.469.3]. This gives, simply enough

$$\lfloor \eta_0 \rceil = -2\pi\delta\, \partial_t (e^{-(\varepsilon/\delta)y_1} + e^{-(\varepsilon/\delta)y_2}).$$

The value of $R \equiv e^{-(\varepsilon/\delta)y_1} + e^{-(\varepsilon/\delta)y_2}$ will attain a minimum when the two vortices are "abreast": $y_1 = y_2 = 0$; and a maximum when one of the vortices is at its closest approach to the wall. In this latter case, $y_1 \approx y_0 - (d/2)$, $y_2 \approx y_0 + (d/2)$. The peak-to-peak range of R is then given approximately by $4e^{-(\varepsilon/\delta)y_0} \sinh^2(\varepsilon\delta^{-1}\, d/4)$. Expecting that the time variations of R are roughly sinusoidal, with a frequency equal to twice the vortex orbital frequency gives:

$$\lfloor \eta_0 \rceil \approx -8\pi\delta\omega\, e^{-(\varepsilon/\delta)y_0} \sinh^2(\varepsilon\delta^{-1}\, d/4) \sin 2\omega t. \tag{29}$$

6.4 The Outer Solutions

Since Kelvin waves travel at the short wave speed, c, the waves generated by the slow motions of the vortex pair will have a long wavelength, $L = \mathrm{O}(\varepsilon^{-1})$. Officially, the outer solutions should be found by rescaling x: $x_\star = \varepsilon x$. (η, u, v, ζ, and q all need to be adjusted too.) But, it has already been guessed that the outer solutions will consist of Kelvin waves. Since the reader has long since grown tired of scaling arguments, the details will skipped.

Kelvin waves have the remarkable properties that they are *non-dispersive*; and that they propagate only in one direction, always keeping the shoreline to their right (in the northern hemisphere). The general form for the outer, Kelvin wave solution in dimensional units is $\eta = e^{-y/\lambda} S(x - ct)$ [Ped87, sec. 3.9]. Non-dimensionalizing by the inner scales, this becomes:

$$\eta = e^{-(\varepsilon/\delta)y} S(\varepsilon x - t),$$

where S is an arbitrary function of its single argument. Note the appearance of the εx (which should really be a $x_\star$), reflecting the long wavelength of the Kelvin waves relative to the inner scales.

6.5 Matching

There are three asymptotic regions in which we have solutions: an inner region ($|\bar{x}| \ll \varepsilon^{-1}$), surrounded by two outer regions; one to the left ($\bar{x} \ll -1$), and one to the right ($\bar{x} \gg 1$).

Since the Kelvin waves of the outer solutions only propagate to the right, there can be no wave in the left outer region. Any waves there would have to have come from $x = -\infty$ — these are disallowed by radiation conditions. The left outer solution is just $\bar{\eta} = 0$.

All that is needed to complete the outer solution on the right side is an boundary condition at $x_\star \to 0^+$. The jump in $\bar{\eta}$ across the inner region (equation 29) provides this boundary condition. The right outer solution is then

$$\bar{\eta} = 8\pi\delta\omega\, e^{-(\varepsilon/\delta)\bar{y}_0} \sinh^2(\varepsilon\delta^{-1}\, d/4)\, e^{-(\varepsilon/\delta)\bar{y}} \sin 2\omega(\varepsilon\bar{x} - \bar{t}).$$

6.6 Radiated Energy Flux

The energy flux carried by the radiated Kelvin waves, $\lim_{x\to\infty} \int_0^\infty \boldsymbol{F}\cdot\hat{\mathbf{x}}\, dy$ may be calculated, much as before. The radiated power is normalized, exactly as in the previous problem, by $c^3\varepsilon^3(d\delta)^{-1}$ (see section 5.5). Finally,

$$\boxed{\dot{\bar{E}} = 16\pi^2\delta^2\omega^2\, e^{-2(\varepsilon/\delta)\bar{y}_0} \sinh^4(\varepsilon\delta^{-1}\, d/4).}$$

With $y_0 = d = \lambda$, $\delta = 0.1$, the non-dimensional radiated power is $\dot{\tilde{E}} = 3.5 \times 10^{-3}$. Yet another *contemptibly small* though *conceivably significant* value. Note that the amplitude of the radiated wave is O(Ro).

7 Remarks

The strength of gravity wave radiation in all of the cases considered above has been shown to be weak. In the case of quasi-geostrophic vortices far from a boundary, coupling is miniscule. The last problem considered, that of forcing of Kelvin waves by vortices near a wall is quite intriguing. It demonstrates relatively significant coupling between vortical eddies and Kelvin waves on a nearby coastline. This sort of process could play an important role in ocean dynamics near coastlines (and presumably other topographic features).

It would be nice to extend the analyses presented here beyond lowest order. Specifically, one would like to carry out the calculations to high enough order to see direct effects on the vortex motion. This was my goal at the beginning of the summer, but my attempts at it so far have been thwarted by the singularities inherent in any point vortex model.

8 Acknowledgments

I would like to thank Rick Salmon for the suggestion of this project, and for his help and encouragement along the way. Glenn Flierl and Joe Keller also deserve special thanks for their efforts at keeping me out of dead-end alleys.

The fellows, staff and other participants in this years GFD program all contributed to an extremely enjoyable and inspiring summer. I would like to express my gratitude to the GFD program for the experience.

References

[AS70] Milton Abramowitz and Irene A. Stegun. *Handbook of Mathematical Functions.* Dover, New York, 1970.

[Bat67] G. K. Batchelor. *An Introduction to Fluid Mechanics.* Cambridge University Press, New York, 1967.

[For93] Rupert Ford. The instability of axisymmetric vortices in shallow water. unpublished, 1993.

[GR80] Izrail Solomonovich Gradshteyn and Iosif Moiseevich Ryzhik. *Table of Integrals, Series and Products.* Academic Press, New York, corrected and enlarged edition edition, 1980. Translated from the Russian by Alan Jeffrey.

[Lig78] James Lighthill. *Waves in Fluids.* Cambridge University Press, New York, 1978.

[Ped87] Joseph Pedlosky. *Geophysical Fluid Dynamics.* Springer-Verlag, New York, 1987.

A periodic orbit expansion of the Lorenz system

Sean McNamara

Scripps Institution of Oceanography, La Jolla CA 92093-0230, USA

The Lorenz system is three coupled first order ordinary differential equations. It was originally developed as a crude model of convection, and is well known to be chaotic. A method has recently been developed for calculating useful and descriptive properties of chaotic systems, called the "periodic orbit expansion". I use this method to calculate the heat flux and kinetic energy of convection, as well as several other quantities.

I. Introduction

In 1963, Lorenz presented a system of equations as a model describing convection which exhibits chaotic behavior for certain parameter values[1]. For this reason, it has proved to be a very interesting system mathematically[2,3], and much work does not consider its humble origin as a simple model of convection. In this paper, I remember its origin and caculate its estimate the heat flux and the kinetic energy of the fluid motion, how frequently the flow direction reverses, as well as the Lyapunov exponent.

In chaotic systems, it is hard to calculate quantities of interest. Recently Cvitanović[4,5,6,7] and others, have developed a method which can be used. This is the periodic orbit expansion. The basic idea is that hidden in the phase space of a chaotic system are an infinite set of unstable periodic orbits. If the system begins on a point *exactly* on one of these orbits, it travels around and around the orbit forever. If it is just slightly off the orbit, it follows the orbit (approximately) for a while, then diverges from it to shadow another. These orbits stand in relation to the nonperiodic trajectories as the rational numbers to the irrational. There is an infinite number of them, and any point is arbitrarily close to one, yet the orbits contain an infinitely small fraction of all points. The periodic orbit expansion computes quantities by constructing a sum over these orbits, weighting each orbit by its stability, and truncating the sum carefully.

In this report, I study the Lorenz system using this method. In Sec. II, I sketch the origin of the Lorenz system and the quantities I will calculate. Sec. III, describes the periodic orbit expansion. Sec. IV describes how the periodic orbits of the Lorenz system were found. Sec. V presents results.

II The Lorenz system

a. Derivation

Figure 1 shows a fluid with viscosity ν, thermal conductivity κ, between two horizontal plates spaced a distance H apart. The upper plate is held at temperature T_0 and the lower at $T_0 + \Delta T$. The density of the fluid depends on temperature: $\rho = \rho_0[1 - \alpha(T - T_0)]$, where α is the coefficient of thermal expansion. Gravitational acceleration, g is downward. Establish a coordinate system with z pointing upwards, and x horizontally.

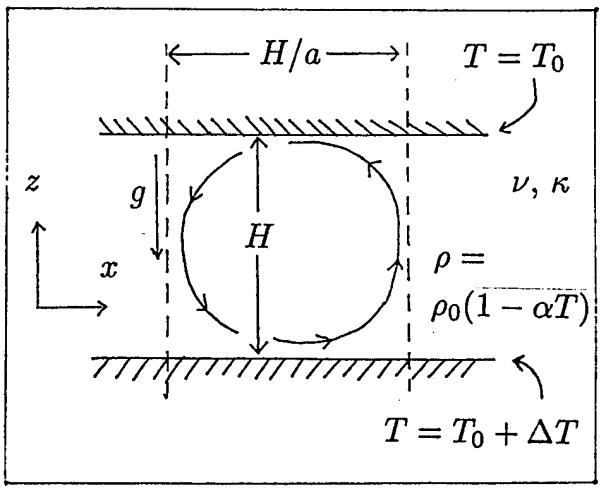

Figure 1. Definition sketch for convection between two parallel plates.

The Boussinesq equations for two–dimensional motion are:

$$\begin{aligned} \nabla^2\psi_t + J(\psi, \nabla^2\psi) &= \nu\nabla^4\psi + g\alpha\theta_x, \\ \theta_t + J(\psi,\theta) &= \kappa\nabla^2\theta + \frac{\Delta T}{H}\psi_x, \end{aligned} \tag{1}$$

where ψ is the streamfunction and θ is the departure of the temperature from the linear profile: $T = T_0 + \Delta T(H-z)/H + \theta$. Assume the solution is two-dimensional rolls of the form

$$\begin{aligned} \psi &= \left(\frac{\kappa}{4a^2b}\right)\left[X(\hat{t})\sqrt{2}\sin\left(\frac{\pi a x}{H}\right)\sin\left(\frac{\pi z}{H}\right)\right], \\ \theta &= \left(\frac{\Delta T}{\pi r}\right)\left[Y(\hat{t})\sqrt{2}\cos\left(\frac{\pi a x}{H}\right)\sin\left(\frac{\pi z}{H}\right) - Z(\hat{t})\sin\left(\frac{2\pi z}{H}\right)\right], \end{aligned} \tag{2}$$

where a is the aspect ratio of the rolls. The dimensionless constants b and r will be defined after the next equation. Time has been nondimensionalized: $\hat{t} = (4\pi^2/bH^2)\kappa t$. Put this solution into Eq. (1). There will be a term containing each of $\dot{X}$, $\dot{Y}$, and $\dot{Z}$. Ignore all terms which do not have the same spatial dependence as these terms. (This involves neglecting the nonlinear terms in the momentum equation, and a nonlinear term proportional to $\sin(3\pi z/H)$ in the temperature equation.) Equating terms with the same spatial dependence gives the *Lorenz equations:*

$$\begin{aligned} \dot{X} &= -\sigma X + \sigma Y, \\ \dot{Y} &= -XZ + rX - Y, \\ \dot{Z} &= XY - bZ. \end{aligned} \tag{3}$$

Here, $\sigma \equiv \nu/\kappa$ is the *Prandtl number*, a property of the fluid. The geometry of the rolls enters through the parameter $b \equiv 4/(1+a^2)$. The parameter $r \equiv R_a/R_c$ measures the strength of the forcing. ($R_a \equiv g\alpha\Delta T H^3/\nu\kappa$ is the Rayleigh number, and $R_c \equiv \pi^4(1+a^2)^3/a^2$ is the critical Rayleigh number; when $R_a > R_c$ ($r > 1$) the solution $\psi = \theta = 0$ is unstable and convection occurs.) The "classical" values which Lorenz first used are $r = 28$, $b = 8/3$ and $\sigma = 10$. In this report, I will vary r but not σ and b.

b. solutions

When $r < 1$, the point $X = Y = Z = 0$ is stable. The system moves from any initial point to the origin and stays there. This corresponds to no fluid motion, with heat transported purely by conduction. At $r = 1$, this fixed point becomes unstable, and bifurcates into two stable, fixed points at $X = Y = \pm\sqrt{b(r-1)}$, $Z = r - 1$. For $1 < r < 24.74$, the system moves from any point towards one of these two points. These fixed points correspond to steady convective rolls. There are two because the fluid can move clockwise or counterclockwise. Finally, for $r > 24.74$, these points become unstable, and the system is chaotic.

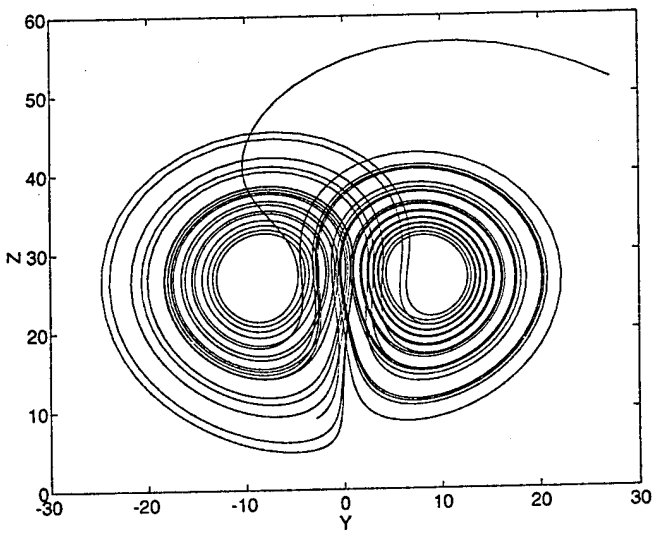

Figure 2. Typical chaotic trajectory at $r = 28$. The initial position is near $(Y, Z) = (30, 50)$.

c. quantities predicted by the Lorenz system

In this paper, I will calculate three physical quantities predicted by the Lorenz system. The first of these is the heat flux q:

$$q = \int_0^{H/a} (wT - \kappa T_z) dx, \tag{4}$$

where w is the vertical velocity, and the integral is taken at some fixed value of z. Using the solution in Eq. (2), we have

$$\frac{\langle q \rangle}{\kappa \Delta T_1 / a} = (r + 2\langle Z \rangle), \tag{5}$$

where $\Delta T_1 \equiv \nu\kappa R_c / g\alpha H^3$ is the temperature difference required to give $r = 1$. The angular brackets denote averages over a long time (they will be more rigorously defined in Sec. III). Deriving Eq. (5) also requires taking the long time average of the third Lorenz equation to get $0 = \langle XY \rangle - b\langle Z \rangle$.

The kinetic energy of the fluid is:

$$KE = \int_0^{H/a} dx \int_0^H dz \; \rho \nabla\psi \cdot \nabla\psi, \tag{6}$$

which becomes

$$\frac{\langle KE \rangle}{M(\kappa/H)^2} = \frac{32\pi^2}{a^2 b^3} \langle X^2 \rangle, \tag{7}$$

where M is the mass of the fluid in the roll, and κ/H has dimensions of velocity.

The third quantity is the "floppiness", $\mathcal{F}$. The floppiness is the number of times X and Y change sign per unit time. Thus, if $\mathcal{F} = 0.65$, it is expected that X and Y change sign 65 times in 100 time units. A change in the sign of X corresponds to a reversal of the flow direction. In Fig. 2, the change in sign of X and Y corresponds to changing the fixed point the system is currently circling.

I also estimate the Lyapunov exponent μ. This quantity measures how fast two neighboring points in phase space seperate. When the two points are close together, the distance between them grows like $e^{\mu t}$.

III. The Periodic Orbit Expansion

In this section, I sketch the periodic orbit expansion. This is not a complete derivation, but it is thorough enough to give a glimpse of the mathematical details. These details are found in the Refs. 4-7. None of this is my original work, but I have not been able to find a simple presentation in the literature.

a. objective

The goal is to compute "long time averages", denoted by angle brackets, and defined by

$$\langle \phi \rangle \equiv \lim_{t \to \infty} \frac{1}{Vt} \int_V d\mathbf{a} \; \Phi^t(\mathbf{a}), \tag{8}$$

where

$$\Phi^t(\mathbf{a}) \equiv \int_0^t dt' \; \phi[\mathbf{f}^{t'}(\mathbf{a})]. \tag{9}$$

Here, boldface denotes positions in phase space. The movement of the system through phase space is given by $\mathbf{f}^t(\mathbf{a})$. If a system is at $\mathbf{a}$, it will have moved to $\mathbf{f}^t(\mathbf{a})$ after time t has passed. V is a fixed volume in phase space in which the system remains, and $\int_V d\mathbf{a} = V$. The quantity we are averaging (the heat flux q for example) is ϕ, and $\Phi^t(\mathbf{a})$ is the integral of ϕ along a trajectory beginning at $\mathbf{a}$ and continuing for a time t. The average of ϕ along one trajectory is $\Phi^t(\mathbf{a})/t$. It is necessary to average over phase-space as well as time because $\Phi^t(\mathbf{a})$ can depend on $\mathbf{a}$ (if $\mathbf{a}$ is on a periodic orbit for example).

b. derivation

We will approach Eq. (8) indirectly. I will dabble with some apparently unrelated equations, when suddenly an expression for $\langle\phi\rangle$ will appear. Let me begin by writing 1 in a very complicated way:

$$\frac{1}{V}\int_V d\mathbf{a}\int_V d\mathbf{x}\;\delta[\mathbf{x}-\mathbf{f}^t(\mathbf{a})] = \Lambda_0 = 1, \tag{10}$$

The δ function has a singularity when a system at $\mathbf{a}$ moves to $\mathbf{x}$ after time t. Thus, for each value of $\mathbf{a} \in V$, the delta function has a singularity at exactly one $\mathbf{x} \in V$. Thus, the integral over $\mathbf{x}$ is 1. The integral over $\mathbf{a}$ is V, giving 1 for the whole expression. I include Λ_0 here, because Eq. (10) is the leading (largest) eigenvalue of the operator

$$\mathcal{L}^t(\mathbf{x},\mathbf{a}) \equiv \delta[\mathbf{x}-\mathbf{f}^t(\mathbf{a})]. \tag{11}$$

$\mathcal{L}^t$ is called the *Perron–Frobenius* operator. It is instructive to compare $\mathcal{L}^t(\mathbf{x},\mathbf{a})$ with a finite dimensional operator L_{ij}:

$$v_i = L_{ij}u_j. \tag{12}$$

L_{ij} operates on vectors, taking one vector into another. The analog of Eq. (12) for $\mathcal{L}^t$ is

$$\rho_2(\mathbf{x}) = \int_V d\mathbf{a}\;\mathcal{L}^t(\mathbf{x},\mathbf{a})\rho_1(\mathbf{a}). \tag{13}$$

The arguments $\mathbf{x}$ and $\mathbf{a}$ play the role of the subscripts i and j. Eq. (12) involves summation over j; Eq. (13) requires integration over $\mathbf{a}$. $\mathcal{L}^t$ operates on phase space density functions such as ρ_1 and ρ_2. In Eq. (13), an initial distribution of points according to ρ_1 will move to a distribution according to ρ_2 after time t. This is the action of $\mathcal{L}^t$. This gives $\mathcal{L}^t$ the special property:

$$\mathcal{L}^{t_1}\mathcal{L}^{t_2} = \mathcal{L}^{t_1+t_2}. \tag{14}$$

This property implies that Λ_0 is the leading eigenvalue of $\mathcal{L}^t$ for large t. To see this, divide t into N parts; $t = N\tau$, where N is large and τ order unity:

$$\Lambda_0 = 1 = \int_V d\mathbf{x}\int_V d\mathbf{a}\;\mathcal{L}^t\frac{1}{V} = \int_V d\mathbf{x}\int_V d\mathbf{a}\;\mathcal{L}^\tau\mathcal{L}^\tau\cdots\mathcal{L}^\tau\frac{1}{V}, \tag{15}$$

where we used Eq. (14) to write $\mathcal{L}^t = [\mathcal{L}^\tau]^N$. Then expand $\rho = 1/V$ in the eigenfunctions of $\mathcal{L}^\tau$: $1/V = c_0\rho_0 + c_1\rho_1 + \cdots$. Here, the ρ_i are the eigenfunctions and the c_i are constants. Let

λ_i be the eigenvalue corresponding to eigenfunction ρ_i. We can show that these eigenvalues are real and can be ordered: † $\lambda_0 > \lambda_1 > \lambda_2 > \cdots$. We then have:

$$\Lambda_0 = 1 = \lambda_0^N \int_V c_0\rho_0(\mathbf{x})d\mathbf{x} + \lambda_1^N \int_V c_1\rho_1(\mathbf{x})d\mathbf{x} + \cdots \approx \lambda_0^N \int_V c_0\rho_0(\mathbf{x})d\mathbf{x}. \tag{16}$$

Applying the operators multiplies each term by the appropriate eigenvalue, raised to the N^{th} power. Finally, the term involving the leading eigenvalue λ_0 dominates since $\lambda_0^N \gg \lambda_1^N$ if N is big enough. If we consider N and t increasing, with τ fixed, we can show $\int_V c_0\rho_0(\mathbf{x})d\mathbf{x} = 1$ so

$$\Lambda_0 = \lambda_0^N = 1. \tag{17}$$

This, combined with the property of $\mathcal{L}^t$ in Eq. (14) shows that Λ_0 is the leading eigenvalue of $\mathcal{L}^t$.

Now, let us write

$$\frac{1}{V}\int_V d\mathbf{a}\int_V d\mathbf{x}\ \exp[\beta\Phi^t(\mathbf{a})]\mathcal{L}^t(\mathbf{x},\mathbf{a}) = \Lambda_0^*(\beta) = \exp[Q(\beta)t]. \tag{18}$$

Here, β is a parameter we have introduced, and Φ^t is the integral of ϕ along the trajectory, defined in Eq. (9). Note that the new operator $\mathcal{L}_*^t = \exp[\beta\Phi^t(\mathbf{a})]\mathcal{L}^t$ has the same property [Eq. (14)] as $\mathcal{L}^t$. Thus, $\Lambda_0^*(\beta)$ is the leading eigenvalue of $\mathcal{L}_*^t$. When $\beta = 0$, Eq. (18) reduces to Eq. (10), implying $Q(0) = 0$. Now, comes the surprise. Differentiate Eq. (18) by β, and set $\beta = 0$. After doing the $\mathbf{x}$ integral, we have

$$\left(\frac{\partial Q}{\partial\beta}\right)_{\beta=0} = \frac{1}{Vt}\int_V d\mathbf{a}\ \Phi^t(\mathbf{a}) = \langle\phi\rangle! \tag{19}$$

c. where the orbits come in

In summary, to find $\langle\phi\rangle$, we must first find $Q(\beta)$ but finding this requires finding the leading eigenvalue of $\mathcal{L}_*^t$. To find this eigenvalue, calculate the trace:

$$\mathrm{tr}\mathcal{L}_*^t = \int_V d\mathbf{a}\ \mathcal{L}_*^t(\mathbf{a},\mathbf{a}) = \int_V d\mathbf{a}\ \delta[\mathbf{a} - \mathbf{f}^t(\mathbf{a})]w(\mathbf{a}). \tag{20}$$

Here, we have used $w(\mathbf{a}) \equiv \exp[\beta\Phi^t(\mathbf{a})]$ for clarity. As with finite matrices, the trace will be the sum of the eigenvalues. In the limit of $t \to \infty$, the leading eigenvalue will dominate, and will simply be equal to the trace.

The δ function in Eq. (20) has a singularity only when a point returns to its original location in phase space. Thus, *only points on periodic orbits contribute* to $\mathrm{tr}\mathcal{L}_*^t$. Therefore, the trace can be rewritten as

$$\mathrm{tr}\mathcal{L}_*^t = \sum_p \int_{\mathcal{D}_p} dx_\parallel\, d\mathbf{x}_\perp\ \delta[x_\parallel - f^t(x_\parallel)]\ \delta[\mathbf{x}_\perp - f^t(\mathbf{x}_\perp)]w(\mathbf{x}). \tag{21}$$

† This is shown using *Fredholm theory*: we consider $\mathcal{L}^t$ as an infinite dimensional matrix, as we did in Eq. (12). The definition of $\mathcal{L}^t$ enables us to deduce enough its matrix representation to prove the eigenvalues are real and can be ordered, as we have assumed.

Here, p indexes the *prime orbits*. Given any orbit, it is possible to find another one with exactly twice the period by traveling around the first orbit twice. The second orbit, however, is not *prime*; a prime orbit cannot be considered as multiple trips around a shorter orbit. The integrals are taken over $\mathcal{D}_p$, a thin tube encircling the orbits. Since only points on periodic orbits contribute, we can establish a new coordinate system, where $x_\parallel$ runs along the orbit, and $\mathbf{x}_\perp$ are the directions perpendicular to the orbit. The delta function involving $x_\parallel$ has a singularity only when t is an integer multiple of an orbital period. This enables us to write

$$\int_{\mathcal{D}_p} \delta[x_\parallel - f^t(x_\parallel)]dx_\parallel = \int_{\mathcal{D}_p} \delta(t - rT_p)\left(\frac{dx_\parallel}{dt}\right)^{-1} dx_\parallel = T_p\delta(t - rT_p). \tag{22}$$

The integral over $\mathbf{x}_\perp$ is

$$\int_{\mathcal{D}_p} \delta[\mathbf{x}_\perp - f^t(\mathbf{x}_\perp)]d\mathbf{x}_\perp = [\det(\mathbf{I} - \mathbf{J}_p^r)]^{-1}, \tag{23}$$

where $\mathbf{I}$ is the identity matrix and $\mathbf{J}_p$ is the linearization of the dynamics around the periodic point. Suppose a system begins a small distance $\Delta\mathbf{x}_\perp$ from the periodic orbit. After one period, its position will be $\mathbf{J}_p\Delta\mathbf{x}_\perp$. The quantity $\det(\mathbf{I} - \mathbf{J}_p)$ is related to the eigenvalues of $\mathbf{J}_p$. In the Lorenz system, $\mathbf{J}_p$ must have at least one unstable (absolute value greater than 1) eigenvalue (denoted Λ_p) since the orbit is unstable. The other eigenvalue (denoted λ_p) is stable, and represents the movement of systems towards the strange attractor. With this notation, we can write

$$\mathrm{tr}\mathcal{L}_*^t = \sum_p \sum_{r=1}^{\infty} \frac{T_p\delta(t - rT_p)w_p^r}{(1 - \Lambda_p^r)(1 - \lambda_p^r)}. \tag{24}$$

At this point, we continue our mathematical odyssey, encountering Fourier series, Wick rotations, complex integration and summation of infinite series. At last, we reach the dynamical ζ function, which defines $Q(\beta)$ implicitly:†

$$\frac{1}{\zeta[\beta, Q(\beta)]} = \prod_p \left(1 - \frac{\exp[\beta\Phi_p - Q(\beta)T_p]}{\Lambda_p}\right) = 0. \tag{25}$$

The product is over the prime orbits, indexed by p. The period of the orbit is T_p, and Φ_p is the integral of ϕ once around the orbit; $\Phi_p = \Phi^{T_p}(\mathbf{a})$ where $\mathbf{a}$ is any point on the orbit.

Expanding the infinite product, and using $\xi_p = \exp[\beta\Phi_p - Q(\beta)T_p]/\Lambda_p$ we have

$$\zeta^{-1} = 1 - \xi_1 - \xi_2 - \cdots + \xi_1\xi_2 + \xi_1\xi_3 + \xi_2\xi_3 + \cdots - \xi_1\xi_2\xi_3 - \cdots = \sum_{\{p_1 p_2 \cdots p_k\}} (-1)^k \xi_{\{p\}}. \tag{26}$$

Where do we truncate this sum? First, we assign an order to each orbit. The order of an orbit is related to its length; more details will be given below. Then, define the order of each term in Eq. (26) to be the sum of the orbits involved. For example, if orbit $p = 1$ is first order, and $p = 2$ third order, the term $\xi_1\xi_2$ is fourth order. Finally, we keep terms up to a certain order. This works because terms of the same order tend to cancel one another. For example, consider the four orbits of Fig. 4. Let ξ_a be the contribution from the orbit of panel a, and so on. Then the third order term is $-\xi_c - \xi_d + \xi_a\xi_b$. But orbit c resembles orbit a superimposed on orbit b, so $\xi_a\xi_b$ nearly cancels $-\xi_c$. At higher orders, the cancellation becomes more complete.

† The ζ function is reached via the *Fredholm determinant* which involves the contracting eigenvalue λ_p as well as Λ_p. It can be written as a product of ζ functions. The Fredholm determinant and the ζ function have the same leading zero.

d. results

The accuracy of the periodic orbit expansion can be checked by recalling $Q(0) = 0$ and Eq. (25):

$$\frac{1}{\zeta(0,0)} = \prod_p \left(1 - \frac{1}{\Lambda_p}\right) = 0. \tag{27}$$

This puts a constraint on the stabilities of the orbits. The orbits are not independent entities, but are related in a strict way. By checking Eq. (27), it is possible to detect missing or duplicated orbits.

Differentiating Eq. (25) with respect to β and setting $\beta = 0$ gives

$$\langle \phi \rangle = \left(\frac{\partial Q}{\partial \beta}\right)_{\beta=0} = \frac{\sum \Phi_{\{p_1 p_2 \ldots p_k\}}/\Lambda_{\{p_1 p_2 \ldots p_k\}}}{\sum T_{\{p_1 p_2 \ldots p_k\}}/\Lambda_{\{p_1 p_2 \ldots p_k\}}}, \tag{28}$$

where the sums are over $\{p_1 p_2 \ldots p_k\}$, as in Eq. (26). Here,

$$\begin{aligned} \Phi_{\{p_1 p_2 \ldots p_k\}} &= \Phi_{p_1} + \Phi_{p_2} + \cdots + \Phi_{p_k}, \\ T_{\{p_1 p_2 \ldots p_k\}} &= T_{p_1} + T_{p_2} + \cdots + T_{p_k}, \\ \Lambda_{\{p_1 p_2 \ldots p_k\}} &= (-1)^k \Lambda_{p_1} \Lambda_{p_2} \cdots \Lambda_{p_k}. \end{aligned} \tag{29}$$

IV. How to find orbits

Next, we turn to the problem of finding the periodic orbits of the Lorenz system. I construct a one dimensional map, and find the periodic orbits of the map. From these orbits, it is possible to accurately estimate the orbits in the full system, which can be refined further.

a. the one–dimensional map

As shown in figure 2, the system is continually looping around one of the two fixed points. For each loop, there is a maximum Z. It turns out that the maximum in Z can be predicted from the Z–maximum in the previous loop. If we solve the equations numerically and plot successive pairs of Z maxima, we get figure 3. † Using figure 3, it is possible to predict the sequence of Z–maxima which will follow any first Z–maximum. For example, if we start with the point where $Z = Z_{\rm next}$ (the fixed point of the map), we stay there forever; the $Z_{\rm max}$ of each loop remains unchanged. This is the first periodic orbit of the map, and is a "first order" orbit. There is a second order orbit where $Z_{\rm max}$ alternates between two values. In an $n^{\rm th}$ order orbit, $Z_{\rm max}$ runs through n values before repeating. The first order orbit and one third order orbit are shown in figure 3.

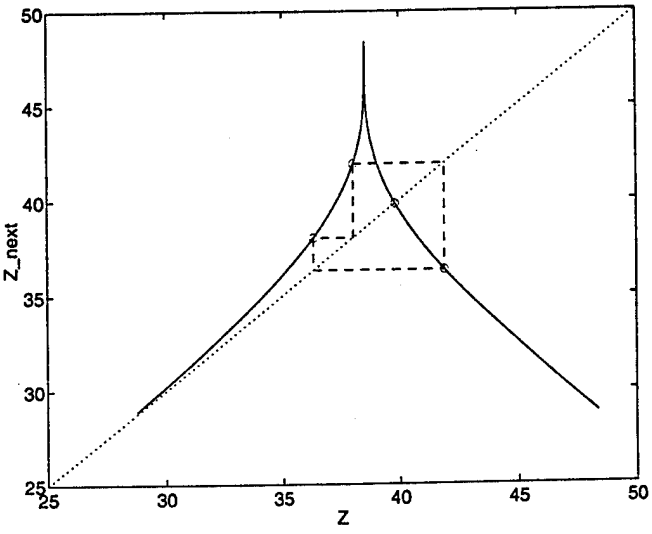

Figure 3. Map for predicting successive Z maxima at $r = 28$. Two orbits are shown: the first order orbit, where the map intersects the diagonal line, and a third order orbit. These orbits are shown in figure 4.

† We interpolate between the "observed" pairs of Z–maxima with a cubic spline.

b. refining the guess from the map

Once we know a Z_{max} associated with a certain orbit, we can estimate the X and Y which occur at this point. Then, using this as an initial condition, we integrate forward in time until n Z maxima later. We will be near the initial point, but not exactly, since the initial guess was not exact. But this initial guess can be refined using a Newton–Raphson technique. In figure 4, I present several low order orbits at $r = 28$. Figure 4a corresponds to the orbit described in the previous paragraph, where $Z = Z_{next}$.

Inspection of Fig. 4 reveals a complication that was not visible in the map. Figure 4a, which is first order in the map, is really *second* order in the differential equation, since it makes two loops before returning to its starting point. There is a whole class of orbits with this property. This happens because the Lorenz system is unchanged by the transformation $(X, Y, Z) \to (-X, -Y, Z)$. This symmetry is invisible to the map, which involves only Z. So, there are two possible ways of determining the order of an orbit: from the map or from the differential equation (defining the order of the orbit as the number of loops around one of the fixed points). If we use the map, the orbit in figure 4a is first order. If we use the differential equation, it is second order, but we must count asymmetric orbits (Fig. 4d) twice to account for its mirror image. In the map, we include it only once. Counting orders according to the map is more efficient because it exploits a symmetry of the dynamics (see Ref. 7 for more details).

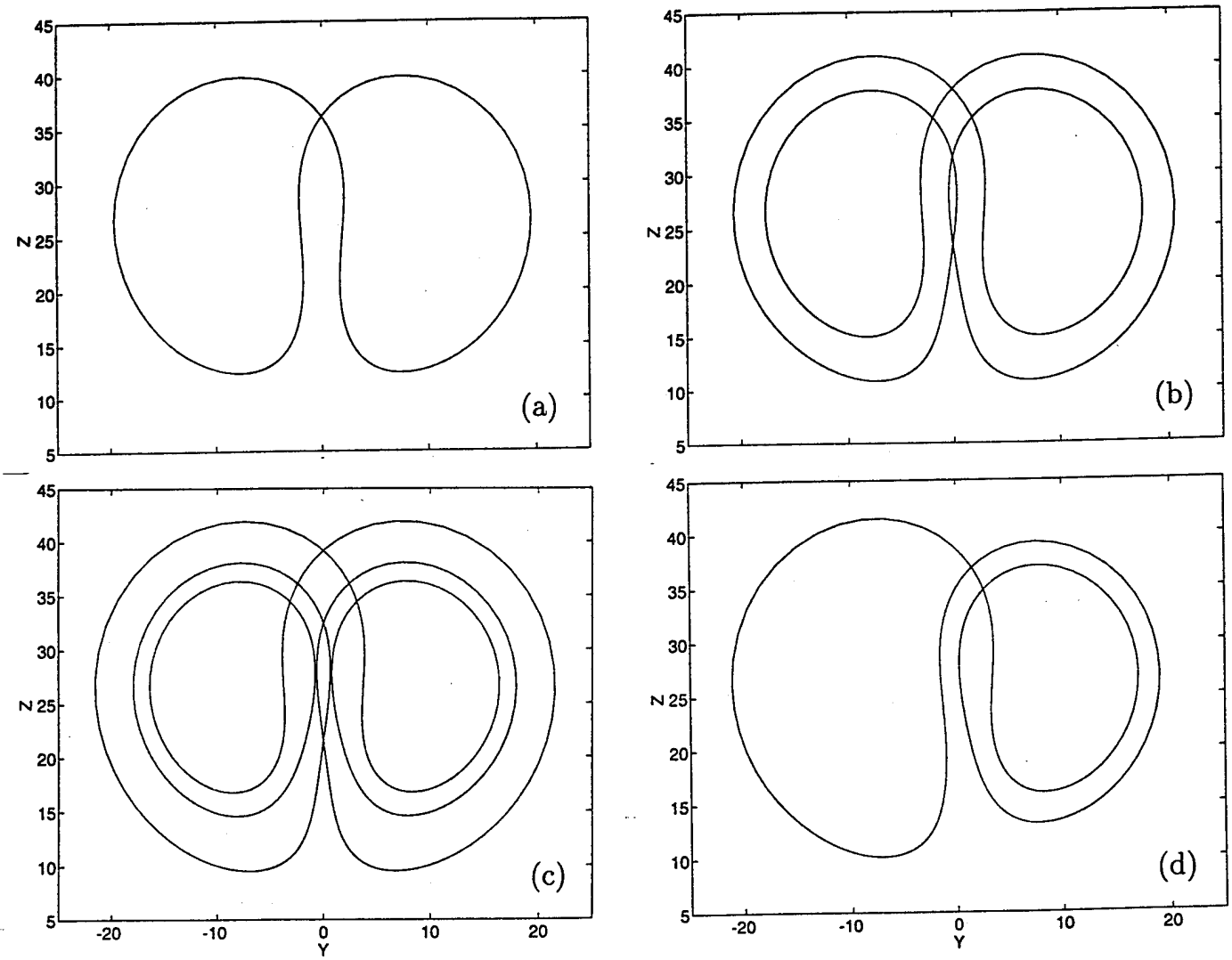

Figure 4. The four lowest order orbits at $r = 28$. (a) the first order orbit, shown also in Fig. 3. (b) the second order orbit. (c) the third order symmetric orbit. (d) the third order antisymetric orbit, also shown in Fig. 3.

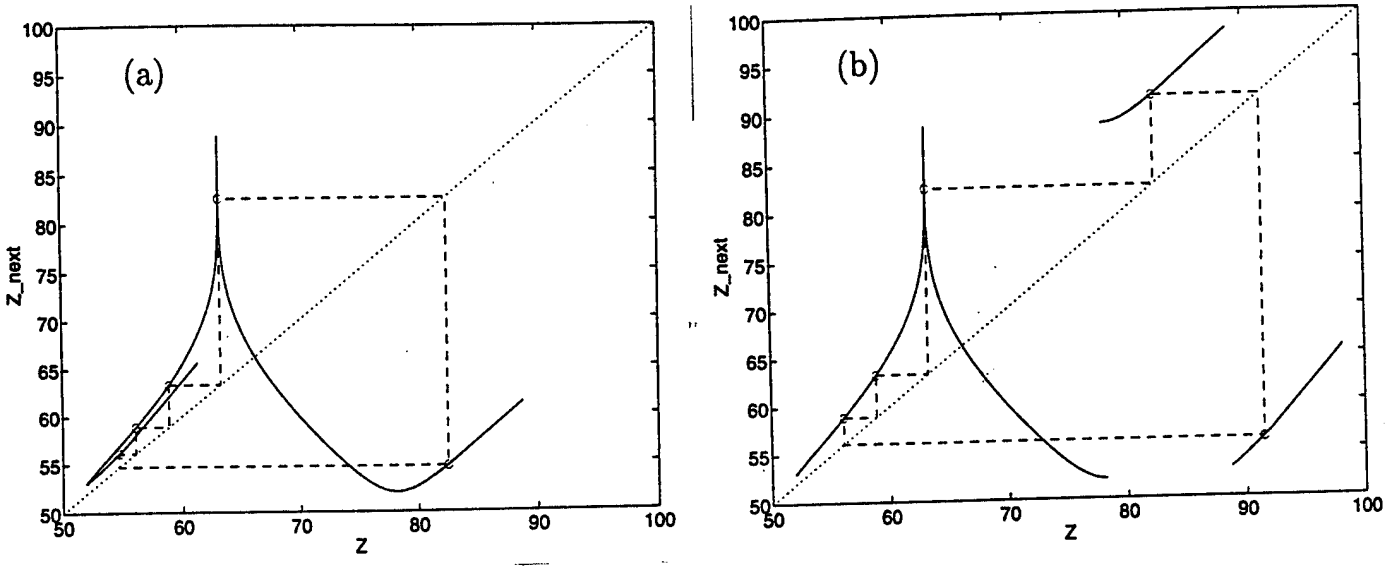

Figure 5. The map for $r = 49$. In (a), the map is double–valued for $52 < Z < 62$. In (b), the map has been "checkerboarded" to make the map single–valued. The same orbit is shown in both panels and in figure 6.

c. Complications at higher r

As r increases, a new class of orbits appear. In figure 5a, we show the Z-maximum map for $r = 49$, and one fifth order orbit. This orbit is different from the orbits of Figs. 3 and 4. First, it travels far up into the cusp, reaching a high value of Z. This sends it to a new branch of the map ($Z > 78$ in figure 5a) not seen at $r = 28$ (Fig. 3). Then, at the next Z–maxima, it visits a new part of the map at small Z before returning to the main map. The map has become double–valued for small Z, and it is very cumbersome to locate the periodic orbits of a double–valued map. One solution is to "checkerboard" the map, as shown in Fig. 5b. Bits of the map are shifted to restore the single-valuedness of the map. I have traced the same orbit in both panels to show how this works. The orbits that visit these shifted segments of the map turn out to be very unstable, and difficult to locate. Figure 6 shows the orbit of Fig. 5 in the YZ plane. Note the broad sweep across the top – this is the passage through large Z to the new parts of the map – nothing like this is seen in the orbits of Fig. 4.

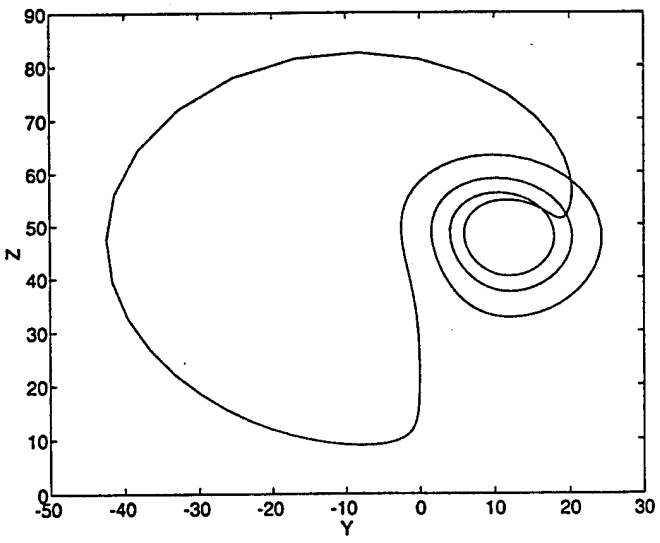

Figure 6. The periodic orbit of Fig. 5 shown in the YZ plane. Compare with the orbits of fig. 4.

V. Results

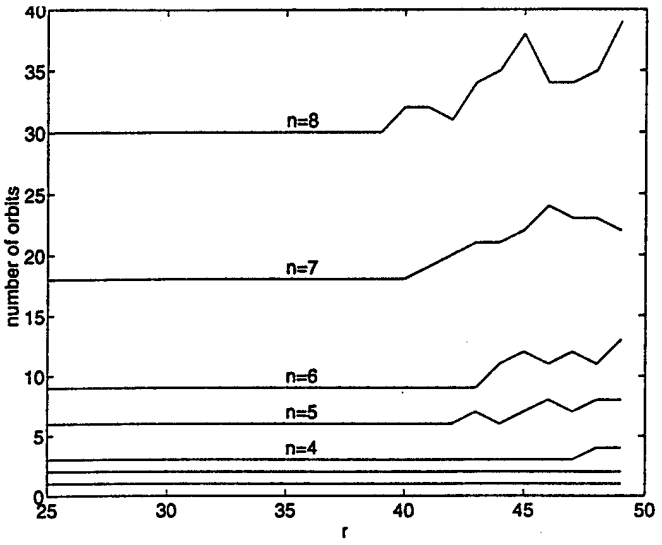

Figure 7. The number of orbits found at each order, vs. r.

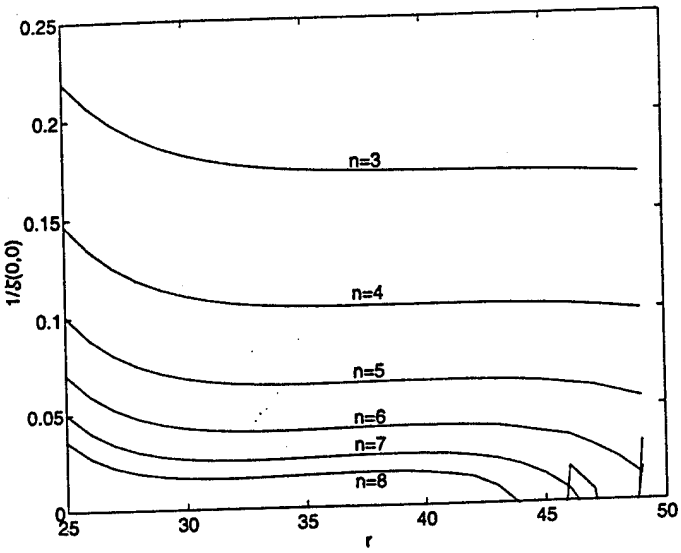

Figure 8. The quantity in Eq. (27). The difference from 0 measures the error in the periodic orbit expansion.

Fig. 7 shows the number of orbits of each order as a function of r. The number of orbits at each order is constant for $r < 40$, when more orbits appear. These new orbits are associated with the map becoming double–valued, and are related to the orbit shown in Fig. 6. These orbits are difficult to locate because the are very unstable. For $r > 40$, there were orbits estimated from the map could not be located in the flow. The lumpiness of Fig. 7 probably could be removed by an improving the method used to find orbits.

In figure 8, I show estimates of $\zeta(0,0) = 0$ for several values of r and orders of approximation. This measures the accuracy of the periodic orbit expansion. Figure 8 shows good behavior for $r < 43$, and then problems appear for higher order estimates. These errors are caused by certain periodic orbits which become stable at special values of r. When this happens, the periodic orbit expansion breaks down because it assumes all orbits are unstable. In figure 9, I show the orbit that is causing problems at $r = 48$. It is a seventh order orbit. Note that one of the points is very near the flat part of the map in Fig. 9b. As r changes continuously, the map changes smoothly, and the points of this orbit move smoothly. For some special r, one point is at the local minimum of the map, and the orbit has $\Lambda_p = 0$, and the periodic orbit expansion doesn't work.

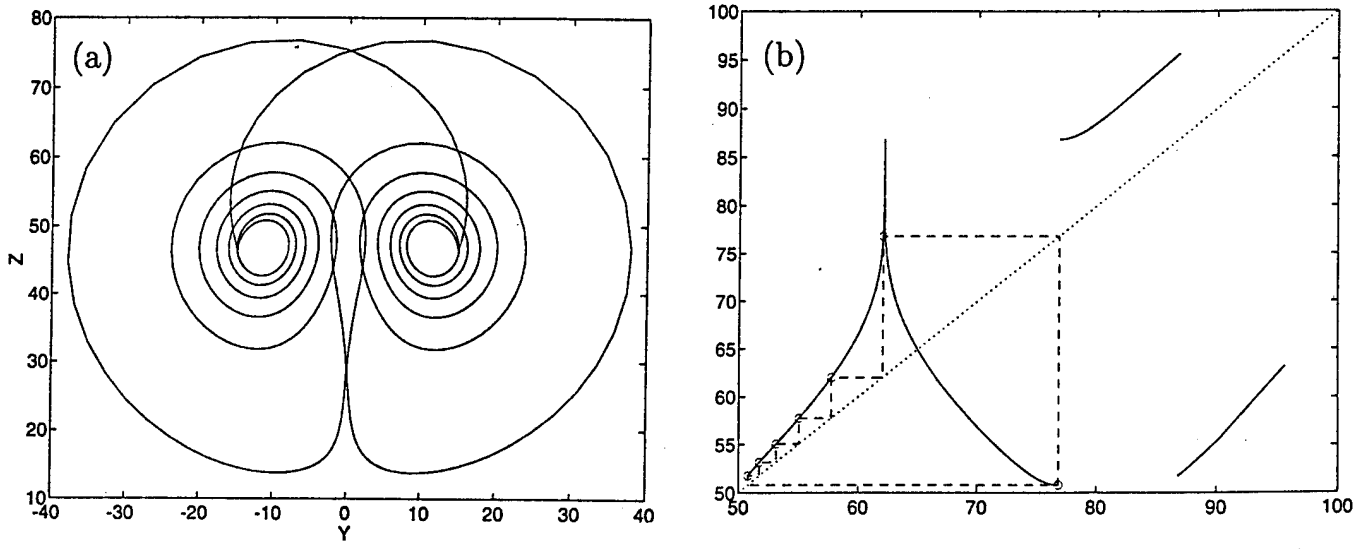

Figure 9. The trouble–making orbit at $r = 48$ in (a) the YZ plane (b) on the map. Note that it touches the map where it is nearly flat.

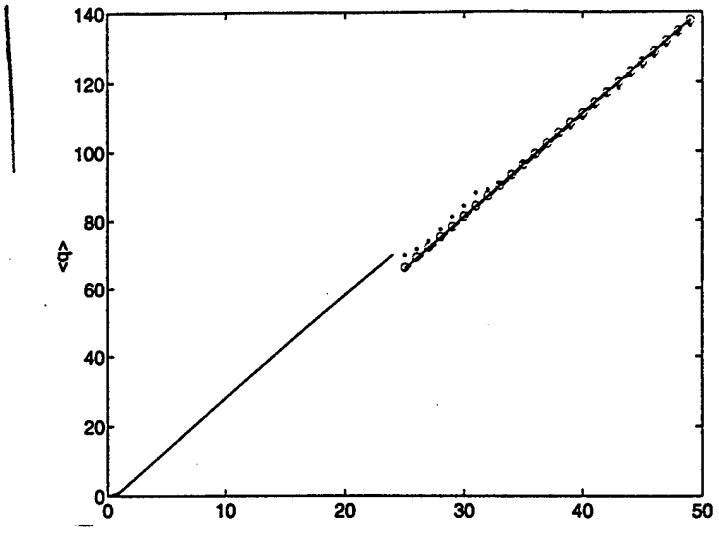

Figure 10. The heat flux. For $r < 24$, the values are calculated from the stable fixed points. For $r > 24$: solid line: eighth order periodic orbit expansion, dashed line: first order periodic orbit expansion; open circles: averaging for $t = 2500$ time units; points: averaging for $t = 25$ time units.

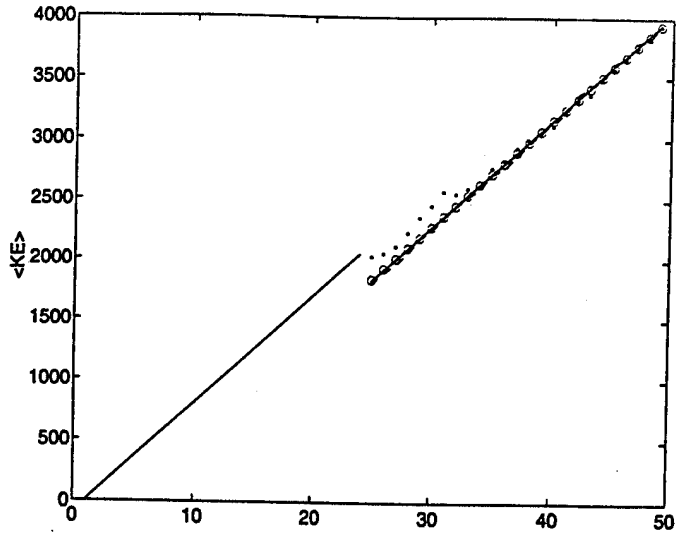

Figure 11. Same as figure 10, except for Kinetic energy of the fluid.

In figures 10 and 11 show the heat flux and and kinetic energy of the flow. For $r \leq 24$, the solid line is the head flux and kinetic energy associated with the stable fixed points. For $r > 25$, there are four different estimates (two from the periodic orbit expansion and two from solving the differntial equations, and averaging), all in good agreement. These quantities are easy to estimate because they don't vary much from orbit to orbit. Note that the the transition to chaos is *not* associated with an increase in kinetic energy or efficiency of heat transport. The transition to chaos should not be thought of as the system finding new ways to transport heat more efficiently; it is less efficient.

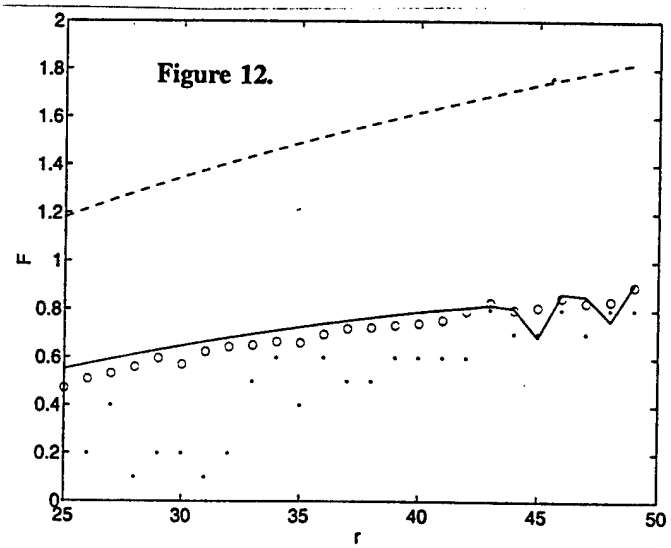

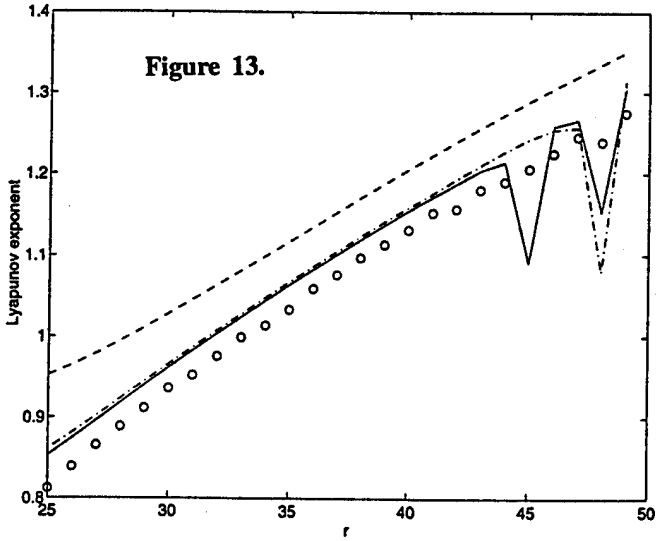

Figure 12 shows four estimates of the "floppiness". Here, the calculations converge much more slowly. The low order periodic orbit expansion estimate is too high because the first orbit (Fig. 4a) is very "floppy" – it flops from one stable point to the other time it circles one of the fixed points. The higher order orbits will often circle the same fixed point several times

before flopping (Fig. 4d or Fig. 6). The contribution from these orbits reduce the floppiness. The floppiness converges slowly, because orbits vary widely in floppiness.

Estimates of the Lyapunov exponent are shown figure 13. This quantity is very difficult to compute by averaging over the flow because it converges slowly. There is a roughly constant offset between the results of the periodic orbit expansion and those of an averaging method. The deep gashes in the periodic orbit estimate are due to almost stable orbits, such as that shown in figure 9. Orbits with unusual properties can confuse the periodic orbit expansion. One the other hand, when there is a stable orbit, the Lyapunov exponent vanishes, so there are special values of r for which Lyapunov exponent plunges to 0. This dramatic behavior is suggested by the periodic orbit expansion, but not the averaging method.

VI. Conclusions

The periodic orbit expansion works, but it requires a lot of effort to find the orbits. To calculate the heat flux or kinetic energy, it is easier just to average while integrating the equations forward in time. But once the orbits are located, it is easy to calculate averages of many different quantities. The periodic orbit expansion also avoids the problem of selecting intial conditions for averaging. The periodic orbit expansion also provides a measure of its accuracy in Eq. (27). This result places a constraint on the stabilities of all the orbits, showing they are all related. Thus, given a set of periodic orbits, it is possible to tell whether they describe a real dynamical system. Finally, examining the periodic orbits is a pleasing way to study the different behaviors a system can have.

Acknowledgements

I would like to thank my summer advisor, Neil Balmforth, for teaching me about this material and providing many of the programs needed. Glenn Ierley unwittingly assisted with the calculations. Comments during the talk by Diego del Castillo, Ed Spiegel and Joe Keller for improved the report. I also thank Rick Salmon for directing the program, and everyone else who made this a fine summer.

References

[1] E. Lorenz:"Deterministic Nonperiodic Flow," J. of the Atmospheric Sciences **20** 244 (1963)
[2]K. Alfsen and J. Froyland: "Systematics of the Lorenz model at $\sigma = 10$," Physica Scripta **31** 15 (1985)
[3]C. Sparrow: *The Lorenz Equations: Bifurcations, Chaos and Strange Atractors*, Springer–Verlag, New York (1982)
[4]R. Artuso, E. Aurell and P. Cvitanović: "Recycling of strange sets I: Cycle expansions," Nonlinearity **3** 325 (1990)
[5]R. Artuso, E. Aurell and P. Cvitanović: "Recycling of strange sets II: Applications," Nonlinearity **3** 361 (1990)
[6]P. Cvitanović: "Notes on dynamical averaging."
[7]P. Cvitanović and B. Eckhardt: "Symmetry decomposition of chaotic dynamics," Nonlinearity **6** 277 (1993)

Elliptical Vortices in Shear: Hamiltonian Formulation, Vortex Merger, and Chaos

Keith Ngan
Department of Physics, University of Toronto

Abstract
The equations of motion for a pair of interacting, elliptical vortices in a background shear flow are derived using a Hamiltonian moment formulation. For no background flow, a 6th order system — identical to that obtained by Melander et al. (1986) — results. These equations are analysed using a variety of methods and implications for vortex merger are examined. A modification of the standard Melnikov method is developed; it is shown that the separatrix for inter-centroid motion exhibits exponentially small splittings. Numerical simulations are performed and chaotic motion is detected.

1 Introduction

The emergence of quasi-elliptical, quasi-uniform vortices in numerical simulations of freely evolving two-dimensional (2D) turbulence has been studied extensively (e.g. McWilliams 1984). Vortices of like-sign *merge* to form persistent coherent structures; it is believed that this phenomenon is essential to the phenomenology of 2D turbulence (e.g. Melander et al. 1988). Vortex merger is a very complicated phenomenon and it is not well-understood.

In this report, a highly idealized model of vortex merger is derived and then analysed. Specifically, the evolution of a pair of elliptical vortices in a background shear flow is considered. This model is an idealized one primarily because it assumes that *at all times*, the vortices are well-separated and elliptical. It is very instructive to compare this model to some simpler ones: the Kida vortex and a pair of point vortices in shear. These models are closely connected to the present one: they underlie the main aspects of this project and they provide a natural overview of this report.

In the Kida problem (Kida 1981), an elliptical patch of constant vorticity evolves in a background shear flow

$$\Psi = \frac{1}{4}\omega(x^2+y^2) + \frac{1}{4}e(x^2-y^2) \tag{1}$$

according to the 2D Euler equations. Kida showed that the ellipse remains elliptical for all time with its centroid fixed and its orientation and aspect ratio varying periodically with time, i.e.

$$\begin{aligned} \dot{\lambda} &= -e\lambda\sin 2\phi \\ \dot{\phi} &= \frac{\lambda}{(1+\lambda)^2} + \frac{\omega}{2} + \frac{1}{2}\frac{1+\lambda^2}{1-\lambda^2}e\cos 2\phi, \end{aligned} \tag{2}$$

where λ is the aspect ratio and ϕ is the orientation. This system can be derived from the equations of motion for the quadratic vorticity moments (Flierl et al. 1993, hereafter FMM); the latter are obtained from the Poisson bracket for 2D Euler flow using the method

FMM); the latter are obtained from the Poisson bracket for 2D Euler flow using the method of reduction (Morrison 1993, hereafter M93). The model which will be derived in section 2 may be thought of as a pair of Kida vortices which are allowed to interact, but in a restricted way. It is obtained by generalizing the analysis of FMM to two uniform elliptical vortices.

The relevance of such a model to vortex merger may be appreciated by considering the simplest model of vortex merger: two point vortices with circulation Γ_i and position $\boldsymbol{x}_i$ in a (Kida) background flow Ψ (e.g. Meacham 1993). The equations of motion for pure shear (i.e. $\omega = -e$) are:

$$\begin{aligned} \dot{X} &= -\left(\frac{1}{2\pi}\frac{1}{X^2+Y^2} + \frac{e}{\Gamma}\right) Y \\ \dot{Y} &= \left(\frac{1}{2\pi}\frac{1}{X^2+Y^2}\right) X, \end{aligned} \tag{3}$$

where $X = x_1 - x_2$ and $Y = y_1 - y_2$. There are hyperbolic points at

$$X = 0, Y = \pm\left(\frac{1}{\pi}\frac{\Gamma}{2e}\right)^{\frac{1}{2}} \tag{4}$$

which are connected by a separatrix (heteroclinic orbit). (For $\omega \neq -e$, there are analogous results.) Regions of unbounded motion are divided from regions of closed motion by the

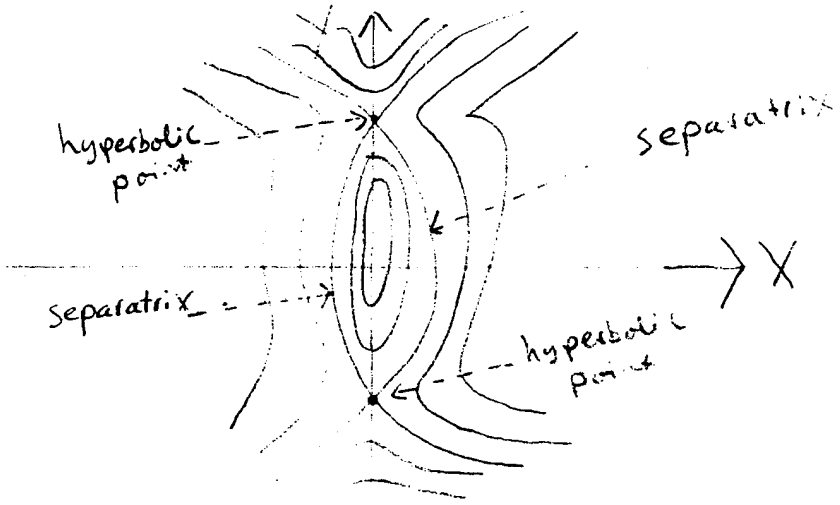

Figure 1: Phase portrait for a point vortex pair in shear.

separatrix and thus merger is impossible. But for the system of two Kida vortices, there are internal degrees of freedom (d.o.f.) and the vortices can merge. The separatrix should also split apart, allowing merger for initial conditions in the unbounded regime. This is examined in section 3 using a Melnikov integral. The Melnikov method for time-periodic, 1 d.o.f. systems is extended to systems with fast and slow time-scales and it is demonstrated that the separatrix splitting is exponentially small. This splitting implies chaotic behaviour and this is studied numerically in section 4. Section 5 presents a summary and outlines possibilities for future work.

2 Hamiltonian Formulation

The equations of motion for two interacting Kida vortices are obtained following FMM. Briefly, FMM: (1) expressed the Poisson bracket for the 2D Euler equations in terms of the quadratic moments — a reduction; (2) determined the cosymplectic matrix J from the bracket; (3) computed the Hamiltonian in terms of the moments; and (4) obtained the equations of motion from H and J. While this procedure is not especially complicated, it is fairly involved; therefore, in the interests of brevity, the derivation will only be outlined: many details will be omitted. (The remaining sections of this report will be abbreviated in a similar fashion. A detailed account of this work will be published elsewhere).

Firstly, some basic notation is established. Our system consists of two elliptical vortices with aspect ratios λ_i, circulation Γ_i, and vorticity q_i' $(i = 1, 2)$ in a background Kida flow, Ψ. The vorticity centroids are located at (x_{i*}, y_{i*}) with respect to some reference frame; Ψ is also defined with respect to this frame. The vortices have orientations ϕ_i with respect to the stationary reference frame; (x_i', y_i') are coordinates in the body frame.

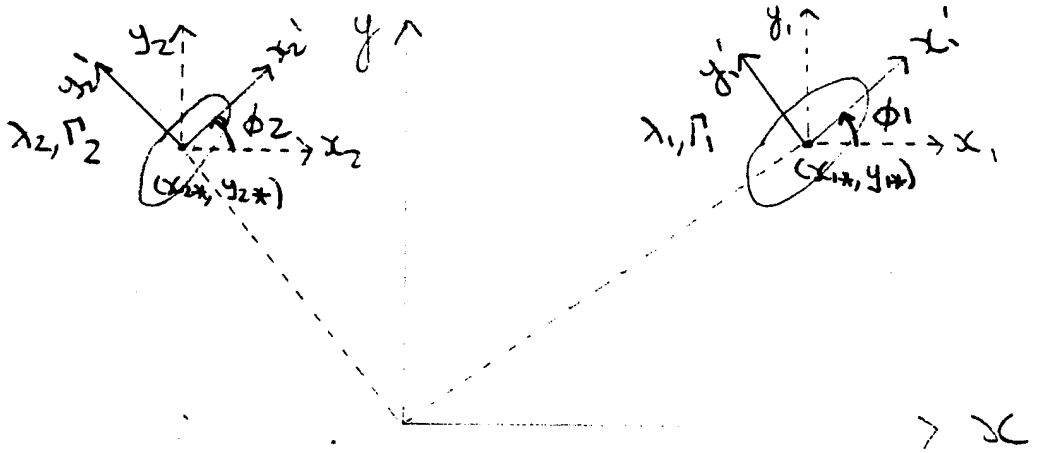

Figure 2: Configuration for the interacting Kida vortices

Because the global centroid will not be fixed when the background flow is present, both first order and quadratic vorticity moments must be considered. The quadratic moments are defined by:

$$\begin{aligned} a_1^i &= \mu_i q_i' \int\int_{D_i} (x - x_{i*})^2 \, dxdy \\ a_2^i &= \mu_i q_i' \int\int_{D_i} (x - x_{i*})(y - y_{i*}) \, dxdy \\ a_3^i &= \mu_i q_i' \int\int_{D_i} (y - y_{i*})^2 \, dxdy \end{aligned} \tag{5}$$

where $\mu_i = 4/A_i$ and D_i is the domain of vortex i. The first order moments are defined by:

$$\begin{aligned} a_{-1}^i &= \mu_i q_i' \int\int_{D_i} x \, dxdy \\ a_{-2}^i &= \mu_i q_i' \int\int_{D_i} y \, dxdy \, . \end{aligned} \tag{6}$$

It is also convenient to define functions m_j^i which are the integrands of the a_j^i: $m_1^i = (x - x_{i*})^2$, etc.

The first step in the derivation proper is the computation of the Poisson bracket. The Poisson bracket for 2D Euler flow is:

$$\{F, G\} = \sum_i \int_{D_i} q_i' \, [\frac{\delta F}{\delta q_i'}, \frac{\delta G}{\delta q_i'}] \, dxdy \, . \tag{7}$$

where $[\cdot, \cdot]$ is the 2D Jacobian and the constant background vorticity has been ignored. From the definition of the a_j^i, it follows that

$$\begin{aligned} \frac{\delta F}{\delta q_i'} &= \sum_j \frac{\partial F}{\partial a_j^i} \frac{\delta a_j^i}{\delta q_i'} \\ &= \sum_j \frac{\partial F}{\partial a_j^i} m_j^i \, \mu_i, \end{aligned} \tag{8}$$

where we have restricted F,G to functions of the a_j^i. It then follows that:

$$\{F, G\} = \sum_{ijk} \int_{D_i} \mu_i^2 q_i' \frac{\partial F}{\partial a_j^i} \frac{\partial G}{\partial a_k^i} \, [m_j^i, m_k^i] \, dxdy \, . \tag{9}$$

It is important to note that this reduction is *exact* because we have restricted F and G to functions of the a_j^i only.

After relabelling indices so that $a_j \equiv a_j^i$ (likewise m_j^i) and so that $q_{jk}' \equiv q_i'$ (likewise μ_i), the cosymplectic matrix J for the Poisson bracket (9) is defined by

$$\{F, G\} = \sum_{jk} \int_D \frac{\partial F}{\partial a_j} J^{jk} \frac{\partial G}{\partial a_k} \, dxdy \, . \tag{10}$$

The relabelling is needed in order for the elements of J^{jk} to define a unique matrix; the precise relabelling is arbitrary. (For convenience, let $j, k = -2 \ldots 3$ be associated with vortex 1 and let all other integers from -4 to 6 be associated with vortex 2; 0 is excluded in both cases.) Thus one obtains that

$$J^{jk} = \int_D \mu_{jk}^2 \, q_{jk}' \, [m_j, m_k]. \tag{11}$$

So in order to determine J all the products $[m_j, m_k]$ must be worked out. This is a straightforward calculation and we omit the details. The essential point is that the m_i constitute an algebra, i.e. $[m_i, m_j] = m_k$. (For instance, $[m_1, m_3] = [(x - x_{1*})^2, (y - y_{1*})^2] = 4m_2$.) This is necessary for $J(a_i)$ to satisfy Jacobi's identity and the reduction to work (M93, lecture 3).

J is a 10×10 matrix with the following form:

$$J = \begin{pmatrix} A & 0 \\ 0 & B \end{pmatrix}, \tag{12}$$

where

$$A = \begin{pmatrix} 0 & 4\mu_1 q_1' & 0 & 0 \\ -4\mu_1 q_1' & 0 & 0 & 0 \\ 0 & .0 & 0 & 4\mu_2 q_2' \\ 0 & 0 & -4\mu_2 q_2' & 0 \end{pmatrix} \tag{13}$$

and

$$B = \begin{pmatrix} C & 0 \\ 0 & D \end{pmatrix}, \tag{14}$$

with

$$C = \begin{pmatrix} 0 & 2\mu_1 a_1 & 4\mu_1 a_2 \\ -2\mu_1 a_1 & 0 & 2\mu_1 a_3 \\ -4\mu_1 a_2 & -2\mu_1 a_3 & 0 \end{pmatrix}, \tag{15}$$

and similarly for D. A is the J for two isolated point vortices and B is the J for two isolated Kida vortices (c.f. FMM). The full J is thus a direct product of the $J's$ associated with the first and second order moments; likewise, it is a direct product of two single-vortex $J's$.

Next, the Hamiltonian is computed in terms of the a_i. By definition,

$$H = \frac{1}{2}\int_D \mid \nabla\Psi + (\nabla\psi_1' + \nabla\psi_2') \mid^2 dxdy\,. \tag{16}$$

Dropping the constant terms and integrating by parts,

$$H = -\sum_i \left\{ \int_{D_i} \Psi q_i'\, dxdy + \frac{1}{2}\int_{D_i} \psi_i' q_i'\, dxdy + \frac{1}{2}\int_{D_i} \psi_j' q_i'\, dxdy \right\}, \tag{17}$$

where $j \neq i$. In order to calculate H, ψ_i', the streamfunction induced by each vortex is needed. Within a vortex, Lamb's (1932) solution for the streamfunction inside a uniform elliptical vortex is used.

$$\psi_i' = q_i' \left[\frac{1}{2}\frac{1}{(1+\lambda_i)^2}(\lambda_i^2 x'^2 + y'^2) - \frac{\lambda_i}{4(1+\lambda_i^2)} + \frac{1}{4}\ln\frac{(1+\lambda_i)^2}{\lambda_i} \right]. \tag{18}$$

In using this solution, it is assumed that the ellipse remains elliptical for all times: this is approximation 1. Outside a vortex, the Green's function for a point vortex in an unbounded domain must be used:

$$G(\boldsymbol{x}\,, \boldsymbol{x}\,') = \frac{1}{2\pi}\ln \mid \boldsymbol{x} - \boldsymbol{x}\,' \mid, \tag{19}$$

where $\boldsymbol{x}\,'$ is a point inside the vortex and the streamfunction is $\psi_i' = -\int_{D_i} q_i' G(\boldsymbol{x}\,, \boldsymbol{x}\,')\, dxdy$.

The first two terms of H are easily computed — they are analogous to the Hamiltonian for an isolated Kida vortex; however, the final term is not quadratic in x, y because of the Green's function, and it cannot be exactly represented using first and second order moments. It can be *approximately* written using the moments by Taylor expanding the Green's function to second order in ϵ_o, where

$$\epsilon_o \equiv x_s/R \ll 1, \tag{20}$$

x_s is the semi-major axis, and R is the intercentroid separation. Thus it is assumed that the ellipses are small and well-separated: this is approximation 2. Finally,

$$
\begin{aligned}
H = & -\frac{1}{4\mu_1}\left[(\omega+e)a_1+(\omega-e)a_3+4q_1'(\omega+e)(\frac{a_{-1}}{4q_1'})^2+4q_1'(\omega-e)(\frac{a_{-2}}{4q_1'})^2\right] \\
& -\frac{1}{4\mu_2}\left[(\omega+e)a_4+(\omega-e)a_6+4q_2'(\omega+e)(\frac{a_{-3}}{4q_2'})^2+4q_2'(\omega-e)(\frac{a_{-4}}{4q_2'})^2\right] \\
& -\frac{\Gamma_1}{8}\ln\left[(a_1+a_3+2)\frac{\pi}{\Gamma_1}\right]-\frac{\Gamma_2}{8}\ln\left[(a_4+a_6+2)\frac{\pi}{\Gamma_2}\right] \\
& -\frac{1}{\pi\mu_1\mu_2}\left[4q_1'q_2'\ln R^2+\frac{2}{R^2}[\frac{1}{2}\cos 2\theta(q_1'(a_6-a_4)+q_2'(a_3-a_1))-\sin 2\theta(q_2'a_2+q_1'a_5)]\right].
\end{aligned}
\tag{21}
$$

From J and H a 10th order system can be obtained for the a_i. However, this system can be simplified further. The global centroid motion decouples from the relative centroid motion (and the internal d.o.f.) since there is a decoupling in J *and* in H. There are two Casimirs $C_1 = a_1a_3 - a_2^2$ and $C_2 = a_4a_6 - a_5^2$; they correspond to circulation preservation of each vortex. And for this report, it is assumed that the vortices are symmetric. These simplifications lead to a 4th order system; recasting it in terms of (R,θ,λ,ϕ), where $x_{2*}-x_{1*} = R\cos\theta$ and $y_{2*}-y_{1*} = R\sin\theta$, one obtains:

$$
\begin{aligned}
\dot{R} &= \frac{1}{2}eR\sin 2\theta - \frac{\Gamma A}{2\pi^2R^3}\frac{1-\lambda^2}{\lambda}\sin 2(\theta-\phi) \\
\dot{\theta} &= \frac{\omega}{2}+\frac{e}{2}\cos(2\theta)+\frac{\Gamma}{\pi R^2}+\frac{\Gamma A}{2\pi^2R^4}\frac{1-\lambda^2}{\lambda}\cos 2(\theta-\phi) \\
\dot{\lambda} &= -\lambda\left\{\frac{\Gamma}{\pi R^2}\sin 2(\theta-\phi)+e\sin 2\phi\right\} \\
\dot{\phi} &= \frac{q'\lambda}{(1+\lambda)^2}-\frac{1}{2}\frac{1+\lambda^2}{1-\lambda^2}\left\{\frac{\Gamma}{\pi R^2}\cos 2(\theta-\phi)-e\cos 2\phi\right\}+\omega/2
\end{aligned}
\tag{22}
$$

We note in passing that the 10th order system can be extended as well as simplified: the equations of motion for N vortices have been worked out.

The 6th order system in $(R,\theta,\lambda_i,\phi_i)$ is — with no background shear — identical to one derived by Melander et al. (1986). This being the case, why is the Hamiltonian formulation useful? Most significantly, it explains why Melander et al. obtained a Hamiltonian system. They showed that their model is Hamiltonian and that it possesses conservation laws analogous to those of the 2D Euler equations; however, these results seem to be very fortuitous: the Hamiltonian formulation demonstrates otherwise. The Hamiltonian approach is simpler than the procedure employed by Melander et al. (who manipulated the moments directly) and some results (e.g. the decoupling between the first and second order moments) are more readily grasped with it.

Although this model is not exact, it is consistent. Deviations from ellipticity are $\mathcal{O}(\epsilon_o^3)$ and will only be significant when ϵ_o is large and the second approximation breaks down. The model cannot provide an exact description of vortex merger, but it should provide insight into

aspects such as the break-up of the separatrix for a point vortex pair in shear. Furthermore, this model is a very interesting dynamical system and it is worth studying in its own right. The background shear introduces many new effects which are not found in the integrable system of Melander et al.

3 A Modified Melnikov Method

For an integrable system, the stable and unstable manifolds associated with the hyperbolic fixed points coincide, forming heteroclinic (homoclinic) orbits. However, under a perturbation, these invariant manifolds no longer coincide and motion (transport) across the separatrix is possible (e.g. Wiggins 1992). The well-known Melnikov method (e.g. Drazin 1992, Wiggins 1988) measures the separation between the stable and unstable manifolds. Zeroes of the Melnikov function are indicative of chaotic motion. In this section, a Melnikov calculation is described for which the integrable basic state corresponds to a point vortex pair in shear and the perturbation corresponds to the internal d.o.f.'s of the interacting Kida vortices. Although other basic states may be chosen, this one is a good choice — notwithstanding the existence of a separatrix! — because it ensures that the results will be physically meaningful for small perturbations (i.e. the model should still be valid).

Before outlining the Melnikov calculation, it is necessary to non-dimensionalize the 4th order system. Defining a perturbation parameter $\epsilon = A/(\pi D^2)$, where D is the semi-major axis), letting $r = RD$, and rescaling time as $t \to t/q'$, one obtains:

$$\begin{aligned}
\dot{r} &= \frac{1}{2}\frac{e}{q'} r \sin 2\theta - \frac{\epsilon^2}{2r^3}\frac{1-\lambda^2}{\lambda}\sin 2(\theta-\phi) \qquad (23)\\
\dot{\theta} &= \frac{\omega}{2q'} + \frac{e}{2q'}\cos(2\theta) + \frac{\epsilon}{r^2} + \frac{\epsilon^2}{2r^4}\frac{1-\lambda^2}{\lambda}\cos 2(\theta-\phi)\\
\dot{\lambda} &= -\lambda\left\{\epsilon\frac{1}{r^2}\sin 2(\theta-\phi) + \frac{e}{q'}\sin 2\phi\right\}\\
\dot{\phi} &= \frac{\lambda}{(1+\lambda)^2} - \frac{1}{2}\frac{1+\lambda^2}{1-\lambda^2}\left\{\frac{\epsilon}{r^2}\cos 2(\theta-\phi) - \frac{e}{q'}\cos 2\phi\right\} + \frac{\omega}{2q'}.
\end{aligned}$$

This system may be interpreted in the following manner: (1) at $\mathcal{O}(1)$ the background shear flow acts on (r,θ) and the internal degrees of freedom; there is also self-rotation (Kirchoff rotation) of the vortices; (2) at $\mathcal{O}(\epsilon)$ the vortices interact, but only as if they were point vortices; and (3) at $\mathcal{O}(\epsilon^2)$ the vortices are now interacting Kida vortices: the internal d.o.f.'s now affect the inter-centroid motion.

While these equations are correct, they cannot be used for a standard Melnikov analysis. Melnikov's method is usually formulated in terms of $\mathcal{O}(\epsilon)$ perturbations to an integrable basic state; for a 1 d.o.f. system,

$$\begin{aligned}
\dot{x} &= f_1(x,y) + \epsilon g_1(x,y,t) \qquad (24)\\
\dot{y} &= f_2(x,y) + \epsilon g_2(x,y,t).
\end{aligned}$$

But in (23), the basic state terms are at $\mathcal{O}(1)$ *and* $\mathcal{O}(\epsilon)$, and there isn't a simple $\mathcal{O}(\epsilon)$ perturbation (it also expands the phase space). If, however, one scales the background flow so that $e/q' = \epsilon\overline{\gamma}$, where $\overline{\gamma}$ is $\mathcal{O}(1)$, then all the basic state terms will indeed be at $\mathcal{O}(\epsilon)$. This scaling is natural because it means that the background shear and the point vortex interactions are equally important — precisely the case near the separatrix.

With this scaling, the first three equations in (23) are $\mathcal{O}(\epsilon)$ and there is fast, $\mathcal{O}(1)$ rotation of the vortices in the $\dot{\phi}$ equation. The dynamics are thus a combination of slow, $\mathcal{O}(\epsilon^{-1})$ time-scale, motion around the unperturbed separatrix and fast, $\mathcal{O}(1)$ perturbations. This coupling between the internal d.o.f. and the inter-centroid motion takes place at $\mathcal{O}(\epsilon^2)$; it can be examined using a multiple time-scale analysis by introducing a slow time-scale $T = \epsilon t$ and expanding the variables in terms of fast and slow components:

$$\begin{aligned} r(t,T) &= r_{os}(T) + \epsilon\{r_{1s}(T) + r_{1f}(t,T)\} + \epsilon^2\{r_{2s}(T) + r_{2f}(t,T)\} + \mathcal{O}(\epsilon^3) \\ \theta(t,T) &= \theta_{os}(T) + \epsilon\{\theta_{1s}(T) + \theta_{1f}(t,T)\} + \epsilon^2\{\theta_{2s}(T) + \theta_{2f}(t,T)\} + \mathcal{O}(\epsilon^3) \\ \lambda(t,T) &= \lambda_o + \epsilon\{\lambda_{1s}(T) + \lambda_{1f}(t,T)\} + \mathcal{O}(\epsilon^2) \\ \phi(t,T) &= \phi_{of}(t) + \phi_{os}(T) + \epsilon\{\phi_{1s}(T) + \phi_{1f}(t,T)\} + \mathcal{O}(\epsilon^2). \end{aligned} \tag{25}$$

By solving the perturbation equations, one can determine the leading order (i.e. $\mathcal{O}(\epsilon^2)$) perturbation to the slow, basic state motion; at this order, λ_1, ϕ_o and ϕ_1 act as time-periodic forcing functions. A Melnikov analysis may now be performed.

It can be shown that an analogue of the time-periodic, 1 d.o.f. Melnikov function exists for this system, viz.

$$\begin{aligned} M(t_o) &= \epsilon^2 \int_{-\infty}^{\infty} -\left\{\frac{1}{2r_o^2} + \frac{1}{2}\overline{\gamma}(\alpha - 1)\right\} y_o \left\{\frac{1}{4r_o^3}\frac{1-\lambda_o^2}{\lambda_o}\left[\cos 3\theta_o \cos 2\phi_o t + \sin 3\theta_o \sin 2\phi_o t\right]\right\} dt \\ &+ \epsilon^2 \int_{-\infty}^{\infty} -\left\{\frac{1}{2r_o^2} + \frac{1}{2}\overline{\gamma}(\alpha + 1)\right\} x_o \left\{\frac{1}{4r_o^3}\frac{1-\lambda_o^2}{\lambda_o}\left[\sin 3\theta_o \cos 2\phi_o t - \cos 3\theta_o \sin 2\phi_o t\right]\right\} dt. \end{aligned}$$

The separatrix co-ordinates (r_o, θ_o) are evaluated at time $T = \epsilon(t - t_o)$, $\phi_o = \lambda_o/(1+\lambda_o)^2$, $x_o = r_o \cos\theta_o$ and $y_o = r_o \sin\theta_o$, t_o parametrizes distance along the unperturbed separatrix, and $\alpha = \omega/e$.

In the limit $\epsilon \to 0$, one can also show that $M(t_o)$ and the splitting between the manifolds are *exponentially small*, i.e. $M(t_o)$ is smaller than any power of ϵ. This is an *asymptotic* result: it suggests that the splitting will be exponentially small for small ϵ, but it is not a rigorous proof. Holmes et al. (1988) showed that the separatrix splitting in the rapidly forced, 1 d.o.f. dynamical system

$$\dot{u} = g(u,\epsilon) + \epsilon^p \delta h(u, \epsilon, t/\epsilon), \quad 0 < \delta \leq 1, \; p > 0 \tag{26}$$

should be exponentially small. Although our Melnikov calculation has been done independently of the theory of Holmes et al., it does seem to be consistent with this general theory. Nevertheless, this result needs to be verified because higher order terms in the perturbation have been neglected.

This result has a number of implications. It suggests that the system is chaotic for non-zero ϵ. And while this is to be expected since this is a 2 d.o.f. system with only 1 integral of motion (the background shear has destroyed the rotational symmetry of the Hamiltonian), it is nice to have some analytical confirmation. There has been some interest in whether or not there are chaotic solutions to the Euler equations: insofar as the model remains valid, this demonstrates that a system of N point vortices ($N \geq 4$; Aref and Pomphrey 1982) is not the only such system. Furthermore, the exponentially small splitting suggests that vortex merger will be rather difficult. Because of the exponential scaling, relatively large values of ϵ are required to produce a large enough splitting for well-separated vortices (i.e. outside the separatrix) to merge. Ordinarily, the splitting would simply scale as ϵ^2.

4 Numerical Simulations

Although the Melnikov result is rather interesting, it only addresses a specific question: how far do the model's stable and unstable manifolds split apart? In order to study its dynamics, numerical simulations are needed. While these equations are easily integrated, they are difficult to visualize: this is a 4 dimensional chaotic system with 4 free parameters (ϵ, q, ω, e). For instance, one could simply plot r, θ, λ and ϕ as functions of time for specified initial conditions; while this provides much information about localized regions of phase space, it is a poor way to study the global dynamics.

In this study, Poincare sections are constructed at constant ϕ ($\phi_o = 0$). The Poincare section projects the 4 dimensional phase space onto a two-dimensional surface and it provides a global picture of the dynamics. It is generated by integrating a set of initial conditions forward in time and plotting (for each initial condition) a point (X, Y) whenever ϕ goes through ϕ_o in a particular sense (clockwise for $q' > 0$). The choice of initial conditions is extremely important: if one just picks random initial conditions, the Poincare section will not exhibit distinct structures but will be smeared out instead.

The initial conditions should be chosen such that they, and their images under a Poincare mapping, are all dynamically accessible to one another (c.f. M93, lecture 2). This is done by choosing points which satisfy $H = H_o$ and $C = C_o$, where C is the Casimir. It is well-known that Hamiltonian dynamics takes place on the intersection of constant H and constant C surfaces (c.f. M93, lecture 2); therefore, H and C should be fixed: changing them amounts to changing the dynamical system. For each initial condition (r, θ), H is fixed at H_o, $\phi = \phi_o$, and λ must be determined. It is trivial to fix the Casimir since it corresponds to the circulation.

Figure 3 is a Poincare section for $A = 0.031416$, $\Gamma = 1$, $\epsilon = 0$. As expected, this case is integrable: one observes a sequence of concentric, closed curves. There are no points around the origin because for r sufficiently small ($r \lesssim 0.6$), the vortices merge before ϕ goes through ϕ_o. Thus the last invariant curve to disappear (i.e. the one nearest the origin) defines a merger threshold. Although this figure isn't particularly exciting, it confirms that the model is integrable without a background flow and it provides a benchmark against which

other Poincare sections may be compared. In what follows, the background shear is fixed ($\omega = -e = -0.318309$; the hyperbolic points are at $(0, \pm 1)$), and ϵ is increased.

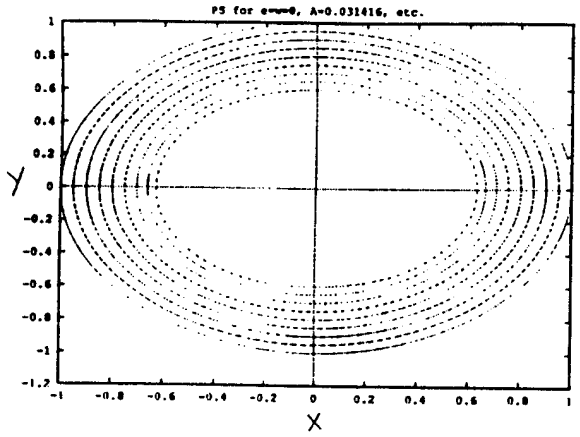

Figure 3: Poincare Section for $\omega = e = 0$.

A Poincare section for $\epsilon = 0.01$ is shown in figure 4. H_o is chosen to be the value of the Hamiltonian on the unperturbed separatrix ($r_o = 1.00$, $\theta_o = 1.57$): this is a reasonable choice for motion near the separatrix. This figure is quite similar to figure 1 (point vortex pair in shear) and to figure 3 — integrable cases both. In this figure, there are no large stochastic regions. This is consistent with an exponentially small separatrix splitting — the stochastic regions should be thin — but the stable and unstable manifolds must be computed numerically in order to verify the Melnikov result. A well-defined invariant torus separating initial conditions which merge from those which do not can be seen. It has been observed that the position of this critical torus moves outwards as ϵ is increased. For this value of ϵ, the critical torus is well-separated from the unperturbed separatrix and the separatrix splitting is not relevant to vortex merger.

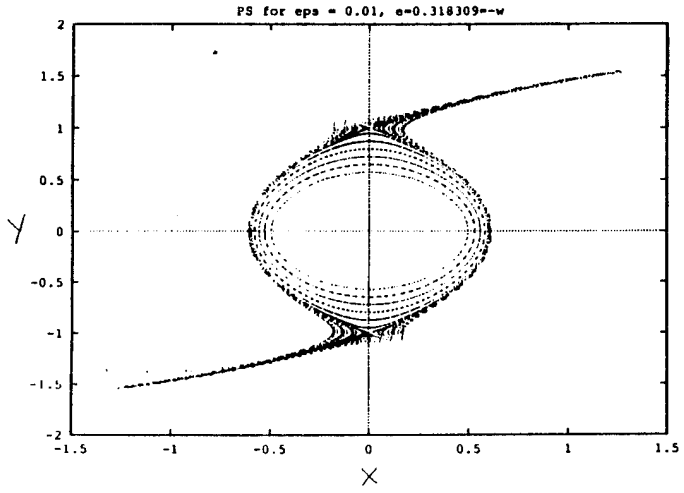

Figure 4 $\epsilon = 0.01$, $\omega = -e = 0.318309$.

Nevertheless, one still expects chaotic behaviour around the unperturbed separatrix. However, for $\epsilon = 0.01$ it is very hard to discern. The inter-centroid separation r has been

plotted against t for initial conditions around the unperturbed separatrix ($\theta = 0, 1.57$) and chaos has not been detected. The absence of any noticeable chaotic behaviour underscores the thinness of the stochastic region. However, an *inner* stochastic region may be found for this value of ϵ. In figures 5a to 5b, $r : t$ is plotted for $\epsilon = 0.01$ and initial conditions

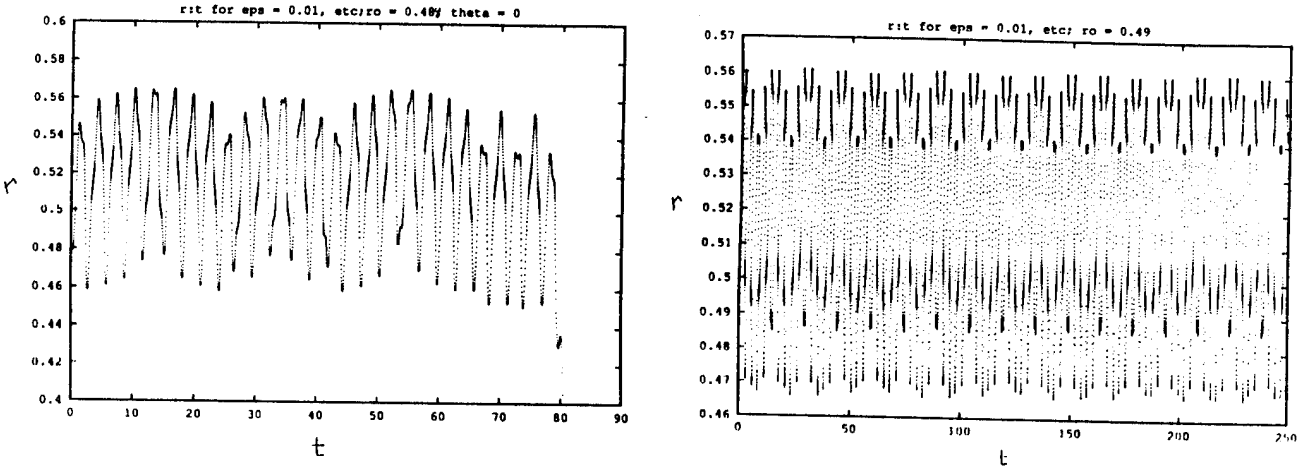

Figure 5: (a) $r : t$ for $r_o = 0.484, \theta_o = 0.0$; (b) $r : t$ for $r_o = 0.49, \theta_o = 0.0$.

successively farther from the origin. As one moves away from the origin there is a transition from regular motion ($r_o = 0.47$), to chaotic motion (figure 5a), and finally to quasi-periodic motion (figure 5b). This stochastic band is associated with a higher order resonance — observe the island chain in figure 6. This stochastic band is much larger than the one near the separatrix: it isn't exponentially small. It is uncommon for an inner stochastic band to be larger than the one around the separatrix: for small perturbations, chaos is usually localized around the separatrix.

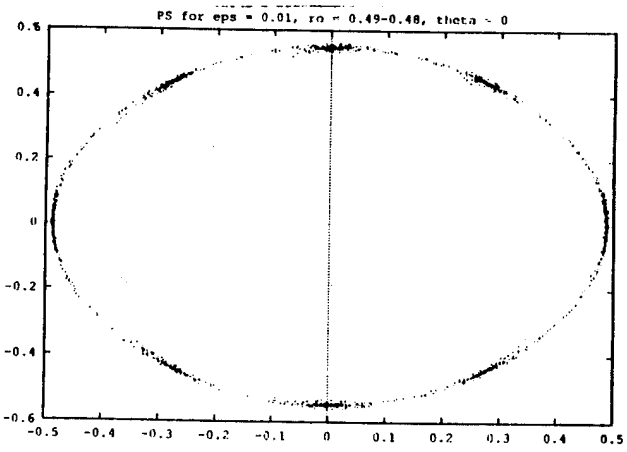

Figure 6: Blow-up of Poincare section near inner stochastic band.

In order to determine whether or not there is actually chaotic motion around the separatrix, a larger value of ϵ is considered. In figure 7, a Poincare section for $\epsilon = 0.03$ is shown. This plot looks quite different from the previous ones: it has a distinct stochastic band and there are folds near the hyperbolic points which are reminiscent of a perturbed (stable) manifold. This unusual structure may be a consequence of exponentially small

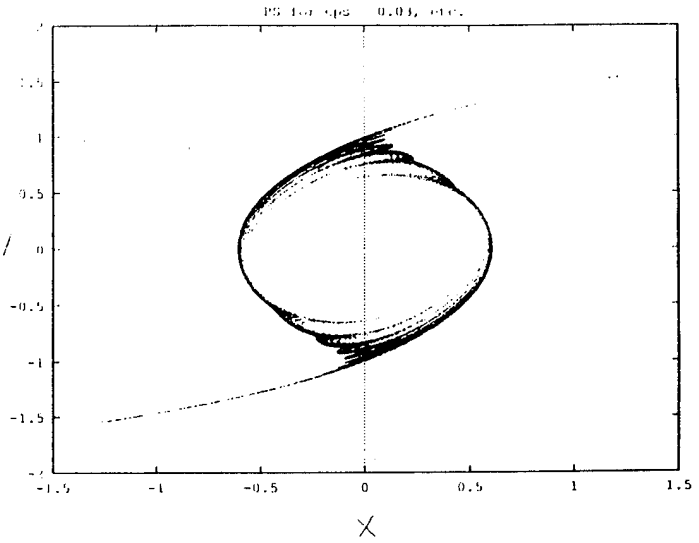

Figure 7: Poincare section for $\epsilon = 0.03$.

splitting: points are constrained from wandering away from the unperturbed separatrix and this may help demarcate the perturbed separatrix. This manifold structure can also be observed for $\epsilon = 0.01$ if one looks closely enough; it's not very prominent because the splitting changes rapidly with ϵ due to the exponential dependence. It is evident that a separatrix no longer remains for this value of ϵ and that there will be transport across what remains of it.

Although the separatrix splitting is not, as hoped, directly connected with vortex merger, it is clear that some interesting things are happening around the separatrix. Specifically, there is *chaotic scattering* of the vortices. Instead of approaching and separating as for two point vortices in shear, the Kida vortices come together and wander about in a chaotic fashion before separating. There has been some work on chaotic scattering, but it has mostly been in the context of molecular physics (e.g. Gutzwiller 1990). For small vortices, chaotic scattering may be more important than vortex merger: the number of initial conditions for which the vortices will scatter is much greater than the number for which they merge.

5 Summary and Future Work

In this report the equations of motion have for a pair of elliptical vortices in background shear (Kida vortices) have been derived using a Hamiltonian formulation and analysed. The derivation follows that of Flierl et al. (1993) and requires the vortices to remain elliptical and well-separated for all time; for no background flow, the 6th order system of Melander et al. (1986) has been recovered. A 4th order system is obtained by assuming symmetric vortices. This system is studied analytically by means of a Melnikov integral for a 1 d.o.f. system with fast and slow time-scales: it is shown that the separatrix splitting is exponentially small. The 4th order system is studied numerically by constructing Poincare sections and plotting r against t. The results are qualitatively consistent with an exponentially small splitting. It is proposed that an empirical merger threshold can be determined from the position of the last invariant torus and that chaotic scattering may be more important than vortex merger.

There is much more work that remains to be done. With regards to numerical work, the Melnikov result should be explicitly verified. A wider range of parameter values should be considered; simplified models other than symmetric vortices should be utilized (e.g. a point vortex and a Kida vortex). The amount of transport across the separatrix should be quantified. As for analytical work, it should be possible to predict the position of the folds from the perturbation equations. The location of the inner stochastic region (i.e. higher order resonances) should be predicted and a physical interpretation should be given. It would also be useful if an analytical criterion for merger could be devised (i.e. the position of the last invariant torus). Finally, the precise relation of the Melnikov calculation to the general result of Holmes et al. should be determined.

Acknowledgements

I would like to thank Steve Meacham and Phil Morrison for all their help and encouragement: it has been a great pleasure working with them. I would also like to thank Glenn Flierl for useful discussions and Rick Salmon for organizing a very enjoyable summer.

References

Aref, H.A. and Pomphrey, N. 1982: Integrable and chaotic motion of four vortices. I. The case of identical vortices. *Proc. Roy. Soc. Lond.* **A380** , 359-387.

Drazin, P.G. 1992: *Nonlinear Systems.* Cambridge: Cambridge University Press.

Flierl, G.R., Meacham, S.P., and Morrison, P.J. 1993. A Hamiltonian formulation of vortices in shear. To be submitted.

Gutzwiller, M.C. 1990. *Chaos in Classical and Quantum Mechanics.* New York: Springer-Verlag.

Holmes, P., Marsden, J. and Scheurle, J. 1988: Exponentially small splittings of separatrices with applications to KAM theory and degenerate bifurcations. *Contemp. Math.* **81**, 213-244.

Kida, S. 1981. Motion of an elliptic vortex in a uniform shear flow. *J. Phys. Soc. Japan* **50** 3517-3520.

Lamb, H. 1932. *Hydrodynamics*, 6th edition. Cambridge: Cambridge University Press.

McWilliams, J.C. 1984. The emergence of isolated vortices in turbulent flow. *J.Fluid Mech.* **146**, 21-43.

Meacham, S.P. 1993. Quasigeostrophic dipoles in strain. To be submitted.

Melander, M.V., Zabusky, N.J., and McWilliams, J.C. 1988. Symmetric vortex merger in two dimensions: causes and conditions. *J. Fluid Mech.* **195**, 303-340.

Melander, M.V., Zabusky, N.J., and Styczek, A.S. 1986: A moment model for vortex interactions of the two-dimensional Euler equations. Part 1: computational validation of a Hamiltonian elliptical representation. *J. Fluid Mech.* **167**, 95-116.

Morrison, P.J. 1993. Generalized Hamiltonian Dynamics and Fluid Mechanics. In these proceeedings.

Wiggins, S. 1988. *Global Bifurcations and Chaos - Analytical Methods.* New York: Springer-Verlag.

Wiggins, S. 1992. *Chaotic Transport in Dynamical Systems.* New York: Springer-Verlag.

A Hamiltonian weak-wave model for Shallow Water flow

Caroline L. Nore

September 14, 1993

The Shallow-Water (SW) model is relevant for the studies of geophysical flows in which the stratification is not crucial. The atmospheric or oceanographic phenomena that it can describe must be characterized by large horizontal scales compared to the vertical scales, and must be conservative to a first approximation. One can write a SW hamiltonian which is cubic in the field variables for a free surface. In order to derive nonlinear stability conditions, this paper presents a simplified SW model characterized by a quadratic hamiltonian with a good bracket; a flow composed of two components: vortical and divergent motions, weakly coupled ;and the two limits of full SW: quasi-geostrophic and gravity-wave limits.

Sufficient stability conditions are obtained for steady basic states admitting an x-invariance or an axisymmetric invariance in the model. Their application to jets, shear flows and vortices is discussed. For hydrodynamically "non stable" profiles, rigorous upper bounds on spontaneous emission of waves (gravity waves and others) are computed.

1 Derivation of the hamiltonian weak-wave model

1.1 Farge and Sadourny's model

Farge and Sadourny ([1]) have studied the turbulent cascades of a flow characterized by two invariants of the motion: an energy and an enstrophy, both quadratic. They have shown that part of the injected energy goes into divergent motion which cascades towards the small scales before being dissipated, while the rest of the energy goes into vortical motion and remains at large scales. They have written down an approximated system of equations for their model in which the approximation is not well defined, dropping some terms appearing at the same order as ones they have kept. Besides, unlike the SW equations, this system does not appear to be hamiltonian.

1.2 Derivation of the hamiltonian weak-wave model

1.2.1 Full SW model

The full SW equations read in terms of the velocity and the depth of the single-layer (v, h) ([2]):

$$\frac{\partial v}{\partial t} + (v \cdot \nabla)v + f\hat{z} \times v = -g\nabla h \tag{1}$$

$$\frac{\partial h}{\partial t} + \nabla \cdot (hv) = 0 \tag{2}$$

This system is equivalently represented by the hamiltonian form

$$\frac{\partial u}{\partial t} = J_1 \frac{\delta H_1}{\delta u} \tag{3}$$

where the vector field $u = (v, h)^T$, the hamiltonian functional is $H_1(v, h) = \frac{1}{2} \iint (h|v|^2 + gh^2) dx\, dy$, and the co-symplectic form J_1 is:

$$J_1 = \begin{pmatrix} 0 & q & -\partial x \\ -q & 0 & -\partial y \\ -\partial x & -\partial y & 0 \end{pmatrix}$$

with $q = (f + \hat{z} \cdot \nabla \times v)/h$ the potential vorticity. J_1 satisfies the Jacobi identity and admits the following Casimirs: $\mathcal{C} = \iint h\, C(q) dx\, dy$. One can transform the system (3) into a new representation $(\tilde{q}, \Delta, h')$ where $\tilde{q} = \hat{z} \cdot \nabla \times v - fh'/H$ is an approximate potential vorticity, $\Delta = \nabla \cdot v$ is the divergence and $h' = h - H$ is the depth perturbation around a constant depth H. The velocity is defined by $v = \hat{z} \times \nabla\psi + \nabla\chi$ where ψ, the stream-function, corresponds to the *vortical* motion and χ, the velocity potential, corresponds to the *divergent* motion. The co-symplectic form reads then:

$$J_2 = \begin{pmatrix} -[\frac{\tilde{q}}{H+h'}, \cdot] & \nabla \cdot \left(\frac{\tilde{q}}{H+h'} \nabla(\cdot)\right) & 0 \\ -\nabla \cdot \left(\frac{\tilde{q}}{H+h'} \nabla(\cdot)\right) & -[\frac{\tilde{q}}{H+h'}, \cdot] & -\nabla^2 \\ 0 & \nabla^2 & 0 \end{pmatrix}$$

with

$$\begin{aligned} H_2 &= \frac{1}{2} \iint h|v|^2 + gh^2 \\ &= \frac{1}{2} \iint h(|\nabla\psi|^2 + |\nabla\chi|^2) + gH^2 + 2gHh' + gh'^2 \end{aligned}$$

By subtracting some Casimirs given by $\mathcal{C} = \iint (H + h') C\left(\frac{\tilde{q}}{H+h'}\right)$, H_2 becomes:

$$H_2 = \frac{1}{2} \iint h(|\nabla\psi|^2 + |\nabla\chi|^2) + gh'^2$$

1.2.2 Approximations

The procedure contains three steps:

- approximation of small Rossby number ϵ
- assumption of timescale separation for the vortical motion and divergent motion
- amplitude of the vortical motion dominating the amplitude of the divergent motion

We non-dimensionalize the bracket with the Rossby number, $\epsilon \equiv U/fL$ and the Rossby deformation radius, $a \equiv \sqrt{gH}/f$. The *'s denote non-dimensional variables : $\omega \equiv \nabla^2\psi = \epsilon f \omega*$, $\Delta = \epsilon f \Delta*$, $h' = \epsilon H h*$, $\tilde{q} = \epsilon f \tilde{q}*$ and $\nabla = \frac{1}{a}\nabla^*$. We then substitute the * variables in J_2 and in rows and columns by the corresponding functional derivatives.

The non-dimensionalized hamiltonian reads:

$$H* = H_1/g\epsilon^2 H^2 = \frac{1}{2}\iint (1+\epsilon h*)(|\nabla^* \psi *|^2 + |\nabla^* \chi *|^2) + h*^2$$

The non-dimensionalized Casimirs read:

$$\mathcal{C}* = \iint (1+\epsilon h*) C\left(\frac{\tilde{q}*}{1+\epsilon h*}\right)$$

Up to order ϵ, the equations are given by:

$$\begin{pmatrix} \frac{\partial \tilde{q}*}{\partial t} \\ \frac{\partial \Delta *}{\partial t} \\ \frac{\partial h*}{\partial t} \end{pmatrix} = \frac{f}{gH^2\epsilon^2} \begin{pmatrix} -\epsilon[\tilde{q}*,\cdot] & \epsilon\nabla\cdot(\tilde{q}*\nabla(\cdot)) & 0 \\ -\epsilon\nabla\cdot(\tilde{q}*\nabla(\cdot)) & -\epsilon[\tilde{q}*,\cdot] & -\nabla^2 \\ 0 & \nabla^2 & 0 \end{pmatrix} gH^2\epsilon^2 \begin{pmatrix} -\psi* \\ -\chi* \\ h*-\psi* \end{pmatrix}$$

In J_2, there are four terms of order ϵ. We will argue to keep only one with the following assumptions.

1.2.3 Separation of amplitudes and timescales

We drop the $\tilde{}$ and $*$. We want to describe a weak but fast divergent flow weakly interacting with a dominant but slow vortical motion ([3]). We keep in each equation the dominant term and rescale the time for the equation in q. Our final system reads then, up to order 1:

$$\begin{aligned} \frac{\partial q}{\partial t} &= -[\psi, q] \\ \frac{\partial \Delta}{\partial t} &= -\nabla^2(h-\psi) \\ \frac{\partial h}{\partial t} &= -\Delta \end{aligned}$$

The corresponding hamiltonian is given by:

$$\mathcal{H} = \frac{1}{2}\iint |\nabla\psi|^2 + |\nabla\chi|^2 + h^2$$

The co-symplectic form is:

$$\mathcal{J} = \begin{pmatrix} -[q,\cdot] & 0 & 0 \\ 0 & 0 & -\nabla^2 \\ 0 & \nabla^2 & 0 \end{pmatrix}$$

We check that the bracket of our system verifies the Jacobi identity (see appendix).

1.3 Tests of the weak-wave model

In the gravity-wave limit, the equations become:

$$\begin{aligned} q &= 0 \Rightarrow \nabla^2\psi = h \\ \Rightarrow \frac{\partial^2\psi}{\partial t^2} &= \nabla^2\psi - \psi \end{aligned}$$

This equation only in ψ corresponds to the non-dimensionalized gravity-wave equation.

In the quasi-geostrophic limit, the equations become:

$$\begin{aligned} \Delta &= 0 \text{ and } h = \psi \\ q &= \nabla^2\psi - \psi \\ \frac{\partial q}{\partial t} &= -[\psi, q] \end{aligned}$$

which corresponds to the material conservation of potential vorticity.

2 Hamiltonian structure

We underline the hamiltonian structure of our model ([4]).

2.1 Good bracket

We check that the co-symplectic form corresponds to a good bracket, i.e. it satisfies the Jacobi identity. It ensures that the dynamics takes place on the leaves where the Casimirs associated to the bracket are constant.

2.2 Conservation of H

We check that our approximate hamiltonian is effectively conserved.

$$\begin{aligned} \frac{d\mathcal{H}}{dt} &= \int \nabla\psi \cdot \nabla\psi_t + \nabla\chi \cdot \nabla\chi_t + hh_t \\ &= \int -\psi q_t - \chi\Delta_t + (h-\psi)h_t = 0 \end{aligned}$$

where integration by parts is used.

2.3 Casimirs

The Casimirs of our weak-wave model are $\mathcal{C}_1 = \int C(q)$, $\mathcal{C}_2 = \int h$ and $\mathcal{C}_3 = \int \Delta$. $\mathcal{C}_4 = \int(\alpha x + \beta y)h$ and $\mathcal{C}_5 = \int(\gamma x + \delta y)\Delta$ might appear to be Casimirs but they are not Casimirs of the full SW system. In fact, they don't satisfy the boundary conditions and so are not admissible functionals. Thus we keep only $\mathcal{C}_1$, $\mathcal{C}_2$ and $\mathcal{C}_3$ which prove to be good Casimirs.

2.4 Zonal momentum invariant

The momentum for an x-invariant flow is seen to be:

$$M = \int yq + h\frac{\partial\chi}{\partial x}$$

Therefore, it appears:

$$\mathcal{J}\begin{pmatrix} \frac{\delta M}{\delta q} \\ \frac{\delta M}{\delta \Delta} \\ \frac{\delta M}{\delta h} \end{pmatrix} = \mathcal{J}\begin{pmatrix} y \\ -\nabla^{-2}\left(\frac{\partial h}{\partial x}\right) \\ \frac{\partial \chi}{\partial x} \end{pmatrix} = \begin{pmatrix} -\frac{\partial q}{\partial x} \\ -\frac{\partial \Delta}{\partial x} \\ -\frac{\partial h}{\partial x} \end{pmatrix}$$

which proves that M is the momentum invariant for a zonal steady flow (Noether's theorem).

2.5 Axisymmetric momentum invariant

The momentum for an axisymmetric invariant flow is seen to be:

$$M = \int -\frac{1}{2}r^2 q + h\frac{\partial \chi}{\partial \theta}$$

Therefore

$$\mathcal{J}\begin{pmatrix} \frac{\delta M}{\delta q} \\ \frac{\delta M}{\delta \Delta} \\ \frac{\delta M}{\delta h} \end{pmatrix} = \mathcal{J}\begin{pmatrix} -\frac{r^2}{2} \\ -\nabla^{-2}\left(\frac{\partial h}{\partial \theta}\right) \\ \frac{\partial \chi}{\partial \theta} \end{pmatrix} = \begin{pmatrix} -\frac{\partial q}{\partial \theta} \\ -\frac{\partial \Delta}{\partial \theta} \\ -\frac{\partial h}{\partial \theta} \end{pmatrix}$$

which proves that M is the momentum invariant for an axisymmetric steady flow.

3 Nonlinear stability conditions

In general, the dynamical equations for geophysical flows are nonlinear partial differential equations and so, to perform a stability analysis is a difficult task. Sometimes it can be computed for some kinds of perturbations, whereas a "physical" steady solution is stable under all kinds of disturbances: no small perturbation can develop and destroy the initial structure. Therefore, it is interesting to obtain an analytical criterion by which to check the stability with respect to any kind of small but finite perturbation. This criterion is obtained by considering the energy or the momentum of a steady state which admits all the relevant symmetries of the problem. If one can show that all perturbations change either the energy or the momentum, or a combination of both, then the flow is stable. That leads to a convexity theorem and therefore to sufficient conditions for nonlinear stability ([5, 6]).

3.1 X-invariant steady flow

We consider an x-invariant steady basic flow. In cartesian coordinates, it reads:

$$\begin{aligned} u_x &= \overline{u}(y) = -\frac{\partial \overline{\psi}}{\partial y} + \frac{\partial \overline{\chi}}{\partial x} \\ u_y &= 0 = \frac{\partial \overline{\psi}}{\partial x} + \frac{\partial \overline{\chi}}{\partial y} \\ h &= \overline{h}(y) \end{aligned}$$

3.1.1 Pseudo-energy

The pseudo-energy is a linear combination of the conserved quantities of the flow. It corresponds to the amount of energy in the fluid when it is perturbed minus the amount in the unperturbed medium.

$$\begin{aligned} A &= \mathcal{A}(\text{perturbed flow}) - \mathcal{A}(\text{unperturbed flow}) \\ &= (\mathcal{H} + \mathcal{C}_1 + \lambda\mathcal{C}_2 + \nu\mathcal{C}_3)(\text{perturbed f.}) - (\mathcal{H} + \mathcal{C}_1 + \lambda\mathcal{C}_2 + \nu\mathcal{C}_3)(\text{unperturbed f.}) \end{aligned}$$

where λ and ν are real numbers.

For the computation, it is equivalent to consider the following $\mathcal{A}$:

$$\begin{aligned} \mathcal{A} &= \mathcal{H} + \mathcal{C}_1 + \lambda\mathcal{C}_2 + \nu\mathcal{C}_3 \\ &= \iint \frac{1}{2}(|\nabla\psi|^2 + |\nabla\chi|^2 + h^2) + C(q) + \lambda h + \nu\Delta \end{aligned}$$

By definition of the basic state, the first variation of $\mathcal{A}$ must be zero:

$$\begin{aligned} \delta\mathcal{A} &= 0 \\ &= \int \delta\nabla\psi \cdot \nabla\psi + \delta\nabla\chi \cdot \nabla\chi + h\delta h + C'(q)\delta q + \lambda\delta h + \nu\delta\Delta \\ &= \int \delta q(-\psi + C') + \delta\Delta(\nu - \chi) + \delta h(h + \lambda - \psi) \end{aligned}$$

That implies:

$$\begin{aligned} C'(\overline{q}(y)) &= \overline{\psi}(y) \Rightarrow C(\overline{q}) = \int^{\overline{q}} \overline{\psi}(\eta)\, d\eta \\ \overline{\chi} &= \nu \\ \overline{h} - \overline{\psi} &= \lambda \end{aligned}$$

where the bar quantities denote the basic state.

We can choose $\lambda = 0 = \nu$ which gives for the second variation of $\mathcal{A}$:

$$\delta^2\mathcal{A} = \int (\delta\nabla\psi)^2 + (\delta\nabla\chi)^2 + (\delta h)^2 + C''(\overline{q})(\delta q)^2$$

This quantity is positive definite if and only if:

$$C''(\overline{q}) \geq 0$$

So a profile is nonlinearly stable if

$$C''(\overline{q}) \geq 0 \Leftrightarrow \left.\frac{d\overline{\psi}}{dq}\right|_{q=\overline{q}} \geq 0 \tag{4}$$

A is then:

$$A = \iint \frac{1}{2}(|\nabla\psi|^2 + |\nabla\chi|^2 + h^2) + \int_0^q (\overline{\psi}(\overline{q} + \eta) - \overline{\psi}(\overline{q}))d\eta,$$

where ψ, χ, h and q are disturbance quantities.

3.1.2 Normed stability

For a stable profile satisfying the conditions (4), if there exist λ_1 and λ_2 such that

$$\lambda_1 = min_q \left(\left. \frac{d\overline{\psi}}{dq} \right|_{q=\overline{q}} \right) > 0 \text{ and } \lambda_2 = max_q \left(\left. \frac{d\overline{\psi}}{dq} \right|_{q=\overline{q}} \right) < \infty$$

then

$$\frac{1}{2}\lambda_1 q^2 \leq \int_0^q (\overline{\psi}(\overline{q}+\eta) - \overline{\psi}(\overline{q}))d\eta \leq \frac{1}{2}\lambda_2 q^2 \text{ for all } t.$$

We choose the *energy-enstrophy* norm such that:

$$||q||_\lambda = \sqrt{\int \frac{1}{2}(|\nabla\psi|^2 + |\nabla\chi|^2 + h^2) + \lambda\frac{q^2}{2}} \text{ with } \lambda_1 \leq \lambda \leq \lambda_2.$$

Then

$$||q(t)||_\lambda^2 \leq \frac{\lambda}{\lambda_1}A(t) = \frac{\lambda}{\lambda_1}A(0) \leq \frac{\lambda_2}{\lambda_1}||q(0)||_\lambda^2$$

So for a given $\beta > 0$, we choose $\delta = \sqrt{\frac{\lambda_1}{\lambda_2}}\beta$ such that if $||q(0)||_\lambda < \delta \Rightarrow ||q(t)||_\lambda < \beta$. That proves Liapunov stability in the *energy-enstrophy* norm and Arnol'd's first theorem.

We are unable to prove Arnol'd's second theorem for this system.

3.1.3 Pseudo-energy-momentum

The pseudo-energy-momentum is a linear combination of $\mathcal{H}$ and M with some Casimirs. It is a conserved quantity for a steady x-invariant basic flow.

$$\begin{aligned} \mathcal{A} &= \mathcal{H} - \alpha M + C_1 \\ &= \iint \frac{1}{2}(|\nabla\psi|^2 + |\nabla\chi|^2 + h^2) - \alpha(yq + h\frac{\partial\chi}{\partial x}) + C(q) \end{aligned}$$

for all α.

$$\begin{aligned} \delta\mathcal{A} &= \int \delta\nabla\psi\cdot\nabla\psi + \delta\nabla\chi\cdot\nabla\chi + h\delta h - \alpha(y\delta q + \delta h\frac{\partial\chi}{\partial x} + h\frac{\partial\delta\chi}{\partial x}) + C'(q)\delta q \\ &= \int \delta q(-\psi - \alpha y + C'(q)) - \chi\delta\Delta + \delta h(h - \psi - \alpha\frac{\partial\chi}{\partial x}) + \alpha\frac{\partial h}{\partial x}\delta\chi \end{aligned}$$

That gives for the basic state:

$$\begin{aligned} C'(\overline{q}) &= \overline{\psi} + \alpha y \\ \overline{\chi} &= 0 \\ \overline{h} - \overline{\psi} &= 0 \end{aligned}$$

For a monotonic profile $Q(y) = \overline{q}(y)$, there exists a function Y such that $y = Y(Q(y))$. So

$$C(q) = \int^q (\overline{\psi}(\eta) + \alpha Y(\eta)) d\eta$$

The second variation of $\mathcal{A}$ is:

$$\begin{aligned}
\delta^2\mathcal{A} &= \int (\delta\nabla\psi)^2 + (\delta\nabla\chi)^2 + (\delta h)^2 + C''(\overline{q})(\delta q)^2 - 2\alpha\delta h\frac{\partial\delta\chi}{\partial x} \\
&= \int (\delta\nabla\psi)^2 + (\delta\frac{\partial\chi}{\partial y})^2 + C''(\overline{q})(\delta q)^2 + (\delta h - \alpha\frac{\partial\delta\chi}{\partial x})^2 + (1-\alpha^2)(\frac{\partial\delta\chi}{\partial x})^2
\end{aligned}$$

This expression is positive-definite if and only if

$$C''(\overline{q}) \geq 0 \text{ and } 1 - \alpha^2 \geq 0$$

This is equivalent to:

$$\frac{\frac{d\overline{\psi}}{dy} + \alpha}{Q'(y)} \geq 0 \text{ and } -1 \leq \alpha \leq 1 \tag{5}$$

That means that, if there exists an α such that the conditions (5) are satisfied, then the flow is nonlinearly stable, i.e. stable under finite rather than infinitesimal perturbations; and no precise information on the basic state is required.

3.2 Axisymmetric steady flow

We consider an axisymmetric steady flow. In cylindrical coordinates, it reads:

$$\begin{aligned}
u_r &= 0 = -\frac{1}{r}\frac{\partial\psi}{\partial\theta} + \frac{\partial\chi}{\partial r} \\
u_\theta &= \overline{u}(r) = \frac{\partial\psi}{\partial r} + \frac{1}{r}\frac{\partial\chi}{\partial\theta} \\
h &= \overline{h}(r)
\end{aligned}$$

3.2.1 Pseudo-energy

$$\begin{aligned}
\mathcal{H} &= \iint \frac{1}{2}(u_r^2 + u_\theta^2 + h^2) r\, dr\, d\theta \\
\mathcal{A} &= \mathcal{H} + C_1 = \iint \frac{1}{2}(|\nabla\psi|^2 + |\nabla\chi|^2 + h^2) + C(q)
\end{aligned}$$

The same procedure as in the x-invariant case gives for the basic state:

$$\begin{aligned}
C'(\overline{q}(r)) &= \overline{\psi}(r) \\
\overline{\chi} &= 0 \\
\overline{h} - \overline{\psi} &= 0
\end{aligned}$$

and for the nonlinear stability condition:

$$C''(\overline{q}) \geq 0$$

The normed stability is proved as in the x-invariant case.

3.2.2 Pseudo-energy-momentum

As in the x-invariant case:

$$\begin{aligned}\mathcal{A} &= \mathcal{H} - \alpha M + \mathcal{C}_1 \\ &= \iint \frac{1}{2}(|\nabla\psi|^2 + |\nabla\chi|^2 + h^2) - \alpha(-\frac{1}{2}r^2 q + h\frac{\partial\chi}{\partial\theta}) + C(q)\end{aligned}$$

for all α.

The θ-invariance gives for the basic state:

$$\begin{aligned}C'(\overline{q}) &= \overline{\psi}(r) - \alpha\frac{r^2}{2} \\ \overline{\chi} &= 0 \\ \overline{h} - \overline{\psi} &= 0\end{aligned}$$

$$\begin{aligned}\delta^2\mathcal{A} &= \int (\delta\nabla\psi)^2 + (\delta\nabla\chi)^2 + (\delta h)^2 + C''(\overline{q})(\delta q)^2 - 2\alpha\delta h\frac{\partial\delta\chi}{\partial\theta} \\ &= \int (\delta\nabla\psi)^2 + (\delta\frac{\partial\chi}{\partial r})^2 + C''(\overline{q})(\delta q)^2 + (\delta h - \alpha\frac{\partial\delta\chi}{\partial\theta})^2 + (\frac{1}{r^2} - \alpha^2)(\frac{\partial\delta\chi}{\partial\theta})^2\end{aligned}$$

This expression is positive-definite if and only if

$$C''(\overline{q}) \geq 0 \text{ and } \frac{1}{r^2} - \alpha^2 \geq 0 \tag{6}$$

For an unbounded domain, the last conditions (6) must be valid for every r. That implies that α must be zero. So an axisymmetric steady flow is nonlinearly stable iff

$$C''(\overline{q}) \geq 0 \quad \Leftrightarrow \frac{\frac{\partial\overline{\psi}}{\partial r}}{\frac{\partial\overline{q}}{\partial r}} \geq 0$$

It means that the pseudo-energy-momentum doesn't contain more information as regards stability than does the pseudo-energy for an unbounded domain. In the case of a bounded domain with a limit $r < L$, the condition (6) would become $0 \leq \alpha \leq 1/L$.

4 Applications

We use the preceding nonlinear stability conditions for testing different flows such as jets, shear-flows and vortices. In the case where the flow is not stable, we compute a rigorous upper bound on the disturbance saturation.

4.1 Stability of jets, shear-flows and vortices

4.1.1 Bickley Jet

We study the stability conditions for the basic state:

$$u(y) = u_0 sech^2(\gamma y) = -\frac{\partial\psi}{\partial y}$$

where γ is the inverse of the half-width of the jet. This jet is stable by the condition (7) iff

$$\frac{\frac{\partial \psi}{\partial y} + \alpha}{q_y} \geq 0 \Leftrightarrow (-u + \alpha) q_y \geq 0 \tag{7}$$

for α s.t. $-1 \leq \alpha \leq 1$.

$$q_y = u - u_{yy} = u_0 sech^2(\gamma y)(1 + 2\gamma^2 - 6\gamma^2 tanh^2(\gamma y))$$

The last term is positive iff $0 \leq \gamma \leq \frac{1}{2}$, for which $q_y > 0$ everywhere. So the condition (7) is satisfied for $1 \geq \alpha \geq u_{max} = u_0 \geq 0$. If not, q_y changes sign and so $(-u + \alpha)$ must change sign for the same $y = y_s$. The only possibility is to take $\alpha = u_0 sech^2(\gamma y_s)$ but then $(-u + \alpha) q_y$ is always negative. So, for $\gamma > \frac{1}{2}$, the Bickley jet is not provably stable under the condition (7).

4.1.2 Shear-flow

We study the shear-flow defined by:

$$u = u_0(a + tanh(\gamma y))$$

which gives:

$$q_y = u_0(a + (1 + 2\gamma^2) tanh(\gamma y) - 2\gamma^2 tanh^3(\gamma y))$$

There are two cases:

- for $0 \leq \gamma \leq \frac{1}{2}$:

if $a \geq 1$, then $q_y > 0$ everywhere. So the shear-flow is stable if $1 \geq \alpha \geq u_{max} = u_0(a + 1)$.

if $a < 1$, q_y changes sign for some $y = y_s$ and so $(-u + \alpha)$ must change sign for the same y_s. The shear-flow is then not provably stable.

- for $\gamma > \frac{1}{2}$:

if $a \geq \frac{2}{3\sqrt{6}} \frac{(1+\gamma^2)^{3/2}}{\gamma}$, then $q_y > 0$ everywhere. So the shear-flow is stable if $1 \geq \alpha \geq u_{max} = u_0(a + 1)$.

if $a < \frac{2}{3\sqrt{6}} \frac{(1+\gamma^2)^{3/2}}{\gamma}$, then q_y changes sign and the shear-flow is not provably stable.

4.1.3 Vortex patch

We study an axisymmetric vortex patch such that:

$$\nabla^2 \psi - \psi = q_0 \text{ for } r \leq a$$
$$\nabla^2 \psi - \psi = 0 \text{ for } r > a$$

in cylindrical coordinates. The solutions are expressed in terms of Bessel functions ([7]). The conditions are the continuity of ψ and $\frac{\partial \psi}{\partial r}$ for $r = a$. The solutions read:

$$\psi = -q_0 + \frac{q_0 K_1(a)}{I_0(a)K_1(a) + I_1(a)K_0(a)} I_0(r) \text{ for } r \leq a$$

$$\psi = -\frac{q_0 I_1(a)}{I_0(a)K_1(a) + I_1(a)K_0(a)} K_0(r) \text{ for } r > a$$

For such a vortex patch, $\frac{d\psi}{dq}$ is always negative which shows that it is not stable under conditions (7).

4.2 Rigorous bounds on the nonlinear saturation of x-invariant unstable flows

The nonlinear stability conditions previously written are used for constraining the evolution of an unstable flow in terms of its vicinity to a stable flow ([8]). The cases of unstable Bickley jets and unstable shear flows are discussed. We bound the amount of *eddy energy* $\mathcal{E}$ which can go into the waves (gravity or vortical waves) when the instability takes place by the amount of pseudo-energy-momentum PEM between the unstable flow and a stable flow (of the same family in practice). For all t, we have

$$\mathcal{E} \leq E$$

with the total disturbance energy E given by

$$E = \iint \frac{1}{2}(|\nabla\psi|^2 + |\nabla\chi|^2 + h^2).$$

We compare E to PEM:

$$\begin{aligned} PEM &= \iint \frac{1}{2}(|\nabla\psi|^2 + |\nabla\chi|^2 + h^2) + C(\overline{q}+q) - C(\overline{q}) - C'(\overline{q})q - \alpha h\frac{\partial\chi}{\partial x} \\ &= \iint \frac{1}{2}(|\nabla\psi|^2 + (\frac{\partial\chi}{\partial y})^2) + C(\overline{q}+q) - C(\overline{q}) - C'(\overline{q})q \\ &\quad + \frac{1}{2}(h - \alpha\frac{\partial\chi}{\partial x})^2 + \frac{1}{2}(1-\alpha^2)(\frac{\partial\chi}{\partial x})^2 \end{aligned}$$

It follows that for all t,

$$E(1-\alpha^2) \leq PEM$$
$$E \leq \frac{PEM}{(1-\alpha^2)} \text{ for } \alpha^2 \leq 1$$

Since PEM is invariant, the rhs provides a rigorous bound on the nonlinear saturation of unstable flows.

4.2.1 Bickley Jet

We consider an unstable jet given by:

$$\begin{aligned} \tilde{\psi} &= -\frac{\tilde{u_0}}{\tilde{\gamma}} tanh(\gamma y) \\ u_\theta &= \tilde{u_0} sech^2(\tilde{\gamma} y) \end{aligned}$$

The same formula holds for the stable jet, with γ and u_0 instead of $\tilde{\gamma}$ and $\tilde{u_0}$. In order that PEM be finite, we must impose the velocity momentum conservation:

$$\int u_\theta dy = \int u dy \Rightarrow \frac{\tilde{u_0}}{\tilde{\gamma}} = \frac{u_0}{\gamma}$$

Besides, in order to minimize PEM, we choose: $\frac{\alpha}{u_0} = 1$. This gives:

$$\begin{aligned} E \leq \mathcal{B} = & \frac{1}{2}(\frac{\tilde{u_0}}{\tilde{\gamma}})^2/(1-(\frac{\tilde{\gamma}}{\gamma}\tilde{u_0})^2) * \\ & \Big[\int (tanh(\tilde{\gamma}y) - tanh(\gamma y))^2 + (\tilde{\gamma} sech^2(\tilde{\gamma}y) - \gamma sech^2(\gamma y))^2 \\ & +(cosh^2(\gamma y) - 1)(tanh(\tilde{\gamma}y)(1 + 2\tilde{\gamma}^2 sech^2(\tilde{\gamma}y)) \\ & -tanh(\gamma y)(1 + 2\gamma^2 sech^2(\gamma y)))/(1 + 2\gamma^2 - 6\gamma^2 tanh^2(\gamma y))\Big] \end{aligned}$$

We want to study the gravity-wave like instability s.t. $\tilde{\gamma} < \frac{1}{2}$ and $\tilde{u_0} = 1 + \epsilon$ are fixed. For fixed $\tilde{\gamma}$ and $\tilde{u_0}$, we compute $\mathcal{B}$ for $0 < \gamma < \frac{\tilde{\gamma}}{1+\epsilon}$ and find its minimum value. Figure 1 shows the stream function for the stable and the unstable jets, figure 2 the velocity and figure 3 the potential vorticity. Figure 4 shows the minimum bound vs ϵ in logarithmic scales.

4.2.2 Shear-flow

We consider an unstable shear-flow given by:

$$\begin{aligned} \tilde{\psi} &= -\tilde{u_0}(\tilde{a}y + \frac{ln(cosh(\tilde{\gamma}y))}{\tilde{\gamma}} + \tilde{const.}) \\ u_\theta &= \tilde{u_0}(\tilde{a} + tanh(\tilde{\gamma}y)) \end{aligned}$$

The same formula holds for the stable shear-flow, with the tildes removed. PEM will be finite if $\tilde{const.} = \frac{ln2}{\tilde{\gamma}}$, $const. = \frac{ln2}{\gamma}$ and $\tilde{u_0} = u_0$. To be stable, u_0 must be smaller than $\frac{1}{1+a}$. So the instability that we can study is a quasi-geostrophic like instability. We fix $a = \frac{2}{3\sqrt{6}}\frac{(1+\gamma^2)^{3/2}}{\gamma}$, which admits two relevant roots γ_{c1} and γ_{c2}. We choose $\tilde{\gamma} = \gamma_{c2} + \epsilon$ and $\gamma = \gamma_{c2} - \delta$ with $\gamma_{c1} \leq \gamma_{c2}$. We fix ϵ and compute the minimum of

$$\begin{aligned} \mathcal{B} = & \frac{1}{2}\frac{u_0^2}{1-4u_0^2}\int \Big[\frac{ln(cosh(\tilde{\gamma}y))}{\tilde{\gamma}} + \frac{ln2}{\tilde{\gamma}} - \frac{ln(cosh(\gamma y))}{\gamma} - \frac{ln2}{\gamma}\Big]^2 \\ & +(tanh(\tilde{\gamma}y) - tanh(\gamma y))^2 + \frac{2}{a-1}\Big(\frac{ln(cosh(\tilde{\gamma}y))}{\tilde{\gamma}} + \frac{ln2}{\tilde{\gamma}} - \tilde{\gamma} sech^2(\tilde{\gamma}y) \\ & -\frac{ln(cosh(\gamma y))}{\gamma} - \frac{ln2}{\gamma} + \gamma sech^2(\gamma y)\Big)^2 \end{aligned}$$

for δ (note: the $\mathcal{B}$ dependence on u_0 is not relevant). Figure 5 shows the stream function for the stable and the unstable shear-flows, figure 6 the velocity and figure 7 the potential vorticity. Figure 8 shows the minimum bound vs ϵ in logarithmic scales.

5 Conclusions

The model derived from the full SW model seems to be the minimum model containing a weak divergent flow (allowing gravity waves) coupled to a slow vortical motion, and characterized by a quadratic hamiltonian and a good bracket.

Some interesting stability conditions were found for finite amplitude disturbances to x-invariant and axisymmetric steady basic flows.

Bounds on saturation of instabilities of jets or shear-flows were computed.

However, when a profile is not provably stable, nothing ensures that an instability will actually develop. To be sure, a perturbation calculation is necessary. A future work.

Acknowledgments

I would like to thank especially Ted Shepherd for supervising my work with patience and enthusiasm. I express my appreciation to Phil Morrison for teaching me how to prove Jacobi's identity, among other things, and to Joe Keller for initiating me to the secrets of Green functions, and to all the staff for this intense summer. I won't forget the fellows, with whom I spent a great summer.

References

[1] M.Farge and R.Sadourny, *Wave-vortex dynamics in rotating shallow water*, J.Fluid Mech., **206**, 433 (1989).

[2] J.Pedlosky, *Geophysical Fluid Dynamics*, Springer (1987).

[3] T.Warn, *Statistical mechanical equilibria of the shallow water equations*, Tellus, **38A**, 1 (1986).

[4] T.G.Shepherd, *Symmetries, conservation laws and Hamiltonian structure in geophysical fluid dynamics*, Adv.in Geop. **32**, 287 (1990).

[5] P.Ripa, *General stability conditions for zonal flows in a one-layer model on the β-plane or the sphere*, J.Fluid Mech., **126**, 463 (1983).

[6] R.Benzi, S.Pierini, A.Vulpiani and E.Salusti, *On nonlinear Hydrodynamic Stability of Planetary Vortices*, GAFD **20**, 293 (1982).

[7] Handbook of mathematical functions, M.Abramowitz and I.Stegun (1970).

[8] T.G.Shepherd, *Rigorous bounds on the nonlinear saturation of instabilities to parallel shear-flows*, J.Fluid Mech., **196**, 291 (1988).

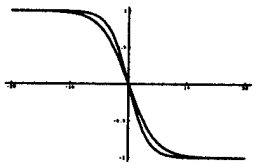

Figure 1. Stream function for the stable and unstable jets.

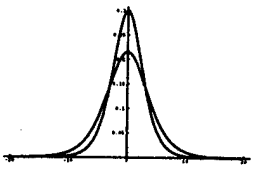

Figure 2. Velocity for the stable and unstable jets.

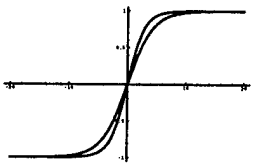

Figure 3. Potential vorticity for the stable and unstable jets.

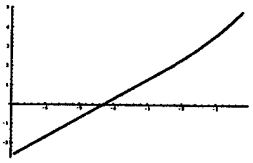

Figure 4. Minimum bound versus ϵ in logaritmic scales.

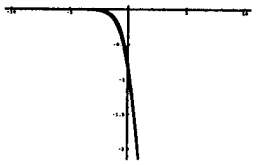

Figure 5. Stream function for the stable and unstable shear-flows

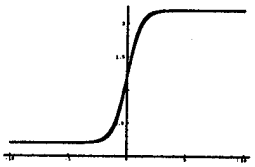

Figure 6. Velocity for the stable and unstable shear-flows.

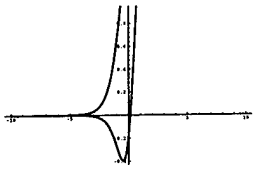

Figure 7. Potential vorticity for the stable and unstable shear-flows.

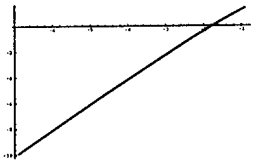

Figure 8. Minimum bound versus ϵ in logaritmic scales.

Appendix: Jacobi identity for the weak-wave model

The bracket reads:

$$\{F,G\} = \int q[F_q, G_q] + F_h \nabla^2 G_\Delta - F_\Delta \nabla^2 G_h$$

where

$$F_q = \frac{\delta F}{\delta q}, \quad \text{etc.}$$

That implies that:

$$\{\{F,G\},H\} = \int q[\{F,G\}_q, H_q] + \{F,G\}_h \nabla^2 H_\Delta - \{F,G\}_\Delta \nabla^2 H_h$$

Then

$$\begin{aligned}
\{F,G\}_q &= [F_q,G_q] + q[F_{qq},G_q] + q[F_q,G_{qq}] + F_{qh}\nabla^2 G_\Delta + F_h \nabla^2 G_{q\Delta} - F_{q\Delta}\nabla^2 G_h - F_\Delta \nabla^2 G_{qh} \\
&= [F_q,G_q] - F_{qq}[q,G_q] + G_{qq}[q,F_q] + F_{qh}\nabla^2 G_\Delta - G_{qh}\nabla^2 F_\Delta + G_{q\Delta}\nabla^2 F_h - F_{q\Delta}\nabla^2 G_h \\
\{F,G\}_h &= q[F_{hq},G_q] + q[F_q,G_{hq}] + F_{hh}\nabla^2 G_\Delta + F_h \nabla^2 G_{h\Delta} - F_{h\Delta}\nabla^2 G_h - F_\Delta \nabla^2 G_{hh} \\
&= -F_{qh}[q,G_q] + G_{qh}[q,F_q] + F_{hh}\nabla^2 G_\Delta - G_{hh}\nabla^2 F_\Delta + G_{h\Delta}\nabla^2 F_h - F_{h\Delta}\nabla^2 G_h \\
\{F,G\}_\Delta &= q[F_{\Delta q},G_q] + q[F_q,G_{\Delta q}] + F_{\Delta h}\nabla^2 G_\Delta + F_h \nabla^2 G_{\Delta\Delta} - F_{\Delta\Delta}\nabla^2 G_h - F_\Delta \nabla^2 G_{\Delta h} \\
&= -F_{q\Delta}[q,G_q] + G_{q\Delta}[q,F_q] + F_{\Delta h}\nabla^2 G_\Delta - G_{h\Delta}\nabla^2 F_\Delta + G_{\Delta\Delta}\nabla^2 F_h - F_{\Delta\Delta}\nabla^2 G_h
\end{aligned}$$

It follows that

$$\{\{F,G\},H\} + (\text{permut.}) = 0$$

Dissipative Quantum Chaos

by Dean Petrich

working with Ed Spiegel

1 Introduction

In the study of classical chaos, one can distinguish two broad classes: Hamiltonian and dissipative. Among other things, Hamiltonian chaos is characterized by a conservation of volume in phase space. Dissipative chaos, on the other hand, is characterized by a contraction of phase space as the system evolves. This implies that all orbits get drawn to a set of measure zero in phase space, a set known as a strange attractor.

The study of quantum chaos is the study of the quantum mechanics of systems that exhibit chaos in the corresponding classical problem. Modulo some uniqueness problems having to do with operator ordering, there is a way of quantizing classical systems possessing a Hamiltonian: the Schrodinger equation. On the other hand, it is not as clear how to quantize a classical system which has dissipation, and as a result, there has been less work done such systems (See, for example, Graham (1987)). Here we will simply choose one such method, explain why it may be a good model for dissipative quantum mechanics, and use it to study the quantum mechanics of a system that exhibits dissipative chaos in the classical limit. The goal is to see how quantum mechanics modifies the classical strange attractor: does quantum mechanics preserve it, smear it, or even destroy it? This report describes the first steps to answering the question for our choice of dissipative quantum mechanics.

2 The Classical System: a Bouncing Ball

The classical system studied here is that of a bouncing ball. The ball bounces on a sinusoidally forced platform. Without dissipation, in almost all cases, the ball would simply gain more and more energy and eventually reach arbitrarily large heights. To balance the forcing, we add dissipation *not* through inelastic bounces, but through a frictional force. Hence the equation of motion for the ball is

$$m\ddot{z} = -mg + \mu\dot{z}, \tag{1}$$

where m is the mass of the ball, g is the gravitational constant, and μ is the coefficient of friction. By dividing by m and rescaling z and t, we can set all the constants equal to one. The boundary conditions on the bounce can be

worked out by momentum and energy conservation and are

$$v_{up} = v_{plat} + |v_{down} - v_{plat}|, \tag{2}$$

where v_{down} is the upward velocity before the bounce, v_{up} is the upward velocity after the bounce, and v_{plat} is the platform velocity at the time of the bounce.

The above equation has to be solved numerically, since the platform moves sinusoidally as a function of time, and therefore the ball generally impacts the platform at different heights on successive bounces.

The most edifying way to view the output is in terms of maps. Figures 1 and 2 are stroboscopic maps; each time the platform reaches its minimum height, the position and velocity of the ball is plotted. The maps have a filamentary structure reminiscent of the Henon map; figure 2 shows an expanded view of a small region of figure 1. This process can be continued, and the filaments look similar to very small length scales.

3 Dissipative Quantum Mechanics

Before introducing the model for dissipative quantum mechanics, we start by reviewing some features of Hamiltonian quantum mechanics. Given a classical system with Hamiltonian $H(x,p)$, the corresponding quantum mechanical system that reduces to the classical system as $\hbar \to 0$ is given by the Schrodinger equation,

$$i\hbar \frac{\partial \psi(x,t)}{\partial t} = H(x,p)\psi(x,t), \tag{3}$$

where p denotes an *operator*, $p = -i\hbar\partial_x$. Moreover, H must be a Hermitian operator, and hence the order of the terms x and p is important. For simplicity, from here on we will set $\hbar = 1$.

The function ψ is the fabled wave function, and it encodes all the information of the system. Note that the equation for ψ is linear, and hence has a complete set of orthogonal eigenfunctions. Each eigenfunction represents a state of a given energy, labeled by its eigenvalue. The probability density for finding the particle at x and t is given by $|\psi(x,t)|^2$. Since this is a probability density, one can use it to define expectation values, as usual. For instance, the expected value of x, written here as $\langle x \rangle$, is

$$\langle x \rangle = \int_{-\infty}^{\infty} x|\psi(x,t)|^2 dx. \tag{4}$$

The expected value of the momentum is given by

$$\langle p \rangle = \int_{-\infty}^{\infty} \psi^*(x,t)(-i\partial_x)\psi(x,t)dx. \tag{5}$$

The dissipative quantum mechanics we intend to study has a similar structure. (See Kostin (1974), or for other possibilities, see Dekker (1981).) To motivate the equation, we follow an argument of Kan and Griffin (1974). They require that the equation have the appropriate classical limit (a particle experiencing a frictional force proportional to the velocity), and that the total energy be given by the sum of the kinetic energy and potential energy pieces. They then note that in the fluid dynamical interpretation of the Schrodinger equation, where the magnitude of ψ represents the density and the phase of represents the velocity potential, the continuity equation is automatically obeyed. Since $F = -\partial V/\partial x$, to get a term proportional to the velocity in the equation of motion, one can add the velocity potential to the true potential. The dissipative Schrodinger equation will thus have a term proportional to the phase in it. To insure that the expectation value of the energy is given by the kinetic energy plus the true potential, we subtract the expectation value of the velocity potential, the phase. Thus we find that if the classical evolution has the form of a Hamiltonian piece plus a friction term (like the bouncing ball problem above), the equation for the wave function time evolution is

$$i\psi_t = H\psi + \mu(\phi - \langle\phi\rangle)\psi, \tag{6}$$

where ϕ is the phase of the wave function, $\psi = Re^{i\phi}$. Note that it is nonlinear, so there is coupling between different energy eigenstates of the zero dissipation problem.

For the problem at hand, the equation of motion for ψ is

$$i\psi_t = -\frac{1}{2}\psi_{zz} + gz\psi + \mu(\phi - \langle\phi\rangle)\psi. \tag{7}$$

There are two boundary conditions. The first is $\psi(z = z_{plat}(t), t) = 0$, where $z_{plat}(t)$ is the platform height at time t. The second we will take to be $\psi(z = L, t) = 0$, which physically represents putting a lid above the ball at height $z = L$. We can put this lid so high that classically it makes no difference for low energy bouncing, as studied here; it is included in the quantum mechanical case only to make the problem easier to solve numerically.

4 Results

Equation (7) was studied numerically using a Crank-Nicholson, finite difference code. Some results are shown in figures 3-7.

Figure 3 shows the evolution of the probability density $|\psi|^2$ as a function of time for the zero dissipation, zero forcing case. In the simulation, $g = 10$. The simulation shows one "bounce" of the quantum-mechanical ball.

Figure 4 shows the evolution of the expectation values $\langle z \rangle$ and $\langle p_z \rangle$ as a function of time for the zero dissipation, zero forcing case. One case see that the quantum ball "bounces" five times. Note that the evolution is not quite periodic, as it would be in the classical case.

To see the effect of including the dissipative term, figure 5 shows the evolution of the expectation values in the zero forcing case. The expectation values indicate that the quantum ball begins to drop, but reaches a terminal velocity as in the classical case.

Figure 6 shows the evolution of the expectation values of z and p_z in the case with both forcing and dissipation: here $g = 10$, $\mu = 1$, $m = 1$, $A = 3$, $\omega = 20$, where the plaform height is given by $z_{plat}(t) = Acos(\omega t)$. This is *not* a stroboscopic map. It simply shows the evolution of the expectation values for a short time. One can see that the quantum ball bounces, but it meanders around even as it moves away from the platform, since the wavefunction interacts with the wall all the time, as opposed to the classical case.

Finally, in figure 7, we show the stroboscopic map of the expectation values, with the same parameters of figure 6. This is the quantum mechanical analogue of figures 1 and 2; there we plotted z and $\dot{z}$, here we plot $\langle z \rangle$ and $\langle p_z \rangle$. The straight vertical line is the mean platform height. The straight horizontal line represents a transient; this is the ball dropping from its initial condition. The simulation has been run for times long enough for the transients to decay, so any structure of an attactor should be apparent. One can see that the structure of the classical strange attractor is totally destroyed for this choice of parameters. Unfortunately, these parameters correspond to the strong quantum limit. By taking g and m larger, the quantum mechanics should approach the classical limit, and figure 7 should look more like figure 1. Moreover, the stroboscopic map of the expectation values is only the first step towards a characterization of a quantum mechanical "strange attractor."

5 Future Work

One possibility for further study has already been mentioned; i.e., take the parameters m and g to be very large and study the quantum mechanics to see if the classical limit is reproduced, at least for short times.

Another direction for future research is to try to answer the general question of what chaos should look like in a dissipative quantum system, or for that matter, any partial differential equation with both forcing and dissipation. The idea is the following: in the classical case, we have a one degree of freedom system, and we can use all the standard lore of nonlinear dynamics and chaos. In the dissipative system studied here, all orbits are drawn onto strange attractors. The quantum mechanical case really represents an *infinite* degree of freedom system, as can be seen by, say, projecting the wave

function onto a complete set of eigenfunctions and writing the dissipative Schrodinger equation as a set of evolution equations for the coefficients. Is there an attractor in this function space, the analogue of the classical strange attractor? Unfortunately, this is a truly difficult problem; turbulence is an example of this type of system! Perhaps there is some simple model for which it is tractable.

Lastly, it should be possible to study this system using the method of periodic orbits. The periodic orbits of a classical chaotic system are dense in the set of all orbits, and as such, can be used as a "basis" in which to expand any orbit. This technique can be used to calculate quantities in classical physics, but in fact, the classical periodic orbits also can be used to calculate quantities in the corresponding quantum mechanical system, too. Using the classical maps shown in section 2, the periodic orbits of the classical system can be determined, and can be further used to calculate any quantity of interest in the classical or quantum mechanical system.

References

H. Dekker, *Physics Reports*, **80** , Number 1, (1981)

R. Graham, *Physica Scripta.* **35** , 111-118, (1987)

K.-K. Kan and J.J. Griffin, *Physics Letters*, **50B**, 241, (1974)

M. D. Kostin, *Journal of Statistical Physics*, **12**, 145, (1975)

Figure 1

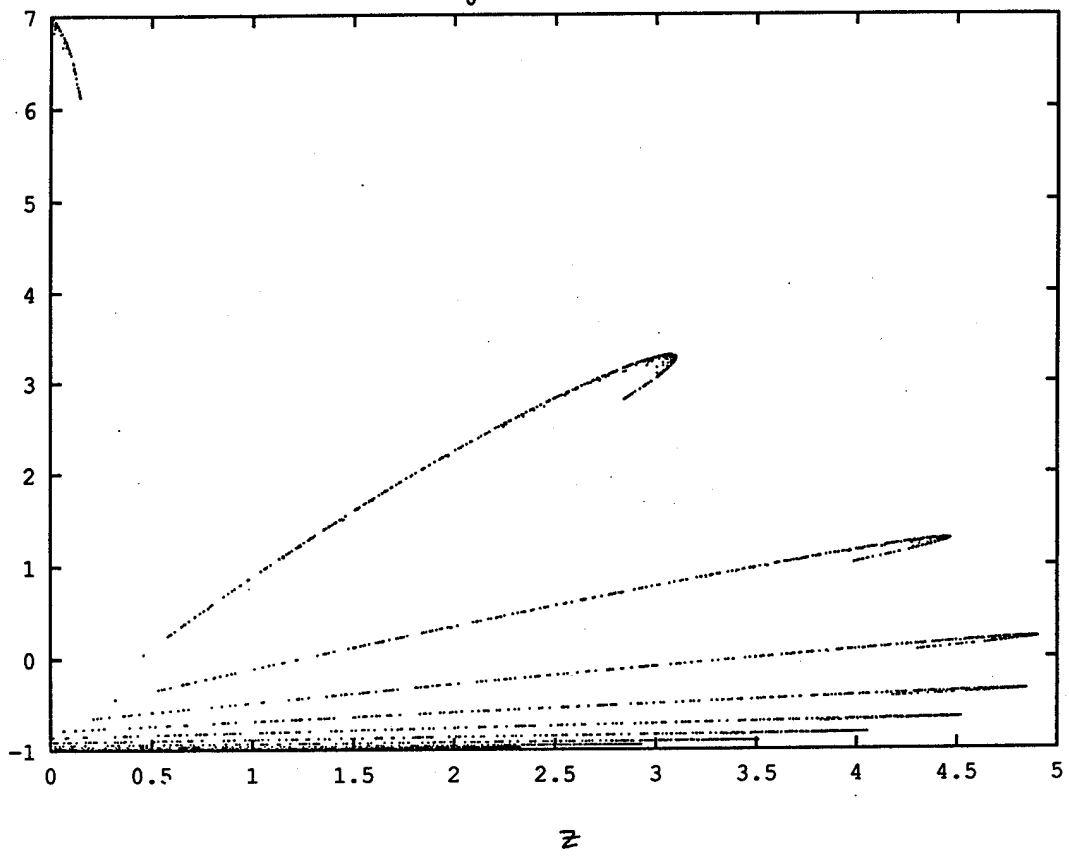

Figure 2

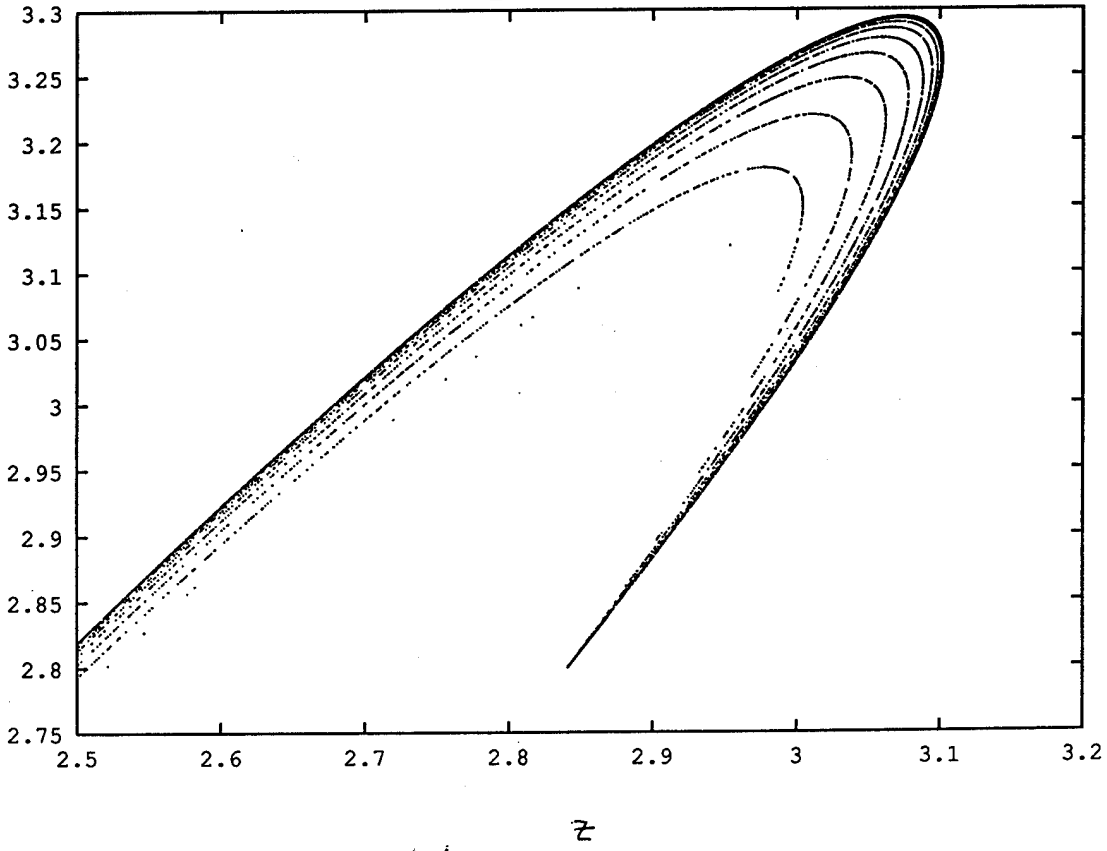

Figure 3

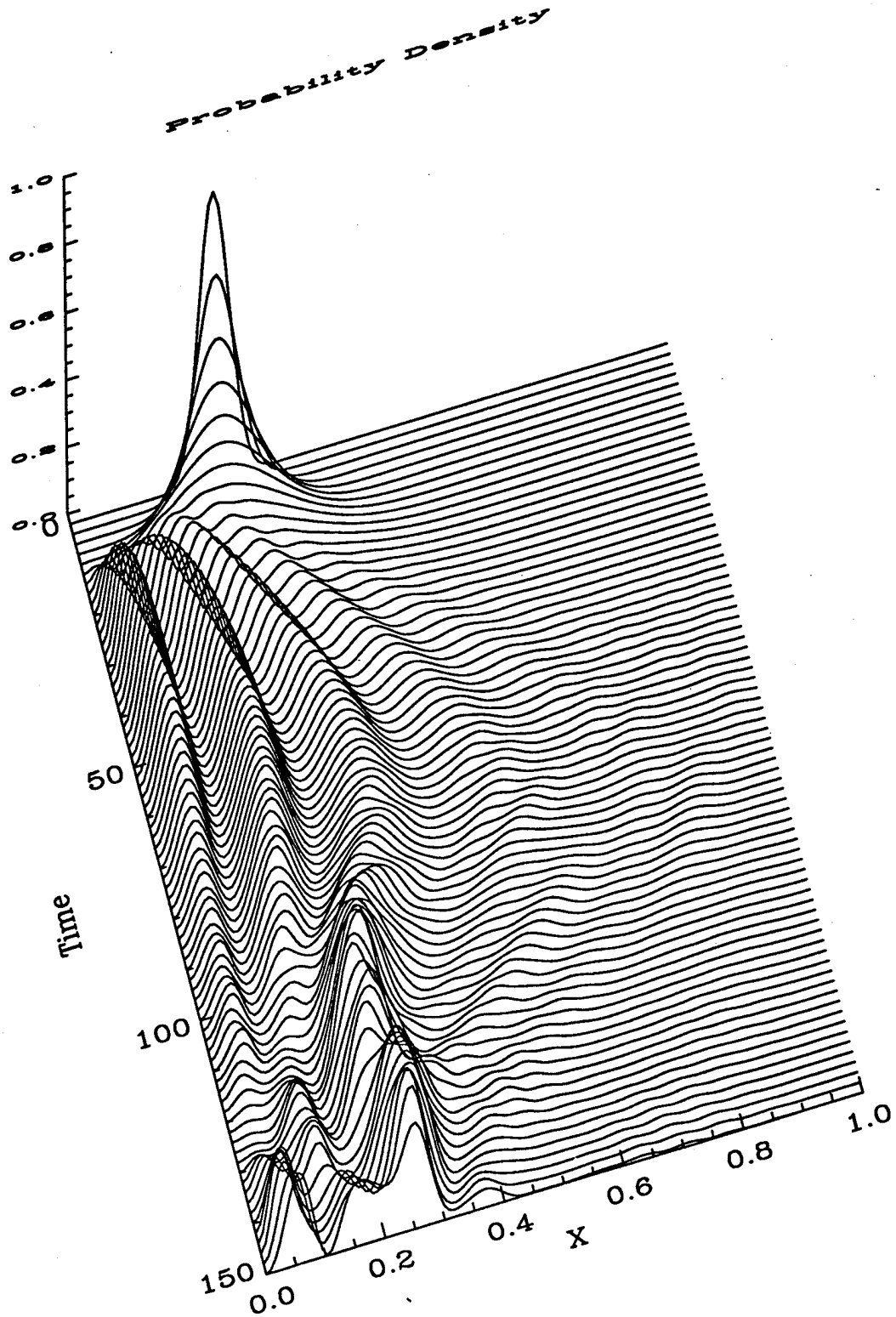
Probability Density
1.0
0.8
0.6
0.4
0.2
0.0
Time
50
100
150
0.0
0.2
0.4
0.6
0.8
1.0
X

Figure 4

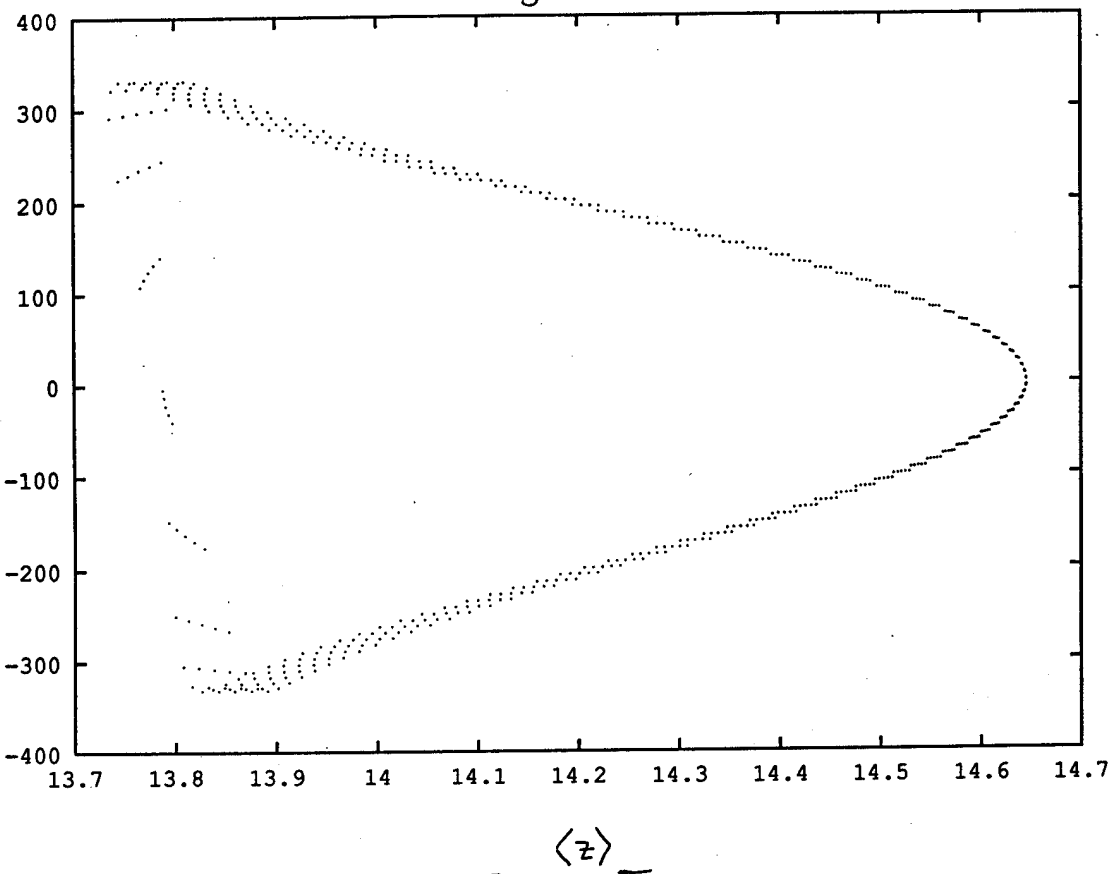

Figure 5

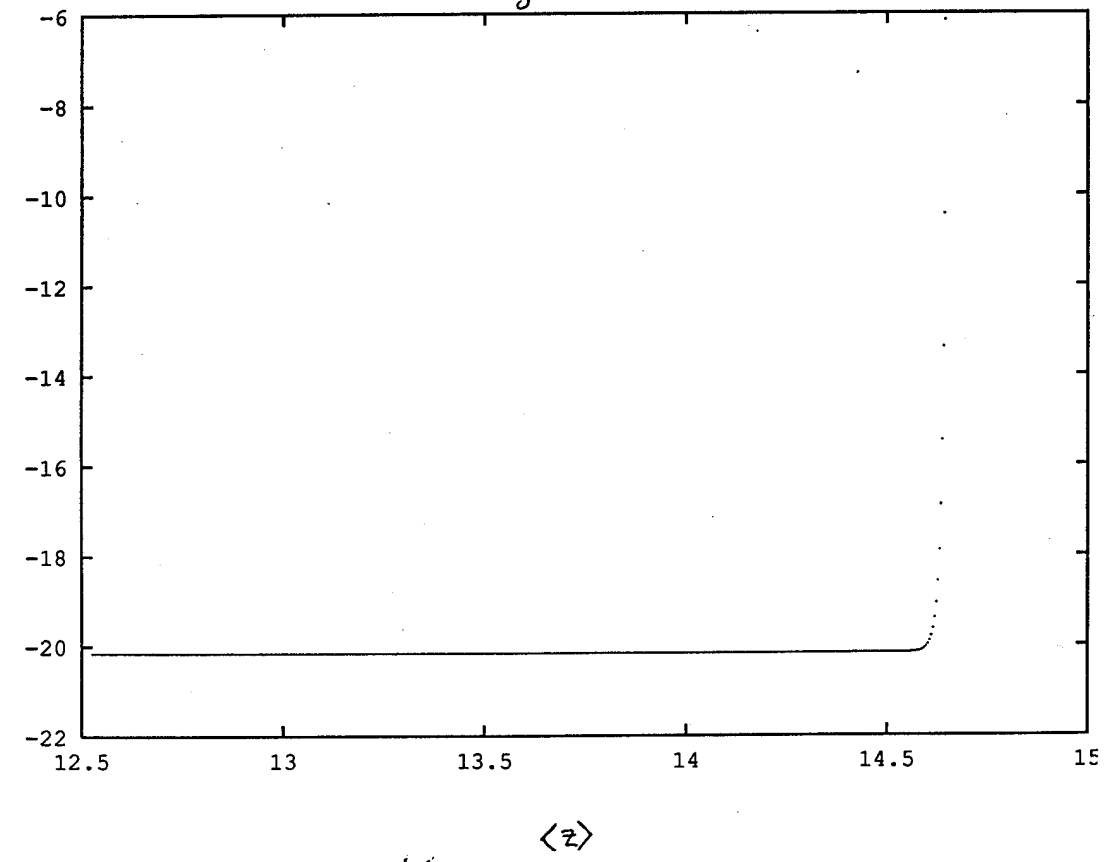

Figure 6

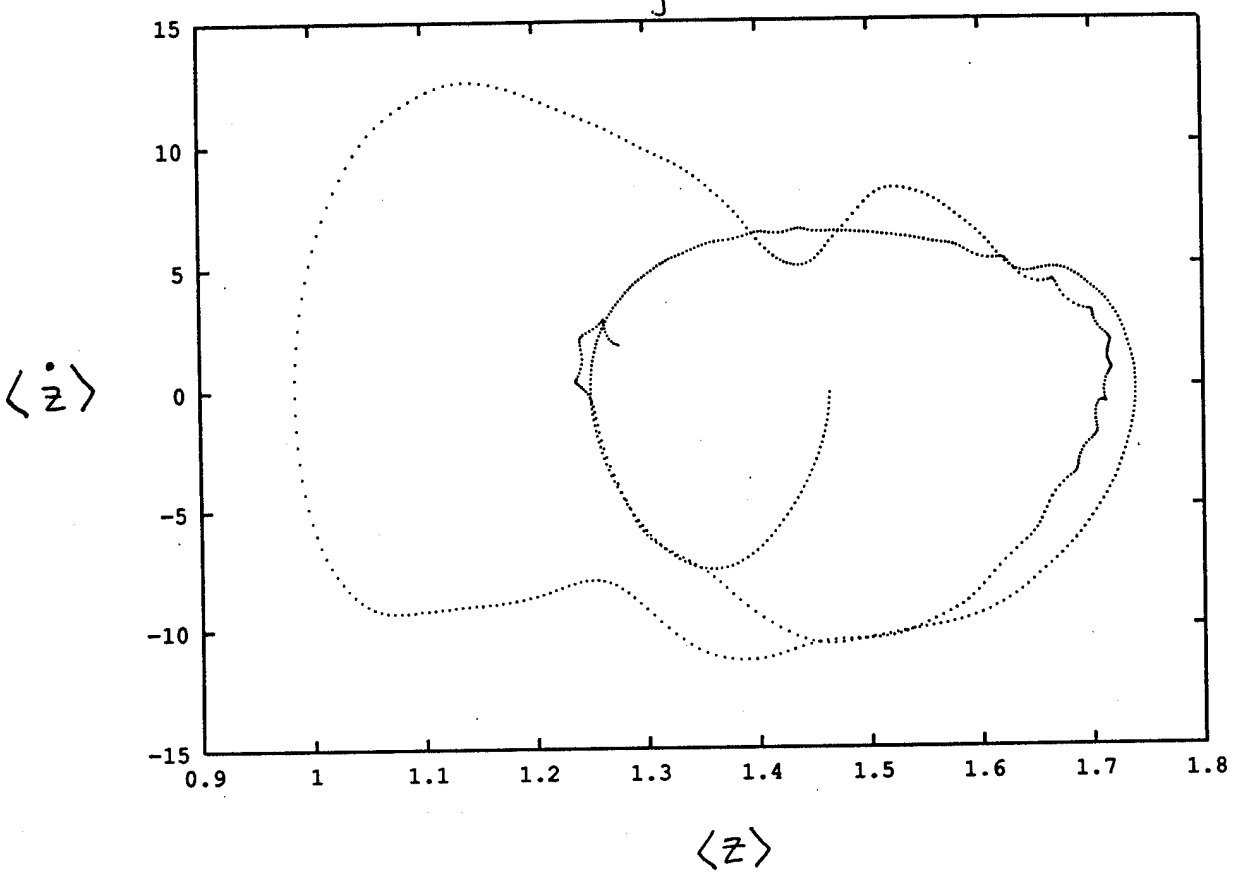

Figure 7

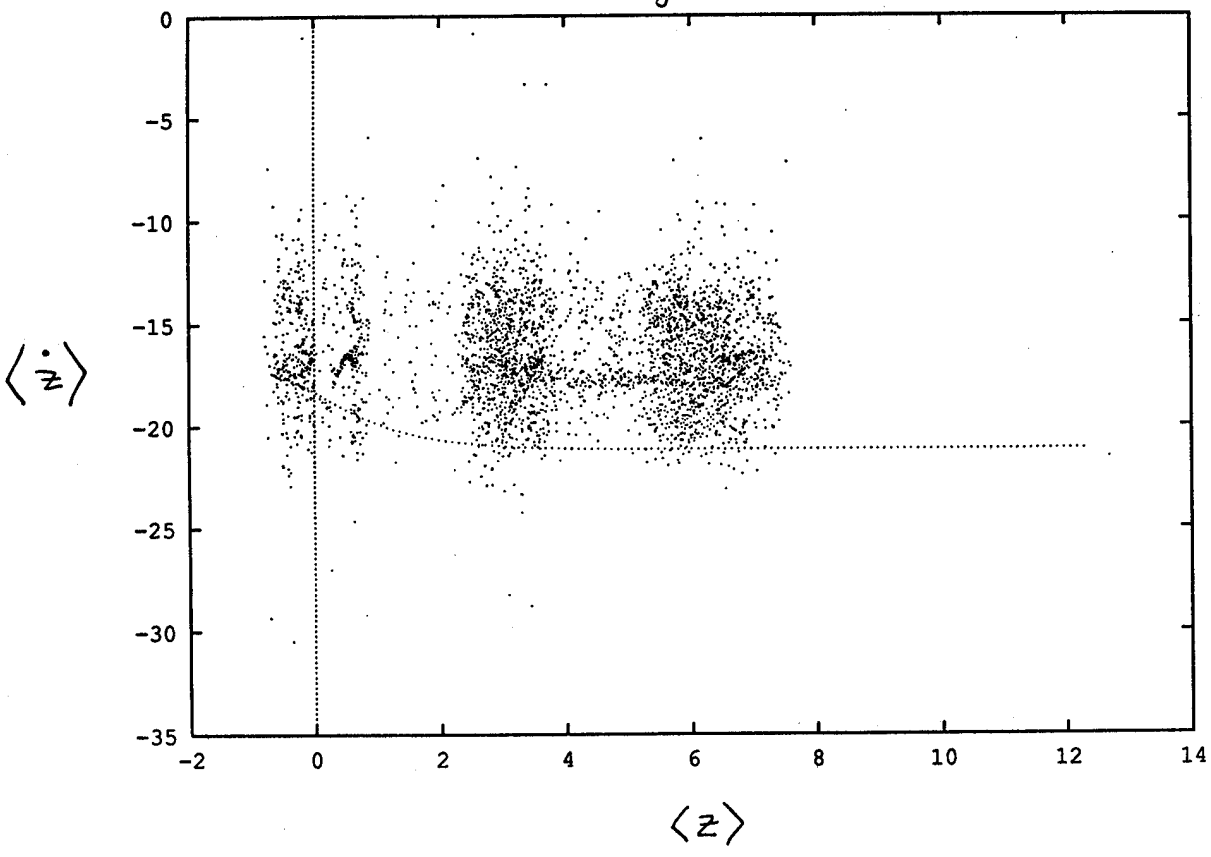

Moisture and Available Potential Energy

Kyle Swanson
1993 Summer Study Program in Geophysical Fluid Dynamics
Fellow Project Report

1. Introduction

The concept of available potential energy (APE) is fundamental to any understanding of instabilities in the Earth's atmosphere. It encompasses phenomena of varying scales; for example, the synoptic–scale eddies which dominate the variability of the extra-tropical troposphere owe their existence to the APE stored in the pole to equator temperature gradient, while on a much smaller scale, buoyancy driven plumes in the planetary boundary layer owe their existence to the APE in an unstable temperature/height profile.

Recently, Shepherd (1993) has shown that a common understanding of APE for a wide variety of systes can be obtained by considering the underlying Hamiltonian structure of those systems. A conserved quantity called the *pseudoenergy* can be constructed from a combination of the Hamiltonian of the system together with its Casimir invariants, and under certain restrictions can be used to construct bounds on the APE available to a disturbance. This generalization is extremely powerful, as it allows one to construct rigorous upper bounds to disturbance energies, which complement the more usual upper bounds calculated by adjustment arguments, in which it is supposed that an unstable flow evolves to some final stable (or neutral) state.

One system in the atmospheric sciences where APE has historically played a large role but the underlying equations are not Hamiltonian is that of non-adiabatic moist convective dynamics. Traditionally, this system has been studied using *parcel dynamics* (Thorpe, et. al. 1989), in which the fluid is seperated into two different entities, namely an infinitessimal parcel and the surrounding fluid environment. The parcel is then assumed to evolve without effecting that fluid environment, which allows for a considerable simplification of the dynamics, and also allows for the construction of an APE for the individual parcels, a quantity known as the convective available potential energy, or CAPE.

This approach, of course, has the draw-back that it is a parcel theory, and in neglecting the feedback between parcel and environment it throws out much useful information. Hence, it would be intriguing if it were possible to extend the methods obtained from APE considerations in a Hamiltonian framework to moist convective systems.

The outline is as follows: First, we will review the Hamiltonian theory of dry, 2-D Boussinesq convection, emphasizing the ideas behind the construction of the APE. We then will quickly review Lagrangian parcel dynamics, and finally, will attempt to extend the Hamiltonian APE concepts to the moist convective case.

2. Hamiltonian bounds and APE: A Boussinesq example

The two-dimensional, non-hydrostatic, dry adiabatic Boussinesq equations can be written

$$\frac{Du}{Dt} = -\frac{p_x}{\rho_0}$$

$$\begin{aligned} \frac{Dw}{Dt} &= -\frac{p_z}{\rho_0} + \frac{g\theta}{\theta_0} \\ u_x + w_z &= 0 \\ \frac{D\theta}{Dt} &= 0. \end{aligned} \tag{1}$$

The notation is standard, with θ the potential temperature, and θ_0 a constant reference value.

As the velocity is nondivergent in the $x-z$ plane, we can introduce the streamfunction ψ defined by

$$u = \psi_z, \qquad w = -\psi_x; \tag{2}$$

it follows that $D/Dt = \partial/\partial t + \partial(\psi, \cdot)$, where $\partial(f,g) = f_z g_x - g_z f_x$ is the two-dimensional Jacobian operator. The pressure can the be consequently eliminated by the introduction of the vorticity $\omega = u_z - w_x$, which reduces (1) to

$$\frac{D\omega}{Dt} = \partial\left(\theta, \frac{gz}{\theta_0}\right), \qquad \frac{D\theta}{Dt} = 0. \tag{3}$$

We shall consider these equations in a simply connected domain D with the nonpenetrative boundary condition

$$\psi = 0 \text{ on } \partial D. \tag{4}$$

a. Hamiltonian structure

The dynamics described by (3) conserves the integral

$$\mathcal{H} = \int\int_D \left\{ \frac{1}{2}|\nabla\psi|^2 - \frac{g\theta z}{\theta_0} \right\} dx\ dz. \tag{5}$$

Evaluation of the functional derivatives of $\mathcal{H}$ with respect to ω and θ shows

$$\begin{aligned} \delta\mathcal{H} &= \int\int_D \left\{ \nabla\psi \cdot \nabla\delta\psi - \frac{gz}{\theta_0}\delta\theta \right\} dx\ dz \\ &= \int\int_D \left\{ -\psi\delta\omega - \frac{gz}{\theta_0}\delta\theta \right\} dx\ dz, \end{aligned} \tag{6}$$

where the second expression follows from integrating by parts. It follows immediately that

$$\frac{\delta\mathcal{H}}{\delta\omega} = -\psi, \qquad \frac{\delta\mathcal{H}}{\delta\theta} = -\frac{gz}{\theta_0}. \tag{7}$$

If we then consider the Poisson tensor

$$J = \begin{pmatrix} -\partial(\omega,\cdot) & \partial(\theta,\cdot) \\ -\partial(\theta,\cdot) & 0 \end{pmatrix} \tag{8}$$

it follows that we can write (3) in the form

$$\frac{\partial u_i}{\partial t} = J_{ij}\frac{\delta\mathcal{H}}{\delta u_j} \tag{9}$$

where $u_1 \equiv \omega$ and $u_2 \equiv \theta$. If J displays the properties of a *Poisson tensor*, i.e. skew-symmetry, Jacobi identity, etc. then (9) is a continuous Hamiltonian system. Proof that J in this case actually satisfies such properties is given in Benjamin (1986).

In addition, the Poisson tensor for this case happens to be singular; there exists a class of functions, the Casimir invariants $\mathcal{C}$, that span the null space of J, *viz*

$$J_{ij}\frac{\delta \mathcal{C}}{\delta u_j} = 0. \tag{10}$$

For this system, the Casimirs have the form

$$\mathcal{C} = \int\int_D C(\theta) dx\ dz \tag{11}$$

for arbitrary C, for which

$$\frac{\delta \mathcal{C}}{\delta \omega} = 0, \qquad \frac{\delta \mathcal{C}}{\delta \theta} = C'(\theta). \tag{12}$$

(There is another Casimir for this system as well, namely $\int\int_D \omega C(\theta) dx\ dz$, but this will not come into play as we are considering disturbances to a resting state.)

To construct the pseudoenergy, consider disturbances to a resting, stably stratified basic state

$$u = w = 0, \qquad \theta = \Theta(z). \tag{13}$$

$\mathcal{C}$ then must satisfy

$$\frac{\delta \mathcal{H}}{\delta \theta} = -\frac{\delta \mathcal{C}}{\delta \theta} \tag{14}$$

which immediately implies

$$C'(\theta) = gz/\theta_0 \iff C(\theta) = \frac{g}{\theta_0}\int^{\theta} \mathcal{Z}(\hat{\theta}) d\hat{\theta}. \tag{15}$$

Note that $\Theta(z)$ stably stratified (i.e. increasing with height) defines the function $\mathcal{Z}(\cdot)$ according to $z = \mathcal{Z}(\Theta)$. This can be seen by considering the second variation of the functional $\mathcal{H} + \mathcal{C}$, which shows immediately that the condition for this state to be and extremum is $\partial^2 C/\partial\theta^2 = \frac{g}{\theta_0}\partial z/\partial\theta > 0$.

The pseudoenergy is then considered to be a functional of the form

$$\mathcal{A}[\mathbf{u}] \equiv \mathcal{H}[\mathbf{u}] - \mathcal{H}[\mathbf{U}] + \mathcal{C}[\mathbf{u}] - \mathcal{C}[\mathbf{U}] \tag{16}$$

where $\mathbf{U}$ is the stable reference state, which in this case is $\mathbf{U} = (0, \Theta(z))$, and $\mathbf{u}$ is a disturbance state. Note that $\mathcal{A}$ is an exact invariant of (9), as it is composed of exact invariants. The APE is defined to be the non-kinetic portion of this pseudoenergy.

For the reference state outlined above, it immediately follows that

$$\mathcal{A} = \int\int_D \left\{ \frac{1}{2}|\nabla\psi|^2 + \int_0^{\theta-\Theta} g[\mathcal{Z}(\Theta + \hat{\theta}) - \mathcal{Z}(\Theta)] d\hat{\theta} \right\} dx\ dz, \tag{17}$$

implying the integral over $\hat{\theta}$ represents the density of APE, as desired.

b. Simple Example

Consider the steady, statically unstable initial profile

$$\theta^{(0)} = -\frac{\theta_0}{H}\epsilon z; \qquad \omega^{(0)} = 0 \tag{18}$$

in the domain $x \in [-L/2, L/2]$, $z \in [-H/2, H/2]$, where $\epsilon > 0$. Now, consider an infinitesimal disturbance $(\theta^{(1)}, \omega^{(1)})$ to this profile, implying

$$\theta = \theta^{(0)} + \theta^{(1)}; \qquad \omega = \omega^{(0)} + \omega^{(1)}. \tag{19}$$

We can now consider (19) to be a finite amplitude disturbance to some stable basic flow $\mathbf{U} \equiv (\Omega, \Theta)$; if we take

$$\Theta = \frac{\theta_0}{H}\delta z; \qquad \Omega = 0, \tag{20}$$

where $\delta > 0$, then the pseudoenergy will be

$$\mathcal{A} = \int\int_D \left\{ \frac{1}{2}|\nabla\psi|^2 + \frac{g}{\theta_0}\int_0^{\frac{\theta_0}{H}(\epsilon+\delta)z} \frac{\hat{\theta}}{\delta} d\hat{\theta} \right\} dx\, dz. \tag{21}$$

Carrying through the $\hat{\theta}$ integration yields an expression for the APE:

$$APE \leq \frac{gH^2L}{24}\frac{(\epsilon+\delta)^2}{\delta}. \tag{22}$$

This is minimized by choosing $\delta = \epsilon$, giving the final bound for the APE, *viz*

$$APE \leq \frac{gH^2L\epsilon}{6}. \tag{23}$$

The important feature to note from this simple calculation is that APE is in a sense a spatially integrated measure of how far each parcel is from its "rest" position given by the choice of the stable state. This idea will become important when we consider moist convective dynamics, where degeneracies will appear that we will be forced to deal with.

3. Lagrangian parcel dynamics: Moisture and CAPE

The addition of phase changes of water and the associated latent heating complicates the theoretical understanding of convective instability immensely, as the effective stability of the fluid to vertical motions depends on the sign and magnitude of the vertical displacement of the fluid. In order to deal with this complexity, the "parcel dynamics" approach to moist convection was formulated. This parcel theory relies on an abandonment of the continuum hypothesis to replace the fluid by *two* distinct entities – the parcel and the undisturbed environment through which it moves. This assumption allows one to neglect the perturbation pressure forces on the parcel, and reduces the original partial differential equations for the entire flow to ordinary differential equations for the parcel.

An important offshoot of parcel dynamics has been the concept of the convective available potential energy (CAPE) of a moist atmosphere. As its name would suggest, CAPE

is a measure of how much energy is available for a parcel to release as it udergoes vertical motion, but it differs from the more traditional concepts of APE as outlined in section 2, as the parcel must meet certain conditions in order to have access to the APE.

The equations of motion for the moist convective system are very similar to those for the dry adiabatic system outlined in section 2. The only change is in the equation for the potential temperature, *viz*

$$\frac{D\theta}{Dt} = \begin{cases} kw & \text{saturated motions} \\ 0 & \text{otherwise} \end{cases} \tag{24}$$

In other words, the potential temperature of the parcel will change *only* if the parcel is saturated, which will usually coincide with rising motions. It follows immediately that if a parcel is rising, it will heat up and has the potential to become more bouyant than its surroundings, leading to an instability.

For the simple thermodynamic systems such as those that will be considered below, we will be considering the saturation moisture profile to be simply a function of height z. Hence, we can define a CAPE appropriate to our model simply as

$$\text{CAPE} = \frac{g}{\theta_0} \int_{z_b}^{z_t} (\theta_p - \theta_e) dz \tag{25}$$

where z_b and z_t have the same meaning as above, and θ_p, θ_e are the parcel and environmental potential temperature profiles, respectively. The CAPE has the basic geometric interpretation shown in Figure 1:

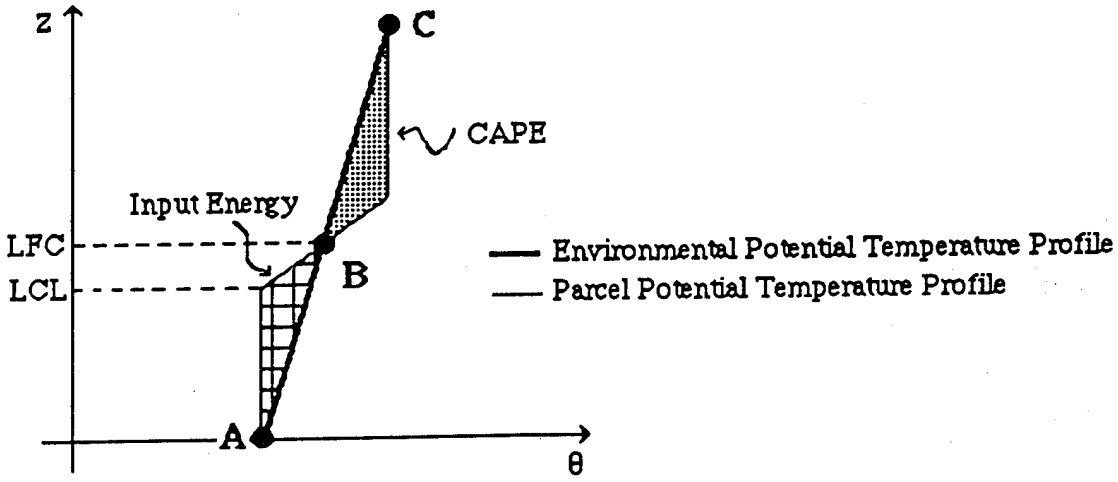

Figure 1: CAPE as defined for the simpler thermodynamic systems herein. Note that A, C are stable equilibrium points and that B is an unstable equilibrium point of the Lagrangian dynamics.

In Figure 1, the parcel undergoes dry (constant θ) motions until it becomes saturated at height LCL, and then begins to warm by the latent conversion of moisture into sensible heat. At height LFC, it reaches a level where it has the same bouyancy as its surrounding environment, and any further upward motion allows the parcel to tap into a source of potential energy, as the latent release of heat as the parcel rises warms it at a rate exceeding

that of the lapse rate of the environment. The shaded area in Figure 1 then represents the amount of kinetic energy the parcel will have when it reaches point C, where it again is neutrally bouyant. It can be seen immediately that points A and C are stable equilibria for the parcel, and point B is an unstable equilibria. Hence, this type of moist instability is referred to as *conditional*, as a certain amount of energy must be supplied to the parcel to get it to point B, where it can release its CAPE.

4. Generalizations of CAPE to finite amplitude perturbations

As it stands, there are several inherently unsatisfying aspects to the Lagrangian CAPE as outlined above. Most disconcerting of these is that the theory is a parcel theory — it does not take into account the effect of the parcel on the environment. Therefore, we would like a generalized theory of CAPE which would allow us to consider all perturbations to the moist atmosphere, analogous to that for dry convection as outlined in section 2.

As such, we would like to define an APE for the moist case analogous to the dry APE defined earlier, *viz*

$$APE \sim \int\int_D \int^{\eta} [C(\bar{\eta}+\eta') - C(\bar{\eta})] d\eta' \, dx \, dz \tag{26}$$

where η is quantity conserved by the flow, $\bar{\eta}$ is a stable reference state of that quantity, and C is analogous to a Casimir. For the moist systems to be considered shortly, the conserved quantity is

$$\eta = \theta + m(z_{sat}) \tag{27}$$

where θ is a usual the potential temperature, and $m(z_{sat})$ represents a temperature perturbation due to the moisture within a given parcel, which is a function of the height at which a given parcel of air becomes saturated.

The quantity $m(z_{sat})$ for a parcel requires defining a saturation moisture profile for our system. This is most simply done in terms of a saturation height, $z_{sat}(x,z,t)$ which is simply the height at which the parcel's thermodynamic evolution shifts from dry to moist adiabatic motion. $z_{sat}(x,z,t)$ can be simply defined as

$$z_{sat}(x,z,t) = \max\{z_{sat}(x_0,z_0,0), \max\{z(t)\}\} \tag{28}$$

where x_0 and z_0 are the initial position of the parcel, where this quantity is considered in a domain $x \in [-L/2, L/2]$, $z \in [-H/2, H/2]$. This then leaves our conserved quantity as

$$\eta = \theta + k(H/2 - z_{sat}) \tag{29}$$

while the thermodynamic equation is simply

$$\frac{D\theta}{Dt} = \begin{cases} kw & z = z_{sat} \\ 0 & z < z_{sat}. \end{cases} \tag{30}$$

This condition on the moisture evolution is equivalent to "raining" out all the moisture above saturation instantaneously, with its latent energy going to heat the parcel.

a. What is a stable basic state?

One of the requirements for the application of Hamiltonian APE ideas to the moist non-adiabatic problem is that we can define a stable basic state. As the example in section 2 showed, it was the ability to define that basic state and treat the unstable state as a finite amplitude perturbation that led to the abililty to construct bounds on the APE.

For the Hamiltonian case, this determination simply amounts to finding whether or not the basic flow is a true extremum of the pseudoenergy $\mathcal{A}$, which can be calculated by examining the second variation $\delta^2\mathcal{A}$. Such a determination for the Hamiltonian case leads to a condition for *arbitrary* perturbations to the flow; in other words, nonlinear stability.

In this moist non-adiabatic case, however, we have no Hamiltonian structure to guide us in defining a stable basic state. Hence, we must confine ourselves to the case of infinitesimal perturbations, as well as defining our basic state from other physical principles. The major point is that we want to use the dry (or moist) adiabatic stability concepts as a guide.

As such, we define a stable basic state as one which is stable to both dry and moist adiabatic disturbances. Under this assumption, several facts are immediately apparent:

1. Any state which has the identical dry and moist saturated profiles as a stable basic state but which is undersaturated will also be stable.

2. Stability depends on the magnitude of the total temperature perturbation η, rather than its slope as in the dry case.

These two results indicate that the moist non-adiabatic case is significantly different from the dry case examined in section 2, so much so that straightforward application of the Hamiltonian APE of the form in equation (26) is impossible! Hence, we must attempt another approach, namely reduction to a dry state and then application of the Hamiltonian APE thinking.

b. Reduction to dry state

In order to reduce our moist system to an equivalent dry system, we must first make a relation between moist and dry states. To do this, we choose to equate the dry neutral state $\theta(z)$ =constant with the moist neutral state $\eta(z)$ =constant. It is perhaps best to first review what assumptions we are making in doing this. From the definition of Lagrangian CAPE, it is immediately apparent that any type of moist APE will be strongly dependent on the mean temperature profile of the atmosphere in which it evolves. Lagrangian parcel dynamics gets around this by assuming that the mean state is fixed. For an atmospheric case which is strongly stably stratified to dry motions, a logical assumption is that dry motions (i.e. vertical mixing of θ) will be strongly inhibited. Hence, the effect of the moist convection will be to simply raise the average temperature of the atmosphere, not adjusting its dry static stability. In a sense, parcels which are warmer by virtue of containing moisture will quickly rise to the top, but downward motions will consist of slow subsidence. Such is the case in active convective regions of the Earth's atmosphere, such as the tropics.

Before we undertake such a procedure, it is useful to lay out our expectations. First, we expect that the Lagrangian CAPE will represent an upper bound to any CAPE we may calculate. Why? Simply because it does not take into account any mean temperature

profile modification. Also, we expect our reduction process to be non-local, that is, it will have to take into account the entire temperature profile of the fluid. This is again due to the non-locality of moist convective processes – the mean temperature of the profile is what determines the accessibility to APE, not the local gradients θ gradients, as in the dry case.

b. Example: Straightforward use of adjusted η profile.

As a first approach, we can simply ignore any mean temperature profile feedbacks, and calculate the APE from the η profile just as we would in the dry case. Consider a basic state consisting of the stable potential profile

$$\theta^{(0)}(z) = \frac{\theta_0}{H}\alpha z \tag{31}$$

and saturation height profile

$$z_{sat}(z) = z, \tag{32}$$

i.e. an initially saturated atmosphere. The stability of our mean state is then controlled by our choice of the moist adiabatic lapse rate k; examination of

$$\eta^{(0)}(z) = \theta^{(0)} + \frac{k\theta_0}{H}(H/2 - z_{sat}) \tag{33}$$

shows that $k > \alpha$ implies instability. Our neutral basic state is $k = \alpha$; this leaves our reduced (dry equivalent) problem as

$$\theta^{(0)}_{red}(z) = \frac{(k-\alpha)\theta_0}{H}z \tag{34}$$

which is the identical problem considered in the example in section 2 if we equate $\epsilon \equiv k - \alpha$, which gives the result for the APE of

$$APE = \frac{gH^2L(k-\alpha)}{6}. \tag{35}$$

This can be compared to the Lagrangian CAPE for the whole domain, which is

$$CAPE = \frac{g}{\theta_0}\int\int_D\int_z^{H/2}(k-\alpha)z'\,dz'\,dx\,\mathrm{dz} \tag{36}$$

$$= \frac{gH^2L(k-\alpha)}{6} \tag{37}$$

As is clear from the above, straightforward application of the "adjusted" profile gives a result identical to the Lagrangian CAPE. Is this true in general? No. An easy example would be to consider a situation where the atmosphere is saturated for $z < 0$ and completely dry for $z > 0$. For such an example, the equivalent dry APE is larger than in the case examined here, but the Lagrangian CAPE is somewhat smaller. Examples where the Lagrangian CAPE is larger than the APE are also easy to come up with.

Note that we expected the Lagrangian CAPE for the whole domain to be an overestimate of the APE available for a moist diabatic disturbance, so it is natural to ask if a correction can be made to this. The answer appears to be no, as doing so removes us from the realm of direct analogy with the dry Hamiltonian case. In addition, the example above showed us that the relationship between Lagrangian CAPE and the equivalent dry profile is not well defined. It appears that a reduction procedure cannot be done rigorously (or even consistently, for that matter), and as the above indicates, the whole question is not well posed.

c. Comments

Some observations about this whole procedure are immediate:

1. Moist convective system vastly different from dry. The profile of the conserved quantity does not determine stability – rather the entire temperature profile does.

2. Hamiltonian APE ideas appear not to be able to be consistently applied.

3. Any calculation will in a sense be ad hoc – without Hamiltonian structure as a guide, it is difficult to see how to proceed. In particular, it is not clear how to work feedbacks into the problem.

4. Discussion

The question of how to fit the diabatic effects of moisture into atmospheric energetics has been a topic of considerable theoretical interest for many years. Insofar as moist processes in the atmosphere are adiabatic, straightforward application of Hamiltonian methods such as those outlined in section 2 should allow for the proper treatment of moisture in constructing APE budgets for various atmospheric fluid systems. However, as has been shown above, the generalization of these methods to diabatic moist convection is not possible in a rigorous or even a consistent manner. Moisture is and will remain a significant barrier to a complete theoretical understanding of energetics in problems where it plays a significant role.

Acknowledgements

I would like to thank Ted Shepherd for introducing me to moisture and Hamiltonian pseudoenergy methods, and the whole GFD staff for providing many new and different perspectives into the diverse field of GFD.

References:

Shepherd, T.G. , 1993: A unified theory of available potential energy. *Atmos. Ocean.*, **31**, 1-26.

Benjamin, T. B., 1986: On the Boussinesq model for two-dimensional wave motions in heterogeneous fluids. *J. Fluid Mech.*, **165**, 445-474.

Thorpe, A. J., B. J. Hoskins and V. Innocentini, 1989: The parcel method in a baroclinic atmosphere. *J. Atmos. Sci*, **46**, 1274-1284.

On Aspects Of Benney's Equation

Rodney A. Worthing
Department of Mathematics, MIT

Introduction

The PDE under investigation is

$$\begin{aligned} u_t + uu_x + \nu u_{xx} + \mu u_{xxx} + u_{xxxx} = 0 \\ -\pi \leq x \leq \pi, \qquad \nu \geq 0,\ \mu \geq 0, \end{aligned} \tag{1}$$

where u is considered to be periodic in x as an apology for the infinite domain. This equation seems rich in character and has been derived in several physical contexts including the flow of thin liquid films (Benney 1966, Topper and Kawahara 1977). Starting from arbitrary initial conditions, the solutions to (1) often ultimately form pulse-like structures that qualitatively maintain their respective positions but may or may not "lock in" to form a steadily traveling pulse train. Should they "lock in", then numerical simulations and asymptotic weak interaction theory show that the final spacings are not unique (Kawahara 1983, Elphic at al. 1991, Balmforth 1993). Also as a certain parameter, ν, is increased these states lose stability and interesting perturbative dynamics result. These dynamics are the focus of this work. By example, the general type of bifurcation is isolated and the responsible mechanism discussed. Though, a general simple theory (like an extension of weak interaction theory which would reduce the dynamics to simply the time-dependent positions of the pulses) is, yet, elusive.

With only two parameters (ν and μ) this equation is actually a nondimensional version of

$$\tilde{u}_{\tilde{t}} + \tilde{u}\tilde{u}_{\tilde{x}} + \tilde{\nu}\tilde{u}_{\tilde{x}\tilde{x}} + \tilde{\mu}\tilde{u}_{\tilde{x}\tilde{x}\tilde{x}} + \tilde{\lambda}\tilde{u}_{\tilde{x}\tilde{x}\tilde{x}\tilde{x}} = 0, \qquad -\tilde{L} \leq \tilde{x} \leq \tilde{L} \tag{2}$$

with

$$\nu = \frac{\tilde{L}^2\tilde{\nu}}{\pi^2\tilde{\lambda}}, \qquad \mu = \frac{\tilde{\mu}\tilde{L}}{\tilde{\lambda}\pi} \tag{3}$$

There are other nondimensional forms but this choice is natural since it necessarily includes the u_{xxxx} term, as it is required to insure solutions remain bounded for $\tilde{\nu} \geq 0$. This point follows by inspection of the following energy equation which is valid for periodic boundary conditions:

$$< \frac{1}{2}u^2 >_t = \nu < u_x{}^2 > - < u_{xx}{}^2 >, \qquad < (\cdot) > \equiv \frac{1}{2\pi}\int_{-\pi}^{\pi}(\cdot)dx \tag{4}$$

Also implied by this equation is that the general role of both the uu_x nonlinear term and the u_{xxx} term is simply to redistribute energy *locally* (a wave-like mechanism), leaving the overall energetics unchanged. In Burgers' equation

$$u_t + uu_x - \nu u_{xx} = 0, \ \ \nu > 0, \ \Rightarrow \ < \frac{1}{2}u^2 >_t = -\nu < u_x^2 > \tag{5}$$

it is precisely this nonlinear term that is solely responsible for the development and propagation of shocks. Likewise, it is solely the dissipative term $-u_{xx}$ that forces *all*

solutions to eventually decay away to zero in the absence of an energy source at the boundaries (as is the case for periodic or $u = 0$ boundary conditions). For Benney's equation, the u_{xxxx} term has acquired the dissipative role but the sign reversal on the u_{xx} term has turned it into an internal energy *source*. Indeed, this is the term responsible for the creation and sustentation of pulses.

Steady Traveling Solutions

In this section we discuss some general features of the steady solutions to (1), construct a few approximate solutions using weakly nonlinear theory (Malkus and Veronis 1958) and discuss their stability. Recall that we are ultimately interested in the dynamics after these solutions go unstable.

Benney's equation has Galilean invariance. That is, if you have a solution $u(x,t) = U(x,t)$ to an initial value problem $u(x,0) = u_0(x)$ then the solution to the initial value problem $u(x,0) = u_0(x) + c$, where c is a constant, is $u(x,t) = U(x - ct, t) + c$. Roughly speaking, lifting up u also speeds it up. Thus, all of the nontrivial dynamics are identical and occur on the same time scale no matter the Galilean boost. With this in mind we are free to choose, say $< u >= 0$, as a restriction on the class of steady solutions we investigate since all others are obviously related. Such steady u are described by an eigen-pair $\{H, c\}$ where $u(x,t) = H(\xi)$, $\xi = x - ct$ and

$$-cH' + HH' + \nu H'' + \mu H''' + H'''' = 0, \qquad < H >= 0. \tag{6}$$

As in (Elphick, et al. 1991) this nonlinear eigenvalue problem is solved numerically using orthogonal expansion techniques.

Unlike both the Burgers and the KdV equations, the zero solution to Benney's equation is usually unstable as a consequence of the inclusion of the energy production term u_{xx}. Instability of the $u = 0$ solution can be demonstrated by linear theory. Normal modes of the form

$$u \propto e^{ikx} e^{i\omega t} e^{\sigma t} \tag{7}$$

solve the linear version of (1) provided

$$\sigma = \nu k^2 - k^4, \quad \omega = \mu k^3, \quad k = 0, 1, 2, \cdots \tag{8}$$

Notice that the $k = 0$ mode is *always* neutral reflecting the fact that $< u >$ is also conserved by the linearized version of (1). To make things simpler, we consider only disturbances having zero mean so that the effect of boosting up and down is factored out. It is clear from (8) that temporal growth of small disturbances is determined only by the struggle between the u_{xx} and u_{xxxx} terms with ν emerging as the relevant bifurcation parameter. Due to the discreteness of k, we see that $u = 0$ is linearly stable if $\nu < 1$ and linearly unstable if $\nu > 1$. Near the marginal point, the least damped disturbance is a long wave e^{ix} that travels at the finite phase speed of roughly $-\mu$ as it grows or decays. To display this point, Figure 1 shows an initial value run starting with energy in several modes at a slightly subcritical value of $\nu = .95$. Actually to obtain Figure 1 we integrated the full equations and we didn't start with initial conditions that were all that small, yet still the zero solution was the long time limit. This will always be the

case, provided $\nu < 1$, as can be shown by energy theory (Elphick et al. 1991). Using the Poincare inequalities (as adapted for this periodic domain)

$$< u^2 > \leq < u_x^2 >, \quad \text{and} \quad < u_x^2 > \leq < u_{xx}^2 >, \tag{9}$$

(5) implies

$$\frac{1}{2} < u^2 >_t \leq (\nu - 1) < u_{xx}^2 > \tag{10}$$

which shows that $< u^2 >$ ever decreases until there is no curvature. In a periodic domain, this means that the solution becomes a constant and since we only admit disturbances with zero mean, then this constant must be zero as a consequence of the conservation of $< u >$ by equation (1). Expecting that these linear instabilities saturate forming equilibrated states, we introduce the expansions

$$\begin{aligned} u &= \epsilon u_1 + \epsilon^2 u_2 + \epsilon^3 u_3 + \cdots \\ \nu &= \nu_0 + \epsilon^2 \nu_2 + \cdots \\ \omega_0 t &= (1 + \epsilon^2 \omega_2 + \cdots)\tau \end{aligned} \tag{11}$$

where ϵ measures the contribution of a fundamental linear eigen-mode in the equilibrated 2π periodic (in τ) steady state. Plugging into (1) and equating terms of equal order in ϵ provides the following sequence of linear PDE's:

$$\begin{aligned} O(\epsilon) &: \ \mathcal{L}_0(u_1) = \omega_0 (u_1)_\tau - L_0(u_1) = 0 \\ O(\epsilon^2) &: \ \mathcal{L}_0(u_2) = \omega_0 (u_2)_\tau - L_0(u_2) = N_2 \\ O(\epsilon^3) &: \ \mathcal{L}_0(u_3) = \omega_0 (u_3)_\tau - L_0(u_3) = L_2(u_1) + \omega_2 L_0(u_1) + N_3 \end{aligned} \tag{12}$$

where we have defined

$$\begin{aligned} L_0 &= -\nu_0 \partial_{xx} - \mu \partial_{xxx} - \partial_{xxxx} & N_2 &= -\tfrac{1}{2}(u_1^2)_x \\ L_2 &= -\nu_2 \partial_{xx} & N_3 &= -(u_1 u_2)_x. \end{aligned} \tag{13}$$

The first equation, of course, has many solutions each corresponding to a different number of pulses, i.e.

$$u_1 = e^{i(\tau + kx)} + \text{ c.c.}, \quad \nu_0 = k^2, \quad \omega_0 = \mu k^3, \quad k = 1, 2, 3... \tag{14}$$

We know that for small enough ϵ any steady state associated with $k > 1$ must be unstable to roughly a $k = 1$ mode. This is inferred from the linear stability theory of the zero state which, of course, is the steady state profile limit as $\epsilon \to 0$. However, should ϵ be larger, then it is possible (and apparently the case) that these higher mode steady states can stabilize, at least for some finite range of ν. We therefore leave k arbitrary for now and continue on to the next order with the reservation that all of the steady branches, with the exception of $k = 1$, must initially be unstable as they branch off the unstable zero state. Using elementary techniques the forced equation for u_2 is easily solved,

$$u_2 = \mathcal{L}_0^{-1} \left\{ -ike^{2i(\tau + kx)} + \text{ c.c.} \right\} = \gamma(k) e^{2i(\tau + kx)} + \text{ c.c.} \tag{15}$$

where

$$\gamma(k) = \frac{6k\omega_0 - i(12k\nu_0^2)}{(12\nu_0^2)^2 + (6\omega_0)^2}. \tag{16}$$

Also note that by the definition of ϵ, we have excluded the homogeneous solution when computing u_2. At the next order we find a forcing that would not permit u_3 to be periodic, unless we choose

$$\nu_2 = \frac{\nu_0^2}{12\nu_0^2 + 3\omega_0^2} \quad \text{and} \quad \omega_2 = \frac{\nu_0}{24\nu_0^4 + 6\omega_0^2} \tag{17}$$

from which we can calculate the approximate amplitude and speed of the resulting steady state,

$$\epsilon = \sqrt{(12k^4 + 3\mu^2 k^2)(\nu - k^2)}, \qquad c = -\mu k^2 + \frac{1}{2}(\nu - k^2). \tag{18}$$

So, at least near the bifurcation points in ν, $H_{\max}$ increases linearly with μ and as the square root of ν. This compliments the observation of Kawahara (1983), based on steady states obtained by time integrating (1), that in general the height of the resulting steady pulse train increases, approximately linearly, with the dispersion parameter μ. For very large μ, evidently, a KdV-like balance between the uu_x and u_{xxx} terms is obtained for each pulse with the final, delicate spatial arrangements determined by higher order contributions from the other terms. By considering some integral consequences of (18), namely

$$\nu < (H')^2 >=< (H'')^2 > \text{ and } \quad c < (H')^2 > - < H(H')^2 > +\mu < (H'')^2 >= 0, \tag{19}$$

we see *any* steady solution must satisfy

$$c + \mu\nu = \frac{< H(H')^2 >}{< (H')^2 >} \tag{20}$$

and therefore

$$H_{\min} \leq c + \nu\mu \leq H_{\max}. \tag{21}$$

At first glance the relation (21) hints at the tendency of $H_{\max}$ to increase with μ and ν but without more information, like useful bounds from below on $c(\mu, \nu)$, no such claims can be made.

For $\mu = 1$, Figure 2 shows three of the branches given by (18) (corresponding to one, two and three pulse solutions) along with some numerically calculated data points (marked with '*', '+' and '*' again) representing the actual range of *stable*, steady solutions[1]. As expected, stable solutions of the two and three pulse type do not extend down to $\epsilon = 0$ yet the finite-amplitude theory still seems useful as it approximates these solutions once they stabilize. Next we provide an estimate for the smallest value of ν for which a stable, two pulse solutions exists by doing an approximate linear stability analysis on the approximate steady states acquired from the weakly nonlinear theory.

The equation governing *small* deviations from an exact steady solution $\{H, c\}$ is

$$v_t - cv_\xi + (Hv)_\xi + \nu v_{\xi\xi} + \mu v_{\xi\xi\xi} + v_{\xi\xi\xi\xi} = 0 \tag{22}$$

[1]These points were calculated by solving the eigenvalue problem (6) plus the appropriate linear stability problem using spectral methods.

where $u = H + v$. Our plan is to substitute approximate steady states into (22) and estimate a stability criterion[2]. Taking $k = 2$ and thus introducing

$$H(\xi) = \epsilon e^{2i\xi} + \text{ c.c.}, \quad c = -4\mu + \frac{1}{2}(\nu - 1), \quad \epsilon = 2\sqrt{(48 + 3\mu^2)(\nu - 4)} \tag{23}$$

into (22), we see two suitable expansions for v are

$$v = e^{\sigma t} e^{i\alpha\xi} \left[\sum c_n e^{2in\xi}\right], \quad \alpha = 0 \text{ or } 1 \tag{24}$$

The choice $\alpha = 1$ is appropriate since for small enough ϵ we can infer from the analysis of the zero solution that the instability ought to have the form $e^{i\xi}$. We radically truncate (24) to

$$v = e^{\sigma t} \left\{c_1 e^{i\xi} + c_{-1} e^{-i\xi}\right\}, \tag{25}$$

insert into (22), neglect higher harmonics produced by $(Hv)_\xi$, and obtain a simple 2 by 2 eigenvalue problem for σ from which it follows that H is unstable if

$$\epsilon^2 \leq (c + \mu)^2 + (\nu - 1)^2. \tag{26}$$

For $\mu = 1$ the transition according to (26) occurs at $\nu \approx 4.1$. If we include the $e^{3i\xi}$ and $e^{-3i\xi}$ modes in (25) we obtain an improved transition value of $\nu \approx 5.1$. Both of these approximations are represented on the 2-pulse branch in Figure 2 by 'o'. These values should be compared to $\nu \approx 5.5$ obtained from an accurate stability analysis of the weakly nonlinear approximate state, and $\nu \approx 5.7$ obtained from an accurate stability analysis of an accurate steady state.

Pulse Dynamics

In this section we discuss the dynamics just after a steady train of pulses go unstable as a result of increasing the parameter ν. For the one, two and three pulse cases, Figure 2 shows where such regions roughly begin by the last point in each of the three sequences of data shown. In all three cases, the linear stability analysis shows that stability is lost as a pair of complex growth rates cross the imaginary axis. Direct numerical simulations, by spectral methods, show that these bifurcations are supercritical with saturation of unstable eigenfunctions easily occurring in regions just beyond the critical points. Figure 5 displays this type of quasi-steady behavior in the case of three pulses at a post-critical value of $\nu = 18$. The dynamics may be described as repeated attempts to bring in one more pulse. This 'extra pulse' appears to move backwards through the pulse train as it tries to pop up where two larger pulses have been sufficiently separated. The larger pulse on its left then seems to overtake the 'extra pulse', but in the process creates room to its left, inducing another growth. Solutions of this type naturally have two distinct time scales (the average propagation speed of the group of pulses, and the frequency of the inter-pulse oscillations) and so cannot appear steady in any reference frame. The resulting

[2]Of course, any *approximate* solution must really be unstable according to the *exact* equations, but by assuming (6) to be satisfied, whether it is or not for our particular choice of $\{H, c\}$, we seem to arrive at a somewhat robust stability problem (22) in which approximate steady states can be meaningfully analyzed.

$u(x,t)$ will be a periodic function in space and most likely only an *almost* periodic function in time. By using weakly nonlinear theory we can provide a fairly simple representation of these time-dependent solutions. We take the three pulse case as an example. At its point of bifurcation, $\nu \approx 17.324$ (for $\mu = 1$), H along with the eigenvalues coming from the associated linear stability problem (22) are plotted in Figures 3 and 4, respectively.[3]

We expand near this solution by carrying out a weakly nonlinear calculation that also provides a description of the time-dependent approach to the final quasi-steady state. As before we set $u(x,t) = H(\xi) + v(\xi,t)$ where $\{H, c\}$ satisfy (6) and therefore v satisfies the complete version of (22),

$$\mathcal{L}(v) = -\frac{1}{2}(v^2)_\xi \quad \text{where} \quad \mathcal{L} = \partial_t - c\partial_\xi + \partial_\xi(H\cdot) + \nu\partial_{\xi\xi} + \mu\partial_{\xi\xi\xi} + \partial_{\xi\xi\xi\xi}. \tag{27}$$

We expand in the following manner

$$\begin{aligned} v &= \epsilon v_1 + \epsilon^2 v_2 + \cdots \\ t &= \tau + \epsilon^2\tau = \tau + T \\ \nu &= \nu_0 + \epsilon^2\nu_2 + \cdots \\ H &= H_0 + \epsilon^2 H_2 + \cdots \\ c &= c_0 + \epsilon^2 c_2 + \cdots \end{aligned} \tag{28}$$

with ν_0, c_0 and H_0 being the marginal values eluded to earlier, and obtain the sequence

$$\begin{aligned} O(\epsilon) &: \ \mathcal{L}_0(v_1) = (v_1)_\tau - L_0(v_1) = 0 \\ O(\epsilon^2) &: \ \mathcal{L}_0(v_2) = (v_2)_\tau - L_0(v_2) = -\tfrac{1}{2}(v_1^2)_\xi \\ O(\epsilon^3) &: \ \mathcal{L}_0(v_3) = (v_3)_\tau - L_0(v_3) = -\mathcal{L}_2(v_1) - (v_1 v_2)_\xi \end{aligned} \tag{29}$$

where

$$\mathcal{L}_0 = \partial_\tau - c_0\partial_\xi + \partial_\xi(H_0\cdot) + \nu_0\partial_{\xi\xi} + \mu\partial_{\xi\xi\xi} + \partial_{\xi\xi\xi\xi} \quad \text{and} \quad \mathcal{L}_2 = \partial_T - c_2\partial_\xi + \partial_\xi(H_2\cdot) + \nu_2\partial_{\xi\xi}. \tag{30}$$

Consistent with the $O(\epsilon)$ equation, we take v_1 to have the form of the marginal Hopf mode, so that

$$v_1 = A(T)\phi(\xi)e^{i\omega\tau} + \text{ c.c.} \qquad \text{where} \quad L_0(\phi) = i\omega\phi, \quad \omega \in \Re. \tag{31}$$

The $O(\epsilon^2)$ equation is a well set BVP for v_2 and so the amplitude evolution equation

$$< \phi^\dagger\phi > A_T + < \phi^\dagger(\nu_2\phi_{\xi\xi} + (H_2\phi)_\xi - c_2\phi_\xi) > A + < \phi^\dagger(\beta\phi + \alpha\phi^*)_\xi > |A|^2 A = 0 \tag{32}$$

is obtained at $O(\epsilon^3)$ as a solvability condition. The two functions $\alpha(\xi)$ and $\beta(\xi)$ originate from the particular solution for v_2 and are determined numerically by the solving the BVPs

$$L_0(\alpha) - 2i\omega\alpha = \phi\phi_\xi \quad \text{and} \quad L_0(\beta) = (\phi\phi^*)_\xi. \tag{33}$$

Also, just as $\{i\omega, \phi\}$ is an eigen-pair of the operator L_0, $\{i\omega, \phi^\dagger\}$ is an eigen-pair of the adjoint operator $L_0^\dagger$ and its existence has been verified numerically. In this formulation

[3] As evident from Figure 3 we have not consistently required $< H >= 0$.

we are free to choose ν_2 from which ϵ, c_2 and H_2 are calculated from (6). The quasi-steady field predicted by these calculations at $\nu = 18$ is shown in Figure 6 and should be compared to Figure 5. We have yet to check whether the quantitative discrepancies are within the expected accuracy of the theory.

Appendix

In this appendix we explore numerically a class of steady solutions to

$$u_t + uu_x + \nu u_{xx} + \lambda u_{xxxx} = 0 \tag{34}$$

with the *fixed* boundary conditions $u(\pm 1) = \mp 1$ and, if $\lambda \neq 0$, $u_x(\pm 1) = 0$. The purpose is to provide another simple setting in which comparisons with the more familiar Burgers equation can be made. Consider the cases:

- $\lambda = 0$, and a range of *negative* ν (Burgers)
- $\nu = 0$, and a range of *positive* λ (Figure 7)
- $\lambda = 1$, and a range of *positive* ν (Figure 8).

Simple *tanh* solutions exist for the case $\lambda = 0$, and so as ν approaches zero, these stationary fronts steepen and always maintain their monotonicity. When the $-u_{xx}$ dissipation is replaced with u_{xxxx} we see the same general steepening of the front as λ is decreased, but we also see an additional oscillatory feature that appears most significant very near the shock interface - see Figure 7. Profiles quite different from these are shown in Figure 8. Those having more oscillations are associated with larger values of ν, a feature reminiscent of the periodic pulses. A remarkable feature of this class of profiles is that drastic changes in amplitude occur during the transitions where the number of oscillations increase. Figure 9 and Figure 10 are intended to display this point. Figure 9 shows this entire class as a surface plot, but perhaps Figure 10, by simply plotting the global measure $< u^2 >$, shows this transition phenomenon most clearly.

Acknowledgements

N.J. Balmforth and I have collaborated to produce much of this work. G.R. Ierley kindly offered access to his computer and his programs, both of which have benefited this work. I appreciate the helpfulness of the entire GFD staff, especially A. Woods and L. Howard.

References

Balmforth, N. J., Ierley, G. R. and Spiegel, E. A. (1993) *Chaotic pulse trains*, to be submitted.

Benney, D. J., (1966) *Long waves on liquid films*, J. Math. Phys. **45**, 150-155.

Elphick, C., Ierley, G. R., Regev, O. and Spiegel, E. A. (1991) *Interacting localized structures with Galilean invariance*, Phys. Rev. A. **44**, 1110-1122.

Kawahara, T. (1983) *Formation of saturated solitons in a nonlinear dispersive system with instability and dissipation*, Phys. Rev. Lett. **51**, 381-383.

Topper, J. and Kawahara, T, (1978) *Approximate equations for the long nonlinear waves on a viscous fluid*, J. Phys. Soc. Japan **44**, 663-666.

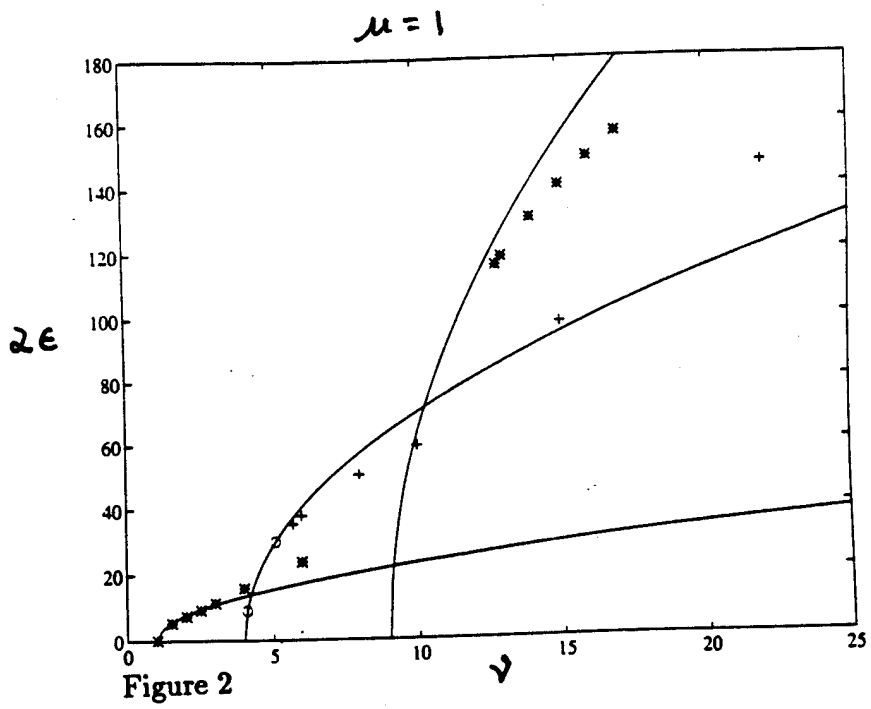

Figure 2

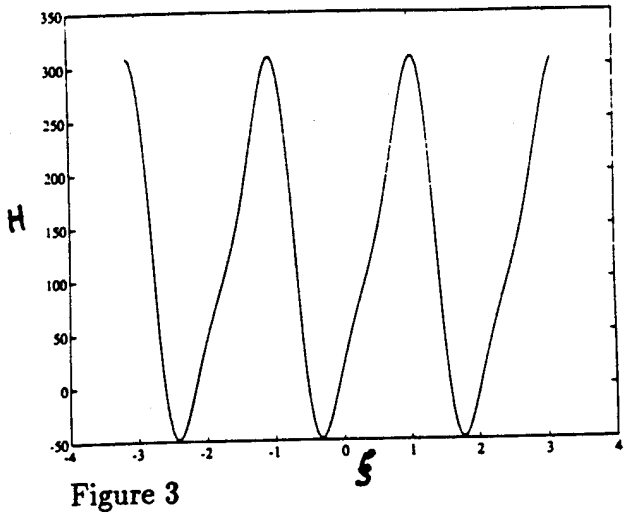

Figure 3

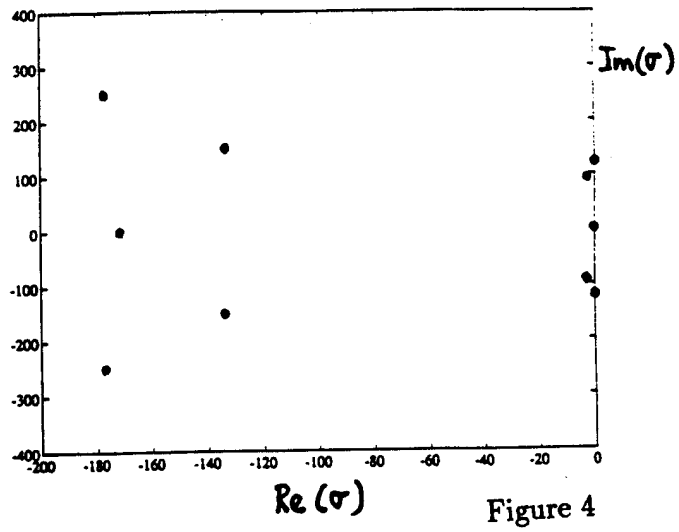

Figure 4

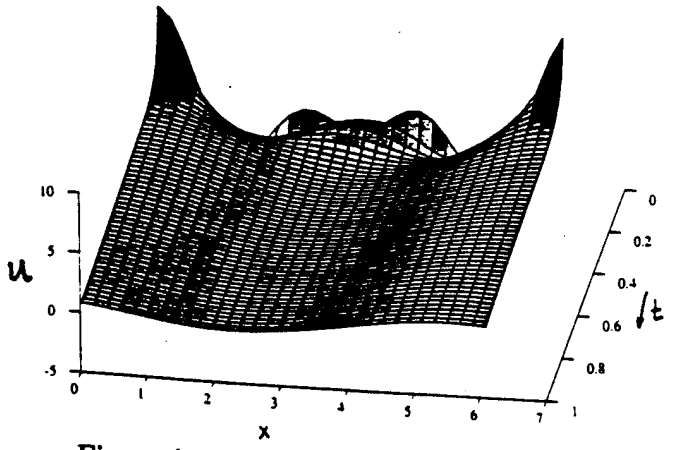

Figure 1

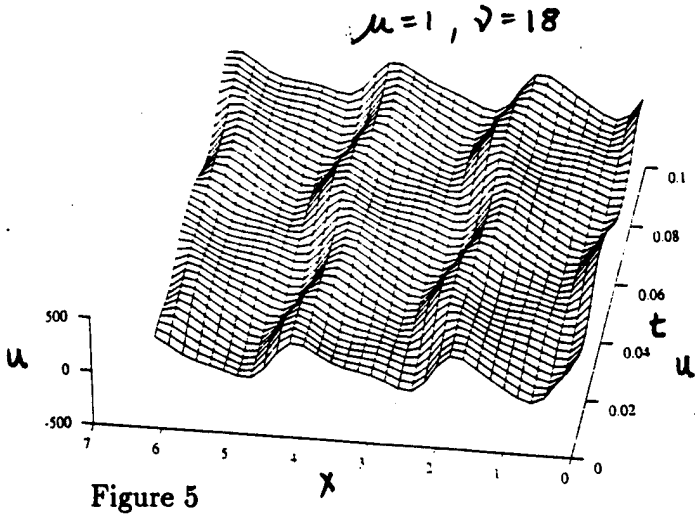

Figure 5

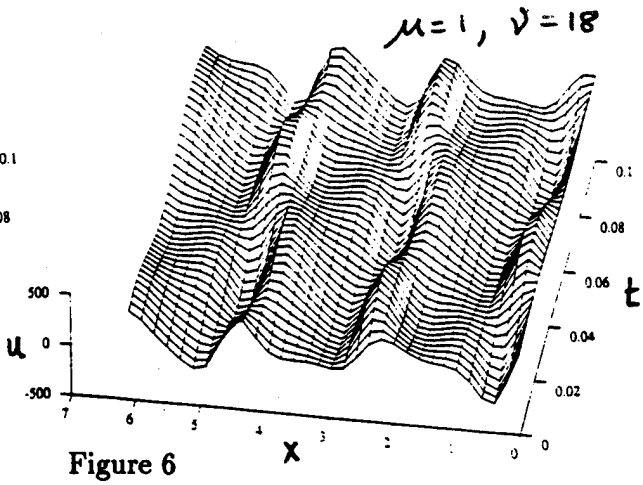

Figure 6

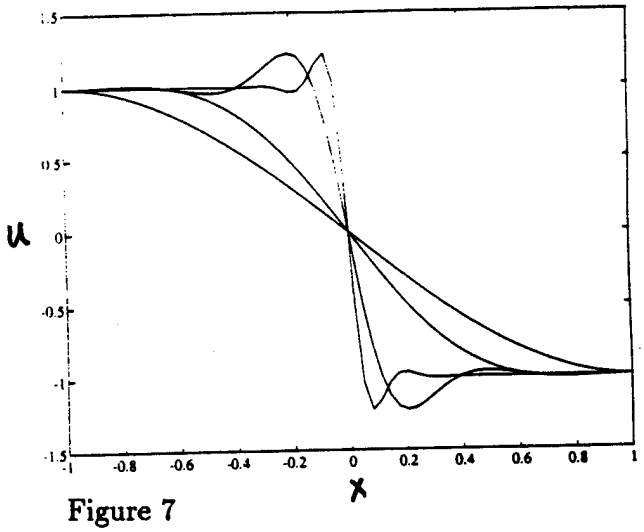

Figure 7

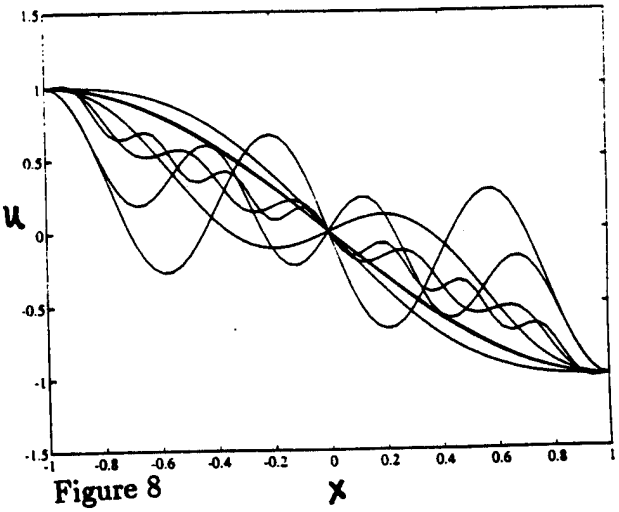

Figure 8

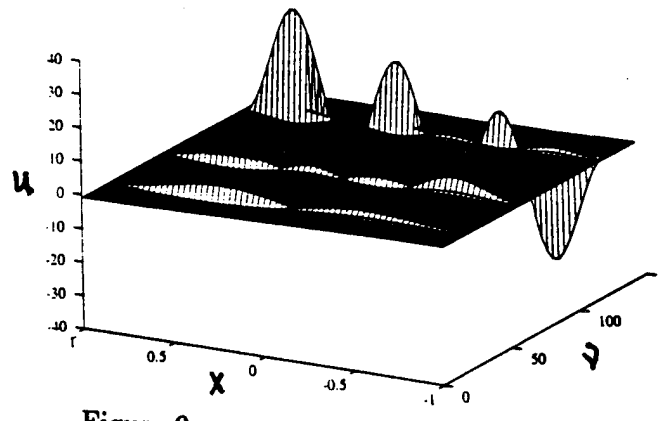

Figure 9

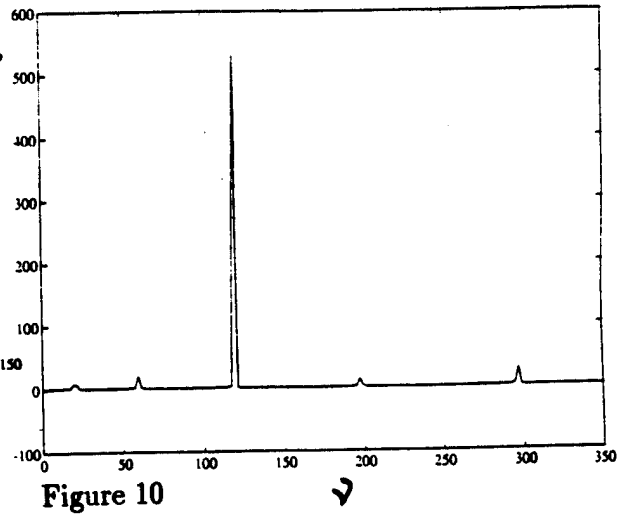

Figure 10

Coherent Structures and Homoclinic orbits

N.J. Balmforth

In the physics of fluids, the dynamics of coherent structures plays a central role. These localized objects appear in laminar flows and persist in turbulent states. In some situations the coherent structures take the form of solitary waves, and this lecture reviewed recent experiments observing the formation and interactions of such objects. It further described the derivation of approximate equations modelling these objects, and discussed the connection between the solitary wave solutions of such equations and the orbits of a dynamical system. Finally, aspects of the theory of pulse interactions were mentioned.

Coherent fluid structures

The concept of a solitary wave, though widespread in physics nowadays, originated first in fluid dynamics after Russell's historic observation of a coherent, propagating structure in the Edinburgh canal. Since that observation, the notion that fluid motion often organizes itself into localized states permeates modern fluid dynamics. In this lecture, specific examples occuring in binary fluid convection and on a falling fluid film were described in some detail.

In binary fluids, sequences of experiments in thin annuli clearly demonstrate the creation of localized states of travelling convection.[1,2] These states consist of a compact pattern of rolls whose envelope moves around the annulus. In many cases, several such "convective pulses" coexist within the annulus, and this leads to an experimental visualization of pulse dynamics, which which range from steady interaction to temporal chaos.

In falling fluid films, solitary structures also occur. These are visible in drying paint and on windows on rainy days. They arise through the linear instability of a film of uniform thickness which grows to a finite-amplitude state of a sequence of propagating solitary waves.[3] These sequences are described by certain solitary wave speeds and particular pulse separations, and can generate spatially disordered patterns. Other states take the form of a succession of rippled, hydraulic jumps.

Model equations

The solitary structures observed in systems like the binary fluid convection occur near the Hopf bifurcation of a spatially extended (one-dimensional) system. In this circumstance, the equations governing the fluid can be asymptotically reduced to a complex Ginzburg-Landau equation governing the spatio-temporal evolution of the envelope of a single wave packet.[4]

A simple example of a system reducing to complex Ginzburg-Landau near marginality is the partial differential equation,

$$\partial_t u + u\partial_x u + \partial_x{}^2 u + \mu\partial_x{}^3 u + \partial_x{}^4 u + \alpha u = 0 \quad , \tag{1}$$

where μ and α are parameters. This equation arises in studies of falling fluid films[5] and in plasma instabilities. For a film, u is the surface displacement about a uniformly thick state, and α is normally zero, but here we vary it continuously through positive values to precipitate a Hopf bifurcation.

The equilibrium state $u = 0$ bifurcates to instability for $\alpha = 0.5$. If we expand about this critical state, $\alpha = 0.5 + \varepsilon^2\alpha_2$, and introduce stretched timescales and lengthscales, then equation (1) can be decomposed into a set of equations of successively higher-order in ε. Applying solvability conditions at each order eventually yields the Ginzburg-Landau equation,

$$\partial_\tau A = \beta A + D\partial_\xi{}^2 A + \gamma|A|^2 A \tag{2}$$

for the amplitude of a propagating wave packet. Here, τ is the slow timescale on which the amplitude evolves and ξ is a corresponding (long) length scale, and the quantities β, γ and D are complex coefficients depending on μ and α_2.

The complex Ginzburg-Landau equation is known to have solitary wave solutions that take the form of pulses or kinks.[5] The former kind of solutions can be comfortably fitted to the experimental data derived from binary fluid convection.[2] Pulses undergoing fission, briefly coherent pulses and spatio-temporally complicated states are more interesting solutions to the complex Ginzburg-Landau equation.[3] All three appear to have experimental counterparts.

Pulses and homoclinic orbits

In a partial differential equation like (1), the propagating, steady solutions take the form, $u(x,t) = U(x-ct) = U(\chi)$, and satisfy the ordinary differential equation,

$$U''' + \mu U'' + U' - cU + U^2/2 = 0 \quad , \tag{3}$$

which arises from (1) on setting $\alpha = 0$ and integrating. This equation can be viewed as a dynamical system whose flow in the phase space, $\mathbf{U} = (U, U', U'')$, defines a velocity field, $\mathbf{V} = \mathbf{U}'$. The divergence of the velocity field is $-\mu$ indicating that, for $\mu > 0$, the flow is volume contracting. Thus the system asymptotically heads towards an attractor of zero volume, which could be a fixed point, a periodic orbit or a strange attractor.

The various attractors of the system, theircharactersitics and bifurcations can all be catalogued to find the many kinds of propagating patterns which solve (1). Of most interest are those that approach a state $U = constant$ as $\chi \to \pm\infty$, for then the time series $U(\chi)$ defines a propagating localized solution in real space and time.

The trajectories that follow such paths are special types of orbits in the dynamical system. They asymptote to the fixed points of the system as "time", χ, runs forward or back. Orbits that connect the same fixed point are homoclinic orbits; they correspond to the pulse of the partial differential equation (see Fig. 1). Heteroclinic orbits join two different fixed points together, and in real space and time, define moving fronts or kinks (or hydraulic jumps).

These special kinds of orbits arise as a result of various bifurcation sequences, and they emerge at certain parameter values in (3). A particularly useful feature of these orbits is that trajectories often spend extended periods of time following them, and this leads us to analyse solutions asymptotically.[7]

Figure 1: A homoclinic orbit. The first panel shows the phase portrait of the orbit, and the second its pulsatile time trace.

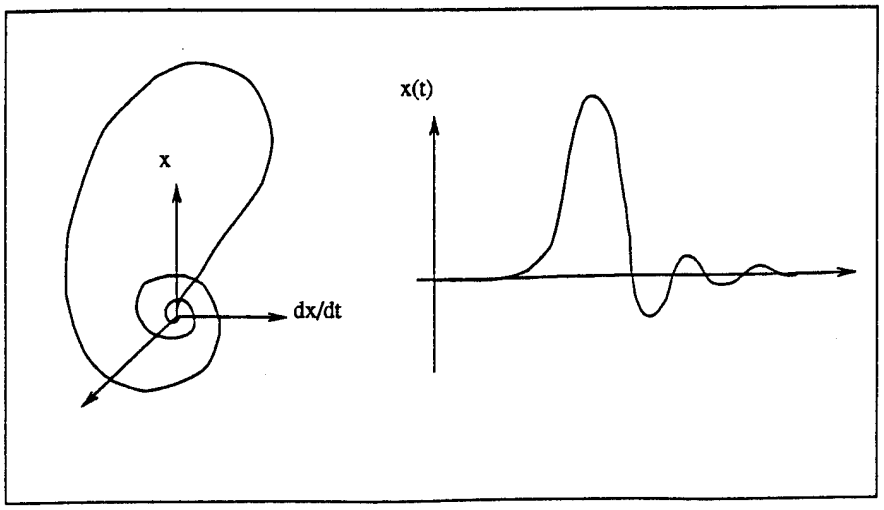

Shil'nikov theory and timing maps

Except for a relatively short interval of time, the homoclinic solution shown in figure 1, $H(\chi)$, is contained within the neighbourhood of the origin. Here, equation (3) can be approximately replaced by its linearization and we find the solution

$$U \simeq ae^{\sigma\chi} + be^{-\rho\chi}\cos(\omega\chi + \psi) \quad , \tag{4}$$

where σ and $-\rho \pm i\omega$ are the eigenvalues of the flow, and a, b and ψ are constants. The homoclinic connection emerges from the origin O at $\chi = -\infty$, escapes the vicinity of the origin, but rapidly returns and spirals back into O at $\chi = \infty$. Thus

$$H(\chi) = \begin{cases} a_0 e^{\sigma\chi} & \chi \to -\infty \\ b_0 e^{-\rho\chi}\cos(\omega\chi + \psi_0) & \chi \to \infty \end{cases} \quad . \tag{5}$$

The two sections of the solution for H correspond to the two invariant manifolds intersecting O (a one-dimensional unstable manifold and a stable two-dimensional manifold).

Nearly homoclinic trajectories typically get caught near the invariant manifolds, and consequently they "skirt" $H(\chi)$ during any excursion away from O. Since they generally do not enter the vicinity of the origin with $a = 0$ identically, however, the trajectories invariably become thrown out from the origin's vicinity along the unstable manifold after spending a lengthy period there. They are reinjected relatively rapidly, however, and so the solution $U(\chi)$ takes on the appearance of a train of widely separated pulses.

Because the nearly-homoclinic solutions spend long durations circulating near the origin, but only relatively short periods away from it, the solution can be approximately described by analytical means in the two representative regions. Near the origin we have solution (4), and away from it, $U(\chi) \sim H(\chi)$. This is equivalent to a matched asymptotic expansion of the solution. For a pulse train, the result of asymptotic analysis is a relation between the successive intervals spent near the origin, or, equivalently, the adjacent spacings between pulses. This can be viewed as a timing map for the pulse train. For certain ranges of parameter values, this map iterates chaotically, and the result is a sequence of irregularly spaced pulses.

For widely separated pulses, the map is of the form,[7]

$$Z_{k+1} = A + BZ_k^{\delta}\sin(\Omega\log Z_k + \Phi) \quad , \tag{6}$$

where $Z_k = \exp(-\sigma\Delta_k)$, Δ_k is the k^{th} pulse spacing, A, B and Φ are constants, and $\delta = \rho/\sigma$. The constant A measures the proximity of the homoclinic connection; it vanishes at homoclinicity.

The map is illustrated in figure 2 for $A = 0$ in the two cases $\delta > 1$ and $\delta < 1$. From it one can construct the spacings of a train of pulses, and knowing the form of a single pulse then provides a complete, approximate solution.

The map also predicts the bifurcation sequence that generates the homoclinic orbit (see the insets of figure 2). The fixed points of the map, $Z_k = Z_{k+1}$, correspond to periodic orbits of (3). When $\delta > 1$, the period of one such orbit monotonically diverges at $A = 0$ and then vanishes. In other words, as A approaches zero, an orbit collides with the origin, annihilates and creates the homoclinic connection. When $\delta < 1$ there is an infinite number of periodic orbits in the map at $A = 0$. Here a periodic orbit winds into homoclinicity creating a dense set of periodic orbits most of which are unstable. Thus Shil'nikov's theory predicts the existence of a chaotic set and this is the region of parameter space in which one expects irregularly spaced pulse trains.

Pulse dynamics

Shil'nikov theory predicts the various kinds of steady solutions of (1) that take the form of patterns of propagating pulses. Calculations using the partial differential equation

Figure 2: Shil'nikov's map for (a) $\delta = 2$ and (b) $\delta = 0.5$. The inset panels indicate the behaviour of a fixed point of the map as A varies, and the distance to homoclinicity changes (so illustrating the bifurcation sequence).

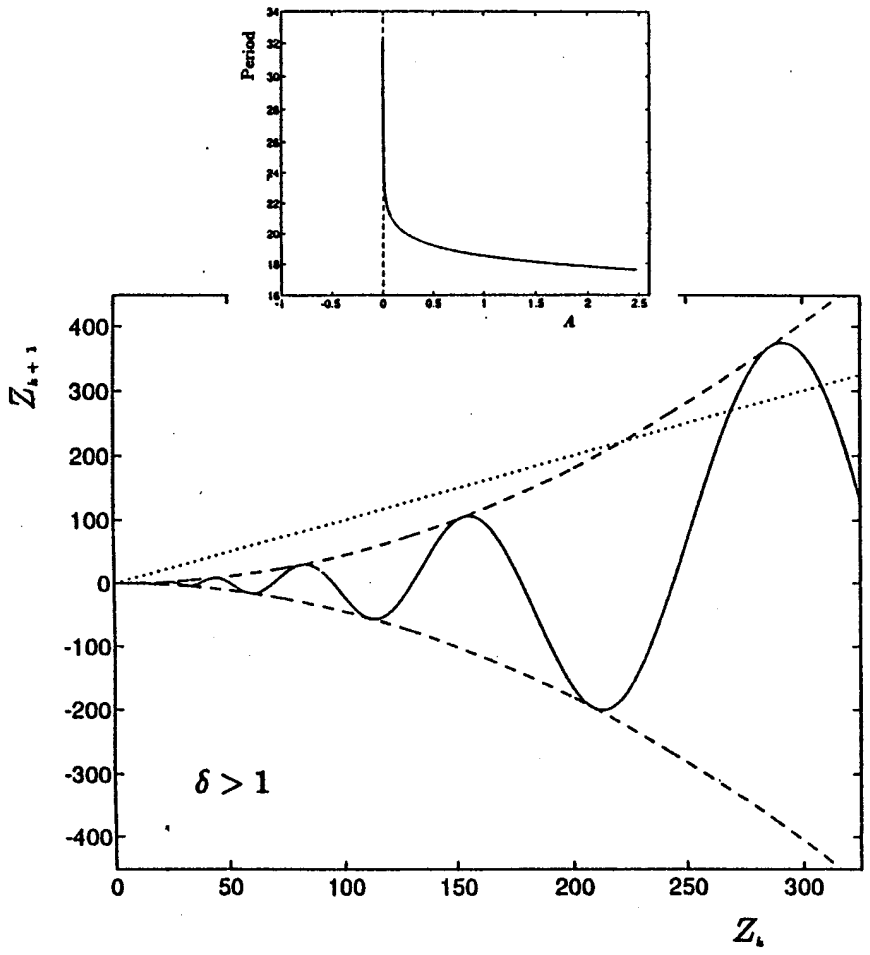

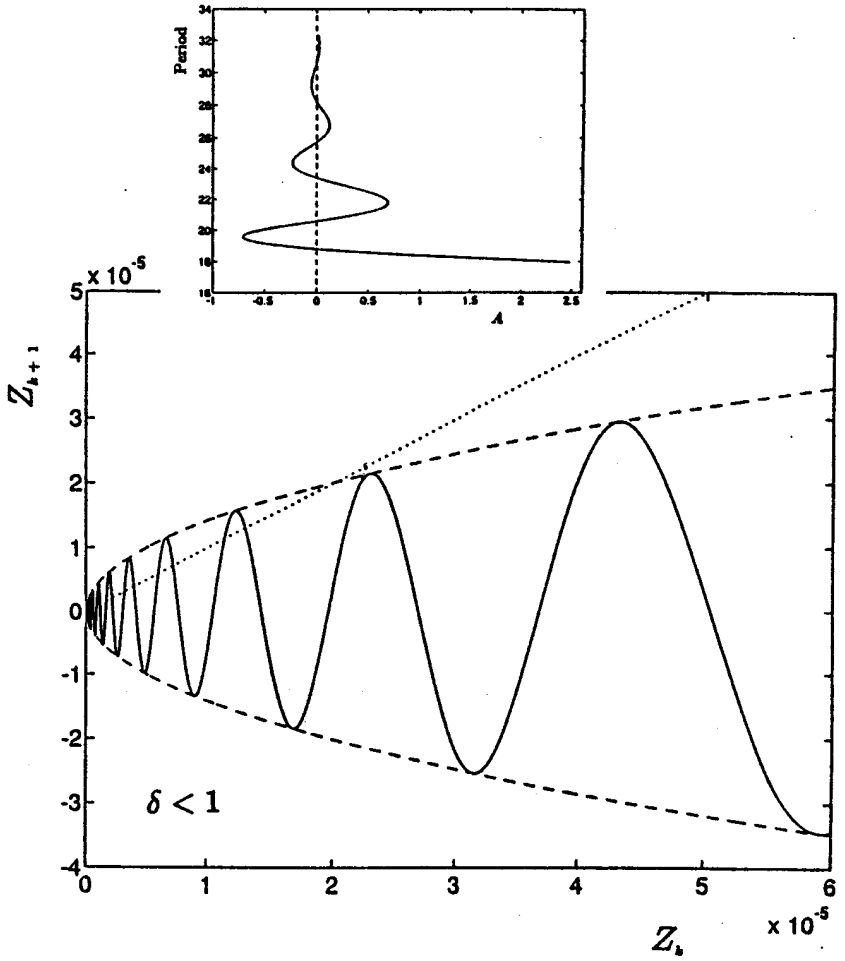

(1) suggest that temporal evolution often leads to solutions that lock into these steady states. Then we have an approximate solution

$$u(x,t) \simeq \sum_{k=1}^{K} H(\chi - \chi_k) \quad , \tag{7}$$

where K is the total number of pulses, $H(\chi)$ is the homoclinic solution and χ_k locates the position of the k^{th} pulse. These pulse positions are related by a map of the form

$$F(\Delta_k) + F(-\Delta_{k+1}) = A \quad , \tag{7}$$

for some function $F(\Delta)$, which for large Δ reduces to (4).[8]

In many problems, however, we typically need more information than just a knowledge of the different kinds of pulse formation is insufficient. For example, we may further need stability information and other aspects of pulse dynamics. To partially account for this we can permit the positions of the pulses vary weakly on a slow time: $\chi_k = \chi_k(\varepsilon t) = \chi_k(\tau)$. Rather than the map (4), we then find a set of coupled ordinary differential equations,[8]

$$F(\Delta_k) + F(-\Delta_{k+1}) = \dot{\chi}_k \quad , \tag{8}$$

which govern the slow evolution of the pulses.

For many partial differential differential systems, this asymptotic description of pulse dynamics works well. One can then describe the interactions between pulses in a practical semi-analytical way and advance to consider many-body systems which would otherwise be computationally intractable. For (1), however, this picture is fatally flawed because pulse interactions are partly mediated by waves and we require further aspects of pulse dynamics (see R. Worthing's report). Nevertheless, this kind of behaviour is at times useful and does point to ways to analyse the multiple solitary-wave solutions in partial differential equations.

References

[1] K.E. Anderson and R.P. Behringer, *Phys. Lett.* A145, 323 (1990); D. Bensimon, P. Kolodner, C.M. Surko, H. Williams and V. Croquette, *J. Fluid Mech* **217**, 441 (1990); E. Moses, F. Fineberg and V. Steinberg, *Phys. Rev. A* **35**, 2757 (1987); Similar experiments have been performed in liquid crystals, see A. Joets and R. Ribotta, *Phys. Rev. Lett.* **60**, 2164 (1988).

[2] J.J. Niemela, G. Ahers and D.S. Cannell, *Phys. Rev. Lett.* **64**, 1365 (1990).

[3] S.V. Alekseenko, V. Ye. Nakoryakov and B.G. Pokusaev, *A.I.Ch.E. Journal* **31**, 1446 (1985).

[4] C.S. Bretherton, *Fellows report, G.F.D. proceedings 1981*; C.S. Bretherton and E.A. Spiegel, *Phys. Lett.* **98A**, 152 (1983); S. Fauve, *G.F.D. proceedings 1991.*

[5] D.J. Benny, *J. Maths. and Phys.* **45**, 150.

[6] B. Malomed and A.A. Nepomnyashchy, *Phys. Rev. A* **42**, 6009 (1990); O. Thual and S. Fauve, *J. Physique* **49**, 1829 (1989); W. van Saarlos and P. Hohenberg, *Physica D* **56**, 303 (1993).

[7] L.P. Shil'nikov, *Soc. Math. Dokl.* **6**, 163 (1965); L.P. Shil'nikov, *Math. USSR Sbornik* **10**, 91 (1970); C. Tresser, *Ann. Inst. H. Poincaré*, **40**, 441 (1984).

[8] C. Elphick, E. Meron and E.A. Spiegel, *SIAM J. Applied Math.* **50**, 490 (1990).

Intergyre Water Exchange of Combined Wind and Buoyancy Forcing

Liang Gui Chen
Scripps Institute of Oceanography La Jolla, CA92093-0230

Water exchange between the subtropical and subpolar gyre is a general feature of the ocean circulation. Recently, several wind driven theories have been proposed to address this problem which allow the baroclinic exchange of water between gyres (*Pedlosky* 1984, *Schopp* and *Arhan* 1986, *Schopp* 1988 and *Chen* and *Dewar* 1993). Chen and Dewar's (referred as CD93 thereafter) study shows that the communication (water exchange) solution is close associated with the baroclinic and barotropic wave interactions and has multiple solution in purely wind driven case. This study is an extension of CD93 which includes the additional buoyancy forcing. The communication equation, which allows the water exchange between gyres, is given as (follow the same notations as CD93):

$$G_1(h_1, h_2, \phi_y)h_{1x} + G_2(h_1, h_2, \phi_y)h_{2x} = G_3(w_{s_1}, w_{s_2}) \tag{1}$$

where G_1 and G_2 are defined as

$$G_1(h_1, h_2, \phi_y) = (1 - 2h_1 - h_2)(\phi_y + 2h_1 + h_2 - (2h_1^2 + h_2^2 + 2h_1h_2))$$
$$G_2(h_1, h_2, \phi_y) = (1 - 2h_1 - h_2)(\phi_y + (h_1 + h_2)(1 - h_1 - h_2)) + h_1(\phi_y + h_2(1 - h_1 - h_2))$$
$$G_3(w_{s_1}, w_{s_2}) = w_{s_2}(3h_1 + h_2 - 1) - w_{s_1}h_1$$

In which h_1 and h_2 are the layer depth and ϕ is the Sverdrup streamfunction ($\phi_y = \tau x$). The cross isopycnal buoyancy fluxes are w_{s_1} and w_{s_2}. This equation is the generalization of the same name equation of CD93. In the limit of the no buoyancy flux, equation (1) results into two kinds of solutions, the traditional non-communication solution and the communicating solution of CD93. An analytical solution of this equation with stagnant third layer condition, has been obtained:

$$x = \frac{\omega(h)}{2(4w_s^2 + \tau^2)} + C_1 e^{\frac{\tau}{w_s}\sin^{-1}(h/c)} \tag{2}$$

in which $h = h_1 + h_2$ and $\omega(h) = (\tau - 2w_s)(c^2 - 2h^2) - 2(\tau + 2w_s)h\sqrt{c^2 - h^2} + c^2(4w_s^2 + \tau^2)/\tau$. The constant C_1 is determined by the boundary conditions:

$$C_1 = -\frac{\omega(h_e)}{2(4w_s^2 + \tau^2)} \exp\left[-\frac{\tau}{w_s}\sin^{-1}(h_e/c)\right] \quad \text{from} \quad x = 0, h = h_e$$

$$C_1 = \left[-1 - \frac{\omega(h_w)}{2(4w_s^2 + \tau^2)}\right] \exp\left[-\frac{\tau}{w_s} \sin^{-1}(h_w/c)\right] \quad \text{from } x = -1, h = h_w$$

The two group of solutions, each associated with the eastern or western boundary conditions, merger at the middle of intergyre boundary, and form a piecewise smooth communication solution. The multiple solutions of the purely wind driven case disappear even with infinitesimal buoyancy flux.

The buoyancy effects on the communication problem can be explained by studying the second layer mass balance, derived from eq. (1) with stagnant third layer:

$$h_x(-u_c) = h_x(\phi_y + h_1 h_2)/h_1 = w_s \tag{3}$$

Eq. (3) is a β-convergent/divergence balance equation. The term $h_x(= v_2)$ represents the second layer meridional velocity, ϕ_y represents the eastward Sverdrup transport and $h_1 h_2$ the westward baroclinic wave speed (CD93). The w_s is the vertical buoyancy flux entering (or leaving) the second layer. This equation states that the horizontal divergence is balanced by the vertical buoyancy flux.

Figures-1,2 illustrate this convergence/divergence concept. The IGB is divided into three different sections. Near the eastern boundary, the Sverdrup transport ϕ_y is almost zero while the baroclinic wave speed $h_1 h_2$ is non-trivial, this results in a finite value of u_c. For small w_s, it means weak horizontal convergence and small meridional transport, $h_x = v_2$, and thus almost flat thermocline. Going westward, the barotropic transport increases while the baroclinic wave speed barely changes due the small h_x. In section II, the barotropic transport finally catches up the baroclinic wave speed and results in near zero u_c. Large meridional transport (h_x) is thus needed so that the horizontal convergence $-h_x u_c$ can balance the vertical buoyancy flux w_s. For zero w_s, u_c becomes zero which corresponds to the communicating solution of CD93. With large h_x, the baroclinic wave speed increases drastically and keeps in pace with the increase of the barotropic transport so that the u_c remains close to zero. This section is defined as the communication window in the CD93. Because the maximal baroclinic wave speed is limited by the eastern boundary condition (Schopp and Arhan [1986], CD93), the barotropic transport finally overcomes the baroclinic wave speed at the end of section II (x_d), where singularity occurs, and results in the changing sign of u_c. In section III, due to the changing sign of u_c, the meridional transport also reverse its direction. Since u_c is no longer small, h_x decreases with small w_s. In the limit of $w_s \to 0$, this corresponds to the non-communicating flat thermocline.

The direction of the cross gyre transport depends also on the sign of the w_s (the β-spiral concept). In sections I and II, where u_c is negative, cooling (negative w_s)

is accompanied by subsurface southward flow and surface northward flow. This is in agreement with general circulation patterns where a large volume of warm water is being transported from the subtropical gyre to the subpolar gyre (in section II) and results in strong surface cooling.

Following the same argument in CD93, the interior solution can be obtained by method of characteristics of which characteristic equations (Luyten and Stommel's 1986a) is:

$$\frac{dh}{ds} = -\left[\frac{\phi_y}{yh_1} + \frac{h_2}{y^2}\right] h_x + \left[\frac{\phi_x}{yh_1}\right] h_y = -w_s \tag{4}$$

The interior is thus divided into three different regions, the eastern, western and the communication regions. The characteristics equation is thus integrated from these boundary to the interior (Figure-3, the trajectories of the characteristic). It is found that with no zero w_s , the characteristics equation must be integrated from the intergyre boundary in order to recover the communicating solution in the interior. The flat thermocline at the intergyre boundary can not recover the communication flow nor can it satisfy the communication equation of (1) and thus are incorrect. When buoyancy flux is weak, the interior flow pattern is similar to that of CD93 (Figure-3).

References

Chen, L. G. and W. K. Dewar 1993: 'Intergyre communication in a three layer model' *J. Phys. Oceanogr.*, **23**, 855-878.

Luyten, J. R., Stommel, 1986a: Gyres driven by combined wind and buoyancy flux. *J. Phys. Oceanogr.*, **16**, 1551-1560.

——, ——, 1986b: Experiments with cross-gyre flow patterns on β-plane. *Deep – Sea Res.*, **33**, 963-972.

Pedlosky, J, 1984: Cross-gyre ventilation of the subtropical gyre: an internal mode in the ventilated thermocline. *J. Phys. Oceanogr.*, **14**, 1172-1178.

Schopp, R. and M. Arhan, 1986: A ventilated middepth circulation model for the Eastern North Atlantic. *J. Phys. Oceanogr.*, **16**, 344-357.

——, 1988: Spin up toward communication between oceanic subpolar and subtropical gyres. *J. Phys. Oceanogr.*, **18**, 1241-1259.

Figure-1

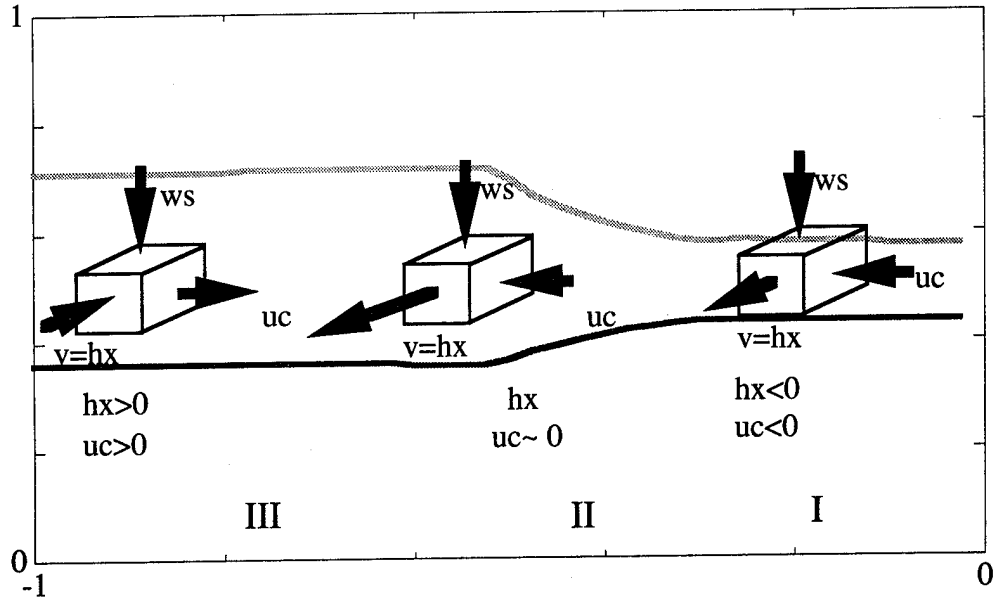

Figure-2

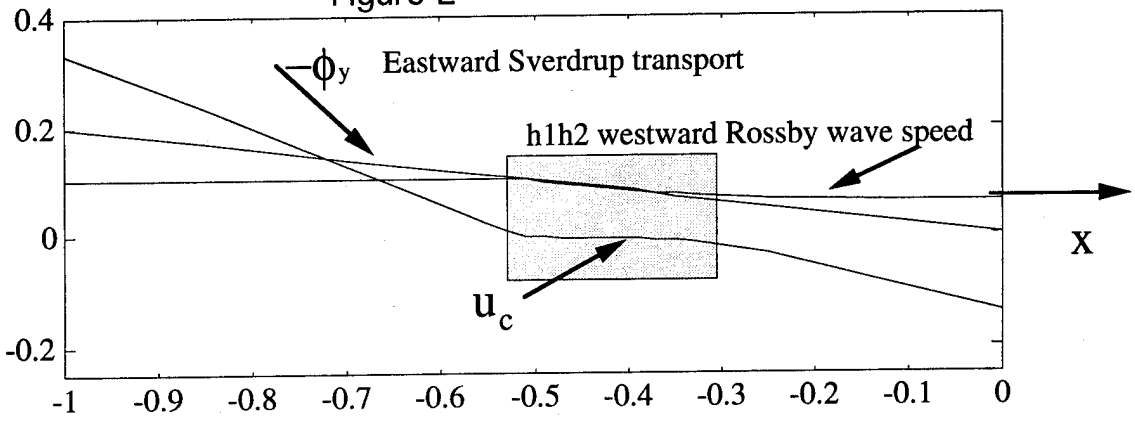

Figure-3

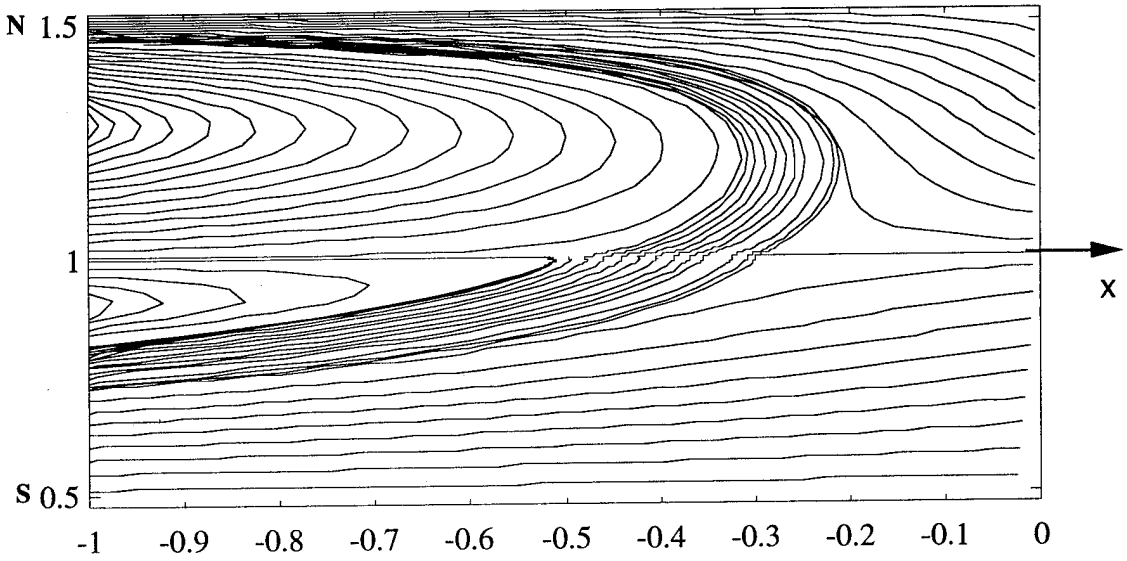

Fast dynamos near integrability

Steve Childress
New York University, Courant Institute, New York, NY 10012 USA

In the study of fluid flows with *small* dissipation, it is natural to consider first a *reduced* problem where the dissipation is identically *zero*. A notable case is steady flow past a bluff body, where the dissipation is viscous and the reduced problem is inviscid flow. The problem is then to select meaningful solutions of the reduced problem, which presumably represent the *limits* of small dissipation, from a generally much larger set of possible solutions. In our example this might select inviscid flows compatible with Prandtl's boundary-layer theory.

A similar problem arises in the context of magnetohydrodynamics, when a magnetic field is present in an electrically conducting fluid and the *magnetic diffusion* is small. The *kinematic dynamo theory* focuses on a subset of this problem, where the velocity field $\mathbf{u}(\mathbf{x},\mathbf{t})$ is *given* and the resulting effects on the magnetic field $\mathbf{B}$ are sought. The equation for the latter field is the *induction equation*,

$$\frac{\partial \mathbf{B}}{\partial t} - \nabla \times (\mathbf{u} \times \mathbf{B}) - \epsilon \nabla^2 \mathbf{B} = \mathbf{0}.$$

We shall assume $\nabla \cdot \mathbf{u} = \mathbf{0}$ so the middle term takes the form $\mathbf{u} \cdot \nabla \mathbf{B} - \mathbf{B} \cdot \mathbf{u}$. The rate of strain of the fluid thus affects the magnetic field. Tubes of flux can be stretched, folded, etc. The small parameter ϵ is one over the magnetic Reynolds number, and is indeed extremely small in stars and galaxies (where the dynamo problem we consider here is of interest). The reduced equation, $\epsilon \equiv 0$, has the well-known property that the flux carried by a flux tube is an invariant of the flow. This leads to a compact representation of the magnetic field in terms of Lagrangian variables of the flow.

Dynamo theory studies solutions of which grow in time, usually exponentially. If we identify a maximal growth rate γ_ϵ for solutions (by setting appropriate boundary conditions and maximizing over initial magnetic fields), we say the flow is a *dynamo* if $\gamma_\epsilon > 0$. We may then take the limit for small ϵ (perhaps as an infimum limit), to obtain γ_0. If $\gamma_0 > 0$ we say $\mathbf{u}$ is a *fast* dynamo. The question then is, can we identify fast dynamos from the reduced problem, and compute γ_0 as equal to the growth rate $\gamma(0)$ obtained from one of its solutions?

To examine this question in a simple setting, we consider the unit square $0 < x, y < 1$ and the *folded Baker's map* $(x,y) \to (2x, y/2)$ or $(2-2x, 1-y/2)$, depending upon whether x is less than or greater than $1/2$. This effectively doubles the aspect ration of the figure, cuts it in two, and folds it back on itself. If we imagine an initial magnetic field $(1,0)$ the field after one operation, by conservation of flux, is $2\,sgn(1/2-y)$. We thus define an operator T describing the effect of the map on a field $(b(y),0)$: $Tb(y) = 2\,sgn(1/2-y)b(\tau(y)$ where $\tau(y) = min(2y, 2-2y)$ is the *tent map*.

N iterations of T on any smooth initial field produce alternating layers of field of strength $\pm 2^N$, with total flux (if $N \geq 1$ exactly zero, while energy grows exponentially. If small dissipation is added by letting $b(y)$ satisfy the heat equation for unit time between applications of T, it is not difficult to show that the field does tend to zero for large t, provided that we extend the problem with period 1 in y.

This suggests that $\gamma_0 = \gamma(0) = -\infty$ in this model. Actually this is not true for other periodic extensions. We can test for other measures of growth by introducing the inner product $(c,b) = \int_0^1 c^* b dy$. Let ϕ be a smooth test function and consider $(\phi, T^N b) = (S^N c, b)$. Here S is the adjoint map, $Sb = b(y/2) - b(1-y/2)$. As Bayly noticed in a related problem [1], the adjoint map has a complete set of smooth eigenfunctions. The eigenvalue 0 is infinitely degenerate since any function of $(y-1/2)^2$ is an eigenfunction. The other eigenvalues are $1/4^k, k = 0,1,2,...$ with eigenfunctions $p_1 = y - 1, ..., p_{2k+1} =$ a polynomial of degree $2k+1$. Thus 0 is the maximal growth rate. If we require the test functions to be at least continuous, then p_1 can be extending to a period 2 eigenfunction of S. The operator T correspondingly has an eigenfunction in the form of a distribution. In fact for finite but small ϵ the eigenfunction of the diffusional version of T, for the eigenvalue 1, is $f_1 = e^{3y^2/16\epsilon} - e^{3(y-1)^2/16\epsilon}$ mod 2. This example shows that the correct measure of growth used in the reduced problem will depend upon the nature of the problem, here the periodic extension used.

More reasonable models of fast dynamo action utilize Beltrami waves of the form

$$\mathbf{u} = \alpha(\mathbf{t})(\mathbf{0}, \sin \mathbf{x}, \cos \mathbf{x}) + \beta(\mathbf{t})(\sin \mathbf{y}, \mathbf{0}, \pm \cos \mathbf{y}),$$

where the - sign gives waves of the same helicity, the + sign of opposite helicity. If $2\alpha, 2\beta = 1 \pm \delta \cos(\omega t)$, where $\delta \ll 1$, the waves describe a flow close to an integrable one with helical streamlines. Fast dynamo action in the reduced problem can be investigated using a variant of Melnikov's method [2]. The distinguishing feature of this model is the hypothesis that the magnetic boundary layers of the steady, integrable flow are replaced by the time-dependent unstable manifolds coming out of each critical point. Based on this hypothesis an approximate method can be found for determining growth rate as measured by the magnetic flux in the manifold. If $\omega \gg 1$ this method offers an extension of conventional laminar boundary-layer methods to nearly-integrable flows with thin bands of chaotic structure. Numerical calculations indicate that in the dynamo phase of growth of the field, the most intense field is indeed concentrated near the heteroclinic tangle on the unstable manifolds.

We have not touched here on the important issue of dynamical equilibration of fast dynamos, which is controlled more by B^2 than by weak measures such as flux, and so is sensitive to the intense small-scale structure of **B**.

[1] Bayly, B. , Childress, S. (1989): Unsteady dynamo effects at large magnetic Reynolds numbers. Geophys. Astrophys. Fluid Dyn. **49** , 23–43.

[2] Childress, S. (1993): On the geometry of fast dynamo action in unsteady flows near the onset of chaos. Preprint.

Pressure fluctuations in swirling turbulent flows

by Stephan Fauve
Ecole Normale Supérieure de Lyon, 69364 Lyon, France

Pressure fluctuations in boundary layers as well as in the bulk of fully developed homogeneous isotropic turbulent flows have been studied for a long time [1-4] and the pressure field is commonly used as a diagnostic in meteorology. However, to the best of my knowledge, it has been emphasized and shown only recently that pressure can be used to locate regions with high vorticity or dissipation in turbulent flows obtained by direct numerical simulations [5]. It has been known for a long time that in an incompressible fluid of density ρ, pressure obeys a Poisson equation obtained by taking the divergenge of the Navier-Stokes equation,

$$\Delta p = -\rho \frac{\partial^2 (v_i v_j)}{\partial x_i \partial x_j} = \frac{\rho}{2}(\omega^2 - \sigma^2), \qquad (1)$$

where ω is the vorticity and σ^2 the squared rate of strain [6], thus showing that low pressures occur in vortex cores (as expected) and high pressures in regions where the effect of strain is large compared to the one of vorticity (stagnation points). Low pressures associated with vorticity filaments were clearly observed in a numerical simulation of the Taylor-Green flow in reference [5], and we performed laboratory experiments to check whether pressure measurements can be used similarly as an experimental tool to study vortical and dissipative structures in turbulent flows. We did find a surprisingly good agreement with the results of numerical simulations [5, 7] concerning the probability density function (PDF) of the pressure, which is strongly asymmetric and displays a long tail toward low pressures whereas the high pressure part shows a sharper cut-off. The low pressure part of the PDF results from random pressure drops which are due to vorticity concentrations in the vicinity of the pressure probe [8]. Let us note that this shape for the pressure PDF is not restricted to the particular geometry of our flow (see below) but has been also observed since in jets [9]. We are now studying some statistical features of the low pressure events in order to get insights in vorticity dynamics in turbulent flows [10].

Von Karman swirling flows

The experimental set-up is shown in figure 1. It consists of a cylindrical container, 20 cm in diameter and 19 cm in height, filled with water. Its temperature is maintained constant with a regulated water circulation. Two co-axial rotating disks of diameter $D = 17.5$ cm, at a distance $H = 8$ cm apart from each other, are rotated independently by two DC motors at angular velocities $\Omega_{1,2}$ in the range [0, 1800] RPM, i.e. [0, 30] Hz for $\Omega_{1,2}/2\pi$. Pressure fluctuations are measured by piezoelectric acceleration-compensated transducers, mounted flush with the lateral wall. We have observed no difference on the shape of the pressure PDF when varying the transducer diameter from 2.5 to 15 mm, although these transducers are all very large compared to the Kolmogorov length. This obviously affects the high-frequency cut-off of the pressure spectrum.

The flows generated between two co-axial rotating disks, known as von Karman swirling flows, are widely studied in fluid mechanics [11]. When the disks are counter-rotating at the same rate, the flow in the median region of the cell looks

rather homogeneous when a turbulent regime is reached. As recently visualized experimentally in water seeded with air bubbles [12], vorticity concentrations in the form of filaments are randomly generated in space and time. This motivated us to choose this flow to perform quantitative pressure measurements.

Let us first give several orders of magnitude which characterize our flow. If one assumes that momentum transfer does not depend on viscosity in a fully developed turbulent regime, dimensional analysis then gives for the torque, $\Gamma \propto \rho L^5 \Omega^2$, which is known as "centrifugal torque" behavior in the engineering literature. Similarly, one has for the dissipated power, $P \propto \rho L^5 \Omega^3$, where L is a characteristic large scale. Note that these laws do not depend on any particular assumption on the turbulent flow, but follow from dimensional analysis as soon as ν is negligible for momentum transfer. For $\Omega/2\pi = 20$ Hz, we have $P \approx 100$ W, thus the average dissipation per unit mass ϵ, is $\epsilon \approx 4$ W/kg. Using $\eta \approx (\nu^3/\epsilon)^{1/4}$, we get for the Kolmogorov length, $\eta \approx 20\,\mu$m. The integral Reynolds number cannot be defined without ambiguity except in the large aspect ratio configuration, $H \ll D$. If one takes $L = 10$ cm for the integral length-scale, and uses $L/\eta \approx Re^{3/4}$, one get $Re \approx 100000$, which shows that the characteristic large scale velocity is roughly 1 m/s, i.e $0.1/, \Omega D/2$. One can also estimate the Taylor scale based Reynolds number, R_λ, with the relation

$$\epsilon = 15\nu < \left(\frac{\partial v}{\partial x}\right)^2 > \approx 15\nu \left(\frac{v_{rms}}{\lambda}\right)^2 .$$

Using the estimate of v_{rms} obtained from pressure measurement (see equation (2) below), $v_{rms} \approx 1$ m/s, we get $\lambda \approx 1$mm. This gives a certainly too large value $R_\lambda \approx 1000$, which is not surprising since R_λ depends on v_{rms}^2 which is only roughly estimated using (2).

fig. 1

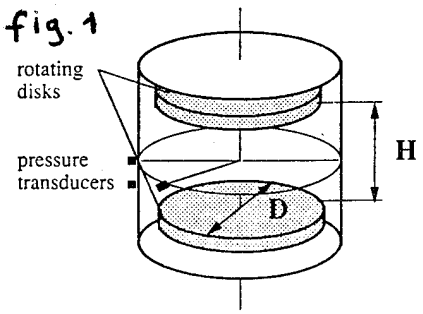

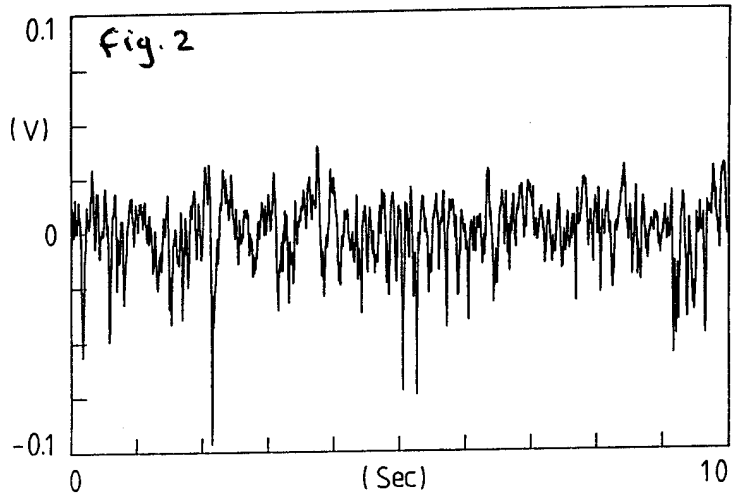

Pressure measurements

A direct time-recording of the pressure is displayed in figure 2. It is clearly visible that pressure fluctuations are asymmetric with random occurrence of strong pressure drops. We relate these low pressure events to random vorticity concentrations in the vicinity of the pressure transducer. Indeed, we have checked that the pressure signals recorded by two transducers, 1 cm far apart, display no coherence. These pressure drops are thus localized in space and do not correspond to a depression on the integral length-scale (or even one tenth of it).

The PDF of p/Ω^2 is displayed in figure 3. It is strongly non-Gaussian with a roughly exponential tail toward low pressures, due to the random occurrence of pressure drops. The low pressure tail becomes stretched at higher Reynolds numbers, i.e. displays a upward concavity in the log-lin plot of figure 3 [13]. It is important to notice that the PDFs of p/Ω^2 for different Ωs (810 and 1250 RPM) roughly collapse on the same curve, showing that pressure fluctuations are mostly governed by the integral scale velocity field, i.e. the large scale velocity fluctuations give the largest contribution to pressure fluctuations, as can be understood from the dimensional relation

$$p_{rms} \propto \rho v_{rms}^2, \tag{2}$$

(see reference [3] for the value of the proportionality constant in the case of homogeneous isotropic turbulence). We checked (2) by measuring the area under the pressure power spectrum as a function of the rotation rate Ω. This leads to a reasonable order of magnitude, $v_{rms} \approx 1$ m/s, for $\Omega/2\pi \approx 20$ Hz. Although the high frequency part of the pressure spectrum may be affected by the large size of the transducers, its high-frequency cut-off is at integral time-scale, $2\pi/\Omega$, and is well resolved; thus most of the power is measured by the transducer.

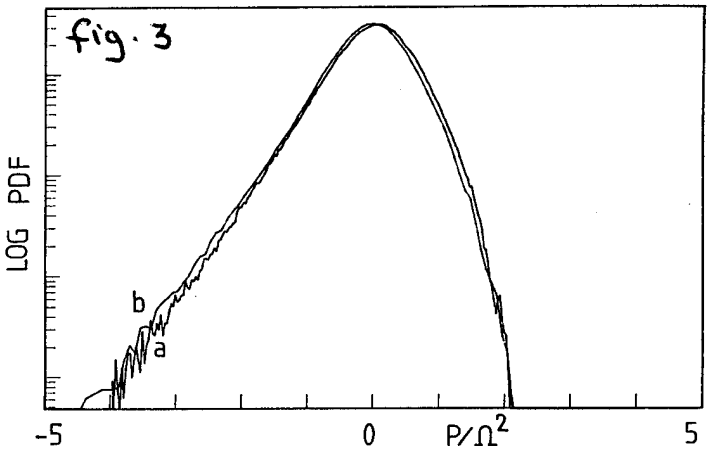

Two possible models for the PDF of the pressure drops

From equation (1) it is clear that the tails of the pressure PDF, should be governed by regions with high velocity-gradients. In particular, the low pressure tail should result from vorticity concentrations. As usual, we have two possibilities to model this : either the shape of the pressure drops, i.e. of the velocity field of the filaments, is enough to explain the functional dependence of the low pressure tail of the PDF, or one should take into account the distribution of pressure drops in time (or space). Let us first consider the first possibility ; assume that on a ball B of size r centered on a vorticity filament, we have

$$\int_B (\omega^2 - \sigma^2) d^3r \propto r. \tag{3}$$

Then Gauss's theorem and equation (1) give, $|\nabla p| \propto 1/r$, thus

$$p = p_0 \mathrm{Log} \frac{r}{r_0}, \tag{4}$$

where r is the distance to the vortex center and r_0 is some scale larger than the characteristic one of the filament. The probability $\pi(p)dp$ of observing a low pressure in the range $[p, p+dp]$ is proportional to the probability of being at a distance r within dr from a filament, which scales as rdr. The PDF for the pressure drops is therefore,

$$\pi(p) \propto \frac{1}{p_0} \exp \frac{2p}{p_0}. \tag{5}$$

However, one needs to check that the velocity field of the filaments satisfies (3). As emphasized by the referee of reference [8], a Burgers vortex (an exact axisymmetric vortex solution of the Navier-Stokes equation) does not satisfy (6) because of the existence of a large dissipation around the core of the vortex. It is not obvious that the filaments in turbulent flows have the same structure, and it would be interesting to check this on numerical data. However, as said in our note [17] of reference [8], it is possible to model the pressure PDF with Burgers vortices if one takes into account their distribution in time (or space).

Let us consider for instance a collection of Burgers vortices, each one stretched by an axially symmetric strain flow [14]. If the size of their core is r_0 and their characteristic vorticity ω_0, the minimum pressure in the core scales as

$$p_{min} \propto (r_0 \omega_0)^2. \tag{6}$$

Now, because of the strain a, ω_0 increases exponentially in time up to a critical value for which the filament is destroyed [14]. Conservation of kinetic momentum implies that

$$r_0{}^2 \omega_0 = \text{constant} \tag{7}$$

during the increase of vorticity. Thus,

$$p_{min} \propto \omega_0. \tag{8}$$

Assume now that these vortices are generated at a constant rate; then, at any time, one has an exponential distribution of ω_0, and consequently of low pressures. Fluctuations of the strain or of the critical ω_0 at which the filaments are destroyed, would give a more stretched PDF than the exponential one.

Note that an exponential distribution of p_{min} in the direct recording of figure 2 does not rule out the first model, since it is precisely what could be expected from filaments sweeping at random distances from the center of the pressure probe. A PDF conditionned on a given value of p_{min} will hopefully discriminate between the above two possible models.

The high pressure part of the PDF was fitted to $(p_{max} - p)^4$ in reference [8], and understood in the spirit of the first model given above. However, a Gaussian fit is equally good for the tail and even better with the smallest pressure probes. A Gaussian behavior for the high pressure part is not understood theoretically, even with a simple model.

Discussion

The low pressure tail of the pressure PDF in this turbulent flow clearly results from vorticity concentrations in the form of nearly 2D filaments. It has been shown recently that a Gaussian velocity field gives a skewed PDF but with exponential tails on both sides [15]. This was also observed numerically for the low pressure tail [7]. I think that this agreement for the shape on the low pressure side is accidental;

the Gaussian velocity field does not involve strong vorticity concentrations, and thus underestimates low pressure fluctuations. For the high pressure part of the PDF, the Gaussian velocity field gives a qualitatively wrong prediction, and it would be interesting to understand why the dynamics imposes a sharper cut-off of the PDF.

Although vorticity filaments do generate the strongest pressure fluctuations, their role in the energy transfers in turbulence is unclear. Filaments seem to have been considered as small scale structures of the turbulent flow, leading to questionable conjectures about their role in direct or inverse cascades of energy. This mistake probably results from the fact that, according to numerical simulations, their mean radius was found to be a few Kolmogorov lengths. However, it is fairly obvious that this does not mean that filaments contribute to the flow kinetic energy mostly at large wavenumbers; they contribute at all wavenumbers between the integral and dissipative scales, and certainly strongly at small wavenumbers; as shown by pressure measurements, they involve a large-scale characteristic velocity difference, which can be easily understood if one considers that they are generated by stretching of a large eddy. This also explains why the pressure PDF scales as the integral velocity, eventhough it contains a dominant contribution due to vorticity filaments in the low pressure tail. It is clear that filaments locally (in space and time) violate isotropy and the mean Kolmogorov scaling, $\Delta v \propto r^{1/3}$; however, further work is needed to claim that they are the source of intermittency.

I acknowledge P. Abry and C. Laroche with whom I am performing the experiments on pressure fluctuations. I have also benefitted from many useful discussions with B. Castaing and A. Pumir.

References

[1] W. W. Willmarth, Ann. Rev. Fluid Mech. **7**, 13-38 (1975).
[2] W. K. George, P. D. Beuther and R. E. A. Arndt, J. Fluid Mech. **148**, 155-191 (1984).
[3] G. K. Batchelor, Proc. Cambridge Philos. Soc. **47**, 359-374 (1951).
[4] R. H. Kraichnan, J. Acoust. Soc. Am. **28**, 64-72, 378-390 (1956).
[5] M. E. Brachet, Fluid Dyn. Res. **8**, 1-8 (1991).
[6] For the last equality in (1) and its interpretation, see P. Bradshaw and Y. M. Koh, Phys. Fluids **24**, 777 (1981) and references therein. However, I was told during this summer program at WHOI, that this formula has been used before by Corrsin (E. Spiegel, private communication).
[7] O. Metais and M. Lesieur, J. Fluid Mech. **239**, 157-194 (1992).
[8] S. Fauve, C. Laroche and B. Castaing, J. Phys. II France **3**, 271-178 (1993).
[9] Y. Gagne, private communication.
[10] P. Abry, S. Fauve, P. Flandrin and C. Laroche, "Analysis of pressure fluctuations in swirling turbulent flows", (preprint 1993).
[11] P. J. Zandbergen and D. Dijkstra, Ann. Rev. Fluid Mech. **19**, 465-491 (1987).
[12] S. Douady, Y. Couder and M. E. Brachet, Phys. Rev. Lett. **67**, 983-986 (1991).
[13] This behavior is also observed in direct numerical simulations; A. Pumir, private communication.
[14] Many models with 2D-vortex have been used to model turbulence; see for instance, T. S. Lundgren, Phys. Fluids **A5**, 1472-1483 (1993), and references therein.
[15] M. Holzer and E. Siggia, "Skewed, exponential pressure distributions from Gaussian velocities" (to be published in Phys. Fluids A, 1993).

Gulf Stream meandering: Some physics and some biology

Glenn Flierl, MIT

and

Cabell Davis, WHOI

Simple models of Gulf Stream physics and biology are used to assess the influence of meandering on the biological populations. For biological dynamics, we use a phytoplankton—zooplankton—nutrient model. However, such models are rather *ad hoc*, and we describe new (for biological modeling) techniques for taking a complex, multi-component set of reaction equations and deriving a reduced set retaining the essential aspects. The full model is solved in a zero-dimensional system under appropriate forcing. The empirical orthogonal eigenfunctions are then used as basis functions for a reduced model. The projection of the equations on this basis set leads to a low-order system which can be incorporated into a two- or even three-dimensional model.

Most of the biological activity occurs in the upper part of the ocean, so we must use some form of mixed layer model in the physical dynamics. We make the assumption that the upper layer is well mixed and average the equations over the mixed layer depth. When the layer is entraining, the nutrients tend to be increased, while the phytoplankton and zooplankton are diluted (under the assumption that these cannot sustain themselves in the deep water.) In contrast, when the mixed layer is detraining, the material just below the interface has the same properties as the mixed layer and the properties in the mixed layer are unaltered. In the summer, the mixed layer depth is fixed by the surface stresses and the entrainment/detrainment is produced by the upward/downward motion at the base (driven by the meandering.) We assume that the properties below the mixed layer reach equilibrium (all nutrients) by the time the water upwells again. The lack of symmetry between upwelling and downwelling regimes implies that not only do fluctuating flows lead to time-dependent biological properties, but the average values are changed as well.

For the physical dynamics, we use a 1-1/2 or two layer contour dynamics model. The 1-1/2 layer model can form rings, if the initial perturbation is large enough; however, the two layer model permits baroclinic instability so that even a small perturbation can grow into an eddy and pinch off. The vertical velocities are much bigger in the baroclinically developing meander. The biological patterns show enhancement of the phytoplankton and reduction in the zooplankton on the northward going branches, as upwelling brings nutrient into the mixed layer and dilutes the plankton. In the southward branches there is downwelling, but the flow is strong enough to carry the enhanced phytoplankton down through most of the meander. The changes in biomass are order 20% and may be difficult to observe since they are, in reality, embedded in significant cross-stream gradients. Yet they are large enough to suggest that meandering and eddy formation can be important modifiers of the biological state.

Generation of Solitary Waves by External Forcing

by Roger Grimshaw

Department of Mathematics, Monash University, Clayton, Vic 3168, Australia

The forced Korteweg–de Vries (fKdV) equation is now established as a canonical model for the generation of solitary waves by the interaction of a flow with a topographic obstacle. In suitable non–dimensional co–ordinates it is

$$-(A_\tau + \Delta A_X) + 6AA_X + A_{XXX} + F_X = 0 \tag{1}$$

Here $\alpha^{\frac{1}{2}}A(X,\tau)$ is the amplitude of the dominant resonant wave mode, $\alpha F(X)$ is a representation of the topographic obstacle, $\alpha^{\frac{1}{2}}\Delta$ is the linear long wave speed of the resonant wave mode, $X = \epsilon x$ and $\tau = \epsilon\alpha^{\frac{1}{2}}t$ where x is a spatial co–ordinate along the wave guide and t is time. The system contains two small parameters α and ϵ where α is a measure of the amplitude of the topographic forcing and ϵ^2 is a measure of linear wave dispersion. The usual nonlinear–dispersive balance holds so that $\epsilon^2 = \alpha^{\frac{1}{2}}$. The fact that in the frame of reference of the topography the linear long wave speed is $\alpha^{\frac{1}{2}}\Delta$ and hence $O(\alpha^{\frac{1}{2}})$ defines the resonant condition here; in traditional hydraulic terminology the flow is supercritical or subcritical according as Δ is positive or negative. Note that in this resonant system a topographic forcing of $O(\alpha)$ produces a response of $O(\alpha^{\frac{1}{2}})$.

The fKdV equation has been shown to describe the generation of solitary waves by flow interaction with topography in a wide variety of physical contexts (see, for instance, the review by Grimshaw, 1992). We note in particular that it describes the critical flow of a homogeneous fluid over topography (Akylas, 1984; Cole, 1985; Wu, 1987; and Lee et al., 1989), or the critical flow of a density stratified fluid over topography (Grimshaw and Smyth, 1986; and Melville and Helfrich, 1987), or the critical flow of a swirling fluid past an obstacle (Grimshaw, 1990), or the resonant generation of Rossby waves by flow interaction with topography (Patoine and Warn, 1982; and Grimshaw and Yi, 1991), or the resonant generation of coastally–trapped waves by the interaction of a coastal current with topography (Grimshaw, 1987; and Mitsudera and Grimshaw, 1990). In general the fKdV equation (1) is not integrable, although it is Hamiltonian with the Hamiltonian invariant

$$H = \int_{-\infty}^{\infty} \{\tfrac{1}{2}\Delta A^2 + \tfrac{1}{2}A_X^2 - A^3 - AF\}\, dX \tag{2}$$

and also possesses the mass invariant $\int_{-\infty}^{\infty} A\,dX$. Solutions must generally be obtained numerically, and so far most interest has focussed on the case of zero initial condition (i.e. $A(X,0) = 0$) and isolated forcing when $F(X)$ is typically modelled by a Gaussian–type function of amplitude F_0. This situation corresponds to the generation of solitary–like waves by the critical flow over topography, and the key parameters are Δ and F_0, measuring respectively the criticality of the flow and the magnitude and sign of the topographic forcing. A representative solution is shown in Figure 1 for $\Delta = 0$ and $F_0 > 0$. The main features of this solution are the generation of an upstream wavetrain, a stationary depression in the lee of the obstacle and a downstream wavetrain. In this Figure, the obstacle (not shown) is located at $X = 86$, and has a half–width of about 3, while the flow is from left to right. Grimshaw and Smyth (1986) describe a comprehensive

et of numerical solutions in which the parameters Δ and F_0 are varied. In general, for subcritical flow when $\Delta < 0$ the upstream wavetrain is weaker and as Δ decreases will eventually detach from the obstacle, while the downstream wavetrain correspondingly intensifies and eventually as Δ decreases stationary lee waves form in the lee of the obstacle. For supercritical flow when $\Delta > 0$, the upstream wavetrain remains attached to the obstacle but each wave takes longer to be generated, while the downstream wavetrain weakens and is swept downstream as Δ increases.

Grimshaw and Smyth (1986) and Smyth (1987) provide a theoretical interpretation of these numerical solutions in which the hydraulic approximation is combined with modulation theory for the periodic solutions of the unforced KdV equation. Consider, for simplicity, the case of positive forcing $(F_0>0)$ and resonant, or critical, flow. The hydraulic approximation omits the linear dispersive term (i.e. A_{xxx}) in (1). It can then be shown that for critical flow when $|\Delta| < (12F_0)^{\frac{1}{2}}$, the hydraulic solution to the initial value problem is a locally steady flow over the topographic obstacle, consisting of an upstream elevation $A_-(>0)$ and a downstream depression $A_+(<0)$ where

$$6A_\pm = \Delta \mp (12F_0)^{\frac{1}{2}} . \tag{3}$$

Within the hydraulic approximation, this steady flow is terminated by upstream and downstream shocks, both propagating away from the obstacle. However, within the context of the KdV equation, now unforced since the constant solutions $A\pm$ occur essentially in the regions outside the isolated obstacle, these shock solutions are not permissable and must be replaced by solutions of the KdV equation which resolve these step discontinuities. Such solutions can conveniently be described asymptotically in terms of modulation theory for the periodic cnoidal wave solutions of the KdV equations, described, for instance, by Whitham (1974, Chapter 16). The details of this application of modulation theory are described by Grimshaw and Smyth (1986) and Smyth (1987). Here we note that the modulated wavetrains range in general from solitary waves of amplitudes $\mp 2A_\pm$ upstream (downstream) at one end to small–amplitude sinusoidal waves at the other (see Figure 1), and occupy the respective zones.

$$\Delta - 4A_- < X/\tau < \min\{0, \Delta + 6A_-\}, \text{ upstream} \tag{3a}$$

$$\text{or } \max\{0, \Delta - 2A_+\} < X/\tau < \Delta - 12A_+, \text{ downstream.} \tag{3b}$$

Combining there relations with the hydraulic estimates (2) for $A_\pm$ we can deduce that the upstream wavetrain is attached to the obstacle for $-\frac{1}{2}(12F_0)^{\frac{1}{2}} < \Delta < (12F_0)^{\frac{1}{2}}$ and detaches for $-(12F_0)^{\frac{1}{2}} < \Delta < -\frac{1}{2}(12F_0)^{\frac{1}{2}}$, while the downstream wavetrain is detached from the obstacle for $-\frac{1}{2}(12F_0)^{\frac{1}{2}} < \Delta < (12F_0)^{\frac{1}{2}}$ and is attached to the obstacle with the formation of stationery lee waves for $-(12F_0)^{\frac{1}{2}} < \Delta < -\frac{1}{2}(12F_0)^{\frac{1}{2}}$. Further, it can be shown that in the upstream wavetrain each individual wave eventually becomes a solitary wave as $\tau \to \infty$, thus leading to the description of this phenomenon as the generation of upstream solitary waves. Similarly, when the downstream wavetrain is detached from the obstacle, each individual wave eventually becomes a solitary wave. Similar interpretations are available for the non–resonant case, $|\Delta| > (12F_0)^{\frac{1}{2}}$ and for the case of negative forcing, $F_0 < 0$.

The fKdV equation (1) combines the ingredients of nonlinearity and linear wave dispersion with external forcing. In Mitsudera and Grimshaw (1991), we describe a model which adds the concept of flow instability to these basic ingredients. The model is a reduction from the two–layer quasigeostrophic equations in which a coastal current can support a baroclinically unstable wave which is simultaneously resonant in the sense described above. The model equations are a fKdV equation for the thin upper layer, coupled to a linear vorticity equation for the deep lower layer, given by, in non–dimensional co–ordinates,

$$-(A_\tau + \Delta A_X) + 6AA_X + A_{XXX} + F_X + \int_{-L}^{0} \psi U_1 \, dy = 0 \tag{4a}$$

$$(\frac{\partial}{\partial \tau} + U_2 \frac{\partial}{\partial X})\,(\psi_{yy} + \gamma A U_1) + Q_{2y}\,\psi_X = 0 \tag{4b}$$

$$\text{where } \psi = 0 \text{ at } y = -L\,, 0 \tag{4c}$$

$$\text{and } Q_{2y} = \beta - U_{2yy} - \gamma U_1\,. \tag{4d}$$

Here the two–layer fluid occupies a channel $-L < y < 0$ in which the basic flow consists of an upper layer current $U_1(y)$ with $U_1(-L) = U_1(0) = 0$ and a lower–layer current $\alpha U_2(y)$. To leading order the upper–layer stream function is $\alpha A(X\,,\,\tau)\,U_1(y)$ and the lower–layer stream function is $\alpha^2\psi\,(X\,,\,\tau\,;\,y)$. Here $\alpha\gamma$ is the ratio of the upper–layer depth to the lower–layer depth, the upper–layer linear long wave speed is $\alpha\Delta$, $\alpha F(X)$ is a measure of some topographic forcing in the coastline $y = 0$, $X = \epsilon x$ and $\tau = \epsilon\alpha t$ where x is a co–ordinate parallel to the coastline and t is the time. The small parameters α and ϵ^2 again measure the amplitude of the topographic forcing and linear wave dispersion respectively, while here the appropriate balance between nonlinearity and dispersion requires that $\alpha = \epsilon^2$.

To determine the linear long–wave stability features of the system (4a–c) we omit the forcing term (F_X), the nonlinear term $(6AA_X)$ and the linear dispersive term (A_{XXX}) in (4a) and then seek solutions in which A is proportional to $exp\,\{\,ik\,(X - c\tau)\}$ while $\psi = A\phi(y)$. We find that

$$c - \Delta + \int_{-L}^{0} \phi U_1 dy = 0 \tag{5a}$$

$$\phi_{yy} + \gamma\, U_1 - \frac{Q_{2y}}{(c - U_2)}\,\phi = 0 \tag{5b}$$

$$\text{and} \quad \phi = 0 \text{ at } y = L, 0 \tag{5c}$$

A necessary condition for baroclinic instability is that $Q_{2y} < 0$ somewhere, and a typical instability diagram is shown in Figure 2 where we see the occurrence of a bubble of instability as function of Δ. Interestingly the unforced system (4a–c) (i.e. $F = 0$ in (4a)) has a solitary wave solution $A = a\,sech^2\,\{\,l\,(X - c\tau)\,\} + d$, where $a = 2l^2$ and $\psi = A\phi(y)$ provided that

$$c - \Gamma + \int_{-L}^{0} \phi U_1 dy = 0 \tag{6a}$$

$$\text{and} \quad \Gamma = \Delta - 2a - 6d\,, \tag{6b}$$

while $\phi(y)$ again satisfies the Rayleigh equation (5b) with boundary conditions (5c). Comparison of (6a, b) with (5a) shows that the only difference is that the linear long wave speed Δ is replaced by the solitary wave speed Γ. Hence we can infer that the solitary waves exist and are stable except when $\Delta_U < \Gamma < \Delta_L$ where $\Delta_U < \Delta < \Delta_L$ defines the instability bubble in Figure 2. But since for solitary waves Γ depends on the amplitude a (see (6b)) and a must be positive (since $a = 2\beta$), we can expect that if unstable solitary waves occur they will increase in amplitude up to a threshold amplitude, beyond which they stabilize. Numerical solutions of the unforced system (4a–c) confirm this expectation.

When the forcing term (F_x) is included in (4a) numerical solutions of the system (4a–c) by Mitsudera and Grimshaw (1991) show that initially the solution develops into an upstream wavetrain, a stationary depression in the lee of the obstacle and a downstream wavetrain, similar to the solution of the fKdV equation (1). Now, however, the baroclinic instability mechanism contained in the system (4a–c) allows for the possibility that either or both of these wavetrains may contain unstable waves. In Figure 3 we show an example of a situation where the downstream waves are unstable, and in Figure 4 a case when it is the upstream waves that are unstable. In these numerical solutions we put the channel width $L = -2$ and let $U_1(y) = (\pi + 4/\pi)^{-1} \{ \cos(\pi/2\,(y+1)) + \frac{1}{8}\sin(\pi/2\,(y+1)) \}$ which describes an asymmetric jet flowing in the positive x–direction. For the non–dimensional depth ratio we choose $\gamma = 2.5\,(\pi + 4/\pi)^{-1}$. The forcing term F(x) is typically modelled with a Gaussian–type function of amplitude F_0. In both cases the unstable waves grow in amplitude but simultaneously decrease in speed and eventually stabilize. Although these waves are only approximately solitary waves the amplitude–speed relation defined by (6b), together with the criterion that the waves are unstable only for $\Delta_U < \Gamma < \Delta_L$, is found to provide a reliable guide to the growth and eventual stabilization of these waves. Finally we note that Mitsudera and Grimshaw (1993a, b) add the effects of interfacial and bottom Ekman friction terms to the system (4a–c). This allows for the additional feature that multiple steady states can occur which describe a balance between nonlinearity, topographic forcing, baroclinic instability and frictional dissipation. Further work on this kind of model is being pursued with the aim of applying the concepts involved to the study of the meandering states of coastal currents, or or to the study of atmospheric blocking systems.

References

T.R. Akylas, 1984: "On the excitation of long nonlinear water waves by a moving pressure distribution", J. Fluid Mech., 141, 455–466.

S.L. Cole, 1985: "Transient waves produced by a blow past a bump", Wave Motion, 7, 579–587.

R. Grimshaw, 1987: "Resonant forcing of barotropic coastally trapped waves", J. Phys.Ocean., 17, 53–65.

R. Grimshaw, 1990: "Resonant flow of a rotating fluid past an obstacle: the general case", Stud. Appl. Math., 83, 249–269.

R. Grimshaw, 1992: "Resonant forcing of nonlinear dispersive waves", in the Conference Proceedings "Nonlinear Dispersive Wave Systems", ed. L. Debnath, World Scientific, 1–11.

R. Grimshaw and N. Smyth, 1986: "Resonant flow of a stratified fluid over topography", J. Fluid Mech., 169, 419–464.

. Grimshaw and Z. Yi, 1991: "Resonant generation of finite–amplitude waves by flow past topography on a beta–plane", Stud. Appl. Math., 88, 89–112.

S–J Lee, G.T. Yates and T.Y. Wu, 1989: "Experiments and analyses of upstream–advancing solitary waves generated by moving disturbances", J. Fluid Mech., 199, 569–593.

W.K. Melville and K.R. Helfrich, 1987: "Transcritical two–layer flow over topography", J. Fluid Mech., 178, 31–52.

H. Mitsudera and R. Grimshaw, 1990: "Resonant forcing of coastally trapped waves in a continuously stratified ocean", Pure Appl. Geophys., 133, 635–664.

H. Mitsudera and R. Grimshaw, 1991: "Generation of mesoscale variability by resonant interaction between a baroclinic current and localized topography", J. Phys. Ocean, 21, 737–765.

H. Mitsudera and R. Grimshaw, 1993a: "Effects of friction on a localized structure in a baroclinic current", J. Phys. Ocean. (to appear).

H. Mitsudera and R. Grimshaw, 1993b: "Capture and resonant forcing of solitary waves by the interaction of a baroclinic current with topography", J. Phys. Ocean. (submitted).

A. Patoine and T. Warn, 1982: "The interaction of long quasi–stationary baroclinic waves with topography", J. Atmos. Sic., 39, 1018–1025.

N. Smyth, 1987: "Modulation theory solution for resonant flow over topography", Proc. Roy. Soc., A409, 79–97.

G.B. Whitham, 1974: "Linear and nonlinear waves", J. Wiley, 636pp.

T.Y. Wu, 1987: "Generation of upstream advancing solitons by moving disturbances", J. Fluid Mech., 184, 75–99.

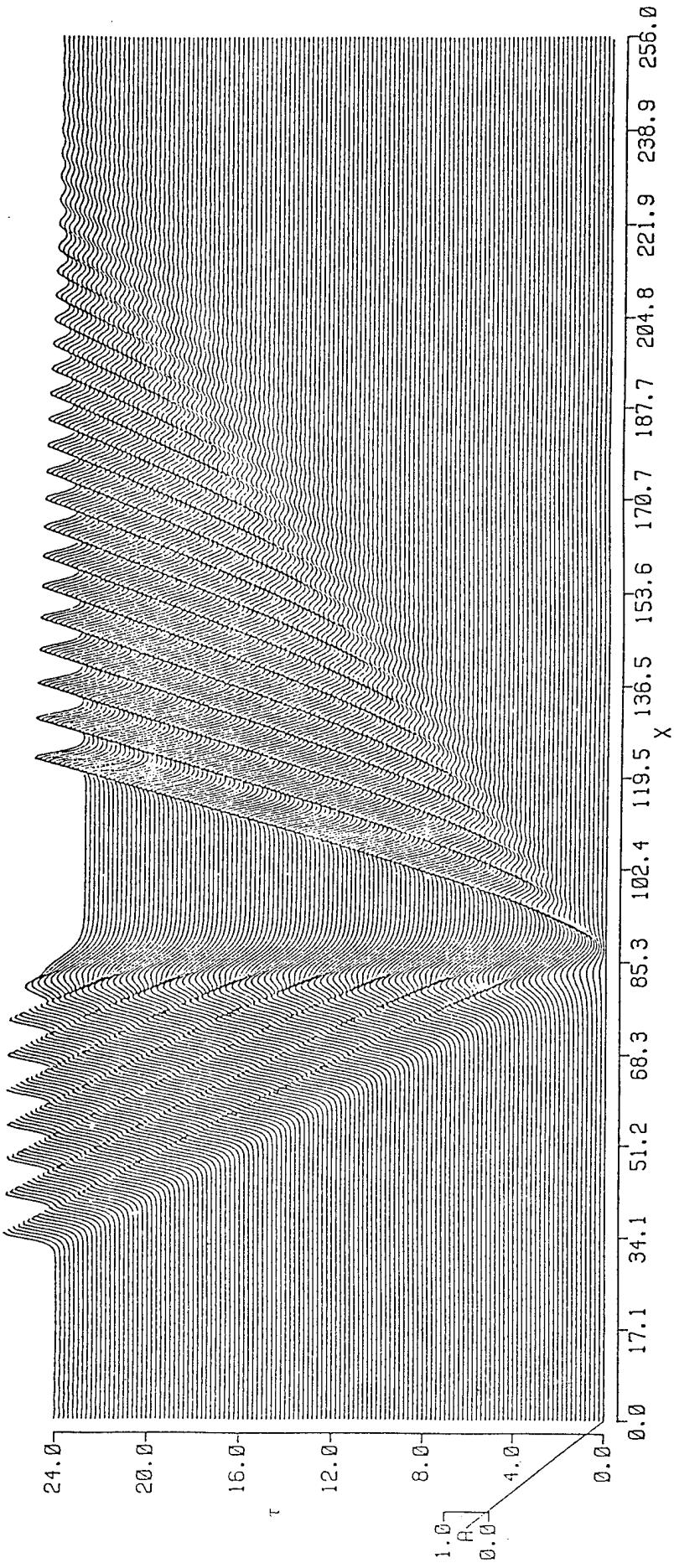

Figure 1: A typical solution of the fKdV equation (1) with $\Delta = 0$ and $F_0 = 1.0$.

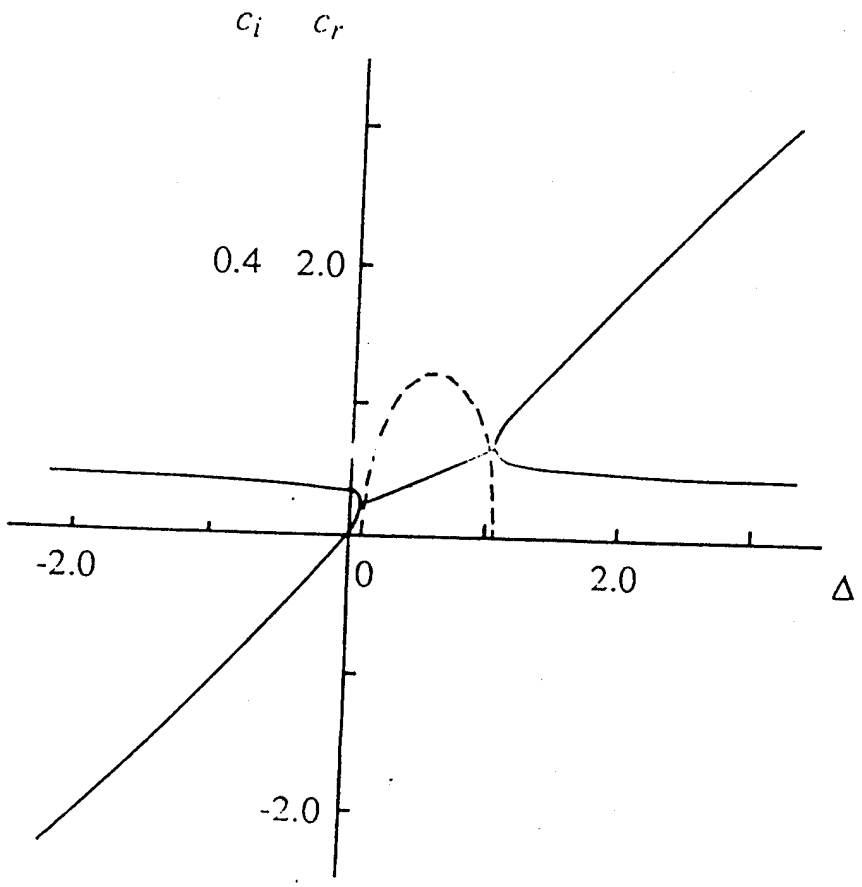

Figure 2: A typical linear long–wave stability diagram for the system (5a–c). Here c_r(–) denotes $Re(c)$ and c_i(——) denotes $Im(c)$. The instability bubble occurs for $\Delta_U < \Delta < \Delta_L$.

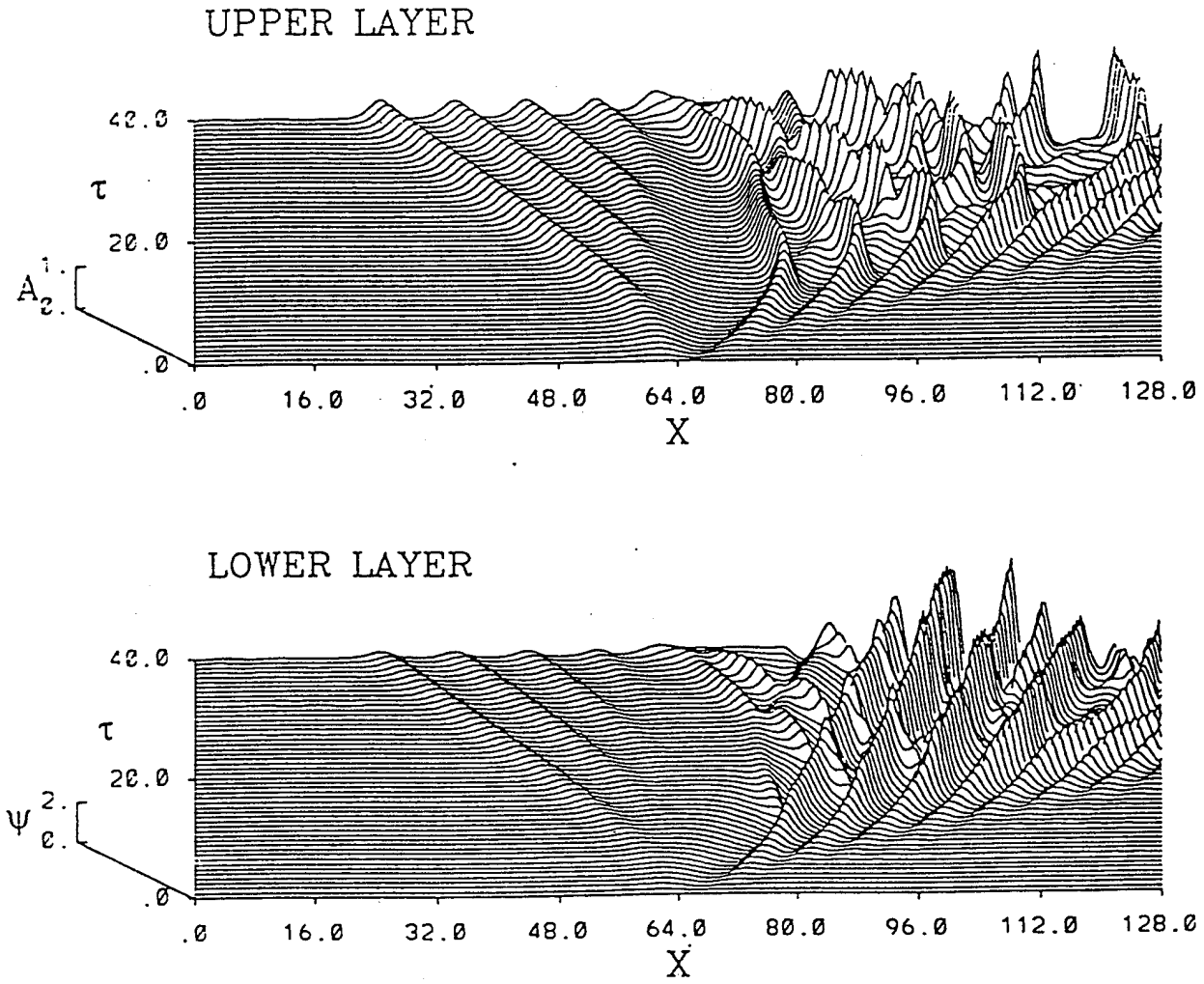

Figure 3: A typical solution of the system (4a–c) showing the development downstream of unstable waves. Here $F_0 = 0.2$, $\Delta = 0$, $\beta = 1$ and $U_2 = 0$. In the lower layer we plot $0.575\psi(x\ ,\ \tau\ ;\ -1)$.

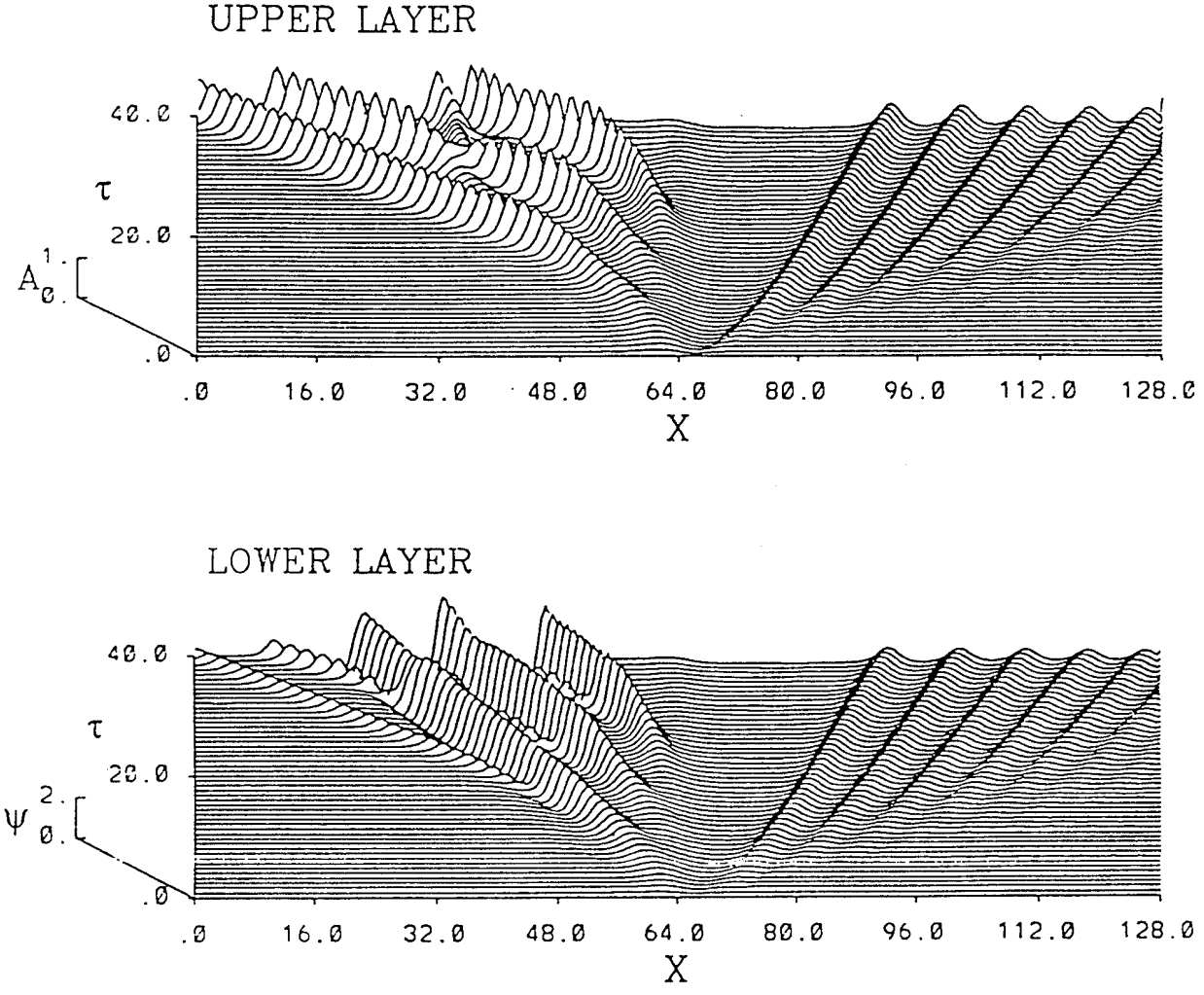

Figure 4: A typical solution of the system (4a–c) showing the development upstream of unstable waves. The parameters are as in Figure 3, except that $U_2 = -1.6$.

Solitary waves with oscillatory tails and exponential asymptotics

by Roger Grimshaw

Department of Mathematics, Monash University, Clayton, Vic. 3168, Australia

Solitary waves are traditionally conceived as localized disturbances of permanent form and propagating with constant speed. One of the classical prototypes is the solitary–wave solution of the Korteweg–de Vries equation

$$u_t + 6uu_x + u_{xxx} = 0 \tag{1}$$

given by $u = u_o(x - c_o t)$ where

$$u_o(x) = a\, sech^2(\gamma x) \tag{2a}$$

and

$$c_o = 2a = 4\gamma^2 \tag{2b}$$

Importantly in the present context we note that in the tail of the solitary wave, as $|x - c_o t| \to \infty$, $u_o \sim 4a\, exp(-\gamma |x - c_o t|)$. Thus the KdV–solitary wave (2a, b) is a genuine solitary wave, with exponential decay in the tail regions.

However, it has recently become recognised that so–called solitary waves may not be genuinely localized and are in fact accompanied by co–propagating oscillatory tails which persist with non–zero amplitudes (see for instance the reviews by Boyd, 1989, 1990, who has called these objects "nanopterons"). This situation may occur in a variety of physical situations including the case of solitary water waves in the presence of surface tension where a combination of numerical work by Hunter and Vanden–broeck (1983), Vanden–broeck (1991) and Vanden–broeck and Dias (1992) and analytical work by Amick and Kirchgassner (1989), Iooss and Kirchgassner (1990), Beale (1991), Sun (1991) and Dias and Iooss (1993) has lead to the following general picture. In the absence of any surface tension, there exist solitary water waves of elevation, which can be described by the KdV–solitary wave (2a, b) in the limit of small amplitude. However, when the Bond number (measuring the effect of surface tension) is greater than $1/3$, there exist solitary gravity–capillary waves of depression, which can again be described by the KdV–solitary wave (2a, b) in the limit of small–amplitude. But when the Bond number lies between 0 and $1/3$ there exist two kinds of solitary wave; one kind contains waves of both depression and elevation with decaying oscillations in the tail region; the other kind consists of a solitary wave core of elevation accompanied by non–decaying tail oscillations. It is this latter non–local solitary wave which is the subject of our attention here.

The first step in determining when non–local solitary waves can be expected to occur is to examine the dispersion relation for small–amplitude waves. For instance, the dispersion relation for gravity–capillary waves of phase speed c and wavenumber k is, in suitable non–dimensional co–ordinates,

$$c^2 = \frac{(1 + \tau k^2)}{k} \tanh k \tag{3}$$

where τ is the Bond number. This is plotted in Figure 1 where we draw attention to the distinction between the cases $0 < \tau < 1/3$ and $\tau > 1/3$. Solitary waves are bifurcations from $k = 0$ at $c = c^{(0)}$ where $c^{(0)} = 1$ is the phase speed in the limit $k \to 0$, and always occur in the opposite direction to the sense of the linear dispersion. Thus when

$0 < \tau < 1/3$ we see that c decreases below $c^{(0)}$ as k increases, and hence solitary waves can be expected with a speed $c > c^{(0)}$. But from Figure 1(a) it is apparent that there is now a possibility of a resonance between this solitary wave and a gravity–capillary wave with a finite wavenumber k_r. It is this resonance which produces the co–propagating tail oscillations for the solitary wave. By contrast, when $\tau > 1/3$ we see from Figure 1(b) that the bifurcation is now for $c < c^{(0)}$ and no such resonance can occur.

This simple consideration establishes when one can expect solitary waves to be non–local and accompanied by co–propagating tail oscillations, and also provides an estimate of k_r of the oscillation wavenumber. However, it remains to establish that the resonance actually occurs, and this requires a calculation to determine the amplitude of the tail oscillations. Often, as in the case of gravity–capillary waves, this amplitude is exponentially small with respect to some small parameter characterizing the amplitude of the solitary wave core. A typical form for the amplitude is

$$\text{(slowly varying function of } \epsilon) \ \exp(-\pi/2\epsilon\gamma)$$

where ϵ is the above–mentioned small parameter, and γ is a physical constant. It follows that the tail amplitude cannot be calculated by conventional means using, for instance, power series expansions in ϵ. Instead, the amplitude calculation requires exponential asymptotics, or "asymptotics beyond all orders" in the terminology of Segur and Kruskal (1987), and Kruskal and Segur (1991) who pioneered this technique in the present context. In this short article we outline a refinement of their method using a model equation as an illustrative example. The method we describe here is similar to the approach of Pomeau et al (1988) and Byatt–Smith (1991) for the same model equation, and fuller details can be found in Grimshaw and Joshi (1993). The same method can be applied to other problems, for instance to solitary waves (Akylas and Grimshaw, 1992) and to the Kuramoto–Sivashinsky equation (Grimshaw 1992, 1993).

Consider then the perturbed Korteweg–de Vries equation

$$u_t + 6uu_x + u_{xxx} + \epsilon^2 u_{xxxxx} = 0 , \tag{4}$$

which has been proposed by Hunter and Scheurle (1988) as a model for gravity–capillary waves when the Bond number is just less than $1/3$. Here we describe the construction of non–local solitary wave solutions of (4) when the parameter ϵ is small. For solutions $u = u(x - ct)$ equation (4) becomes

$$-cu + 3u^2 + u_{xx} + \epsilon^2 u_{xxxx} = 0 \tag{5}$$

where a constant of integration can be effectively ignored in this context. The dispersion relation for the linearization of (5) is

$$c = -k^2 + \epsilon^2 k^4 \tag{6}$$

The graph of (6) is similar to that of Figure 1(a) and hence we can expect a resonance to occur between solitary–like waves of speed $c > 0$ and oscillatory waves of wavenumber $k_r \approx \epsilon^{-1}$, noting that here the long–wave phase speed $c^{(0)} = 0$. Further, for a given $c > 0$ the solution of (6) for k has two real solutions, and two pure imaginary solutions, where real solutions correspond to oscillatory behaviour in the tail regions ($|x| \to \infty$) and the pure imaginary solutions correspond respectively to exponential growth or decay as $|x| \to \infty$. Hence a pure solitary wave solution of (5) would require three boundary conditions as $x \to \infty$, and a further three as $x \to \infty$, leading to an overdetermined problem since (5) is only a fourth–order differential equation. We can conclude that pure solitary wave solutions of (5) are extremely unlikely, and indeed the argument which follows

demonstrates that there are no local solitary wave solutions of (5), at least when ϵ^2 is sufficiently small.

First we seek a regular asymptotic expansion u_s of (5) where

$$u_s \sim \sum_{n=0}^{\infty} \epsilon^{2n} u_n(x), \quad c \sim \sum_{n=0}^{\infty} \epsilon^{2n} c_n \tag{7}$$

Here u_o, c_o are given by (2a, b) and correspond to the KdV–solitary wave, while $u_1 = -5au_o + 15u_o^2/2$ and $c_1 = 4a^2$. The general terms u_n, c_n are readily calculated by a recursion formula (in fact $c_n = 0$ for $n \geq 2$). It is found that this asymptotic expansion u_s contains no tail oscillations, and satisfies the symmetry condition that $u(x) = u(-x)$. However, as already noted, the tail oscillations are exponentially small with respect to ϵ, and hence cannot be detected by asymptotic expansions of the form (7). To find these tail oscillations we observe that u_s is singular in the complex x–plane at $x = \pm(2n + 1)\ i\pi/2\gamma$ $(n = 0, 1, 2 \ldots)$, and motivates us to consider the solution structure near these points. Thus let

$$x = \frac{i\pi}{2\gamma} + \epsilon q \tag{8}$$

and we then find that

$$u_s \sim \frac{1}{\epsilon^2}\left\{-\frac{2}{q^2} + \frac{30}{q^4} - \frac{930}{q^6} + \ldots\right\} + 0(1). \tag{9}$$

Next, motivated by the form of (9) we put $v = \epsilon^2 u$ and change independent variables from x to q using (8). Omitting an $0(\epsilon^2)$ term we get

$$v_{qqqq} + v_{qq} + 3v^2 = 0 \tag{10}$$

Our aim now is to solve equation (10) subject to a matching condition obtained from (9),

$$v \sim -\frac{2}{q^2} + \frac{30}{q^6} - \frac{930}{q^6} + \ldots, \text{ as } |q| \to \infty \text{ in } Re(q) \geq 0, \quad Im(q) < 0, \tag{11}$$

and the symmetry condition that $Im\{v(q)\} = 0$ on $Re(q) = 0$, $Im(q) < 0$. To solve (10) we use a Laplace transform

$$v = \int_{\gamma} exp(-sq)\ V(s)\ ds, \tag{12}$$

where the contour γ runs from $s = 0$ to infinity in the half–plane $Re(q) \geq 0$, $Im(q) < 0$. Substituting (12) into (10) we obtain the Volterra integral equation

$$(s^4 + s^2)\ V(s) + 3\int_0^s V(\lambda)\ V(s-\lambda)\ d\lambda = 0 \tag{13}$$

From the form of (13) we can anticipate that $V(s)$ has singularities at $s = \pm i, \pm 2i, \ldots$. (but not at $s = 0$) and the contour γ must be chosen to avoid these. Standard iteration techniques can now be used to establish the existence of a unique solution $V(s)$ of (13). To construct this solution we first try

$$V(s) = \sum_{0}^{\infty} a_n s^{2n+1} \quad . \tag{14}$$

and substitution into (13) yields the recurrence relation

$$\left\{ \frac{(2n-1)(2n+6)}{(2n+2)(2n+3)} \right\} a_n + a_{n-1} + 3 \sum_{r=1}^{n-1} a_r \, a_{n-r} \frac{(2r+1)! \ (2n-2r+1)!}{(2n+3)!} = 0 \, ,$$

$$\text{for } n = 2, 3 \ldots \tag{15}$$

where $a_0 = -2$, $a_1 = 5$. Also substitution of (14) into (12) and term–by–term evaluation verifies that the matching condition (11) is satisfied. But as $n \to \infty$, $a_n \sim (-1)^n K$ where K is a constant, found numerically such at $K \approx -19.97$. It follows that the series (14) converges only for $|s| < 1$ and for $|s| \geq 1$ on the contour γ , $V(s)$ must be determined by analytic continuation using (13). But since $a_n \sim (-1)^n K$ as $n \to \infty$ we can infer that $V(s)$ has a singularity at $s = \pm i$ where

$$V(s) \approx \frac{Ks}{1+s^2} \quad \text{as} \quad s \to \pm \, i \tag{16}$$

In particular the contour γ must now be chosen to pass to the right or left of the singularity at $s = i$. To fix ideas we let γ pass to the right (i.e. γ lies in $Re(s) \geq 0$) .

It remains to satisfy the symmetry condition on the imaginary q–axis. Further, it is immediately apparent that with $V(s)$ given by (14) for $|s| <$ | implying in turn the pole singularity at $s = i$ (16), the expression (12) cannot satisfy the symmetry condition. The remedy is to add a subdominant asymptotic term to (12) so that now

$$v \sim \int_{\gamma} exp\,(-sq)\ V(s) ds \ + \ \tfrac{1}{2}\, ibexp\,(-iq \ + \ i\delta), \tag{17}$$

where b , δ are real constants to be determined. Note here that $|exp\,(-iq)|$ is smaller than any power of q^{-2n} as $|q| \to \infty$ in $Re(q) \geq 0$, and hence this exponential term does not affect the matching condition (11), and further $exp(-iq)$ is an approximate solution of (10), again as $|q| \to \infty$ in $Re(q) \geq 0$, $Im(q) < 0$. The symmetry condition is now applied by moving the contour γ to the imaginary s–axis, deforming the contour around the singularity at $s = i$. We find that

$$b \cos \delta = -\pi K \tag{18}$$

The final step is to bring the solution v (17) back to the real x–axis using (8). Taking account of a corresponding contribution from the singularity at $x = -i\pi/2\gamma$ we get, in $x \geq 0$,

$$u \sim u_s + \frac{b}{\epsilon^2} \, exp\,(-\frac{\pi}{2\epsilon\gamma}) \, \sin\,(\frac{x}{\epsilon} - \delta) \, , \tag{19}$$

where we recall that u_s is given by (7) and defines the solitary wave core. It is obtained from the integral term in (17), while the tail oscillation term in (19) comes from the subdominant exponential term in (17). The expression (19) defines a one–parameter family of non–local solitary wave solutions of (4), and this result compares well with the numerical solutions of (5) obtained by Boyd (1991).

As a final comment we recall that the non–local solitary wave solution (19) is symmetric, and contains tail oscillations, both as $x \to \infty$ and as $x \to -\infty$. It follows that this solution has an energy flux both as $x \to \infty$ and as $x \to -\infty$, and since here the group velocity is approximately $2/\epsilon^2$ (obtained from (6)), this is positive. Hence this solution can only be generated by appropriate energy sources and sinks as $x \to -\infty$ and $x \to \infty$. If instead equation (4) is solved with a localized initial condition, we expect the solution to consist of solitary waves accompanied by radiating oscillations to the right only. Such solitary waves cannot be exactly steady since they continue to lose energy to this radiation. These aspects are discussed further by Benilov et al (1993).

References

C.J. Amick and K. Kirchgässner, 1989: "A theory of solitary waves in the presence of surface tension", Arch. Rat. Mech. Anal., **105**, 1–49.

T.R. Akylas and R.H.J. Grimshaw, 1993: "Solitary internal waves with oscillatory tails", J. Fluid Mech., **242**, 279–298.

J.T. Beale, 1991: "Exact solitary water waves with capillary waves at infinity", Comm. Pure Appl. Maths., **44**, 211–247.

E.S. Benilov, R. Grimshaw and E.P. Kuznetsova, 1993: "The generation of radiating waves in a singularly perturbed Korteweg–de Vries equation", Physica D, (to appear).

J.P. Boyd, 1989: "Weakly nonlocal solitary waves", in Mesoscale/Synoptic Coherent Structures in Geophysical Turbulence, ed. J.C.J. Nihoul and B.M. Jamart, Elsevier, 103–112.

J.P. Boyd, 1990: "New directions in solitons and nonlinear periodic waves: polycnoidal waves, imbricated solitons, weakly nonlocal solitary waves, and numerical boundary value algorithms", Adv. Appl. Mech., **27**, 1–82.

J.P. Boyd, 1991: "Weakly non–local solitons for capillary–gravity waves: fifth–degree Korteweg–de Vries equation", Physica D, **48**, 119–146.

J.G. Byatt–Smith, 1991: "On the existence of homoclinic and heteroclinic orbits for differential equations with a small parameter", Eur. J. Appl. Maths, **2**, 133–159.

F. Dias and G. Iooss, 1993: "Capillary–gravity in waves with damped oscillations", Physica D, **65**, 399–423.

R. Grimshaw, 1992: "The use of Borel–summation in the establishment of non–existence of certain travelling–wave solutions of the Kuramoto–Sivashinsky equation", Wave Motion, **15**, 393–395.

R. Grimshaw, 1993: "Exponential asymptotics in the reduced Kuramoto–Sivashinsky equation", in Proceedings of the meeting on Nonlinear Diffusion Phenomena, Bangalore, 1992, (to appear).

R. Grimshaw and N. Joshi, 1992: "Weakly non–local solitary waves in a singularly perturbed Korteweg–de Vries equation", SIAM J. Appl. Maths., (submitted).

J.K. Hunter and J–M. Vandenbroeck, 1983: "Solitary and periodic gravity–capillary waves of finite–amplitude", J. Fluid Mech., **134**, 205–219.

J.K. Hunter and J. Scheurle, 1988: "Existence of perturbed solitary wave solutions to a model equation for water waves", Physica D, 253–268.

G. Iooss and K. Kirchgässner, 1990: "Bifurcation d'ondes solitaires en présence d'une faible tension superficielle", C.R. Acad. Sci. Paris, **311**, 265–268.

M.D. Kruskal and H. Segur, 1991: "Asymptotics beyond all orders in a model of crystal growth", Stud. Appl. Math., **85**, 129–181.

Y. Pomeau, A. Ramani and B. Grammaticus, 1988: "Structural stability of the Korteweg–de Vries solitons under a single perturbation", Physica D, **31**, 127–134.

H. Segur and M.D. Kruskal, 1987: "Non–existence of small amplitude breather solutions in ϕ^4 theory", Phys. Rev. Lett., **58**, 747–750.

S.M. Sun, 1991: "Existence of a generalized solitary wave with positive Bond number smaller than 1/3", J. Math. Anal. Appl., **156**, 471–504.

J–M. Vandenbroeck, 1991: "Elevation solitary waves with surface tension", Phys. Fluids, **A3**, 2659–2663.

J–M. Vandenbroeck and F. Dias, 1992: "Gravity–capillary solitary waves in water of infinite depth and related flows", J. Fluid Mech., **240**, 549–577.

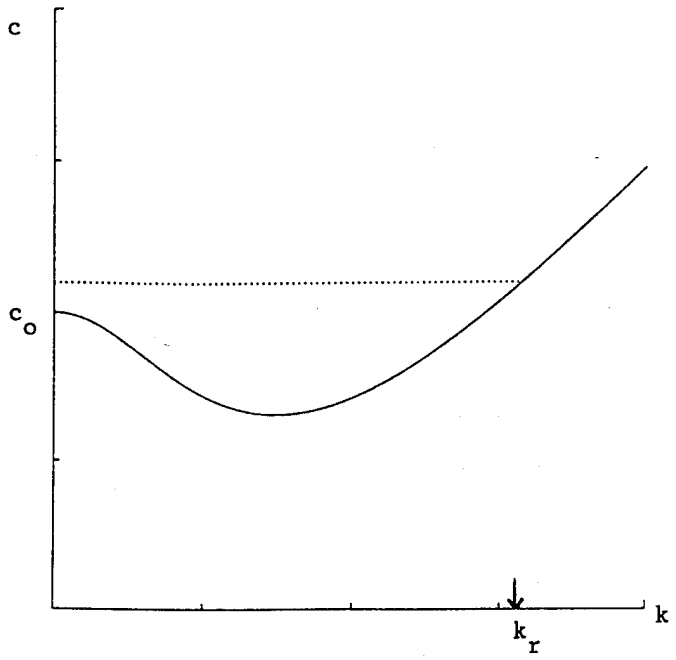

Figure 1(a): Plot of dispersion relation (3) for $\tau = 0.2$

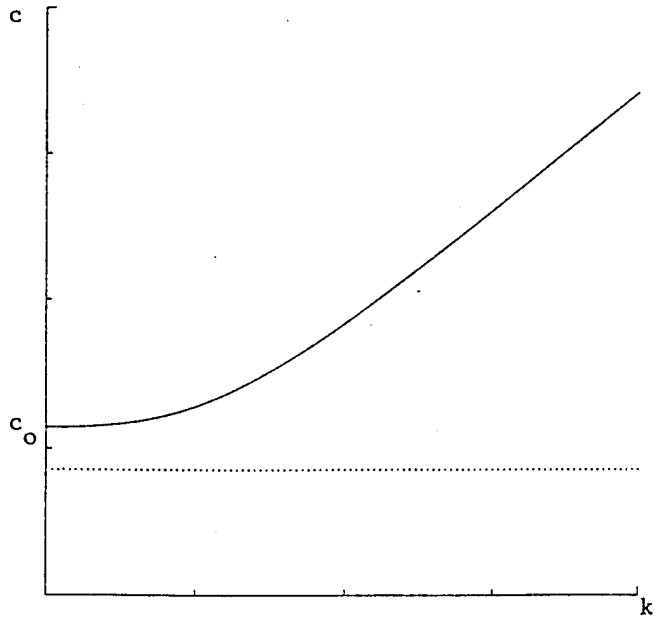

Figure 1(b): Plot of dispersion relation (3) for $\tau = 0.35$

Vertical Temperature Gradient Finestructure Spectra in the Gulf of California

Juan A. Rodrigues-Sero, Myrl C. Hendershott

Vertical temperature gradient finestructure in the upper kilometer of the water column in the Gulf of California was studied by making CTD vertical yoyos lasting a semidiurnal period at locations ranging from the center of Guaymas Basin (tens of km from coasts and thousands of m deep) to the shallow sills (a few hundred m deep) that separate Guaymas Basin from the shallow northern Gulf and over which spring tidal currents are likely to be supercritical with respect to internal wave speeds. Spring tide vertical temperature gradient (VTG) spectra observed at these yoyo locations show internal wave levels (defined below) that rise from near open ocean values in central Guaymas Basin to values about 15 times open ocean values very near the sills. Spring tide VTG spectra in central Guaymas Basin closely resemble open ocean spectra, being nearly flat at the lowest wavenumbers $k < O(0.1$ cpm) and then falling off nearly as k^{-1}. Further towards the sills the transition between the flat region and the k^{-1} falloff occurs at smaller wavenumbers, and the k^{-1} region itself terminates with a region of increase towards very high wavenumbers.

The differences in shape between different Gulf VTG spectra and between Gulf and open ocean VTG spectra are accountable for in a composite model of ocean vertical gradient spectra which connects the Garret-Munk internal wave spectra (flat at low wavenumbers k) with the Kolmogoroff and Obukhov Universal spectra (varying as $k^{1/3}$ at high wavenumber) through an intervening saturated internal wave region (varying as k^{-1} between an internal wave saturation wavenumber k_R and a higher wavenumber k_{OZ} corresponding to the largest vertical scale at which overturning can occur). The composite spectral model is largely conventional, the new ingredients are (1) use of Gregg's recent suggestion that kinetic energy dissipation ε has the simple dependance N^2E^2 on local Vaisala frequency N and Garret-Munk internal wave level E, and (2) care with constants in patching the spectra together. In the Gulf of California, where stratification is primarily determined by temperature, the resulting VTG spectra $F_{TZ}(k)$ vary with local mean vertical temperature gradient T_o' and with E as:

$$F_{TZ}(k) \approx (T_o'^2)\, E \qquad k^* < k < k_R, \qquad (1)$$

$$k_R \approx E^{-1}, \qquad (2)$$

$$F_{TZ}(k) \approx (T_o'^2)/k \qquad k_R < k < k_{OZ}, \qquad (3)$$

$$k_{OZ} \approx E^{-1}\,(T_o'^2)^{1/4}, \qquad (4)$$

$$F_{TZ}(k) \approx E^{4/3}\,(T_o'^2)^{5/3}\,k^{1/3} \qquad k_{OZ} < k, \qquad (5)$$

in which k^* is a wavenumber corresponding to a low mode internal wave vertical scale.

The scaling (1, 2, 3) with with T_o' and with E (estimated from the low wavenumber part of the spectra) successfully collapses all the Gulf VTG spectra that have an approximately flat internal wave region followed by a k^{-1} saturated internal wave region. The scaling (3, 4, 5) successfully predicts the wavenumber k_{OZ} at which the k^{-1} region terminates, but only qualitatively predicts the dependance on T_o' of VTG spectra for $k > k_{OZ}$.

A further consequence of the composite spectral model is an estimate of internal wave induced diapycnal diffusivity K_V of heat or salt. In the open ocean this estimate yields $K_V \approx 0.15$ cm^2/s, but in the high internal wave energy region just south of the sills it yields $K_V \approx 34$ cm^2/s. This is roughly a third of the value that would be required to completely account for spring-neap changes in vertical profiles of temperature recently observed in this part of the Gulf.

On the representation of a magnetic field as vector product of two gradients.

Louis N. Howard

Suppose α and β are scalars evolving according to the scalar advection equation

$$\left(\frac{\partial}{\partial t} + \mathbf{v}\cdot\nabla\right)(\alpha,\beta) = 0$$

and let $\mathbf{A} = \nabla\alpha \times \nabla\beta$. To show that then $\mathbf{A}$ satisfies the induction equation [$\mathbf{A}_t = \nabla\times(\mathbf{v}\times\mathbf{A}) = \mathbf{A}\cdot\nabla\mathbf{v} - \mathbf{v}\cdot\nabla\mathbf{A}$ (when div $\mathbf{v} = 0$)], we may calculate as follows:

$$\begin{aligned}
\mathbf{A}_t &= \nabla\alpha_t \times \nabla\beta + \nabla\alpha \times \nabla\beta_t \\
&= -\nabla(\mathbf{v}\cdot\nabla\alpha)\times\nabla\beta - \nabla\alpha\times\nabla(\mathbf{v}\cdot\nabla\beta) \\
&= -\nabla\times((\mathbf{v}\cdot\nabla\alpha)\nabla\beta) + \nabla\times((\mathbf{v}\cdot\nabla\beta)\nabla\alpha) \\
&= \nabla\times[(\mathbf{v}\cdot\nabla\beta)\nabla\alpha - (\mathbf{v}\cdot\nabla\alpha)\nabla\beta] \\
&= \nabla\times[\mathbf{v}\times(\nabla\alpha\times\nabla\beta)] = \nabla\times[\mathbf{v}\times\mathbf{A}]
\end{aligned}$$

Now if we have a *magnetic* field $\mathbf{B}(\mathbf{x},t)$ which at $t = 0$ has the representation $\mathbf{B}(\mathbf{x},0) = \nabla\alpha_0 \times \nabla\beta_0$, then we may take α_0 and β_0 as initial conditions for α and β, which are to evolve according to the scalar advection equation. Then the field $\mathbf{A} = \nabla\alpha\times\nabla\beta$ will satisfy the induction equation, as above, and assuming $\mathbf{v}$ such that this equation has a unique solution to the initial value problem (continuity and boundedness of $\mathbf{v}$ and its first derivatives would suffice, though considerably less would do), we conclude that $\mathbf{B} = \mathbf{A}$: i.e., the representation $\mathbf{B} = \nabla\alpha\times\nabla\beta$ persists.

If the region of interest is not all space and the flow crosses its boundary at some points, there are some further issues. Both the initial value problems for the advection equation and for the induction equation will require the specification of boundary data at inflow points in order to have unique solutions. If $\mathbf{B}$ and $\mathbf{v}$ are defined in all space but the region in which $\mathbf{B}(\mathbf{x},0) = \nabla\alpha_0\times\nabla\beta_0$ is not all space, these boundary issues can to some extent be avoided by restricting attention not to the same region in space as at $t = 0$, but to the same set of fluid particles. Then the region in which we continue to have $\mathbf{B} = \nabla\alpha\times\nabla\beta$ would itself move with the fluid.

On being frozen-in

If some region in space is occupied by a fluid continuum moving with velocity $\mathbf{v}(\mathbf{x},t)$, the *particle paths* are perhaps most clearly described as curves in the 4-dimensional space-time which are integral curves of the equations

$$\begin{aligned}
\frac{d\mathbf{x}}{d\tau} &= \mathbf{v}(\mathbf{x},t) \\
\frac{dt}{d\tau} &= 1
\end{aligned} \tag{1}$$

the 'world lines' of the fluid particles. The projections of these curves onto the space may be very complicated curves with many self-intersections, but in principle we can imagine the differential equations solved and the results expressed in the form $\mathbf{x} = \mathbf{P}(\mathbf{x}_0, t_0; t)$, this $\mathbf{P}$ giving the position at time t of the particle which at time t_0 was at $\mathbf{x}_0$.

For any vector field $\mathbf{A}(\mathbf{x})$ (which may also depend on t) we can define the 'lines' of the field as the integral curves (in space) of the system

$$\frac{d\mathbf{x}}{ds} = \mathbf{A}(\mathbf{x}).$$

The lines in this sense of the velocity field $\mathbf{v}(\mathbf{x}, t)$, at time t, are the 'instantaneous streamlines'; while they coincide with the projections onto space of the particle paths when the velocity field is independent of time, they are in general not the same at all. The lines of a vector field $\mathbf{A}(\mathbf{x}, t)$ are integral curves of

$$\frac{d\mathbf{x}}{ds} = \mathbf{A}(\mathbf{x}, t) \tag{2}$$

and may be described by functions of the form $\mathbf{x} = \mathbf{X}(t, \mathbf{x}_0; s)$, in which t appears simply as an extra parameter, $\mathbf{x}_0$ being the value of $\mathbf{X}$ when $s = 0$, the initial condition for the system (2) (in which t is arbitrary but fixed). Under fairly weak assumptions about the field $\mathbf{A}$; e.g., Lipschitz continuity in $\mathbf{x}$, the lines of the field exist and are unique. (If $\mathbf{x}_0$ is a critical point of (2) — where $\mathbf{A} = 0$ — the 'line' through $\mathbf{x}_0$ is of course just the point $\mathbf{x}_0$ itself.) The solutions of the equation can be extended from $s = 0$ forward and backward either for all s, or until the integral curve reaches the boundary of the region of definition of $\mathbf{A}$.

Now a vector field $\mathbf{A}$ may be described as *frozen-in* (with respect to the given velocity field $\mathbf{v}(\mathbf{x}, t)$), if the following is the case: Take an arbitrary line of $\mathbf{A}$ at time t_0, follow the fluid particle paths starting on this line at t_0 to an arbitrary (different) time t_1; if the resulting curve of particle positions remains a line of $\mathbf{A}$ — now of $\mathbf{A}(\mathbf{x}, t_1)$ — and if this is true for all t_0, t_1 and original lines, then call $\mathbf{A}$ "frozen-in."

This geometrical or kinematic concept of being frozen-in is evidently a property of the *lines* of $\mathbf{A}$, and not precisely of $\mathbf{A}$ itself, in the sense that if $\mathbf{A}$ is frozen-in so is any other field $\lambda(\mathbf{x}, t)\mathbf{A}(\mathbf{x}, t)$ which has the same lines. To express this concept of being frozen-in in an infinitesimal form, we first solve the particle path equations (1) with the initial conditions (at $\tau = 0$): $\mathbf{x} = \hat{\mathbf{x}}_0$, $t = t_0$. This may be done, for instance, by Picard iteration for small τ with the result (assuming suitable differentiability)

$$\begin{aligned} \mathbf{x} &= \hat{\mathbf{x}}_0 + \tau \mathbf{v}(\hat{\mathbf{x}}_0, t_0) + O(\tau^2) \\ t &= t_0 + \tau \end{aligned} \tag{3}$$

Similarly, we solve (2) to compute the line of $\mathbf{A}$ through the point $\mathbf{x}_0$ at $t = t_0$ as:

$$\mathbf{x} = \mathbf{x}_0 + s\mathbf{A}(\mathbf{x}_0, t_0) + \frac{1}{2}s^2 \mathbf{A}(x_0, t_0) \cdot \nabla \mathbf{A}(\mathbf{x}_0, t_0) + O(s^3) \tag{4}$$

Now taking the initial point $\hat{\mathbf{x}}_0$ in (3) as a point on this line of $\mathbf{A}$ corresponding to some (small) value of s in (4); i.e.,

$$\hat{\mathbf{x}}_0 = \mathbf{x}_0 + s\mathbf{A}(\mathbf{x}_0, t_0) + \frac{1}{2}s^2 \mathbf{A}(\mathbf{x}_0, t_0) \cdot \nabla \mathbf{A}(\mathbf{x}_0, t_0) + \ldots$$

(3) gives for some fixed (small) value of τ a parametrization by s of the curve occupied at $t_0 + \tau$ by the particles which at t_0 were on the line of $\mathbf{A}$. The tangent to this curve thus has the direction $\frac{d\hat{\mathbf{x}}_0}{ds} + \tau \frac{d\hat{\mathbf{x}}_0}{ds} \cdot \nabla \mathbf{v}(\hat{\mathbf{x}}_0, t_0) + O(\tau^2)$ in which

$$\frac{d\hat{\mathbf{x}}_0}{ds} = \mathbf{A}(\mathbf{x}_0, t_0) + s\mathbf{A}(\mathbf{x}_0, t_0) \cdot \nabla \mathbf{A}(\mathbf{x}_0, t_0) + O(s^2)$$

so to first order in s and τ this tangent has the direction

$$\mathbf{A}(\mathbf{x}_0,t_0)+s\mathbf{A}(\mathbf{x}_0,t_0)\cdot\nabla\mathbf{A}(\mathbf{x}_0,t_0)+\tau\mathbf{A}(\mathbf{x}_0,t_0)\cdot\nabla\mathbf{v}(\mathbf{x}_0,t_0) \tag{5}$$

If A is to be frozen-in, this vector should be parallel to the vector $\mathbf{A}$ at the corresponding point, namely (to first order) $\mathbf{x}_0+s\mathbf{A}(\mathbf{x}_0,t_0)+\tau\mathbf{v}(\mathbf{x}_0,t_0)$, and at time $t_0+\tau$, which is

$$\mathbf{A}(\mathbf{x}_0,t_0)+(s\mathbf{A}(\mathbf{x}_0,t_0)+\tau\mathbf{v}(\mathbf{x}_0,t_0))\cdot\nabla\mathbf{A}(\mathbf{x}_0,t_0)+\tau\mathbf{A}_t(\mathbf{x}_0,t_0)=\mathbf{A}+s\mathbf{A}\cdot\nabla\mathbf{A}+\tau(\mathbf{A}_t+\mathbf{v}\cdot\nabla\mathbf{A}) \tag{6}$$

(Here $\mathbf{A}$ and $\mathbf{v}$, and their derivatives, are to be evaluated at $\mathbf{x}_0$, t_0.) The cross product of the vectors (5) and (6), to first order in s and τ, is thus $\tau\mathbf{A}\times(\mathbf{A}_t+\mathbf{v}\cdot\nabla\mathbf{A}-\mathbf{A}\cdot\nabla\mathbf{v})$ and so if $\mathbf{A}$ is frozen-in we must have, at each interior point of the relevant space-time region,

$$\mathbf{A}\times(\mathbf{A}_t+\mathbf{v}\cdot\nabla\mathbf{A}-\mathbf{A}\cdot\nabla\mathbf{v})=0 \tag{7}$$

To demonstrate the converse, namely that if (7) holds, or equivalently if $\mathbf{A}$ satisfies an evolution equation of the form

$$\mathbf{A}_t+\mathbf{v}\cdot\nabla\mathbf{A}-\mathbf{A}\cdot\nabla\mathbf{v}=\lambda\mathbf{A} \tag{8}$$

for some scalar field $\lambda(\mathbf{x},t)$, then $\mathbf{A}$ is frozen-in, we may proceed as follows. (To avoid consideration of flow across boundaries, we here just assume the fields are defined in all of the $\mathbf{x}$-space. We also assume that $\mathbf{v}$ and $\mathbf{A}$ and their first $\mathbf{x}$-derivatives are continuous.)

Let $\mathbf{X}(s)$ be the solution of (2) for $t=t_0$, with $\mathbf{x}(0)=\mathbf{x}_0$; ($\mathbf{X}(s)$ gives a parametric description of the line of $\mathbf{A}$ through the arbitrary point $\mathbf{x}_0$ at time t_0).

Let $\mathbf{P}(\mathbf{x}_1,t)$ be the solution of $\dfrac{d\mathbf{x}}{dt}=\mathbf{v}(\mathbf{x},t)$, $\mathbf{x}(t_0)=\mathbf{x}_1$; ($\mathbf{P}(\mathbf{x}_1,t)$ is the position at time t of the particle which at t_0 was located at $\mathbf{x}_1$).

Let $Q_{ij}(\mathbf{x}_1,t)=\dfrac{\partial P_i(\mathbf{x}_1,t)}{\partial x_j}$. Then Q_{ij} satisfies $\dfrac{\partial Q_{ij}}{\partial t}=\dfrac{\partial v_i}{\partial x_k}(\mathbf{P}(\mathbf{x}_1,t),t)Q_{kj}$ with $Q_{ij}(\mathbf{x}_1,t_0)=\delta_{ij}$.

Let $\mathbf{Y}(s,t)=\mathbf{P}(\mathbf{X}(s),t)$. $\mathbf{Y}$ gives a curve, parametrized by s, which is the locus at t of the particles which at t_0 occupied the line $\mathbf{X}(s)$. We want to show that provided (7) (or (8)) holds then this curve is a *line* of $\mathbf{A}(\mathbf{x},t)$; i.e., $\dfrac{\partial\mathbf{Y}(s,t)}{\partial s}$ is parallel to $\mathbf{A}(\mathbf{Y}(s,t),t)$. Now $\dfrac{\partial Y_i}{\partial s}=Q_{ik}(\mathbf{X}(s),t)A_k(\mathbf{X}(s),t_0)$. We consider the antisymmetric tensor

$C_{ij}(s,t)=\dfrac{\partial Y_i}{\partial s}A_j(\mathbf{Y}(s,t),t)-\dfrac{\partial Y_j}{\partial s}A_i$, whose vanishing implies the parallelism. Evidently $C_{ij}(s,t_0)=0$, since Q_{ij} is δ_{ij} at $t=t_0$. We compute

$$\begin{aligned}\frac{\partial C_{ij}}{\partial t}&=\frac{\partial}{\partial t}\left[Q_{ik}(\mathbf{X}(s),t)A_k(\mathbf{X}(s),t_0)A_j(\mathbf{Y}(s,t),t)-Q_{jk}(\mathbf{X},t)A_k(\mathbf{X},t_0)A_i(\mathbf{Y},t)\right]\\&=\frac{\partial v_i}{\partial x_\ell}(\mathbf{Y}(s,t),t)Q_{\ell k}(\mathbf{X}(s),t)A_k(\mathbf{X}(s),t_0)A_j(\mathbf{Y}(s,t),t)+Q_{ik}(\mathbf{X},t)A_k(\mathbf{X},t_0)\\&\quad\cdot\left(\frac{\partial A_j}{\partial x_\ell}(\mathbf{Y},t)v_\ell(\mathbf{Y},t)+A_{jt}(\mathbf{Y},t)\right)\\&\quad-\frac{\partial v_j}{\partial x_\ell}(\mathbf{Y}(s,t),t)Q_{\ell k}(\mathbf{X}(s),t)A_k(\mathbf{X}(s),t_0)A_i(\mathbf{Y}(s,t),t)-Q_{jk}(\mathbf{X},t)A_k(\mathbf{X},t_0)\\&\quad\cdot\left(\frac{\partial A_i}{\partial x_\ell}(\mathbf{Y},t)v_\ell(\mathbf{Y},t)+A_{it}(\mathbf{Y},t)\right)\end{aligned}$$

Using (8), this is

$$\begin{aligned}\frac{\partial C_{ij}}{\partial t} &= \frac{\partial v_i}{\partial x_\ell}(\mathbf{Y},t)Q_{\ell k}A_k(\mathbf{X},t_0)A_j(\mathbf{Y},t) + Q_{ik}A_k(\mathbf{X},t_0)(A_\ell(\mathbf{Y},t)\frac{\partial v_j}{\partial x_\ell}(\mathbf{Y},t) + \lambda A_j(\mathbf{Y},t))\\ &\quad - \frac{\partial v_j}{\partial x_\ell}(\mathbf{Y},t)Q_{\ell k}A_k(\mathbf{X},t_0)A_j(\mathbf{Y},t) - Q_{jk}A_k(\mathbf{X},t_0)(A_\ell(\mathbf{Y},t)\frac{\partial v_i}{\partial x_\ell}(\mathbf{Y},t) + \lambda A_j(\mathbf{Y},t))\\ &= \frac{\partial v_i}{\partial x_\ell}(\mathbf{Y},t)[Q_{\ell k}A_k(\mathbf{X},t_0)A_j(\mathbf{Y},t) - Q_{jk}A_k(\mathbf{X},t_0)A_\ell(\mathbf{Y},t)]\\ &\quad + \frac{\partial v_j}{\partial x_\ell}(\mathbf{Y},t)[Q_{ik}A_k(\mathbf{X},t_0)A_\ell(\mathbf{Y},t) - Q_{\ell k}A_k(\mathbf{X},t_0)A_i(\mathbf{Y},t)]\\ &\quad + \lambda(\mathbf{Y},t)[Q_{ik}A_k(\mathbf{X},t_0)A_j(\mathbf{Y},t) - Q_{jk}A_k(\mathbf{X},t_0)A_i(\mathbf{Y},t)]\\ &= \frac{\partial v_i}{\partial x_\ell}(\mathbf{Y},t)C_{\ell j} + \frac{\partial v_j}{\partial x_\ell}(\mathbf{Y},t)C_{i\ell} + \lambda(\mathbf{Y},t)C_{ij}.\end{aligned}$$

Thus $C_{ij}(s,t)$ satisfies a linear homogeneous system of differential equations in t with zero initial conditions, hence is identically zero. Consequently $\dfrac{\partial \mathbf{Y}}{\partial s}$ is indeed parallel to $\mathbf{A}(\mathbf{Y},t)$, and the field $\mathbf{A}$ is frozen-in.

Remarks:

a) The condition (7) is clearly weaker than the induction equation, though it is satisfied if $\mathbf{A}$ *does* satisfy the latter. There are, in fact, *divergence free* fields $\mathbf{A}$ which are frozen-in in this kinematic sense but do not satisfy the induction equation, for instance a field satisfying (8) with λ not zero but a function only of t (when div $\mathbf{v} = 0$), or a field evolving according to $\mathbf{A}_t + \nabla \times (\mathbf{A} \times \mathbf{v}) = \lambda(t)\mathbf{A}$ (which also preserves div $\mathbf{A} = 0$ if it holds initially) even if div $\mathbf{v} \neq 0$.

b) The meaning of the induction equation satisfied by a magnetic field $\mathbf{B}$ is not merely that the field *lines* are carried by the flow into field lines, but the stronger condition that the *flux* of $\mathbf{B}$ through any piece of surface which is carried with the flow is preserved.

c) The induction equation is satisfied by the vorticity vector of an incompressible Euler flow, and from this we may conclude that the flux of vorticity through any piece of surface carried with the flow is preserved. Kelvin's circulation theorem follows from this, for any circuit which is the boundary of a surface lying in the flow domain. If the latter is not simply-connected, however, we cannot in this way deduce Kelvin's theorem for circuits which are not such boundaries, though it is in fact true for them: it follows directly from the Euler equations and the single-valued character of the pressure, independent of the connectivity of the domain. Thus Kelvin's circulation theorem is, for fluid dynamics, more fundamental than the vorticity equation. It does not seem that a similar extension, to the "circulation of the magnetic vector potential," is possible for magnetohydrodynamics, however, since presumably the flux through a circuit surrounding a hole could be externally altered; e.g., if a toroidal flow domain were one winding of a transformer.

Why do synoptic scale eddies like to go to the tropics?

R.Kimura and H.B.Cheong
(Ocean Research Institute of Tokyo Univ., Tokyo)

Observational analysis: Synoptic eddies and the background pressure fields are separated in weather charts at 500hPa to investigate the characteristics of propagation of disturbances produced by the baroclinic instability. The geopotential height data used in this analysis are objectively analysed data set from 1985 to 1991 provided by ECMWF. The weather charts for synoptic eddies and the background pressure fields were made with filtered data of periods from 2.5 to 6.5 days and of periods longer than 7 days, respectively.

Spatial correlation of synoptic eddies were calculated at a base grid point at 45N. The correlation pattern depends upon the choice of the base grid point. We calculated 36 correlation patterns by changing the longitude of the base grid points by 10 degrees(at 45N). Fig.1 is the result made by composite of all correlation patterns so that all base points are the center of the figure to eliminate longitudinal effects as done by Randel(1988). Since the synoptic eddies are produced by the baroclinic instability of the westerly, it is not surprising to get a wave train of a low and high pressure system propagating to the east direction along the latitude circle. However, there is a slight tendency for the wave to propagate equatorward.

This tendency was confirmed by calculating the propagation-velocity vectors of the center

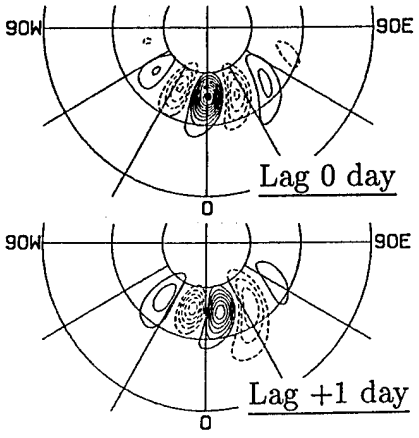

Fig.1 One-point correlation map at 45N in winter season 500hPa. Contour interval is 0.1.

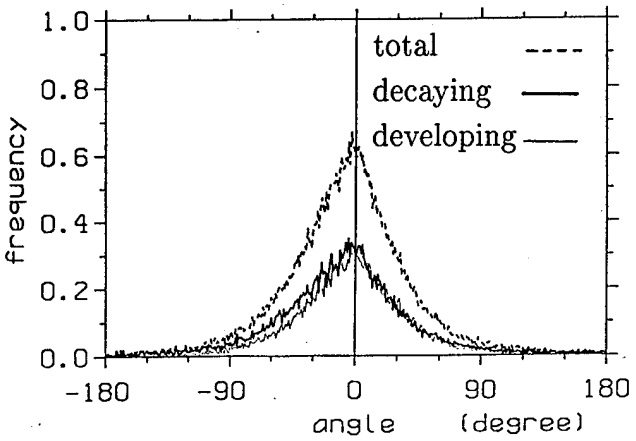

Fig.2 Frequency distributions of angle with zonal direction, normalized by total frequency divided by 50.

of individual pressure anomalies(both positive and negative) by comparing two weather charts with 12 hours interval. Fig.2 shows frequency distributions of angle between each propagation-velocity vectors and the latitude line(negative values mean equatorward propagation). In this figure we separate eddies in the developing stage from the decaying stage. Note that the distribution is not symmetric: The frequency of the equatorward propagation is greater than that of the poleward propagation. Besides, the deviation from the

symmetric distribution is greater for the eddies in the decaying stage than for the eddies in the developing stage. This result implies that the equatorward propagation is caused by the barotropic process, because the baroclinic eddies turn out to be barotropic in the decaying stage. Encouraged by this fact, we try to explain this tendency by means of the non-divergent barotropic vorticity equation.

Propagation of wave-packet and phase tilt: The linearized non-divergent barotropic vorticity equation with a zonal flow $\overline{u}$ on a sphere is written as

$$\frac{\partial \zeta'}{\partial t} = -\frac{\overline{u}}{\cos\theta}\frac{\partial \zeta'}{\partial \lambda} - v'\frac{d}{d\theta}(f+\overline{\zeta}), \tag{1}$$

where all variables are non-dimensional, time being scaled by Ω^{-1} and length by the radius of the earth. λ is longitude, θ is latitude and f is the Coriolis parameter, $2\sin\theta$. Let us introduce the stream function to express $u = -\frac{\partial \psi}{\partial \theta}$, $v = \frac{1}{\cos\theta}\frac{\partial \psi}{\partial \lambda}$ and $\zeta = \nabla^2\psi$. If Eq.(1) is multiplied by $\zeta'\cos\theta$ and averaged in the zonal direction

$$\frac{\partial V}{\partial t} = -2\gamma \cdot \overline{v'\zeta'}\cos\theta \tag{2}$$

$$= +2\gamma \cdot \frac{d}{d\mu}(\overline{u'v'}\cos^2\theta), \tag{3}$$

where μ is sine of latitude, $V = \overline{\zeta'^2}$, and $\gamma = \frac{d}{d\mu}(f+\overline{\zeta})$. The posivive value of γ makes the mean flow free from barotropic instability(Baines,1976). The zonally averaged enstrophy, V, represents the meridional distribution of amplitude of eddies when they are composed of only one zonal wavenumber or an isolated one. We are interested in the propagation of eddies rather than the wave activity discussed in Held and Hoskins(1985).

• **Meridional phase tilt:** Let the stream function with single zonal wavenumber m be written as

$$\psi'(\lambda,\theta) = C_m(\theta)\cos(m\lambda) + S_m(\theta)\sin(m\lambda)$$

$$= \sqrt{C_m^2 + S_m^2}\cos\{m\lambda - m\Xi(\theta)\}, \tag{4}$$

where $m\Xi$ is the longitudinal phase angle at latitude θ i.e. $m\Xi = \tan^{-1}\frac{S_m}{C_m}$. Then, the meridional gradient of phase or the phase tilt is expressed as

$$\frac{\partial \Xi}{\partial \theta} = \frac{1}{m^2}\frac{\overline{u'v'}\cos\theta}{\overline{\psi'^2}}. \tag{5}$$

When a vorticity anomaly is isolated, let (λ_0,θ_0) be a point where $\frac{\partial \psi'}{\partial \lambda} = 0$ i.e. the location of maximum amplitude. If the latitude is increased by infenitesimal amount $\delta\theta$, the longitudinal location of the maximum amplitude will be shifted by $\delta\lambda$.

$$\frac{\partial \psi'}{\partial \lambda}(\lambda_0+\delta\lambda,\theta_0+\delta\theta) = \frac{\partial \psi'}{\partial \lambda} + \frac{\partial^2\psi'}{\partial \lambda^2}\cdot\delta\lambda + \frac{\partial^2\psi'}{\partial\lambda\partial\theta}\cdot\delta\theta \equiv 0, \tag{6}$$

where the first term in rhs vanishes by definition, and the differentiation in rhs is taken at (λ_0, θ_0). If the rhs of Eq.(7) is multiplied by ψ' and averaged,

$$\frac{\delta\lambda}{\delta\theta} \equiv \frac{\partial\Xi}{\partial\theta} = \frac{\overline{u'v'}\cos\theta}{\overline{v'^2}\cos^2\theta}. \tag{7}$$

When the stream function is represented by a single wavenumber m, Eq.(7) is identical to Eq.(5).

In the Eqs.(5) and (7), the NE-SW phase tilt is defined as positive and NW-SE is as negative. Then, the Eq.(3) can be used as a prognostic equation on wave-packet propagation in the meridional direction. Suppose that a wave-packet of zonal wavenumber m whose phase tilt is exactly NE-SW i.e. contant with latitude is located in mid-latitude. In this case the meridional gradient of $\overline{u'v'}\cos\theta$ is positive to the south and negative to the north of the center of it. Form Eq.(3) this means that the wave-packet will propagate into low latitude. Therefore, the wave-packet with NE-SW(NW-SE) phase tilt is expected to propagate into low latitude(high latitude).

•**Phase tilt and wave-packet propagation with $\overline{u} = 0$, $m = 6$:** Eq.(1) is represented by spectral method with truncation N and time integrated with an appropriate initial condition. We consider an initial vorticity field given by

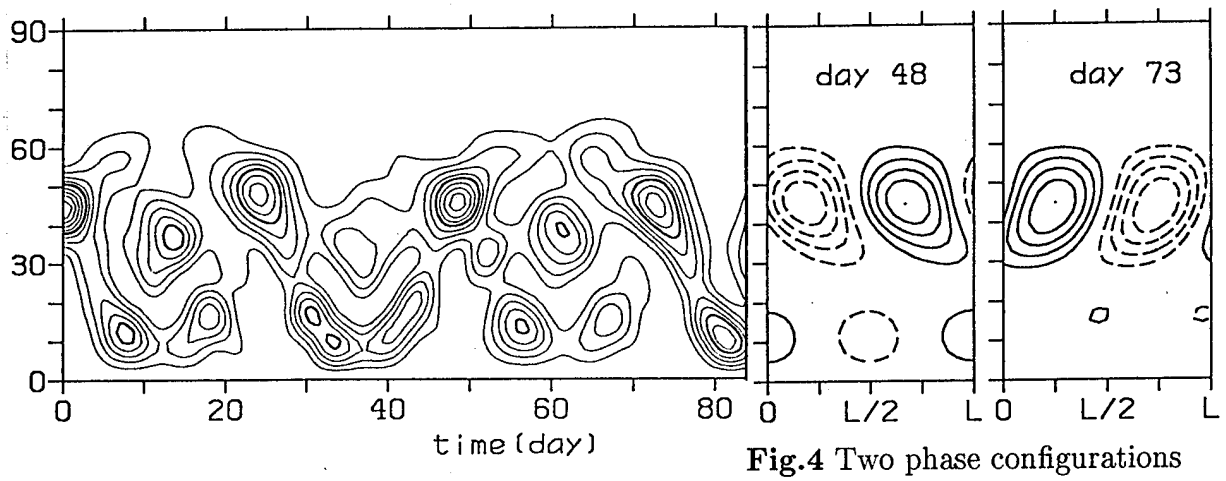

Fig.3 Time evolution of V. Contour interval is 1/10 of the maximum of day 0

Fig.4 Two phase configurations , NW-SE and NE-SW. CI is 1/5 of maximum of initial condition.

$$\zeta' = C\frac{\cos\theta}{\cos\theta_0}\cos(m\lambda)\exp\{-(\frac{\theta-\theta_0}{10^\circ})^2\}, \tag{8}$$

with $m = 6$, $\theta_0 = 45^\circ$ and $C = 0.1$. This vorticity field is symmetric with respect to the equator. Notice that this initial eddy field has no phase tilt. Fig.3 shows time evolution of V. The wave-packet initially located in mid-latitude propagate into low or high latitude, continuously changing the phase tilt. The initial vorticity field is dispersed by the dispersion relation of each modes of Rossby-Haurwitz waves; $\sigma_n^m = -\frac{2m}{n(n+1)}$. The

local maximum of the eddy amplitude propagates into high or low latitudes, by the interference of Rossby-Haurwitz waves. Around the day 73 the wave-packet shows an apparent tendency to propagate toward low latitude, while around the day 48 the wave-packet propagates toward high latitude. Vorticity fields of day 48 and 73 are shown in Fig.4. The phase tilt of them is NW-SE and NE-SW, respectively.

• **Effect of zonal flow:** If the initial eddy given by Eq.(8) is located in a zonal flow, the phase is tilted by the meridional shear of it. Fig.5 shows the time evolutions of the initial eddy in the 4 zonal flows shown in Fig.6. The most striking feature in the presence of the zonal flow is that once the wave-packet propagates into high or low latitude, they are trapped there or reflected and eventually reach a certain latitude. These features can be explained qualitatively. The wave-packet 'A' is splitted into two parts by the zonal flow. The northern part whose phase tilt is NW-SE propagates poleward and the southern part whose phase tilt is NE-SW propagates equatorward. During the propagation the phase tilt is steepened more and more; the phase tilt of the northern part tends to be close W-E and the southern E-W. Before reaching the pole region the phase tilt of the northern part becomes NE-SW, the inverse phase tilt of initial stages, which means the turning of the propagation direction. The wave-packet 'a' is splitted into two parts also, but in this case with the reversed phase tilt compared with the wave-packet 'A'. The wave-packet 'a' tends to back to the mid-latitude forming a waveguide. In case of $m = 6$ the shear effect dominates over that of latitudinally varing Coriolis effect. The simple prognostic Eq.(3)

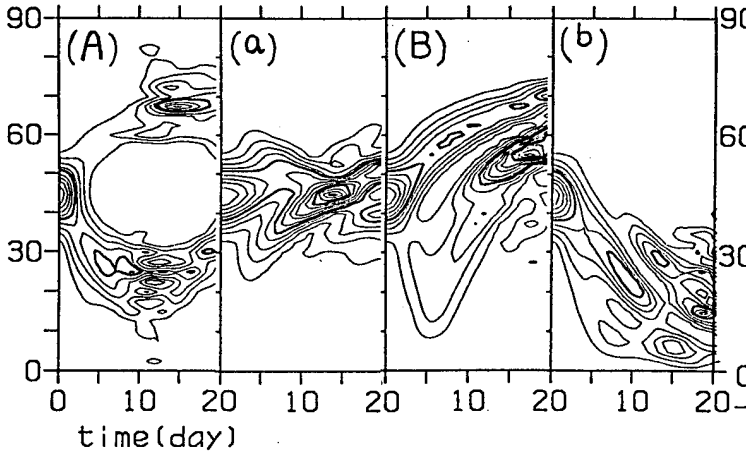

Fig.5 Time evolution of V. The zonal flow type is written on each panel.

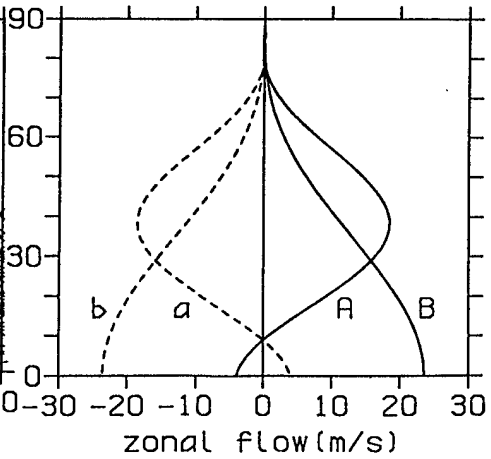

Fig.6 Zonal flows used here.

is useful in interpreting the propagation of Rossby wave-packet in horizontal shear flow as in Yamagata(1976), where the trajectory of the wave-packet was calculated by the ray path theory.

Packet velocity: The usual concept of group velocity cannot be used for the meridional energy propagation in our problem. Instead, we can define a 'packet velocity' on the basis

of the basic concept. The latitudinal location of largest amplitude is solely due to the zonal phase propagation of Rossby-Haurwitz waves in the absence of the zonal flow. In the presence of the shear flow, however, the location of largest amplitude is determined by both the shear flow and the dispersion of Rossby-Haurwitz waves due to the Coriolis factor. Which factor will dominate depends on the detailed profile of the zonal flow as well as the zonal wavenumber of the vorticity field. We define the 'packet velocity' as the propagation speed of the location of local maximum. Let the vorticity field be

$$\zeta' = \sum_{n=m}^{m+N} \hat{\zeta}_n^m P_n^m(\mu) \cos(m\lambda + \alpha_n^m) \tag{9}$$

, where $\alpha_n^m = \sigma_n^m t + \alpha_n^{m0}$, α_n^{m0} is the initial phase in the longitude. Then, by definition and from Eq.(2)

$$V = \frac{1}{2} \sum_{l,n} \hat{\zeta}_l^m \hat{\zeta}_n^m P_l^m(\mu) P_n^m(\mu) \cos(\alpha_l^m - \alpha_n^m), \tag{10}$$

$$\frac{\partial V}{\partial t} = \frac{1}{2} \gamma(\mu) \sum_{l,n} \hat{\zeta}_l^m \hat{\zeta}_n^m P_l^m(\mu) P_n^m(\mu) \sigma_l^m \sin(\alpha_l^m - \alpha_n^m). \tag{11}$$

Let μ_0 be where $\frac{\partial V}{\partial \mu} = 0$ at t_0. Then the packet velocity can be written as

$$V_{gy} \cdot \cos\theta = \frac{\delta\mu}{\delta t} = -\frac{\partial^2 V}{\partial \mu \partial t} \left(\frac{\partial^2 V}{\partial \mu^2} \right)^{-1}. \tag{12}$$

The differentiation with respect to μ can be evaluated directly by using the recursion relation of Legendre polynomials. Once μ_0 is known, the packet velocity can be calculated for any zonal flow. We show the calculated 'packet velocity' of vorticity field of day 73 in Fig.7. The presence of the zonal flow alters the packet velocity to a large extent. The zonal flow of 'A' enhances the equatorward propagation of eddies into low latitude, while 'a' does not.

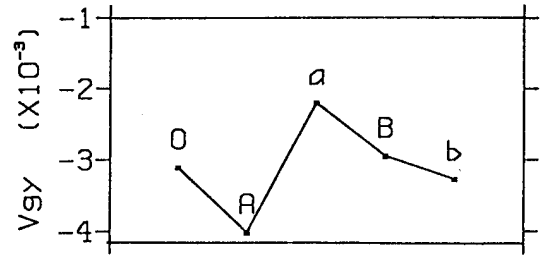

Fig.7 The packet velocity. The letters A,a,B and b represent zonal flow types. O denotes the case without zonal flow.

References

Baines,P.G.(1976): *J.Fluid Mech.*,**73**,193-213.

Held,I.M. and B.J.Hoskins(1985): *Issues in Atmospheric and Oceanic Modelling. Part A: Climate Dynamics*, Academic Press, 3-31

Randel,W.J.(1988): *Tellus*,**40A**,257-271.

Yamagata,T.(1976): *J.Oceanogr.Soc.Japan*,**32**,162-168

Short Wavelength Instabilities of Riemann Ellipsoids

Norman R. Lebovitz
The University of Chicago, Chicago, IL 60637

We consider families of astrophysical flows that are stable under the assumption that they are axially symmetric, but are unstable under even a small departure from axial symmetry. We adopt as models families of Riemann ellipsoids. These figures of uniform density are the only known exact models of self-gravitating fluids that depart from axial symmetry. Their stability has been the subject of many investigations, going back to Riemann [1] himself. Despite this long history, very little is known about their stability to perturbations of length less than, say, one-fourth the average radius. We use the geometrical-optics approximation to study the limit of short wavelengths.

We consider a restricted class of steady-state Riemann ellipsoids, the so-called S-type family (see [2] for a description). In a frame of reference rotating with angular velocity ω about the x_3 axis relative to inertial space, their semiaxes are aligned with the coordinate axes and they have further fluid motions with a velocity, relative to the rotating frame, given by

$$U_1 = \lambda\frac{a_1}{a_2}x_2, \quad U_2 = -\lambda\frac{a_2}{a_1}x_1, \quad U_3 = 0. \tag{1}$$

Here λ is a constant parameter. The parameters λ and ω are related to to the semiaxes a_1, a_2 and a_3 of the ellipsoid through the equations of fluid equilibrium. By virtue of Eq. (1) the vorticity of the flow is constant, having the value $\zeta_R = -\lambda[(a_1/a_2) + (a_2/a_1)]$ relative to the rotating frame, and the value $\zeta_T = 2\omega + \zeta_R$ relative to inertial space. The parameter space is conveniently taken to be the plane of $(a_2/a_1, a_3/a_1)$. The permissible steady state figures occupy a horn-shaped region of the unit square in the first quadrant ([2]). In fact, they occupy two such regions because, for each ellipsoidal shape, there are two choices of the parameters λ and ω. One choice, for which $|\lambda/\omega| \leq 1$, leads to the so-called direct configurations ; the opposite choice leads to the adjoint configurations.

The stability of any one of these figures to small perturbations is governed by the Euler equations of fluid dynamics linearized about the steady-state solution. If the Eulerian perturbation of the Eulerian velocity field is denoted by $u(x,t)$, the geometrical-optics approximation to u is achieved, to leading order, by the ansatz

$$u(x,t) = \exp\{\frac{i\Phi}{\varepsilon}\}a(x,t), \tag{2}$$

where Φ represents a real phase, the small parameter ϵ is a nondimensional measure of the wavelength, and a is the amplitude, which may be spatially localized. We refer to $k = \nabla\Phi$ as the wavenumber, regarded as of order unity. On substitution of this ansatz into the linearized Euler equations under the assumption that the fluid is incompressible, one obtains the eikonal and transport equations (*cf.* [3])

$$\frac{dk}{dt} = -L^t k \tag{3}$$

and

$$\frac{da}{dt} = \left(-(L + 2\Omega) + 2k^{-2}kk^t(L + \Omega)\right)a = Aa, \tag{4}$$

which are compatible with the incompressibility condition $a \cdot k = 0$. Here the matrices L and Ω given by the formulas

$$L = \begin{pmatrix} 0 & \lambda a_1/a_2 & 0 \\ -\lambda a_2/a_1 & 0 & 0 \\ 0 & 0 & 0 \end{pmatrix}, \quad \Omega = \begin{pmatrix} 0 & -\omega & 0 \\ \omega & 0 & 0 \\ 0 & 0 & 0 \end{pmatrix},$$

are constant. The general solution of Eq. (3) is

$$k = k_0(\sqrt{1-\mu^2}\sqrt{\frac{a_2}{a_1}}\cos(\lambda(t-t_0)), -\sqrt{1-\mu^2}\sqrt{\frac{a_1}{a_2}}\sin(\lambda(t-t_0)), \mu), \tag{5}$$

where μ is a parameter representing the angle between the wave-vector k and the x_3 axis at $t = t_0$. As a result, the equation for the amplitude has periodic coefficients. Since the instability or stability of the flow depends on whether the amplitude a grows with time or not, the mathematical problem is one of analyzing a certain linear differential equation with periodic coefficients (see [4],[5],[6]). This has been done with a combination of analytic and numerical methods.

We now turn to the specific results of this analysis, beginning by considering certain special cases that can be treated analytically.

The rigidly rotating ellipsoids of Maclaurin (for which $a_2 = a_1$) and Jacobi (for which $\lambda = 0$ and $a_2 < a_1$) have been the objects of numerous investigations over a period of centuries (*cf.* [7]). The Maclaurin figures are known to be stable to collective modes provided a_3/a_1 exceeds the critical value 0.303 (this is the so-called point of dynamical instability, where the Maclaurin family becomes unstable, in the absence of dissipation, to perturbations described by spheroidal harmonics of order two). The Jacobi family is known to be stable to collective modes from its intersection with the Maclaurin line (at $a_3/a_1 = 0.583$) to the point where $(a_2/a_1, a_3/a_1) = (0.432, 0.345)$ (the point of "pear-shaped" instability to perturbations belonging to ellipsoidal harmonics of order three).

The transport equations reduce significantly in these cases of rigid rotation: $\lambda = 0$ so the wave-vector k is constant and Eq. (4) has constant coefficients. The analysis is easy and shows that no further instabilities are added to those previously known: the Maclaurin and Jacobi families are stable to short wavelength perturbations.

If the total vorticity relative to inertial space vanishes, the transport equations can be integrated explicitly, and the solutions are periodic in time, so these figures are stable. A more complete analysis shows that the curve in parameter space of these irrotational ellipsoids is embedded in a narrow band throughout which all solutions are bounded. These are therefore stable to short wavelength perturbations.

A complete mapping of the domains of stability and instability can only be carried out numerically. The band of stability is found to occupy only a small fraction of the parameter space ([2]); the much larger region of instability abuts the line of Maclaurin spheroids, except near the region where the latter tend to a sphere. Consequently, the smallest departure from axial symmetry implies the instability of the corresponding motion. When these results are combined with the known instabilities to collective modes belonging to the second, third, and fourth ellipsoidal harmonics, even less of the parameter space is occupied by stable figures.

References

[1] B. Riemann, Gött. Abh. **IX**, 3 (1860)

[2] S. Chandrasekhar, *Ellipsoidal Figures of Equilibrium* (Yale, New Haven, 1969).

[3] A. Lifschitz and E. Hameiri, Phys. Fluids A **3**, 2644 (1991).

[4] R.T. Pierrehumbert, Phys. Rev. Lett. **57**, 2157 (1986).

[5] B.J. Bayly, Phys. Rev. Lett. **57**, 2160 (1986).

[6] A.D.D. Craik, J. Fluid. Mech. **198**, 275 (1989).

[7] R.A. Lyttleton, *The Theory of Rotating Liquid Masses* (Cambridge University Press, Cambridge, 1953).

VORTICITY COORDINATES AND A CANONICAL FORM FOR BALANCED MODELS

by Gudrun Magnusdottir
Department of Applied Mathematics and Theoretical Physics,
University of Cambridge, Silver Street, Cambridge CB3 9EW, U.K.

The shallow water equations on an f-plane

The shallow water equations on an f-plane can be written

$$\frac{\partial u}{\partial t} - \zeta v + \frac{\partial}{\partial x}\left[gh + \tfrac{1}{2}(u^2 + v^2)\right] = 0, \tag{1}$$

$$\frac{\partial v}{\partial t} + \zeta u + \frac{\partial}{\partial y}\left[gh + \tfrac{1}{2}(u^2 + v^2)\right] = 0, \tag{2}$$

$$\frac{Dh}{Dt} + h\left(\frac{\partial u}{\partial x} + \frac{\partial v}{\partial y}\right) = 0, \tag{3}$$

where u and v are the eastward and northward components of the velocity, h is the fluid depth,

$$\frac{D}{Dt} = \frac{\partial}{\partial t} + u\frac{\partial}{\partial x} + v\frac{\partial}{\partial y} \tag{4}$$

the total derivative, and

$$\zeta = f + \frac{\partial v}{\partial x} - \frac{\partial u}{\partial y} \tag{5}$$

the absolute vorticity.

Now consider a transformation from the coordinates (x, y, t) to the new coordinates $(X, Y, \mathcal{T})$, where $\mathcal{T} = t$. The symbol $\mathcal{T}$ has been introduced to distinguish the time derivative at fixed (X, Y) from the time derivative at fixed (x, y). We require the new coordinates to be vorticity coordinates in the sense that the Jacobian of (X, Y) with respect to (x, y) is the dimensionless absolute vorticity, i.e.,

$$\zeta = f\frac{\partial(X, Y)}{\partial(x, y)}. \tag{6}$$

If we eliminate ζ between (5) and (6), the resulting expression can be rearranged into the form

$$\frac{\partial}{\partial x}\left\{v - \tfrac{1}{2}f\left[(X - x)\left(\frac{\partial Y}{\partial y} + 1\right) - (Y - y)\frac{\partial X}{\partial y}\right]\right\}$$
$$-\frac{\partial}{\partial y}\left\{u - \tfrac{1}{2}f\left[(X - x)\frac{\partial Y}{\partial x} - (Y - y)\left(\frac{\partial X}{\partial x} + 1\right)\right]\right\} = 0. \tag{7}$$

Thus, the first term in braces can be expressed as $\partial\chi/\partial y$ and the second term in braces by $\partial\chi/\partial x$, where $\chi(x, y, t)$ is a scalar potential. This results in

$$u = \frac{\partial\chi}{\partial x} + \tfrac{1}{2}f\left[(X - x)\frac{\partial Y}{\partial x} - (Y - y)\left(\frac{\partial X}{\partial x} + 1\right)\right], \tag{8}$$

$$v = \frac{\partial \chi}{\partial y} + \tfrac{1}{2} f \left[(X - x) \left(\frac{\partial Y}{\partial y} + 1 \right) - (Y - y) \frac{\partial X}{\partial y} \right]. \tag{9}$$

We can regard (8) and (9) as a Clebsch representation of the velocity field (Lamb 1932, page 248; Seliger and Whitham 1968) or as generalizations of the geostrophic coordinates of semigeostrophic theory (Schubert and Magnusdottir 1993, hereafter SM, and references therein).

To transform the original momentum equations we now take $\partial/\partial t$ of (8) and (9) to obtain

$$\frac{\partial u}{\partial t} + \frac{\partial}{\partial x} \left[gh + \tfrac{1}{2}(u^2 + v^2) \right] = f \frac{\partial (X, Y)}{\partial (t, x)} + g \frac{\partial \mathcal{H}}{\partial x}, \tag{10}$$

$$\frac{\partial v}{\partial t} + \frac{\partial}{\partial y} \left[gh + \tfrac{1}{2}(u^2 + v^2) \right] = f \frac{\partial (X, Y)}{\partial (t, y)} + g \frac{\partial \mathcal{H}}{\partial y}, \tag{11}$$

where

$$g\mathcal{H} = gh + \tfrac{1}{2}(u^2 + v^2) + \frac{\partial \chi}{\partial t} + \tfrac{1}{2} f \left[(X - x) \frac{\partial Y}{\partial t} - (Y - y) \frac{\partial X}{\partial t} \right]. \tag{12}$$

Adding $-\zeta v$ to both sides of (10) and ζu to both sides of (11), then using (6) and the original momentum equations (1) and (2), we obtain

$$f \left(\frac{\partial Y}{\partial x} \frac{DX}{Dt} - \frac{\partial X}{\partial x} \frac{DY}{Dt} \right) + g \frac{\partial \mathcal{H}}{\partial x} = 0, \tag{13}$$

$$f \left(\frac{\partial Y}{\partial y} \frac{DX}{Dt} - \frac{\partial X}{\partial y} \frac{DY}{Dt} \right) + g \frac{\partial \mathcal{H}}{\partial y} = 0. \tag{14}$$

Together (13) and (14) imply that

$$U \equiv \frac{DX}{Dt} = -\frac{g}{f} \frac{\partial \mathcal{H}}{\partial Y}, \tag{15}$$

$$V \equiv \frac{DY}{Dt} = \frac{g}{f} \frac{\partial \mathcal{H}}{\partial X}. \tag{16}$$

Equation (15) has been obtained by eliminating DY/Dt between (13) and (14), and (16) by eliminating DX/Dt between (13) and (14). These are the canonical shallow water equations where $\mathcal{H}$ involves the temporal variation of the Clebsch variables and where the derivatives of $\mathcal{H}$ are taken in $(X, Y, \mathcal{T})$ space. The total time derivative (4) can be written in vorticity coordinates as

$$\frac{D}{Dt} = \frac{\partial}{\partial \mathcal{T}} + U \frac{\partial}{\partial X} + V \frac{\partial}{\partial Y}. \tag{17}$$

The advantage of (17) over (4) is that the horizontal advecting velocity is expressed in terms of derivatives of $\mathcal{H}$ by (15) and (16), which are mathematically analogous to the geostrophic formulae.

The governing equation for the absolute vorticity can be derived from (15) and (16) or, in the usual way, from (1) and (2). Combining the vorticity equation with the continuity equation (3) so as to eliminate the divergence, we obtain

$$\frac{Dh^*}{Dt} = 0, \tag{18}$$

where $h^* = (f/\zeta)h$ is the potential thickness (or the reciprocal of the potential vorticity), which is simply the thickness a fluid column would acquire if the absolute vorticity ζ were changed to the constant reference value f.

We can now summarize the above as follows. In vorticity coordinates the independent variables are $(X, Y, \mathcal{T})$ and the transformed governing equations are

$$h = \left(\frac{\partial(x,y)}{\partial(X,Y)}\right)^{-1} h^*, \tag{19}$$

$$u = \frac{h}{h^*}\left\{-\left[\frac{\partial\chi}{\partial Y} + \tfrac{1}{2}f(X-x)\right]\frac{\partial y}{\partial X} + \left[\frac{\partial\chi}{\partial X} - \tfrac{1}{2}f(Y-y)\right]\frac{\partial y}{\partial Y}\right\} - \tfrac{1}{2}f(Y-y), \tag{20}$$

$$v = \frac{h}{h^*}\left\{\left[\frac{\partial\chi}{\partial Y} + \tfrac{1}{2}f(X-x)\right]\frac{\partial x}{\partial X} - \left[\frac{\partial\chi}{\partial X} - \tfrac{1}{2}f(Y-y)\right]\frac{\partial x}{\partial Y}\right\} + \tfrac{1}{2}f(X-x), \tag{21}$$

$$U = -\frac{g}{f}\frac{\partial\mathcal{H}}{\partial Y}, \tag{22}$$

$$V = \frac{g}{f}\frac{\partial\mathcal{H}}{\partial X}, \tag{23}$$

$$\frac{D\chi}{Dt} = g(\mathcal{H}-h) + \tfrac{1}{2}(u^2+v^2) - \tfrac{1}{2}f\left[(X-x)(V+v) - (Y-y)(U+u)\right], \tag{24}$$

$$\frac{Dx}{Dt} = u, \tag{25}$$

$$\frac{Dy}{Dt} = v, \tag{26}$$

$$\frac{Dh^*}{Dt} = 0. \tag{27}$$

Equations (20) and (21) are simply the vorticity coordinate versions of (8) and (9). Equation (24) is derived by combining (8), (9) and (12). Taken together, (19)–(27) constitute a system of nine equations for the six diagnostic variables h, u, v, $\mathcal{H}$, U, V and the four prognostic variables χ, x, y, h^*, with the total derivative given in $(X, Y, \mathcal{T})$-space by (17). Obviously, an additional relation is required. If the additional relation is simply a definition of $\mathcal{H}$, and if this definition is inserted between (21) and (22), then the time evolution of the prognostic fields χ,x,y,h^* can be found by sequential calculations in the order given.

In fact, we have some freedom in choosing the additional relation. For example, the choice $\mathcal{H} = 0$ leads to the conclusion that $DX/Dt = U = 0$ and $DY/Dt = V = 0$, i.e., the vorticity coordinates move with the flow so that $D/Dt = \partial/\partial\mathcal{T}$. In addition, the right hand side of (24) is simplified and we now have three diagnostic equations, in addition to the four prognostic equations.

Notice three interesting features of the transformed system (19)–(27). Firstly, the system consists of four predictive equations rather than three, as in the original shallow water equations (1)–(3). The additional prognostic equation is due to the added information content in the solutions of the transformed system. This is most apparent in (25) and (26), which determine Lagrangian particle trajectories. This trajectory information is not directly available from solutions of the Eulerian equations (1)–(3). The second interesting feature of (19)–(27)

is the natural way in which the predictive equation for potential thickness emerges. The third interesting feature is the freedom in choosing how the vorticity coordinates move. This last feature is useful in the derivation of balanced models through approximation of the primitive set (19)–(27). One such balanced model is the semigeostrophic model, the derivation of which is discussed in SM.

There is a certain arbitrariness to the system (19)–(27) in the sense that the representation (8)–(9) is not the only representation leading to (6). In fact (8)–(9) is only unique to within a canonical transformation. We can regard (8)–(9) as the definitions of the vorticity coordinates, (X, Y), in terms of u, v and χ. Our choice in (8)–(9) was in part motivated by the desire to represent both directions on the f-plane equally.

The quasi-static primitive equations in spherical coordinates and a general structure for balanced theories

When considering the quasi-static primitive equations in spherical and isentropic coordinates we proceed similarly to the previous section (for details see SM). In particular, we now require the three components of vorticity to satisfy:

$$(\xi, \eta, \zeta) = 2\Omega \sin\Phi \left(\frac{a\partial(\Lambda, \sin\Phi)}{\partial(\phi, s)}, \frac{a\partial(\Lambda, \sin\Phi)}{\cos\phi\partial(s, \lambda)}, \frac{\partial(\Lambda, \sin\Phi)}{\partial(\lambda, \sin\phi)} \right), \tag{28}$$

where (λ, ϕ, s, t) are the original coordinates, $(\Lambda, \Phi, S, \mathcal{T})$ are the new coordinates and $S = s$, $\mathcal{T} = t$. This leads to a Clebsch representation of the velocity field expressed as:

$$u\cos\phi = \frac{\partial\chi}{a\partial\lambda} + \tfrac{1}{2}\Omega a(\Lambda - \lambda)\frac{\partial(\sin^2\Phi)}{\partial\lambda} - \tfrac{1}{2}\Omega a(\sin^2\Phi - \sin^2\phi)\frac{\partial(\Lambda + \lambda)}{\partial\lambda}, \tag{29}$$

$$v = \frac{\partial\chi}{a\partial\phi} + \tfrac{1}{2}\Omega a(\Lambda - \lambda)\frac{\partial(\sin^2\Phi + \sin^2\phi)}{\partial\phi} - \tfrac{1}{2}\Omega a(\sin^2\Phi - \sin^2\phi)\frac{\partial\Lambda}{\partial\phi}. \tag{30}$$

$$0 = \frac{\partial\chi}{\partial s} + \tfrac{1}{2}\Omega a^2(\Lambda - \lambda)\frac{\partial(\sin^2\Phi)}{\partial s} - \tfrac{1}{2}\Omega a^2(\sin^2\Phi - \sin^2\phi)\frac{\partial\Lambda}{\partial s}. \tag{31}$$

Transforming the two momentum equations and the hydrostatic equation, we obtain

$$(2\Omega V \sin\Phi, -2\Omega U \sin\Phi, T) = \left(\frac{\partial\mathcal{M}}{a\cos\Phi\partial\Lambda}, \frac{\partial\mathcal{M}}{a\partial\Phi}, \frac{\partial\mathcal{M}}{\partial S} \right), \tag{32}$$

where $U = a\cos\Phi\, D\Lambda/Dt$, $V = aD\Phi/Dt$, and $\mathcal{M}$ involves the temporal variation of the Clebsch variables, Λ, Φ and χ. These are the canonical quasi-static equations. Now, the total derivative in $(\Lambda, \Phi, S, \mathcal{T})$ space can be written as

$$\frac{D}{Dt} = \frac{\partial}{\partial\mathcal{T}} + U\frac{\partial}{a\cos\Phi\partial\Lambda} + V\frac{\partial}{a\partial\Phi} + \dot{S}\frac{\partial}{\partial S}, \tag{33}$$

where $\dot{S} = \dot{s}$ since $S = s$, resulting in the same advantage as before; that of being able to express the horizontal advecting velocity in terms of derivatives of $\mathcal{M}$, which by (32) are mathematically analogous to the geostrophic formulae.

Consider the potential pseudodensity, defined by

$$\sigma^* = \left(\frac{2\Omega \sin \Phi}{\zeta}\right) \sigma, \tag{34}$$

where $\sigma = -\partial p/\partial s$ is the pseudodensity. The potential vorticity, P, and the potential pseudodensity are related by $P\sigma^* = 2\Omega \sin \Phi$. The potential pseudodensity equation, which can be easily obtained from the potential vorticity equation, has the flux form

$$\frac{\partial \sigma^*}{\partial \mathcal{T}} + \frac{\partial(\sigma^* U)}{a \cos \Phi \partial \Lambda} + \frac{\partial(\sigma^* V \cos \Phi)}{a \cos \Phi \partial \Phi} + \frac{\partial(\sigma^* \dot{S})}{\partial S} = 0. \tag{35}$$

This is identical to the form of the potential pseudodensity equation found in many balanced model studies mentioned in SM. Here, it has been derived from the quasi-static primitive equations on the sphere. An advantage of (35) is that the velocity that accomplishes the flux is simply expressed in terms of derivatives of $\mathcal{M}$ by (32).

The potential pseudodensity defined by (34) can also be expressed in terms of a Jacobian. To obtain this Jacobian form we first note that from the definition of pseudodensity we can write

$$\begin{aligned} \sigma = -\frac{\partial p}{\partial s} = -\frac{\partial(\lambda, \sin\phi, p)}{\partial(\lambda, \sin\phi, s)} &= -\frac{\partial(\Lambda, \sin\Phi, S)}{\partial(\lambda, \sin\phi, s)} \frac{\partial(\lambda, \sin\phi, p)}{\partial(\Lambda, \sin\Phi, S)} \\ &= -\left(\frac{\zeta}{2\Omega \sin\Phi}\right) \frac{\partial(\lambda, \sin\phi, p)}{\partial(\Lambda, \sin\Phi, S)}. \end{aligned} \tag{36}$$

Then, comparing (36) with (34), we obtain the Jacobian form

$$\frac{\partial(\lambda, \sin\phi, p)}{\partial(\Lambda, \sin\Phi, S)} + \sigma^* = 0. \tag{37}$$

Using the gas law and the form of the hydrostatic equation given in the last entry of (32), we can write (37) as

$$R \begin{vmatrix} \frac{\partial \lambda}{\cos\Phi \partial\Lambda} & \frac{\partial \sin\phi}{\cos\Phi \partial\Lambda} & \frac{\partial}{\cos\Phi \partial\Lambda}\left(\rho \frac{\partial \mathcal{M}}{\partial S}\right) \\ \frac{\partial \lambda}{\partial \Phi} & \frac{\partial \sin\phi}{\partial \Phi} & \frac{\partial}{\partial \Phi}\left(\rho \frac{\partial \mathcal{M}}{\partial S}\right) \\ \frac{\partial \lambda}{\partial S} & \frac{\partial \sin\phi}{\partial S} & \frac{\partial}{\partial S}\left(\rho \frac{\partial \mathcal{M}}{\partial S}\right) \end{vmatrix} + \sigma^* = 0. \tag{38}$$

If approximations to (29) and (30), along with a balance assumption, allow λ and $\sin\phi$ to be expressed in terms of $\mathcal{M}$, then (38) becomes an invertibility relation, relating σ^* and $\mathcal{M}$. This invertibility relation and the predictive equation (35) then give a succinct mathematical description of the dynamics. Thus, the pair of equations (35) and (38) constitute what might be called the canonical form for balanced models.

References

Lamb, H., 1932: *Hydrodynamics.* Dover Publications, 738 pages.

Schubert, W. H., and G. Magnusdottir, 1993: Vorticity coordinates, transformed primitive equations and a canonical form for balanced models. Submitted to *J. Atmos. Sci.* in June, 1993. (Preprints available upon request.)

Seliger, R. L., and G. B. Whitham, 1968: Variational principles in continuum mechanics. *Proc. R. Soc. Lond.*, **A305**, 1–25.

Necessary Conditions for Statistical Stability: with Applications to Large Scale Flow Due to Convection

Willem V. R. Malkus
Department of Mathematics
Massachusetts Institute of Technology, Cambridge, MA 02139

ABSTRACT

In this study, the mean properties of solutions associated with the statistically steady states are sought. A necessary condition that the Reynolds stress and its equivalent thermal transport term are time independent is that global integrals of the square of all perturbative departures from these transport terms decay with time. For that special set of perturbative departures from a statistically stable mean which have the spatial and temporal form of any one of the other solutions to this problem, and have no global correlation with other solutions, it is possible to determine a first set of integral properties of the solutions characterizing stability. For example, in the symmetry breaking large scale shear flows observed in high Rayleigh number convection, the first condition found is that the sum of the mean squared convective terms and a function of the Rayleigh number times the mean squared Reynold stresses must be maximum among all possible solutions. For these criteria to be usefully sharp, it is speculated that the necessary conditions "approach" the sufficient conditions as the density of adjacent solutions in the phase space becomes large. Of course, these many solutions include the observed highly disordered flows in space and time. How can one estimate their properties?... One quantitative approach is upper bound theory. A recent study by L. N. Howard (1990) determines the minimum Rayleigh number for a prescribed heat and momentum flux in plane parallel convection. Here one can use these results to make a first estimate of the large scale mean flow and the corresponding heat flux (less than the maximum possible) which lead to optimal statistical stability for a given Rayleigh number. The very limited experimental data support the theory, but begs for further data to determine the theory's limits of validity.

INTRODUCTION

In turbulent pipe flow one is confident that the average velocity profile for a given Reynolds number will be the same profile tomorrow – and next year. Yet the detailed fluid motions responsible for this local average will never be the same. Such a statistically steady state is also critically balanced, in that a small change in Reynolds number leads to a (non-linearly) different average velocity profile. However, no deductive approach from the basic equations to this statistical stability problem is to be found in the literature.

The question raised above lies in a small domain of the general problem of non-equilibrium statistical mechanics. There are at least two schools of inquiry. The Brussels school would start with Newton or Schrödinger and follow the path of Boltzmann. Deductive advance beyond dilute gas kinetic theory has been slight. The second school following from Gibbs, has a Bayesian base, but similar objects of inquiry, with similar success. Most physical scientists find little comfort in either the Brussels or Bayesian approach. They appear to believe that the questions as posed are "bad questions", that is that the rate of occupancy of the phase space and initial conditions determine the

observations – and that no general quantitative results will be forthcoming. Yet the Bogoliubov-Kolmogorov work and much of modern turbulence theory fall in one or the other of these schools.

The example of pipe flow given in the first paragraph, in idealized form, is a well-posed problem in the Hadamar sense, and suggests a different approach to determining the properties of the statistically steady state ($\equiv s^3$) in a macroscopic continuum. The alternative explored here is to presume knowledge of the average features of the many macroscopic solutions including and adjacent to a particular s^3 and seek to establish the properties of the subset of these solutions which can survive disturbances of arbitrary amplitude and form. Having established at least some of the properties characterizing this s^3, one can then use formal bound theory to predict their dependence on the (forcing) parameters, without the introduction of empirical functions or constants. Hence the adequacy of these properties to define the s^3 can be "falsified", or more generously, the "limits of validity" can be determined.

Determination of a Necessary Condition for the s^3.

The Boussineq equations for plane parallel convection with a large scale horizontal flow are written

$$(\frac{\partial}{\partial t} - \nu\nabla^2)\mathbf{V} = -\frac{1}{\rho}\nabla P - \mathbf{V}\cdot\nabla\mathbf{V} + \alpha g T\hat{k} \tag{1}$$

$$\nabla\cdot\mathbf{V} = 0 \tag{2}$$

$$(\frac{\partial}{\partial t} - \kappa\nabla^2)T = -\mathbf{V}\cdot\nabla T \tag{3}$$

where $\mathbf{V}$ is the velocity, P the pressure, T the temperature, and $\nu, \kappa, \rho, \alpha, g$, are constants determining viscosity, conductivity, density, coefficient of expansion, gravity, and $\hat{k}$ is the unit vector in the z direction. Consider the horizontal average of eq. (3) (over $x, y \to \infty$), written as $(-)$,

$$\frac{\partial}{\partial t}\overline{T} - \kappa\overline{T}_{zz} = -(\overline{w\theta})_z \tag{4}$$

where $w = \mathbf{V}\cdot\hat{k}$, and $\theta(\mathbf{r},t) = T(\mathbf{r},t) - \overline{T}(z,t)$.

Now for all initial conditions

$$\frac{\partial\overline{T}}{\partial t} \to 0 \text{ only if } \frac{\partial}{\partial t}(\overline{w\theta})_z \to 0, \text{ or } \frac{\partial}{\partial t}(\overline{w\theta}) \to 0 \tag{5}$$

This state is (believed to be) realized in real geometries. The resulting thermal "profile" $\overline{T}(z)$ appears to be unique and is akin to the average velocity profile in the pipe of the introductory paragraph.

The idealized statistically steady state, s^3, is defined here to be stable against all possible disturbances. A necessary and sufficient condition for the fields $w_0(\mathbf{r},t)$ and $\theta_0(\mathbf{r},t)$ to have an s^3 horizontal average is that for all possible disturbance $w'(\mathbf{r},t)$ and $\theta'(\mathbf{r},t)$, where $\nabla\cdot\mathbf{v}' = 0$ and $w' = \theta' = 0$ on the boundaries,

$$\frac{\partial}{\partial t}|\overline{w_0\theta_0} + \overline{w_0\theta'} + \overline{w'\theta_0} + \overline{w'\theta'}| \le 0 \tag{6}$$

at any instant $t = t_0$. Note that the time development of w, θ due to the basic equations (1), (2), (3), will lead to other w', θ' from among all possible disturbances, which in turn are required to satisfy (6) if $\overline{w_0(\mathbf{r},t) \cdot \theta_0(\mathbf{r},t)}$ is to be a s^3.

It follows from (6) that a necessary condition for $\overline{w_0\theta_0}$ to be one of the realizations of a unique s^3 is that

$$\frac{\partial}{\partial t} < [\overline{w_0\theta} + \overline{w'\theta_0} + \overline{w'\theta'}]^2 > \quad \leq 0 \text{ at each } t = t_0, \tag{7}$$

where $<\quad>$ indicates an average over the entire system.

Condition (7) must be met also by that subset of disturbances w', θ' which have arbitrary amplitudes but the spatial and temporal form of other solutions to the basic equations which can equilibrate but are unstable (e.g., the many steady cellular solutions which are not realized at large Rayleigh number.)

Here, (7) will be used to seek a primary selection criteria for a s^3 among the many (unknown) solutions. To implement this search the subset of test disturbances is further reduced to include only solutions which are not spatially correlated over the (infinite) horizontal domain. That is, where $w' = Aw_1$ and $\theta' = B\theta_1, A$ and B are arbitrary amplitudes, and $w_1 = w_1(\mathbf{r}, t = t_0), \theta_1 = \theta_1(\mathbf{r}, t = t_0)$ is another solution to the problem at some arbitrary initial instant, then $\overline{w_0, \theta_1} = \overline{w_1\theta_0} = 0$. It follows from eq. (7) that at any instant $t = t_0$

$$A^2B^2\frac{\partial}{\partial t} < (\overline{w_1\theta_1})^2 > \leq 0. \tag{8}$$

For the selection criteria which emerges from (8) to be usefully sharp, it is speculated that the density of adjacent solutions in the phase space must become very large.

For the large scale mean flow observed in convection, consider $\mathbf{V} = \overline{\mathbf{V}}(z,t) + \mathbf{v}$, and from Eq. (1)

$$\frac{\partial \overline{V}}{\partial t} - \nu \overline{V}_{zz} = -(\overline{wu})_z \tag{9}$$

paralleling eq. (4), where here $u = \mathbf{v} \cdot \hat{i}$.

Then paralleling the discussion leading to eq. (8), in a first instant

$$\frac{\partial}{\partial t} < (\overline{w'u'})^2 >_t \leq 0 \tag{10}$$

where $\mathbf{v}' = A\mathbf{v}_1$. First integrals of eqs. (4) and (9) for equilibrated solutions are

$$H = -\kappa \overline{T}_z + \overline{w\theta} \text{ and } M = -\nu \overline{V}_z + \overline{wu}. \tag{11}$$

where H and M are constants for plane convection.

Using the Schwarz inequality it follows that eqs. (8) and (10) are met if $\partial < \mathbf{v}'^2 > /\partial t \leq 0$ and $\partial < \theta'^2 > /\partial t \leq 0$ in the first instant.

From the basic equations (1), (2) and (3) the disturbance integrals for this case are written

$$\frac{\partial < v'^2 >}{\partial t} = \nu < \mathbf{v}' \cdot \nabla^2 \mathbf{v}' > + \alpha g < \overline{w'\theta'} > - < \overline{u'w'}(\overline{V}_0)_z > \leq 0 \qquad (12)$$

and

$$\frac{\partial < \theta'^2 >}{\partial t} = \kappa < \theta' \cdot \nabla^2 \theta' > - < \overline{w'\theta'}(\overline{T}_0)_z > \leq 0. \qquad (13)$$

It is convenient to scale the variables at this point, writing,

$$\theta_0 = (\Delta T)\theta, \mathbf{v}_0 = (\frac{\kappa}{d})\mathbf{v}, \qquad R = \frac{\alpha g \Delta T d^3}{\kappa \nu}, \qquad \sigma = \frac{\nu}{\kappa}, \qquad h \equiv \overline{w\theta}, \qquad m \equiv \frac{\overline{wu}}{\sigma},$$

where d is the vertical dimension of the convecting layer and ΔT is the temperature contrast between its boundaries. Then, from eqs. (10), (11), (12), so scaled, the condition for s^3 is written

$$< h_1 \cdot (h - h_1) > + \frac{1}{R}(\frac{< -h_1(\overline{T}_1)_z) >}{< h_1 >}) < m_1(m - m_1) > \quad \geq 0$$

from which it follows that a necessary property which characterizes s^3 is that

$$< h^2 > + \frac{1}{R}\left\{1 - \frac{< (< h > - h)^2 >}{< h >}\right\} < m^2 > \equiv Q \qquad (14)$$

is a maximum.

Implementing the necessary conditions for s^3.

An upper bound on (14), subject to derived integral constraints on $< v^2 >$ and $< \theta^2 >$ can be found which leads to Euler-Lagrange equations describing an entire field of temperature and velocity which will generate this bound. This study is under way, and like the earlier work, Busse (1978), contains an entire spectrum of motions. Yet, there is the observed remarkable gap between the many small scale motions which drive the flow and the very large scale flow, seemingly symmetry breaking, but reflecting the large scale geometry (e.g., Krishnamurti and Howard (1981), Zocchi et al. (1990). Here, by great good fortune, a recent study by Howard (1990) can be applied to find a formal maximum to (14) directly from the integral constraints. Howard determined the minimum R for given $< h >$ and $< m >$, in a paper entitled "Convection with Shear has its Limits". This observation is apparent in eq. (1), where one sees that the last term, involving $\overline{V}_z$ "uses up" buoyancy, hence reducing the convective heat flux. Although there are many interesting bifurcations along the way to high R, only that high R limit will be described here. Howard established relations between $< h >, < m >$, and R for $< h > \gg 1$ and $< m > \gg 1$, subject to two integral constraints. In this limit the bracket $\{\ \}$ function of h in eq. (14) approaches the value 1/2, and

$$\begin{aligned} < h^2 > &= < h >^2 + 0(< h >) \\ < m^2 > &= < m >^2 + 0(< m >) \\ R < h > &\geq < m >^2 / < h > + (64/3) < h^3 > \end{aligned} \qquad (15)$$

for the special case $\sigma = 1$. From eq. (14) one finds that the maximum value of Q, eq. (14), occurs for maximum $< m >$. In this limit, and for $\sigma = 1$, Howard's study leads to

$$< m >_{\max} \leq \frac{1}{2}\sqrt{\frac{3}{64}}R \tag{16}$$

From Busse's (1978) upper bounds for shear flow applied to this case, which use the same integral constraints used by Howard, and for $\sigma = 1$, one finds that

$$< m > \simeq < \overline{V}^2 > /(\frac{d}{\kappa})^2 \tag{17}$$

Therefore, from eqs. (16) and (17), redimensionalizing,

$$< \overline{V}^2 > \leq \frac{1}{2}\sqrt{\frac{3}{64}}R(\frac{\kappa}{d})^2 = \frac{1}{2}\sqrt{\frac{3}{64}}(\alpha g \Delta T d)/\sigma. \tag{18}$$

It is seen that $< \overline{V}^2 >$ is a fraction of the "free-fall" velocity squared, $(\alpha g \Delta T d)$. Although the preceding bounds were made for $\sigma = 1, \sigma$ is retained in eq. (17) as a first determination of the σ dependence for $\sigma = 0(1)$. This result, eq. (17), as an upper bound, is in such good agreement with the limited observations that a fortuitous element in the reasoning or data is suspected, which one will now endeavor to remove with a more complete theory and new experiments.

Conclusions and Acknowledgments

The search continues for the most revealing physical hypothesis which leads to further optimal properties for the statistically steady state (s^3). The path described here may point the way. Combined with the formal tools of upper bound theory, now supplemented by new constraints made accessible by computer, many qualitative and quantitative features of the *organization* of turbulent flows may be revealed, (e.g., the "origin", from stability theory, of large scale magnetic fields).

The critical comments of L. N. Howard, J. Keller, E. A. Speigel, R. Worthing, and F. Waleffe, on a first draft of this work were most appreciated as is support under NSF grant ATM-9208373.

References

Howard, L. N., "Limits on the Transport of Heat and Momentum by Turbulent Convection with Large-Scale Flow", *Studies in Applied Math.*, 1990, **83**, 273.

Krishnamurti, R. and Howard, L. N., "Large-Scale Flow Generation in Turbulent Convection" *Proc. Natl. Acad. Sci.*, 1981, **4**, 1981.

Zocchi, G., Moses, E. and Libchauber, A., "Coherent Structures in Turbulent Convection on Experimental Study", *Physics A*, 1990, **166**, 387.

Three-Dimensional, Hamiltonian Vortices.

Steve Meacham
Dept. of Oceanography, Florida State University.

Abstract.

I demonstrate a Hamiltonian-moment method of approximating flows dominated by coherent concentrations of vorticity, developed by Flierl, Meacham & Morrison (1993), by applying it to an ellipsoidal quasigeostrophic vortex in a shear flow. In this particular case, the approach yields *exact*, as opposed to approximate, equations of motion.

1. Introduction.

As one possible model of an intrathermocline vortex in a shear flow, one can consider a blob of uniform potential vorticity embedded in an unbounded, uniformly stratified, quasigeostrophic flow. Such a model was examined by Meacham et al. (1993) (hereafter, MPSZ) who showed that when the background flow was given by a streamfunction of the form

$$\Psi = \frac{1}{4}\omega(x^2 + y^2) + \frac{1}{4}e(x^2 - y^2) - \tau yz \qquad (1)$$

an initially ellipsoidal blob of potential vorticity will remain ellipsoidal for all future times. This result and its proof is really a generalisation of a result from the theory of vortices in 2D Euler flow – that an elliptical patch of uniform vorticity in a background strain flow will remain elliptical (Kida, 1981).

The motivation for the work of Meacham et al. was a desire to try and understand the conditions under which a shear flow might cause a vortex to break up. In MPSZ, it was shown that the motion of the ellipsoid was described by a six-dimensional system of nonlinear ODEs. These were written in terms of three variables that describe the shape of the ellipsoid – the semi-axis lengths, $a(t)$, $b(t)$, $c(t)$ – and three that describe its orientation – the Euler angles $\phi(t)$, $\theta(t)$, $\psi(t)$. These equations are rather complicated, a fact which limits their utility and makes it difficult to classify all of the modes of behavior of the vortex. It was conjectured (MPSZ) that these equations correspond to a Hamiltonian system but while it is possible to show this directly for certain particular forms of Ψ, MPSZ were unable to do this for the general case, (1).

It was also noted in MPSZ that their dynamical system posesses several conserved quantities – *i)* vortex volume, *ii)* particle height, and *iii)* excess energy. Volume conservation can be exploited quite readily to reduce the system from sixth-order to fifth-order but it is very difficult to achieve any further reduction of order by exploiting the remaining integrals of motion, *(ii)* and *(iii)*.

Working with Phil Morrison and Glenn Flierl, I have come up with a better representation of the same system. Here, I define better to mean more useful in the sense that

one can better exploit the integrals of motion and more easily classify the behavior of the vortex. I achieve this by using a Hamiltonian-moment formulation in which a truncated set of spatial moments of the vorticity distribution are used as dynamical variables and substituted into a non-canonical Hamiltonian representation of the equations governing the evolution of continuously stratified quasigeostrophic flows. This approach provides a general method for obtaining finite-dimensional approximations to flows dominated by coherent but separated blobs of vorticity. For the case considered here, it leads to an *exact* set of evolution equations. A more comprehensive treatment of this problem can be found in Flierl, Meacham and Morrison (1993).

2. Derivation of the moment equations.

We begin with Morrison's Poisson bracket for continuously stratified quasigeostrophic flow (see Morrison's lectures earlier in this volume.)

$$\{F,G\} = \int q \left[\frac{\delta F}{\delta q}, \frac{\delta G}{\delta q}\right] dxdydz \tag{2}$$

where $[A,B]$ is the horizontal Jacobian $\partial_x A \partial_y B - \partial_y A \partial_x B$ and q is the potential vorticity

$$q = \left\{\partial_x^2 + \partial_y^2 + \partial_z \frac{f^2}{N^2}\partial_z\right\}\psi$$

We assume uniform stratification and scale z by N/f so that the potential vorticity relation becomes isotropic

$$q = \nabla^2\psi \tag{3}$$

We consider a compact vortex consisting of an ellipsoidal volume of uniform unit potential vorticity anomaly (formally q') embedded in a uniform potential vorticity background flow. We will use two Cartesian coordinate systems. One, $Oxyz$, fixed with respect to the underlying f-plane and the other, $O\tilde{x}\tilde{y}\tilde{z}$, moving with the principle axes of the ellipsoid. In both cases, the origin coincides with the center of the ellipsoid. The background flow is described by a streamfunction of the form

$$\Psi = \frac{1}{4}\omega(x^2+y^2) + \frac{1}{4}e(x^2-y^2) - \tau yz \tag{4}$$

while the vortex generates an additional contribution ψ'. Provided that the shape of the vortex is ellipsoidal initially, it will remain ellipsoidal in such a flow. This shape can be described by a set of time-dependent semi-axis lengths, $\{a(t),\ b(t),\ c(t)\}$, while its orientation can be expressed in terms of Euler angles $\{\phi(t),\ \theta(t),\ \psi(t)\}$. We define these so that the transformation between the fixed and co-rotating reference frames is

$$\tilde{\boldsymbol{x}} = \mathcal{M}^T \boldsymbol{x} \tag{5}$$

where

$$\mathcal{M}^T = \begin{pmatrix} \cos\psi & \sin\psi & 0 \\ -\sin\psi & \cos\psi & 0 \\ 0 & 0 & 1 \end{pmatrix} \begin{pmatrix} \cos\theta & 0 & -\sin\theta \\ 0 & 1 & 0 \\ \sin\theta & 0 & \cos\theta \end{pmatrix} \begin{pmatrix} \cos\phi & \sin\phi & 0 \\ -\sin\phi & \cos\phi & 0 \\ 0 & 0 & 1 \end{pmatrix} \tag{6}$$

The state (shape and orientation) of an ellipsoid is uniquely determined by the values of its six quadratic moments $\{a_i |\ i = 1, \ldots, 6\}$ defined by

$$m_1 = x^2, \qquad m_2 = xy, \qquad m_3 = y^2, \qquad m_4 = yz, \qquad m_5 = zx, \qquad m_6 = z^2$$

$$a_i = \mu \int q' m_i dx dy dz.$$

Here, $\mu = 15/(4\pi abc)$. Thus,

$$\delta F = \int \frac{\delta F}{\delta q} \delta q = \sum_j \frac{\partial F}{\partial a_j} \delta a_j = \sum_j \frac{\partial F}{\partial a_j} \mu \int \delta q m_j$$

We see that, for variations that preserve the ellipsoidal property of the vortex,

$$\frac{\delta F}{\delta q} = \mu \sum \frac{\partial F}{\partial a_i} m_i$$

It can be shown that in a background flow of the form (4), an initially ellipsoidal vortex will remain ellipsoidal (MPSZ). Within this restricted class of variations in q, the Poisson bracket may be rewritten in the form

$$\{F, G\} = \mu^2 \sum_{j,k} \int q \frac{\partial F}{\partial a_j} \frac{\partial G}{\partial a_k} [m_j, m_k] \qquad \text{i.e.} \quad \{F, G\} = \frac{\partial G}{\partial a_i} J^{ij} \frac{\partial F}{\partial a_j} \tag{7}$$

where the symplectic matrix J is

$$J^{ij} = \mu^2 \int q [m_i, m_j] \tag{8}$$

Applying this to the moments, we obtain

$$\dot{a}_i = \{a_i, H\} = J^{ij} \frac{\partial H}{\partial a_j} \tag{9}$$

We note that $[m_i, m_j]$ is itself proportional to some $m_{k(i,j)}$ and find that J takes the form

$$\mu \begin{pmatrix} 0 & 2a_1 & 4a_2 & 2a_5 & 0 & 0 \\ -2a_1 & 0 & 2a_3 & a_4 & -a_5 & 0 \\ -4a_2 & -2a_3 & 0 & 0 & -2a_4 & 0 \\ -2a_5 & -a_4 & 0 & 0 & -a_6 & 0 \\ 0 & a_5 & 2a_4 & a_6 & 0 & 0 \\ 0 & 0 & 0 & 0 & 0 & 0 \end{pmatrix}$$

We now assume that the excess energy for the system, defined as

$$H = -\int q' (\Psi + \frac{1}{2} \psi') \tag{10}$$

is the appropriate Hamiltonian for this system. Evaluating the integral in (10) yields

$$\mu H = \left\{ R + \frac{V_0}{2} I \right\}$$

where $V_0 = abc$,

$$R = \frac{1}{4}(\omega + e)a_1 + \frac{1}{4}(\omega - e)a_3 - \tau a_4$$

and

$$I = -\int_0^\infty ds K(s), \qquad K(s) = \left[(a^2+s)(b^2+s)(c^2+s)\right]^{-\frac{1}{2}}$$

We introduce the related integrals, I_1 and I_2, where

$$I_j = \frac{1}{2}\int_0^\infty ds s^j K^3(s) \tag{11}$$

After some manipulation, the equations of motion are

$$\begin{aligned}
\dot{a}_1 &= -(\omega - e)a_2 + 2\tau a_5 - 2V_0\left\{(a_2a_6 - a_4a_5)I_1 + a_2I_2\right\} \\
\dot{a}_2 &= \frac{1}{2}(\omega + e)a_1 - \frac{1}{2}(\omega - e)a_3 + \tau a_4 + V_0\left\{[a_6(a_1 - a_3) + (a_4^2 - a_5^2)]I_1 + (a_1 - a_3)I_2\right\} \\
\dot{a}_3 &= (\omega + e)a_2 + 2V_0\left\{(a_2a_6 - a_4a_5]I_1 + a_2I_2\right\} \\
\dot{a}_4 &= \frac{1}{2}(\omega + e)a_5 + V_0\left\{[a_3a_5 - a_4a_2]I_1 + a_5I_2\right\} \\
\dot{a}_5 &= -\frac{1}{2}(\omega - e)a_4 + \tau a_6 - V_0\left\{[a_1a_4 - a_5a_2]I_1 + a_4I_2\right\} \\
\dot{a}_6 &= 0
\end{aligned} \tag{12}$$

With the formulation (7), we can search for Casimirs, quantities, C, that satisfy

$$\{C, F\} = 0$$

for arbitrary F. From (12), a_6 (= C_1, say) is a Casimir; it corresponds to the conservation of particle height in the quasigeostrophic system. A second Casimir, C_2, can be found by looking for a second null vector of the symplectic matrix J. We find

$$C_2 = a_1a_3a_6 + 2a_2a_4a_5 - a_1a_4^2 - a_3a_5^2 - a_6a_2^2 \tag{13}$$

This is proportional to the square of the volume of the ellipsoid so that we recover volume conservation. There are only two independent Casimirs for this system.

One of the coordinates, a_6 is already a Casimir, C_1. We can introduce a change of coordinates $\boldsymbol{a} \rightarrow \boldsymbol{b}$ so that the second Casimir is also used as a coordinate. This allows us to reduce to system to fourth order, since $\dot{C}_2 = 0$, and $J^{ij}\partial C_2/\partial b_j = 0$ so that $\partial H/\partial C_2$ will not appear on the right-hand side.

Set

$$b_1 = a_1, \quad b_2 = a_3, \quad b_3 = a_4, \quad b_4 = a_5, \quad b_5 = C_2, \quad b_6 = a_6 = C_1$$

then

$$\dot{\boldsymbol{b}} = \begin{pmatrix} 0 & 4a_2 & 2b_4 & 0 & 0 & 0 \\ -4a_2 & 0 & 0 & -2b_3 & 0 & 0 \\ -2b_4 & 0 & 0 & -b_6 & 0 & 0 \\ 0 & 2b_3 & b_6 & 0 & 0 & 0 \\ 0 & 0 & 0 & 0 & 0 & 0 \\ 0 & 0 & 0 & 0 & 0 & 0 \end{pmatrix} \frac{\partial H}{\partial \boldsymbol{b}} \tag{14}$$

Here a_2 is a known function of $\boldsymbol{b}$ that may be deduced from (13). Going further, (14) can be put into a canonical form by the change of variables

$$e_1 = b_4^2 - b_1 b_6; \quad e_2 = b_3^2 - b_2 b_6; \quad e_j = b_j, \; j = 3,4,5,6.$$

Then

$$\begin{aligned} \dot{e}_1 &= -4e_6 w \frac{\partial H}{\partial e_2}, & \dot{e}_3 &= -e_6 \frac{\partial H}{\partial e_4}, & \dot{e}_5 &= 0 \\ \dot{e}_2 &= 4e_6 w \frac{\partial H}{\partial e_1}, & \dot{e}_4 &= e_6 \frac{\partial H}{\partial e_3}, & \dot{e}_6 &= 0 \end{aligned} \tag{15}$$

where $w = \pm(e_1 e_2 - e_5 e_6)^{\frac{1}{2}}$. The double-branched structure of the square root does not pose any problem as w satisfies a well-behaved auxiliary equation

$$\dot{w} = F(e_1, ..., e_4; e_5, e_6) \tag{16}$$

in which F is a single-valued function of its arguments. This is useful when trying to integrate (15) numerically.

3. Summary.

The use of the Hamiltonian-moment method allows one to derive the evolution equations for an ellipsoidal, quasigeostrophic vortex in shear in a Hamiltonian form. This method is much simpler than the approach used by MPSZ and permits one to employ more easily the constraints embodied in the available integrals of motion to reduce the order of the system.

4. Acknowledgements.

I'd like to thank Rick Salmon for organising a superb summer, Keith Ngan for being such good company on an excursion into dynamical chaos, Phil Morrison & Ted Shepherd for their inspiring sets of lectures, and Phil Morrison & Glenn Flierl for a very enjoyable collaboration of which this work forms a part.

References

Flierl, G.R., Meacham, S.P. and Morrison, P.J. (1993) In preparation.

Kida, S. (1981) *J. Phys. Soc. Japan*, **50**, 3517-3520.

Meacham, S.P., Pankratov, K.K., Shchepetkin, A.S. and Zhmur, V.V. (1993) *Dyn. of Atmos. and Oceans.* In press.

Higher Order Models for Water Waves

Peter J. Olver
School of Mathematics
University of Minnesota
Minneapolis, MN 55455
olver@ima.umn.edu

In this note I would like to discuss some new perspectives on the construction of model equations for physical systems, with particular emphasis on the role of Hamiltonian structure and solitary waves. The ideas, which have a wide applicability, will be presented in the specific context of higher order model equations for water waves, valid in the shallow water regime. Details can be found in the references [5], [8], [9].

We begin with the standard free boundary problem for incompressible, irrotational fluid flow in a channel. We restrict attention to two-dimensional motions, taking x as the horizontal and y as the vertical coordinate, the (flat — for simplicity) bottom at $y = 0$, and the free surface at $y = h + \eta(x,t)$, where h is the undisturbed fluid depth. In terms of the velocity potential $\varphi(x, y, t)$, the full water wave problem takes the well-known form

$$\varphi_{xx} + \varphi_{yy} = 0, \qquad 0 < y < h + \eta(x, t), \tag{1}$$

$$\varphi_y = 0, \qquad y = 0, \tag{2}$$

$$\left.\begin{aligned} &\varphi_t + \tfrac{1}{2}\varphi_x^2 + \tfrac{1}{2}\varphi_y^2 + g\,\eta = 0, \\ &\eta_t = \varphi_y - \eta_x\,\varphi_x, \end{aligned}\right\} \qquad y = h + \eta(x, t), \tag{3}$$

where g is the gravitational constant. For simplicity, I have omitted surface tension, although this can be readily incorporated in both the full equations as well as the models discussed below. In the standard Boussinesq (shallow water) approximation to the water wave problem, one begins by introducing the small parameters

$$\varepsilon = \frac{a}{h} \qquad \kappa = \frac{h^2}{\ell^2} = O(\varepsilon),$$

where a is the wave amplitude, ℓ the wave length. The equations (1-3) are rescaled according to $(x, y, t, \eta, \varphi) \longmapsto (\ell x, h y, a \eta, c^{-1} g a \ell \varphi)$, where $c = \sqrt{g h}$ is the (linearized) wave speed. The boundary value problem (1-2) (in the rescaled variables) is then solved for the potential, and the resulting series expansion substituted into the free surface conditions (3). The resulting bidirectional system of equations is typically expressed in terms of the surface elevation $\eta(x, t)$ and the horizontal velocity $u(x, t) = \varphi_x(x, \theta h, t)$ at a fraction $0 \le \theta \le 1$ of the undisturbed depth. Truncating to some specified order, one finds a variety of Boussinesq-type systems of model equations for waves propagating in both directions. To specialize to waves moving in a single direction, one resticts to an "approximate" unidirectional function surface, and re-expands the system. The result, to first order, is the celebrated Korteweg-deVries approximation

$$\eta_t + \eta_x + \frac{3}{2}\varepsilon\,\eta\,\eta_x - \frac{1}{2}\kappa\,\eta_{xxx} = 0, \tag{4}$$

which we have written in terms of η, although the horizontal velocity u satisfies the same equation to first order. (The higher order approximations, though, are different, [8], [9].)

The water wave problem was shown by Zakharov, [11], to be a Hamiltonian system with the total energy serving as the required Hamiltonian functional. Also, as is well known, [10; Chapter 7], the Korteweg-deVries equation (4) has two distinct Hamiltonian structures — indeed, the fact that it is a biHamiltonian system implies, by Magri's theorem, that it is, in fact, a completely integrable Hamiltonian system in the sense that it has an infinite sequence of independent conservation laws and associated (generalized) symmetries. On the other hand, in collaboration with Benjamin, [2], [7], the full water wave problem (1–3) was shown to possess precisely eight (seven if surface tension is included) local conservation laws, corresponding to nine (eight if surface tension is included) independent one-parameter symmetry groups. (The "extra" scaling group is not being "canonical", and thus does not lead to a conserved quantity.) In the course of trying to understand which of the Korteweg-deVries conservation laws correspond to true water wave laws, I found, much to my surprise, that *neither* of the Hamiltonian structures for the Korteweg-deVries equation arises directly from the Hamiltonian structure for the full water wave problem. The crucial feature is that the Boussinesq expansion is *not* canonical, and so cannot lead to a first order Hamiltonian approximation. Indeed, the first order truncation of the water wave energy functional is *not* one of the conserved quantities for the Korteweg-deVries model (4).

The easiest way to appreciate this phenomenon is through an appeal to a simple form of "noncanonical perturbation theory". Consider a Hamiltonian system

$$\frac{dv}{dt} = J(v)\,\nabla H(v), \tag{5}$$

which, in our application, would represent the full water wave problem. In standard perturbation theory, which ignores any additional structure the model may possess — such as Hamiltonian structure, conservation laws, etc., one derives approximate models by substituting the physically motivated perturbation expansion $v = u + \varepsilon\,\varphi(u) + \varepsilon^2\,\psi(u) + \dots$ into the system, and then truncating the resulting system to some desired order in ε. However, this procedure must now be correlated with the Hamiltonian structure of (5). Indeed, if the expansion is not canonical then we must not only expand the Hamiltonian function(al) $H(v) = H_0(u) + \varepsilon\,H_1(u) + \varepsilon^2\,H_2(u) + \dots$, but also the Hamiltonian operator $J(v) \longmapsto J_0(u) + \varepsilon\,J_1(u) + \varepsilon^2\,J_2(u) + \dots$. If we truncate to just first order, the resulting perturbed system

$$\frac{du}{dt} = J_0\,\nabla H_0 + \varepsilon\,\{\,J_1\,\nabla H_0 + J_0\,\nabla H_1\,\} \tag{6}$$

is not Hamiltonian in any obvious way. Indeed, as was remarked above in the context of the water wave problem, the first order truncation of the Hamiltonian, $H_0(u) + \varepsilon\,H_1(u)$, is not a conserved quantity for (6). A *Hamiltonian* first order approximation to (5) can be given by retaining some (but not all) of the second order terms:

$$\begin{aligned} \frac{du}{dt} &= [\, J_0 + \varepsilon J_1 \,] \nabla [\, H_0 + \varepsilon H_1 \,] \\ &= J_0 \nabla H_0 + \varepsilon \{\, J_1 \nabla H_0 + J_0 \nabla H_1 \,\} + \varepsilon^2 J_1 \nabla H_1 . \end{aligned} \tag{7}$$

(Technically, since the Jacobi identity imposes a quadratic constraint on the Hamiltonian operator, the combination $J_0 + \varepsilon J_1$ is not guaranteed to be Hamiltonian; however, in many cases, including the Korteweg-deVries approximation, this is not a problem.)

In certain situations, the first order model (6) may turn out to be Hamiltonian "by accident". One way in which this can occur is if the two terms in braces are constant multiples of each other, so $J_1 \nabla H_0 = \lambda J_0 \nabla H_1$. If this happens, the associated first order approximation (6) is in fact biHamiltonian, and hence completely integrable. This observation, which does apply to the Korteweg-deVries equation, can be offered as an explanation of the surprising prevalence of completely integrable soliton equations appearing as models for a wide variety of complicated nonlinear physical systems — it is because they arise from non-canonical perturbation expansions of Hamiltonian systems, while, at the same time, retaining some form of Hamiltonian structure.

Both the Hamiltonian models constructed using the preceding non-canonical perturbation theory, as well as the complete second order models for unidirectional shallow water waves, are evolution equations of the general form

$$u_t + c u_x + \varepsilon \{\mu u_{xxx} + 2 q u u_x\} + \varepsilon^2 \{\alpha u_{xxxxx} + \beta u u_{xxx} + \delta u_x u_{xx} + 3 r u^2 u_x\} = 0. \tag{8}$$

Such models arise in a wide variety of other physical situations, including wave interactions, elastic media with microstructure, and soliton. The precise formulas for the coefficients vary, and I refer the reader to [5] for a survey of (most of the) models of this form in current use, including all water wave models, both first order Hamiltonian, and second order, with and without surface tension. Some analytical results are known for such fifth order models, although much remains unknown. In particular, numerical solutions have not, as far as I know, been implemented. Here I would like to comment on some recent results concerning the existence of solitary wave solutions. For small ε, equation (8) should be regarded as a perturbation of the Korteweg-deVries model, cf. [4], obtained by omitting the $O(\varepsilon^2)$ terms entirely. Therefore, one would expect that the model admits a one-parameter family of solitary wave solutions which would look like small perturbations of the standard sech^2 solitons of the Korteweg-deVries equation. This point of view would be additionally bolstered by the fact that the full water wave model also admits a family of solitary wave solutions, up to a wave of maximal height which satisfies the Stokes' phenomena of exhibiting a 120° corner. Indeed, Kunin, [6], introduces models, using only $\varepsilon^2 \beta u u_{xxx}$ in the second order terms, which *do* have solitary waves of maximal height, although these waves have a 0° cusp. Remarkably, the expectation of solitary wave solutions is not correct, and, indeed, most of the fifth order models (8) do not have the expected property. Indeed, in joint work with S. Kichenassamy, [5], it was proved that, subject to a technical analyticity hypothesis, the only models (8) which admit a one-parameter family of solitary wave solutions which, in the $\varepsilon \longrightarrow 0$ limit, reduce to Korteweg-deVries solitons, are the models which admit a one-parameter family of exact sech^2 solitary wave solutions!

In the case of the water wave models, only at the "magic depth" $\theta = \sqrt{\frac{11}{12} - \frac{3}{4}\tau}$ do the higher order models possess solitary wave solutions. In this case, the Hamiltonian model is, in fact a fifth order Korteweg-deVries equation, having soliton solutions. (The many remakable properties of the models at this depth has been noted before, [8], [9], but no explanation is as yet forthcoming.) This fact brings into sharp focus our preconceived notions concerning the construction of model equations for solitary wave phenomena. According to work of Friedrichs and Hyers, [4], and Amick and Toland, [1], the full water wave problem possesses a one-parameter family of exact solitary wave solutions, up to a wave of maximal height. The Korteweg-deVries equation also has a one-parameter family of exact sech^2 solitary wave solutions (of all amplitudes), which, for small amplitudes, are fairly good approximations to the exact solitary water waves, [3]. However, if one tries to improve the approximation by including higher order terms, or maintaining Hamiltonian structure, one in fact does much worse, destroying the solitary wave solutions entirely. At first glance, this is very surprising. However, what should really be surprising is that the models to a physical system have solitary wave solutions in the first place! Indeed, since the $O(\varepsilon^k)$ model is (presumably) only valid for time $O(\varepsilon^{-k})$, the fact that it has a solitary wave solution valid for all time is certainly not guaranteed, even if the full physical system has solitary wave solutions. In fact, all we have a right to expect is a solution which looks like a solitary wave for a long time, but then, possibly, has some completely different behavior, e.g. dissipation, break-up, blow-up, or something else, which is irrelevant for the physical system being modelled. The fact that almost all popular models for wave phenomean *do* have solitary wave solutions is, therefore, an accident that has lulled us into a false sense of security.

The details of the proof of this result are to be found in [5]. The method is to first determine which of the models have exact sech^2 solitary wave solutions. Substituting the explicit formula $u(x, t) = a \operatorname{sech}^2 \lambda(x - c\,t)$ into the model (8), we find that the coefficients $a, \lambda, c,$ must satisfy the compatibility conditions

$$\alpha\rho^2 + \mu\rho + (p - c) = 0, \quad 15\alpha\rho\sigma + 2(\beta+\gamma)\rho + 3\mu\sigma + 2q = 0, \quad 15\alpha\sigma^2 + (3\beta + 2\gamma)\sigma + 2\rho = 0, \tag{9}$$

where $\rho = 4\lambda^2$, $\sigma = -4\lambda^2 / a$. Note that $\sigma < 0$ gives a wave of elevation, $\sigma > 0$ a wave of depression. Analysis of the algebraic system (9) proves that a general fifth order model (8) possesses either 0, 1, 2, ∞, or $\infty + 1$ explicit sech^2 solitary wave solutions, where ∞ denotes a one-parameter family of such solutions. In particular, the model admits a one-parameter family of explicit sech^2 solitary wave solutions if and only if the coefficients satisfy the two algebraic relations

$$(\beta + \gamma)\mu = 5q\alpha, \qquad 15\alpha r = \beta(\beta + \gamma). \tag{10}$$

It should be remarked that these are not enough to guarantee that the model is completely integrable! Interestingly, there may be more than one sech^2 solitary wave solution for subcritical wave speeds if $\alpha\mu < 0$.

In order to prove non-existence, we first construct a suitable solitary wave tail (i.e. for $|x| \longrightarrow \infty$) by proving the convergence of the appropriate formal series solution. On

the other hand, there exists a formal expansion of any solitary wave solutions in a series in power of sech, which, if it converged, would actually give a solitary wave solution. However, except when the coefficients of the equation satisfy the algebraic constraints (10) guaranteeing a family of sech^2 solitary wave solutions, the recurrence relations for the formal series solutions introduce poles in the coefficients in the complex ε-plane converging to $\varepsilon = 0$, which serve to violate our underlying analyticity hypothesis. This gives a brief outline of the essence of the proof — the reader can find the full details in [5].

References

[1] Amick, C.J. and Toland, J.F., On solitary water waves of finite amplitude, *Arch. Rat. Mech. Anal.* **76** (1981), 9-95.

[2] Benjamin, T.B. and Olver, P.J., Hamiltonian structure, symmetries and conservation laws for water waves, *J. Fluid Mech.* **125** (1982), 137-185.

[3] Craig, W., An existence theory for water wave, and the Boussinesq and Korteweg-deVries scaling limits, *Commun. Partial Diff. Eq.* **10** (1985), 787-1003.

[4] Frierichs, K.O., and Hyers, D.H., The existence of solitary waves, *Commun. Pure Appl. Math.* **7** (1954), 517-550.

[5] Kichenassamy, S., and Olver, P.J., Existence and non-existence of solitary wave solutions to higher order model evolution equations, *SIAM J. Math. Anal.* **23** (1992), 1141-1166.

[6] Kunin, I.A., *Elastic Media with Microstructure I*, Springer-Verlag, New York, 1982.

[7] Olver, P.J., Conservation laws of free boundary problems and the classification of conservation laws for water waves, *Trans. Amer. Math. Soc.* **277** (1983), 353-380.

[8] Olver, P.J., Hamiltonian perturbation theory and water waves, *Contemp. Math.* **28** (1984), 231-249.

[9] Olver, P.J., Hamiltonian and non-Hamiltonian models for water waves, in: *Trends and Applications of Pure Mathematics to Mechanics*, P.G. Ciarlet and M. Roseau, eds., Lecture Notes in Physics No. 195, Springer-Verlag, New York, 1984, pp. 273-290.

[10] Olver, P.J., *Applications of Lie Groups to Differential Equations*, Second Edition, Graduate Texts in Mathematics, vol. 107, Springer-Verlag, New York, 1993.

[11] Zakharov, V.E., Stability of periodic waves of finite amplitude on the surface of a deep fluid, *J. Appl. Math. Tech. Physics* **2** (1968), 190-194.

Hamiltonian GFD and Stability

by Pedro Ripa

C.I.C.E.S.E., 22800 Ensenada, B.C., México

Most GFD models are Hamiltonian when dissipation is excluded; this is a structural property which provides a unified picture of different systems, three of which I would like to compare here. We envision the state of a Hamiltonian system as a point φ in a certain state space E; in practice we deal with a particular set of fields $\varphi^a(\mathbf{x},t)$ $\mathbf{x} \in D$, but it must be remembered that the Hamiltonian formalism is covariant under changes of representation. Given any *admissible functional of state* $\mathcal{F}[\varphi,t]$ its gradient $D\mathcal{F}$ is a covector, which is represented by a set of functional derivatives $\delta\mathcal{F}/\delta\varphi^a$, calculable from the first variation $\delta\mathcal{F} =: \langle\delta\varphi, D\mathcal{F}\rangle$. The rate of change φ_t of the state point is a vector field which is constructed by a linear operation of a tensor $\mathbb{J}[\varphi]$ on the gradient of the *Hamiltonian functional* $\mathcal{H}[\varphi,t]$, namely $\varphi_t = \mathbb{J}D\mathcal{H}$. Thus

$$\frac{d\mathcal{F}}{dt} = \frac{\partial\mathcal{F}}{\partial t} + \{\mathcal{F},\mathcal{H}\}, \quad \forall\ \mathcal{F}[\varphi,t], \tag{1}$$

where $\{\mathcal{A},\mathcal{B}\} := \langle D\mathcal{A}, \mathbb{J}D\mathcal{B}\rangle$. This bracket allows for the definition of a one-parameter (say s) group of transformations, generated by some functional of state (say $\mathcal{M}[\varphi,t]$), namely

$$\frac{d\mathcal{F}}{ds} = -\{\mathcal{F},\mathcal{M}\}, \quad \forall\ \mathcal{F}[\varphi,t]. \tag{2}$$

Let $\mathcal{A}$ & $\mathcal{B}$ be any two functionals of state which generate transformations represented by the vector fields $\mathbb{J}D\mathcal{A}$ & $\mathbb{J}D\mathcal{B}$. Their Lie bracket $(\mathbb{J}D\mathcal{A})(\mathbb{J}D\mathcal{B}) - (\mathbb{J}D\mathcal{B})(\mathbb{J}D\mathcal{A})$ is another vector field: if one *demands* it to be also of the form (2) and, moreover, to be generated by the bracket of both functionals (i.e. to be equal to $-\mathbb{J}D\{\mathcal{A},\mathcal{B}\}$) then it follows that $\mathbb{J}$ must be skew-symmetric and satisfy the Jacobi identity [1] (the converse is also true). A $\mathbb{J}$ with those properties is called a *Poisson* tensor and $\{\ ,\ \}$ a Poisson bracket; only this type of brackets is considered here. If the $\mathbb{J}$ is *singular*, its null space is spanned by the gradients of the Casimirs, $\mathbb{J}D\mathcal{C} = 0$ (or $\{\mathcal{F},\mathcal{C}\} = 0\ \forall\mathcal{F}$); using this in (2) shows that the Casimirs generate no transformation. Equations (1) and (2) are invariant under the addition of Casimirs to $\mathcal{H}$ and $\mathcal{M}$.

One of the most powerful properties of a Hamiltonian system is given by Noether's theorem, which links symmetries to conservation laws. A *symmetry* of a dynamical system represents the existence of an operation that transforms any solution into another solution; the transformation may be done at any fixed time, without knowledge of the future -or previous- state of the system. In the particular case that the symmetry transformation of an arbitrary functional $\mathcal{F}$ has the form (2), skew-symmetry and Jacobi property of $\mathbb{J}$ yield $\{\mathcal{F}, d\mathcal{M}/dt\} = 0\ \forall\mathcal{F}$, which in turn implies that

$d\mathcal{M}/dt$ is -at most- equal to a function of time and the Casimirs (this is called a *distinguished function*). Redefining $\mathcal{M}$ by substracting the time integral of that function, the transformation (2) is not changed and the new $\mathcal{M}$ is conserved, $d\mathcal{M}/dt = 0$. This derivation of Noether's theorem requires neither $\partial\mathcal{H}/\partial t = 0$ nor $\partial\mathcal{M}/\partial t = 0$; $\mathcal{H}[\varphi,t]$ may not be conserved even if $\mathcal{M}[\varphi,t]$ is.

Let me now present the three models to be compared. In all cases D is some horizontal domain with a rigid boundary ∂D, and the vertical structure is that of a single active layer of fluid.

The first model is a generalization of the shallow water equations, allowing for lateral -but not vertical- density inhomogeneities [1]. The φ^a fields are the flotability ϑ, the layer thickness h, and the horizontal velocity $\mathbf{u}$; the latter has Cartesian components (u,v) along the the eastward and northward coordinates (x,y). The external fields are the *Coriolis parameter* $f = f_0 + \beta y$ and a topography $h_0(\mathbf{x})$; $\tilde{h} := h_0 + h/2$ is the mean depth of the water column. The evolution equations are

$$\vartheta_t = -\mathbf{u}\cdot\nabla\vartheta,\quad h_t = -\nabla(h\mathbf{u}),\quad \mathbf{u}_t = -qh\hat{\mathbf{z}}\times\mathbf{u} - \nabla b + \tilde{h}\nabla\vartheta. \tag{3}$$

where $q := (f+\hat{\mathbf{z}}\cdot\nabla\times\mathbf{u})/h$ is the *potential vorticity* and $b := \vartheta(h+h_0) + \mathbf{u}^2/2$ is the *Bernoulli function*. This rrotational force field comes from calculating the pressure profile in the active layer -using the hydrostatic balance- and then vertically averaging its horizontal gradient. In this system, potential vorticity is not conserved following fluid particles, indeed

$$q_t + \mathbf{u}\cdot\nabla q = h^{-1}\hat{\mathbf{z}}\cdot\nabla\tilde{h}\times\nabla\vartheta. \tag{4}$$

Boundary conditions for (3) are $\mathbf{u}\cdot\mathbf{n} = 0$ and $\nabla\vartheta\times\mathbf{n} = 0$ at ∂D, where $\mathbf{n}$ is the outward normal; the last one guarantees that the circulations γ_ν are constant.

The condition ϑ = constant (=: g_r) defines a submanifold which is preserved by the dynamics: (3) reduces to the *classical* shallow water equations (SWE): $h_t = -\nabla(h\mathbf{u})$ and $\mathbf{u}_t = -qh\hat{\mathbf{z}}\times\mathbf{u} - \nabla b$, with $b := g_r(h+h_0) + \mathbf{u}^2/2$. This constitutes the second model discussed here. For this system, the right hand side of (4) vanishes, i.e., potential vorticity is conserved, but ϑ is lost as a lagrangian label.

The third model is the so called *equivalente barotropic* one. It is set up from the SWE writing $h+h_0 = H+\eta$, for some constant H, and assuming $\eta, h_0 \ll H$ and $\hat{\mathbf{z}}\cdot\nabla\times\mathbf{u}, \beta y \ll f_0$. To lowest order, the potential vorticity takes the linearized form

$$q := f + \hat{\mathbf{z}}\cdot\nabla\times\mathbf{u} - f_0(\eta-h_0)/H, \tag{5}$$

where $1/H$ has been factored from this definition. The evolution equations for this model express that the circulations γ_ν are

time independent and that potential vorticity is conserved following fluid particles, $q_t + \mathbf{u}\cdot\nabla q = 0$. This equation requires to solve for $(\mathbf{u},\eta)$ as functionals of (q,γ_ν), which is done assuming $\mathbf{u} = \hat{\mathbf{z}}\times\nabla\psi$ and $p\ (\equiv g_r\eta) = f_0\psi$. Notice that this implies not only a geostrophic balance, $f_0\hat{\mathbf{z}}\times\mathbf{u} = -\nabla p$, but also a vanishing horizontal divergence, $\nabla\cdot\mathbf{u} = 0$, in spite of the vertical stretching $\eta - h_0$ in the last term of (5).

The three models presented are but the one-layer cases of larger families, namely primitive equations with inhomogeneous [1] or homogeneous [2] layers and the quasi-geostrophic approximation of the latter [3][4]. All these are singular Hamiltonian systems. For instance, (3) may be obtained from

$$\mathcal{H} := \tfrac{1}{2}\int_D h(\mathbf{u}^2 + \vartheta\tilde{h}) \quad \& \quad \mathbb{J} := \begin{pmatrix} 0 & 0 & -h^{-1}\nabla\vartheta \\ 0 & 0 & -\nabla\cdot \\ h^{-1}\nabla\vartheta & -\nabla & -q\ \hat{\mathbf{z}}\times \end{pmatrix}. \tag{6}$$

If and only if the boundary ∂D is invariant under x-translations, then the momentum

$$\mathcal{M} := \int_D h(u - f_0 y - \tfrac{1}{2}\beta y^2) \tag{7}$$

may be used in (2) to generate the transformation $\varphi^a(x,..) \longmapsto \varphi^a(x+s,..)$, keeping x fixed elsewhere (e.g. in h_0). $\mathcal{H}$ is conserved because $\partial\mathcal{H}/\partial t = 0$, whereas in order for $\mathcal{M}$ to be conserved one requires $\partial h_0/\partial x = 0$. Expressions for $\mathcal{H}$ and $\mathcal{M}$ for the other two models are very similar to these ones. The main difference between the three models is in the geometry of state space, reflected in the form of their respective Casimirs:

$$\mathcal{C} := \int_D qhC_1(\vartheta) + hC_2(\vartheta),\ \int_D hC_3(q),\ \int_D C_4(q), \tag{8}$$

where the $C_j(\ )$ are arbitrary. (The circulations γ_ν are also Casimirs.)

Assume that for certain Casimirs $\mathcal{C}_E$ & $\mathcal{C}_M$ it is $\delta(\mathcal{H}+\mathcal{C}_E) = 0$ @ $\varphi = \Phi_E$ and $\delta(\mathcal{M}+\mathcal{C}_M) = 0$ @ $\varphi = \Phi_M$. The particular states Φ_M & Φ_E could be the same one, and must satisfy $\partial_t\Phi_E = \mathbb{J}D\mathcal{H} = \mathbb{J}D(\mathcal{H}+\mathcal{C}_E) = 0$ and $\partial_x\Phi_M = -\mathbb{J}D\mathcal{M} = -\mathbb{J}D(\mathcal{M}+\mathcal{C}_M) = 0$. The converse (i.e. given Φ_M & Φ_E such that $\partial_t\Phi_E = \partial_x\Phi_M = 0$, find $\mathcal{C}_E$ & $\mathcal{C}_M$ such that $\delta(\mathcal{H}+\mathcal{C}_E) = \delta(\mathcal{M}+\mathcal{C}_M) = 0$) is not guaranteed, as shown below. Take for instance the second model (classical shallow water equations) and search for $\mathcal{C}_M$ such that $\mathcal{M}+\mathcal{C}_M$ is quadratic to lowest order in $\mathbf{u}$ in η ($:= h+h_0-H$, for some constant H), i.e. $\delta(\mathcal{M}+\mathcal{C}_M) = 0$ at the resting ocean. Using $h_0 = 0$ for simplicity (one only needs an x-independent topography), the *pseudomomentum* obtained is [5]

$$\mathcal{P} := \mathcal{M} - \frac{H}{2\beta}\int_D h(q^2 - f_0^2/H^2) + \frac{1}{\beta}\oint_{\partial D} f\mathbf{u}\cdot d\mathbf{x}$$
$$= \int_D u\eta - (v_x - u_y - f\eta/H)^2 \, H/2\beta(H+\eta), \qquad (9)$$

where trivially constant terms have been suppressed. Notice that there are higher order terms in $\mathcal{P}$, on account of the $1/(H+\eta)$. However, for the third model (quasi-geostrophic) $\mathcal{P}$ is exactly quadratic and equal to $-1/2\beta$ times the *enstrophy* $\int(v_x - u_y - f\eta/H)^2$ [6], since the integral of $u\eta$ vanishes because of geostrophy. On the other hand, for the first model (shallow water equations with lateral inhomogeneities) this trick is not posible: in order to be able to construct $\mathcal{P}$ one would need a monotonous ambient buoyancy profile $\Theta(y)$.

Notice that $\mathcal{P}$ cannot be obtained if $\beta = 0$ (or, more generally, $d[f/(H-h_0)]/dy = 0$), for lack of an appropriate Casimir. The reason being that for the degenerate cases (uniform ambient potential vorticity and/or density) there are not enough natural conserved scalars that could serve as Lagrangian labels [7]. From the Eulerian point of view, both $\mathcal{M}$ and $\mathcal{P}$ may serve as x-momentum. From the Lagrangian point of view, $\mathcal{M}$ and $\mathcal{P}$ conservation are obtained from homogeneity of position x and label x_0, but one cannot have one symmetry without the other. Moreover, different equivalent Lagrangians give conservation of different combinations of $\mathcal{M}$ and $\mathcal{P}$ for the independent variations δx and δx_0, so it is not possible to say, in a unique way, which one of the two invariants is related to which symmetry transformation [7].

For a steady basic state Φ_E one can use the pseudoenergy $\mathcal{I}_E := \mathcal{H}+\mathcal{C}_E$, $\delta\mathcal{I}_E = 0$, to derive Arnol'd's first ($\delta^2\mathcal{I}_E > 0$) or second ($\delta^2\mathcal{I}_E < 0$) formal stability theorems. Even better, one may use the total variation $\Delta\mathcal{I}_E$ to find finite amplitude (nonlinear) stability criteria. Table III in Ref. [1] shows that this program has not had much success, except for the very restrictive class of horizontally non-divergent models (quasi-geostrophic and 2D Euler). These are also the only models for which an instability can be characterized by energy transfer terms; for the other two classes discussed here, the perturbation may have zero or negative energy and therefore its growth is related to an increase in the energy of the mean flow [2][8].

Primitive equations models with homogeneous layers (e.g., the classical shallow water equations) only have Arnol'd's first formal stability theorem [2], and this condition is harder and harder to satisfy as the number of layers increases. Moreover, there is no formal stability theorem for the cases with either inhomogeneous layers [1] or continuous stratification [8]; for the latter, however, there is the Miles-Howard criterium for normal mode perturbations. Failure of the strict application of Arnol'd's method does not mean that there are not stable states, it only means that their stability will have to be proved by

special methods.

The condition $\delta(\mathcal{H}+\mathcal{C}_E) = 0$ defines an extreme of the Hamiltonian on the Casimir leaf $\delta\mathcal{H}|_C = 0$ (or vice versa, $\delta\mathcal{C}|_H = 0$). In Ref. [4] it is argued that sign definiteness of $\delta^2\mathcal{H}|_C$ is enough to guarantee stability for general perturbations, even if $\delta^2(\mathcal{H}+\mathcal{C}_E)$ is not sign definite. The reason for this being that nearby constant-$\mathcal{C}_E$ leaves have similar dynamics. A different situation arises when leaving a sheet changes the physics, like going from $\nabla\Theta \equiv 0$ (second model) to $\nabla\delta\vartheta \not\equiv 0$ (first model).

Finally, let me comment on the role of invariants in the instability problem. Consider the case of a symmetric system: by Andrew's theorem [9] one can only consider steady and symmetric basic states. Not only the pseudoenergy, but also the pseudomomentum $\mathcal{I}_M := \mathcal{M}+\mathcal{C}_M$ are quadratic (and higher order) invariants. Formal stability is guaranteed if there is any α such that $\delta^2\mathcal{I}_E - \alpha\delta^2\mathcal{I}_M$ is sign definite. (This combination is the Hamiltonian for the linearized dynamics, in a frame moving with speed α.) On the other hand, if the basic state is unstable then there is a perturbation for which $\delta^2\mathcal{I}_E - \alpha\delta^2\mathcal{I}_M = 0$ for any α, i.e. both terms vanish. This represents a balance between positive and negative parts, which may be used to characterize growing perturbations [10]. Typification of an instability by energy transfer terms only works for non-divergent models.

For lack of space I am only listing some of my contributions to these subjects. Further references may be found in these papers and in the Lecture Notes by Phill Morrison and Ted Shepherd, in this volume.

References

[1] Ripa P., **Geophys. & Astrophys. Fluid Dyn., 70:** 85-111 (1993).

[2] Ripa P., **J. Fluid Mech., 222:** 119-137 (1991).

[3] Ripa P., **J. Fluid Mech., 235:** 379-398 (1992).

[4] *Arnol'd's second stability theorem for the equivalent barotropic model*, P. Ripa, **J. Fluid Mech.,** in press (1993).

[5] Ripa P., **J. Phys. Ocean., 12**: 97-111 (1982).

[6] Ripa P., **Journal Fluid Mechanics, 103**: 87-115 (1981).

[7] Ripa P., **A.I.P. Proceedings, 76:** 281-306 (1981).

[8] Ripa P., **Pure and Applied Geophysics, 133:** 713-732 (1990).

[9] Ripa P.,**Rev. Méx. Fís., 38**: 229-243 (1992).

[10] Ripa P., **J. Fluid Mech., 242:** 395-417 (1992).

STRUCTURE OF THE CANONICAL TRANSFORMATION

Ian Roulstone [1] *Michael J. Sewell* [2]

1 Introduction

The aim of this work (Sewell & Roulstone 1992) has been to conduct a fresh study of the canonical transformation. This transformation is widely known to be a classical and time-honoured device in mechanics, but we have found that an understanding of it may be no more than formal without a reasonable variety of explicit examples. The literature on this subject is often stereotyped and rather uncritical, or sophisticated and unduly difficult. One of our aims has been to investigate some of these apparently sophisticated ideas with some explicit examples which we have not found available elsewhere.

We have found that the expression for the transformation in terms of gradients of generating functions reveals much about the *anatomy* of the transformation. In turn, the variety of possible structures of generating functions (e.g. multivaluedness), suggests that some of the other definitions are ambiguous if stated in the forms that are often found in the literature. We shall elucidate this point further in §5.

The importance of the canonical transformation derives from the fact that it is intrinsic in any part of mathematics, mechanics or numerical analysis (applied to symplectic integrators), where Hamilton's equations appear. The trigger for this present work lay within our investigation of the semi-geostrophic equations of meteorology. Previous papers (Chynoweth & Sewell 1989, 1990, 1991) showed that topic to contain convexifications of multivalued Legendre dual functions such as the swallowtail, which are adapted to provide examples of canonical transformations.

2 Definition

It is clearest to deal with the lowest dimensional case, because this offers fully explicit examples in a way which higher dimensions, despite their importance, cannot. We use the neutral notation of Carathéodory (1982), which is not biased towards any particular context. Thus we suppose that a pair x, y of real scalars is related to another such pair X, Y by

$$X = X(x, y), \quad Y = Y(x, y) \ . \tag{1}$$

This is a dependence or transformation $\mathbf{R}^2 \mapsto \mathbf{R}^2$. Let j denote the jacobian of (1). For some particular transformations (1), j has a constant value over some domain in x, y space.

[1]Meteorological Office, Bracknell, RG12 2SZ, U.K.
[2]Department of Mathematics, University of Reading, Reading, RG6 2AX, U.K.

We adopt the following definition for the purpose of this paper. If the transformation (1) has

$$j = 1 \tag{2}$$

over a two-dimensional domain, we define the transformation to be *canonical over that domain.* The domain need not be the whole space.

3 Anatomy

A canonical transformation has a locally unique inverse in the neighbourhood of every point of its domain, because $j = 1$ is sufficient for the inverse function theorem to apply. Even when the functions in (1) are single valued, however, the global inverse of the transformation, which we write as

$$x = x(X, Y), \quad y = y(X, Y) \tag{3}$$

in terms of differentiable functions on the right, need not be single valued.

We now seek to explore some of the variety of *anatomical detail* which gives the canonical transformation its structure. It is convenient to define an *internal singularity* of a canonical transformation to be a location where one or more of $\partial X/\partial x$, $\partial X/\partial y$, $\partial Y/\partial x$, $\partial Y/\partial y$ is zero or infinite.

Theorem 1 *A canonical transformation (1) with (2) can be expressed locally in one or more of the following versions, when the indicated sufficient condition holds.*
(i) If $\partial Y/\partial y \neq 0, \pm\infty$, *then* $X = X(x, Y)$, $y = y(x, Y)$ *such that* $\partial X/\partial x = \partial y/\partial Y$.
(ii) If $\partial X/\partial y \neq 0, \pm\infty$, *then* $y = y(x, X)$, $Y = Y(x, X)$ *such that* $\partial y/\partial X + \partial Y/\partial x = 0$.
(iii) If $\partial X/\partial x \neq 0, \pm\infty$, *then* $x = x(X, y)$, $Y = Y(X, y)$ *such that* $\partial x/\partial X = \partial Y/\partial y$.
(iv) If $\partial Y/\partial x \neq 0, \pm\infty$, *then* $X = X(Y, y)$, $x = x(Y, y)$ *such that* $\partial X/\partial y + \partial x/\partial Y = 0$.

In the case of thermodynamics, the last equations in (i)-(iv) are called Maxwell's relations.

Theorem 2 *For each part of Theorem 1 which is available, there exists a scalar* generating function *listed below, allowing the canonical transformation to be expressed in gradient form as follows, and locally so in the first instance.*
(i) $A(x, Y)$ *such that* $X = \partial A/\partial Y, y = \partial A/\partial x$. *(ii)* $B(x, X)$ *such that* $y = -\partial B/\partial x, Y = \partial B/\partial X$. *(iii)* $C(X, y)$ *such that* $x = -\partial C/\partial y, Y = -\partial C/\partial X$. *(iv)* $D(Y, y)$ *such that* $X = -\partial D/\partial Y, x = \partial D/\partial y$.

The generating functions in Theorem 2 are available locally and as single valued functions in the first instance, but we shall give an example, later in this section, showing how they can be available globally, and as multivalued functions.

Theorem 3 *When any two of the generating functions having one argument in common exist, they are connected by a Legendre transformation which relates the non-common arguments as active variables, while the common one is passive.*

To illustrate some of the features of Theorems 1, 2 and 3, consider the following example. The transformation

$$X = x, \quad Y = x^2 + y \ , \tag{4}$$

is canonical and possesses a quartet of generating functions (as in Theorem 2). There are no internal singularities associated with $\partial X/\partial x = 1$ and $\partial Y/\partial y = 1$, so (i) and (iv) of Theorem 2 with (4) can be integrated to give the generating functions A and C, over the whole x, Y and X, y planes respectively. These two functions each have the form of a fold catastrophe potential: $A = -1/3x^3 + xY$, $C = -1/3X^3 - Xy$. The internal singularity of $\partial Y/\partial x = 0$ at $x = 0$ is an isolated singularity of the $A \leftrightarrow D$ and $C \leftrightarrow D$ relationships, but this does not inhibit the construction of the double-valued function $D = \mp\frac{2}{3}(Y - y)^{\frac{3}{2}}$ with cusped edge of regression along $Y = y$. The internal singularity $\partial X/\partial y \equiv 0$ of (4) is not an isolated singularity, so that the inverse function theorem cannot be resurrected in the way that is possible for the foregoing isolated singularities. Parts (ii) of Theorems 1 and 2 fail in the stated forms. Nevertheless, the $A \leftrightarrow B$ and $B \leftrightarrow C$ relationships can still be constructed using the more basic definition of a Legendre transformation in terms of points and planes, or poles and polars respectively (see Sewell, 1987, §2.2). Each of $A(x, Y)$ and $C(X, y)$ is linear in the variable now required to be active, namely Y and y respectively, and the dual of these polars is the single point, with abscissa $x = X$ and ordinate $\frac{1}{3}x^3 = \frac{1}{3}X^3$, and only has restricted differentiability. The generating function $B(x, X)$ still exists, therefore, but only over a domain of lower dimension. One may not know in advance which generating functions have this limitation.

4 Semi-geostrophic theory

The semi-geostrophic theory of meteorology provides a recent example of a Legendre quartet given by Chynoweth & Sewell (1989, 1991), which can contain singularities. Here $\mathbf{x}$ is a horizontal position vector in physical space, and the scalar z is a measure of height; $\mathbf{M}$ is a horizontal momentum vector, and θ is a measure of temperature (see Chynoweth & Sewell, 1991, for further discussion of these variables). Note that there is a Legendre transformation between $R(\theta, \mathbf{M})$ and $P(z, \mathbf{x})$, with all arguments active, having the property $R + P = \mathbf{M} \cdot \mathbf{x}$, and

$$\partial R/\partial\theta = z(\theta, \mathbf{M}), \qquad \partial R/\partial \mathbf{M} = \mathbf{x}(\theta, \mathbf{M}), \tag{5}$$

$$\partial P/\partial z = \theta(z, \mathbf{x}), \qquad \partial P/\partial \mathbf{x} = \mathbf{M}(z, \mathbf{x}) \tag{6}$$

(see Purser & Cullen 1987).

Consider the case of flow in a single vertical plane. The vectors $\mathbf{M}$ and $\mathbf{x}$ are replaced by their scalar components M and x. In general $(5)_1$ can now be inverted and substituted into $(5)_2$ to give a canonical transformation, $M = M(\theta, -z)$, $x = x(\theta, -z)$, generated, for example, by $R(\theta, M)$.

A mathematically simple illustration is provided by the parabolic umbilic polynomial,

$$R(\theta, M) = \frac{1}{4}M^4 + M\theta^2 + \alpha M^2 + \beta\theta^2 \ , \tag{7}$$

in which α and β are given parameters. This leads via (5) to $z = 2\theta(M + \beta)$, $x = M^3 + 2\alpha M + \theta^2$, which can be rearranged as the canonical transformation

$$M = z/2\theta - \beta, \ \ x = (z/2\theta - \beta)^3 + 2\alpha(z/2\theta - \beta) + \theta^2 \ . \tag{8}$$

The function (7) was used by Chynoweth & Sewell (1989) as a starting point for calculating its Legendre dual function $P(z, x)$, because the latter has a self-intersection line whose projection onto the physical x, z plane models the trace of an atmospheric front. From the viewpoint of canonical transformations, (8) is therefore an example of one which is derivable from a multivalued generating function P possessing self-intersections.

5 Alternative definitions

Here we comment briefly on the invariance of a circuit integral and its relationship to (2).

If a differentiable function $B(x, X)$ exists, and is single valued, and if (ii) of Theorem 2 holds, then its first differential is unambiguously $\mathrm{d}B = Y\mathrm{d}X - y\mathrm{d}x$. In particular, if it has a single-valued branch over a closed circuit γ drawn in its domain, then it follows that

$$\oint_\gamma Y \ \mathrm{d}X = \oint_\gamma y \ \mathrm{d}x \ , \tag{9}$$

where the circuit integrals are each evaluated around the lifted version of γ on the considered branch. This result expresses the invariance of the circuit integral under the transformation (1).

One motivation for the use of the circuit integral is that it can be related via Stokes' theorem to the $j = 1$ definition, which can be illustrated by results of the following type.

Theorem 4 *If fully differentiable B(x,X) exists, and if there exists another, intermediate, uniquely invertible mapping*

$$x = x(a, b), \ \ X = X(a, b) \ ,$$

to a third pair of variables a, b, then

$$\int_D \frac{\partial(x, y)}{\partial(a, b)} (j - 1) \ \mathrm{d}a\mathrm{d}b = 0 \ , \tag{10}$$

where D is the interior of the single valued image ∂D of the circuit γ.

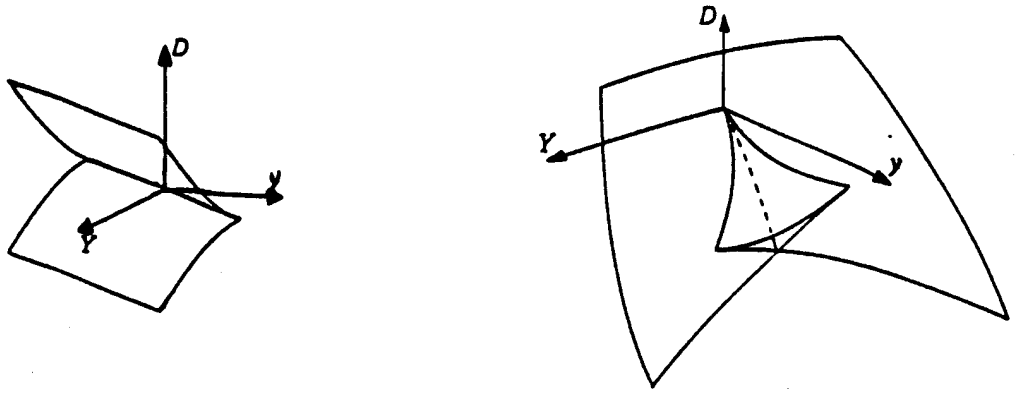

Figure 1: (a) D(Y, y) of §(3), (b) The swallowtail surface.

Proof. We write (9) in terms of a and b

$$\oint_{\partial \mathcal{D}} Y \left(\frac{\partial X}{\partial a} \mathrm{d}a + \frac{\partial X}{\partial b} \mathrm{d}b \right) = \oint_{\partial \mathcal{D}} y \left(\frac{\partial x}{\partial a} \mathrm{d}a + \frac{\partial x}{\partial b} \mathrm{d}b \right) \quad . \tag{11}$$

Using Stokes' theorem (11) becomes

$$\int_{\mathcal{D}} \frac{\partial(X,Y)}{\partial(x,y)} \frac{\partial(x,y)}{\partial(a,b)} \, \mathrm{d}a\mathrm{d}b = \int_{\mathcal{D}} \left(\frac{\partial x}{\partial a} \frac{\partial y}{\partial b} - \frac{\partial x}{\partial b} \frac{\partial y}{\partial a} \right) \mathrm{d}a\mathrm{d}b \ , \tag{12}$$

which is (10). □

A common definition in the literature (Arnol'd, 1989, p. 239) is: 'The transformation (1) is canonical if the property (9), or one of its alternatives, holds', but this is subject to the following qualifications. It must be reasonable to expect a generating function to have global multivaluedness, e.g. of the type encountered with the example in §3, or the swallowtail (see figure 1), or worse in higher dimensions. In such circumstances, one must decide which single-valued part of the multivalued generating function is to receive the lifted circuit. It may be that at least one of the four generating functions is always globally single valued, but in the absence of a theorem which identifies in advance which one, there is an inherent ambiguity in the use of the circuit integral.

References

ARNOL'D, V.I. (1989) Mathematical Methods of Classical Mechanics. *Springer Graduate Texts*, **60**. 2nd edition.

CARATHÉODORY, C. (1982) Calculus of variations and partial differential equations of the second order. *New York: Chelsea.*

CHYNOWETH, S. and SEWELL, M.J. (1989) *Proc. Roy. Soc. Lond.*, **A424**, 155-186.

CHYNOWETH, S. and SEWELL, M.J. (1990) *Proc. Roy. Soc. Lond.*, **A428**, 351-377.

CHYNOWETH, S. and SEWELL, M.J. (1991) *Q. J. Roy. Met. Soc.*, **117**, 1109-1128.

PURSER, R.J. and CULLEN, M.J.P. (1987) *J. Atmos. Sci.* **44**, 3449-3468.

SEWELL, M.J. (1987) Maximum and Minimum Principles. *C.U.P.*

SEWELL, M.J. and ROULSTONE, I. (1992) *Met. Office Sci. Note No. 6.* To appear in *Phil. Trans. Roy. Soc. Lond.* (1993).

ON THE HAMILTONIAN STRUCTURE OF SEMI-GEOSTROPHIC THEORY.

Ian Roulstone [1] *John Norbury* [2]

1 Introduction

A description of the canonical form for the semi-geostrophic (SG) equations within the context of Generalized Hamiltonian systems was given by Salmon (1988). In this work a canonical Hamiltonian structure for the semi-geostrophic equations is presented and from this, a reduced, noncanonical Hamiltonian structure is derived, providing a fully nonlinear version of the approximate linearised vorticity-streamfunction representation. This paper constitutes a synopsis of Roulstone & Norbury (1992). For reasons of brevity the propositions are given here with only sketch proofs, however we attempt to convey some of the essential geometric ideas.

Here we work with Lagrangian and Eulerian formulations of the equations. The SG equations of motion may be written either as an infinite set of coupled ordinary differential equations or, as in the formulation of the geometric model, an advection equation based on the Monge-Ampere operator. The geometry of the Monge-Ampere equation together with convex analysis and their application to atmospheric flows offers a new perspective on balanced systems.

2 Semi-Geostrophic Dynamics

2.1 *Equations of motion*

The three-dimensional Boussinesq equations of semi-geostrophic theory given by Hoskins & Draghici (1977) on an f-plane, can be written using the following coordinates

$$\mathbf{X} \equiv (X,\, Y,\, Z) \equiv \left[x + \frac{v_g}{f},\, y - \frac{u_g}{f},\, \frac{g\theta}{f^2\theta_0}\right] , \tag{1}$$

in the form

$$\frac{\mathrm{D}\mathbf{X}}{\mathrm{D}t} = \mathbf{u}_g \equiv (u_g,\, v_g,\, 0) \ ; \tag{2}$$

that is, the motion in these transformed coordinates is exactly geostrophic. The material derivative is $\mathrm{D}/\mathrm{D}t \equiv \partial/\partial t + \mathbf{u}\cdot\nabla_x$. In these transformed coordinates a consistent approximation to the energy integral can be derived and the condition for the integral to be stationary under virtual displacements, may be expressed in terms of a convexity condition on a streamfunction for the geopotential (Cullen *et. al.* (1987)). We will introduce such a function in the next subsection. The Jacobian $q = \partial(X,Y,Z)/\partial(x,y,z)$, defines a consistent form of the Ertel potential vorticity in SG, satisfying $\mathrm{D}q/\mathrm{D}t = 0$.

[1] Meteorological Office, Bracknell, RG12 2SZ, U.K.
[2] Mathematical Institute, Oxford, OX1 3LB, U.K.

2.2 *The Legendre Transform*

The equations of motion have a particular duality structure. The vector $\mathbf{X}$ may be expressed as the gradient of some scalar function $P(\mathbf{x})$, $\mathbf{X} = \nabla_x P$. Within an arbitrary additive constant this function is uniquely defined by, from (1) $P = \phi/f^2 + (x^2 + y^2)/2$, where ϕ is the geopotential. Define $\mathbf{Q}(\mathbf{x}) \equiv \nabla_x \mathbf{X}$, then $\mathbf{Q}$ is the Hessian of P with respect to $\mathbf{x}$. $\mathbf{Q}$ is symmetric, so when it is non-singular its inverse exists, and the inverse Jacobian is symmetric also, implying that $\mathbf{x}$ is the gradient of some scalar function $R(\mathbf{X})$:

$$\mathbf{x} = \nabla_X R \ . \tag{3}$$

R is given to within an additive constant by $R(\mathbf{X}) = \mathbf{x} \cdot \mathbf{X} - P(\mathbf{x})$, which is the expression for the *Legendre transform* between R and P. We can show that the motion is non-divergent in $\mathbf{X}$-space and therefore, being constrained to Z-surfaces since (2) has $\dot{Z} = 0$, is expressible in terms of a streamfunction Ψ by $(u_g,\ v_g,\ 0) = (-\partial\Psi/\partial Y, \partial\Psi/\partial X,\ 0)/f$. From (1) and (3) we deduce that the simplest form for Ψ is given by

$$\Psi = f^2 \left(\frac{1}{2}(X^2 + Y^2) - R(\mathbf{X}) \right) \ . \tag{4}$$

The particular duality structure described above is but *one* realization of a *quartet* of Legendre transformations described in Chynoweth & Sewell (1989).

2.3 *A solution strategy*

We outline the numerical method as discussed by Purser & Cullen (1987) and Cullen, Norbury & Purser (1991) to show that the above formulation leads to a natural phase space description.

At each timestep define a *distribution* of $\rho(\mathbf{X}) = q^{-1}(\mathbf{x}) = \det(\mathbf{Q}^{-1})$, and solve the nonlinear elliptic or parabolic (Monge-Ampere) equation for R:

$$\det |\mathrm{Hes}(R)| = \rho \tag{5}$$

subject to suitable boundary conditions. The boundary conditions are imposed with respect to the domain in which the fluid motion takes place and need to be translated into conditions on ∇R. The next step is to use Ψ defined in (4) in terms of R given by (5) to update the conserved density ρ, according to the advection equation

$$\frac{\partial \rho}{\partial t} = -\mathbf{u}_g \cdot \nabla_X \rho \equiv \frac{1}{f} \frac{\partial(\rho,\ \Psi)}{\partial(X,\ Y)} \ . \tag{6}$$

In this model we seek to construct a solution by solving a sequence of time independent elliptic problems.

3 Hamiltonian Structure

3.1 *Kinematics and Dynamics*

For any differentiable function R of $\mathbf{X}$ for which we write the relationship (3), we can define the Hamiltonian functional, using (4) and an appropriate normalization for the geopotential, as

$$\mathcal{H}[\mathbf{X}] = \int_\Gamma \mathrm{d}\gamma\, \Psi(\mathbf{X}) = f^2 \int_D \mathrm{dx} \left(\frac{1}{2} \left[(y-Y)^2 + (X-x)^2 \right] - zZ \right) \ , \tag{7}$$

where $\mathrm{d}\gamma$ is the measure over the Lagrangian particle labelling coordinates $(a,b,c) \equiv \mathbf{a}$, assigned at $\tau = 0$, $\mathbf{X}(\mathbf{a},\, \tau) : \mathbf{X}(\mathbf{a},\, 0) = \mathbf{a}$. The coordinates $\mathbf{x} \equiv (x,y,z)$ are locally cartesian on a domain D. The dual space mass density $\rho(\mathbf{X})$, becomes the Jacobian of the map $\mathbf{X} \mapsto \mathbf{a}$, and is taken to have compact support in Γ to avoid later difficulties with boundary conditions. For incompressible flow, $\partial(\mathbf{a})/\partial(\mathbf{x}) = 1$. We now write our equations of motion (2) in Lagrangian phase space variables $\mathbf{X}$ as a canonical Hamiltonian system by means of a Poisson bracket defined as follows.

Proposition 1 *The equations of motion (2) take the form on surfaces of constant Z*

$$\frac{\partial X}{\partial \tau} = \{\mathcal{H},\, X\}_C, \quad \frac{\partial Y}{\partial \tau} = \{\mathcal{H},\, Y\}_C \ , \tag{8}$$

where $\{\ ,\ \}_C$ is given by

$$\{\mathcal{F},\, \mathcal{G}\}_C = \int_\Gamma \mathrm{d}\gamma \left(\frac{\delta \mathcal{F}}{\delta X(\mathbf{a})} \frac{\delta \mathcal{G}}{\delta Y(\mathbf{a})} - \frac{\delta \mathcal{F}}{\delta Y(\mathbf{a})} \frac{\delta \mathcal{G}}{\delta X(\mathbf{a})} \right) \ .$$

One can show directly in these variables that the $\mathbf{X}$-space mass density ρ is conserved, $\{\rho,\, \mathcal{H}\}_C = 0$. Conservation of potential vorticity may be established using the same procedure by noting $\rho = q^{-1}$.

3.2 *Symplectic structure and particle labels*

Qualitatively, a Hamiltonian system possesses a volume element called the *symplectic form*, which we denote by Ω, and this is an invariant in the sense that its Lagrangian derivative along the flow vanishes. We express the symplectic structure Ω in canonical bases for the particle label description. One can identify a natural dual to Ω, such that their inner product is a scalar. We refer to this object as Θ, known as the cosymplectic structure. It turns out that the abstract statement of the conservation of the symplectic inner product $\langle \Omega | \Theta \rangle$, is equivalent to the conservation of *potential vorticity* on fluid particles. This is, therefore, an important relationship between the dynamical invariant $q\,|_Z$ and the canonical kinematic structure Ω.

3.3 *A noncanonical Hamiltonian approach to the advection equation*

We make some brief remarks concerning the generalization of the results to *noncanonical systems.* Suppose that a system has densities $\mathcal{F}$, $\mathcal{G}$,which are functionals of canonical coordinates z^i. It may be possible to write the Poisson brackets in terms of noncanonical coordinates $\bar{z}^\alpha$, where $\alpha < i$, in the following manner

$$\{\mathcal{F},\, \mathcal{G}\}_E = \int \mathrm{d}\bar{\mathbf{z}}_1 \int \mathrm{d}\bar{\mathbf{z}}_2 \frac{\delta \mathcal{F}}{\delta \bar{z}_{1\alpha}} \{\bar{z}_{1\alpha},\, \bar{z}_{2\beta}\}_C \frac{\delta \mathcal{G}}{\delta \bar{z}_{2\beta}} \,. \tag{9}$$

We will show that this structure leads to an appropriate generalization of (6).

In the following calculations the canonical coordinates z^i will be identified with the Lagrangian coordinates $X^i \leftrightarrow (X, Y)$, while the noncanonical variable $\bar{z}$ will be identified with $\rho(\bar{X}^i)$. We use the overbar to distinguish the use of the dual space coordinates here from that employed in §3.1: The partial derivative with respect to time is taken at constant $\bar{X}$. It is the symmetry invariance (commonly referred to as gauge invariance) with respect to the particle relabelling that enables the kinematics of the system to be described in terms of a single observable $\bar{z}$, together with a noncanonical structure.

We use our previous Hamiltonian (7), but evaluated in phase space solely as a functional of ρ. The Hamiltonian is given by

$$\mathcal{H}[\rho] \;=\; \int \mathrm{d}\bar{\mathbf{X}} \rho(\bar{\mathbf{X}}) \Psi(\bar{\mathbf{X}}) \;. \tag{10}$$

The functional derivative $\delta\mathcal{H}/\delta\rho$ is calculated using the Legendre Transformation and may be related to the energy minimization condition. The result is

$$\frac{\delta \mathcal{H}}{\delta \rho} \;=\; f^2 \left(\frac{1}{2} (\bar{X}^2 + \bar{Y}^2) \;-\; R \right) \;. \tag{11}$$

The key to understanding the variation in (11) is the use of the *contact structure* of the Legendre transformation. The salient feature of a contact space which is of importance here is the idea of a lifted curve (Arnol'd (1989), appendix 4). A curve $R = \mathcal{C}(\mathbf{X})$ in the 'base space', spanned by the coordinates (X, R), has an image or *lift* denoted $\mathcal{C}'$ in the space spanned by the coordinates $(X, R, \nabla_X R)$. This is the structure of phase space for the reduced SG model. At a fixed point (X_0, R_0) on a curve $\mathcal{C}$, we can vary $\mathcal{C}'$ with respect to x (using (3)) and thus the Legendre Transformation gives $\delta\mathcal{C} = \delta_x R = X\delta x - \nabla_x P \delta x \equiv 0$. The integrand of the Hamiltonian (10) may thus be varied with respect to $\mathbf{x}$, with the result $\delta\mathcal{H} = \Psi\delta\rho + \rho\delta\Psi$. But at fixed $\mathbf{X}$, $\delta_{\mathbf{x}}\Psi = \delta_{\mathbf{x}} R = 0$. Consequently we get (11). It is the contact geometry that distinguishes the dynamics of SG theory from that of perfect incompressible fluids (e.g. Marsden & Weinstein (1983)).

We may now formulate the Hamiltonian structure of (6).

Proposition 2 *The equation of motion (6) may be written in the following Hamiltonian form*

$$\frac{\partial \rho(\bar{\mathbf{X}})}{\partial t} = \{\mathcal{H},\, \rho(\bar{\mathbf{X}})\}_E \ ,$$

with

$$\{\mathcal{F},\, \mathcal{G}\}_E = \int_\Gamma \mathrm{d}\bar{\mathbf{X}} \frac{\delta \mathcal{G}}{\delta \rho(\bar{\mathbf{X}})} \left(\frac{\partial \left(\rho(\bar{\mathbf{X}}), \dfrac{\delta \mathcal{F}}{\delta \rho(\bar{\mathbf{X}})} \right)}{\partial (\bar{X},\, \bar{Y})} \right) \tag{12}$$

and Hamiltonian given by (10). Γ is taken to be a union of bounded components in $\bar{\mathbf{X}}$ in which the defining relation for R (5) holds.

Sketch of Proof: With an appropriate functional form for ρ, we evaluate the canonical bracket in (6) and obtain the result

$$\{\rho(\bar{\mathbf{X}}_1), \rho(\bar{\mathbf{X}}_2)\}_C = -\frac{\partial \delta(\bar{\mathbf{X}}_2 - \bar{\mathbf{X}}_1)}{\partial \bar{Y}_1} \frac{\partial \rho(\mathbf{X}_1)}{\partial \bar{X}_1} + \frac{\partial \delta(\bar{\mathbf{X}}_2 - \bar{\mathbf{X}}_1)}{\partial \bar{X}_1} \frac{\partial \rho(\mathbf{X}_1)}{\partial \bar{Y}_1} \ ,$$

and substitute this into (6). Integrating by parts and discarding boundary terms which are of the form $\delta(\bar{\mathbf{X}}_2 - \bar{\mathbf{X}}_1)|_\partial$, because of compact supports, we get (12). Identify $\mathcal{F}$ with $\mathcal{H}$ and $\mathcal{G}$ with ρ, and use the results of §2.2 to get the right hand side of (6). □

We note that the form of (12) means that the bracket of functionals depending on ρ alone will be in *involution* with respect to $\{\ ,\ \}_E$ (i.e. their Poisson Brackets all vanish). We identify the bilinear skew adjoint operator $\mathcal{J}$ and write it

$$\mathcal{J}^{\bullet\circ} = \circ \frac{\partial (\rho,\, \bullet)}{\partial (\bar{X},\, \bar{Y})} \ .$$

References

ARNOL'D, V.I. (1989). Mathematical Methods of Classical Mechanics. *Springer Graduate Texts*, **60**.

CHYNOWETH, S. and SEWELL, M.J. (1989). *Proc. Roy. Soc. Lond.* Ser. A **424**, 155-186.

CULLEN, M.J.P., NORBURY, J., PURSER, R.J. and SHUTTS, G.J. (1987). *Quart. J. Roy. Met. Soc.*, **113**, 735-757.

CULLEN, M.J.P., NORBURY, J. and PURSER, R.J. (1991). *SIAM J. Appl. Math.*, **51**, 20-31.

HOSKINS, B.J. and DRAGHICI, I. (1977). *J. Atmos. Sci.*, **34**, 1859-1867.

MARSDEN, J.E. and WEINSTEIN, A. (1983). *Physica*, **7D**, 305-323.

PURSER, R.J. and CULLEN, M.J.P. (1987). *J. Atmos. Sci.* **44**, 3449-3468.

ROULSTONE, I and NORBURY, J. (1992). *Preprint, submitted for publication.*

SALMON, R. (1988). *J. Fluid Mech.*, **196**, 345-358.

Linear and Nonlinear Baroclinic Wave Packets: Atmospheric Cyclogenesis and Storm Tracks

Kyle Swanson
Department of the Geophysical Sciences
University of Chicago

Our present understanding of the dynamics of synoptic scale structures in the midlatitude regions of the Earth is based on quasi-geostrophic theory, with its roots in the works of Charney [1] and Eady [2]. These researchers found that the linearized equation expressing conservation of quasi-geostrophic potential vorticity in a vertically sheared mean flow, together with the appropriate boundary conditions, results in eigenmode solutions resembling midlatitude cyclones in scale and structure. Furthermore, for some spatial scales and mean flow parameters there exist associated eigenvalues corresponding to an exponential increase in perturbation amplitude with time, at least while the structures evolve according to the linear dynamics.

While this theory elucidates the primary mechanism of the instability (see [3:7.1-7.6] for a review), namely the baroclinic conversion of mean flow potential energy into perturbation energy, there remains much to be explained as far as the role of these synoptic scale structures or ``baroclinic eddies'' in the general circulation of the Earth's atmosphere is concerned. As far as the role of baroclinic instability in this circulation is concerned, this boils down to two questions: First, how does baroclinic instability effect the mean flow profile of the atmosphere (essentially a question of mean flow interaction), and secondly, what are the fluxes in heat, moisture, etc. brought about by the instabilities themselves (a question of the structure and temporal frequency of the instabilities themselves). This presentation will deal with some preliminary results regarding the second of these points, namely trying to understand the evolution of baroclinic wave packets, i.e. coherent groups of synoptic-scale eddies, which have been shown to compose a large portion of variability in both the Northern and Southern Hemispheres [5].

Linear Theory: Absolute Instability and Wave Packets

We first want to consider the linear stability of a strictly zonal (i.e. x - independent) flow, which can be given in terms of a geostrophic streamfunction $\varphi = \Psi(y,z)$, corresponding to the basic state zonal velocity $U_0 = -\partial\Psi/\partial y$. If we let ϕ be a small amplitude perturbation to that zonal flow, i.e. $|\phi| << 1$, then neglecting terms of $O(\phi^2)$ in the quasi-geostrophic equations yields the linear equation

$$\frac{\partial q}{\partial t} + L(\phi, q) = 0 \qquad (1)$$

where $q = \phi_{xx} + \phi_{yy} + V(\phi_z, \phi_{zz})$ is the perturbation potential vorticity (V being a vertical coupling term) and $L(\phi,q)$ is a linear operator representing advection of perturbation potential vorticity by the mean flow U_0. Equation (1) has solutions of the form $\phi(x,y,z,t) = \Phi(y,z)\exp[i(kx - \omega t)]$; upon substitution this yields an eigenvalue problem, wherein modal solutions Φ exits only if ω and k are constrained to satisfy a dispersion relation $D[\omega,k] = 0$. Together, these allow the linear description of the evolution of a single wave. As stated above, $\omega = \omega(k)$ is in general complex, implying the flow profile $\Psi(y,z)$ has the potential for instability. Typical examples $\omega = \omega(k)$ for the Charney and Eady profiles can be found in [3:7.7-7.11]; these examples mimic quite well more realistic profiles [6]. We will confine ourselves to the case where $\Psi(y,z)$ is unstable.

Generic disturbances, of course, are not composed of a single wavenumber, but rather can be thought of a Fourier superposition of a (possibly infinite) number of modes. In such a case, one expects the disturbance to develop spatially as well as temporally. The development of an initially localized disturbance (in the long time limit) can be calculated using *absolute*

stability analysis [4]. By taking the Laplace and then the Fourier transform of (1), we can state the solution for ϕ in terms of integrals, *viz*

$$\phi(x,t) = \int_{-\infty+i\gamma}^{\infty+i\gamma} d\omega \int_{-\infty}^{\infty} dk \, \frac{G(\omega,k)e^{i(kx-\omega t)}}{D[\omega,k]} \qquad (2)$$

where the y and z dependence of ϕ has been suppressed for clarity. $G(\omega,k)$ contains information about the mean flow, initial conditions, etc., but is analytic in the upper half ω plane, and γ must be larger than the largest positive imaginary part of $\omega = \omega[\text{Real}(k)]$.

The long time asymptotics of (2) are evaluated simply by making γ as small as possible, i.e. moving the contour in the Laplace integral toward the real ω axis. For a given ω, the integrand will have poles where $D[\omega,k] = 0$, i.e. at $k=k(\omega)$, where $k(\omega)$ is generally multi-valued. As γ is reduced to zero, several things may happen: First, a given $k = k(\omega)$ which started on one side of the real k axis may cross to the other, which will require the Fourier contour in the complex k plane to be deformed to avoid the singularity. If the crossing is from above, (2) will receive contribution from negative Im(k) for $x > 0$, representing spatially amplifying disturbances, with the opposite holding as well; a crossing from below leads to spatially amplifying disturbances for $x < 0$. The second thing that may happen (which requires the first as a precursor) is that two poles originating from opposite sides of the real k axis may coalesce. If this occurs, the Fourier contour in the complex k plane cannot be deformed so as to avoid the singularity, and it can be shown that the contribution from this singularity grows exponentially with time for any x. Such a system is then called "absolutely unstable." If no such coalescence occurs, the system is then called "convectively unstable." The difference between these two cases is illustrated in Figure 1.

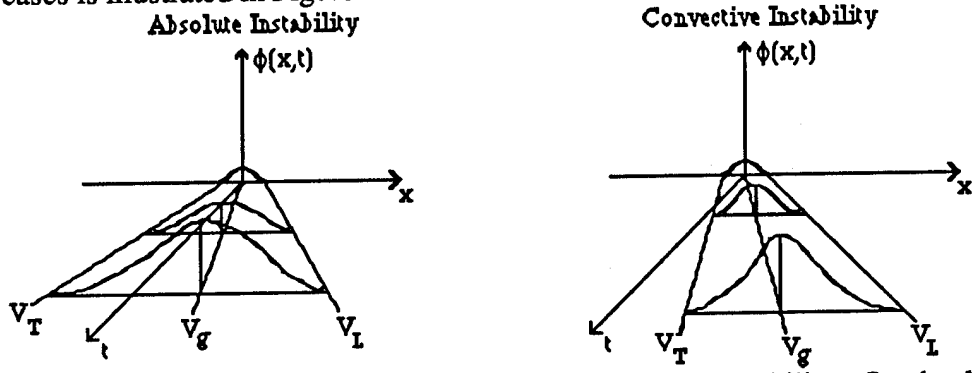

Figure 1: Difference between absolute and convective instability. In absolute instability, the initially localized disturbance radiates both up and downstream from its initial source, whereas convective instability only affects regions downstream from its initial location. V_L, V_G, and V_T represent the leading edge, group, and trailing edge velocities of the packet, respectively.

Technically, whether or not one sees an absolute instability in a given system is strongly dependent on the Galilean reference frame in which one is observing the system. However, the term "absolutely unstable" is reserved for those systems in which exponential growth is observed for all x in the resting frame. This ambiguity resulting from the freedom of choice of Galilean frame turns out to be useful, however, as the wave packet emanating from an initially localized disturbance is defined asymptotically by those Galilean frames in which exponential growth occurs; this defines a wedge-shaped region in the x-t plane confined by the leading and trailing edge velocities as in Figure 1. Within such a region, absolute stability analysis allows the calculation of all relevant quantities; wavenumber, frequency, growth rate, and modal structure, all as a function of x/t, the velocity of a given Galilean observer.

Such an analysis applied to a "typical" atmospheric midlatitude flow profile reveals the following [6]: Dimensional growth rates following the packet peak are on the order of one day,

dimensional phase velocities are about 15% the maximum flow velocity and are relatively constant throughout the wave packet, and the group velocity is about twice that of the phase speed, implying that individual crests and troughs will move toward the trailing edge of the packet. Secondly, the leading edge of the packet tends to move with a velocity about that of the mean flow, while the trailing edge velocity is nearly stationary. Also, the modal structures tend to be "deeper" (i.e. maximum modal amplitude occurs at a greater height) at the leading edge of the packet, while the waves near the leading edge also tend to be longer in wavelength than those near the trailing edge.

When one applies the results of this linear analysis to flows in the real atmosphere, an interesting picture is obtained. Flows which are baroclinically unstable in the atmosphere tend to be zonally confined (i.e. are of finite length in the x direction). Hence, one would expect that the amplification rate, which can be defined as the growth rate a function of position within the packet times the Galilean velocity characterizing that position, to give a meaningful picture of which portions of the wave packet should dominate the evolution. Applying such a criteria to the results of the absolute stability analysis for the atmospheric-like flows indicates that the short, shallow waves toward the trailing edge of the packet should dominate.

Nonlinear Results

To test whether or not this conclusion of linear theory holds in the nonlinear domain, we used a numerical model, namely the two-layer truncation of the quasigeostrophic equations (see [3:6.16] for a derivation) with a flow consisting of a narrow (~5 Rossby deformation radii in the meridional (y) direction) jet in the upper layer and no flow in the lower layer. Such numerics were necessary, as we are concerned with mean flow conditions which mimic the atmosphere (i.e. growth rate the same order of magnitude as advection time) whereas analytical approaches to the problem are only tractable in the range where the growth rate is asymptotically smaller than the advection time scale.

The results of one of these integrations is shown in Figure 2. Several things are quite obvious: First, the largest amplitude structures in the nonlinear domain are located at the leading edge of the wave packet, rather than at the trailing edge as would be indicated by linear theory. This is because the nonlinear equilibration takes place solely by homogenization of the mean-state potential vorticity gradient in the lower layer, and since the modal structures are "deeper" near the leading edge of the wave packet than near the trailing edge, the upper layer perturbation can grow much larger.

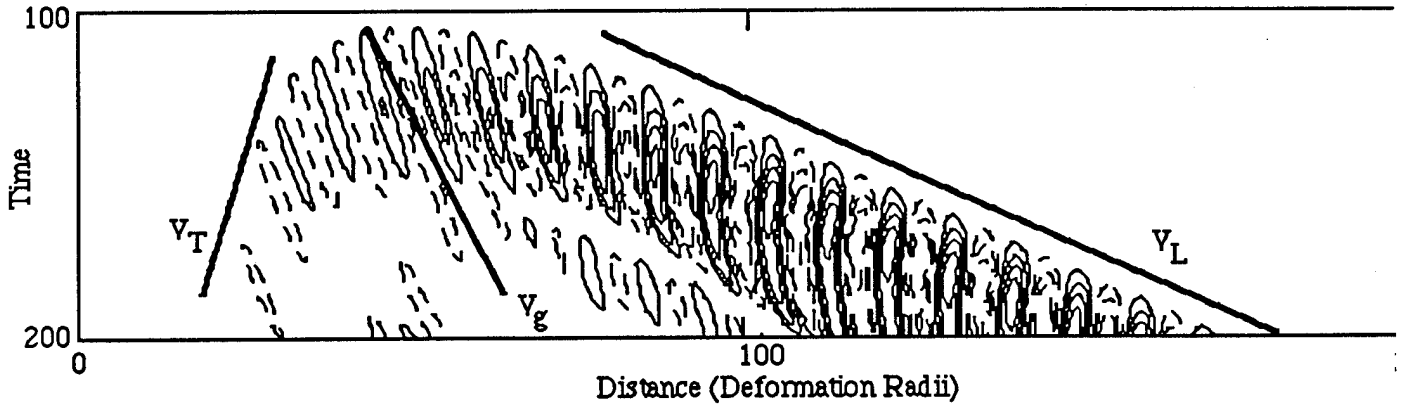

Figure 2: Time development of upper layer streamfunction of wave packet along the basic state jet symmetry axis. Contour interval is .5, with the zero contour omitted. A typical atmospheric radius of deformation is 700 km, which along with a typical flow speed of 70 m/s implies approximately 10 model time steps correspond to one day of actual time.

Secondly, there is no spreading of the packet outside its linear theory boundaries even in the strongly nonlinear stage. One can certainly imagine the scenario where nonlinear wave-wave interactions would "seed" new disturbances well upstream of the linear theory packet boundaries,

but such interactions do not take place here. Finally, there is no "global" decay stage for the disturbance; it continues forward at nearly constant amplitude as long as there is undisturbed flow to supply it with energy.

An additional consequence of the lifecycle of the wave packet is shown in Figure 3. The mean flow modification is confined for the most part to the region well *upstream* of the developing packet. Hence, the generation of a strong barotropic flow component will not act to stabilize the packet from which it was spawned. However, we would expect that its existence would tend to wipe out any absolute instabilities (if any are there) and act to suppress incipient upstream disturbances. Hence, the role of mean flow modification may be to enforce a temporal spacing between successive wave packets in the atmosphere.

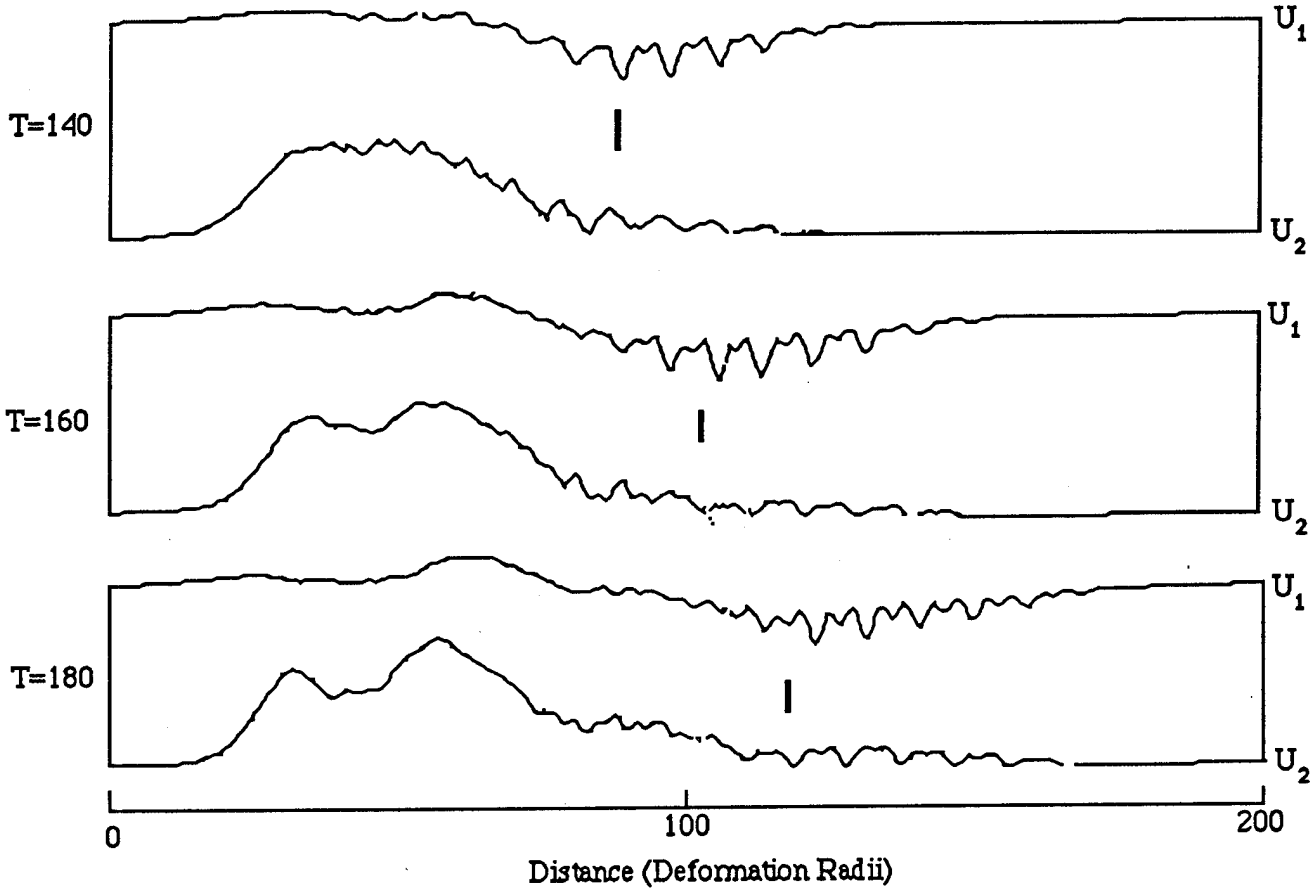

Figure 3: Alteration in mean flow along the basic state jet symmetry axis. The mean state values (shown on the right side of the graph) are $U_1 = 1$ and $U_2 = 0$. The vertical dashes for each time step represent the position of the linear theory group velocity.

References:

[Main Reference] Swanson, K. and R. T. Pierrehumbert 1993: Nonlinear wave packet evolution on baroclinically unstable jet. *Journal of the Atmospheric Sciences* , in press.

[1] Charney, J. G. 1947: The dynamics of long waves in a baroclinic westerly current. *Journal of Meteorology* **4**, 125-162.

[2] Eady, E. T. 1949: Long waves and cyclone waves. *Tellus* **1**, 33-52.

[3] Pedlosky, J. 1987: *Geophysical Fluid Dynamics* (2nd edition), Springer-Verlag, 710 pp.

[4] Briggs, R. J. 1964: Electron-stream interaction with plasmas, chap. 2, 8-46. *Research Monographs* **29**, MIT Press.

[5] Chang, E. 1993: Downstream development of baroclinic instabilities as inferred from regression analysis. *Journal of the Atmospheric Sciences*, in press.

[6]Lin, S-J. and R. T. Pierrehumbert 1993: Is the midlatitude zonal flow absolutely unstable? *Journal of the Atmospheric Sciences* **50**, 505-517.

INSTABILITY IN EXTENDED SYSTEMS

L. TAO[†] AND E. A. SPIEGEL[‡]

Abstract. The elimination of fast modes from mildly unstable systems is complicated by the problem of resonances among the stable modes. In extended systems, where the spectrum of normal modes is continuous, this is a typical difficulty. We illustrate this problem with an example.

Introduction. Bifurcation theory is reasonably well understood for finite systems whose linear theories produce discrete spectra of normal modes, even when several modes are nearly marginal for the same parameter values. One approach to this problem of multiple bifurcation is based on the ideas that Bogoliubov and collaborators have used in nonlinear dynamics and statistical physics [3]. However, when the systems studied are extended in one or more spatial directions, the eigenvalues of the linear theory become closely spaced. In the limit of infinite spatial extent, when we have to deal with continuous spectra, problems are encountered in applying the procedures for systems with discrete spectra [4].

The first difficulty that arises in the case of continuous spectra, or even for closely spaced discrete spectra, comes early in the attempt to parallel the derivation of amplitude equations for the situation with sparse spectra. When trying to eliminate the fast modes to get equations for the slow modes, we have to decide how to distinguish the two kinds of mode. A natural choice is suggested when the system is finite in one spatial dimension (coordinate z) and infinite in the transverse ones (x and y). In this configuration, commonly studied in fluid dynamics, the system has discrete mode numbers associated with z, the vertical coordinate. When there is translational invariance in x and y, the horizontal coordinates, we have a continuum of horizontal wave vectors associated with the Fourier modes for that case. Typically, instability occurs for a few vertical mode numbers and here we assume that there is only one unstable vertical mode, the gravest. This gravest mode occurs for a continuum of horizontal wave numbers, k, and there is no way to divide this continuum reliably into fast modes and slow modes. Hence the best procedure seems to be to eliminate the relatively fast higher vertical modes and keep the gravest vertical modes for all k [4,7].

The trouble that normally arises in this reduction is that resonant nonlinear interactions among stable modes are often unavoidable in the case of continuous spectra, no matter how we tune parameters [4]. Moreover, in the present state of understanding, it is not clear whether these effects represent physics or come from the methods. Here we shall describe the problem in terms of a model system.

A Model Problem. Consider a pair of equations for two functions $f(x,t)$ and $g(x,t)$, bounded for all x. These are stand-ins for the vertical modes of convection theory, mentioned in the introduction. The model equations are

$$\partial_t f = \sigma f - (\partial_x^2 - k_1^2)^2 f - fg. \tag{1}$$

$$\partial_t g = \gamma g - (\partial_x^2 - k_2^2)^2 g + f^2. \tag{2}$$

Here σ and γ are constants with $\gamma < 0$ and $|\sigma| << |\gamma|$.

The linear theory of these equations has two solutions for the eigenvector $(f,g)^T$; these are of the form $(A,B)^T exp(st - ikx)$, where the wave number k is arbitrary in the case of infinite spatial domain. The two solutions are $(1,0)^T$ with $s = \sigma - (k^2 - k_1)^2$ and $(0,1)^T$ with $s = \gamma - (k^2 - k_2)^2$, where k_1 and k_2 are constants and k_1 is the critical wavenumber.

† Physics Department, University of Chicago, Chicago IL 60637

‡ Astronomy Department, Columbia University, New York, NY 10027

The mode $(0,1)^T$ is never critical and always suffers finite damping under the conditions prescribed. Thus g is becomes a slave of f, which controls it through the nonlinear terms.

Since (2) is linear, we could write down a formal solution with $g = \mathcal{G}[f]$. Then we would substitute that functional into (1) to obtain an integrodifferential equation for f of the type studied in pattern dynamics [7]. This is a prototypical case of the problem we are talking about and we want to use a generalizable method on it.

In the discrete case, which we get from this problem by making the spatial domain finite, there are (at least) two straightforward procedures that work nicely and give Landau's amplitude equation. We can simply assume that $|g|$ is small everywhere and solve by successive approximations for $\mathcal{G}[f]$. Or we can use normal form theory to transform (1)-(2) into the desired form. In each case, there is trouble when $2\sigma = \gamma$. This is not a real difficulty since we are usually interested in $\sigma > 0$ and $\gamma < 0$, , but it does foreshadow the problems that arise when these methods are applied to the continuous case ([2] and [4], respectively). Let us see what happens in the continuous case when we apply (for instance) the second procedure.

The Functional Center Manifold. For any suitable function $h(x,t)$ we write

$$h(x,t) = \int_{-\infty}^{\infty} \hat{h}_k(t)\, e^{ikx} dk. \tag{3}$$

With this notation, the Fourier transforms of (1) and (2) are

$$\partial_t \hat{f}_k(t) = \sigma_k \hat{f}_k(t) + \int_{-\infty}^{\infty} \hat{g}_q(t)\hat{f}_{k-q}(t)dq, \tag{4}$$

and

$$\partial_t \hat{g}_k(t) = \gamma_k \hat{g}_k(t) + \int_{-\infty}^{\infty} \hat{f}_q(t)\hat{f}_{k-q}(t)dq, \tag{5}$$

where $\sigma_k = \sigma - (k^2 + k_1^2)^2$ and $\gamma_k = \gamma - (k^2 + k_2^2)^2$.

The dynamics of this system takes place in a phase space with coordinates $\hat{f}_k(t)$ and $\hat{g}_k(t)$ $(-\infty < k < \infty)$. If $\hat{f}_k(t)$ were zero, $\hat{g}_k(t)$ would decay away and so we expect $\hat{f}_k(t)$ to be larger than $\hat{g}_k(t)$ in magnitude for most k, and will formulate expansions accordingly. Moreover, this picture leads us to look for dynamics approximately confined to a subspace with only one important coordinate at each k, at any rate near the origin of phase space, where the system will linger for the mildly unstable case, $\sigma \approx 0$.

Given these expectations, we look for new phase space coordinates, $\hat{F}_k(t)$ and $\hat{G}_k(t)$, related to old the coordinates by a functional power series with the idea that $\hat{F}_k(t)$ is the coordinate in the invariant subspace and $\hat{G}_k(t)$ is transverse to it. That is, we introduce the coordinate transformation

$$\hat{f}_k(t) = \hat{F}_k(t) + \int_{-\infty}^{\infty}\int_{-\infty}^{\infty} \mathcal{I}_k(p,q)\hat{F}_p(t)\, \hat{F}_q(t)\, dpdq + \dots\,, \tag{6}$$

$$\hat{g}_k(t) = \hat{G}_k(t) + \int_{-\infty}^{\infty}\int_{-\infty}^{\infty} \mathcal{J}_k(p,q)\hat{F}_p(t)\, \hat{F}_q(t)\, dpdq + \dots\,. \tag{7}$$

This near-identity transformation preserves the structure of the linear problem. We want it also to turn (4) and (5) into this standard form:

$$\partial_t \hat{F}_k(t) = \sigma_k \hat{F}_k(t) + \int_{-\infty}^{\infty}\int_{-\infty}^{\infty} \Phi_k(p,q)\hat{F}_p(t)\hat{F}_q(t)dq + \dots \tag{8}$$

and

$$\partial_t \hat{G}_k(t) = \left(\gamma_k + \int_{-\infty}^{\infty} \Psi_k(p)\, \hat{F}_p(t)\, dp + \dots\right) \hat{G}_k(t) + \dots \,. \tag{9}$$

Even though (8), the desired equation for $\hat{F}_k$ alone, is generally the main aim, for now we want to know whether we can get an equation like (9). For this equation says that, to leading order, once $\hat{G}_k(t) = 0$, it remains so. The dots in the parentheses of (9) represent higher terms in $\hat{F}_k$ that complete the renormalization of γ_k. More important are the dots at the end which must represent terms that vanish to reasonably high order for $\hat{G}_k(t) = 0$. For now, we are content to develop the results in the leading order of this formal procedure to see whether a transformation of the form of (6)-(7) can produce (9) and give the desired form to the dynamics.

We substitute the transformations into the equations for $\hat{f}_k(t)$ and $\hat{g}_k(t)$ and use (9). Then we equate like orders in the functional power series. The first significant result comes at order two:

$$\int_{-\infty}^{\infty}\int_{-\infty}^{\infty} [\mathcal{D}_k(p,q)\, \mathcal{J}_k(p,q) - \delta(p+q-k)]\, \hat{F}_p \hat{F}_q\, dpdq = 0 \tag{10}$$

where

$$\mathcal{D}_k(p,q) = \sigma_p + \sigma_q - \gamma_k. \tag{11}$$

When we solve this for $\mathcal{J}_k(p,q)$, we find that it must contain the delta function and so we are interested in the condition $p+q-k=0$. Even with this restriction, there are many wave number triplets for which $\mathcal{D}_k(p,q) = 0$. As in plasma physics, where a similar problem arises [6] we write the formal solution as

$$\mathcal{J}_k(p,q) = \left(\mathcal{P}\frac{1}{\mathcal{D}_k(p,q)} - \lambda\delta(\mathcal{D}_k(p,q))\right)\delta(p+q-k), \tag{12}$$

where λ is a constant (or set of constants should $\mathcal{D}$ have many zeros) and $\mathcal{P}$ means principal value. Now we put this into (7) and obtain

$$\hat{g}_k = \hat{G}_k - \mathcal{P}\int_{-\infty}^{\infty} \frac{1}{\mathcal{D}_k(p,k-p)} \hat{F}_p \hat{F}_{k-p}\, dp$$

$$+ \sum_{\{p_0\}} \lambda_{p_0} \int_{-\infty}^{\infty} \frac{1}{D'_k(p,k-p)} \hat{F}_p \hat{F}_{k-p}\, \delta(p-p_0)\, dp \; + \dots, \tag{13}$$

where $\{p_0\}$ is the set of all zeros of $\mathcal{D}_k(p,k-p)$ for given k and $D'_k(p,k-p)$ is the derivative of $\mathcal{D}_k(p,k-p)$ with respect to p. On referring to equation (11) we see that

$$\mathcal{D}'_k(p,k-p) = -4(p^2 - k_1^2)p - 4((k-p)^2 - k_1^2)(k-p). \tag{14}$$

Now $\hat{G}_k = 0$ is the invariant manifold in which the dynamics is played out, after the transients decay away and, once the system is in it, the dynamics is simplified. To leading order, this "functional center manifold" is given by

$$\hat{g}_k = \int_{-\infty}^{\infty} \frac{1}{\mathcal{D}_k(p,k-p)} \hat{f}_p \hat{f}_{k-p}\, dp + \sum_{\{p_0\}} \frac{\lambda_{p_0}}{\mathcal{D}'_k(p_0,k-p_0)} \hat{f}_{p_0} \hat{f}_{k-p_0} \; + \dots, \tag{15}$$

where p_0 is a function of k. The problem that is as yet unsolved is the determination of the λ_{p_0}. In previous work on this subject, they have been implicitly set to zero. The way this has been done has been to assume either implicitly or explicitly [4] that f_k vanishes outside narrow intervals containing $k = \pm k_1$.

A singular expression like that for $\mathcal{J}_k(p,q)$ arises in plasma physics and it had been avoided in the past by the assumption of compact support of the one-particle distribution function, f_0 that arises there. But this approach was questioned by van Kampen [6] who remarked that "the assumption of a rigorously cut off f_0 is rather artificial, and it is unsatisfactory that the calculation should fail for an f_0 that decreases rapidly without actually vanishing." This view is appropriate here. However, van Kampen also pointed out that [6]: "Vlasov decreed that the Cauchy principal value has to be taken without trying to justify this choice. The present article will show that this choice was indeed correct." Van Kampen [6] (see also [1]) determined λ by a normalization condition which we do not see how to use here. We shall instead describe what happens when we abide by the Vlasov decree and set $\lambda_k(p,q) = 0$. However, there is probably more to be said on this matter [8] and we hope to return to it at another time.

The Evolution Equation. If we do set the $\lambda_{p_0} = 0$, then we omit the second term in (15). Moreover, we can approximate the finite P.V. integral, by noting that f_k is peaked around $\pm k_1$, even though it does not have compact support. Then, since σ_{k_1} is close to zero, (15) is well approximated by

$$\hat{g}_k = \frac{1}{\gamma_k} \int_{-\infty}^{\infty} \hat{f}_p \hat{f}_{k-p} dp + \dots \,. \tag{16}$$

When we introduce this into (4), we get, to leading order,

$$\partial_t \hat{f}_k = \sigma_k \hat{f}_k - \int_{-\infty}^{\infty} \int_{-\infty}^{\infty} \frac{1}{\gamma_q} \hat{f}_{k-q} \hat{f}_p \hat{f}_{q-p} \, dpdq. \tag{17}$$

If we continue to assume that $\hat{f}_k$ is sharply peaked at k_1, we consider this equation only near this critical circle. When $k \approx k_1$ in the integral, we must have $q \approx 0$ and we may approximate γ_q by $\gamma_0 = \gamma - k_2^4 =: 1/\alpha$. Then, when we take the Fourier transform of (13), we get

$$\partial_t f = \sigma f - (\partial_x^2 - k_1^2)^2 f - \alpha f^3 \,, \tag{18}$$

This is the Swift-Hohenberg model familiar in convection theory [9].

In the next section we shall give some numerical solutions for the full model equations and for the Swift-Hohenberg model and see that the qualitative agreement is satisfactory.

Numerical Experiments. We compare the periodic solutions of equations (1) and (2) (the full model system) to those of equation (18) (the Swift-Hohenberg model). Using a pseudospectral code, we calculate the exponential damping in time from the linear terms exactly for each Fourier mode and we compute the nonlinear terms in real space. The timestepping scheme is explicit second-order Adams-Bashforth. The advantage of such a spectral code over conventional finite difference methods is the ease of comparison to the ordinary differential equations we obtained analytically. To test our code, we chose parameters for which the ordinary differential equations for each Fourier mode obtained by normal theory give us a system of predator-prey equations. In this test case, we indeed observe that the numerical solutions follow the classical predator-prey models.

In figures 1-8 and 9-16 we show results from two calculations. In all figures, the solid line are the numerical solution of the full model system and the dotted lines the solutions of the Swift-Hohenberg model. Initially we start with finite amplitudes in the first 40

Fourier modes (our parameter values were $\sigma = 0.0005$, $\gamma = 1.023$, $k_1 = 16$ and $k_2 = 32$ and were chosen so that $f_{k=0}$, $f_{k=32}$ and $g_{k=32}$ form a resonating triad). The initial values of each Fourier mode were random with some weighting so that the f_k's near $k_1 = 16$ have higher amplitude than the rest. We contrast the transient dynamics of the Swift-Hohenberg model with its asymptotic behavior and show the space dependence of the f-mode at times $t = 0, 10, 20, 30$ and at $t = 50, 100, 150, 200$. As we see from Figures 5-8 and 13-16 the approximate Swift-Hohenberg system asymptotically approaches the correct nonlinear state selected out by the full dynamics. Even though the Swift-Hohenberg model gets the transients wrong, eventually the system locks into the correct asymptotic state with the same decay rate as the solutions of the full model system. The approximate dynamics of the Swift-Hohenberg model mimics that of the full model system which is what we expect of the correct center manifold description. A variety of other parameter values were tried and we have not been able to detect the complicated time dependence shown in the analogous discrete spectrum ode model of Cessi, Spiegel and Young [2]. Our numerical results so far justify our choice in setting the λ_{p_0}'s equal to zero.

Conclusions. Our goal in this note was to understand the effects of stable resonant modes in spatially extended systems. The Vlasov decree from plasma physics of taking the P.V. to deal with resonant denominators produces noncatastrophic results and leads to the usual Swift-Hohenberg model. The numerical results from this approximation are in good agreement with those from the full model system. Formally, the possibility of analogues to the van Kampen modes remains open. However, lacking proper normalization conditions, we have not yet seen how to include the resonant contribution to the determination of the functional center manifold. We hope that further work will shed light on this matter.

This work was supported by the U.S. Air Force under contract number F49620-92-J-0061 to Columbia University.

References.

[1] K.M Case, *Plasma Oscillations*, Ann. Phys. **7** (1981) 349-364.

[2] P. Cessi, E.A. Spiegel and W.R. Young *Small-Scale Excitations in Large Systems*, in *Nonlinear Evolution of Spatio-Temporal Structures in Dissipative Continuous Systems*, F.H. Busse and L. Kramer, eds. (Plenum Press, 1990) pp. 231-236.

[3] P.H. Coullet and E.A. Spiegel , *Amplitude Equations for Systems With Competing Instabilities*, SIAM J. Appl. Math **43** (1983) pp. 774-821.

[4] P.H. Coullet and E.A. Spiegel , *Evolution equations for extended systems*, in *Energy Stability and Convection*, G.P. Galdi & B. Straughan, eds., *Pitman Research Notes in Math.*, **168**, (Longman Sci. and Tech., 1988) pp. 22-43.

[5] M.C. Cross *Derivation of the amplitude equation at the Rayleigh-Bénard instability*, Phys. Fluids **23** (1980) pp. 1727-1731.

[6] N.G. Van Kampen *On The Theory Of Stationary Waves in Plasmas*, *Physica* **XXI** (1955) pp. 949-963.

[7] P. Manneville, *Dissipative Structures and Weak Turbulence*, (Academic, New York, 1990).

[8] P.J. Morrison and D. Pfirsch, *Dielectric energy versus plasma energy, and Hamiltonian action-angle variables for the Vlasov equation*, Phys. Fluis B **4** (1992) pp. 3038-3057.

[9] J. Swift and P.C. Hohenberg, *Hydrodynamic fluctuations at the convective instability*, Phys. Rev. A **15** (1977) pp. 319-328.

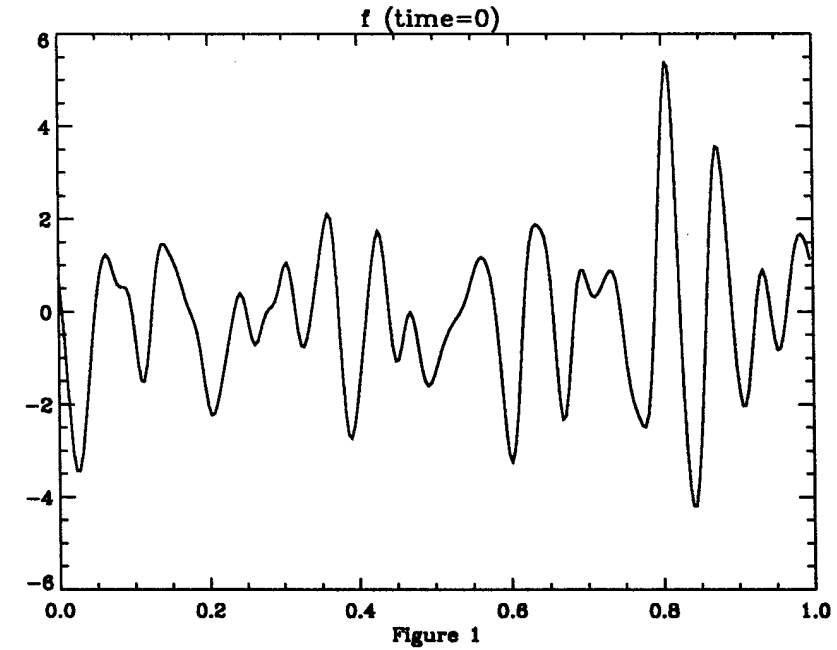

Figure 1

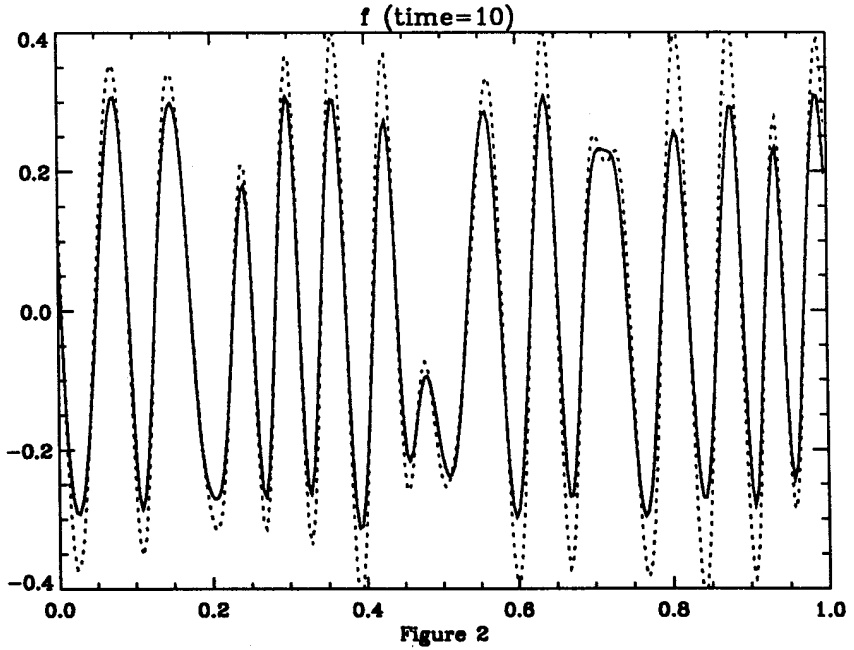

Figure 2

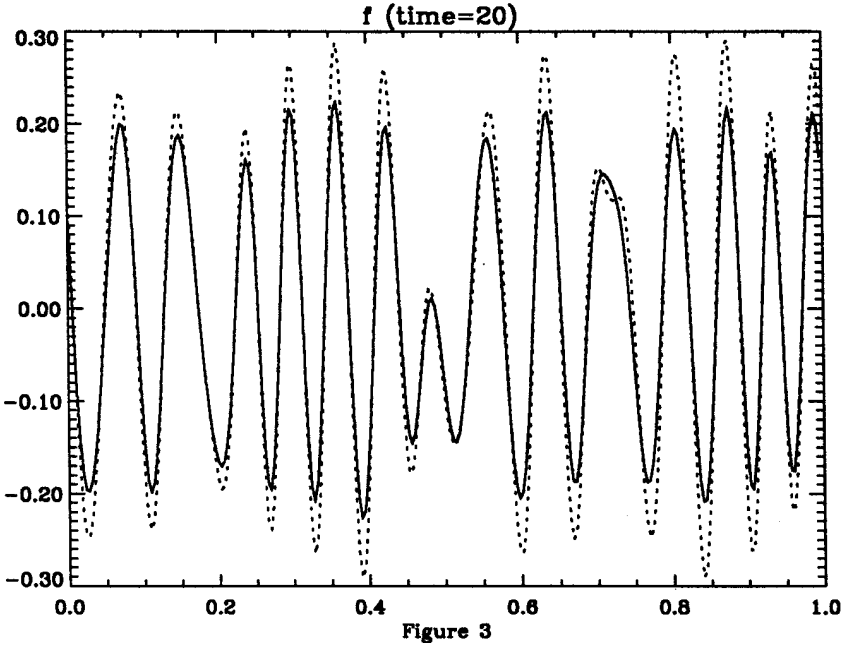

Figure 3

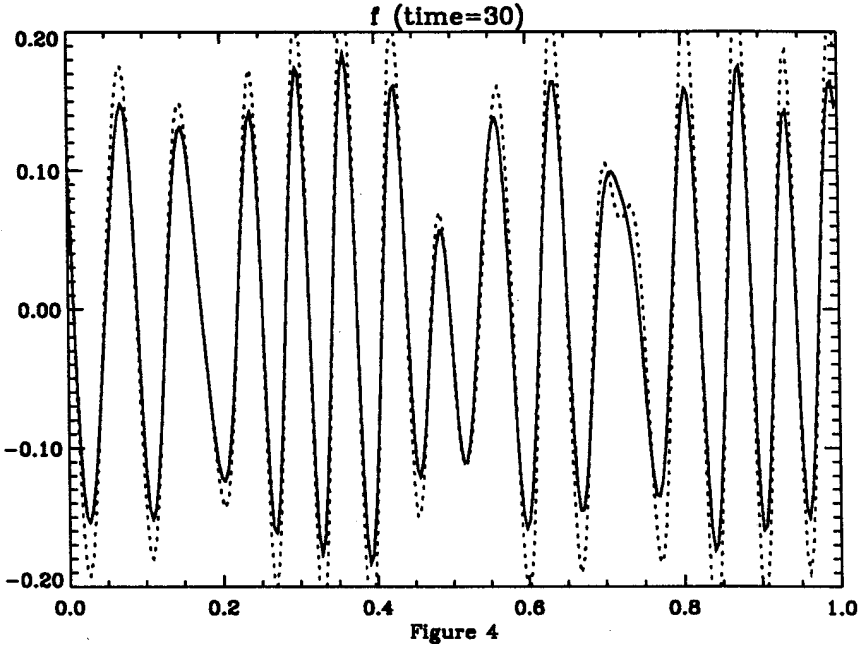

Figure 4

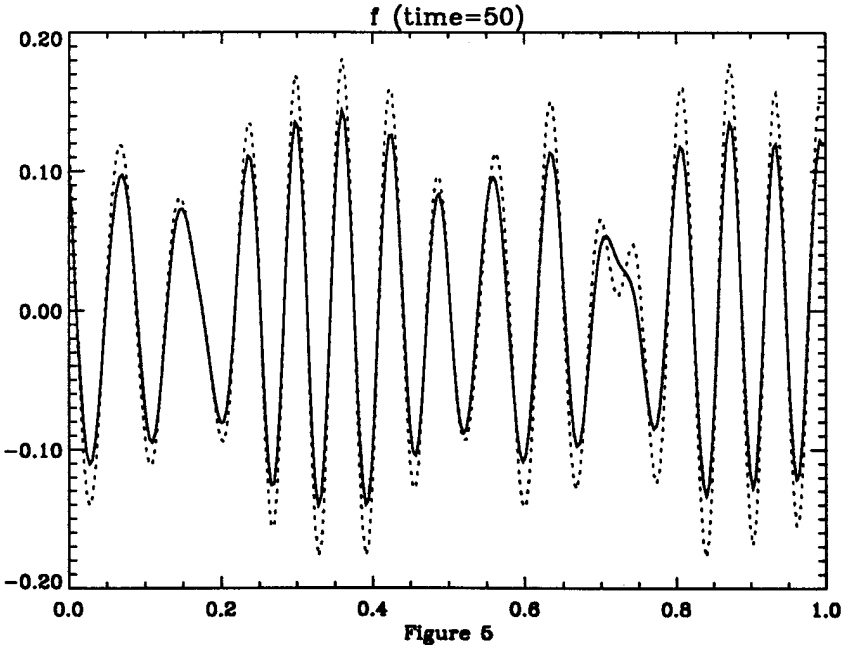

Figure 5

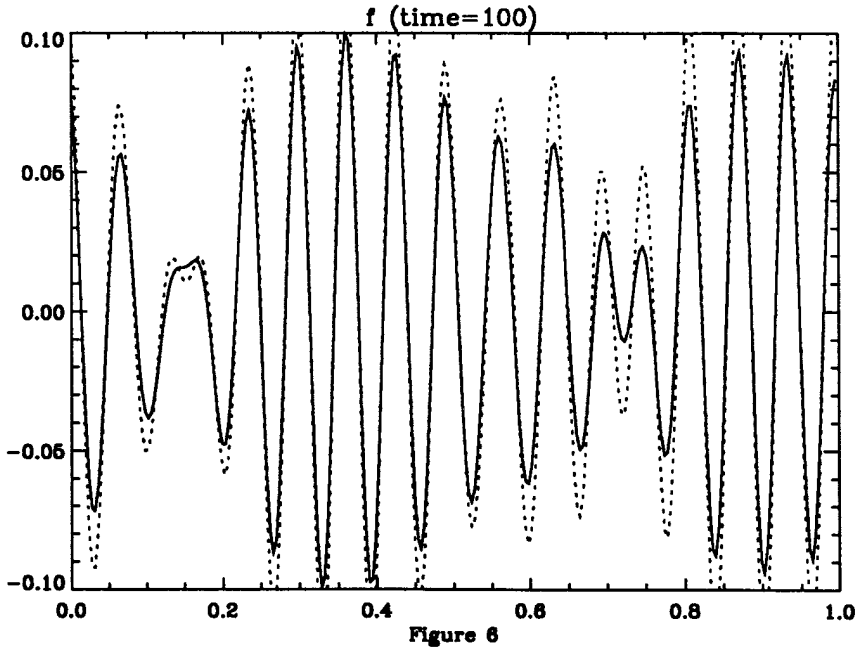

Figure 6

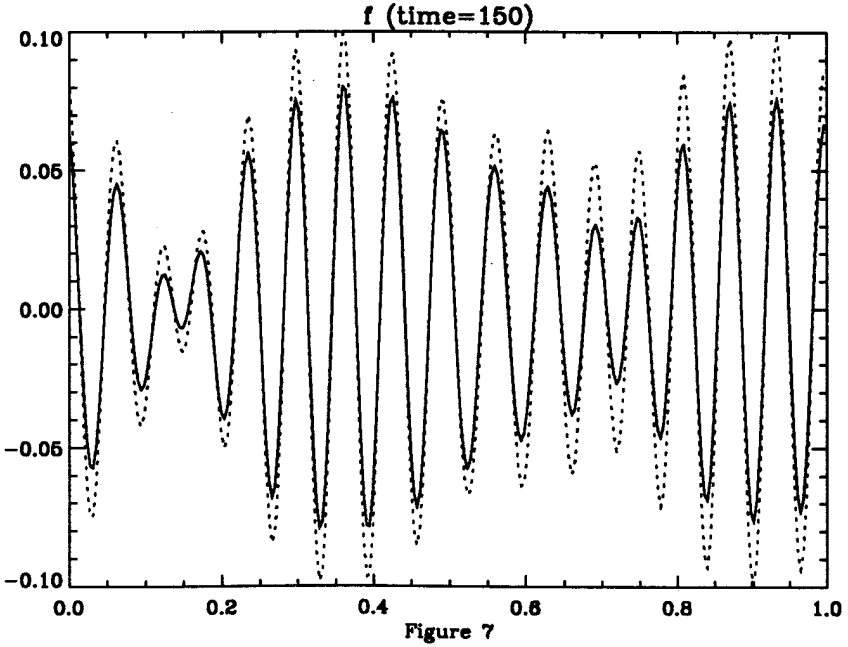

Figure 7

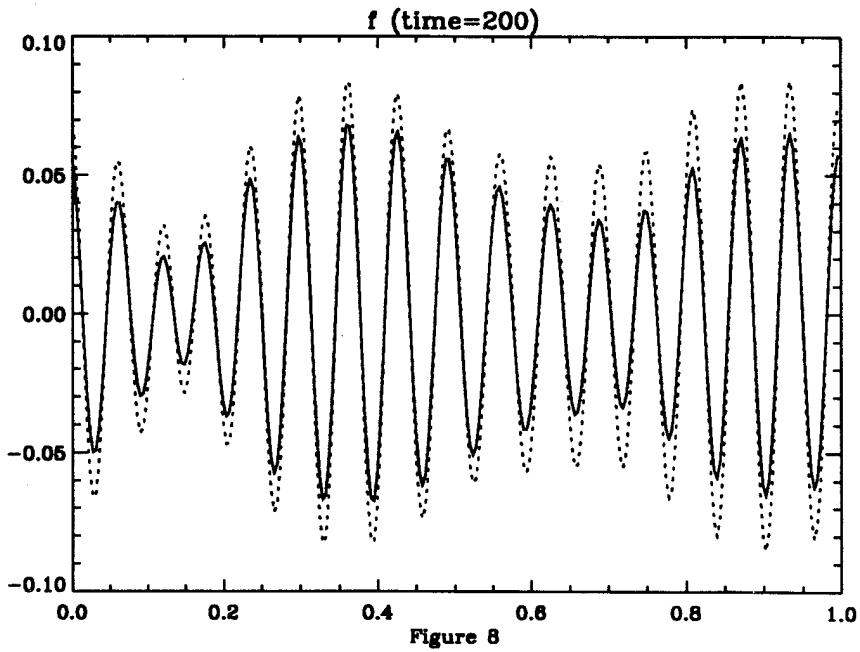

Figure 8

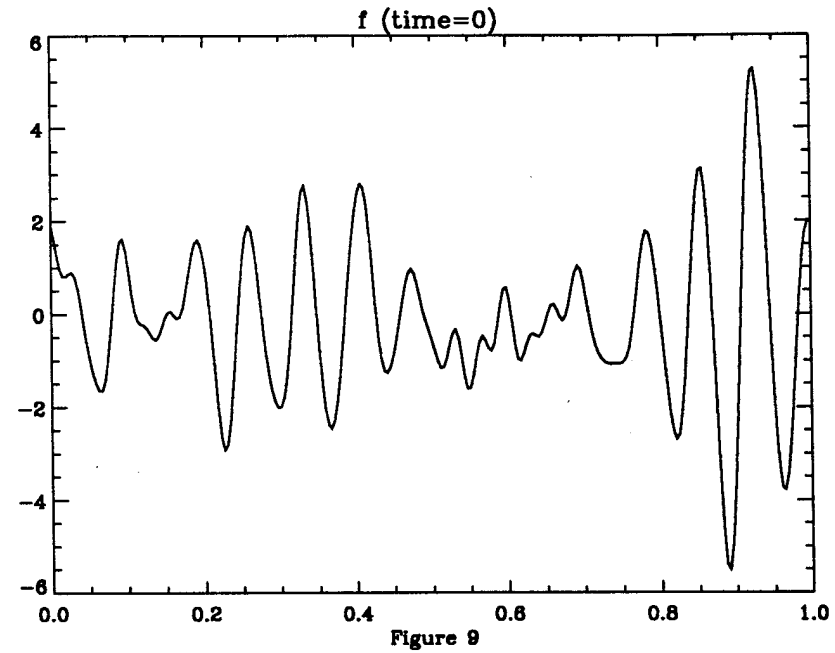

Figure 9

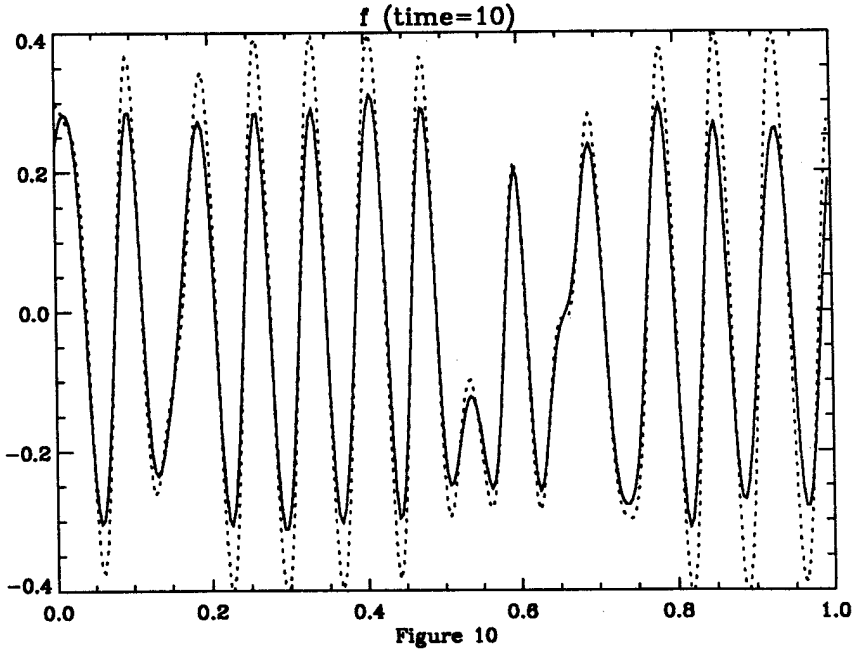

Figure 10

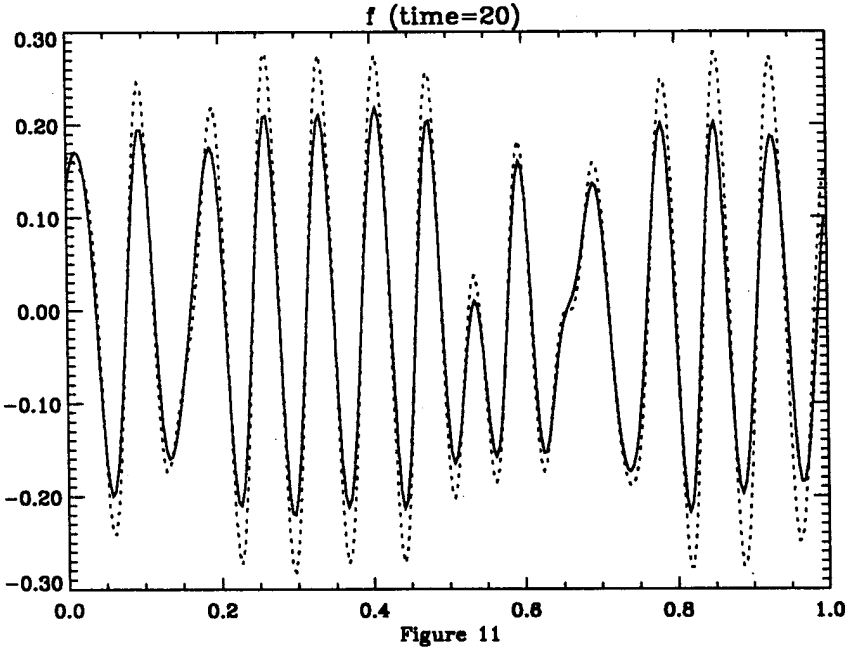

Figure 11

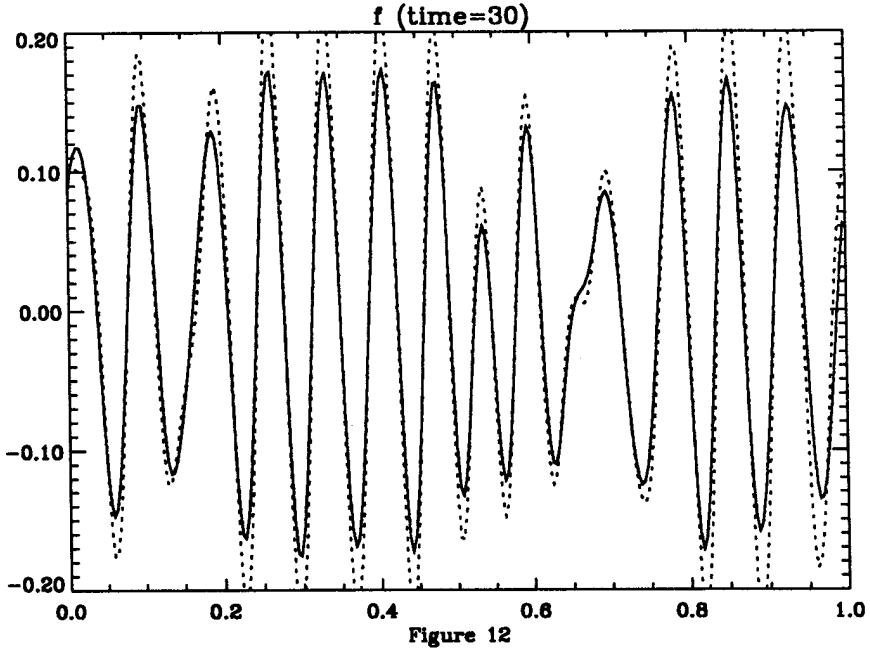

Figure 12

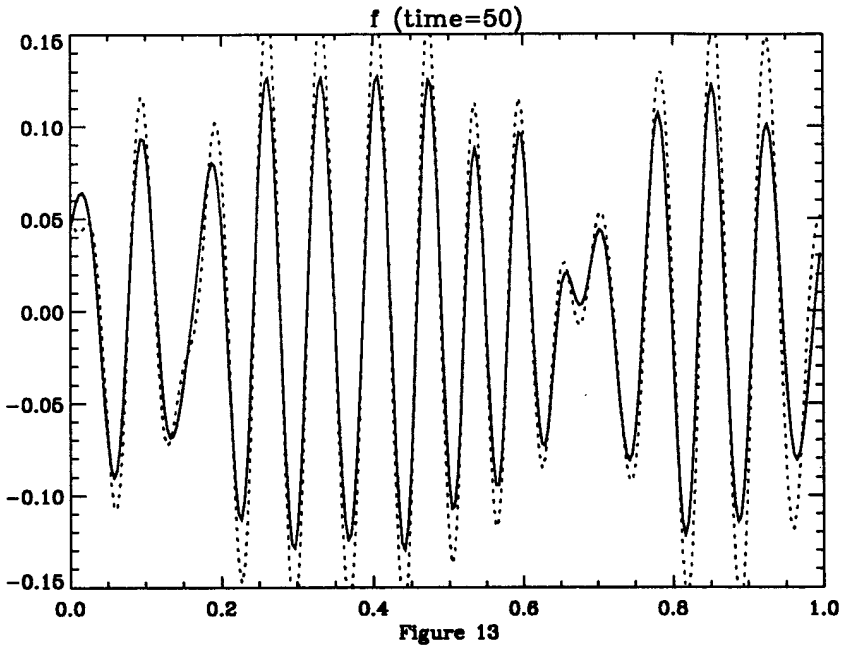

Figure 13

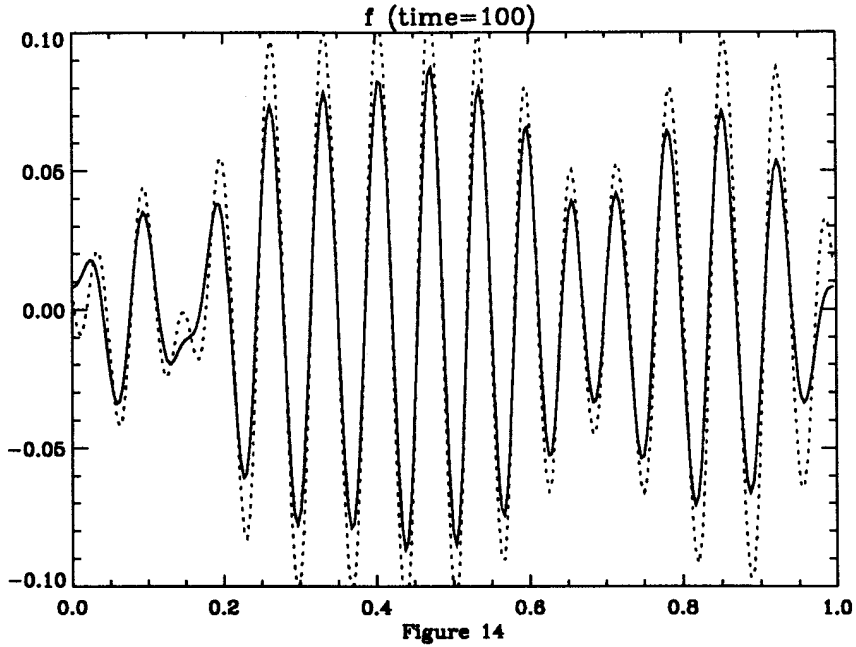

Figure 14

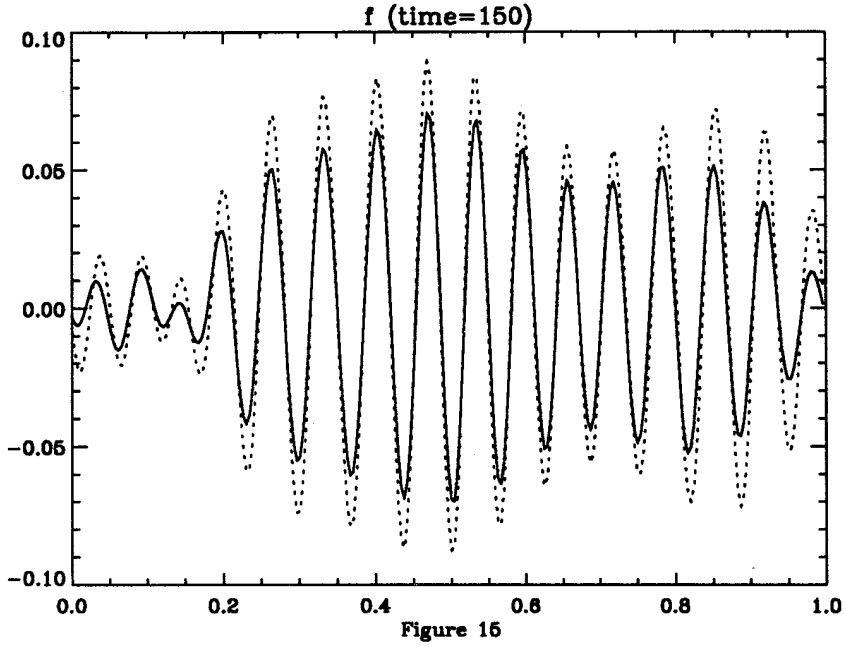

Figure 15

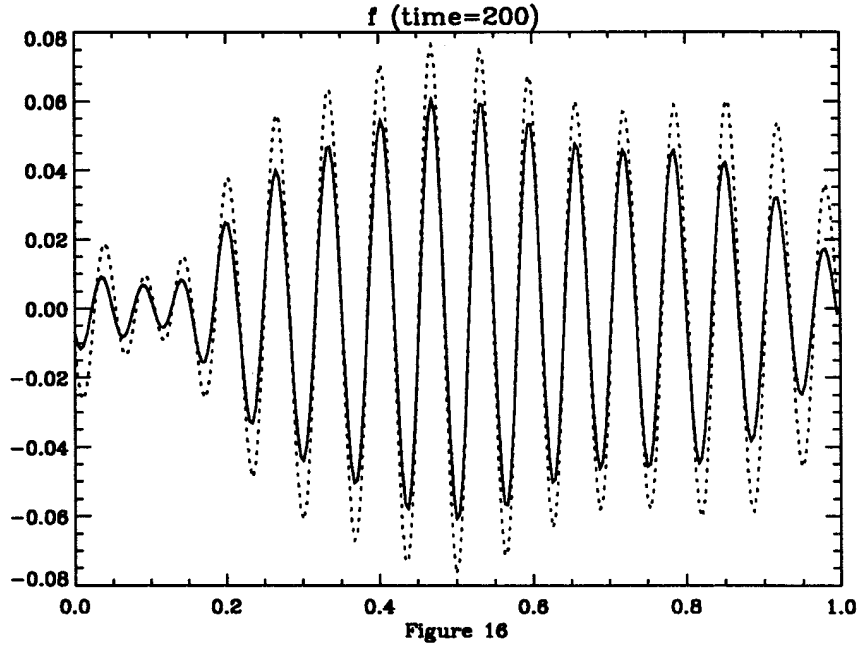

Figure 16

The fluid dynamics of crystal slurries

Andrew W. Woods and Richard A. Jarvis

In this presentation, a model of the nucleation, growth and sedimentation of crystals in a vigorously convecting and cooling binary melt was described. The model is based upon the conservation of heat and mass in the melt, and explicitly accounts for the crystal size distribution and its evolution with time. The model can be used to predict the rate of accumulation of crystals on the floor of the chamber housing the melt, and also the variation of the mean crystal size with height in the deposit. The model was compared with some simple laboratory experiments in which a melt of aqueous ammonium chloride was cooled from an overlying layer of light oil. As the melt was cooled, crystals which nucleated near the upper cold boundary sank from into the main body of melt and eventually accumulated in a pile on the floor of the chamber.

The model is based upon the conservation of heat in the chamber

$$(H-h)\rho c_p \frac{\partial T}{\partial t} = -F + \rho L (H-h) R_p$$

where $H-h$ is the depth of the melt, h is the depth of the crystal pile, T is the melt temperature and F is the convective heat flux extracted from the upper boundary of the melt. Also, R_p is the rate of production of the crystals, and L the latent heat of crystallisation. The rate of accumulation of the crystals on the base of the chamber is

$$\frac{dh}{dt} = (H-h) R_p$$

where we assume the crystals are close packed on the base of the chamber.

The crystal size distribution $\phi(a,t)$ is governed by the equation

$$\frac{\partial \phi}{\partial t} + \frac{\partial V \phi}{\partial a} = -\lambda a^2 \phi$$

where V is the growth rate of the crystals, a is the crystal size and t is the time. In the limit in which the residence time of the crystals is much smaller than the cooling time of the magma, the solution of this equation has the simple form

$$\phi(a,t) = \frac{N(t)}{V(t)} \exp\left(-\frac{\lambda(t) a^3}{3V(t)}\right)$$

and this may be used to develop expressions for the crystal fraction in suspension and the production rate of the crystals in terms of the crystal nucleation and growth laws. In the model, the crystal nucleation was assumed to occur in the upper cooled boundary layer. The growth laws were specified by simple functional forms, incorporating the constraint that there be a finite undercooling before nucleation occurs.

The coupled model of the cooling together with the nucleation, growth and settling of the crystals was solved to examine the different controls upon the process. The dimensionless form of the equations describing the conservation of heat and solute and the thickness of the cumulate pile are

$$(1-d)\dot{\theta} = -f + AS(1-d)r_p$$

$$\dot{\theta}_L = -A(1-k_D)(\theta_\alpha - \theta_L)r_p$$

$$\dot{d} = A(1-d)r_p$$

Here, the parameter A which is of order 10^4, denotes the ratio of the cooling time of the magma to the crystal nucleation, growth and settling time. Two cases were examined to elucidate the controls upon the cooling. In the first, the upper boundary of the melt was lowered to a fixed value below the saturation temperature of the melt. It was found that during the initial stages of the cooling, crystals could readily nucleate in the upper boundary. Therefore, in order that the melt continues to cool, the growth of the crystals and hence the latent heat release, was suppressed by maintaining the melt close to saturation conditions - this is termed the growth limited regime. However, as the melt cooled so that the melt in the upper boundary approached the critical undercooling for nucleation, the nucleation rate decreased. Subsequently, the melt became supercooled since the limited supply of crystals suppressed the production of latent heat as these crystals grew in the melt. This is termed the nucleation limited regime.

In the second case examined, the material overlying the turbulently convecting melt was assumed to be of a lower fusion temperature than the initial temperature of the melt. As a result, the upper layer melted while the lower layer cooled and crystallised. The upper layer was taken to be less dense than the lower layer, so that it remained separate from the initial melt. We found that if the upper layer is sufficiently viscous, then the initial temperature of the interface between the two layers is very close to the initial temperature of the lower layer and no nucleation occurs. Only after some time, when the upper layer has cooled sufficiently, was the critical undercooling for nucleation attained. Beyond this time, the system remained in the nucleation limited regime described above. In contrast, when the overlying melt was not sufficiently viscous, the system evolved from the growth limited to the nucleation limited regimes.

We then described a series of laboratory experiments in which crystal piles were grown by cooling a binary melt from above, with a thin layer of overlying oil to prevent attachment of the crystals to the cold upper boundary. It was shown that within experimental error, the experiments were well modelled with the above theory of cooling and crystallisation, subject to the modification that the solid fraction in the crystal pile had a fixed value of 0.1-0.3 rather than unity.

One important prediction of the model concerns the variation of the crystal size with depth in the crystal pile. During the growth limited regime the model predicts that the crystal size steadily decreases with height in the deposit. This is a result of the decrease in the residence time of the crystals in suspension as the depth of the melt layer decreases. However, this crystal size grading is relatively weak compared to that associated with the nucleation limited regime. In that case, the mean grain size increases steadily with height as a result of the increasing viscosity and hence increasing residence time of the crystals as

the melt cools. The increase of grain size with height in the main portion of the intrusion is broadly consistent with geological observations from the Stillwater complex in Montana and the Palisades Sill in New York.

A Laboratory Model of Cooling over the Continental Shelf
J. A. Whitehead, Woods Hole Oceanographic Institution

A laboratory experiment is conducted where hot water is cooled by exposure to air in a cylindrical rotating tank with a flat shallow outer "continental shelf" region next to a sloping "continental slope" bottom and a flat "deep ocean" center. It is taken to be a model of wintertime cooling over a continental shelf. The flow on the shelf consists of cellular convection cells descending from the top cooled surface into a region with very complicated baroclinic eddies. Extremely pronounced fronts are found at the shelf break and over the slope. Associated with these are sizable geostrophic currents along the shelf and over shelf break contours. Eddies are particularly energetic there. Cooling rate of the hot water is determined and compared with temperature difference between "continental shelf" and "deep ocean". The results are compared with scaling arguments to produce an empirical best fit formula that agrees with the experiment over a wide range of experimental parameters. A relatively straight trend of the data causes a good collapse to a regression line for all experiments. These experiments have the same range of governing dimensionless numbers as actual ocean continental shelves in some Arctic regions. Therefore this formula can be used to estimate how much temperature decrease between shelf and offshore will be produced by a given cooling rate by wintertime cooling over continental shelves. The formula is also generalized to include brine rejection by ice formation. It is found that for a given ocean cooling rate, shelf water will be made denser by brine rejection than by thermal contraction. Estimates of water density increase implied by these formulas are useful to determine optimum conditions for deep water formation in polar regions. For instance, shelves longer than the length scale $0.09\ f\ W^{5/3}/B^{1/3}$ (where f is the Coriolis parameter, W is shelf width and B is buoyancy flux) will produce denser water than shorter shelves. In all cases, effects of Earth rotation are very important, and the water will be much denser than if the fluid was not rotating.

DOCUMENT LIBRARY

Distribution List for Technical Report Exchange – May 5, 1994

University of California, San Diego
SIO Library 0175C (TRC)
9500 Gilman Drive
La Jolla, CA 92093-0175

Hancock Library of Biology & Oceanography
Alan Hancock Laboratory
University of Southern California
University Park
Los Angeles, CA 90089-0371

Gifts & Exchanges
Library
Bedford Institute of Oceanography
P.O. Box 1006
Dartmouth, NS, B2Y 4A2, CANADA

Commander
International Ice Patrol
1082 Shennecossett Road
Groton, CT 06340-6095

NOAA/EDIS Miami Library Center
4301 Rickenbacker Causeway
Miami, FL 33149

Library
Skidaway Institute of Oceanography
10 Ocean Science Circle
Savannah, GA 31411

Institute of Geophysics
University of Hawaii
Library Room 252
2525 Correa Road
Honolulu, HI 96822

Marine Resources Information Center
Building E38-320
MIT
Cambridge, MA 02139

Library
Lamont-Doherty Geological Observatory
Columbia University
Palisades, NY 10964

Library
Serials Department
Oregon State University
Corvallis, OR 97331

Pell Marine Science Library
University of Rhode Island
Narragansett Bay Campus
Narragansett, RI 02882

Working Collection
Texas A&M University
Dept. of Oceanography
College Station, TX 77843

Fisheries-Oceanography Library
151 Oceanography Teaching Bldg.
University of Washington
Seattle, WA 98195

Library
R.S.M.A.S.
University of Miami
4600 Rickenbacker Causeway
Miami, FL 33149

Maury Oceanographic Library
Naval Oceanographic Office
Building 1003 South
1002 Balch Blvd.
Stennis Space Center, MS 39522-5001

Library
Institute of Ocean Sciences
P.O. Box 6000
Sidney, B.C. V8L 4B2
CANADA

Library
Institute of Oceanographic Sciences
Deacon Laboratory
Wormley, Godalming
Surrey GU8 5UB
UNITED KINGDOM

The Librarian
CSIRO Marine Laboratories
G.P.O. Box 1538
Hobart, Tasmania
AUSTRALIA 7001

Library
Proudman Oceanographic Laboratory
Bidston Observatory
Birkenhead
Merseyside L43 7 RA
UNITED KINGDOM

IFREMER
Centre de Brest
Service Documentation - Publications
BP 70 29280 PLOUZANE
FRANCE

50272-101

REPORT DOCUMENTATION PAGE	1. REPORT NO. WHOI-94-12	2.	3. Recipient's Accession No.

4. Title and Subtitle
"Geometrical Methods In Fluid Dynamics"
1993 Summer Study Program in Geophysical Fluid Dynamics

5. Report Date
Summer 1993

6.

7. Author(s)
Rick Salmon, Director and Barbara Ewing-Deremer, Staff Assistant

8. Performing Organization Rept. No.
WHOI-94-12

9. Performing Organization Name and Address

Woods Hole Oceanographic Institution
Woods Hole, Massachusetts 02543

10. Project/Task/Work Unit No.

11. Contract(C) or Grant(G) No.
(C) OCE-8901012
(G)

12. Sponsoring Organization Name and Address

National Science Foundation

13. Type of Report & Period Covered
Technical Report

14.

15. Supplementary Notes
This report should be cited as: Woods Hole Oceanog. Inst. Tech. Rept., WHOI-94-12.

16. Abstract (Limit: 200 words)

"Geometrical methods in fluid dynamics" were the subject of the 1993 GFD session. Participants explored the applications of Hamiltonian fluid mechanics and related ideas about symmetry and conservation laws to problems in geophysical fluid dynamics. Phil Morrison and Ted Shephere offered an intensive introductory course (of which a detailed summary appears in this volume.) Subsequent lecturers explored a full range of currently interesting topics in geophysical fluid dynamics.

17. Document Analysis **a. Descriptors**
Hamiltonian
symplectic
fluid

b. Identifiers/Open-Ended Terms

c. COSATI Field/Group

18. Availability Statement
Approved for public release; distribution unlimited.

19. Security Class (This Report)
UNCLASSIFIED

20. Security Class (This Page)

21. No. of Pages
366

22. Price

(See ANSI-Z39.18) *See Instructions on Reverse*

OPTIONAL FORM 272 (4-77)
(Formerly NTIS-35)
Department of Commerce